# *Synthesis, Characterisation, Reactivity and Computational Study of Cobalt and Palladium Complexes of bis(Diphenylphosphino)amines*

ADAM CARRICK

# Synthesis, Characterisation, Reactivity and Computational Study of Cobalt and Palladium Complexes of *bis*(Diphenylphosphino)amines

Department of Chemistry, Durham University

2020 – 2024

Thesis submitted for the degree of Doctor of Philosophy

By

**Adam Carrick, MChem (Dunelm), MRSC, AFHEA**

## Statement of Originality

This thesis if based on work conducted by the author, in the Department of Chemistry at Durham University, during the period October 2020 to March 2024. All the work described in this thesis is original, unless otherwise acknowledged in the text or in the references. None of this work has been submitted for any other degree in this or any other University.



Signed: A Carrick Date: 29/04/24

This thesis is for Mam, Dad, our Alex, Nana, Grandad and Gran.

In loving memory of

My Grandad

Thomas Mallaby

30/08/1939 – 22/12/2023

Thank you for everything

“You show them what people where we are from can do”

## Abstract

This thesis presents the synthesis and characterisation of a range of cobalt(I) and cobalt(II) complexes of narrow bite angle *bis*(diphenylphosphino)amine-type ('PNP') and associated ligands.

**Chapter 1** outlines the importance of bite angle in the coordination chemistry and reactivity of cobalt complexes, with particular emphasis on 'PNP' and related ligands.

**Chapter 2** describes the synthesis of an array of 'PNP' and associated ligands and their corresponding phosphine selenides.

**Chapter 3** presents the coordination chemistry of 'PNP' and 'PCNCP' ligands with $[(MeCN)_2PdCl_2]$. The reactivity of $[\{Ph(CH_2)_2N(PPh_2)_2\}PdCl_2]$ with MeOH (affording $[(PhCH_2CH_2NHPPh_2)(MeOPPh_2)PdCl_2]$) and $[\{Py\text{-}o\text{-}(CH_2)_2N(PPh_2)_2\}PdCl_2]$ with trifluoroacetic acid (affording $[(H\text{-}Py\text{-}o\text{-}(CH_2)_2N(PPh_2)_2)PdCl_2][CF_3CO_2]$) as well as $CoCl_2$ and $[N(n\text{-}Pr)_4]Cl$ (affording $[N(n\text{-}Pr)_4][(\{Cl_3Co\}Py\text{-}o\text{-}(CH_2)_2N(PPh_2)_2)PdCl_2]$) is probed.

**Chapter 4** discusses the coordination of 'PNP' ligands with $CoX_2$ (X = Cl, Br, and I), in particular describing the formation of zwitterionic (*e.g.*, $[CoX(Py\text{-}o\text{-}(CH_2)_2N\{PPh_2\}_2)(\{X_3Co\}Py\text{-}o\text{-}(CH_2)_2N\{PPh_2\}_2)]$) or ionic (*e.g.*, $[CoX(Ph(CH_2)_2N\{PPh_2\}_2)_2]_2[Co_2X_6]$) complexes. The pathway to zwitterionic cobalt(II) complexes *via* an ionic cobalt(II) complex formed *in situ* is verified through the synthesis of $[CoBr(Ph(CH_2)_2N\{PPh_2\}_2)_2][PyCoBr_3]$ obtained from reacting $[CoBr(Ph(CH_2)_2N\{PPh_2\}_2)_2]_2[Co_2Br_6]$ with pyridine.

**Chapter 5** outlines the synthesis and zinc reduction of cobalt(II) complexes $[CoBr('PNP')_2][BAr^F{}_4]$ to afford cobalt(I) complexes of the form $[Co('PNP')_2][BAr^F{}_4]$. Attempts at other strategies to access cobalt(I) complexes, as well as the reactivity of $Py\text{-}o\text{-}(CH_2)_2N(PPh_2)_2$ and $Ph(CH_2)_2N(PPh_2)_2$ with $ZnBr_2$, are presented.

**Chapter 6** explores the reactivity of $[Co\{Ph(CH_2)_2N(PPh_2)_2\}_2][BAr^F{}_4]$ with ethylene, CO and $H_2$, and describes the formation of $[Co\{Ph(CH_2)_2N(PPh_2)_2\}_2(\eta^2\text{-}CH_2CH_2)][BAr^F{}_4]$, $[Co\{Ph(CH_2)_2N(PPh_2)_2\}_2CO][BAr^F{}_4]$ and an equilibrium mixture of $[Co\{Ph(CH_2)_2N(PPh_2)_2\}_2(\eta^2\text{-}H_2)][BAr^F{}_4]$ and $[Co\{Ph(CH_2)_2N(PPh_2)_2\}_2(cis\text{-}(H)_2)][BAr^F{}_4]$, respectively (primarily studied by $^{31}P\{^1H\}$ NMR and computational studies).

**Chapter 7**, **Chapter 8** and the **Appendices** contain all experimental details, conclusions and future outlook, and supplementary information, respectively.

## Acknowledgements

Thank you to Mam, Dad, our Alex, Nana, Grandad, Gran, Uncle Raymond, our Derek, Uncle Thomas (and the dogs!) and the rest of my family for all of their support, love and kindness during my PhD. I'm fortunate to be able to call County Durham hyem (that's 'home' for those not lucky enough to be from the North East), and having my family close-by has been a lifeline during my PhD. Thank you in particular to Mam for all the teas, carpooling to work, and for listening to me moan – a lot!

Thank you to my supervisor Prof. Phil Dyer for giving me the opportunity to do a PhD in his group, for listening to and discussing my ideas, for supporting my development, for asking and answering questions, for giving feedback on everything you can possibly imagine, and for being an exceptionally kind and selfless supervisor. Anyone wanting to do a PhD in the field of catalysis would be lucky to have Phil as a supervisor.

Thank you to the Dyer group, especially Jake, Alana, Hannah and Sherry. Special thanks to Jake (who started and finished his PhD on the same dates as me, and was also a Dyer MChem 2019-20) for being a great mate of mine since the 2nd year of our MChem's at Durham. Thank you for everything mate, I appreciate it. Thank you to Alana for teaching me Schlenk chemistry many moons ago and for falling off the stool that one time – that was really funny – and to Hannah for being a great MSc student during the last 6 months of my PhD and bringing 'youthfulness' to the group.

Thank you to: Dr Juan Aguilar Malavia for all of his help running 'sophisticated' NMR experiments on my often tricky samples; Dr's Andrei Batsanov, Dmitry Yufit and Toby Blundell for their excellent crystallographic work, which features heavily in this thesis; my secondary supervisor Dr Mark Fox for all of his help and advice relating to computational chemistry; Dr Pippa Coffer for supporting my teaching in the undergraduate laboratory (which I really enjoyed); Becky for being a nice familiar face on the technical team face from my MChem days; Aaron Brown and Malcolm Richardson for fixing numerous Schlenk lines and flame sealing many NMR tubes, and Mr Len Lauchlan and Dr Emily Unsworth for collecting IR and CHN data, respectively.

## Table of Contents

## Abbreviations

Å – Angstrom

Ar – Aryl

atm – Atmosphere

B – Field adjacent from the nuclei

$B_0$ – Applied magnetic field

$Ar^F$ – 3,5-*bis*(trifluoromethyl)phenyl

*β*-H – Beta hydrogen

br – Broad

Bu – Butyl

B3LYP – Becke three-parameter Lee-Yang-Parr functional

$C_n$ – Moles of polymer with n carbon atoms

CHN – Carbon, Hydrogen, Nitrogen

CSD – Cambridge Structural Database

Cy – Cyclohexyl

d – Doublet

*δ* – Chemical shift

DCM – Dichloromethane

Dcype – 1,2-*bis*(dicyclohexylphosphino)ethane

DFT – Density Functional Theory

DME – Dimethoxyethane

Dedpe – $Et_2PCH_2CH_2PPh_2$

DIOP – 2,3-*O*-isopropylidene-2,3-dihydroxy-1,4-*bis*(diphenylphosphino)butane

DPPA – Diphenylphosphinoamine

Dppb – 1,4-*bis*(diphenylphosphino)butane

Dppbz – 1,2-*bis*(diphenylphosphino)benzene

Dppe – 1,2-*bis*(diphenylphosphino)ethane

Dppf – 1,1'-*bis*(diphenylphosphino)ferrocene

Dppm – 1,1-*bis*(diphenylphosphino)methane

Dppp – 1,2-*bis*(diphenylphosphino)propane

Dppv – *cis*-1,2-*bis*(diphenylphosphino)ethylene

ESI – Electrospray ionisation

Et – Ethyl

equiv. – Equivalents

FT-IR – Fourier transform infrared

G – Gibbs free energy

HBPin – Pinacolborane

HOMO – Highest occupied molecular orbital

$^{(i)}Pr$ – (*iso*)propyl

$^nJ_{AB}$ – n-bond coupling constant between nuclei A and B

$k_x$ – Rate constant

K – Equilibrium constant

L – neutral ligand (2 electron donor)

$L_nM^{(n+)}$ – Ligated metal

LUMO – Lowest unoccupied molecular orbital

m – Multiplet or Meta (italics)

MAO – Methyaluminoxane

Me – Methyl

MeCN – Acetonitrile

MHHB – Metal Halogen Hydrogen Bond

MMAO – Modified methylaluminoxane

MO – Molecular Orbital

Mol – Moles

MS – Mass Spectrometry

*m/z* – Mass per charge

n – Number

*N,N* – Bidentate nitrogen-based ligand

$N_A$ – Avogadro's constant

*N,S* – Bidentate nitrogen sulfur ligand

NMR – Nuclear Magnetic Resonance

NOESY – Nuclear Overhauser effect spectroscopy

*o* – Ortho

OPh – Phenoxy group

*p* – para

PCNCP – $RN(CH_2PR'_2)_2$

Ph – Phenyl

*P,N* – Bidentate phosphorus nitrogen ligand

PNP – $RN(PR'_2)_2$

*P,P* – Bidentate phosphine

ppm – Parts per million

*P,S* – Bidentate phosphorus sulfur ligand

PPN – *Bis*(triphenylphosphine)iminium

Py – Pyridyl

q – Quartet

quin – Quintet

R – Gas constant

s – Singlet

S – Solvent

sF – Shape factor

SPNP – $RN(S=PR'_2)(PR'_2)$

SPNPS – $RN(S=PR'_2)_2$

spt – Septet

t – Triplet

T – Temperature

$T_1$ – Spin-lattice relaxation

$T_2$ – Spin-spin relaxation

$\mu_{eff}$ – Effective magnetic moment

TFA – Trifluoroacetic acid

TMS – Trimethylsilyl

THF – Tetrahydrofuran

UV-Vis – Ultraviolet-visible

$\upsilon$ – Frequency

$\%V_{bur}$ – Percentage buried volume

VT – Variable temperature

XRD – X-Ray Diffraction

2D – Two dimensional

°C – Degrees Celsius

## Experimentally Studied Compounds and Complexes in Chapter 2

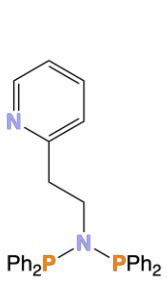

**2.1**

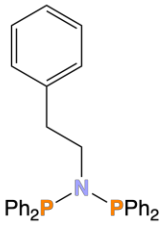

**2.2**

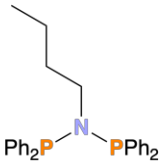

**2.3**

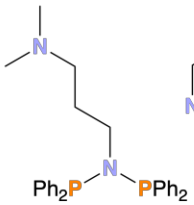

**2.4**

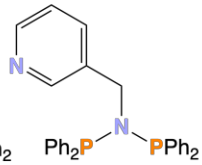

**2.5**

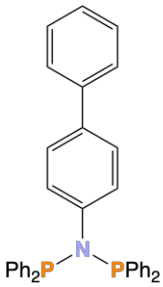

**2.6**

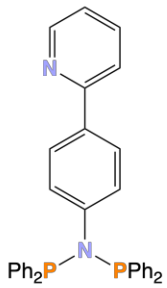

**2.7**

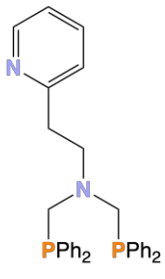

**2.8**

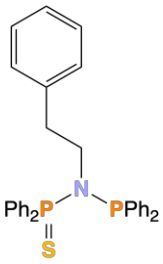

**2.9**

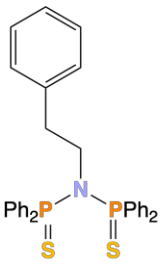

**2.10**

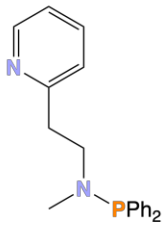

**2.11**

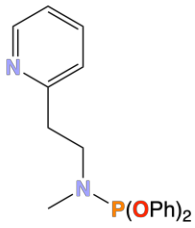

**2.12**

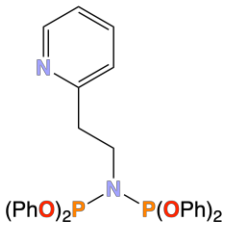

**2.13**

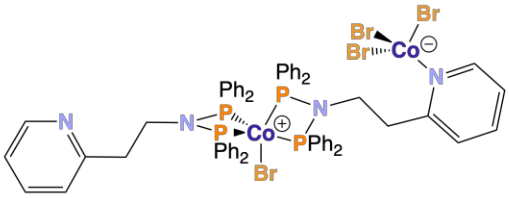

**2.14**

**Phosphine Selenides of 2.2 – 2.9, 2.11 and 2.12**

## Experimentally Studied Compounds and Complexes in Chapter 3

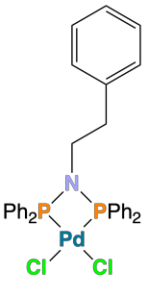

**3.1**

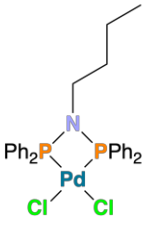

**3.2**

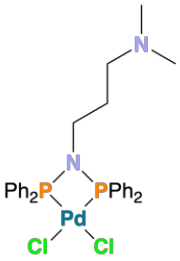

**3.3**

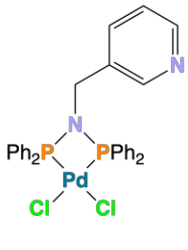

**3.4**

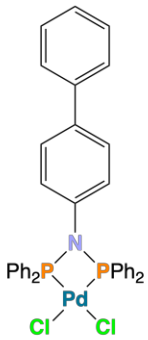

**3.5**

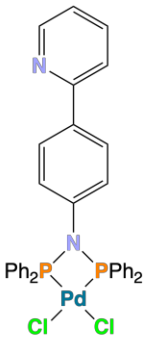

**3.6**

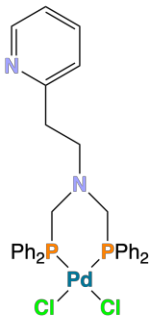

**3.7**

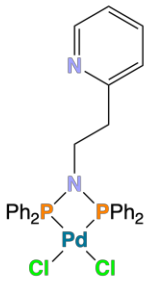

**3.8**

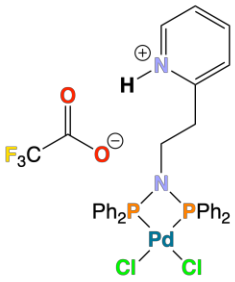

**3.9**

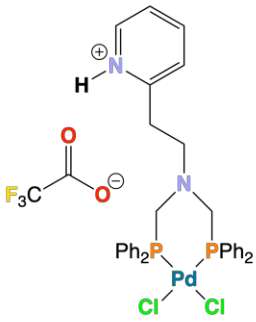

**3.10**

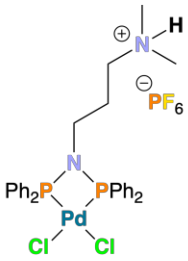

**3.11**

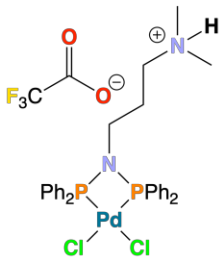

**3.12**

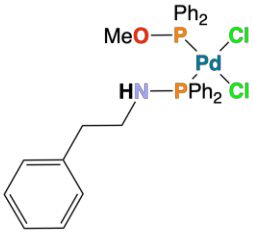

**3.23**

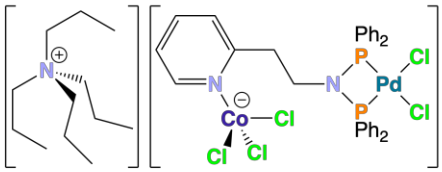

**3.25**

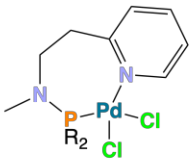

**3.29** (R = Ph)
**3.30** (R = OPh)

## Experimentally Studied Compounds and Complexes in Chapter 4

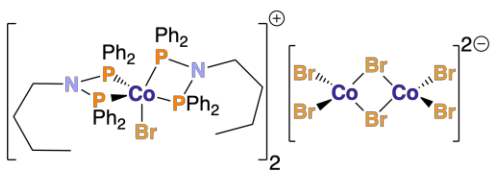

4.1

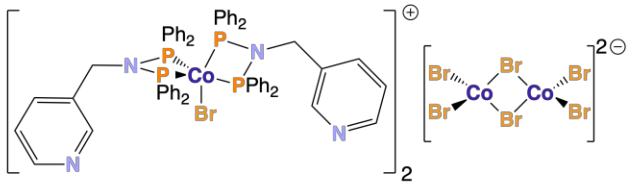

4.2

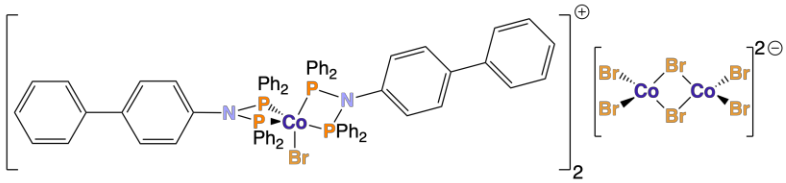

4.3

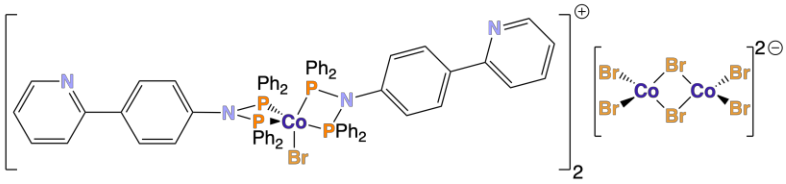

4.4

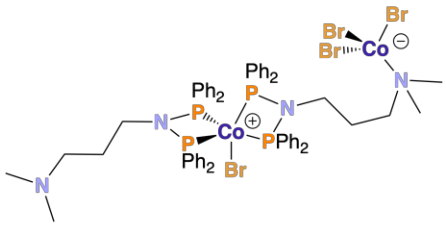

4.5

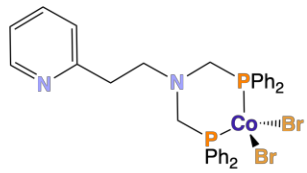

4.6

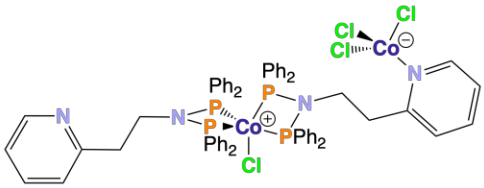

4.7

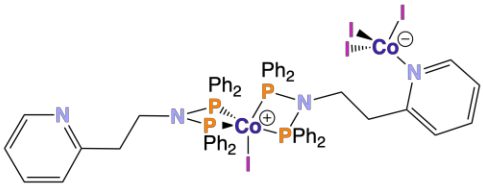

4.8

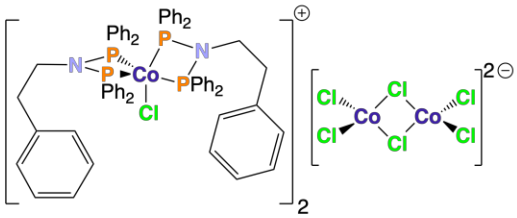

4.9

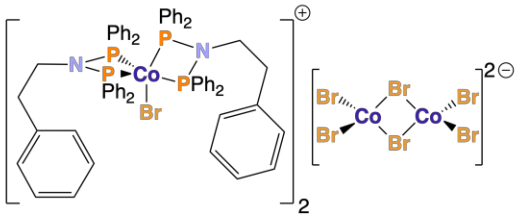

4.10

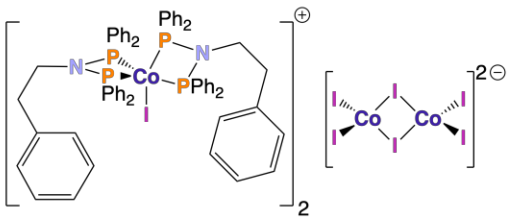

4.11

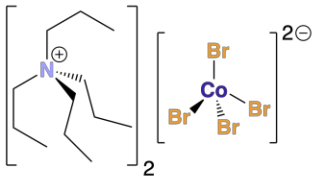

**4.13**

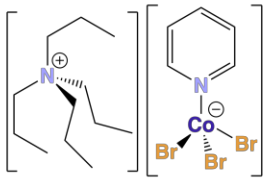

**4.14**

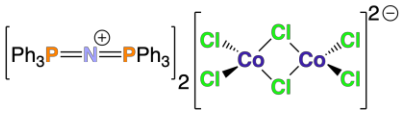

**4.15**

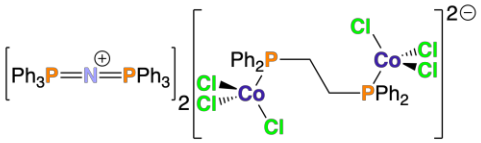

**4.16**

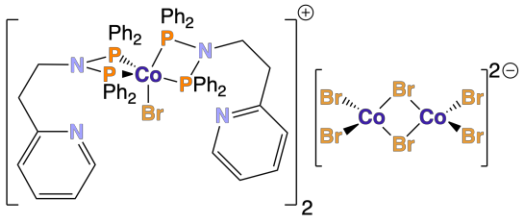

*In situ* ionic intermediate **4.18**

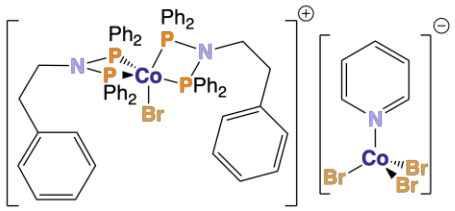

**4.19**

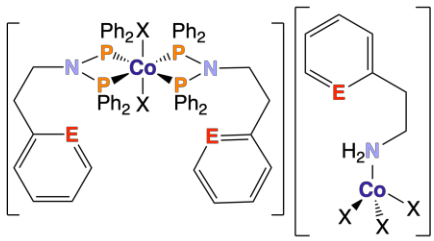

**4.20** {**E** = **N**} (X = **Cl**); **4.21** {**E** = **N**} (X = **Br**)
**4.22** {**E** = CH} (X = **Cl**); **4.23** {**E** = CH} (X = **Br**)

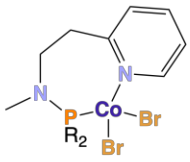

**4.24** (R = Ph)
**4.25** (R = **O**Ph)

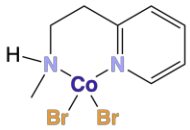

**4.26**

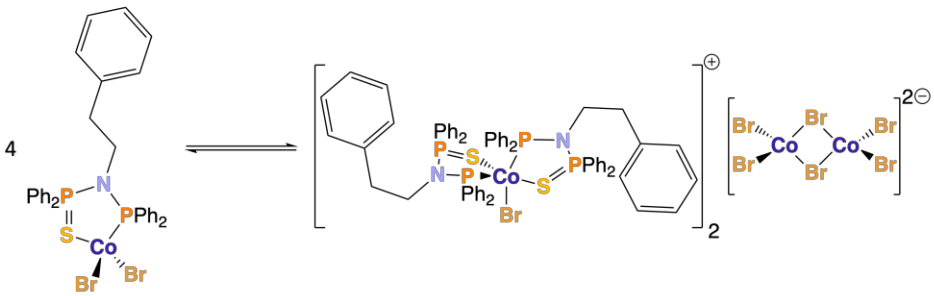

**4.27** **4.28**

# Experimentally Studied Compounds and Complexes in Chapter 5

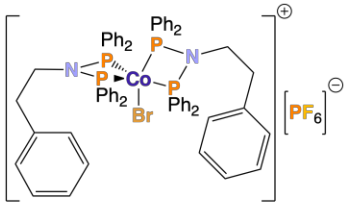

**5.1**

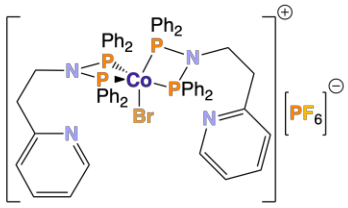

**5.2**

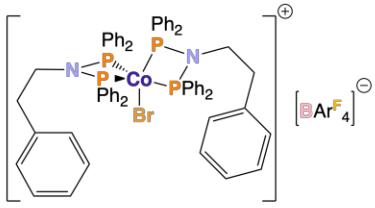

**5.3**

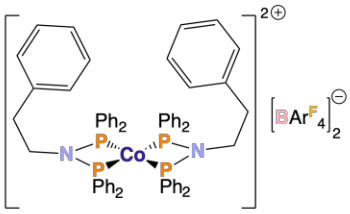

**5.4**

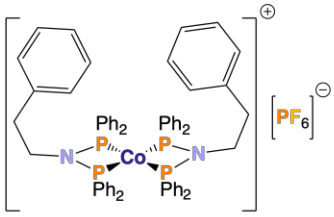

**5.5**

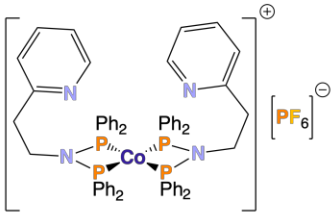

**5.6**

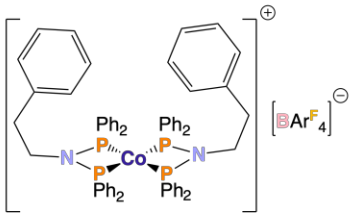

**5.7**

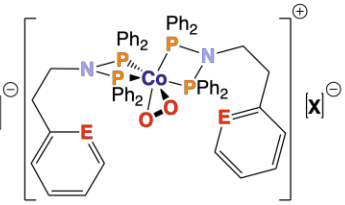

**5.11** {E = CH}, X = $PF_6$
**5.12** {E = N}, X = $PF_6$
**5.13** {E = CH}, X = $BAr^F_4$

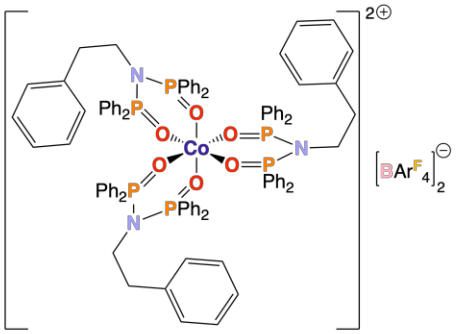

**5.16**

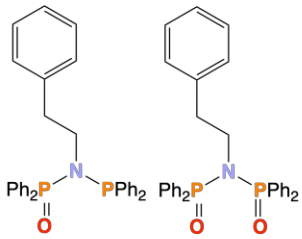

**5.17**



**5.18**

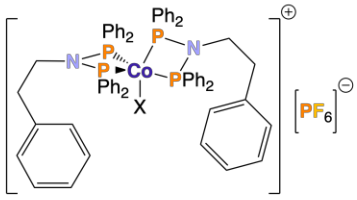

**5.19** (X = 0.75Cl : 0.25Br)
**5.20** (X = Cl)

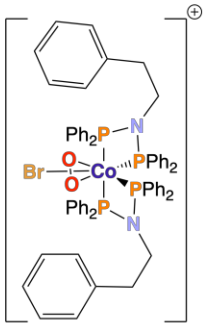

**5.23 Cation**

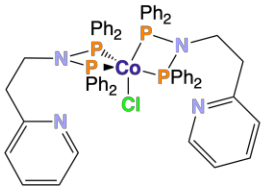

**5.27**

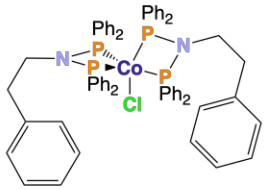

**5.28**

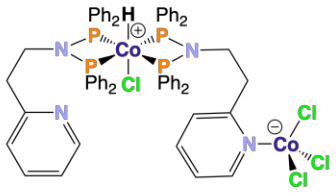

**5.32**

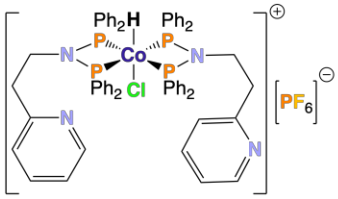

**5.33**

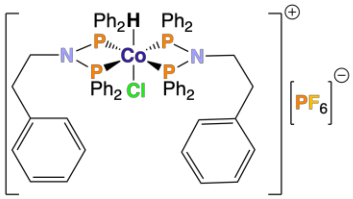

**5.34**

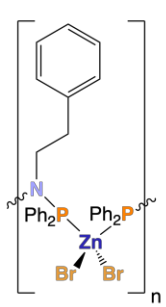
N
Ph2P
Ph2P
Zn
Br
Br
n

**5.44**

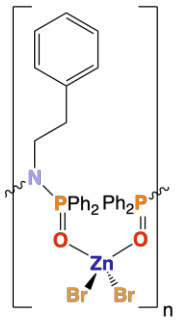
N
PPh2
Ph2P
O
O
Zn
Br
Br
n

**5.47**

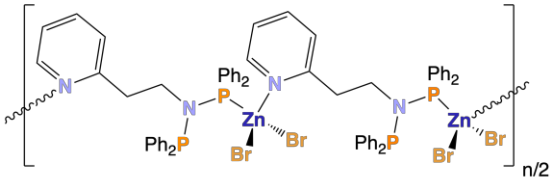
N
N
Ph2P
Ph2
P
N
Zn
Br
Br
N
Ph2P
Ph2
P
Zn
Br
Br
n/2

**5.54**

# Experimentally Studied Compounds and Complexes in Chapter 6

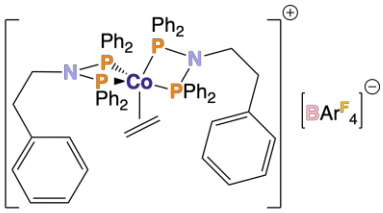

6.1

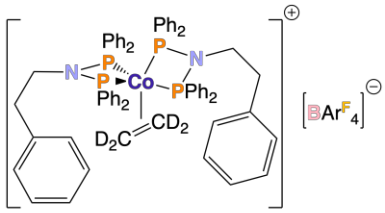

6.9

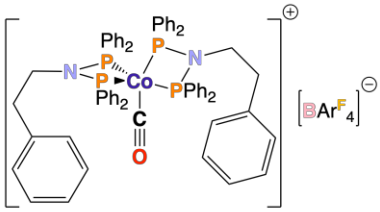

6.21

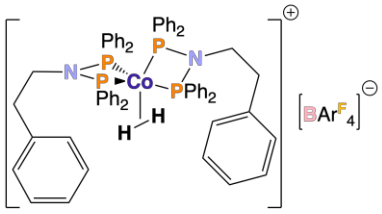

6.26

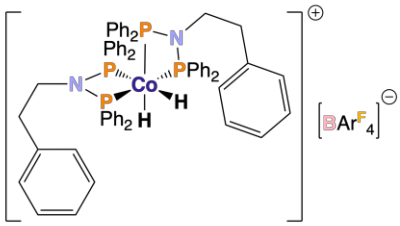

6.29

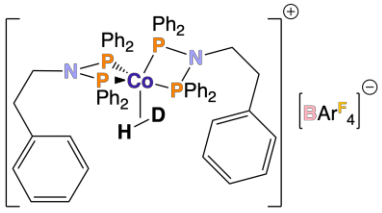

6.27

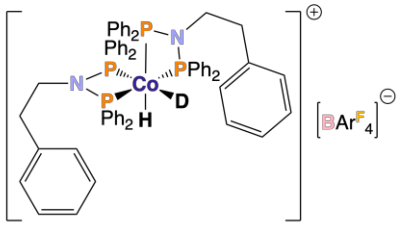

6.30

# Chapter 1 – Introduction

The main aim of this work is to gain an understanding of the effect of ligands with < 90° bite angles on the structure and reactivity of cobalt complexes. Hence, this thesis explores aspects of the fundamental coordination chemistry of narrow bite angle 'PNP' ligands ($RN\{PPh_2\}_2$, where R = alkyl, aryl, *etc*.,) and associated analogues (*i.e*., 'PCNCP', 'SPNP' and 'SPNPS') with cobalt using a combination of synthetic, spectroscopic and computational approaches. Subsequently, the reactivity of synthesised 'PNP' cobalt complexes with activated zinc and gaseous substrates (ethylene, carbon monoxide and dihydrogen) is probed. The synthesis of zinc and palladium complexes of 'PNP' ligands is also presented. The overarching theme of **Chapter 1** is a discussion of the importance of bidentate ligand bite angle in metal complex reactivity. An overview of the use of low valent cationic diphosphine cobalt(I) complexes in catalysis and a summary of the fundamental chemistry established in relation to 'PNP' ligands are also presented.

## 1.1 An Overview of Ligand Bite Angle

The bite angle ($\beta$, **a)**, **Figure 1.1**) is the angle subtended at the metal between the two coordinating donors of chelating ligands in metal complexes. This angle has significant effects on metal complex reactivity and the subsequent application of metal complexes as catalysts by altering reaction selectivity and catalytic activity. Preferences for geometries adopted by (and accessible to) metal complexes are dictated by the bite angle of the chelating ligand as the bite angle is heavily dependent on the nature and number of atoms in the backbone between the donor atoms. The ability of a ligand to enforce specific bite angles enables access to reaction pathways through the stabilisation of particular metal complex geometries present in the initial, transition and final states, as well as in intermediates in catalytic cycles.[1–7]

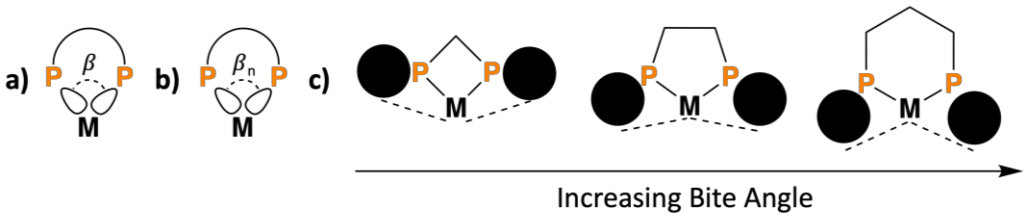


**Figure 1.1. a)** the bite angle of (*P,P*)M; **b)** natural bite angle of (*P,P*)M; **c)** the steric bite angle effect, increasing with increasing bite angle, where black spheres represent phosphorus substituents.[1]

For diphosphine complexes, the P-M-P angle (**a)**, **Figure 1.1**) is often measured from solid-state structures of complexes determined by XRD analysis, but increasingly the bidentate ligand bite angle is also being determined computationally. For example, the natural bite angle, $\beta_n$, as defined by Casey and Whiteker[8] (**b)**, **Figure 1.1**), is computed using molecular mechanics by placing the phosphine donor at an average distance (*e.g.*, 2.315 Å for M = rhodium)[2] away from a "dummy" metal centre (necessary to ensure the phosphorus atom lone pairs are orientated in the correct direction).[2,8,9] $\beta_n$ is defined as the preferred chelation angle determined not by metal valence angles, but only by the ligand backbone, *i.e.*, dependent only on ligand sterics and not electronic considerations imposed by the metal centre.[8] In reality, the determined P-M-P angle $\beta_n$ is a compromise between the P-M-P angles preferred by the metal centre (determined by the metal valence orbitals, generally d-orbitals, involved in the P-M bond molecular orbitals) and the ligand (determined by steric repulsion arising from the phosphorus substituents and the backbone, and geometric constraints arising from the ligand backbone).[10]

Two effects can be observed in a series of related metal complexes stemming from the influence of the P-M-P bite angle: the steric bite angle and the electronic bite angle effects.[2] The steric bite angle effect (**c)**, **Figure 1.1**) is observed for a series of bidentate diphosphine ligands with the same phosphorus substituents, but with different ligand backbones.[2] Bidentate ligands with wider bite angles can be regarded as being more sterically demanding, occupying more of the coordination sphere around the metal centre and exerting more steric repulsion upon other ligands or substrates coordinating at the metal centre.[1,2] The electronic bite angle effect is orbital in origin as the P-M-P angle determines metal orbital energies as a result of metal hybridisation.[6] As a result, a particular P-M-P angle electronically favours and stabilises a preferred geometry, which is exhibited by the complex. For example, square planar and tetrahedral complexes prefer ligands with bite angles of approx. 90° and 109.5°, respectively.[1]

The P-M-P angle can also impact the structures of obtained complexes. For example, diphosphines $^{i}Pr_2P(CH_2)_xP^{i}Pr_2$ with $x \geq 4$ have enough flexibility to reduce the statistical likelihood of chelation,[11] allowing instead for the formation of bridged bimetallic complexes, for example **1.2** (**Figure 1.2**), a structure that is quite different to that of complex **1.1** (**Figure 1.2**) containing two bidentate $^{i}Pr_2P(CH_2)_xP^{i}Pr_2$ ligands with x = 2.[11] In contrast, rigid linkers can be used in order to achieve chelation with large bite angle

ligands, something well-established for ligands such as Xantphos and DPEphos (**Figure 1.2**).[2]

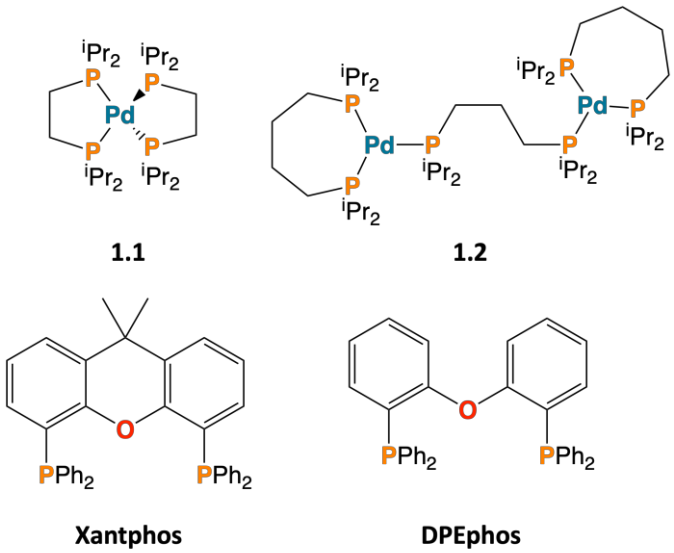


**Figure 1.2.** Structures of complexes **1.1** and **1.2**,[11] and of so-called "wide bite angle" diphosphine ligands Xantphos and DPEphos.[2]

## 1.1.1 Low Valent Cationic Diphosphine Cobalt Complexes in Catalysis

The effect of the P-M-P angle upon catalyst selectivity in a range of metal complex-mediated reactions is well-established. For example, complexes **1.3** – **1.6** have been utilised as pre-catalysts, in combination with $Me_3Al$, to afford catalytically active cationic cobalt(II) species (believed to be $[(P\text{^}P)CoH]^+$), active for the hydrovinylation of 1,3-(*E*)-nonadiene.[12] The systems incorporating diphosphine ligands with larger bite angles, *i.e.*, n = 2, 3, 4, afforded almost exclusively the 4,1-(*Z*)-diene **1.7**, whereas the derivatives with smaller bite angle diphosphines, *i.e.*, n = 1, gave mostly 2,1-(*E*)-diene **1.8** (**Scheme 1.1**).[12]

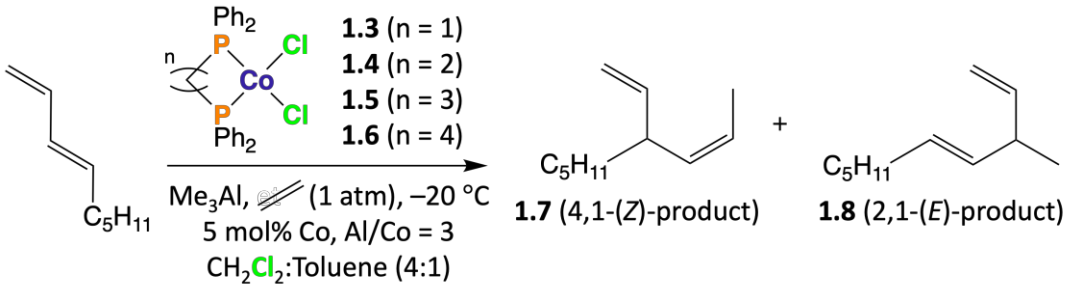


**Scheme 1.1.** Major products **1.7**, 4,1-(*Z*)-product, when n = 1, and **1.8**, 2,1-(*E*)-product when n = 2, 3, or 4, of the hydrovinylation of 1,3-(*E*)-nonadiene.[12]

Complexes **1.3** – **1.6**, in combination with MAO (or activated zinc and $NaBAr^F_4$), have also been used as pre-catalysts for the hydroboration of 1,3-(*E*)-nonadiene.[13] The

catalytic system, using MAO, with complex **1.3** (n = 1, smallest bite angle) provided 82% regioselectivity for compound **1.10** in 4 hours (**1.9**:**1.10**:**1.11** of 6:82:12), whereas the catalytic system with complex **1.5** (n = 3, *i.e.*, a larger bite angle) afforded compound **1.9** with 95% regioselectivity in 15 minutes (**1.9**:**1.10**:**1.11** of >95:5:0), further evidencing the impact that bite angle can have upon reactivity (**a)**, **Scheme 1.2**).[13] The catalytic system incorporating complex **1.5**, alongside activated zinc and $NaBAr^F_4$, still affords compound **1.9** as the major product, but only with 82% regioselectivity (**1.9**:**1.10**:**1.11** of 82:14:4), with the proportion of compound **1.11** (isomerisation product) increasing with time.[13] Activation of complex **1.5** with zinc (in the absence of $NaBAr^F_4$) and subsequent reaction with 1,3-(*E*)-nonadiene did not result in any reaction, but utilising $NaBAr^F_4$ (in the absence of zinc) again afforded compound **1.9** as the major product (**1.9**:**1.10**:**1.11** of 82:13:5), with a cationic cobalt(I) catalyst presumably being produced through HBPin serving as a reducing agent.[13] Synthesis and catalytic application of isolated cobalt(I) complex **1.12** (**b)**, **Scheme 1.2**) with $NaBAr^F_4$ resulted in compound **1.9** being afforded as the major product (**1.9**:**1.10**:**1.11** of 83:14:3) in a 5 minute reaction. The role of a cationic cobalt(I) species in the catalytic hydroboration process (**Scheme 1.2**) was verified by the observation that utilising complex **1.12** in the absence of $NaBAr^F_4$ resulted in no reaction.[13]

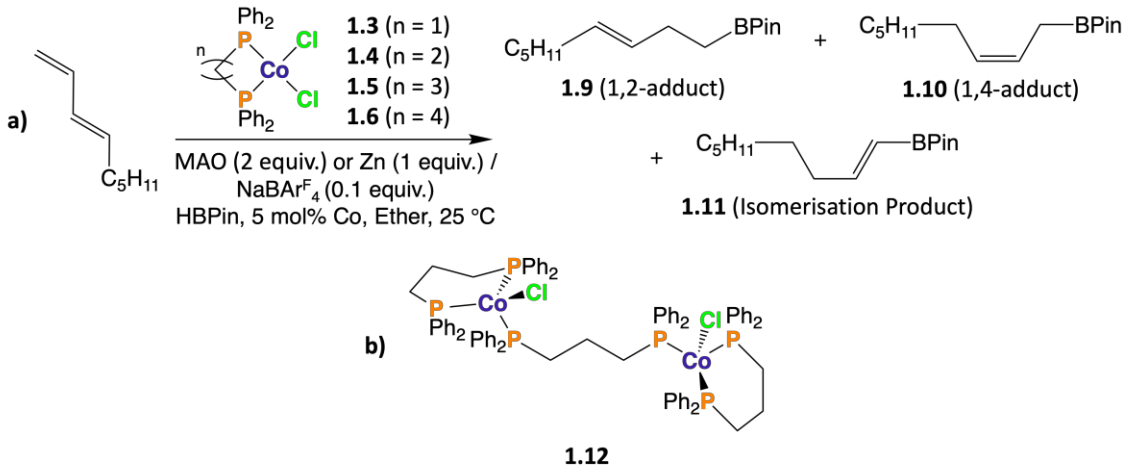


**Scheme 1.2. a)** major products **1.9**, 1,2-product when n = 3 and 4, and **1.10**, 1,4-product when n = 1 and 2, and isomerisation product **1.11** for the hydroboration of 1,3-(*E*)-nonadiene; **b)** structure of complex **1.12**.[13]

The cationic cobalt(I) complex generated from the reduction of complex **1.13** (**Scheme 1.3**) with activated zinc, in the presence of $NaBAr^F_4$, has been identified to be the active species for enantioselective heterodimerisation of acrylates and 1,3-dienes.[14,15] The proposed catalytic mechanism (**Scheme 1.3**) is supported by a detailed kinetic study that

found reaction rate orders with respect to the catalyst, 2,3-dimethylbutadiene and methyl acrylate, are first, first and zeroth order, respectively.[14] The observation of an induction period was also confirmed by stirring complex **1.13** (**Scheme 1.3**), zinc and $ZnBr_2$ before the addition of methyl acrylate and 2,3-dimethylbutadiene. An initial activation time of 5 minutes is observed during which only a slow decrease in the alkene substrate concentration occurs.[14] It is proposed that this is due to incomplete catalyst activation, *i.e.*, production of **A** (**Scheme 1.3**) not taking place until after 5 minutes of reaction.

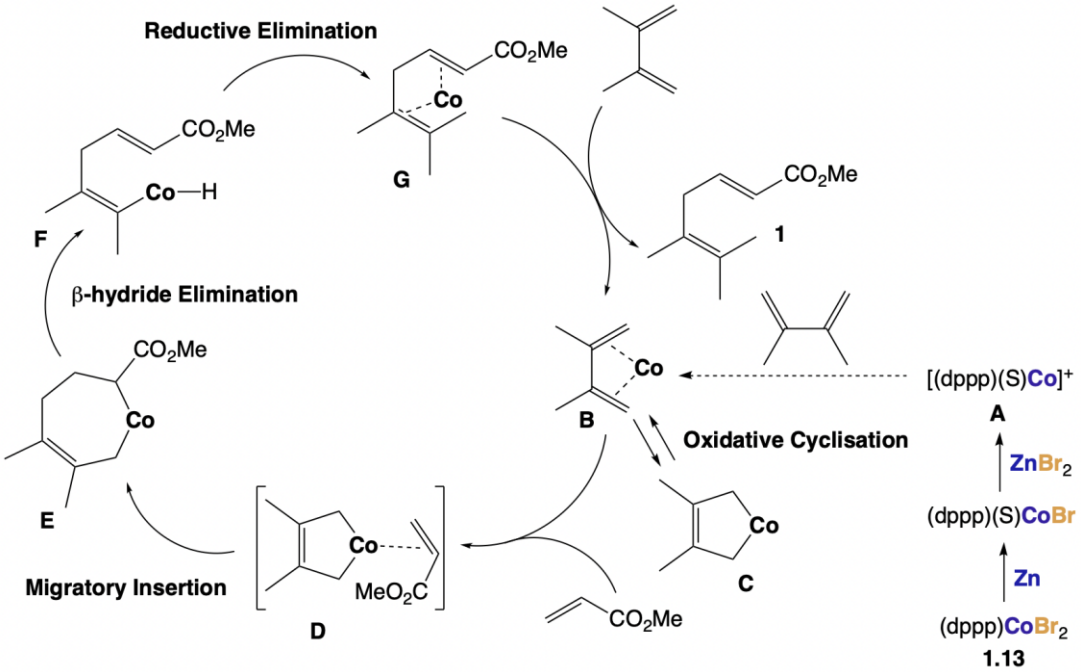


**Scheme 1.3.** Proposed catalytic cycle for the cobalt-dppp complex catalysed heterodimerisation reaction of methyl acrylate and 2,3-dimethylbutadiene. *NB.* S = solvent, **Co** = $[(dppp)Co]^+$ and dppp = 1,3-*bis*(diphenylphosphino)propane.[14]

The role of a cobalt(I) species in the catalytic cycle shown in **Scheme 1.3** has been elucidated spectroscopically. Comparison of the UV-Vis spectra of a stirred mixture of complex **1.13**, zinc and $ZnBr_2$ (*i.e.*, the reaction used for *in situ* catalyst generation) over a period of time revealed that the absorbance of bands characteristic of cobalt(I) species (namely at 740 nm and a broad band above 900 nm) increased up until 240 minutes after initial mixing.[14] It was shown that the cobalt(I) complex must be cationic by running two parallel reactions; one reaction included (dppp)CoBr (isolated from the reduction of complex **1.13** with zinc), methyl acrylate and 2,3-dimethylbutadiene, and the other reaction included (dppp)CoBr, methyl acrylate, 2,3-dimethylbutadiene and $ZnBr_2$. Only the reaction containing (dppp)CoBr, methyl acrylate, 2,3-dimethylbutadiene and $ZnBr_2$

showed conversion of the alkene substrates to the desired product.[14] Hence, it is implied that a cationic cobalt(I) complex is the active species for heterodimerisation (and related catalytic processes), since the role of $ZnBr_2$ is to generate a cationic cobalt(I) complex.

### 1.1.2 Importance of Bidentate Ligand Bite Angle in Cobalt Complex Coordination Chemistry

Systematic variation in the P-M-P bite angle can result in drastic changes in the structure of metal complexes. For example, utilising acute bite angle ligands can result in metal complexes exhibiting unique coordination chemistry. Ionic complexes of the form $[CoX(dppe)_2]_2[X_3Co\text{-}dppe\text{-}CoX_3]$ (where X = Cl, Br, I, **Figure 1.3**) are obtained upon reaction of $CoX_2$ with dppe,[16] with the cationic cobalt(II) centre having a trigonal bipyramidal (**1.14**) or square-based pyramidal (**1.15**) geometry (**Figure 1.3**). The structures of complexes **1.14** and **1.15** differ significantly from the structure of complex **1.4** proposed in **Scheme 1.1/1.2**. In contrast, the neutral molecular structure $[(dppp)CoCl_2]$ is obtained upon reaction of dppp (with a larger natural bite angle than dppe) with $CoCl_2$,[17] agreeing with the structure of complex **1.5** proposed in **Scheme 1.1/1.2**. The differing regioselectivities outlined for the catalytic processes described in **Scheme 1.1/1.2**[12,13] are likely implications of the differing geometries around the cobalt centre and structure types of the pre-catalyst species $[CoX(dppe)_2]_2[X_3Co\text{-}dppe\text{-}CoX_3]$ and $[(dppp)CoCl_2]$ (and analogously for the catalytically active species).

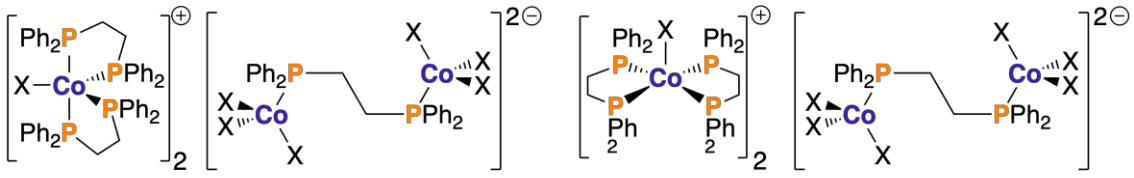

**1.14** **1.15**

**Figure 1.3.** Structures of complexes **1.14** and **1.15**, where X = Cl, Br and I for complex **1.14** and X = Br and I for complex **1.15**.[16]

A comparison of the structures of complexes **1.16**,[18] **1.17**,[19] **1.18**[20]/**1.19**[21] and **1.21** – **1.27**[21,22] shows that increasing the bite angle in a series of ligands ranging from 'PNP' in complex **1.16**, 'PCNCP' in complexes **1.17** – **1.19**, to 'PCCNCCP' in complexes **1.21** – **1.27** results in a significant change in the structure of the associated cobalt complexes (**Figure 1.4**). Zwitterionic complex **1.16** (with a distorted trigonal bipyramidal cationic cobalt(II) centre, with two equivalents of diphosphine coordinating, and a distorted tetrahedral

anionic cobalt(II) centre) is obtained from the 1:1 reaction of $CoCl_2$ with acute bite angle 'PNP' ligand $MeS(CH_2)_3N(PPh_2)_2$. In contrast, neutral [(*P^P*)$CoX_2$] complexes **1.21** – **1.27** (with distorted tetrahedral cobalt(II) centres) are afforded from the 1:1 reactions of $CoX_2$ (X = Cl, I) with large bite angle 'PCCNCCP' ligands. This suggests that the acute bite angle of 'PNP' ligands promotes zwitterionic complex formation. In contrast, the larger bite angle of 'PCCNCCP' ligands disfavours this, instead preferring neutral cobalt(II) complexes of the form [(*P^P*)$CoX_2$]. However, both zwitterionic (complex **1.17**) and neutral (complexes **1.18** and **1.19**) cobalt(II) halide complexes are accessible from the 1:1 reactions of $CoX_2$ (X = Cl, I) with 'PCNCP' ligands (**Figure 1.4**), suggesting that 'PCNCP' ligands have an intermediate bite angle that can support both types of cobalt(II) complex. Hence, unique cobalt complex structures can be achieved using acute bite angle 'PNP' ligands (including co-crystal **1.20**),[23] although elucidation of the exact reasoning requires further study.

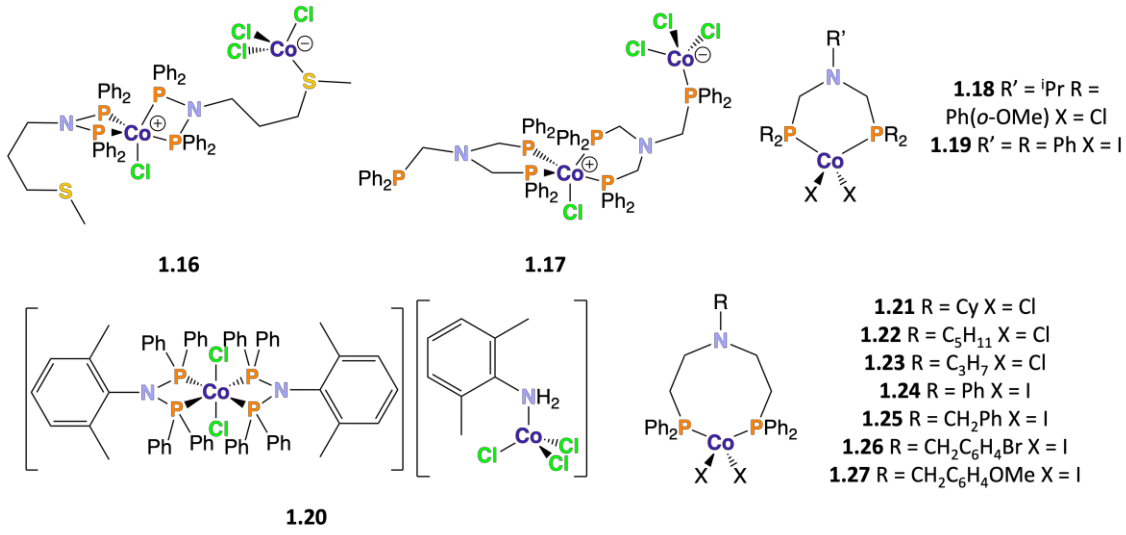


**Figure 1.4.** Structures of complexes **1.16** – **1.19** and **1.21** – **1.27**, and co-crystal **1.20**.[18 – 23]

## 1.2 An Overview of 'PNP' ligands

As highlighted in **Section 1.1.1** – **1.1.2**, cobalt complexes with acute bite angle diphosphine ligands exhibit unique reaction selectivity when utilised as pre-catalysts in catalytic processes[12,13] and unique coordination chemistry compared to their larger bite angle analogues.[16 – 23] Hence, metal complexes containing acute bite angle diphosphine ligands are interesting targets for further study. Complex **1.16**[18] and co-crystal **1.20**[23] (**Figure 1.4**) contain acute bite angle 'PNP' ligands (*bis*(diphenylphosphino)amine

ligands, *i.e.*, **1.28** in **Scheme 1.4**) which have been identified as a suitable ligand scaffold for future investigation. 'PNP' ligands are easy to synthesise (although incorporation of sterically demanding motifs on the bridging N-atom can be synthetically challenging) from cheap, readily available amine and chlorophosphine starting materials (**Scheme 1.4**). 'PNP' ligands are also readily structurally tuneable through variation of ligand substituents (on the amine and chlorophosphine starting materials).[18,24 – 30]

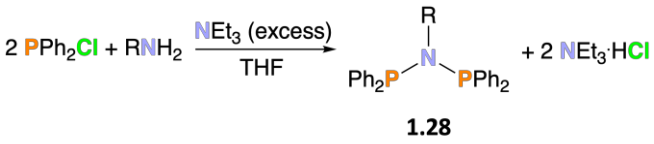


**Scheme 1.4.** Generic synthesis of 'PNP' compounds.

'PNP' ligands feature prominently in the literature due to the unique steric and electronic properties they offer, combined with the constrained coordination geometries they confer as a result of their acute bite angle.[1] 'PNP' metal scaffolds evidence a range of coordination modes, including bridging (dashed box, **Scheme 1.5**)[24] and chelating[25,26,27] (containing one,[25] *e.g.*, complex **1.30**,[26] or two,[27] *e.g.*, complex **1.31**, chelate rings at the same metal centre), exhibited with a variety of transition metals.[28]

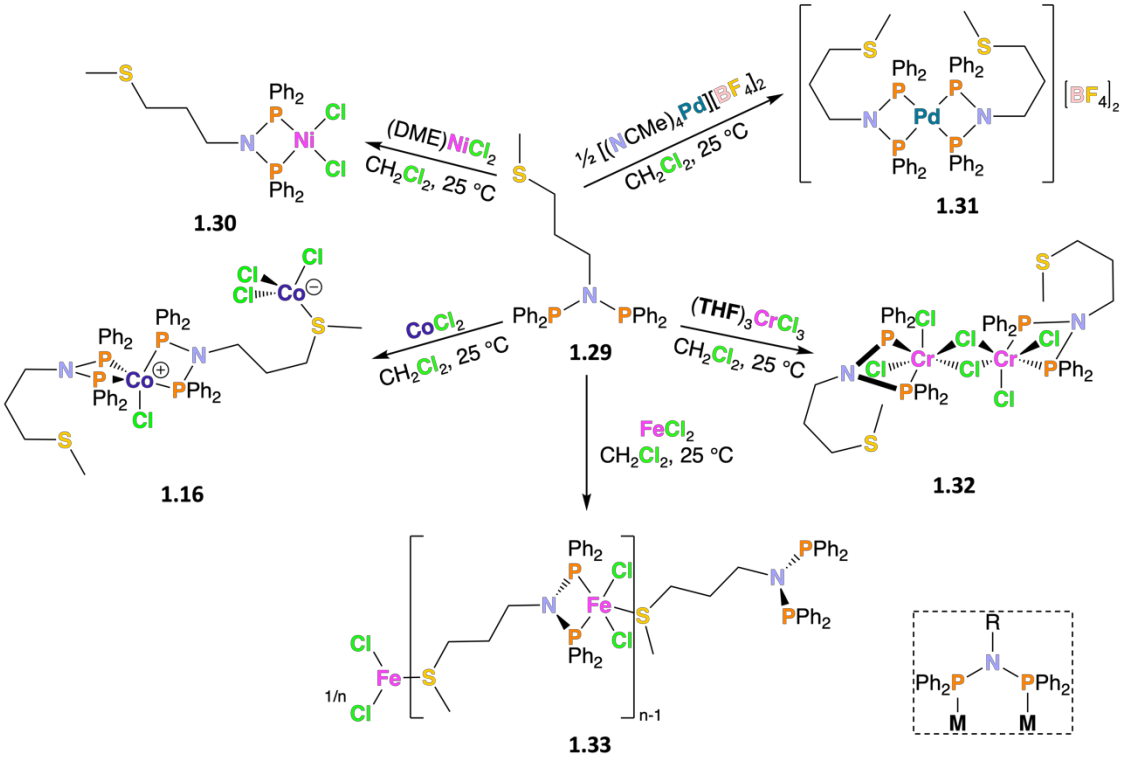


**Scheme 1.5.** Synthesis of complexes **1.30** – **1.33** and **1.16**.[18,26,27,29,30]

Polynuclear complexes (*e.g.*, complex **1.16**),[18] and coordination polymers (*e.g.*, complex **1.33**),[29] shown in **Scheme 1.5**, are accessible with 'PNP' ligands containing a nitrogen substituent with an additional coordinating heteroatom, *e.g.*, R' = $(CH_2)_3SMe$ in **1.28** (**Scheme 1.4**). Complex **1.32** (**Scheme 1.5**) contains two chromium(III) metal centres in the same environment,[30] with analogous complex **1.34** (**Figure 1.5**) being utilised as a pre-catalyst by Sasol for ethylene oligomerisation. This catalyst system affords $C_8$ olefins with 68.3% selectivity and a productivity of 272400 g/g Cr/h at 45 bar, 45 °C alongside 300 equivalents of MAO.[31] Indeed, various 'PNP' metal complexes have been employed for an array of catalytic applications. For example, palladium(II) complexes are utilised for Suzuki-Miyaura coupling,[32] rhodium(II) and ruthenium(II) complexes have been used for transfer hydrogenation of ketones,[25] and chromium(III) and nickel(II) complexes are well-established as effective catalysts for ethylene oligomerisation.[31,33 – 38]

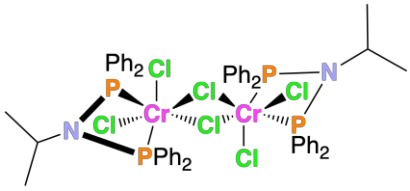


**1.34**

**Figure 1.5.** Structure of complex **1.34**.[31]

## 1.2.1 An Overview of 'SPNP' and 'SPNPS' ligands

Modification of the 'PNP' scaffold, for example to produce 'SPNP' and 'SPNPS' ligands, leads to variation in bite angle, ligand donor atoms available to coordinate at the metal centre, and, accordingly, the structure of obtained metal complexes. 'SPNP' and 'SPNPS' compounds are synthesised by reacting the parent 'PNP' compound with either $^1/_8$ or $^1/_4$ equivalents of $S_8$, respectively,[26,39,40] as shown in **Scheme 1.6** for parent 'PNP' **1.35**.[41] The palladium complexes of 'SPNP' compound **1.36** and 'SPNPS' compound **1.37**, complexes **1.38** and **1.39**, respectively, evidence the expected $\kappa^2$-*P,S* and $\kappa^2$-*S,S* coordination modes, respectively.

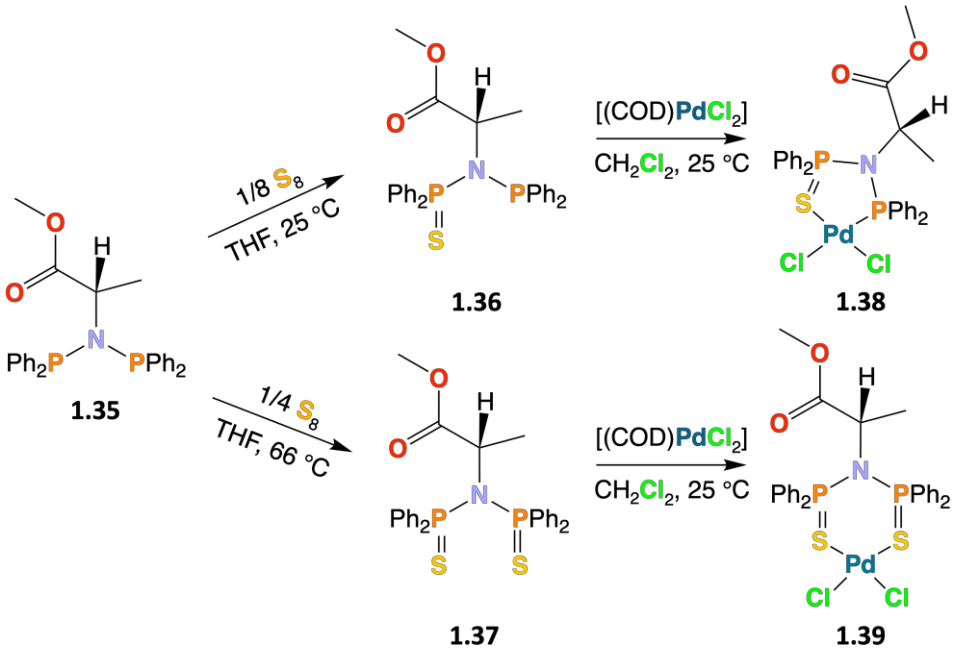


**Scheme 1.6.** Synthesis of compounds **1.36** ('SPNP') and **1.37** ('SPNPS') and their corresponding palladium complexes **1.38** and **1.39**, respectively.[41]

The reactions of the 'SPNP' and 'SPNPS' derivatives of compound **1.29** (**Scheme 1.5**) with (DME)$NiCl_2$, however, do not necessarily proceed as would be expected.[26,39] Compound **1.41** could not be obtained in a pure form due to formation of about 30% of compound **1.40** during the synthesis of compound **1.41** (**Scheme 1.7**).[26] Hence, compound **1.41** was generated *in situ* for the synthesis of complexes **1.42** and **1.43**. Excess compound **1.40** was removed from the crude mixture of complexes **1.42** and **1.43** by washing with toluene, implying (as study of the reaction of compound **1.40** with (DME)$NiCl_2$ is not reported)[26] that compound **1.40** did not react with (DME)$NiCl_2$ (**a**), **Scheme 1.7**). Compound **1.41** reacts with (DME)$NiCl_2$ to afford complex **1.42** (P-Ni-P = 94.12(6)°, *cf*. 73.69(3)° measured for complex **1.30**, **Scheme 1.5**)[26] as evidenced by a solid-state structure. Complex **1.42** is in an equilibrium in solution with complex **1.43** (**b**), **Scheme 1.7**); complex **1.43** is afforded through reversible ligand exchange of compound **1.29** ($MeS(CH_2)_3N(PPh_2)_2$) and chloride migration. An analogous equilibrium is not observed for complex **1.30**, which is found to be stable in solution.[26,39]

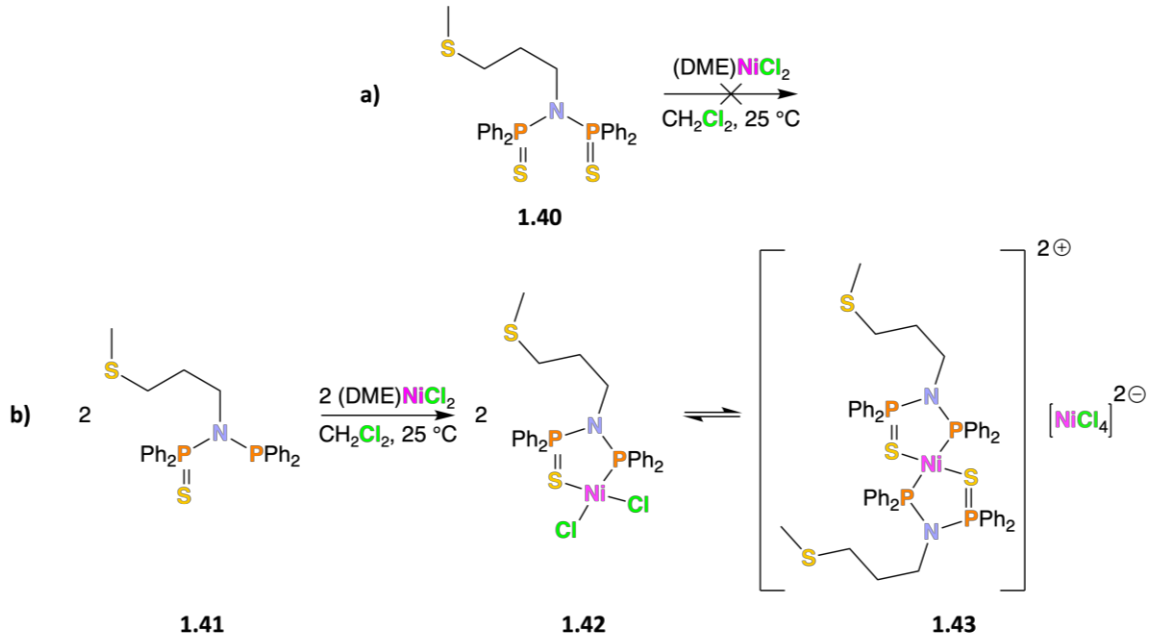


**Scheme 1.7. a)** attempted reaction of compound **1.40** with $NiCl_2$(DME); **b)** reaction of compound **1.41** with $NiCl_2$(DME) producing complexes **1.42** and **1.43** in equilibrium.[26]

## 1.3 Summary

The bite angle ($\beta$) is the angle subtended at the metal between the two coordinating donors of chelating ligands in metal complexes. Acute bite angle cobalt diphosphine complexes exhibit unique catalytic reaction selectivity (**Section 1.1.1**)[12,13] and coordination chemistry (**Section 1.1.2**)[18,19] relative to their large bite angle analogues. 'PNP' ligands are an example of an acute bite angle ligand structurally related to dppm, $H_2C(PPh_2)_2$, with their synthesis and vast coordination chemistry featuring prominently in the literature.[24 – 38] The 'PNP' ligand scaffold can be modified to produce 'SPNP' and 'SPNPS' ligands, leading to changes in ligand bite angle, the nature of the donor atoms, and coordination chemistry relative to their 'PNP' analogues.[26,39 – 41]

Cobalt has been selected as the primary metal of choice for the work presented in this thesis as low valent cationic cobalt(I) species have been utilised for a range of catalytic applications, including [2+2] cycloadditions,[42] hydrovinylation,[42] hydroalkenylation,[43] alkene coupling,[44] hydroacylation,[45] and hydrogenation.[46] The low valent cationic cobalt(I) species employed for the aforementioned applications all have relatively large P-Co-P bite angles due to there being at least two atoms in the backbone between the two phosphorus donor atoms. However, the application of low valent cationic cobalt(I) diphosphine species containing acute P-Co-P bite angle ligands in

catalytic processes is a vastly overlooked area.[13] Hence, further study of the synthesis and reactivity of cobalt(I) complexes containing acute bite angle 'PNP' ligands is required (and will be the focus of this thesis). Further study would establish greater insight into fundamental underpinning coordination chemistry, which can be used, for example, to guide design of highly active and selective catalytic systems.

Cobalt complexes are suitable targets for study in the context of homogeneous catalysis. Cobalt-alkyl intermediates have a reduced tendency to undergo $\beta$-H elimination (relative to, *e.g.*, palladium-alkyl intermediates) due to their high spin electronic configuration with five or more d-electrons (cobalt(I), cobalt(II) and cobalt(III) are $d^8$, $d^7$ and $d^6$, respectively) having no empty d-orbitals (an empty d-orbital is a requirement for $\beta$-H elimination). Hence, it has been shown that cobalt-based catalysts are very efficient at $sp^3C$–$sp^3C$ coupling.[47] Furthermore, cobalt has various accessible oxidation states, allowing for the application of cobalt complexes as catalysts in catalytic processes involving oxidation and reduction of a cobalt centre in a catalyst to be pursued.[48]

However, there are difficulties associated with utilising cobalt in synthetic chemistry and catalytic study. A large proportion of cobalt is extracted by mining to meet the demand of cobalt being utilised as a component of Lithium ion batteries for electric vehicles.[49] Cobalt mining involves child labour and very primitive health and safety measures, resulting in many of the miners and their families developing severe health conditions.[49] Post-extraction, the experimental application of cobalt complexes can exhibit further disadvantages. The reactivity of cobalt complexes can be unpredictable as cobalt can access multiple spin states[50] and undergo single-electron transfer processes (which can subsequently generate highly reactive carbon-based radicals, if the criteria of persistent radicals is not met).[51] Hence, reaction control is required to exploit the aforementioned advantages that cobalt has to offer. One strategy to control cobalt complex reactivity is through the bite angle present in cobalt complexes containing bidentate phosphine ligands, and highlighted in **Section 1.1.1** – **1.1.2**.

## 1.4 Thesis Aims

The aim of the work presented in this thesis is to study the structures and reactivity of acute bite angle ligand cobalt complexes, allowing for an understanding of the effects of acute bite angle ligands on the chemistry of cobalt complexes to be gained. In order to achieve this aim, **Chapter 2** will present the synthesis of a range of 'PNP' ligands and associated derivatives (*e.g.,* 'PCNCP, 'SPNP' and 'SPNPS' ligands). The coordination chemistry of the synthesised ligands with $CoX_2$ will be presented in **Chapter 4**. Low valent cationic cobalt(I) species of 'PNP' ligands are accessed in **Chapter 5**, and their reactivity with a range of substrates of interest for a variety of catalytic processes, *e.g*., ethylene, carbon monoxide and hydrogen, will be probed in **Chapter 6**. Additionally, the coordination chemistry of 'PNP' compounds with palladium(II), zinc(II) and selenium (to determine their basicity *via* measurement of $|^1J_{SeP}|$) will be outlined in **Chapter 3**, **Chapter 5** and **Chapter 2**, respectively. Palladium(II) complexes of 'PNP' compounds are well-established to evidence $\kappa^2$-*P,P* coordination of the 'soft' phosphorus donor atoms with 'soft' palladium(II), contrasting the coordination chemistry illustrated in complex **1.16** ($[CoCl(MeS(CH_2)_3N\{PPh_2\}_2)(\{Cl_3Co\}MeS(CH_2)_3N\{PPh_2\}_2)]$, **Figure 1.4**) with 'hard' cobalt(II). Palladium(II) complexes will be accessed *via* reaction of the 'PNP' ligands with $[(MeCN)_2PdCl_2]$. The coordination chemistry of 'PNP' compounds with zinc(II) halides has also been scarcely studied,[52] and will be studied due to the use of activated zinc in the reduction of cobalt(II) halide species to cobalt(I) species producing zinc(II) halides which may coordinate to 'PNP' compounds in solution. Zinc(II) complexes will be accessed *via* reaction of the 'PNP' ligands with $ZnBr_2$.

## References


1. S. M. Mansell, *Dalton Trans*., **2017**, *46*, 15157 – 15174. 10.1039/C7DT03395H
2. P. W. N. M. van Leeuwen, P. C. J. Kamer, J. N. H. Reek, P. Dierkes, *Chem. Rev*., **2000**, *100*, 2741 – 2770. 10.1021/cr9902704
3. P. W. N. M. van Leeuwen, P. C. J. Kamer, J. N. H. Reek, *Pure Appl. Chem*., **1999**, *71*, 1443 – 1452. 10.1351/pac199971081443
4. P. Dierkes, P. W. N. M. van Leeuwen, *J. Chem. Soc., Dalton Trans*., **1999**, 1519 – 1530. 10.1039/A807799A
5. M-N. Birkholz (née Gensow), Z. Freixa, P. W. N. M. van Leeuwen, *Chem. Soc. Rev*., **2009**, *38*, 1099 – 1118. 10.1039/B806211K
6. Z. Freixa, P. W. N. M. van Leeuwen, *Dalton Trans*., **2003**, 1890 – 1901. 10.1039/B300322C

7. L. A. van der Veen, P. C. J. Kamer, P. W. N. M. van Leeuwen, *CATTECH*, **2002**, *6*, 116 – 120. 10.1023/A:1020137607125
8. C. P. Casey, G. T. Whiteker, *Isr. J. Chem*., **1990**, *30*, 299 – 304. 10.1002/ijch.199000031
9. J. A. Gillespie, D. L. Dodds, P. C. J. Kamer, *Dalton Trans*., **2010**, *39*, 2751 – 2764. 10.1039/B913778E
10. P. W. N. M. van Leeuwen, *Homogeneous Catalysis: Understanding the Art*, Springer, Netherlands, **2004**. ISBN: 978-1-4020-2000-1
11. M. Portnoy, D. Milstein, *Organometallics*, **1993**, *12*, 1655 – 1664. 10.1021/om00029a025
12. R. K. Sharma, T. V. RajanBabu, *J. Am. Chem. Soc*., **2010**, *132*, 3295 – 3297. 10.1021/ja1004703
13. K. Duvvuri, K. R. Dewese, M. M. Parsutkar, S. M. Jing, M. M. Mehta, J. C. Gallucci, T. V. RajanBabu, *J. Am. Chem. Soc*., **2019**, *141*, 7365 – 7375. 10.1021/jacs.8b13812
14. M. Gray, M. T. Hines, M. M. Parsutkar, A. J. Wahlstrom, N. A. Brunelli, T. V. RajanBabu, *ACS Catal*., **2020**, *10*, 4337 – 4348. 10.1021/acscatal.9b05455
15. S. M. Jing, V. Balasanthiran, V. Pagar, J. C. Gallucci, T. V. RajanBabu, *J. Am. Chem. Soc*., **2017**, *139*, 18034 – 18043. 10.1021/jacs.7b10055
16. G. Kiefer, H. Vrubel, R. Scopelliti, K. Severin, *Eur. J. Inorg. Chem*., **2013**, 4916 – 4921. 10.1002/ejic.201300551
17. K. Heinze, G. Huttner, L. Zsolnai, P. Schober, *Inorg. Chem*., **1997**, *36*, 5457 – 5469. 10.1021/ic9705352
18. C. Fliedel, V. Rosa, B. Vileno, N. Parizel, S. Choua, C. Gourlaouen, P. Rosa, P. Turek, P. Braunstein, *Inorg. Chem.*, **2016**, *55*, 4183 – 4198. 10.1021/acs.inorgchem.5b02889
19. U. Omoruyi, S. J. Page, S. L. Apps, A. J. P. White, N. J. Long, P. W. Miller, *J. Organomet. Chem*., **2021**, *935*, 121650 – 121661. 10.1016/j.jorganchem.2020.121650
20. R. Pehn, J. Pann, K. Ehrmann, W. Viertl, H. Roithmeyer, M. Bendig, C. Strabler, H. Kopacka, T. Müller, T. Hofer, P. Brüggeller, *Eur. J. Inorg. Chem*., **2020**, 4358 – 4372. 10.1002/ejic.202000778
21. Q. Dong, M. J. Rose, W-Y. Wong, H. B. Gray, *Inorg. Chem*., **2011**, *50*, 10213 – 10224. 10.1021/ic201213c
22. D. Naicker, H. B. Friedrich, B. Omondi, *RSC Adv*., **2015**, *5*, 63123 – 63129. 10.1039/C5RA07365K
23. K. Naktode, R. K. Kottalanka, H. Adimulam, T. K. Panda, *J. Coord. Chem*., **2014**, *67*, 3042 – 3053. 10.1080/00958972.2014.953071
24. N. Biricik, Z. Fei, R. Scopelliti, P. J. Dyson, *Eur. J. Inorg. Chem*., **2004**, 4232 – 4236. 10.1002/ejic.200400439
25. F. Ok, M. Aydemir, F. Durap, A. Baysal, *Appl. Organomet. Chem*., **2014**, *28*, 38 – 43. 10.1002/aoc.3068
26. A. Ghisolfi, C. Fliedel, V. Rosa, R. Pattacini, A. Thibon, K. Y. Monakhov, P. Braunstein, *Chem. Asian J*., **2013**, *8*, 1795 – 1805. 10.1002/asia.201300687
27. C. Fliedel, V. Faramarzi, V. Rosa, B. Doudin, P. Braunstein, *Chem. – Eur. J*., **2014**, *20*, 1263 – 1266. 10.1002/chem.201303626
28. K. G. Gaw, M. B. Smith, A. M. Z. Slawin, *New J. Chem*., **2000**, *24*, 429 – 435. 10.1039/B001458N

29. C. Fliedel, V. Rosa, A. Falceto, P. Rosa, S. Alvarez, P. Braunstein, *Inorg. Chem.*, **2015**, *54*, 6547 – 6559. 10.1021/acs.inorgchem.5b00834
30. Z. Weng, S. Teo, T. S. A. Hor, *Dalton Trans*., **2007**, 3493 – 3498. 10.1039/B702636F
31. A. Bollmann, K. Blann, J. T. Dixon, F. M. Hess, E. Killian, H. Maumela, D. S. McGuinness, D. H. Morgan, A. Neveling, S. Otto, M. Overett, A. M. Z. Slawin, P. Wasserscheid, S. Kuhlmann, *J. Am. Chem. Soc*., **2004**, *126*, 14712 – 14713. 10.1021/ja045602n
32. M. R. Crawley, A. E. Friedman, T. R. Cook, *Inorg. Chem*., **2018**, *57*, 5692 – 5700. 10.1021/acs.inorgchem.8b00787
33. G. J. P. Britovsek, D. S. McGuinness, *Chem. Eur. J*., **2016**, *22*, 16891 – 16896. 10.1002/chem.201603909
34. K. Song, H. Gao, F. Liu, J. Pan, L. Guo, S. Zai, Q. Wu, *Eur. J. Inorg. Chem*., **2009**, 3016 – 3024. 10.1002/ejic.200900256
35. P. R. Elowe, C. McCann, P. G. Pringle, S. K. Spitzmesser, J. E. Bercaw, *Organometallics*, **2006**, *25*, 5255 – 5260. 10.1021/om0601596
36. S. Sa, S. M. Lee, S. Y. Kim, *J. Mol. Catal. A: Chem*., **2013**, *378*, 17 – 21. 10.1016/j.molcata.2013.05.015
37. M. J. Overett, K. Blann, A. Bollmann, R. de Villiers, J. T. Dixon, E. Killian, M. C. Maumela, H. Maumela, D. S. McGuinness, D. H. Morgan, A. Rucklidge, A. M. Z. Slawin, *J. Mol. Catal. A: Chem*., **2008**, *283*, 114 – 119. 10.1016/j.molcata.2007.11.036
38. K. Blann, A. Bollmann, H. de Bod, J. T. Dixon, E. Killian, P. Nongodlwana, M. C. Maumela, H. Maumela, A. E. McConnell, D. H. Morgan, M. J. Overett, M. Prétorius, S. Kuhlmann, P. Wasserscheid, *J. Catal*., **2007**, *249*, 244 – 249. 10.1016/j.jcat.2007.04.009
39. A. Ghisolfi, C. Fliedel, V. Rosa, K. Y. Monakhov, P. Braunstein, *Organometallics*, **2014**, *33*, 2523 – 2534. 10.1021/om500141k
40. J. W. Faller, J. Lloret-Fillol, J. Parr, *New J. Chem*., **2002**, *26*, 883 – 888. 10.1039/B111422K
41. A. M. Z. Slawin, J. D. Woollins, Q. Zhang, *J. Chem. Soc., Dalton Trans*., **2001**, 621 – 632. 10.1039/B009074N
42. M. E. Farmer, L. E. Ehehalt, T. P. Pabst, M. T. Tudge, P. J. Chirik, *Organometallics*, **2021**, *40*, 3599 – 3607. 10.1021/acs.organomet.1c00473
43. J. H. Herbort, R. F. Lalisse, C. M. Hadad, T. V. RajanBabu, *ACS Catal*., **2021**, *11*, 9605 – 9617. 10.1021/acscatal.1c02530
44. S. Biswas, J. P. Page, K. R. Dewese, T. V. RajanBabu, *J. Am. Chem. Soc*., **2015**, *137*, 14268 – 14271. 10.1021/jacs.5b10364
45. M. M. Parsutkar, T. V. RajanBabu, *J. Am. Chem. Soc*., **2021**, *143*, 12825 – 12835. 10.1021/jacs.1c06245
46. C. S. MacNeil, H. Zhong, T. P. Pabst, M. Shevlin, P. J. Chirik, *ACS Catal*., **2022**, *12*, 4680 – 4687. 10.1021/acscatal.2c01059
47. S. M. Bellows, T. R. Cundari, P. L. Holland, *Organometallics*, **2013**, *32*, 4741 – 4751. 10.1021/om400325x
48. F. Kreyenschmidt, S. E. Meurer, K. Koszinowski, *Chem. Eur. J*., **2019**, *25*, 5912 – 5921. 10.1002/chem.201805964
49. S. H. Farjana, N. Huda, M. A. P. Mahmud, *J. Sustain. Min*., **2019**, *18*, 150 – 161. 10.1016/j.jsm.2019.03.002

50. P. Kumar, Y-M. Lee, L. Hu, J-W. Chen, Y. J. Park, J. Yao, H. Chen, K. D. Karlin, W. Nam, *J. Am. Chem. Soc*., **2016**, *138*, 7753 – 7762. 10.1021/jacs.6b04040
51. B. E. Daikh, R. G. Finke, *J. Am. Chem. Soc*., **1992**, *114*, 2938 – 2942. 10.1021/ja00034a028
52. T. S. Sukhikh, R. M. Khisamov, D. A. Bashirov, V. Y. Komarov, M. S. Molokeev, A. A. Ryadun, E. Benassi, S. N. Konchenko, *Cryst. Growth Des*., **2020**, *20*, 5796 – 5807. 10.1021/acs.cgd.0c00406

# Chapter 2 – Design and Synthesis of 'PNP', 'PCNCP', 'SPNP' and 'SPNPS' Ligands

## 2.1 Introduction

As highlighted in **Chapter 1**, the research presented in this thesis involves the synthesis and coordination study of a range of 'PNP', 'PCNCP', 'SPNP' and 'SPNPS' compounds. 'PNP' compounds are generally easily synthetically accessible (see **Section 2.2**) from reaction of a primary amine with two equivalents of a chlorophosphine of choice, *i.e*., readily available and cheap starting materials. Notably, the potentially unique coordination chemistry and reactivity (arising from the acute P-Co-P angle) of cobalt halide complexes containing 'PNP' ligands has been scarcely studied.[1 – 3] Hence, further study of the fundamental chemistry associated with the cobalt complexes of 'PNP' ligands (*i.e*., their synthesis, coordination chemistry, and reactivity) is required to develop low valent cationic cobalt(I) complexes with 'PNP' ligands for potential catalytic applications.

Structures of the various 'PNP' (**2.2** – **2.7**), 'PCNCP' (**2.8**), 'SPNP' (**2.9**), 'SPNPS' (**2.10**), aminophosphines (**2.11** and **2.12**) and **2.13** (phosphite variant of compound **2.1**) compounds explored in this thesis are shown in **Figure 2.1**. Compound **2.1** (with a pendant donor pyridyl group) has been established to react with $CoBr_2$ to afford complex **2.14** (**Figure 2.1**).[4] Since no structures of cobalt complexes containing 'PNP' ligands without pendant donor groups have been reported in the literature, the study of the coordination chemistry of compounds **2.2**, **2.3** and **2.6** with cobalt halides is informative. Probing the coordination chemistry of compounds **2.4**, **2.5** and **2.7** with cobalt halides is hoped to evidence the structures of cobalt complexes accessible with 'PNP' compounds containing a range of potential pendant donor groups and linkers (*e.g*., aryl compound **2.7** and alkyl in compound **2.4**) between the pendant donor group and the $-N(PPh_2)_2$ moiety. Notably, it is of interest to determine if cobalt complexes with structures differing from that exhibited by complex **2.14** are obtained from the reaction

of cobalt halides with 'PNP' compounds containing suitable pendant donor groups, or if only cobalt complexes analogous to complex **2.14** are afforded.

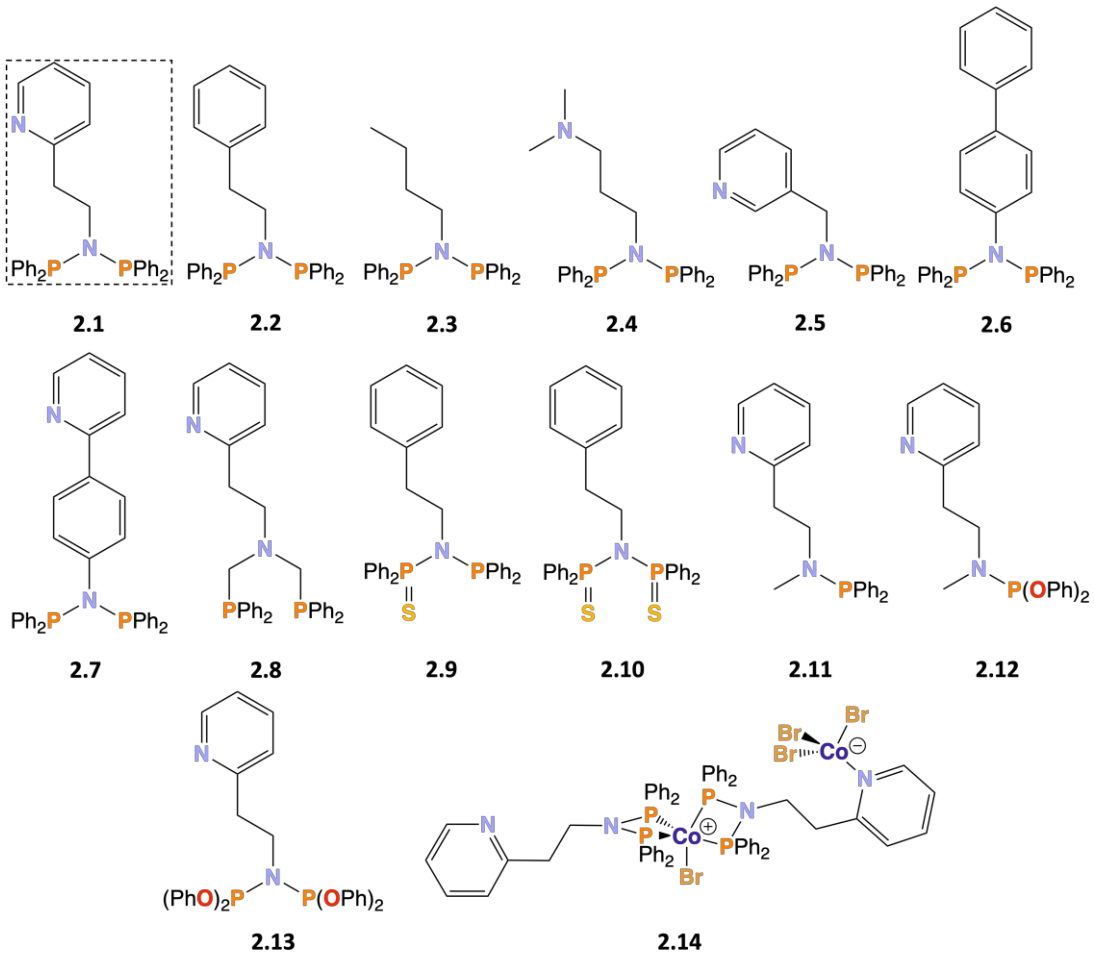


**Figure 2.1.** Structures of compounds (potential ligands) **2.1** – **2.13** and complex **2.14**.

Comparison of the coordination chemistry of compounds **2.8**, the 'PCNCP' analogue of compound **2.1**, and **2.1** with $CoBr_2$ will evidence the impact of chelate ring size. Similarly, the study of the coordination of compounds **2.9** and **2.10** ('SPNP' and 'SPNPS' analogues of compound **2.2**, respectively) with $CoBr_2$ will reveal the impact of the addition of one and two sulfur atoms to the $-N(PPh_2)_2$ moiety. The impact of the addition of sulfur atom(s) to the $-N(PPh_2)_2$ moiety is likely to be related to both bite angle and the change in the nature of the coordinating atoms, *i.e.*, sulfur is 'softer' than phosphorus. Compound **2.13** contains electron-withdrawing OPh substituents and hence may better stabilise the electron-rich cobalt(I) oxidation state relative to compound **2.1**. Compounds **2.11** and **2.12**, the mono-P analogues of compounds **2.1** and **2.13**, respectively, may coordinate in a $\kappa^2$-*P,N* manner with $CoBr_2$ (as coordination $\kappa^2$-*P,P* is not possible) *via* the $PR_2$ (R = Ph, OPh) and pyridyl moieties.

The synthesis of compounds **2.2**,[5] **2.3**,[6] **2.4**,[7] **2.5**[8] and **2.11**[9] has been reported previously (ligands used in a variety of different applications). New compounds **2.6** – **2.10**, **2.12** and **2.13** were prepared using adaptations of methods for related compounds reported in the literature.[5 – 13]

## 2.2 Synthesis of 'PNP' Compounds $Ph(CH_2)_2N(PPh_2)_2$ (2.2), *n*-$BuN(PPh_2)_2$ (2.3), $NMe_2(CH_2)_3N(PPh_2)_2$ (2.4), Py-*m*-$CH_2N(PPh_2)_2$ (2.5), Ph-$C_6H_4N(PPh_2)_2$ (2.6) and Py-*o*-$C_6H_4N(PPh_2)_2$ (2.7)

Compounds **2.2** – **2.7** (**c)**, **Scheme 2.1**) are synthesised by reaction of the appropriate primary amine with two equivalents (**a)**, **Scheme 2.1**) of $Ph_2PCl$ (R' = Ph in **a)**, **Scheme 2.1**; $\delta_P$ = 81 ppm in $CD_2Cl_2$)[14] in the presence of an excess of triethylamine base.[5 – 8] The reactions described in **a)**, **Scheme 2.1**, were monitored by $^{31}P\{^1H\}$ NMR spectroscopy. A singlet in the range of $\delta_P$ = 55 – 70 ppm is observed for 'PNP' compounds $RN(PPh_2)_2$ (**a)**, **Scheme 2.1**), whereas a singlet in the range $\delta_P$ = 20 – 30 ppm corresponds to aminophosphines $RN(PPh_2)H$ (**b)**, **Scheme 2.1**).

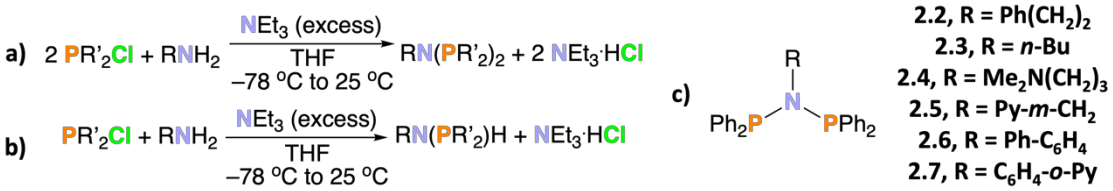


**Scheme 2.1. a)** generic synthesis of $RN(PR'_2)_2$; **b)** generic synthesis of $RN(PR'_2)H$; **c)** structures of compounds **2.2** – **2.7** (R' = Ph in **a)**).

During the synthesis of 'PNP' compounds, *e.g.,* **2.2** – **2.7**, trace amounts of the corresponding aminophosphine (R' = Ph in **b)**, **Scheme 2.2**) and iminobiphosphine products (**2.18** in **Scheme 2.2**) are produced. The iminobiphosphine impurity, formed by the deprotonation and subsequent reaction of **2.17** (the prototropomer of **2.16**) with $Ph_2PCl$, gives rise to the expected AB system by $^{31}P\{^1H\}$ NMR spectroscopy; one doublet is centred at approx. $\delta_P$ = 15 – 20 ppm and the other at approx. $\delta_P$ = –15 to –25 ppm, with $^1J_{PP}$ = 220 – 290 Hz (values comparable to those reported for related compounds in the literature).[15]

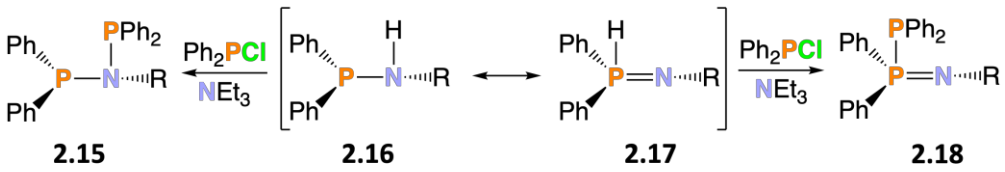


**Scheme 2.2.** Prototropism of an aminophosphine resulting in tautomers **2.16** and **2.17**, which can react with $Ph_2PCl$ affording **2.15** and iminobiphosphine **2.18**, respectively.[15]

## 2.3 Synthesis of 'PCNCP' Compound Py-*o*-$(CH_2)_2N(CH_2PPh_2)_2$ (2.8)

Compound **2.8** (**b)**, **Scheme 2.3**) is synthesised by heating a solution of $HPPh_2$ (R' = Ph, **a)**, **Scheme 2.3**, $\delta_P$ = –40 ppm)[16] with paraformaldehyde at reflux, generating a hydroxymethylphosphine intermediate. Subsequently, two equivalents of the hydroxymethylphosphine react with one equivalent of the desired amine, generating the 'PCNCP' compound in a Mannich-type condensation. The hydroxymethylphosphine intermediate can either be isolated or formed *in situ* in the presence of the desired amine; [10] for the synthesis of compound **2.8**, the latter 'one pot' method was followed. The reaction described in **a)**, **Scheme 2.3**, was monitored by $^{31}P\{^1H\}$ NMR spectroscopy. For R' = Ph, a singlet in the range of approx. $\delta_P$ = –15 to –50 ppm is observed for *bis*(diphenylphosphinomethyl)amine 'PCNCP' compounds (n = 2, **a)**, **Scheme 2.3**), whereas a singlet in the range of approx. $\delta_P$ = –10 to –20 ppm is observed for (diphenylphosphinomethyl)amine 'PCNH' compounds (n = 1, **a)**, **Scheme 2.3**).

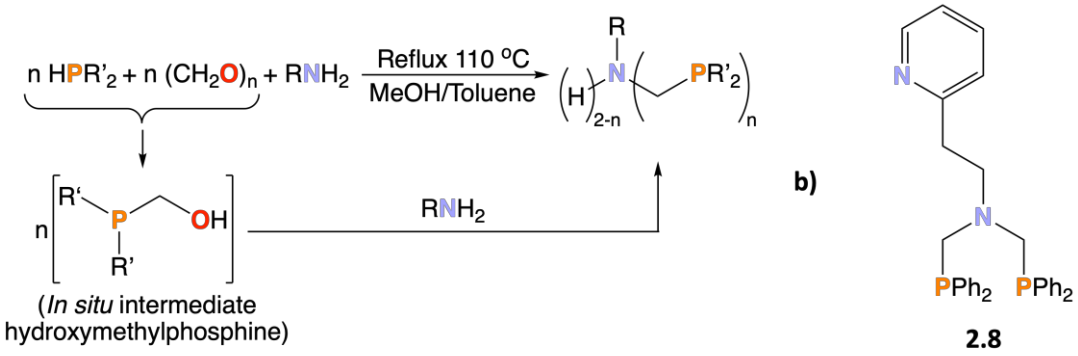


**Scheme 2.3. a)** Generic synthesis of 'PCNCP' (n = 2) and 'PCNH' compounds (n = 1);[10] **b)** structure of compound **2.8**.

## 2.4 Synthesis of 'SPNP' Compound $Ph(CH_2)_2N(SPPh_2)(PPh_2)$ (2.9) and 'SPNPS' Compound $Ph(CH_2)_2N(SPPh_2)_2$ (2.10)

Compounds **2.9** and **2.10** (**c)**, **Scheme 2.4**) are synthesised by reacting a solution of compound **2.2** ($Ph(CH_2)_2N(PPh_2)_2$) with either $^1/_8$ or $^1/_4$ equiv. of $S_8$ (**a)** and **b)**, **Scheme 2.4**), respectively, an extension of previously published methodologies.[11–13] The $^{31}P\{^1H\}$

NMR spectrum of the crude reaction mixture for the synthesis of compound **2.9** evidenced 69% purity, with unreacted **2.2** and compound **2.10** being the major by-products. Recrystallisation from THF/MeOH increased the purity to 93%. Compound **2.9** exhibits the expected AB system in its $^{31}P\{^{1}H\}$ NMR spectrum, with doublets ($^{2}J_{PP}$ = 88 Hz) at 71.0 ppm ('SPNP') and 51.9 ppm ('SPNP') . Compound **2.10** exhibits a singlet at 69.0 ppm (*cf*. a singlet at 62.7 ppm for compound **2.2**). IR spectroscopic analysis shows $\nu$(P=S) stretches at 697 and 685 $cm^{-1}$ for compounds **2.9** and **2.10**, respectively.

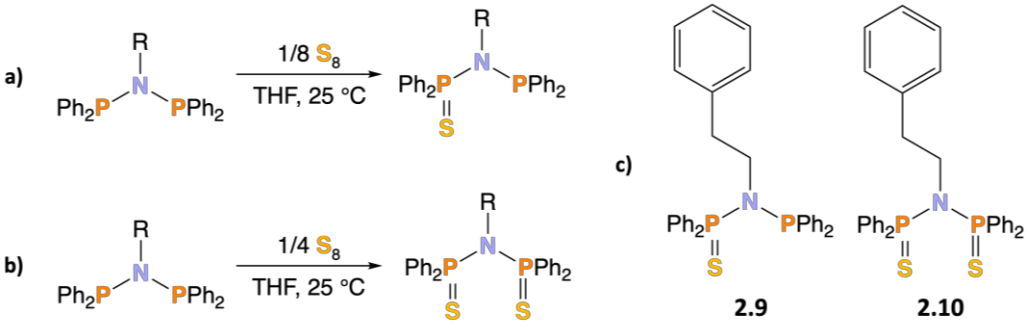


**Scheme 2.4.** Generic synthesis of **a)** 'SPNP' compounds and **b)** 'SPNPS' compounds, and **c)** structures of 'SPNP' compound **2.9** and 'SPNPS' compound **2.10**.

## 2.4.1 Solid-State Structures of 'SPNP' Compound $Ph(CH_2)_2N(SPPh_2)(PPh_2)$ (2.9) and 'SPNPS' Compound $Ph(CH_2)_2N(SPPh_2)_2$ (2.10)

Single crystals of compounds **2.9** and **2.10** (**Figure 2.2**) were obtained and molecular structures determined. Analysis of the molecular structure of compound **2.9** reveals that P1 is partially oxidised, *i.e*., the mixed phosphine oxide/sulfide is present in 12% of the asymmetric units. Oxidation likely occurred as the single crystals of compound **2.9** were grown under air.

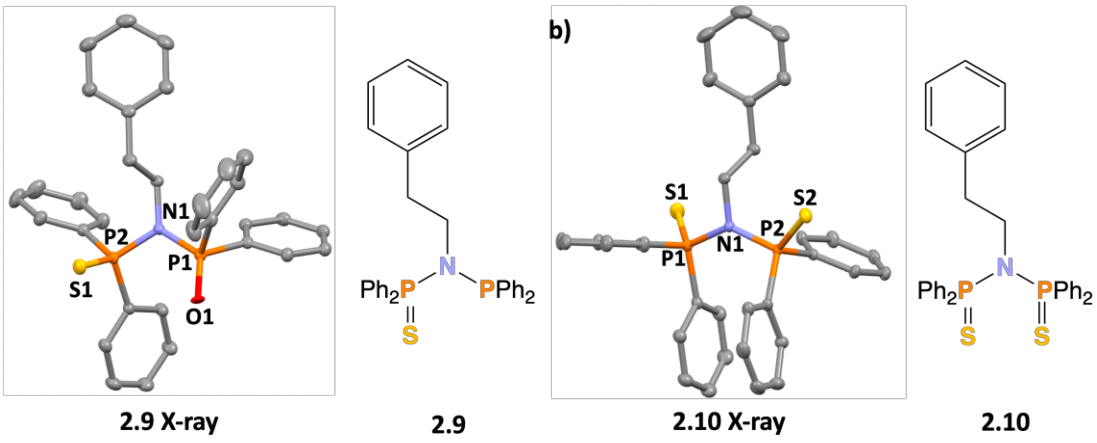


**Figure 2.2.** Solid-state molecular structures determined from XRD analysis of single crystals of **a) 2.9** and **b) 2.10**. Hydrogen atoms are omitted for clarity. Thermal ellipsoids are shown at the 50 % probability level. O1 in the solid-state structure of **2.9** is only present in 12% of asymmetric units. Atom colour key: carbon – grey; nitrogen – blue; phosphorus – orange; sulfur – yellow and oxygen – red.

**Table 2.1.** Key bond lengths and angles measured from the solid-state molecular structures of compounds **2.9** and **2.10**.

| Parameter | 2.9 | 2.10 |
|---|---|---|
| N1-P1 / Å | 1.732(1) | 1.7042(9) |
| N1-P2 / A | 1.687(1) | 1.7012(9) |
| P1-S1 / Å | – | 1.9460(4) |
| P2-S2 / Å | – | 1.9521(4) |
| P1-O1 / Å | 1.558(8) | – |
| P2-S1 / Å | 1.9516(5) | – |
| P1-N1-P2 / ° | 114.77(8) | 131.89(6) |

The key bond lengths and angles measured from the solid-state structures of compounds **2.9** and **2.10** are shown in **Table 2.1**. Compound **2.9** has measured N1-P2 and N1-P1 distances of 1.687(1) Å and 1.732(1) Å, respectively, whereas compound **2.10** has P-N bond lengths of 1.704(1) Å and 1.701(1) Å. The 'PNP' moiety of 2-{N=$PPh_2$-$PPh_2$}-3-{$N(PPh_2)_2$}-$C_5H_3N$ has P-N bond distances of 1.725(2) Å and 1.737(2) Å,[17] showing good similarity to the N1-P1 distance of compound **2.9**. Thiolation of the phosphorus atom (*i.e.*, forming N-P=S) results in a reduction in the P-N bond distance, indicating greater P-N multiple bond character and likely reflecting the greater electron deficiency of the phosphorus(V) atom in N-$P^{V}$=S relative to the phosphorus(III) atom in N-$P^{III}$. The N1-P2 bond distance (1.687(1) Å) measured for complex **2.9** is the shortest of the aforementioned distances, potentially as delocalisation of the N1 lone pair occurs onto the N-$P^{V}$2=S1 moiety to a greater extent relative to the $P^{III}$1-N1 bond, favouring the $^{+}$N=P-$S^{-}$ canonical form (**a)**, **Scheme 2.5**). The P-N bond distances (1.704(1) Å and 1.701(1) Å) in compound **2.10** are the next shortest as delocalisation of the N1 lone pair occurs onto both N1-$P^{V}$1=S1 and N1-$P^{V}$2=S2 moieties (**b)**, **Scheme 2.5**) equally in compound **2.10**, as both P1 and P2 are phosphorus(V). This is unlike compound **2.9**, which contains only one N-P=S motif (with delocalisation of the N1 lone pair not being shared over two N-P=S moieties). Hence, the P-N bond distances in compound **2.10** increase relative to N1-P2 bond distance in compound **2.9**. The N1-P1 distance measured for compound **2.9** (1.732(1) Å) is the longest, reflecting the lesser N1-P1 multiple bond character due to reduced N1 lone pair delocalisation onto the N1-P1 as P1 is phosphorus(III), *i.e.*, more electron rich.

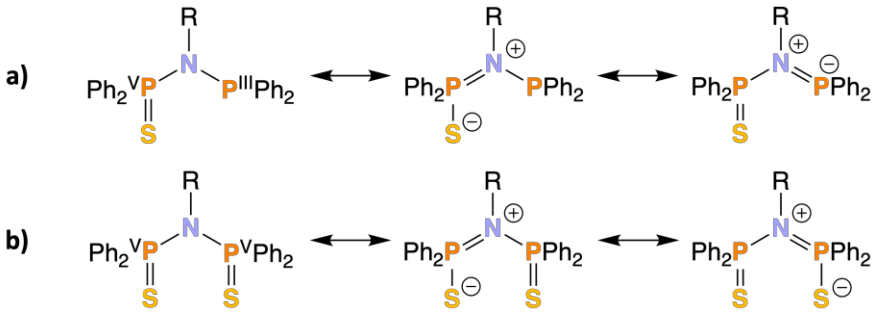

**Scheme 2.5.** Resonance canonicals of **a)** a S-P-N-P moiety and **b)** a S-P-N-P-S moiety.

The measured P1-N1-P2 bond angles of compounds **2.9** and **2.10** are 114.77(8)° and 131.89(6)°, respectively. The P-N-P bond angle compresses with the addition of one sulfur atom (*i.e.*, in compound **2.9**) and expands with the addition of two sulfur atoms (*i.e.*, in compound **2.10**) relative to the approx. 120° P-N-P angle of a 'PNP' ligand, *e.g.*, in 2-{N=$PPh_2$-$PPh_2$}-3-{N($PPh_2$)$_2$}-$C_5H_3N$ with a P-N-P bond angle of 120.48(11)°.[17] The compression of the P-N-P bond angle in compound **2.9** is likely due to the shortening of the N1-P2 bond distance to 1.687(1) Å upon thiolation. The P-N-P bond angle of 'SPNPS' compound **2.10** likely expands relative to the approx. 120° angle present in 'PNP' compounds to reduce the greater steric clash between the two (S)$PPh_2$ moieties.

Good similarity is seen between the key bond lengths and angles of compound **2.9** with those of Ph(Me)CHN($PPh_2$)({S}$PPh_2$), which are: P1-N1-P2 = 112.0(2)°; P1-N1 = 1.748(5) Å; P2-N2 = 1.694(4) Å and P2-S1 = 1.955(2) Å.[18] The key bond lengths and angles of compound **2.10** show good similarity to those of ($Ph_2$P{S})$_2$N$CH_2CH_2$N({S}$PPh_2$)$_2$, which are (for one S-P-N-P-S moiety): P2-N1-P1 = 133.3(1)°; S1-P2 = 1.953(1) Å; P2-N1 = 1.719(2) Å; P1-N1 = 1.706(2) Å and P1-S2 = 1.9441(8) Å.[19]

## 2.5 Synthesis of Aminophosphines Py-*o*-$(CH_2)_2$N($PPh_2$)(Me) (2.11) and Py-*o*-$(CH_2)_2$N(P{OPh}$_2$)(Me) (2.12)

Compounds **2.11** and **2.12** (**b)**, **Scheme 2.6**) were synthesised as described in **a)**, **Scheme 2.6** and exhibit singlets in their $^{31}P\{^1H\}$ NMR spectra at 64.4 ppm ($CD_2Cl_2$) and 140.1 ppm ($CDCl_3$), respectively. These chemical shifts are consistent with previously reported data for comparable systems: **2.11** 61.7 ppm[9] and $Me_2NP(OPh)_2$ at 139.0 ppm,[20] respectively.

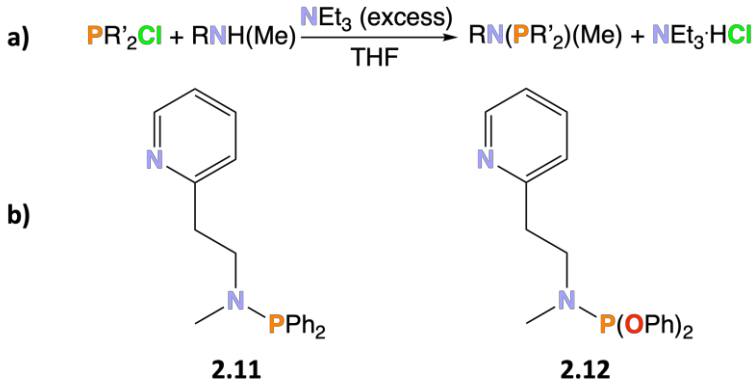


**Scheme 2.6. a)** generic aminophosphine synthesis; **b)** structures of compounds **2.11** and **2.12**.

## 2.6 Attempted Synthesis of Py-*o*-$(CH_2)_2N(P\{OPh\}_2)_2$ (2.13)

The synthesis of compound **2.13** (Py-*o*-$(CH_2)_2N\{P(OPh)_2\}_2$) was attempted through the reaction of two equivalents of $P(OPh)_2Cl$ ($\delta_P$ = 158.2 ppm; synthesised following a published procedure in **a)**, **Scheme 2.7**)[21] with 2-(aminoethyl)pyridine, in the presence of an excess of $NEt_3$ (**a)**, **Scheme 2.1** with R' = OPh and R = Py-*o*-$(CH_2)_2$). $^{31}P\{^1H\}$ NMR spectroscopic analysis of the crude reaction mixture from the attempted synthesis of compound **2.13** revealed a mixture of compounds with signals at $\delta_P$ = 138.1 ppm (assigned to Py-*o*-$CH_2CH_2NH(P\{OPh\}_2)$) and $\delta_P$ = 126.2 ppm (tentatively assigned to compound **2.13**), as well as unreacted $P(OPh)_2Cl$. Since heating the reaction mixture at reflux in THF did not increase conversion, a route to compound **2.13** utilising Py-*o*-$(CH_2)_2N(TMS)_2$[22] was implemented. It was hoped that the formation of TMSCl upon reaction with $P(OPh)_2Cl$ would drive the reaction to completion (**b)**, **Scheme 2.7**).

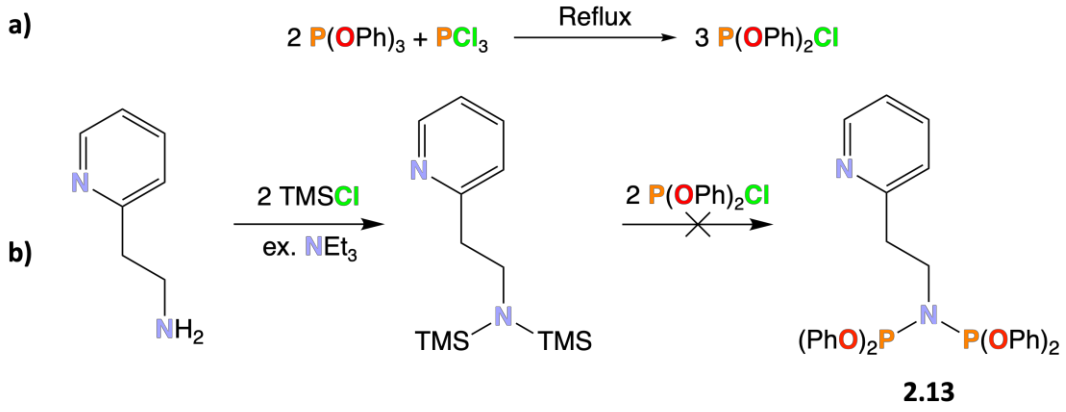


**Scheme 2.7. a)** synthesis of $P(OPh)_2Cl$; **b)** two-step attempted synthesis of compound **2.13** *via* *o*-$PyCH_2CH_2N(TMS)_2$.

The isolated product from the attempted reaction (**b)**, **Scheme 2.7**) was exposed to elemental selenium in an NMR tube in order to produce the corresponding phosphine

selenide (see **Section 2.7**), but no reaction took place. A lack of reaction suggests that compound **2.13** (Py-*o*-$(CH_2)_2N\{P(OPh)_2\}_2$) is indeed not the isolated product as $PhN\{P(OC_6H_4OMe\text{-}o)_2\}_2$) (a 'PNP' compound with phosphite substituents) reacts with elemental selenium to form $PhN\{P(Se)(OC_6H_4OMe\text{-}o)_2\}_2$) with $|^1J_{SeP}|$ = 1004 Hz,[23] hence compound **2.13** would be expected to exhibit analogous reactivity. Research relating to compound **2.13** was halted at this point.

## 2.7 Measuring $|^1J_{SeP}|$ to Estimate the Basicity of the Phosphorus Donor Atoms

Phosphine selenides are prepared by reaction of elemental grey selenium with the desired phosphine (**Scheme 2.8**). The synthesis of phosphine selenides allows for the basicity, and hence donor ability, of the phosphorus donor atoms of compounds **2.2** – **2.9**, **2.11** and **2.12** to be estimated by measuring $|^1J_{SeP}|$ gained from $^{31}P\{^1H\}$ NMR spectroscopic analysis of the corresponding phosphorus(V) selenides.


**Scheme 2.8.** Generic reaction of elemental grey selenium with a phosphine to generate a phosphine selenide.

The NMR-active $^{77}Se$ nucleus ($I$ = ½) has a natural abundance of 7.6%. Accordingly, the $^{31}P\{^1H\}$ NMR spectrum of phosphine selenides shows two satellites of 3.8% intensity originating from $^{77}Se\text{-}^{31}P$ coupling. The satellites are observed as doublets (* in **Figure 2.3** for compound **2.19**) due to $^2J_{PP}$ coupling in the phosphine selenides of compounds **2.2** – **2.7** arising from the inequivalence of the two phosphorus atoms in the $Ph_2P(Se)NR(^{77}Se)PPh_2$ isotopomer. Phosphorus atom inequivalence in the phosphine selenide of 'SPNP' compound **2.9** ($Ph_2P(S)N\{(CH_2)_2Ph\}(^{77}Se)PPh_2$) results in satellites observed as doublets in the corresponding $^{31}P\{^1H\}$ NMR spectrum. Analogously, $^4J_{PP}$ coupling in the phosphine selenide of compound **2.8** and phosphorus atom inequivalence in the $Ph_2P(Se)CH_2N(R)CH_2(^{77}Se)PPh_2$ isotopomer is responsible for the satellites being observed as doublets for the phosphine selenide of compound **2.8**. The phosphine selenides of compounds **2.11** and **2.12** only have one phosphorus atom, hence the satellites in these $^{31}P\{^1H\}$ NMR spectra are singlets. *NB* a $J_{PP}$ coupling constant ($^2J_{PP}$ for compounds **2.2** – **2.7** and **2.9** and $^4J_{PP}$ for compound **2.8**) of approx. 9 – 12 Hz is measured for the phosphine selenides of compounds **2.2** – **2.9**.

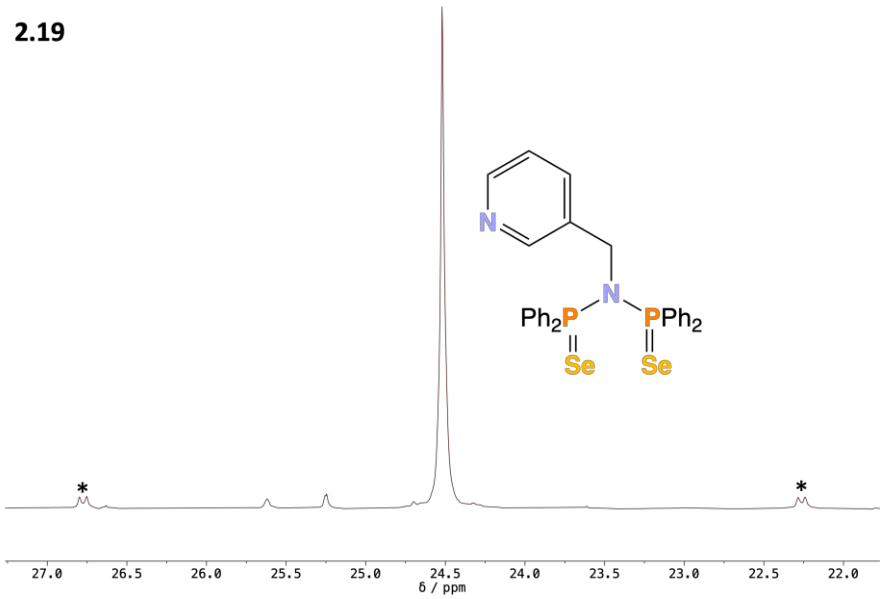


**Figure 2.3.** $^{31}P\{^{1}H\}$ NMR (162 MHz, 290 K, $CDCl_3$) spectrum for compound **2.19**. * indicates satellites originating from $^{77}Se$-$^{31}P$ coupling.

**Table 2.2** shows the measured $|^{1}J_{SeP}|$ values for the phosphine selenides of compounds **2.2** – **2.9**, **2.11, 2.12** and **2.21** – **2.26**.[24 – 28]

**Table 2.2.** Experimentally determined $|^{1}J_{SeP}|$ coupling constants for the phosphine selenides of compounds **2.2** – **2.9**, **2.11**, **2.12** and **2.21** – **2.26**.[24 – 28] $|^{1}J_{SeP}|$ values of the phosphine selenides of compounds **2.2** – **2.9**, **2.11** and **2.12** are measured in $CDCl_3$ from the relevant $^{31}P\{^{1}H\}$ NMR spectrum (162 MHz, 290 K). On average, the peak width at half maximum for the singlets in the $^{31}P\{^{1}H\}$ NMR spectra of compounds **2.2** – **2.9**, **2.11** and **2.12** is approx. 4 Hz.

| Phosphine Selenide | Corresponding Parent Phosphine | $\|^{1}J_{SeP}\|$ / Hz |
|---|---|---|
| **$Ph(CH_2)_2N(\{Se\}PPh_2)_2$** | **$Ph(CH_2)_2N(PPh_2)_2$ (2.2)** | 772 |
| ***n*-$BuN(\{Se\}PPh_2)_2$** | ***n*-$BuN(PPh_2)_2$ (2.3)** | 770 |
| **$Me_2N(CH_2)_3N(\{Se\}PPh_2)_2$** | **$Me_2N(CH_2)_3N(PPh_2)_2$ (2.4)** | 771 |
| **Py-*m*-$CH_2N(\{Se\}PPh_2)_2$** | **Py-*m*-$CH_2N(PPh_2)_2$ (2.5)** | 777 |
| **Ph-$C_6H_4N(\{Se\}PPh_2)_2$** | **Ph-$C_6H_4N(PPh_2)_2$ (2.6)** | 794 |
| **Py-*o*-$C_6H_4N(\{Se\}PPh_2)_2$** | **Py-*o*-$C_6H_4N(PPh_2)_2$ (2.7)** | 796 |
| **Py-*o*-$(CH_2)_2N(CH_2PPh_2\{Se\})_2$** | **Py-*o*-$(CH_2)_2N(CH_2PPh_2)_2$ (2.8)** | 730 |
| **$Ph(CH_2)_2N(SPPh_2)(\{Se\}PPh_2)$** | **$Ph(CH_2)_2N(SPPh_2)(PPh_2)$ (2.9)** | 783 |
| **Py-*o*-$(CH_2)_2N(\{Se\}PPh_2)(Me)$** | **Py-*o*-$(CH_2)_2N(PPh_2)(Me)$ (2.11)** | 759 |
| **Py-*o*-$(CH_2)_2N(\{Se\}P\{OPh\}_2)(Me)$** | **Py-*o*-$(CH_2)_2N(P\{OPh\}_2)(Me)$ (2.12)** | 951 |
| **$SePPh_3$** | **$PPh_3$ (2.20)** | 736[24] |
| **$(Ph_2P\{Se\})_2N(CH_2$-*o*-pyridine)** | **$(Ph_2P)_2N(CH_2$-*o*-pyridine) (2.21)** | 776[25] |
| **$(Ph_2P\{Se\})_2N(CH_2Ph)$** | **$(Ph_2P)_2N(CH_2Ph)$ (2.22)** | 772[25] |
| **$(Ph_2P\{Se\})_2N$(2-fluorene)** | **$(Ph_2P)_2N$(2-fluorene) (2.23)** | 796[26] |
| **9-adenine$(CH_2)_2N(CH_2\{Se\}PPh_2)_2$** | **9-adenine$(CH_2)_2N(CH_2PPh_2)_2$ (2.24)** | 730[27] |
| **9-adenine$(CH_2)_3N(CH_2\{Se\}Ph_2)_2$** | **9-adenine$(CH_2)_3N(CH_2PPh_2)_2$ (2.25)** | 730[27] |
| **$HN(SPPh_2)(\{Se\}PPh_2)$** | **$HN(SPPh_2)(PPh_2)$ (2.26)** | 790[28] |

The relationship shown (**Equation 2.1**) illustrates that a greater $|^1J_{SeP}|$ corresponds to a greater amount of phosphorus atom lone pair s-character and therefore a lower basicity of the phosphine, translating to a phosphine with a greater $|^1J_{SeP}|$ being a weaker $\sigma$-donor.

$$|^1J_{SeP}| \propto \%\text{ s-character of P lone pair} \propto \frac{1}{\text{basicity of } PR_3} \qquad \textbf{(2.1)}$$

$PPh_3$, due to its wide usage, has been deemed a suitable benchmark phosphine to allow for interpretation of the measured $|^1J_{SeP}|$ values listed in **Table 2.2**. Compounds **2.2** – **2.7**, **2.9**, **2.11** and **2.12** contain phosphorus atoms directly bonded to an electron-withdrawing nitrogen atom (*i.e.*, P-N bonds), resulting in a decrease in basicity relative to $PPh_3$ by increasing the s-character of the phosphorus lone pair (**Equation 2.1**). 'PCNCP' compound **2.8** does not contain phosphorus atoms directly bonded to electron withdrawing nitrogen atoms. Hence, the electron-withdrawing effect of the P-C-N-C-P nitrogen atom on the phosphorus atoms is reduced relative to the 'PNP' compounds. Accordingly, this leads to a decrease in s-character of the phosphorus lone pairs and therefore leads to an increase in basicity, resulting in compound **2.8** being more basic than compounds **2.2** – **2.7**, **2.9**, **2.11**, **2.12** and $PPh_3$. The $|^1J_{SeP}|$ values for the phosphine selenides of compounds **2.2** – **2.5**, compounds **2.6** and **2.7**, compound **2.8**, and compound **2.9** are consistent with the $|^1J_{SeP}|$ values for the phosphine selenides of compounds **2.21** – **2.22**,[25] compound **2.23**,[26] compounds **2.24** – **2.25**[27] and compound **2.26**,[28] respectively (**Figure 2.4**).

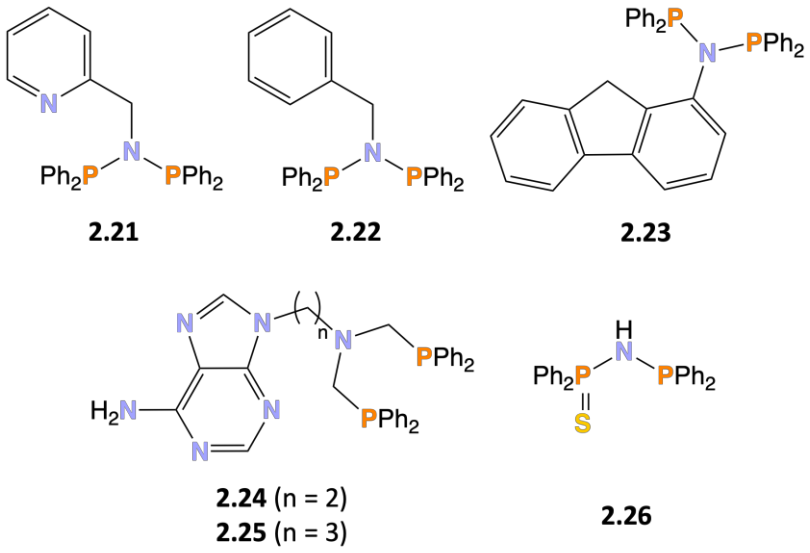


**Figure 2.4.** Structures of compounds **2.21** – **2.26**.[25 – 28]

Comparison of the $|^1J_{SeP}|$ values for compounds **2.2** – **2.9**, **2.11** and **2.12** (**Table 2.2**) identifies that compound **2.8** is the most basic (as explained above), followed by aminophosphine compound **2.11** (the nitrogen atom lone pair is delocalised over one P-N bond as opposed to two P-N bonds in a 'PNP' compound, resulting in a more electron dense phosphorus atom). Compounds **2.2** – **2.5** exhibit measured $|^1J_{SeP}|$ values which can be regarded as the same (approx. 1 Hz difference), as do compounds **2.6** – **2.7** (*cf*. the measured approx. 4 Hz peak width at half maximum from **Figure 2.3**). Compounds **2.2** – **2.7** and **2.9** exhibit similar $|^1J_{SeP}|$ values in the small range of 770 – 796 Hz, and can be regarded as having the same basicity. Compound **2.12** is the least basic due to containing strongly electron-withdrawing OPh substituents.

## 2.8 Summary

$Ph(CH_2)_2N(PPh_2)_2$ (**2.2**), *n*-$BuN(PPh_2)_2$ (**2.3**), $Me_2N(CH_2)_3N(PPh_2)_2$ (**2.4**), Py-*m*-$CH_2N(PPh_2)_2$ (**2.5**), Ph-$C_6H_4N(PPh_2)_2$ (**2.6**), Py-*o*-$C_6H_4N(PPh_2)_2$ (**2.7**), Py-*o*-$(CH_2)_2N(CH_2PPh_2)_2$ (**2.8**), $Ph(CH_2)_2N(SPPh_2)(PPh_2)$ (**2.9**), $Ph(CH_2)_2N(SPPh_2)_2$ (**2.10**), Py-*o*-$(CH_2)_2N(PPh_2)(Me)$ (**2.11**) and Py-*o*-$(CH_2)_2N(P\{OPh\}_2)(Me)$ (**2.12**) have been synthesised (**Section 2.2** – **2.5**), and the synthesis of Py-*o*-$(CH_2)_2N\{P(OPh)_2\}_2$ (**2.13**) was attempted (**Section 2.6**). Compound **2.13** was not afforded from its attempted synthesis, as evidenced by a lack of reactivity between the isolated product with elemental selenium. The basicity of compounds **2.2** – **2.9**, **2.11** and **2.12** was estimated *via* the synthesis of the corresponding phosphine selenides and measurement of $|^1J_{SeP}|$ coupling constants (**Section 2.7**).

### References


1. C. Fliedel, V. Rosa, B. Vileno, N. Parizel, S. Choua, C. Gourlaouen, P. Rosa, P. Turek, P. Braunstein, *Inorg. Chem.*, **2016**, *55*, 4183 – 4198. 10.1021/acs.inorgchem.5b02889
2. D. Naicker, H. B. Friedrich, B. Omondi, *RSC Adv*., **2015**, *5*, 63123 – 63129. 10.1039/C5RA07365K
3. K. Naktode, R. K. Kottalanka, H. Adimulam, T. K. Panda, *J. Coord. Chem*., **2014**, *67*, 3052 – 3053. 10.1080/00958972.2014.953071
4. A. Carrick, MChem Thesis, Durham University, **2020**.
5. P. Wang, H. Liu, Y-Q. Li, X-L. Zhao, Y. Lu, Y. Liu, *Catal. Sci. Technol*., **2016**, *6*, 3854 – 3861. 10.1039/C5CY01827G
6. H. Lee, S. H. Hong, *Appl. Catal., A*, **2018**, *560*, 21 – 27. 10.1016/j.apcata.2018.04.030

7. P-H. Zhao, M-Y. Hu, J-R. Li, Z-Y. Ma, Y-Z. Wang, J. He, Y-L. Li, X-F. Liu, *Organometallics*, **2019**, *38*, 385 – 394. 10.1021/acs.organomet.8b00759
8. L-C. Song, L. Feng, Y-Q. Guo, *Dalton Trans*., **2019**, *48*, 1443 – 1453. 10.1039/C8DT04211J
9. Y. Shaikh, J. Gurnham, K. Albahily, S. Gambarotta, I. Korobkov, *Organometallics*, **2012**, *31*, 7427 – 7433. 10.1021/om3007135
10. M. K. Penney, R. Giang, K. K. Klausmeyer, *Polyhedron*, **2015**, *85*, 275 – 283. 10.1016/j.poly.2014.08.017
11. A. Ghisolfi, C. Fliedel, V. Rosa, R. Pattacini, A. Thibon, K. Y. Monakhov, P. Braunstein, *Chem. Asian J*., **2013**, *8*, 1795 – 1805. 10.1002/asia.201300687
12. A. Ghisolfi, C. Fliedel, V. Rosa, K. Y. Monakhov, P. Braunstein, *Organometallics*, **2014**, *33*, 2523 – 2534. 10.1021/om500141k
13. J. W. Faller, J. Lloret-Fillol, J. Parr, *New J. Chem*., **2002**, *26*, 883 – 888. 10.1039/B111422K
14. M. M. Wade Wolfe, M. D. Pluth, *Inorg. Chem*., **2023**, *62*, 14339 – 14343. 10.1021/acs.inorgchem.3c01976
15. Z. Fei, R. Scopelliti, P. J. Dyson, *Dalton Trans*., **2003**, 2772 – 2779. 10.1039/B303645F
16. A. Benny, D. Sharma, Ankur, T. Rajeshkumar, L. Maron, A. Venugopal, *Chem. Eur. J*., **2023**, *29*, e202300588. 10.1002/chem.202300588
17. Z. Fei, E. Păunescu, W. H. Ang, R. Scopelliti, P. J. Dyson, *Eur. J. Inorg. Chem.,* **2014**, 1745 – 1750. 10.1002/ejic.201301143
18. E. Simón-Manso, M. Valderrama, P. Gantzel, C. P. Kubiak, *J. Organomet. Chem*., **2002**, *651*, 90 – 97. 10.1016/S0022-328X(02)01317-7
19. R. Kumar, S. Kumar, M. K. Pandey, V. S. Kashid, L. Radhakrishna, M. S. Balakrishna, *Eur. J. Inorg. Chem*., **2018**, 1028 – 1037. 10.1002/ejic.201701414
20. Z. Dinev, C. T. Gannon, C. Egan, J. A. Watt, M. J. McConville, S. J. Williams, *Org. Biomol. Chem*., **2007**, *5*, 952 – 959. 10.1039/B616450A
21. Y. Xu, Y. J. Hong, D. J. Tantillo, M. K. Brown, *Org. Lett*., **2017**, *19*, 3703 – 3706. 10.1021/acs.orglett.7b01420
22. J. R. Ascenso, C. G. de Azevedo, A. R. Dias, M. T. Duarte, I. Eleutério, M. J. Ferreira, P. T. Gomes, A. M. Martins, *J. Organomet. Chem*., **2001**, *632*, 17 – 26. 10.1016/S0022-328X(01)00837-3
23. M. S. Balakrishna, P. P. George, J. T. Mague, *J. Organomet. Chem*., **2004**, *689*, 3388 – 3394. 10.1016/j.jorganchem.2004.08.003
24. W. McFarlane, D. S. Rycroft, *J. Chem. Soc., Dalton Trans.*, **1973**, *20*, 2162 – 2166. 10.1039/DT9730002162
25. N. Biricik, F. Durap, C. Kayan, B. Gümgüm, N. Gürbüz, I. Özdemir, W. H. Ang, Z. Fei, R. Scopelliti, *J. Organomet. Chem.*, **2008**, *693*, 2693 – 2699. 10.1016/j.jorganchem.2008.05.010
26. C. Kayan, N. Biricik, M. Aydemir, *Transition Met. Chem*., **2011**, *36*, 513 – 520. 10.1007/s11243-011-9497-8
27. Q. Zhang, G. Hua, P. Bhattacharyya, A. M. Z. Slawin, J. D. Woollins, *Eur. J. Inorg. Chem*., **2003**, *2003*, 2426 – 2437. 10.1002/ejic.200300037
28. P. Sekar, J. A. Ibers, *Inorg. Chim. Acta*, **2001**, *319*, 117 – 122. 10.1016/S0020-1693(01)00456-X

# Chapter 3 – Synthesis and Reactivity of Palladium(II) Complexes of 'PNP' and 'PCNCP' Ligands

## 3.1 Introduction

In order to offer a contrast to the coordination chemistry exhibited by 'PNP' and 'PCNCP' ligands with 'hard' cobalt(II), *i.e.*, zwitterionic complexes (further studied in **Chapter 4**),[1] the synthesis of square planar [(RN(PPh$_2$)$_2$)PdCl$_2$] complexes, with 'soft' palladium(II) centres will be pursued. Exploitation of the well-established κ$^2$-*P,P* coordination chemistry and diamagnetic nature of [(RN(PPh$_2$)$_2$)PdCl$_2$] complexes[2 – 4] allows for their $^{31}$P{$^1$H} NMR spectroscopic study, a technique not readily applicable to paramagnetic cobalt complexes.

Although the synthesis of [(RN(PPh$_2$)$_2$)PdCl$_2$] complexes is well-established, their reactivity has been scarcely studied. For example, some of the reactions of [(RN(PPh$_2$)$_2$)PdCl$_2$] that have been studied include reaction with R'-OH (mainly when R' = Me) affording [{RNH(PPh$_2$)}(R'OPPh$_2$)PdCl$_2$],[5] and chloride ligand exchange (to iodide ligands,[6] $SO_3CF_3^-$ ligands,[7] or L-type ligands[7,8]). In order to further study the reactivity of [(RN(PPh$_2$)$_2$)PdCl$_2$] complexes, [(RN(PPh$_2$)$_2$)PdCl$_2$] complexes containing a pendant donor group, *e.g.*, the pendant and non-coordinating pyridyl group of [(Py-*o*-CH$_2$N(PPh$_2$)$_2$)PdCl$_2$],[3] will be studied. A pendant donor group could serve as a reactive site to allow for the functionalisation of [(RN(PPh$_2$)$_2$)PdCl$_2$] complexes through Lewis or Brønsted base behaviour. Hence, the reactivity of the potential pendant pyridyl and amine groups in the palladium(II) complexes of compounds **2.1** (Py-*o*-(CH$_2$)$_2$N(PPh$_2$)$_2$), **2.4** (Me$_2$N(CH$_2$)$_3$N(PPh$_2$)$_2$) and **2.8** (Py-*o*-(CH$_2$)$_2$N(CH$_2$PPh$_2$)$_2$) will be pursued.

Note that the reactivity of 'SPNP' compound **2.9** (Ph(CH$_2$)$_2$N(SPPh$_2$)(PPh$_2$)) and 'SPNPS' compound **2.10** (Ph(CH$_2$)$_2$N(SPPh$_2$)$_2$) with [(MeCN)$_2$PdCl$_2$] has not been studied. However, the κ$^2$-*P,S* and κ$^2$-*S,S* coordination modes (which would be evidenced in the palladium(II) complexes of compounds **2.9** and **2.10**, respectively) have been described previously for complexes **1.38** and **1.39** ([{(CO$_2$Me)(Me)HCN(PPh$_2$)(SPPh$_2$)}PdCl$_2$] and [{(CO$_2$Me)(Me)HCN(SPPh$_2$)$_2$}PdCl$_2$], respectively, **Scheme 1.6**, **Section 1.2.1**).[9]

## 3.2 Coordination Chemistry of $Ph(CH_2)_2N(PPh_2)_2$ (2.2), *n*-$BuN(PPh_2)_2$ (2.3), $NMe_2(CH_2)_3N(PPh_2)_2$ (2.4), Py-*m*-$CH_2N(PPh_2)_2$ (2.5), Ph-$C_6H_4N(PPh_2)_2$ (2.6), Py-*o*-$C_6H_4N(PPh_2)_2$ (2.7) and Py-*o*-$(CH_2)_2N(CH_2PPh_2)_2$ (2.8) with Palladium(II) Dichloride

To assess their coordination chemistry with palladium(II) dichloride, 'PNP' compounds **2.2** – **2.7** and 'PCNCP' compound **2.8** were reacted with 1 equivalent of $[(MeCN)_2PdCl_2]$, affording complexes **3.1** – **3.7** (**Scheme 3.1**).

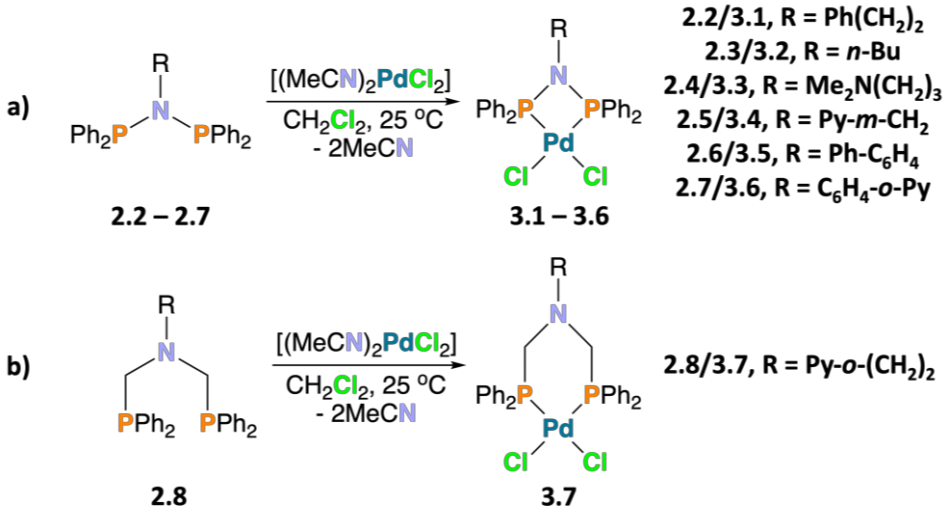


**Scheme 3.1.** Synthesis of **a)** complexes **3.1** – **3.7** and **b)** complex **3.7**.

The $^{31}P\{^1H\}$ NMR spectra of the $[(RN(PPh_2)_2)PdCl_2]$ complexes **3.1** – **3.6** show singlet resonances at approx. $\delta_P$ = 30 – 40 ppm evidencing $\kappa^2$-*P,P* coordination, as illustrated in **Scheme 3.1**. In contrast, singlet $^{31}P\{^1H\}$ resonances at slightly higher frequency, approx. $\delta_P$ = 55 – 70 ppm, are observed for uncoordinated 'PNP' $(RN(PPh_2)_2)$ compounds **2.2** – **2.7** (**Scheme 3.1**). The $^{31}P\{^1H\}$ NMR spectra of compound **2.2** and complex **3.1**, illustrating the negative coordination chemical shift (–Δδ), are shown in **Figure 3.1**.

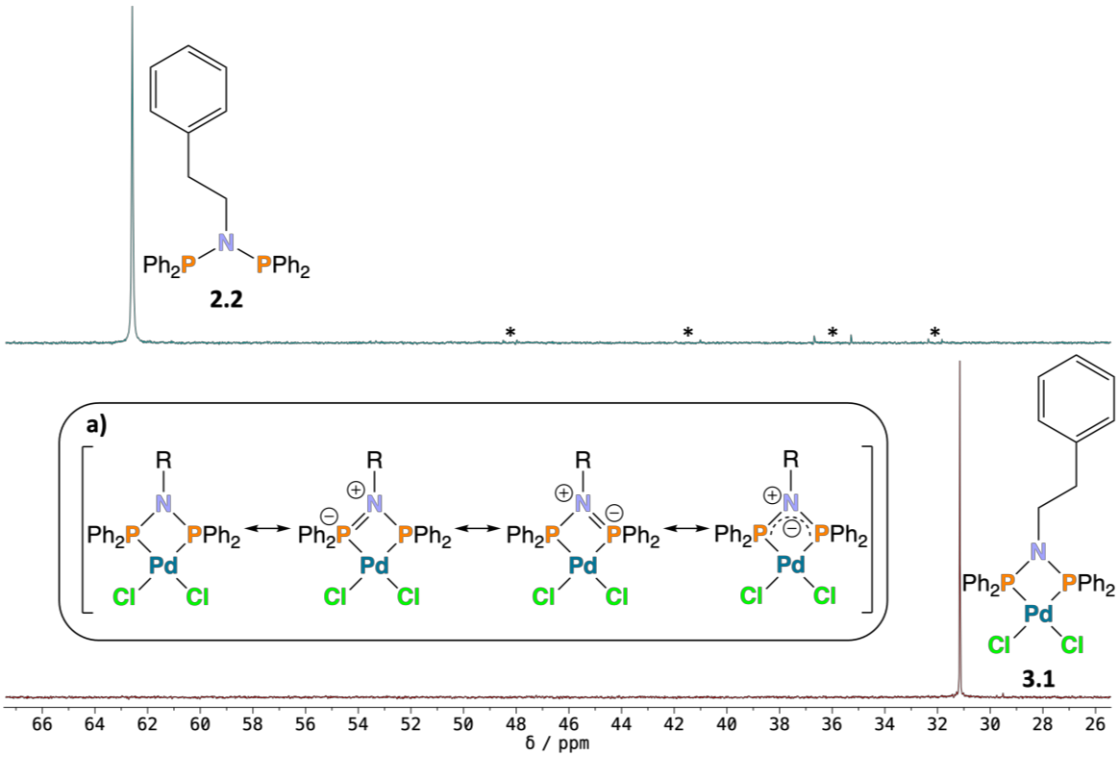


**Figure 3.1.** $^{31}P\{^{1}H\}$ NMR (162 MHz, 290 K, $CDCl_3$) spectra for compound **2.2** and complex **3.1**. **a)** shows resonance canonicals of $[RN(PPh_2)_2PdCl_2]$. * indicates trace impurities.

The lower frequency $^{31}P\{^{1}H\}$ NMR shifts of $[(RN(PPh_2)_2)PdCl_2]$ complexes **3.1** – **3.6** relative to uncoordinated 'PNP' $(RN(PPh_2)_2)$ compounds **2.2** – **2.7** likely arises from enhanced delocalisation of the 'PNP' nitrogen atom lone pair upon complexation. This results in both phosphorus atoms having formal associated negative charges (**a)**, **Figure 3.1**),[2] providing further shielding from the applied magnetic field and resulting in a negative coordination chemical shift, –Δδ.

Coordination of Py-*o*-$(CH_2)_2N(CH_2PPh_2)_2$ (**2.8**) to afford complex [{Py-*o*-$(CH_2)_2N(CH_2PPh_2)_2$}$PdCl_2$]) (**3.7**) occurs with a positive coordination chemical shift (+Δδ) with singlet resonances in their $^{31}P\{^{1}H\}$ NMR spectra at –28.6 and 8.1 ppm, respectively, (**Figure 3.2**). The $N(\underline{CH_2}PPh_2)_2$ $CH_2$ spacers preclude nitrogen atom lone pair delocalisation to the phosphorus atoms. Hence, the phosphorus nuclei of compound **2.8** are less shielded, compared to those of compounds **2.2** – **2.7**, upon coordination due to lone pair donation to the palladium(II) centre, resulting in +Δ$\delta$.

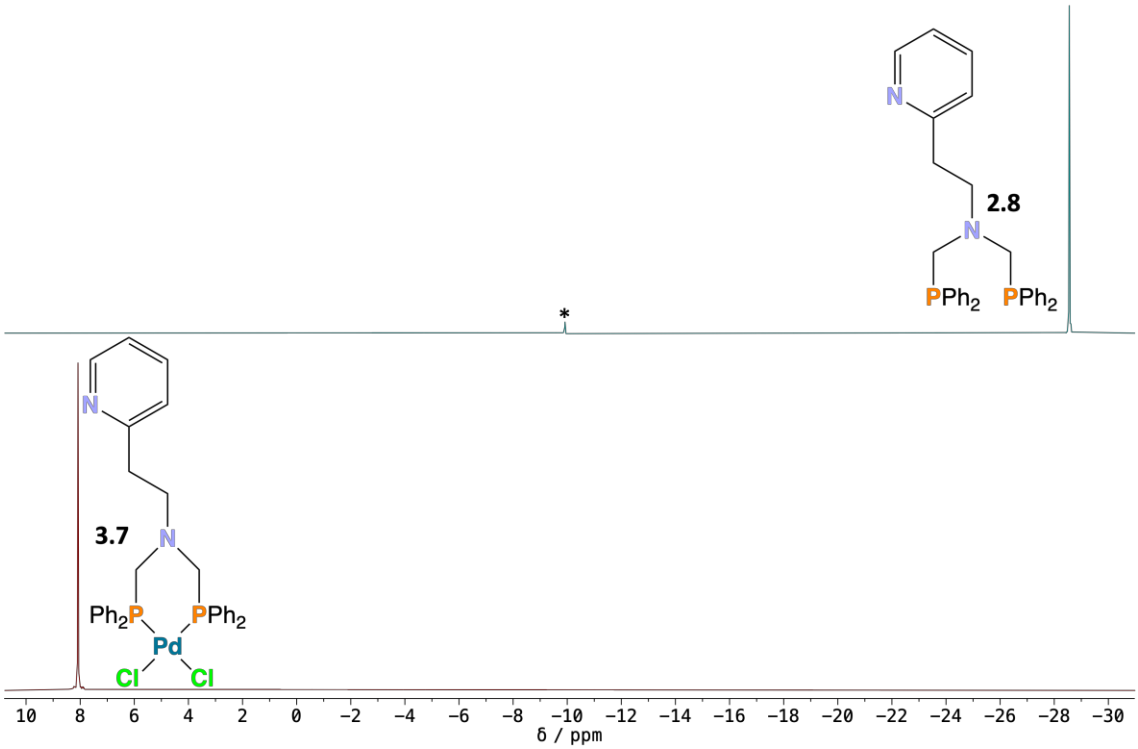


**Figure 3.2.** $^{31}P\{^{1}H\}$ NMR (162 MHz, 290 K, $CDCl_3$ for **2.8**, $CD_2Cl_2$ for **3.7**) spectra for compound **2.8** and complex **3.7**. * indicates a trace impurity.

### 3.2.1 Solid-State Molecular Structures of [(Ph(CH$_2$)$_2$N(PPh$_2$)$_2$)PdCl$_2$] (3.1), [(*n*-BuN(PPh$_2$)$_2$)PdCl$_2$] (3.2), [(NMe$_2$(CH$_2$)$_3$N(PPh$_2$)$_2$)PdCl$_2$] (3.3), [(Py-*m*-CH$_2$N(PPh$_2$)$_2$)PdCl$_2$] (3.4), [(Ph-C$_6$H$_4$N(PPh$_2$)$_2$)PdCl$_2$] (3.5), [(Py-*o*-C$_6$H$_4$N(PPh$_2$)$_2$)PdCl$_2$] (3.6) and [(Py-*o*-(CH$_2$)$_2$N(CH$_2$PPh$_2$)$_2$)PdCl$_2$] (3.7)

Single crystals of complexes **3.1** – **3.7** were obtained and molecular structures determined. Each of the solid-state molecular structures (**Figure 3.3**) shows $\kappa^2$-*P,P* coordination, in agreement with the structures established from $^{31}P\{^{1}H\}$ NMR analysis (**Section 3.2**). The solid-state structures of complexes **3.3**, **3.4**, **3.6** and **3.7** confirm that the potential nitrogen donor atoms are non-coordinating.

The key bond lengths and angles for complexes **3.1** – **3.6** are very similar (**Table 3.1** and **Table 3.2**), and are very similar to those previously reported for [(Ph(CH$_2$)N(PPh$_2$)$_2$)PdCl$_2$].[3] Similarly, the key bond angles and lengths determined for complex **3.7** (**Table 3.2**) are very similar to those previously reported for [(o-CH$_3$C(=CH$_2$)C$_6$H$_4$N(CH$_2$PPh$_2$)$_2$)PdCl$_2$].[4]

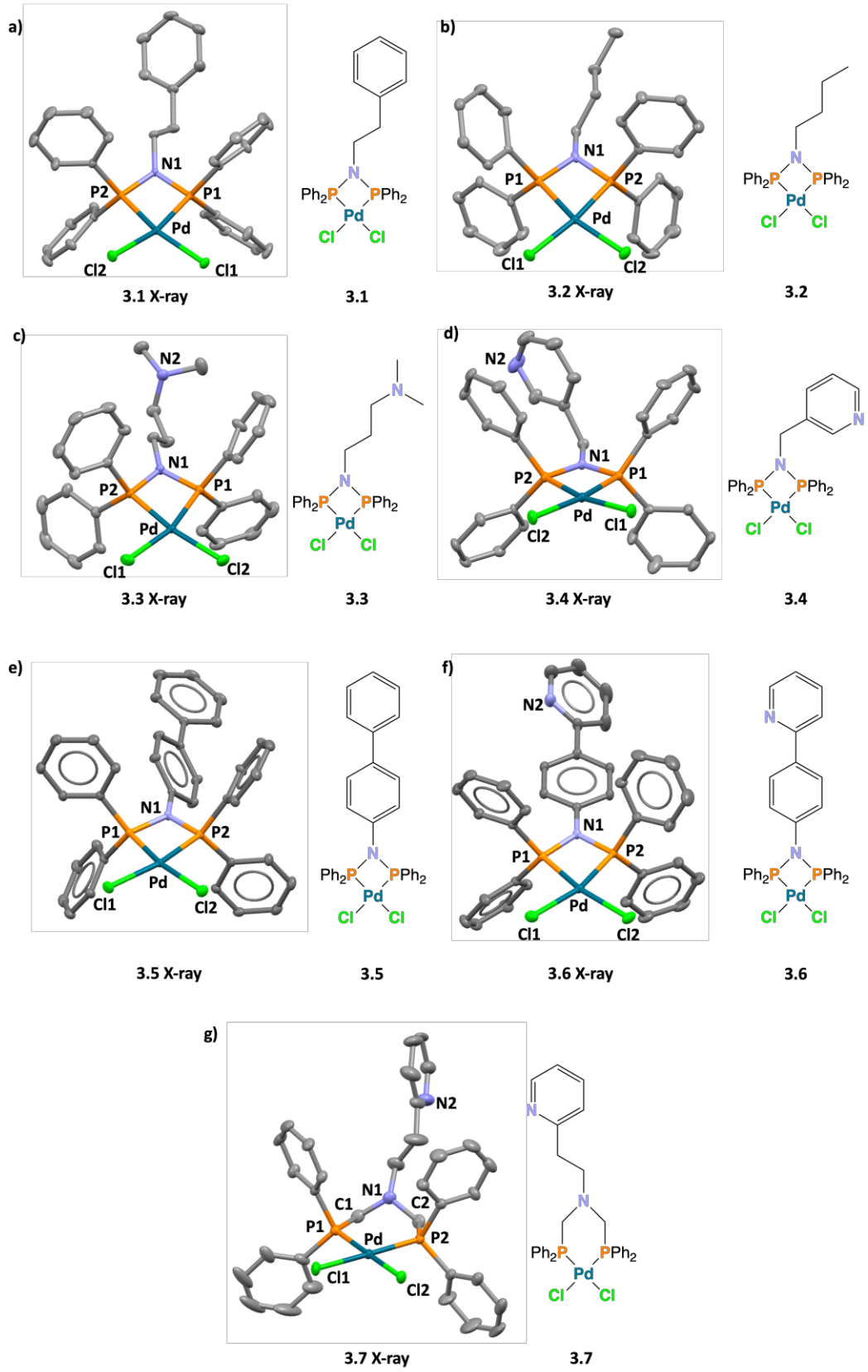


**Figure 3.3.** Solid-state molecular structures of complexes **3.1** – **3.7**. *NB* hydrogen atoms (for **3.1** – **3.7 X-rays**) and DCM molecules (for **3.1**, **3.4, 3.5**, **3.6** and **3.7 X-rays**) are omitted for clarity. Thermal ellipsoids are shown at the 50 % probability level. Atom colour: carbon – grey; nitrogen – blue; phosphorus – orange; chlorine – green and palladium – blue-green. *NB* the molecular structure of **3.2** has not been completely refined due to the crystal being twinned, however the connectivity is certain and bond lengths/angles can be measured. Accordingly, the crystallographic data have been omitted from **Appendix 4**.

Complexes **3.1** – **3.7** adopt a distorted square planar geometry around the palladium(II) centre. As expected, complexes **3.1** – **3.6** are significantly more distorted from the ideal square planar geometry (**3.1** – **3.6** : P1-Pd-P2 ~71°) than complex **3.7** (P1-Pd-P2 ~95°) arising from the smaller P-Pd-P angle. The distortion of a square planar geometry is quantified by the $\tau_4$ geometry index[10] (**Table 3.1** and **Table 3.2**); for a perfect square planar geometry, $\tau_4$ has a value of 0. $\tau_4$ is calculated by **Equation 3.1**:

$$\tau_4 \approx -0.00709\alpha - 0.00709\beta + 2.55 \qquad \textbf{(3.1)}$$

where $\alpha$ and $\beta$ are the two largest valence angles around the four-coordinate centre.[10] The calculated $\tau_4$ value for complex **3.7** is 0.03993, which is much closer to 0 ($\alpha = \beta =$ 180°) than the $\tau_4$ values for complexes **3.1** – **3.6** in the range of ~0.15 – 0.18.

**Table 3.1.** Key bond lengths and angles measured from the solid-state molecular structures of complexes **3.1** – **3.3**, and calculated $\tau_4$ parameters for complexes **3.1** – **3.3**.

| Parameter | 3.1 | 3.2 | 3.3 |
|---|---|---|---|
| N1-P1 / Å | 1.700(1) | 1.695(2) | 1.697(1) |
| N1-P2 / Å | 1.695(1) | 1.700(8) | 1.682(1) |
| P1-Pd / Å | 2.2112(5) | 2.227(2) | 2.2255(6) |
| P2-Pd / Å | 2.2038(5) | 2.209(2) | 2.2017(5) |
| Pd-Cl1 / Å | 2.3602(5) | 2.340(2) | 2.3653(5) |
| Pd-Cl2 / Å | 2.3548(5) | 2.357(2) | 2.3566(6) |
| N1-C1 / Å | – | – | – |
| N1-C2 / Å | – | – | – |
| P1-N1-P2 / ° | 98.43(6) | 99.6(4) | 100.19(9) |
| P1-Pd-P2 / ° | 71.20(2) | 71.51(7) | 71.69(2) |
| P1-Pd-Cl1 / ° | 96.11(2) | 100.76(7) | 98.70(2) |
| P2-Pd-Cl2 / ° | 97.93(2) | 93.90(7) | 92.51(2) |
| Cl1-Pd-Cl2 / ° | 94.90(2) | 93.86(7) | 97.06(2) |
| P1-Pd-Cl2 / ° | 166.81(2) | 165.24(8) | 164.07(2) |
| P2-Pd-Cl1 / ° | 167.17(2) | 172.23(8) | 170.34(2) |
| C1-N1-C2 / ° | – | – | – |
| $\tau_4$ | 0.18 | 0.12 | 0.18 |

**Table 3.2.** Key bond lengths and angles measured from the solid-state molecular structures of complexes **3.4** – **3.7**, and calculated $\tau_4$ parameters for complexes **3.4** – **3.7**.

| Parameter | 3.4 | 3.5 | 3.6 | 3.7 |
|---|---|---|---|---|
| N1-P1 / Å | 1.697(4) | 1.7083(7) | 1.714(2) | – |
| N1-P2 / Å | 1.699(5) | 1.7083(7) | 1.705(2) | – |
| P1-Pd / Å | 2.209(1) | 2.2143(2) | 2.1979(7) | 2.240(1) |
| P2-Pd / Å | 2.215(1) | 2.2143(2) | 2.2058(6) | 2.244(1) |
| Pd-Cl1 / Å | 2.365(1) | 2.3548(2) | 2.3666(5) | 2.351(1) |
| Pd-Cl2 / Å | 2.359(1) | 2.3548(2) | 2.3556(7) | 2.352(1) |
| N1-C1 / Å | – | – | – | 1.447(5) |
| N1-C2 / Å | – | – | – | 1.453(5) |
| P1-N1-P2 / ° | 99.7(2) | 99.79(6) | 99.0(1) | – |
| P1-Pd-P2 / ° | 71.83(4) | 72.33(13) | 72.40(2) | 95.22(4) |
| P1-Pd-Cl1 / ° | 96.46(4) | 96.52(9) | 95.63(3) | 86.12(4) |
| P2-Pd-Cl2 / ° | 96.67(4) | 96.52(9) | 94.11(3) | 86.87(4) |
| Cl1-Pd-Cl2 / ° | 95.02(4) | 94.63(14) | 97.95(3) | 91.69(4) |
| P1-Pd-Cl2 / ° | 168.50(4) | 168.83(9) | 165.92(3) | 176.40(4) |
| P2-Pd-Cl1 / ° | 167.66(4) | 168.83(9) | 167.90(3) | 177.63(4) |
| C1-N1-C2 / ° | – | – | – | 111.1(3) |
| $\tau_4$ | 0.17 | 0.16 | 0.18 | 0.04 |

The P1-N1-P2 bond angle (∼98°) in complexes **3.1** – **3.6** is significantly smaller than the expected 120° P-N-P bond angle in non-coordinated 'PNP' compounds, *e.g.,* in 2-{N=$PPh_2$-$PPh_2$}-3-{N($PPh_2$)$_2$}-$C_5H_3N$ where P-N-P = 120.48(11)°,[11] resulting in significant strain in the planar Pd-P-N-P four-membered chelate rings in complexes **3.1** – **3.6**. The six-membered chelate ring in complex **3.7** adopts a typical puckered conformation, with C1-N1-C2 ∼111° being close to the ideal 109.5° tetrahedral bond angle.

The square planar geometry of palladium(II) complexes **3.1** – **3.7** is further evidenced by considering the distance between the palladium(II) centre and the mean plane containing the two phosphorus atoms and the two chloride ligands (**Figure 3.4**) – the shorter the distance, the more planar the geometry around the palladium(II) centre. For complexes **3.1** and **3.7** (**Figure 3.4**), these measured distances are short at 0.063 Å and 0.048 Å, respectively.

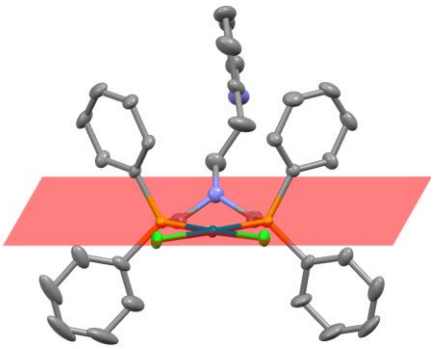

**Figure 3.4.** The mean plane (red) calculated from the positions of P1, P2, Cl1 and Cl2 in complex **3.7**. Thermal ellipsoids are shown at the 50 % probability level.

## 3.3 Protonation and Deprotonation of [(Py-*o*-$(CH_2)_2N(PPh_2)_2$)$PdCl_2$] (3.8), [(Py-*o*-$(CH_2)_2N(CH_2PPh_2)_2$)$PdCl_2$] (3.7) and [$(NMe_2(CH_2)_3N(PPh_2)_2)PdCl_2$] (3.3)

To explore the potential reactivity of the pendant nitrogen donor groups present in complexes **3.3**, **3.7** and **3.8** (previously prepared),[12] they were treated with one equivalent of trifluoroacetic acid (TFA), affording complexes **3.9**, **3.10** and **3.12** (**Scheme 3.2**). Complex **3.3** was also treated with one equivalent of $NH_4PF_6$, affording complex **3.11** (**Scheme 3.2**). Additionally, complexes **3.9** – **3.12** were deprotonated with $NEt_3$ to regenerate the corresponding complexes **3.3**, **3.7** and **3.8** (**Scheme 3.2**).

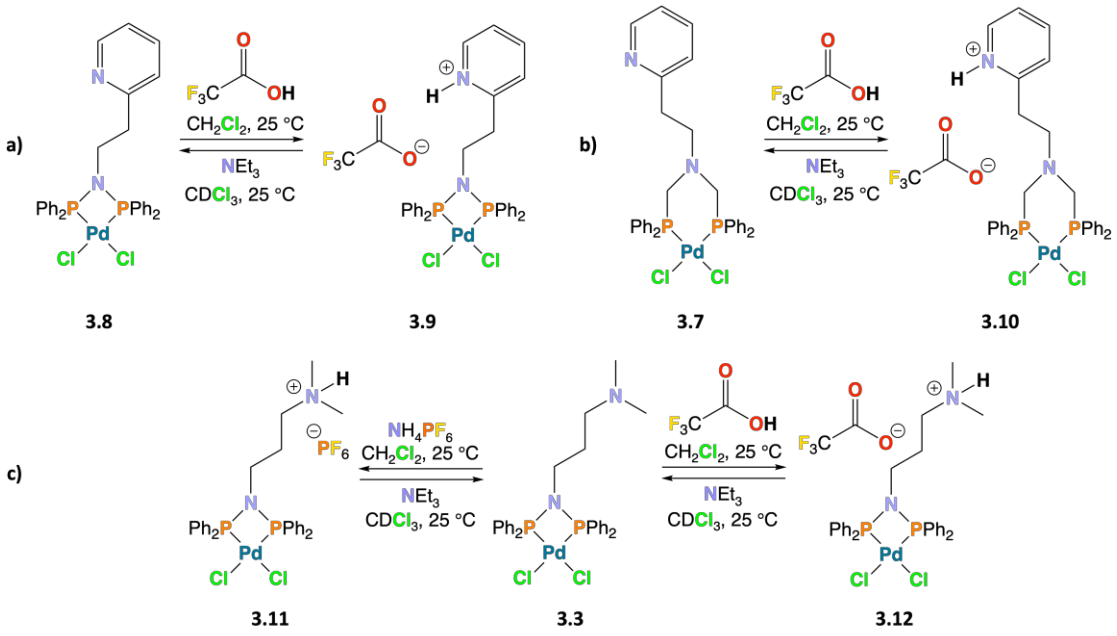


**Scheme 3.2.** Reactions of complexes **a) 3.8** with TFA, **b) 3.7** with TFA, and **c) 3.3** with $NH_4PF_6$ or TFA, affording complexes **3.9**, **3.10**, **3.11** and **3.12**, respectively, and the corresponding deprotonations with $NEt_3$.

TFA ($pK_a$ = –0.25 in $H_2O$)[13] was chosen as a suitable acid to probe the reactions of the pendant amine and pyridine motifs (**Scheme 3.2**) due to being more acidic than $Py^+H$

($pK_a$ = 5.21 in $H_2O$)[13] and $Et_3N^+H$ ($pK_a$ = 10.75 in $H_2O$).[13] Pyridine and $NEt_3$ are suitable models for the pyridyl groups present in complexes **3.7** and **3.8** and the tertiary amine groups in compounds **3.3** and **3.7** (the P-C-N-C-P nitrogen atom), respectively. Previous studies have explored reaction of complex **3.13** with triflic acid ($pK_a$ = –14 in $H_2O$)[13] (**a)**, **Scheme 3.3**).[14] However, triflic acid was avoided in this work, in favour of TFA, due to concerns of additional reactivity being possible between triflic acid and P-N bonds arising from triflic acid's greater acidity. Additionally, $NH_4PF_6$ was also used to protonate complex **3.3** to afford compound **3.11**, as $H_4N^+$ has $pK_a$ = 9.2 in $H_2O$.[13] Similar protonation of complexes **3.15** and **3.16** (**b)**, **Scheme 3.3**) with $NH_4PF_6$ has been reported.[15]

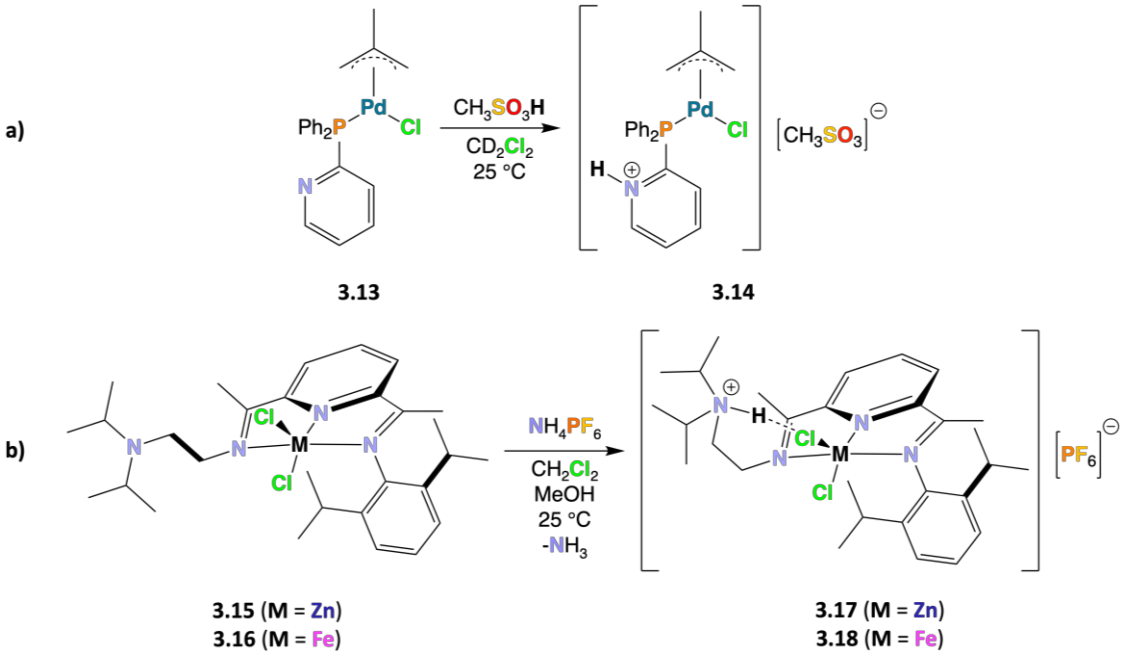


**Scheme 3.3. a)** synthesis of complex **3.14**;[14] **b)** synthesis of complexes **3.17** and **3.18**.[15]

The $^{31}P\{^1H\}$ NMR spectra of complexes **3.8** and **3.9** evidence singlet resonances at $\delta_P$ = 31.5 and 32.0 ppm, respectively, *i.e.*, the same chemical shift. Comparison of the $^1H$ NMR spectra of complexes **3.8** and **3.9** (**Figure 3.5**) shows that the pyridyl proton resonances move to higher frequency upon protonation of complex **3.8**, with $\Delta\delta$(H-4Py) > $\Delta\delta$(H-5Py) >> $\Delta\delta$(H-6Py) > $\Delta\delta$(H-3Py), where $\Delta\delta = \delta_{protonated} - \delta_{unprotonated}$ . Similar changes in chemical shift are observed on protonation of 2-pyridyldiphenylphosphine[14] and pyridine,[16] further supporting that protonation occurs at the pyridyl nitrogen atom of complex **3.8**. A broad singlet centred at approx. 12 ppm ($\nu_{1/2}$ ~440 Hz), corresponding to the $Py^+\underline{H}$ proton, is observed in the $^1H$ NMR spectra of complex **3.9**, agreeing with the

broad singlet at 11.9 ppm seen in the $^1$H NMR spectrum of complex **3.14** (**a**), **Scheme 3.3**).[14]

Deprotonation of complex **3.9** with $NEt_3$ results in the signals for the pyridyl protons returning essentially to the original chemical shifts determined for complex **3.8** prior to protonation (with $\Delta\delta'$ ranging from ~0.05 – ~0.07 ppm, where $\Delta\delta' = \delta_{\text{unprotonated}} - \delta_{\text{deprotonated}}$). Complete return to the original chemical shifts of the unprotonated complex is not observed upon deprotonation since there is exchange with $[NEt_3H]Cl$ generated during deprotonation.[17] The behaviour evidenced from the $^1$H NMR spectra (**Figure 3.5**) is consistent with the protonation of the pyridyl nitrogen atom being reversible as expected.

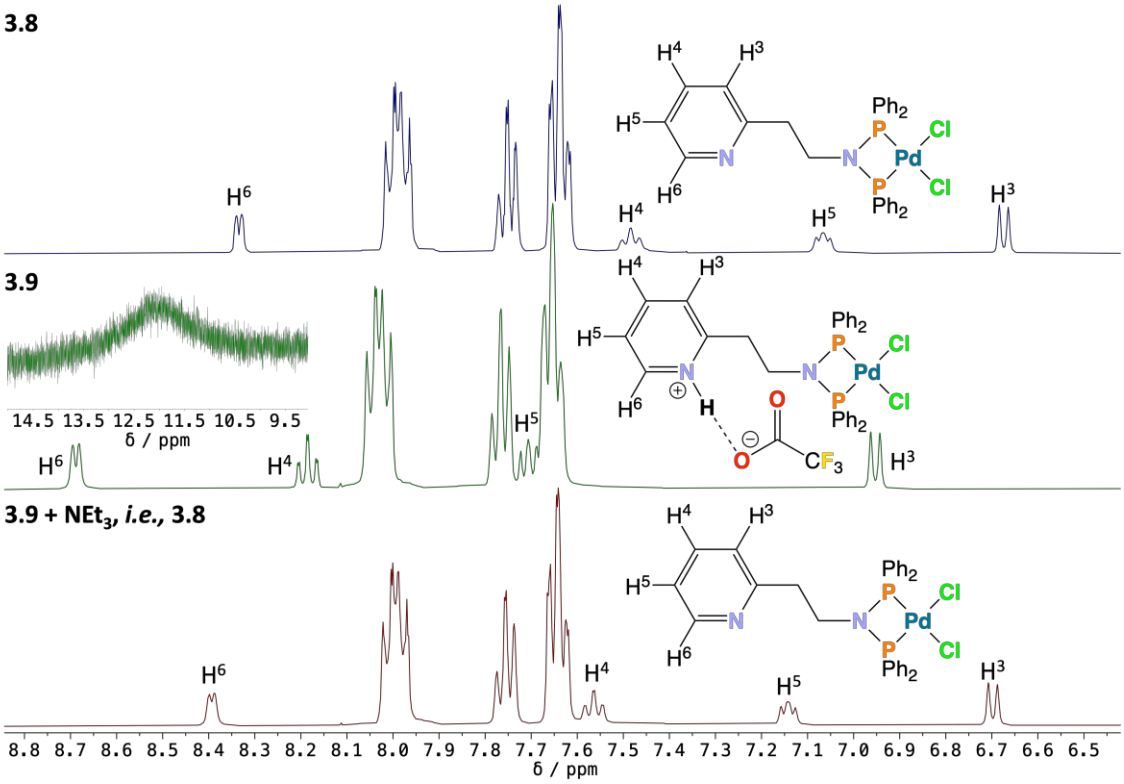


**Figure 3.5.** Partial $^1$H NMR (400 MHz, 290 K, $CD_2Cl_2$) spectra for complexes **3.8**, **3.9** and **3.9 + NEt$_3$**, *i.e.,* the deprotonation of **3.9** to reform **3.8**. $H^3$ – $H^6$ corresponding to the pyridyl protons.

The $^1$H NMR spectrum of the complex $[(Me_2N(CH_2)_3N(PPh_2)_2)PdCl_2]$ (**3.3**) shows a singlet at 1.96 ppm corresponding to both $N(C\underline{H}_3)_2$ and $C\underline{H}_2NMe_2$. The $^1$H NMR spectrum of the $PF_6^-$ complex $[(Me_2N(H)(CH_2)_3N(PPh_2)_2)PdCl_2][PF_6]$ (**3.11**), obtained following reaction of complex **3.3** with $NH_4PF_6$ (**Scheme 3.2**), shows an analogous singlet at 2.36 ppm. In contrast, the $^1$H NMR spectrum of $CF_3CO_2^-$ complex $[(Me_2N(H)(CH_2)_3N(PPh_2)_2)PdCl_2][CF_3CO_2]$ (**3.12**), isolated following reaction of complex

**3.3** with TFA (**Scheme 3.2**), presents a doublet at 2.49 ppm for $N(C\underline{H}_3)_2$ and a multiplet at 2.80 ppm for $C\underline{H}_2NMe_2$, consistent with protonation occurring at the non-coordinating tertiary amine site. The origin of the difference in the $^1$H NMR spectra of complexes **3.11** and **3.12** is most likely due to the $PF_6^-$ counter-anion of complex **3.11** being weakly coordinating relative to the $CF_3CO_2^-$ counter-anion (which can coordinate and interact with the Py-$N^+$-H proton; see **Section 3.3.1**) of complex **3.12**.

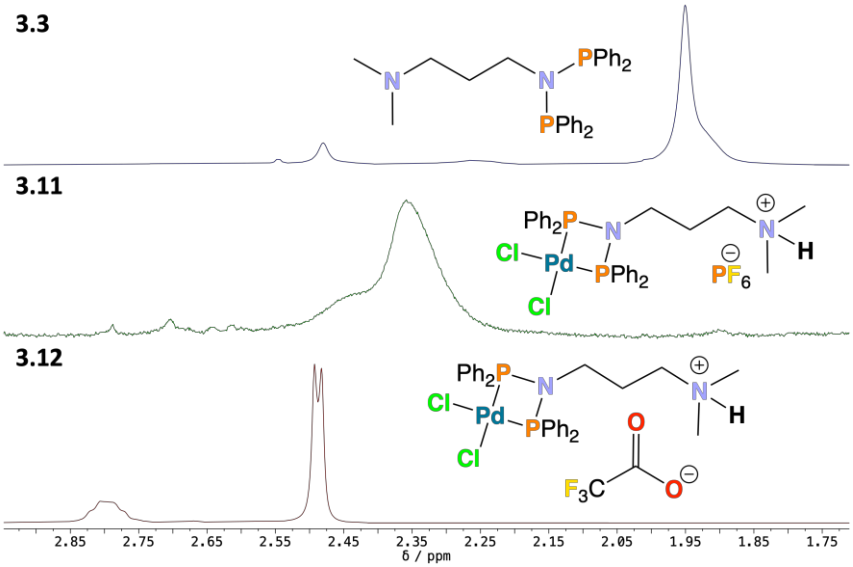


**Figure 3.6.** Partial $^1$H NMR (400 MHz, 290 K, $CD_2Cl_2$ for complexes **3.3** and **3.11**, $CDCl_3$ for complex **3.12**) spectra for complexes **3.3**, **3.11** and **3.12**.

In conclusion, the reactions in **Scheme 3.2** illustrate the Brønsted basicity and reversible protonation of the pendant non-coordinating nitrogen atoms in the complexes $[(Me_2N(CH_2)_3N(PPh_2)_2)PdCl_2]$ (**3.3**), $[(Py\text{-}o\text{-}(CH_2)_2N(CH_2PPh_2)_2)PdCl_2]$ (**3.7**), and $[(Py\text{-}o\text{-}(CH_2)_2N(PPh_2)_2)PdCl_2]$ (**3.8**). This evidences the potential behaviour of these groups as *in situ* bases. *In situ* base functionality has proven useful in alkoxycarbonylation (the reaction of an alkene/alkyne, carbon monoxide and an alcohol); deprotonating the alcohol, hence making the alcohol more nucleophilic, increases the rate of catalysis (**Scheme 3.4**).[18,19]

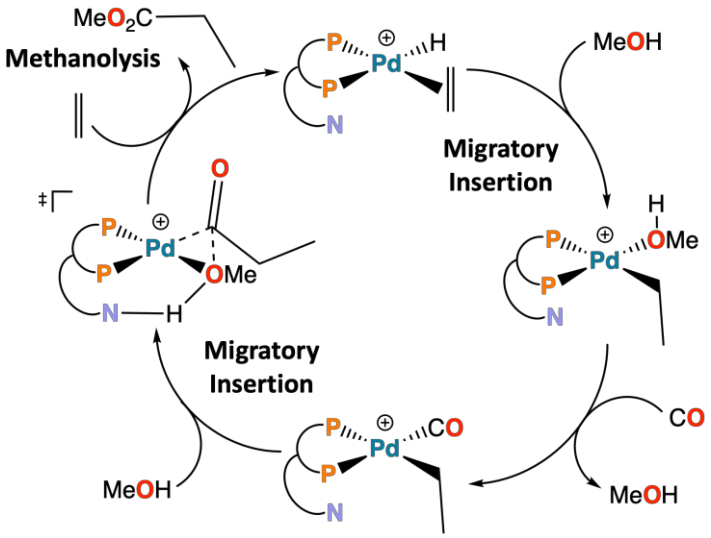


**Scheme 3.4.** Catalytic mechanism of methoxycarbonylation of ethene, showing a nitrogen donor behaving as an *in situ* base. Adapted from Dong *et al*.[18]

### 3.3.1 Solid-State Molecular Structures of [(H-Py-*o*-$(CH_2)_2N(PPh_2)_2)PdCl_2][CF_3CO_2]$ (3.9), [(H-Py-*o*-$(CH_2)_2N(CH_2PPh_2)_2)PdCl_2][CF_3CO_2]$ (3.10) and [(H-$NMe_2(CH_2)_3N(PPh_2)_2)PdCl_2][PF_6]$ (3.11)

Single crystals of complexes **3.9** – **3.11** (**Figure 3.7**) were obtained and molecular structures determined. The solid-state molecular structures (**Figure 3.7**) show the retention of the $\kappa^2$-*P,P* coordination present in the parent non-protonated complexes **3.3** ([$(Me_2N(CH_2)_3N(PPh_2)_2)PdCl_2$]), **3.7** ([(Py-*o*-$(CH_2)_2N(CH_2PPh_2)_2)PdCl_2$]) and **3.8** ([(Py-*o*-$(CH_2)_2N(PPh_2)_2)PdCl_2$]). These molecular structures also reveal that the tertiary amine nitrogen atom of complex **3.3** and the pyridyl nitrogen atoms of complexes **3.7** and **3.8** are indeed the protonated sites, agreeing with the $^1$H NMR spectroscopic analysis described in **Section 3.3**. Note that bond angles and lengths of complexes **3.9**/**3.11** and **3.10** are very similar to the metric parameters determined for complexes **3.1** and **3.7**, respectively.

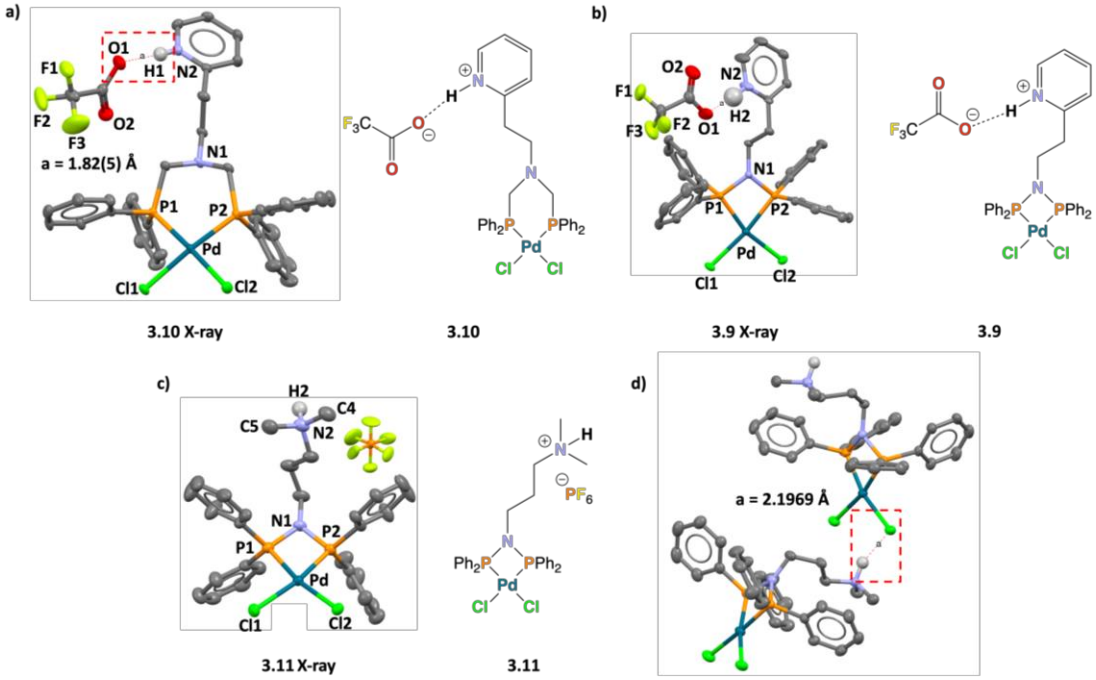


**Figure 3.7.** Solid-state molecular structures of **a) 3.10**, **b) 3.9** and **c) 3.11**. **d)** shows the intermolecular metal halogen hydrogen bond (MHHB) between the protonated tertiary amine site of one molecule of **3.11** and a chloride ligand present in a different molecule of **3.11**. Thermal ellipsoids are shown at the 50 % probability level. *NB* hydrogen atoms (except the hydrogen atoms at the protonated pyridyl and tertiary amine sites in complexes **3.9**, **3.10** and **3.11**, respectively) and DCM molecules are omitted for clarity. Atom colour: carbon – grey; nitrogen – blue; phosphorus – orange; chlorine – green; palladium – blue-green; hydrogen – white and fluorine – yellow.

The key bond lengths and bond angles measured from the solid-state structures of complexes **3.9**, **3.10** and **3.11** are presented in **Table 3.3** and **Table 3.4**, respectively.

**Table 3.3.** Key bond lengths measured from the solid-state molecular structures of complexes **3.9** – **3.11**.

| Parameter | 3.9 | 3.10 | 3.11 |
|---|---|---|---|
| N1-P1 / Å | 1.705(3) | – | 1.691(3) |
| N1-P2 / Å | 1.706(2) | – | 1.706(3) |
| P1-Pd / Å | 2.2171(9) | 2.2409(8) | 2.204(1) |
| P2-Pd / Å | 2.3687(9) | 2.234(1) | 2.215(1) |
| Pd-Cl1 / Å | 2.3540(9) | 2.360(1) | 2.359(1) |
| Pd-Cl2 / Å | 2.3687(9) | 2.3440(9) | 2.3655(9) |
| N1-C1 / Å | – | 1.454(5) | – |
| N1-C2 / Å | – | 1.458(5) | – |
| O1-H2 / Å | 1.58(7) | 1.82(5) | – |
| N2-H2 / Å | 1.02(7) | 0.83(5) | 1.000 |
| N2-C4 / Å | – | – | 1.489(5) |
| N2-C5 / Å | – | – | 1.490(5) |

**Table 3.4.** Key bond angles measured from the solid-state molecular structures of complexes **3.9** – **3.11**.

| Parameter | 3.9 | 3.10 | 3.11 |
|---|---|---|---|
| P1-N1-P2 / ° | 98.4(1) | – | 99.5(1) |
| P1-Pd-P2 / ° | 71.50(3) | 92.63(3) | 71.85(3) |
| P1-Pd-Cl1 / ° | 99.49(3) | 86.93(3) | 96.70(4) |
| P2-Pd-Cl2 / ° | 93.28(3) | 90.11(3) | 94.58(3) |
| Cl1-Pd-Cl2 / ° | 95.89(3) | 90.73(3) | 97.09(3) |
| P1-Pd-Cl2 / ° | 164.13(3) | 176.65(4) | 165.38(4) |
| P2-Pd-Cl1 / ° | 170.68(3) | 169.45(4) | 168.16(4) |
| C1-N1-C2 / ° | – | 113.4(3) | – |
| N2-H2-O1 / ° | 157(5) | 174(5) | – |

The solid-state molecular structures of complexes **3.10** and **3.9** (**a)** and **b)**, **Figure 3.7**) show that there is hydrogen bonding between one of the oxygens of the $CF_3CO_2^-$ anion, O1, and the Py-$N^+$-H proton, H2. For complexes **3.9** and **3.10**, O1-H2 is 1.58(7) Å and 1.82(5) Å (same value), respectively, and H2-N2 is 1.02(7) Å and 0.83(5) Å (same value), respectively. The measured O1-H2 and H2-N2 bond distances show excellent agreement with the analogous bond distances reported for complexes **3.19** (O1-H2 = 1.82(2) Å, H2-N2 = 0.90(2) Å)[20] and **3.20** (O1-H2 = 1.580 Å, H2-N2 = 1.040 Å)[21] in **a)**, **Figure 3.8**.

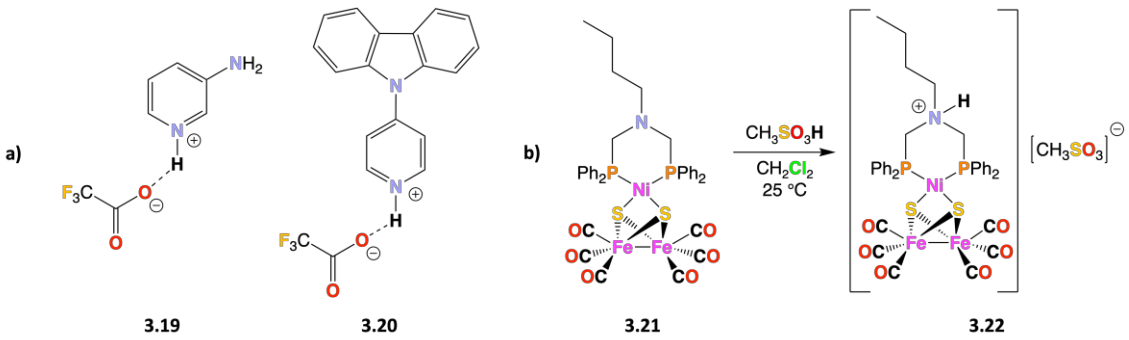


**Figure 3.8. a)** structures of compounds **3.19**[20] and **3.20**;[21] **b)** synthesis of complex **3.22**.[22]

Together, the solid-state structure of complex **3.10** and the accompanying solution-state $^1$H NMR spectroscopic analysis (**Figure 3.9**) confirm exclusive protonation at the pyridyl moiety, despite the P-C-N-C-P nitrogen atom being the more basic site in uncoordinated compound **2.8**. Protonation at the P-C-N-C-P nitrogen atom is possible (*e.g.*, triflic acid has previously been shown to protonate complex **3.21**; **b)**, **Figure 3.8**).[22] Hence, for complex **3.10**, exclusive protonation at the pyridyl site likely arises due to the P-C-N-C-P

nitrogen atom's basicity being reduced in complex **3.7** relative to compound **2.8**, resulting in the pyridyl site of complex **3.7** being the more basic site. The NMR spectral analysis summarised in **Figure 3.9** shows that the resonances of the pyridyl protons (*e.g.*, pyridyl resonances indicated by ^ and ', **Figure 3.9**) in complex **3.10** are at higher frequencies relative to the analogous resonances in complex **3.7** (indicative of protonation at the pyridyl nitrogen atom, as discussed in **Section 3.3**).

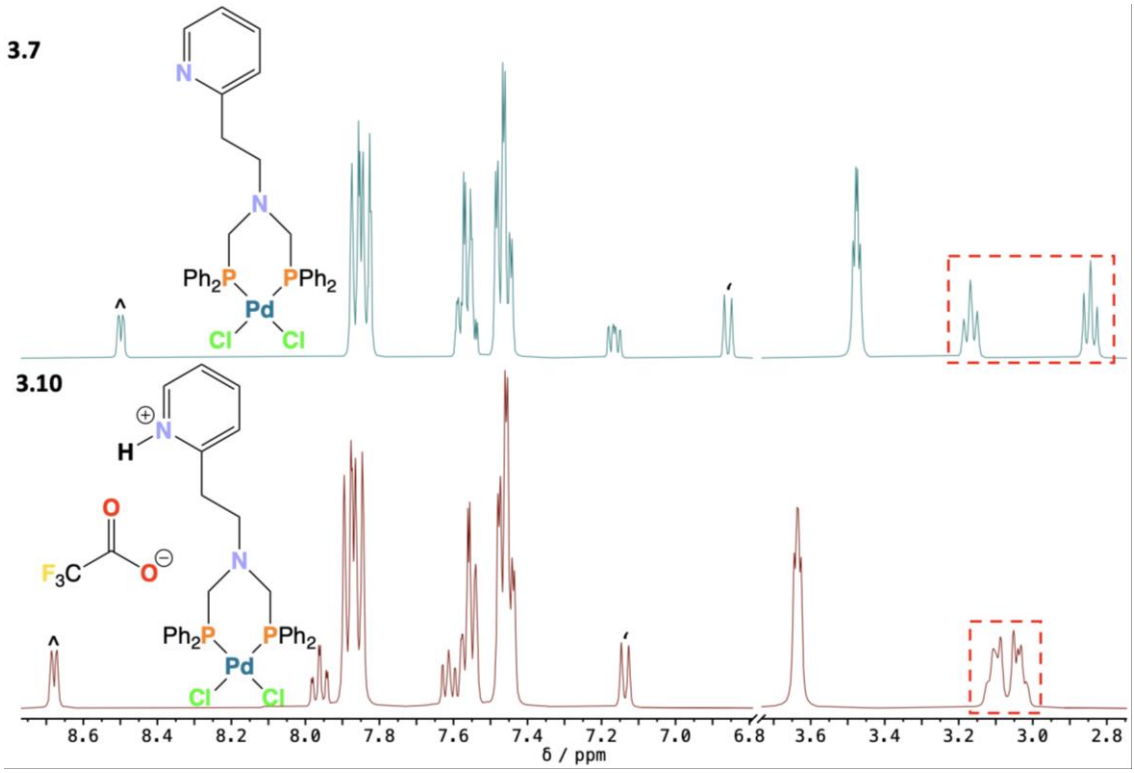


**Figure 3.9.** $^{1}$H NMR (400 MHz, 290 K, $CD_2Cl_2$) spectra for complexes **3.7** and **3.10**. The region between approx. 3.7 – 6.8 ppm has been removed for clarity. ^ and ' label two of the pyridyl proton resonances. Red dashed boxes highlight the signals corresponding to the $(CH_2)_2$ protons.

Comparison of the solid-state molecular structures of complexes **3.7** ([(Py-*o*-$(CH_2)_2$N($CH_2PPh_2)_2$)$PdCl_2$]) and **3.10** ([(HPy-*o*-$(CH_2)_2$N($CH_2PPh_2)_2$)$PdCl_2$][$CF_3CO_2$]) shows that the $(CH_2)_2$ linker (red dashed box in **Figure 3.10**) between the P-C-N-C-P moiety and the pyridyl group has rotated in complex **3.10** relative to complex **3.7**. Rotation of the $(CH_2)_2$ linker likely facilitates the formation of the O1-H2 hydrogen bond, and results in the shifting of the signals corresponding to the $CH_2$ protons in the 2.8 – 3.7 ppm region of the $^{1}$H NMR spectrum of complex **3.10** (relative to the $^{1}$H NMR spectrum of complex **3.7**) such that the signals in the red dashed boxes (**Figure 3.9**) almost have the same chemical shift.

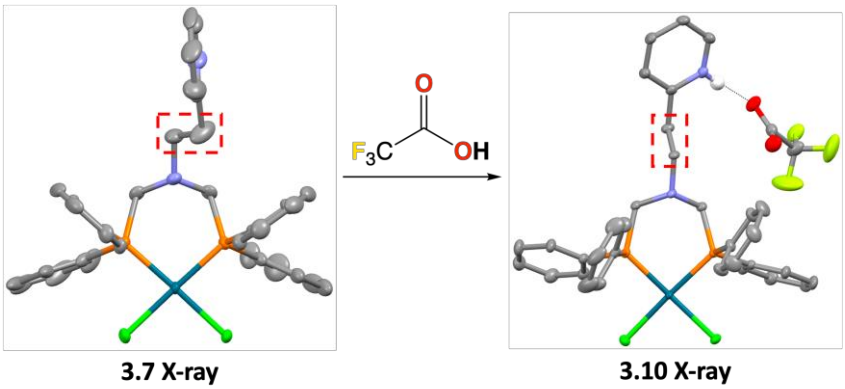


**Figure 3.10.** Solid-state structures of complexes **3.7** and **3.10**, highlighting the effect of protonation on the $(CH_2)_2$ linker (red dashed boxes). Thermal ellipsoids are shown at the 50 % probability level.

H2 of the solid-state structure of complex **3.11** ($[(Me_2N(H2)(CH_2)_3N(PPh_2)_2)PdCl_2][PF_6]$, **c), Figure 3.7**) could not be located reliably and had to be placed into a calculated position. The presence of H2 at the specified location is in agreement with the measured distance of the intramolecular metal–halogen hydrogen bond (MHHB) of 2.1969 Å (**d)**, **Figure 3.7**). This is consistent with the intramolecular metal–halogen hydrogen bond distances of 2.17(6) Å and 2.18(3) Å determined for complexes **3.17** ($[Zn(Hdidpa)Cl_2][PF_6]$) and **3.18** ($[Fe(Hdidpa)Cl_2][PF_6]$), respectively (**Scheme 3.5**).[15] Additionally, the N2-C4/C5 bond lengths in complex **3.11** (with an average of 1.490(2) Å) increase very slightly relative to the analogous bond lengths (with an average of 1.456(2) Å) in complex **3.3**, $[(Me_2N(CH_2)_3N(PPh_2)_2)PdCl_2]$. Comparison of the solid-state structures of complexes **3.15** ($[Zn(didpa)Cl_2]$) and **3.17** ($[Zn(Hdidpa)Cl_2][PF_6]$) also evidences an increase in N-C bond distance (respective average N-C bond distances for complexes **3.15** and **3.17** are 1.485(7) Å and 1.531(7) Å),[15] supporting that H2 is in the specified location in the solid-state structure of complex **3.11** (**c), Figure 3.7**).

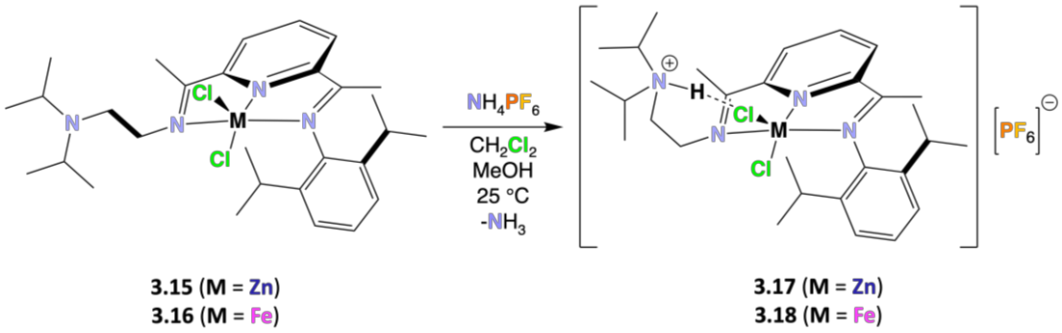


**Scheme 3.5.** Synthesis of complexes **3.17** and **3.18**.[15]

## 3.4 Reaction of $[(Ph(CH_2)_2N(PPh_2)_2)PdCl_2]$ (3.1) with MeOH

Complexes of the type $[(RN(PPh_2)_2)PdCl_2]$ are known to react with alcohols, *via* alcoholysis of a P-N bond, as shown in **Scheme 3.6**.[5] This reaction has been shown to only occur for linear alcohols, and generally leads to only one P-N bond being cleaved.[5] In order to further probe the alcoholysis reaction, complex **3.1** (R = $(CH_2)_2Ph$ in **Scheme 3.6**) was reacted with MeOH (R' = Me in **Scheme 3.6**) to afford complex **3.23**.

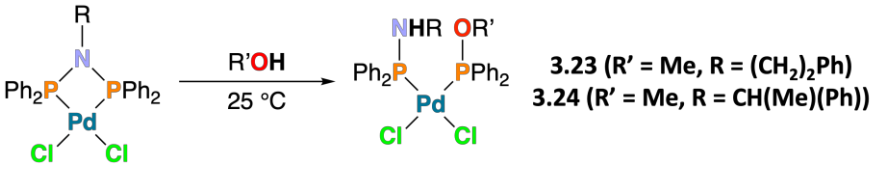


**Scheme 3.6.** Alcoholysis of $[(RN(PPh_2)_2)PdCl_2]$ to afford complex **3.23** (when R' = Me, R = $(CH_2)_2Ph$), and the structure of complex **3.24**.[5]

The $^{31}P\{^1H\}$ NMR spectrum of synthesised complex **3.23** (**Figure 3.11**) shows two doublet resonances ($^2J_{PP}$ = 30 Hz) at 108.8 ppm (*cis*-$[(PhCH_2CH_2NHPPh_2)(MeOPPh_2)PdCl_2]$) and 58.1 ppm (*cis*-$[(PhCH_2CH_2NHPPh_2)(MeOPPh_2)PdCl_2]$), which is in contrast to the singlet resonance observed at $\delta_P$ = 30.4 ppm for complex **3.1** ($[(Ph(CH_2)_2N(PPh_2)_2)PdCl_2]$). The NMR spectroscopic data for complex **3.23** are very similar to those for the previously reported complex **3.24** (**Scheme 3.6**), the corresponding data being: $^{31}P\{^1H\}$ (162 MHz, $CDCl_3$) 56.44 (d, N-P-Pd, $^2J_{PP}$ = 27 Hz), 109.19 (d, O-P-Pd, $^2J_{PP}$ = 27 Hz).[5]

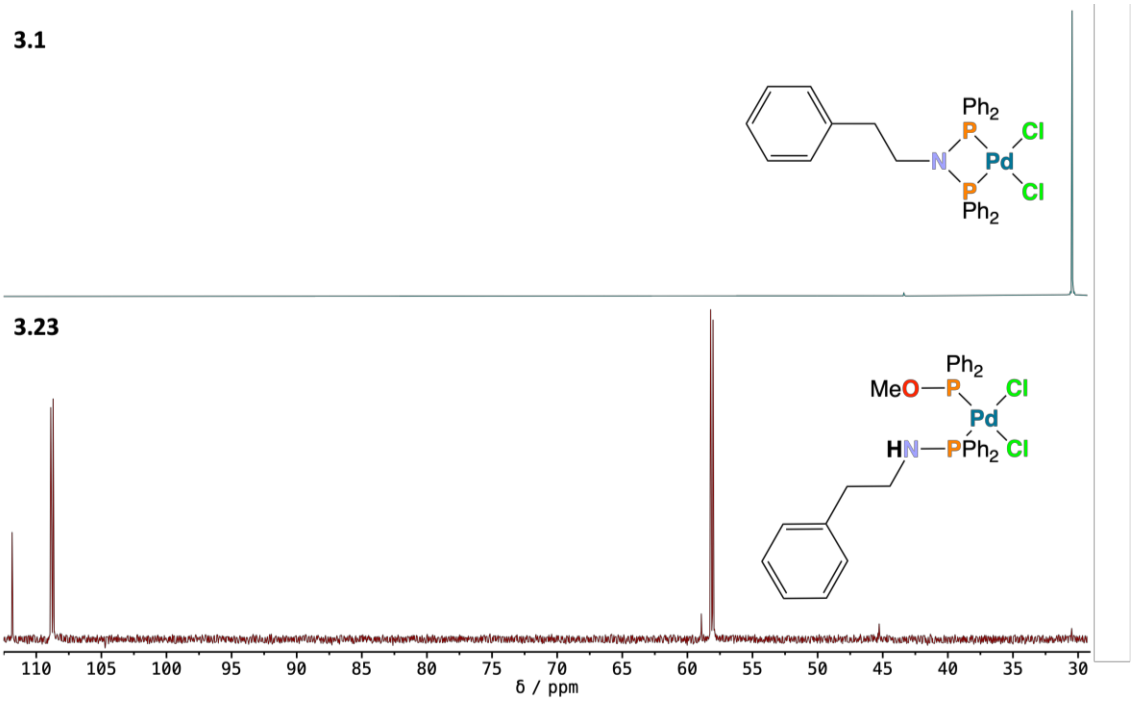


**Figure 3.11.** $^{31}P\{^1H\}$ NMR (162 MHz, 290 K, $CD_2Cl_2$) spectra for complexes **3.1** and **3.23**. *NB* the signal at 111.9 ppm corresponds to known complex $[(MeOPPh_2)_2PdCl_2]$.[23]

The difference in reactivity of complex **3.1** (reacts with MeOH) and parent ligand compound **2.2** ($Ph(CH_2)_2N(PPh_2)_2$; no reaction with MeOH) suggests that at least in part, the driving force for methanolysis of **3.1** is relief of strain in the four-membered Pd-P-N-P chelate ring. Additionally, only one of the two P-N bonds is cleaved, despite MeOH being present in excess (reaction solvent). This has been attributed to the remaining P-N bond in complex **3.23** being stronger than the P-N bonds in complex **3.1**, since the P-N-P nitrogen lone pair is no longer delocalised over two P-N bonds (discussed in **Section 3.2**), but instead is involved in bonding with one of the phosphorus atoms (N lp → PRσ*).[5,24] Ultimately, the reactivity of complex **3.1** with MeOH suggests that complexes of the form of $[(RN(PPh_2)_2)PdCl_2]$ will not be suitable for alkoxycarbonylation.

## 3.5 Reaction of $[(Py\text{-}o\text{-}(CH_2)_2N(PPh_2)_2)PdCl_2]$ (3.8) with $CoCl_2$ and $[N(n\text{-}Pr)_4]Cl$

Since pyridyl groups can behave as Lewis bases, complex **3.8** was reacted with one equivalent of $CoCl_2$ and $[N(n\text{-}Pr)_4]Cl$ affording heterobimetallic complex **3.25**, as shown in **a)**, **Scheme 3.7**. To the best of the author's knowledge, this is the first synthesis of a complex containing both $[(\kappa^2\text{-}P,P)PdCl_2]$ and Py-$CoCl_3^-$ moieties.

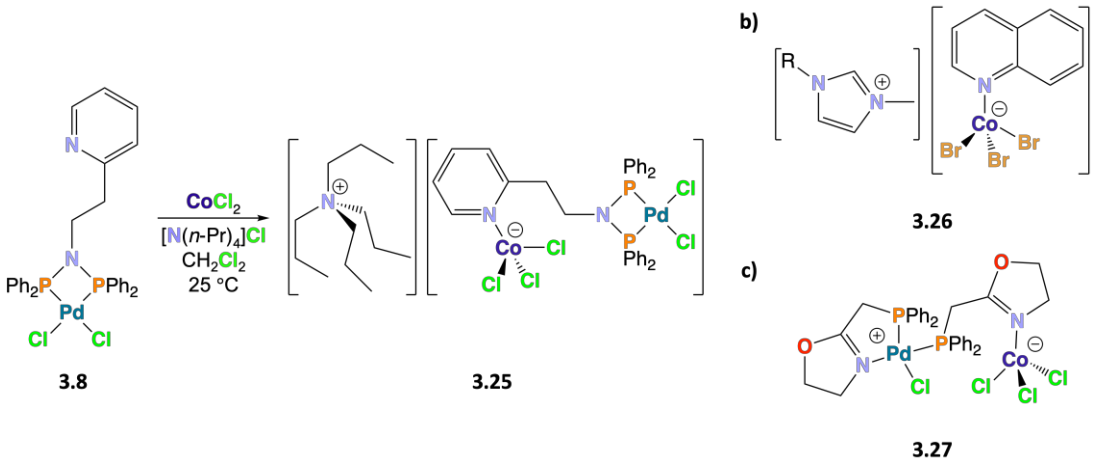


**Scheme 3.7. a)** Synthesis of complex **3.25**; **b)** structure of complex **3.26**, where R = ethyl, *n*-butyl, *n*-hexyl, *n*-heptyl, *n*-octyl, *n*-nonyl, allyl, propargyl;[25] **c)** structure of complex **3.27**.[26]

The structures of previously reported complexes **3.26**[25] and **3.27**[26], with similarities to complex **3.25**, are shown in **b)** and **c)** of **Scheme 3.7**, respectively. Complex **3.26** possesses a quinoline motif (*cf.* pyridyl group of complex **3.25**) bound to the $CoBr_3$ fragment, alongside a 1-alkyl-3-methylimidazolium cation (*cf.* tetrapropylammonium cation of complex **3.25**). Complex **3.27** is zwitterionic containing an anionic $CoCl_3$

fragment coordinated by a pyridine ligand (analogous to complex **3.25**). However, the palladium(II) centre has a formal positive charge, unlike the neutral palladium(II) centre in complex **3.25** (the tetrapropylammonum cation is the source of positive charge in complex **3.25**). It is noteworthy that during the synthesis of heterobimetallic complex **3.25**, there is no ligand exchange between the palladium(II) and the cobalt(II) centres.

### 3.5.1 Solid-State Molecular Structure of [N(*n*-Pr)$_4$][({Cl$_3$Co}Py-*o*-(CH$_2$)$_2$N(PPh$_2$)$_2$)PdCl$_2$] (3.25)

Single crystals of complex **3.25** were obtained and a molecular structure determined (**Figure 3.12**), evidencing the Py-CoCl$_3$ moiety and hence the Lewis basicity of the pyridyl group of complex **3.8** ([(Py-*o*-(CH$_2$)$_2$N(PPh$_2$)$_2$)PdCl$_2$]). The core bond angles and bond lengths related to the P-N-P-Pd four-membered chelate ring for complex **3.25** are essentially identical to those for complex **3.1** ([(Ph(CH$_2$)$_2$N(PPh$_2$)$_2$)PdCl$_2$]). The anionic Py-CoCl$_3$ moiety has a slightly distorted tetrahedral geometry (with N-Co-Cl and Cl-Co-Cl bond angles deviating slightly from the ideal 109.5° tetrahedral angle), N1-Co1 bond distance of 2.077(3) Å (*cf*. N$_{Py}$-Co = 2.084(3) Å measured for complex **3.28**),[27] and Co-Cl distances of 2.239(2) Å, 2.238(2) Å and 2.265(1) Å (*cf*. Co-Cl distances varying from 2.2421(13) – 2.2653(13) Å measured for complex **3.28**).[27] The slightly distorted tetrahedral geometry is evidenced by a calculated (using **Equation 3.1**) $\tau_4$ value of 0.94057 which is very close to 1, *i.e*., the $\tau_4$ value for a perfect tetrahedron.[10]

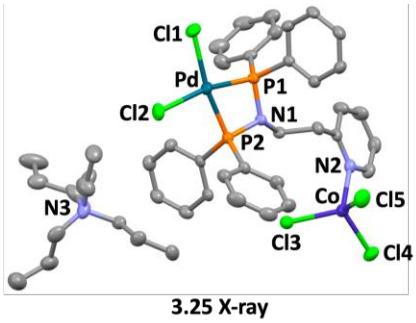


3.25 X-ray

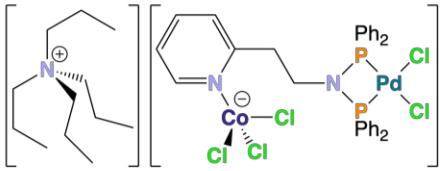


3.25

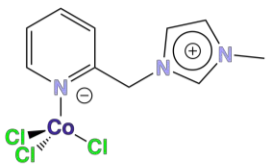


3.28

**Figure 3.12.** Solid-state molecular structure determined from XRD analysis of single crystals of **3.25**. Thermal ellipsoids are shown at the 50 % probability level. *NB* hydrogen atoms are omitted for clarity. Atom colour: carbon – grey; nitrogen – light blue; phosphorus – orange; palladium – blue-green; cobalt – dark blue, and chlorine – green. Structure of previously reported complex **3.28** is also shown.[27]

The key bond lengths and bond angles measured from the solid-state structure of complex **3.25** are presented in **Table 3.5** and **Table 3.6**, respectively.

**Table 3.5.** Key bond lengths measured from the solid-state molecular structure of complex **3.25**.

| Bond | Bond Length / Å |
|---|---|
| N1-P1 | 1.698(3) |
| N1-P2 | 1.703(4) |
| P1-Pd | 2.208(1) |
| P2-Pd | 2.214(1) |
| Pd-Cl1 | 2.372(2) |
| Pd-Cl2 | 2.360(1) |
| N2-Co1 | 2.077(3) |
| Co-Cl3 | 2.239(2) |
| Co-Cl4 | 2.238(2) |
| Co-Cl5 | 2.265(1) |

**Table 3.6.** Key bond angles measured from the solid-state molecular structure of complex **3.25**.

| Angle | Bond Angle / ° |
|---|---|
| P1-N1-P2 | 98.7(2) |
| P1-Pd-P2 | 71.39(5) |
| P1-Pd-Cl1 | 96.24(5) |
| P2-Pd-Cl2 | 95.96(5) |
| Cl1-Pd-Cl2 | 96.36(5) |
| P1-Pd-Cl2 | 167.31(5) |
| P2-Pd-Cl1 | 167.44(5) |
| N2-Co-Cl3 | 106.5(1) |
| N2-Co-Cl4 | 107.0(1) |
| N2-Co-Cl5 | 108.4(1) |
| Cl3-Co-Cl4 | 114.14(6) |
| Cl3-Co-Cl5 | 112.86(6) |
| Cl4-Co-Cl5 | 107.65(6) |

## 3.6 Coordination Chemistry of Py-*o*-$(CH_2)_2N(PPh_2)(Me)$ (2.11) and Py-*o*-$(CH_2)_2N(P\{OPh\}_2)(Me)$ (2.12) with Palladium(II) Dichloride

Compounds **2.11** and **2.12** were reacted with $[(MeCN)_2PdCl_2]$ to afford complexes **3.29** and **3.30**, respectively (**Scheme 3.8**). Complexes **3.29** and **3.30**, due to the presence of only one $PR_2$ moiety, are forced to exhibit $\kappa^2$-*P,N* coordination through coordination of the pyridyl moiety.

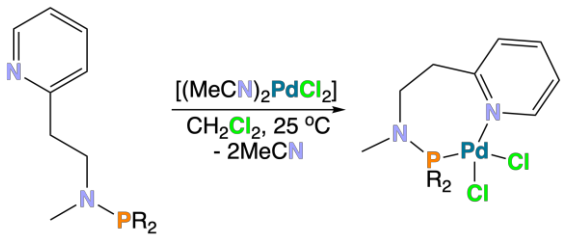


**2.11** (R = Ph)
**2.12** (R = OPh)

**3.29** (R = Ph)
**3.30** (R = OPh)

**Scheme 3.8.** Synthesis of complexes **3.29** and **3.30**.

The $^{31}P\{^{1}H\}$ NMR spectra of complexes **3.29** and **3.30** show singlet resonances at 59.7 ppm and 83.8 ppm, respectively. In the case of complex **3.29**, the chemical shift differs only slightly from that determined for the parent ligand compound **2.11** (64.4 ppm), whereas complex **3.30** shows a significant shift to lower frequency for the chemical shift relative to that determined for compound **2.12** (140.1 ppm). The origins of the small $\Delta\delta_P$ (where $\Delta\delta_P = \delta_{P\text{-uncoordinated}} - \delta_{P\text{-coordinated}}$) of 4.7 ppm between **2.11** and **3.29**, but approximately ten times larger $\Delta\delta_P$ of 56.3 ppm between **2.12** and **3.30**, is unclear, but may relate to the fact that $^{31}P\{^{1}H\}$ chemical shift is very sensitive to bond angles around the phosphorus atom[28] and hence phosphorus atom substituents (OPh in **3.30** and Ph in **3.29**). While the phosphorus centre of complex **3.30** bearing phenoxy groups is likely to be at least partially $\pi$-accepting in nature, it is unlikely that there is significant Pd → P $\pi$-backbonding for geometric reasons.

Evidence of pyridyl group coordination is clear from comparison of the $^{1}H$ NMR spectra of the uncoordinated ligands **2.11** and **2.12** and their corresponding metal complexes **3.29** and **3.30**, specifically considering the chemical shift of the *ortho*-pyridyl proton. For Py-*o*-N($PPh_2$)(Me) and the corresponding palladium(II) complex [{Py-*o*-N($PPh_2$)(Me)}$PdCl_2$], the *ortho*-pyridyl protons have $^{1}H$ chemical shifts of 8.29 ppm and 9.65 ppm, respectively, illustrating a shift to a higher frequency in $\delta_H$ of 1.36 ppm upon ligand coordination.[29] The *ortho*-pyridyl protons of compound **2.11** and complex **3.29** have $\delta_H$ = 8.56 ppm and $\delta_H$ = 8.80 ppm, respectively, evidencing a $\Delta\delta_H$ = 0.24 ppm (where $\Delta\delta_H = \delta_{H\text{-complex}} - \delta_{H\text{-free ligand}}$). The *ortho*-pyridyl protons of compound **2.12** and complex **3.30** have $\delta_H$ = 8.57 ppm and $\delta_H$ = 9.11 ppm, respectively, exhibiting a $\Delta\delta_H$ = 0.54 ppm (**Figure 3.13**). The change in $\delta_H$ ($\Delta\delta_H$) of the *ortho*-pyridyl proton in conjunction with the aforementioned change in $\delta_P$ ($\Delta\delta_P$) upon complexation indicates that compounds **2.11** and **2.12** coordinate to the palladium(II) centre in a $\kappa^2$-*P,N* fashion.

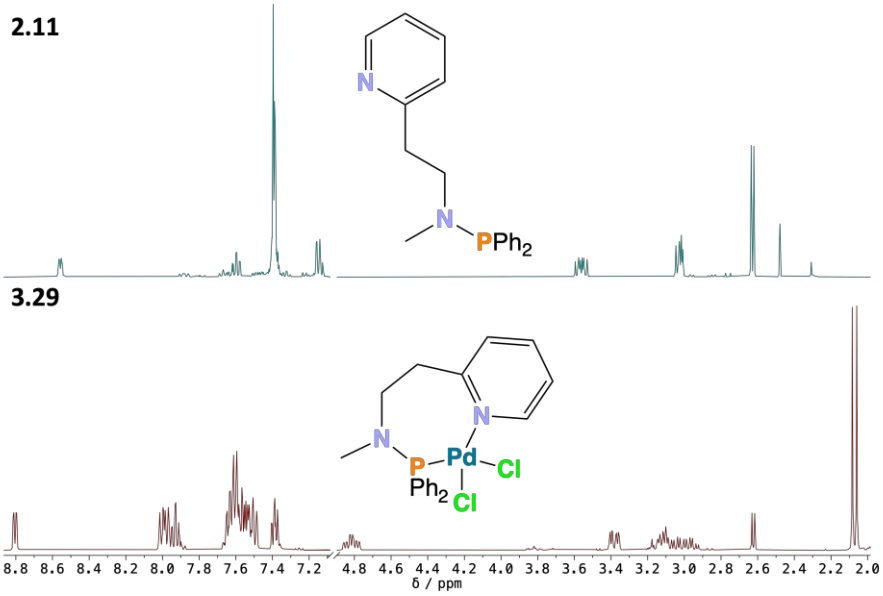


**Figure 3.13.** $^{1}$H NMR (400 MHz, 290 K, $CDCl_3$) spectra for compound **2.11** and complex **3.29**, with the 4.9 – 7.1 ppm region removed for clarity.

The $^{1}$H NMR spectrum of compound **2.11** presents two signals corresponding to the four protons of the two $CH_2$ groups in the 2.8 – 3.7 ppm range. The $^{1}$H NMR spectrum of complex **3.29**, however, shows four signals corresponding to the same four protons in the 2.8 – 4.8 ppm region (**Figure 3.13**). This is attributed to coordination of the pyridyl group resulting in conformational locking of the $CH_2$ chain, causing the individual hydrogen atoms of the $CH_2$ groups to be in different chemical environments and have different chemical shifts in complex **3.29** relative to compound **2.11**.

### 3.6.1 Solid-State Molecular Structure of [(Py-*o*-$(CH_2)_2$N($PPh_2$)(Me))$PdCl_2$] (3.29) and [(Py-*o*-$(CH_2)_2$N(P{OPh}$_2$)(Me))$PdCl_2$] (3.30)

Single crystals of complexes **3.29** and **3.30** have been obtained and molecular structures determined (**Figure 3.14**), evidencing the $\kappa^2$-*P,N* coordination mode inferred from $^{1}$H and $^{31}$P{$^{1}$H} NMR spectroscopies (**Section 3.6**). The 7-membered chelate rings of complexes **3.29** and **3.30** are less strained than the 4-membered chelate rings of complexes **3.1** – **3.6**; this is reflected in the N1-Pd1-P1 bite angles of complexes **3.29** and **3.30** being 91.97(6)° and 91.11(3)°, respectively (*cf.* approx. 71° for complexes **3.1** – **3.6**). The other bond angles around the palladium(II) centres of complexes **3.29** and **3.30** (Cl1-Pd1-Cl2, N1-Pd1-Cl1 and P1-Pd1-Cl2) are also very close to the ideal 90° bond angle (**Table 3.7**), suggesting that the square planar geometry around the palladium(II) centres is not

significantly distorted (quantified by the calculated values for complexes **3.29** and **3.30**, **Table 3.7**, being very close to 0).[10]

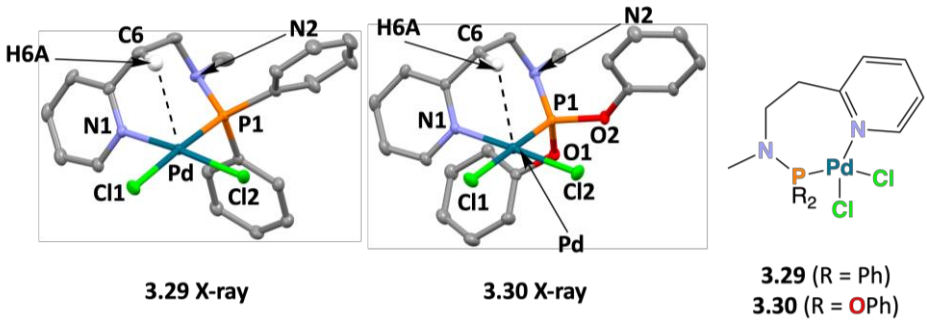


**Figure 3.14.** Solid-state molecular structure determined from XRD analysis of single crystals of complexes **3.29** and **3.30**. Thermal ellipsoids are shown at the 50 % probability level. *NB* hydrogen atoms (except H6A) and a DCM molecule (for complex **3.29**) is omitted for clarity. Atom colour: carbon – grey; nitrogen – blue; phosphorus – orange; palladium – blue-green; oxygen – red, chlorine – green. Black dashed line indicates interaction between H6A and Pd.

The key bond lengths and bond angles measured from the solid-state structures of complexes **3.29** and **3.30** are presented in **Table 3.7**.

**Table 3.7.** Key bond lengths and angles measured from the solid-state molecular structures of complexes **3.29** and **3.30**, and calculated $\tau_4$ values for complexes **3.29** and **3.30**.

| Parameter | 3.29 | 3.30 |
|---|---|---|
| N1-Pd | 2.041(2) | 2.041(1) |
| P1-Pd | 2.2260(8) | 2.2125(4) |
| Pd-Cl1 | 2.3546(7) | 2.3379(4) |
| Pd-Cl2 | 2.2859(8) | 2.2923(4) |
| N2-P1 | 1.682(2) | 1.637(1) |
| Pd-H6A | 2.6366 | 2.5683 |
| P1-O1 | – | 1.608(1) |
| P1-O2 | – | 1.609(1) |
| N1-Pd-P1 | 91.97(6) | 91.11(3) |
| N1-Pd-Cl1 | 89.86(6) | 87.54(3) |
| P1-Pd-Cl2 | 85.83(3) | 89.82(2) |
| Cl1-Pd-Cl2 | 92.08(3) | 91.47(2) |
| N1-Pd-Cl2 | 171.96(6) | 178.44(3) |
| P1-Pd-Cl1 | 177.23(3) | 177.24(2) |
| C6-H6A-Pd | 114.7 | 115.98 |
| $\tau_4$ | 0.0074 | 0.0028 |

The P1-Pd bond lengths of 2.2260(8) Å and 2.2125(4) Å for complexes **3.29** and **3.30**, respectively, are very similar to those of complexes **3.1** ([(Ph$(CH_2)_2$N$(PPh_2)_2$)Pd$Cl_2$]) and **3.7** ([(Py-*o*-$(CH_2)_2$N$(CH_2PPh_2)_2$)Pd$Cl_2$]). The N1-Pd bond lengths are identical (**3.29**: 2.041(2) Å; **3.30**: 2.041(1) Å). The N2-P1 bond length is shorter in complex **3.30** (1.637(1) Å) than in complex **3.29** (1.682(2) Å) due to P1 having OPh substituents in complex **3.30**. The P$(OPh)_2$ moiety of complex **3.30** is more electron-withdrawing than the $PPh_2$ moiety of complex **3.29**, hence there is greater P-N multiple bond character in complex **3.30** resulting in a shorter P1-N2 distance.

Notably, there is a Pd-H6A interaction (H6A-Pd distances: 2.6366 Å (**3.29**); 2.5683 Å (**3.30**). C6-H6A-Pd angles: 114.7° (**3.29**); 115.98° (**3.30**)), which is retained in solution as evidenced by $\delta_H$ H6A ~4.7 – 4.8 ppm for complexes **3.29** and **3.30** (*cf*. 2.99 – 3.06 for Py-C$\underline{H}_2$ in compound **2.11** in **Figure 3.13**, hence $\Delta\delta_H$ ~1.73 ppm). The aforementioned Pd-H distances and C-H-Pd angles are within the general ranges of 2.3 – 2.9 Å and 110 – 170°, respectively, accepted to describe anagostic Pd···H-C interactions.[30,31] Anagostic interactions are poorly understood compared to their agostic counterparts (with a M---H distance of ~1.8 – 2.3 Å), but have been established to control polymer microstructure during catalytic polymerisation processes.[32] Agostic interactions are an interaction between the two electrons in a C-H bond and an empty d-orbital on a transition metal, forming a three-centre two-electron bond. Anagostic interactions are more electrostatic in character relative to their agostic counterparts.[32] Indeed, a similar H-Pd distance (2.8875 Å), C-H-Pd angle (116.3°) and $\Delta\delta_H$ (~1.08 ppm; this may be smaller than the $\Delta\delta_H$ for complexes **3.29** and **3.30** as an *ortho*-aryl proton is involved in the anagostic interaction in complex **3.31**, *cf*. an alkyl proton in complexes **3.29** and **3.30**) value have been reported for complex **3.31** (**Figure 3.15**).[33]

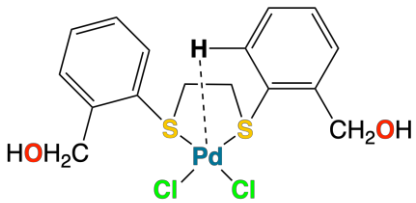


**3.31**

**Figure 3.15.** Structure of complex **3.31**, highlighting the anagostic Pd---H-C interaction.[33]

## 3.7 Summary

The various 'PNP' and 'PCNCP' compounds $Ph(CH_2)_2N(PPh_2)_2$ (**2.2**), *n*-$BuN(PPh_2)_2$ (**2.3**), $Me_2N(CH_2)_3N(PPh_2)_2$ (**2.4**), Py-*m*-$CH_2N(PPh_2)_2$ (**2.5**), Ph-$C_6H_4N(PPh_2)_2$ (**2.6**), Py-*o*-$C_6H_4N(PPh_2)_2$ (**2.7**), Py-*o*-$(CH_2)_2N(CH_2PPh_2)_2$ (**2.8**), Py-*o*-$(CH_2)_2N(PPh_2)(Me)$ (**2.11**) and Py-*o*-$(CH_2)_2N(P\{OPh\}_2)(Me)$ (**2.12**) were reacted with $[(MeCN)_2PdCl_2]$ in order to afford complexes $[(Ph(CH_2)_2N(PPh_2)_2)PdCl_2]$ (**3.1**), $[(n\text{-}BuN(PPh_2)_2)PdCl_2]$ (**3.2**), $[(Me_2N(CH_2)_3N(PPh_2)_2)PdCl_2]$ (**3.3**), $[(Py\text{-}m\text{-}CH_2N(PPh_2)_2)PdCl_2]$ (**3.4**), $[(Ph\text{-}C_6H_4N(PPh_2)_2)PdCl_2]$ (**3.5**), $[(Py\text{-}o\text{-}C_6H_4N(PPh_2)_2)PdCl_2]$ (**3.6**), $[(Py\text{-}o\text{-}(CH_2)_2N(CH_2PPh_2)_2)PdCl_2]$ (**3.7**), $[(Py\text{-}o\text{-}(CH_2)_2N(PPh_2)(Me))PdCl_2]$ (**3.29**) and $[(Py\text{-}o\text{-}(CH_2)_2N(P\{OPh\}_2)(Me))PdCl_2]$ (**3.30**), respectively. Complexes **3.1** – **3.7** exhibit $\kappa^2$-*P,P* coordination, evidenced through $^{31}P\{^1H\}$ NMR and solid-state molecular structure studies (**Section 3.2** – **3.2.1**). The reactivity of complexes **3.3**, **3.7** and **3.8** (previously prepared)[12] with pendant nitrogen donors has been studied. Complexes $[(Py\text{-}o\text{-}(CH_2)_2N(PPh_2)_2)PdCl_2]$ (**3.8**), **3.3** and **3.7** were protonated using TFA (and $NH_4PF_6$ for complex **3.3**, affording $[(Me_2N(H)(CH_2)_3N(PPh_2)_2)PdCl_2][PF_6]$, *i.e.*, complex **3.11**), affording $[(HPy\text{-}o\text{-}(CH_2)_2N(PPh_2)_2)PdCl_2][CF_3CO_2]$, $[(Me_2N(H)(CH_2)_3N(PPh_2)_2)PdCl_2][CF_3CO_2]$, and $[(HPy\text{-}o\text{-}(CH_2)_2N(CH_2PPh_2)_2)PdCl_2][CF_3CO_2]$ (complexes **3.9**, **3.12** and **3.10**, respectively), verified by $^1H$ NMR spectroscopic analysis and solid-state structures for complexes **3.11**, **3.9** and **3.10** (**Section 3.3** – **3.3.1**), evidencing the Brønsted basicity of the pendant nitrogen atoms. The Lewis basicity of the pyridyl moiety of complex **3.8** was evidenced by the reaction of complex **3.8** with $CoCl_2$ and $[N(n\text{-}Pr)_4]Cl$ affording heterobimetallic complex $[N(n\text{-}Pr)_4][(\{Cl_3Co\}Py\text{-}o\text{-}(CH_2)_2N(PPh_2)_2)PdCl_2]$ (**3.25**), with the pyridyl moiety of complex **3.8** coordinating to $CoCl_3^-$ (**Section 3.5** – **3.5.1**). The reactivity of complex **3.1** (as a representative $[\{RN(PPh_2)_2\}PdCl_2]$ complex) with MeOH to afford $[(PhCH_2CH_2NHPPh_2)(MeOPPh_2)PdCl_2]$ (complex **3.23**), *via* the established P-N alcoholysis reaction, has been verified by $^{31}P\{^1H\}$ NMR analysis (**Section 3.4**). Complexes **3.29** and **3.30** exhibited $\kappa^2$-*P,N* coordination and an anagostic C6-H6A···Pd interaction, both evidenced by $^1H$ NMR and solid-state molecular structure studies (**Section 3.6** – **3.6.1**).

## References


1. C. Fliedel, V. Rosa, B. Vileno, N. Parizel, S. Choua, C. Gourlaouen, P. Rosa, P. Turek, P. Braunstein, *Inorg. Chem.*, **2016**, *55*, 4183 – 4198. 10.1021/acs.inorgchem.5b02889
2. M. R. Crawley, A. E. Friedman, T. R. Cook, *Inorg. Chem*., **2018**, *57*, 5692 – 5700. 10.1021/acs.inorgchem.8b00787
3. N. Biricik, F. Durap, C. Kayan, B. Gümgüm, N. Gürbüz, I. Özdemir, W. H. Ang, Z. Fei, R. Scopelliti, *J. Organomet. Chem.*, **2008**, *693*, 2693 – 2699. 10.1016/j.jorganchem.2008.05.010
4. B. Cao, M. R. J. Elsegood, N. Lastra-Calvo, M. B. Smith, *J. Organomet. Chem*., **2017**, *853*, 159 – 167. 10.1016/j.jorganchem.2017.10.029
5. A. Badia, L. R. Falvello, R. Navarro, E. P. Urriolabeitia, *J. Organomet. Chem*., **1997**, *547*, 121 – 128. 10.1016/S0022-328X(97)00206-4
6. I. K. Stamatopoulos, M. Kapsi, M. Roulia, G. C. Vougioukalakis, C. P. Raptopoulou, V. Psycharis, I. D. Kostas, L. Kollár, P. Kyritsis, *Polyhedron*, **2018**, *151*, 292 – 298. 10.1016/j.poly.2018.05.041
7. U. Anandhi, T. Holbert, D. Lueng, P. R. Sharp, *Inorg. Chem*., **2003**, *42*, 1282 – 1295. 10.1021/ic025987f
8. X. Morise, P. Braunstein, R. Welter, *Inorg. Chem*., **2003**, *42*, 7752 – 7765. 10.1021/ic030032y
9. A. M. Z. Slawin, J. D. Woollins, Q. Zhang, *J. Chem. Soc., Dalton Trans*., **2001**, 621 – 632. 10.1039/B009074N
10. L. Yang, D. R. Powell, R. P. Houser, *Dalton Trans*., **2007**, 955 – 964. 10.1039/B617136B
11. Z. Fei, E. Păunescu, W. H. Ang, R. Scopelliti, P. J. Dyson, *Eur. J. Inorg. Chem.,* **2014**, 1745 – 1750. 10.1002/ejic.201301143
12. A. Carrick, MChem Thesis, Durham University, **2020**.
13. J. March, *Advanced Organic Chemistry: Reactions, Mechanisms, and Structure*, Wiley, New York, **1985**. ISBN: 9780070402478
14. A. Scrivanti, M. Bertoldini, V. Beghetto, U. Matteoli, A. Venzo, *J. Organomet. Chem*., **2009**, *694*, 131 – 136. 10.1016/j.jorganchem.2008.09.063
15. M. Delgado, S. K. Sommer, S. P. Swanson, R. F. Berger, T. Seda, L. N. Zakharov, J. D. Gilbertson, *Inorg. Chem*., **2015**, *54*, 7239 – 7248. 10.1021/acs.inorgchem.5b00633
16. R. J. Pugmire, D. M. Grant, *J. Am. Chem. Soc*., **1968**, *90*, 697 – 706. 10.1021/ja01005a025
17. B. Prusti, M. Chakravarty, *ACS Omega*, **2019**, 4*,* 16963 – 16971. 10.1021/acsomega.9b02277
18. K. Dong, R. Sang, Z. Wei, J. Liu, R. Dühren, A. Spannenberg, H. Jiao, H. Neumann, R. Jackstell, R. Franke, M. Beller, *Chem. Sci.*, **2018,** *9*, 2510 – 2516. 10.1039/C7SC02964K
19. R. I. Pugh, E. Drent, *Adv. Synth. Catal.,* **2002**, *344*, 837 – 840. 10.1002/1615-4169(200209)344:8<837::AID-ADSC837>3.0.CO;2-1
20. S. L. Huth, T. L. Threlfall, M. B. Hursthouse, *University of Southampton, Crystal Structure Report Archive*, **2008**, 698. 10.5258/ecrystals/698
21. E. Taipale, N. A. Durandin, J. K. Salunke, N. R. Candeias, T.-P. Ruoko, J. S. Ward, A. Priimagi, K. Rissanen, *Mater. Adv*., **2022**, *3*, 1703 – 1712. 10.1039/D1MA00438G

22. L. Duan, M. Wang, P. Li, N. Wang, F. Wang, L. Sun, *Inorg. Chim. Acta*, **2009**, *362*, 372 – 376. 10.1016/j.ica.2008.04.011
23. K. G. Gaw, M. B. Smith, J. B. Wright, A. M. Z. Slawin, S. J. Coles, M. B. Hursthouse, G. J. Tizzard, *J. Organomet. Chem*., **2012**, *699*, 39 – 47. 10.1016/j.jorganchem.2011.11.003
24. P. W. Dyer, J. Fawcett, M. J. Hanton, R. D. W. Kemmitt, R. Padda, N. Singh, *Dalton Trans*., **2003**, 104 – 113. 10.1039/B208886J
25. T. Peppel, M. Köckerling, *Cryst. Growth Des*., **2011**, *11*, 5461 – 5468. 10.1021/cg2010419
26. S. Zhang, R. Pattacini, S. Jie, P. Braunstein, *Dalton Trans*., **2012**, *41*, 379 – 386. 10.1039/C1DT11352F
27. X. Wang, S. Liu, L. Weng, G-X. Jin, *J. Organomet. Chem*., **2005**, *690*, 2934 – 2940. 10.1016/j.jorganchem.2005.03.015
28. D. J. Purdela, *J. Magn. Reson*., **1971**, *5*, 23 – 36. 10.1016/0022-2364(71)90059-X
29. P. A. Aguirre, C. A. Lagos, S. A. Moya, C. Zúñiga, C. Vera-Oyarce, E. Sola, G. Peris, J. C. Bayón, *Dalton Trans*., **2007**, 5419 – 5426. 10.1039/B704615B
30. M. Brookhart, M. L. H. Green, *J. Organomet. Chem*., **1983**, *250*, 395 – 408. 10.1016/0022-328X(83)85065-7
31. D. Braga, F. Grepioni, E. Tedesco, K. Biradha, G. R. Desiraju, *Organometallics*, **1997**, *16*, 1846 – 1856. 10.1021/om9608364
32. M. P. Mitoraj, M. G. Babashkina, K. Robeyns, F. Sagan, D. W. Szczepanik, Y. V. Seredina, Y. Garcia, D. A. Safin, *Organometallics*, **2019**, *38*, 1973 – 1981. 10.1021/acs.organomet.9b00062
33. S. González-Montiel, D. Martínez-Otero, N. Andrade-López, J. G. Alvarado-Rodríguez, M. Carmona-Pichardo, J. Cruz-Borbolla, T. Pandiyan, L. W. Pineda, *Polyhedron*, **2015**, *87*, 181 – 193. 10.1016/j.poly.2014.11.007

# Chapter 4 – Synthesis and Reactivity of Cobalt(II) Complexes of 'PNP', 'PCNCP', 'SPNP' and 'SPNPS' Ligands

## 4.1 Introduction

The coordination chemistry of 'PNP' and 'PCNCP' ligands with cobalt halides has been scarcely studied.[1 – 6] Previously, syntheses of zwitterionic complex **1.16**[1] and co-crystal **1.20**[3] (**Figure 4.1**) have been reported, with their structures confirmed by XRD analysis of single crystals. Complex **1.16** is obtained by the 1:1 reaction of $CoCl_2$ with $MeS(CH_2)_3N(PPh_2)_2$,[1] whereas co-crystal **1.20** is afforded from the 1:2 reaction of $CoCl_2$ with $\{2,6\text{-}Me_2C_6H_3N(PPh_2)_2\}$.[3] Co-crystal **1.20** contains tetrahedral cobalt(III) complex $[Cl_3Co\{NH_2(2,6\text{-}Me_2Ph)\}]$ (with $NH_2(2,6\text{-}Me_2Ph)$ forming from P-N bond cleavage in a molecule of $\{2,6\text{-}Me_2C_6H_3N(PPh_2)_2\}$). The origin of the change in cobalt oxidation state and P-N bond cleavage is not established.[3]

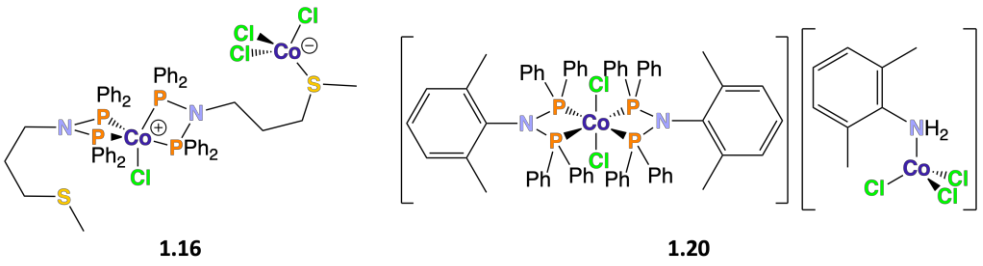


**Figure 4.1.** Structures of complex **1.16** and co-crystal **1.20**.[1,3]

To further establish the fundamental coordination chemistry of 'PNP' ligands with cobalt halides evidenced by complex **1.16** and co-crystal **1.20**, the corresponding coordination chemistry of 'PNP' compounds **2.2** – **2.7** was studied. The 1:1 reactions of compounds **2.4** ($Me_2N(CH_2)_3N(PPh_2)_2$), **2.5** (Py-*m*-$CH_2N(PPh_2)_2$) and **2.7** (Py-*o*-$C_6H_4N(PPh_2)_2$), containing pendant donor groups, with cobalt halides are predicted to afford zwitterionic complexes based on the complex **1.16** being obtained from the 1:1 reaction of $CoCl_2$ with $MeS(CH_2)_3N(PPh_2)_2$ (**Figure 4.1**).[1] In contrast, the complexes obtained from the 1:1 reactions of compounds **2.2** ($Ph(CH_2)_2N(PPh_2)_2$), **2.3** (*n*-$BuN(PPh_2)_2$) and **2.6** (Ph-$C_6H_4N(PPh_2)_2$) with cobalt halides are likely to adopt a structure different from that exhibited by complex **1.16** since there is no pendant donor group on the 'PNP' ligand.

Additionally, reactions of 'PNP' ligands with cobalt halides with various 'PNP':$CoX_2$ stoichiometries (1:1 and 2:1) will be probed to elucidate potential changes in cobalt complex structure upon changing reaction stoichiometry.

The reactivity of 'PCNCP' compounds with cobalt halides has been probed to a limited extent, with the potential for both zwitterionic[4] and [($\kappa^2$-*P,P*)$CoX_2$] complexes being established (**Figure 1.4**, **Section 1.1.2**, **Chapter 1**).[5,6] Study of the coordination chemistry of 'PCNCP' compound **2.8** (Py-*o*-$(CH_2)_2N(CH_2PPh_2)_2$) with cobalt dibromide aims to elucidate the factors governing the structure of the cobalt complexes obtained with 'PCNCP' ligands. In contrast, the coordination chemistry of 'SPNP' and 'SPNPS' compounds has not been previously studied with cobalt. Study of the reactivity of 'SPNP' compound **2.9** ($Ph(CH_2)_2N(SPPh_2)(PPh_2)$) and 'SPNPS' compound **2.10** ($Ph(CH_2)_2N(SPPh_2)_2$) with cobalt dibromide is predicted to establish the impact of the addition of sulfur atoms to a 'PNP' scaffold on the coordination chemistry with cobalt. To the best knowledge of the author, the coordination chemistry of aminophosphine compounds with cobalt is also unstudied. Consequently, the reactions of aminophosphine compounds **2.11** (Py-*o*-$(CH_2)_2N(PPh_2)(Me)$) and **2.12** (Py-*o*-$(CH_2)_2N(P\{OPh\}_2)(Me)$) with cobalt halides are hoped to establish if $\kappa^2$-*P,N* coordination is exhibited in the resultant cobalt complexes.

## 4.2 Coordination Chemistry of Py-*o*-$(CH_2)_2N(PPh_2)_2$ (2.1), $Ph(CH_2)_2N(PPh_2)_2$ (2.2), *n*-$BuN(PPh_2)_2$ (2.3), $NMe_2(CH_2)_3N(PPh_2)_2$ (2.4), Py-*m*-$CH_2N(PPh_2)_2$ (2.5), Ph-$C_6H_4N(PPh_2)_2$ (2.6), Py-*o*-$C_6H_4N(PPh_2)_2$ (2.7), and Py-*o*-$(CH_2)_2N(CH_2PPh_2)_2$ (2.8) with Cobalt(II) Halides

The previously prepared compound Py-*o*-$(CH_2)_2N(PPh_2)_2$ (**2.1**)[7] and compound **2.2** were each reacted in a 1:1 molar ratio with $CoX_2$ (X = Cl, Br and I) allowing for the effect of halide on cobalt(II) complex structure to be probed. In contrast, compounds **2.3** – **2.8** were reacted with $CoBr_2$, only, in a 1:1 molar ratio in THF (or DCM for the reaction involving compound **2.8**) solution. The corresponding cobalt(II) halide complexes **4.1** – **4.11** were afforded (**Scheme 4.1**).

This coordination study revealed, for the first time, that ionic cobalt(II) complexes (**4.1** – **4.4**, **4.9** – **4.11**) of the form $[CoX(RN\{PPh_2\}_2)_2]_2[Co_2X_6]$ (X = Cl, Br, I) are obtained

when no suitable pendant donor is present in R of $RN\{PPh_2\}_2$, as is the case for compounds **2.2**, **2.3**, **2.5** – **2.7**. The reaction of compound **2.4** with $CoBr_2$ affords the expected zwitterionic complex **4.5**, with similar reactivity observed for compound **2.1** with $CoCl_2$ and $CoI_2$ (analogous to previously prepared complex **2.14**,[7] **d)**, **Scheme 4.1**, evidencing zwitterionic complex formation regardless of the halide ligand present).

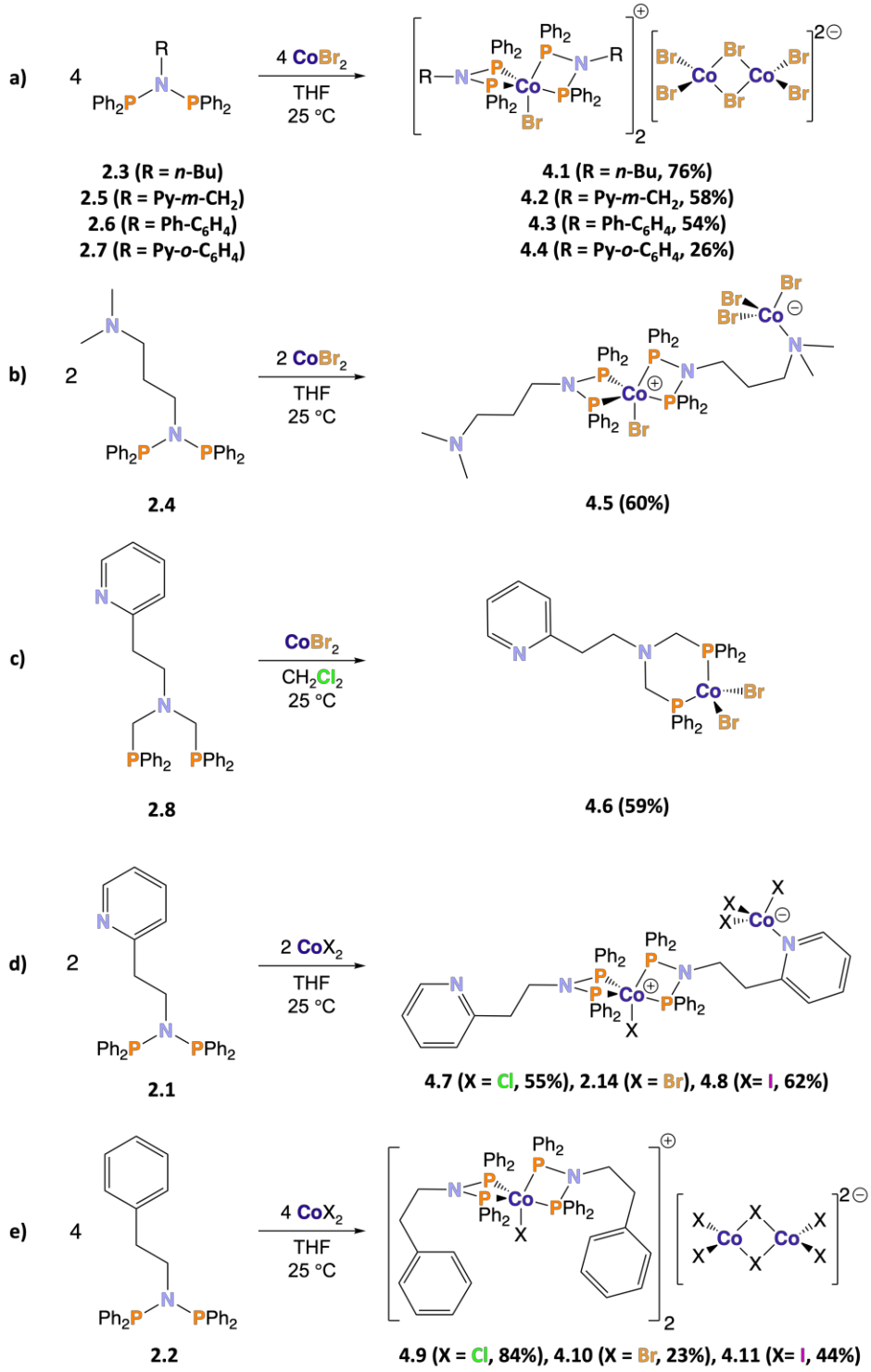


**Scheme 4.1.** Reactions of various 'PNP' and 'PCNCP' compounds with cobalt halides. *NB* complex **2.14** (previously prepared)[7] is included for completeness. Percentage yields included.

Single crystal XRD analyses have confirmed the solid-state molecular structures of complexes **4.1**, **4.5**, and **4.7** – **4.11** (see **Section 4.2.1**). The $[Co_2X_6]$ (X = Cl, Br, I) dianion of complexes **4.1** – **4.4** and **4.9** – **4.11** (**Scheme 4.1**) is of interest as a search using the CSD Conquest Software[8] (31/01/24) reveals a limited number of reports of the $[Co_2X_6]$ dianion in the literature. Indeed, there are several reported molecular structures containing the $[Co_2Cl_6]$ dianion,[9 – 19] only three reported molecular structures containing the $[Co_2Br_6]$ dianion,[20,21] with complex **4.11** being the first mention of the $[Co_2I_6]$ dianion (to the best knowledge of the author). In each case, the $[Co_2X_6]$ dianion is formed from the breakdown of polymeric $CoX_2$.[9] Single crystals of complexes **4.2** and **4.4**[1.1]***** could not be obtained, despite numerous attempts. Hence, their molecular structures (required in order to determine the ionic, *cf*. complex **4.1**, **Scheme 4.1**, or zwitterionic, *cf*. complex **4.5**, **Scheme 4.1**, nature of the complex) could not be determined.

More generally, the characterisation of cobalt(II) complexes is challenging due to the paramagnetic nature of these $d^7$ species. For example, the presence of paramagnetic cobalt(II) species results in very large NMR spectroscopic chemical shift ranges due to the dependence of the chemical shift of a given nucleus on shielding and the chemical environment.[22] The actual magnetic field at a given nucleus is not simply equal to the applied magnetic field, but instead is given by **Equation 4.1**:

$$\text{Actual Field} = B_0 + B \qquad \textbf{(4.1)}$$

$B_0$ is the applied magnetic field and B is the field from adjacent nuclei, to which paramagnetic nuclei contribute significantly.[22] Hence, paramagnetic nuclei result in a large range of magnetic field values experienced by neighbouring nuclei and very large chemical shift ranges.[22] Additionally, paramagnetic nuclei have very short spin-spin, *i.e.,* $T_2$, relaxation times, and therefore have short excited state lifetimes; the shorter the lifetime of a nucleus in a given state, the greater the uncertainty in the energy of that given state. This greater uncertainty arising from short $T_2$ relaxation results in broader NMR resonances (often broadened to the point of invisibility).[22] Consequently, NMR spectroscopy is often not suitable to characterise complexes described in **Scheme 4.1**.

[1.1]***** Single crystals of complex **4.3** also could not be obtained, but complex **4.3** can only have an ionic structure due to the lack of a pendant donor group in the 'PNP' nitrogen atom's substituent.

CHN, ESI mass spectrometry and measurement of the magnetic susceptibility of the complexes *via* the Evans Method[23] have been employed to study complexes **4.1** – **4.11**, but cannot distinguish between ionic and zwitterionic structures. Obtained CHN analyses reflects the 1:1 ratio of 'PNP' compound to $CoX_2$ present in both ionic and zwitterionic complexes. Positive ion ESI mass spectra evidence clear signals for the $[CoX(RN\{PPh_2\}_2)_2]$ cation and the $[M\text{-}CoX_3]^+$ fragment of ionic (*e.g.*, complex **4.4 Ionic**, **Figure 4.2**) and zwitterionic (*e.g.*, complex **4.4 Zwitterionic**, **Figure 4.2**) complexes, respectively, with the same *m/z* value (1214.20 *m/z*, **Figure 4.2**, hence equivalence of $[CoX(RN\{PPh_2\}_2)_2]^+$ and $[M\text{-}CoX_3]^+$). Negative ion ESI mass spectra show signals for the equivalent $[CoX_3]^-$ and $[Co_2X_6]^{2-}$ anions for zwitterionic and ionic complexes, respectively. The aforementioned signals are not observed in the positive and negative ion ESI mass spectra of complex **4.6**, suggesting a neutral structure; a fragment at 656.3 *m/z* has been assigned as $[M\text{-}Br]^+$, consistent with the proposed structure (**Figure 4.2**).

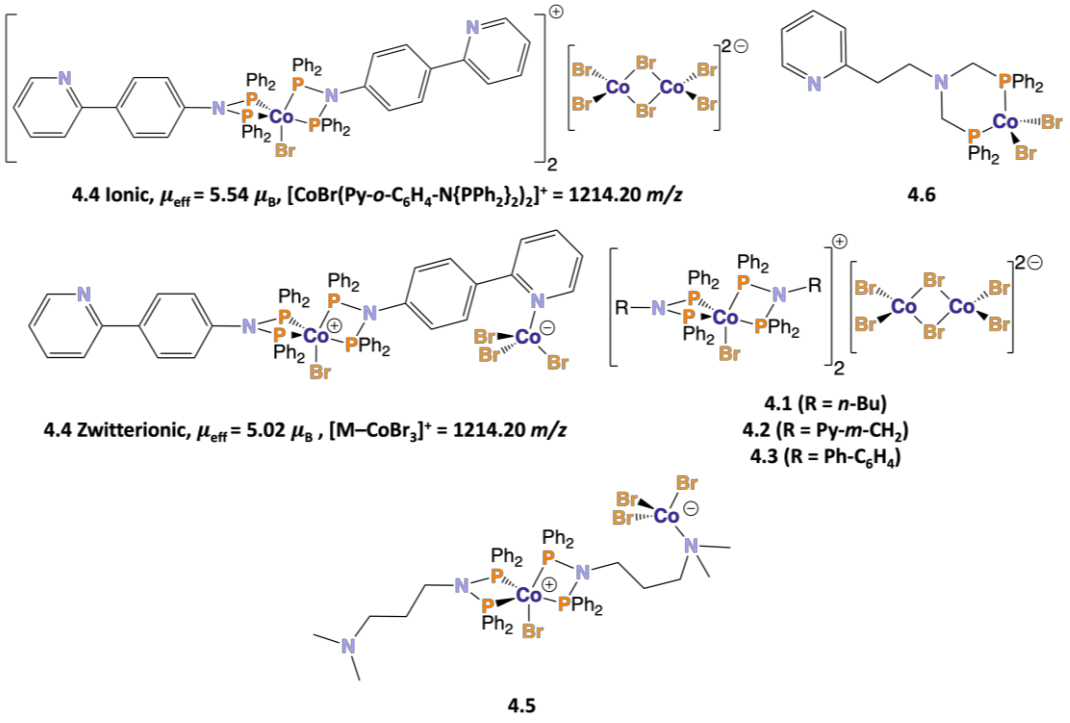


**Figure 4.2.** Structures of complexes **4.1** – **4.5**.

Probing the magnetic susceptibility of complexes **4.1** – **4.11** *via* the Evans Method[23] (see **Section 4.9**) has proven to be unable to distinguish between zwitterionic and ionic structures; for example, $\mu_{eff}$ values of 5.02 and 5.54 $\mu_B$ were measured for the possible complexes **4.4 Zwitterionic** and **4.4 Ionic**, respectively (**Figure 4.2**). However, $\mu_{eff}$ values

of 5.02 and 5.54 $\mu_B$ agree with measured values for analogous zwitterionic and ionic complexes (see **Section 4.9**), respectively.

Given the difficulty in obtaining structural information in the absence of single crystal XRD analyses, the exact structures of complexes **4.2** and **4.4** cannot be confirmed. Consequently, complexes **4.2** and **4.4** have been tentatively assigned ionic structures (**Scheme 4.1**) since the formation of zwitterionic complexes (as described in **Section 4.4**) has been shown to occur *via* an intramolecular reaction of a pendant donor moiety present in the cation of an intermediate ionic cobalt(II) complex and the $[Co_2X_6]$ dianion. Since zwitterionic complex formation might not occur, the intermediate ionic cobalt(II) complex is assumed to be the isolated product during the synthesis of complexes **4.2** and **4.4**.

### 4.2.1 Solid-State Molecular Structures of $[CoBr(n\text{-}BuN\{PPh_2\}_2)_2]_2[Co_2Br_6]$ (4.1), $[CoBr(Me_2N(CH_2)_3N\{PPh_2\}_2)(\{Br_3Co\}Me_2N(CH_2)_3N\{PPh_2\}_2)]$ (4.5), $[CoCl(Py\text{-}o\text{-}(CH_2)_2N\{PPh_2\}_2)(\{Cl_3Co\}Py\text{-}o\text{-}(CH_2)_2N\{PPh_2\}_2)]$ (4.7), $[CoI(Py\text{-}o\text{-}(CH_2)_2N\{PPh_2\}_2)(\{I_3Co\}Py\text{-}o\text{-}(CH_2)_2N\{PPh_2\}_2)]$ (4.8), $[CoCl(Ph(CH_2)_2N\{PPh_2\}_2)_2]_2[Co_2Cl_6]$ (4.9), $[CoBr(Ph(CH_2)_2N\{PPh_2\}_2)_2]_2[Co_2Br_6]$ (4.10) and $[CoI(Ph(CH_2)_2N\{PPh_2\}_2)_2]_2[Co_2I_6]$ (4.11)

Single crystals of complexes **4.1**, **4.5**, and **4.7** – **4.11** were obtained and molecular structures determined (**Figure 4.3**). *NB* the structure of the analogous previously prepared complex **2.14** has been included here for comparison.[7] As anticipated, the metric parameters of the $[CoX(P,P)_2]^+$ motif are very similar for complexes **4.1**, **4.5**, **4.7** – **4.11** and **2.14**.

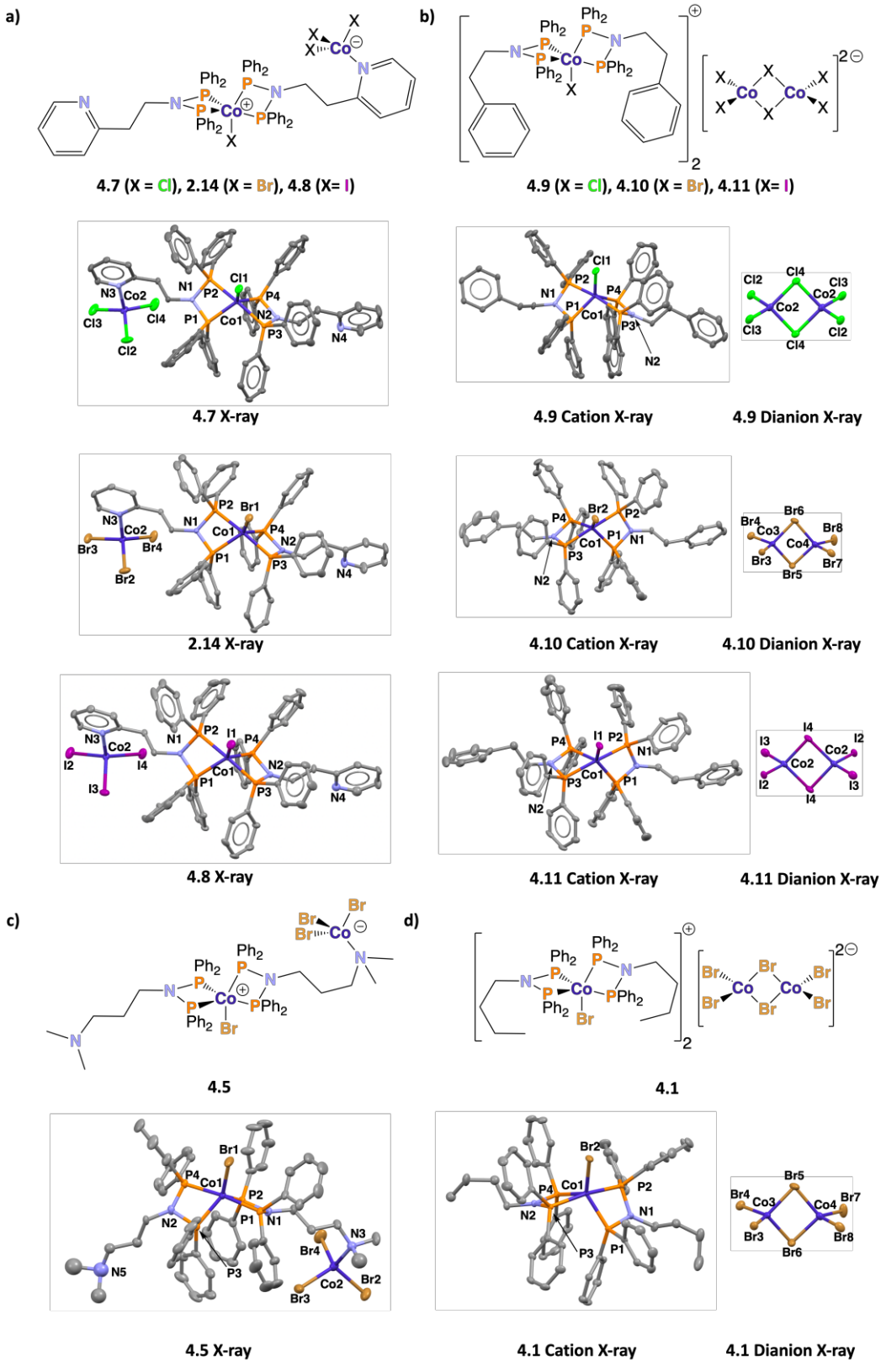


**Figure 4.3.** Solid-state molecular structures of complexes **4.7**, **2.14**, **4.8** and **4.5**, and the cations and dianions of complexes **4.9**, **4.10**, **4.11** and **4.1**. Thermal ellipsoids are shown at the 50 % probability level. *NB* for **4.9** and **4.11** the asymmetric unit contains only one equivalent of cation and half of the $[Co_2X_6]$ dianion (X = Cl, I), whereas for **4.10** and **4.1** the asymmetric unit contains two equivalents of cation and the entire $Co_2Br_6^{2-}$ anion, hence only one cation is shown as a representative example of both in **Figure 4.3**. Hydrogen atoms and DCM molecules are omitted for clarity. Atom colour: carbon – grey; nitrogen – light blue; phosphorus – orange; cobalt – dark blue; chlorine – green; bromine – orange-brown, and iodine – purple.

The key bond lengths and bond angles measured from the solid-state structures of complexes **4.5**, **4.7**, **2.14** and **4.8** are shown in **Table 4.1**, with analogous data for complexes **4.1** and **4.9** – **4.11** being presented in **Table 4.2**. The cationic cobalt(II) centre in complexes **4.1**, **4.5**, and **4.7** – **4.11** and **2.14** adopts a distorted trigonal bipyramidal geometry (evidenced by equatorial-equatorial bond angles of Cl1-Co1-P4 ~132° and P1-Co1-P4 ~108°, *cf*. 120°, and axial-equatorial bond angles of Cl1-Co1-P2/3 ~95°, *cf*. 90°, for complex **4.7**) bearing a single halide ligand and two 'PNP' ligands coordinating in a $\kappa^2$-*P,P* manner, *i.e*., $[CoX(P,P)_2]^+$. Distortion arises due to small P1-Co1-P2 and P3-Co1-P4 angles of ~71.2 – 71.5°. Taking the molecular structure of complex **4.5** (**Figure 4.3**) as an example, the Br1, P2 and P3 atoms are coplanar, with P1 and P4 occupying the apical positions. Indeed, the distortion of a trigonal bipyramidal geometry can be probed be calculating the $\tau_5$ value[24] using **Equation 4.2**:

$$\tau_5 \approx -0.01667\alpha + 0.01667\beta \qquad \textbf{(4.2)}$$

where $\alpha$ and $\beta$ are the two largest valence angles around the five-coordinate centre and $\beta > \alpha$. For a perfect trigonal bipyramidal geometry, $\alpha$ = 120° and $\beta$ = 180°, resulting in a $\tau_5$ value of 1.[24] The range of $\tau_5$ values obtained for complexes **4.1**, **4.5**, and **4.7** – **4.11** are ~0.61 – 0.72, indicating significant distortion from the ideal trigonal bipyramidal geometry.

Ionic complexes **4.1** and **4.9** – **4.11** contain the $[Co_2X_6]$ dianion with two distorted tetrahedral cobalt(II) centres joined by two bridging halide ligands and completed by two terminal halide ligands. In the case of zwitterionic complexes **4.5**, **4.7**, **4.8** and **2.14**, the anionic charge exists on a distorted tetrahedral cobalt(II) centre with three halide ligands and one nitrogen donor ligand, either pyridyl or tertiary amine-based, with the pyridyl or tertiary amine moiety being present in the nitrogen substituent of the 'PNP' ligand. This same 'PNP' ligand is coordinating to the cationic cobalt(II) centre in complexes **4.5**, **4.7**, **4.8** and **2.14**, resulting in a zwitterionic complex.

**Table 4.1.** Key bond lengths and angles measured from the solid-state molecular structures of complexes **4.5**, **4.7**, **2.14** and **4.8**, and calculated $\tau_5$ values for complexes **4.5**, **4.7**, **2.14** and **4.8**.

| Parameter | 4.5 (X = Br) | 4.7 (X = Cl) | 2.14 (X = Br) | 4.8 (X = I) |
|---|---|---|---|---|
| Co1-X1 / Å | 2.3568(7) | 2.2264(7) | 2.3638(5) | 2.5461(5) |
| Co1-P1 / Å | 2.242(1) | 2.2687(7) | 2.2692(9) | 2.2804(8) |
| Co1-P2 / Å | 2.250(1) | 2.2396(7) | 2.235(1) | 2.239(1) |
| Co1-P3 / Å | 2.249(1) | 2.2411(7) | 2.238(1) | 2.238(1) |
| Co1-P4 / Å | 2.232(1) | 2.2397(5) | 2.2400(8) | 2.2497(9) |
| N1-P1 / Å | 1.683(3) | 1.708(2) | 1.707(3) | 1.716(3) |
| N1-P2 / Å | 1.709(4) | 1.694(2) | 1.695(2) | 1.701(2) |
| N2-P3 / Å | 1.707(4) | 1.691(2) | 1.687(2) | 1.692(2) |
| N2-P4 / Å | 1.683(4) | 1.698(2) | 1.698(3) | 1.709(4) |
| N3-Co2 / Å | 2.121(7) | 2.077(2) | 2.075(2) | 2.073(2) |
| Co2-X2 / Å | 2.436(2) | 2.250(1) | 2.3836(7) | 2.5954(8) |
| Co2-X3 / Å | 2.40(1) | 2.2662(9) | 2.3977(8) | 2.5887(6) |
| Co2-X4 / Å | 2.374(2) | 2.2530(6) | 2.3894(6) | 2.5788(6) |
| X1-Co1-P1 / ° | 94.54(4) | 119.57(3) | 120.25(3) | 123.26(3) |
| X1-Co1-P2 / ° | 123.40(4) | 95.16(2) | 95.35(3) | 96.17(3) |
| X1-Co1-P3 / ° | 128.73(4) | 95.26(2) | 94.70(3) | 93.57(3) |
| X1-Co1-P4 / ° | 94.08(4) | 132.33(3) | 131.90(3) | 129.50(3) |
| P1-Co1-P2 / ° | 71.46(4) | 71.35(2) | 71.49(3) | 71.27(3) |
| P1-Co1-P3 / ° | 103.77(4) | 103.71(2) | 103.84(3) | 104.06(4) |
| P1-Co1-P4 / ° | 171.26(5) | 108.09(2) | 107.83(3) | 107.22(4) |
| P2-Co1-P3 / ° | 107.83(4) | 169.57(3) | 169.82(3) | 170.21(4) |
| P2-Co1-P4 / ° | 102.44(4) | 100.96(2) | 100.98(3) | 101.34(4) |
| P3-Co1-P4 / ° | 71.71(4) | 71.45(2) | 71.46(3) | 71.44(3) |
| P1-N1-P2 / ° | 101.3(2) | 101.3(1) | 101.3(1) | 100.8(1) |
| P3-N2-P4 / ° | 101.5(2) | 101.0(1) | 101.1(1) | 100.8(2) |
| N3-Co2-X4 / ° | 103.2(2) | 114.01(6) | 115.59(7) | 117.73(9) |
| X3-Co2-X4 / ° | 109.9(2) | 111.03(3) | 109.31(2) | 113.62(2) |
| X2-Co2-X4 / ° | 117.5(1) | 113.27(3) | 113.44(2) | 106.19(2) |
| $\tau_5$ | 0.71 | 0.62 | 0.63 | 0.68 |

**Table 4.2.** Key bond lengths and angles measured from the solid-state molecular structures of complexes **4.1** and **4.9** – **4.11**, and calculated $\tau_5$ values for complexes **4.1** and **4.9** – **4.11**. *NB* ‘ is 2, * is 2, ^ is 3, and ‘’ is 4 for complexes **4.9** and **4.11**, and ‘ is 3, * is 3, ^ is 4, and ‘’ is 5 for complexes **4.1** and **4.10**.

| Parameter | 4.1 (X = Br) | 4.9 (X = Cl) | 4.10 (X = Br) | 4.11 (X = I) |
|---|---|---|---|---|
| Co1-X1 / Å | 2.3819(6) | 2.2296(6) | 2.3708(6) | 2.5561(7) |
| Co1-P1 / Å | 2.2645(10) | 2.2650(5) | 2.2512(9) | 2.253(1) |
| Co1-P2 / Å | 2.2606(10) | 2.2194(5) | 2.2265(9) | 2.227(1) |
| Co1-P3 / Å | 2.2310(10) | 2.2430(4) | 2.2312(8) | 2.259(1) |
| Co1-P4 / Å | 2.2495(10) | 2.2722(5) | 2.2577(8) | 2.30(2) |
| N1-P1 / Å | 1.699(3) | 1.707(1) | 1.58(2) | 1.705(4) |
| N1-P2 / Å | 1.689(3) | 1.680(1) | 1.81(2) | 1.679(4) |
| N2-P3 / Å | 1.684(3) | 1.685(1) | 1.692(2) | 1.684(4) |
| N2-P4 / Å | 1.717(3) | 1.700(1) | 1.712(2) | 1.71(2) |
| Co’-X* / Å | 2.3431(6) | 2.2340(5) | 2.3452(6) | 2.5713(7) |
| Co’-X^ / Å | 2.3726(6) | 2.2371(7) | 2.3602(8) | 2.5516(7) |
| Co’-X’’ / Å | 2.4660(6) | 2.3377(5) | 2.4541(9) | 2.6368(8) |
| X1-Co1-P1 / ° | 122.13(3) | 127.64(2) | 126.90(3) | 133.67(4) |
| X1-Co1-P2 / ° | 97.23(3) | 93.17(2) | 94.47(3) | 92.88(4) |
| X1-Co1-P3 / ° | 92.41(3) | 96.19(2) | 96.43(3) | 96.36(4) |
| X1-Co1-P4 / ° | 129.25(3) | 125.66(2) | 125.17(3) | 123.1(5) |
| P1-Co1-P2 / ° | 71.30(3) | 71.18(2) | 71.34(3) | 71.18(4) |
| P1-Co1-P3 / ° | 103.01(4) | 102.15(2) | 101.62(3) | 102.72(5) |
| P1-Co1-P4 / ° | 108.43(4) | 106.67(2) | 107.92(3) | 103.0(5) |
| P2-Co1-P3 / ° | 170.34(4) | 170.59(2) | 169.10(3) | 170.72(5) |
| P2-Co1-P4 / ° | 102.89(4) | 103.76(2) | 102.39(3) | 102.8(5) |
| P3-Co1-P4 / ° | 71.07(4) | 71.33(2) | 71.38(3) | 71.3(5) |
| P1-N1-P2 / ° | 102.26(15) | 100.83(7) | 101(2) | 100.8(2) |
| P3-N2-P4 / ° | 99.93(15) | 102.11(7) | 100.6(1) | 103.0(7) |
| X*-Co’-X^ / ° | 116.59(3) | 114.18(2) | 109.80(3) | 116.99(3) |
| X’’-Co’-X’’ / ° | 97.19(2) | 93.76(2) | 96.48(2) | 99.48(3) |
| Co’-X’’-Co’ / ° | 82.64(2) | 86.24(2) | 82.95(2) | 80.52(2) |
| $\tau_5$ | 0.68 | 0.72 | 0.70 | 0.62 |

## 4.3 Attempted Synthesis of $[N(n\text{-}Pr)_4]_2[Co_2Br_6]$ (4.12)

In order to provide a model complex for the $[Co_2Br_6]$ dianion, *i.e.,* for reactivity and magnetic studies, $[N(n\text{-}Pr)_4]Br$ was reacted with one equivalent of $CoBr_2$ in an attempt to prepare complex **4.12** (**Scheme 4.2**). However, despite the 1:1 reaction stoichiometry, the reaction afforded the complex $[N(n\text{-}Pr)_4]_2[CoBr_4]$ (**4.13**), **Scheme 4.2**, *i.e.,* the 2 $[N(n\text{-}Pr)_4]Br$ : 1 $CoBr_2$ reaction product, with one equiv. of unreacted $CoBr_2$. The outcome of this reaction was verified by obtaining a solid-state molecular structure (**Section 4.3.1**) of complex **4.13**. CHN analysis supports the isolated product having the chemical formula $C_{24}H_{56}Br_6Co_2N_2$, *i.e.,* $[N(n\text{-}Pr)_4]_2[CoBr_4]\cdot CoBr_2$ containing an unreacted equivalent of $CoBr_2$. The formation of complex **4.13**, as opposed to complex **4.12**, highlights the preference to form complexes containing the $[CoBr_4]$ dianion when tetraammonium-based cations are present, possibly due to more efficient packing in the solid-state arising from both the cation and anion having distorted tetrahedral geometries. Complexes of the form $[NR_4]_2[CoBr_4]$ (where R = alkyl, aryl, H) are prevalent in the literature, with well-established syntheses (*i.e.*, a 2:1 ratio of $NR_4Br:CoBr_2$).[25]

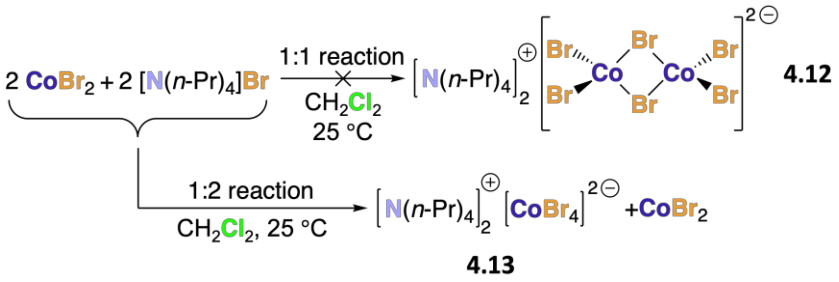


**Scheme 4.2.** Attempted synthesis of complex **4.12** and formation of complex **4.13**.

### 4.3.1 Solid-State Molecular Structure of $[N(n\text{-}Pr)_4]_2[CoBr_4]$ (4.13)

Single crystals of complex **4.13** were obtained and the molecular structure determined (**Figure 4.4**).

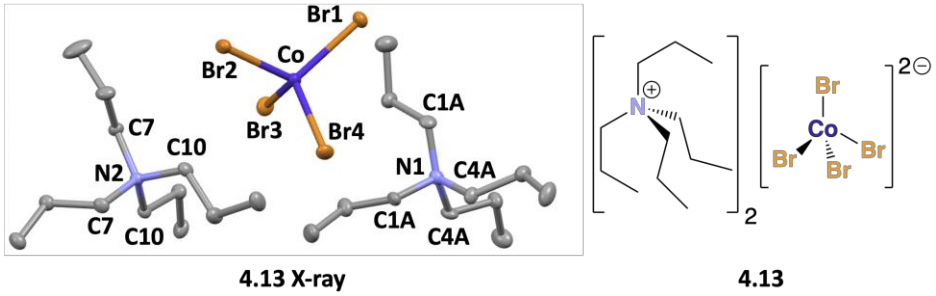


**Figure 4.4.** Solid-state molecular of complex **4.13**. Thermal ellipsoids are shown at the 50 % probability level. *NB* hydrogen atoms are omitted for clarity. Atom colour: carbon – grey; nitrogen – light blue; cobalt – dark blue and bromine – orange-brown.

The direct synthesis and molecular structure of complex **4.13** has very recently been published,[26] and the key bond lengths (**Table 4.3**) and bond angles (**Table 4.4**) between the published molecular structure and the molecular structure determined during this thesis work (**Figure 4.4**) show good similarity (*e.g.,* Co-Br bond lengths vary from 2.403(1) – 2.433(1) Å,[26] *cf*. 2.4041(6) – 2.4347(8) Å for the molecular structure in **Figure 4.4**).

**Table 4.3.** Key bond lengths measured from the solid-state molecular structure of complex **4.13**.

| Bond | Bond Length / Å |
|---|---|
| Co-Br1 | 2.4347(8) |
| Co-Br2 | 2.4290(6) |
| Co-Br3 | 2.4217(4) |
| Co-Br4 | 2.4041(6) |

**Table 4.4.** Key bond angles measured from the solid-state molecular structure of complex **4.13**.

| Angle | Bond Angle / ° |
|---|---|
| Br1-Co-Br2 | 113.11(2) |
| Br1-Co-Br3 | 110.36(2) |
| Br1-Co-Br4 | 108.84(2) |
| Br2-Co-Br3 | 109.29(2) |
| Br2-Co-Br4 | 107.08(2) |
| Br3-Co-Br4 | 108.00(2) |

## 4.3.2 Synthesis of [N(*n*-Pr)$_4$][PyCoBr$_3$] (4.14)

In order to provide a model of the [PyCoX$_3$]$^-$ moiety present in complexes **4.7**, **4.8** and **2.14**, *i.e.,* for magnetic studies, without the complex being zwitterionic, [N(*n*-Pr)$_4$]Br was reacted with one equivalent of CoBr$_2$ and one equivalent of pyridine to afford complex **4.14** (**Scheme 4.3**). With the addition of pyridine, CoBr$_2$ and [N(*n*-Pr)$_4$]Br do react in the desired 1:1 ratio (unlike the reaction described in **Scheme 4.2**). The reaction outcome was verified by a solid-state molecular structure (**Section 4.3.3**) and CHN analysis.

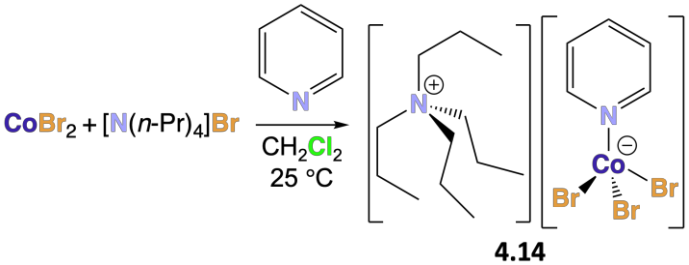


**4.14**

**Scheme 4.3.** Synthesis of complex **4.14**.

## 4.3.3 Solid-State Molecular Structure of [N(*n*-Pr)$_4$][PyCoBr$_3$] (4.14)

Single crystals of complex **4.14** were obtained and a molecular structure determined (**a)**, **Figure 4.5**). Complex **4.14** is analogous to complex **3.26**[27] (**b)** in **Figure 4.5**). The metric parameters of the anion of complex **4.14** (key bond lengths and bond angles are given in **Table 4.5** and **Table 4.6**, respectively) are very similar to those of **3.26**. Complex **4.14** has N1-Co = 2.047(2) Å and Co-Br ~2.39 Å with complex **3.26** (R = Et) evidencing N1-Co1 = 2.058(2) Å and Co-Br ~2.40 Å; both complexes **4.14** and **3.26** (R = Et) exhibit Br-Co-Br and Br-Co-N angles in the range of 103 – 118°.[27]

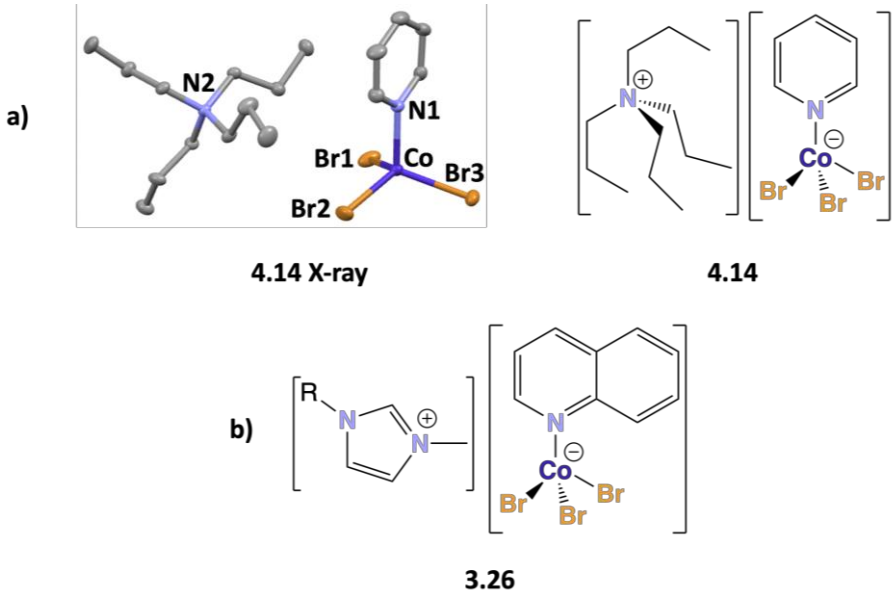


**Figure 4.5.** Solid-state molecular structure of complex **4.14**. Thermal ellipsoids are shown at the 50 % probability level. *NB* hydrogen atoms are omitted for clarity. Atom colour: carbon – grey; nitrogen – light blue; cobalt – dark blue and bromine – orange-brown. Structure of complex **3.26** also shown.[27]

**Table 4.5.** Key bond lengths measured from the solid-state molecular structure of complex **4.14**.

| Bond | Bond Length / Å |
|---|---|
| Co-Br1 | 2.3965(5) |
| Co-Br2 | 2.3898(5) |
| Co-Br3 | 2.3879(5) |
| Co-N1 | 2.047(2) |

**Table 4.6.** Key bond angles measured from the solid-state molecular structure of complex **4.14**.

| Angle | Bond Angle / ° |
|---|---|
| Br1-Co-Br2 | 111.99(2) |
| Br1-Co-Br3 | 113.73(2) |
| Br2-Co-Br3 | 111.71(2) |
| N1-Co-Br1 | 106.55(7) |
| N1-Co-Br2 | 104.74(7) |
| N1-Co-Br3 | 107.46(7) |

### 4.3.4 Synthesis of $[PPN]_2[Co_2Cl_6]$ (4.15) and Reaction with 1,2-*bis*(diphenylphosphino)ethane

Since the previous attempt to prepare complex **4.12** was unsuccessful (**Scheme 4.2**), an alternative approach was employed. The structure of complex **4.15** was found in the aforementioned CSD Conquest Software[8] search (**Section 4.2**), and was synthesised using an adapted literature procedure (**Scheme 4.4**).[9] $[PPN]_2[Co_2Cl_6]$ (complex **4.15**) and $[PPN]_2[Co_2Br_6]$ (containing the $[Co_2Br_6]$ dianion like complex **4.12**) are both complexes of the form $[PPN]_2[Co_2X_6]$. Since the reactivity of the $[Co_2X_6]$ dianion is not affected by the halide ligand (X), complex **4.15** was synthesised (as opposed to $[PPN]_2[Co_2Br_6]$) due to easier synthetic accessibility arising from [PPN]Cl availability. The structure of complex **4.15** contains the $[Co_2Cl_6]$ dianion, contrasting with reactions utilising tetraalkyl ammonium cations, which afford the $[CoCl_4]$ dianion, allowing for the study of the reactivity and the magnetic properties of the 'isolated' $[Co_2Cl_6]$ dianion, *i.e.,* in a complex where the cation is not cobalt-containing.

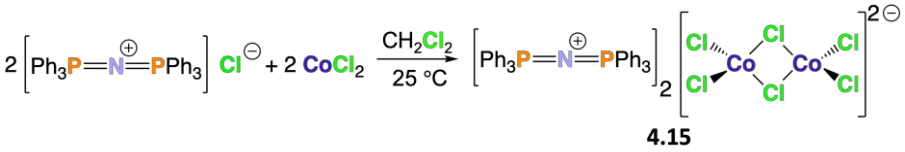


**Scheme 4.4.** Synthesis of complex **4.15**.

The $[X_3Co\text{-}PPh_2CH_2CH_2Ph_2P\text{-}CoX_3]$ dianion of complex **1.14**[28] is likely afforded upon reaction the $[Co_2X_6]$ dianion of *in situ* complex **4.17** with one equivalent of dppe (**b)**, **Scheme 4.5**). To verify the reactivity described in **b)** in **Scheme 4.5**, complex **4.15** was reacted with one equivalent of dppe to afford complex **4.16** (**a)**, **Scheme 4.5**).

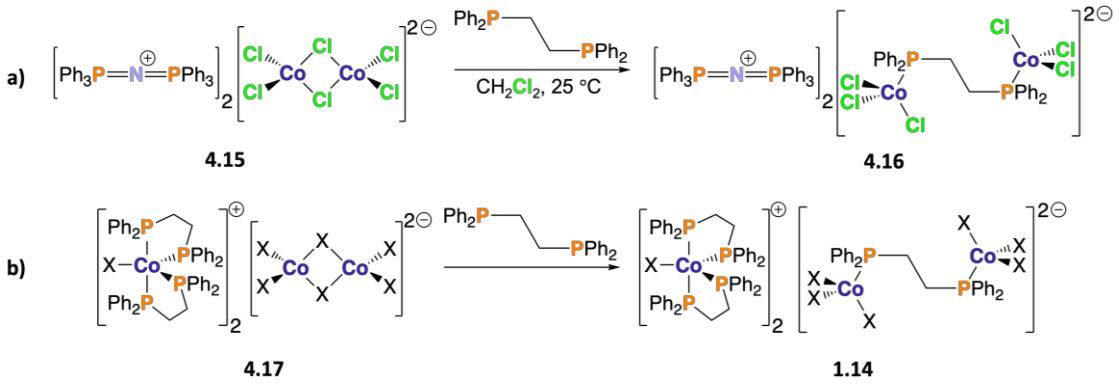


**Scheme 4.5. a)** reaction of dppe and complex **4.15** to afford complex **4.16**; **b)** predicted reaction of complex **4.17** with dppe to afford complex **1.14**.

Confirmation of the successful synthesis of complex **4.16** by obtaining a molecular structure (**Section 4.3.5**) reveals that the $[Co_2X_6]$ dianion can react with dppe. Hence, complex **1.14** is afforded *via* the reaction described in **b)** in **Scheme 4.5**.

### 4.3.5 Solid-State Molecular Structures of $[PPN]_2[Co_2Cl_6]$ (4.15) and $[PPN]_2[Cl_3Co\text{-}dppe\text{-}CoCl_3]$ (4.16)

Single crystals of complexes **4.15** and **4.16** were obtained and molecular structures determined (**Figure 4.6**).

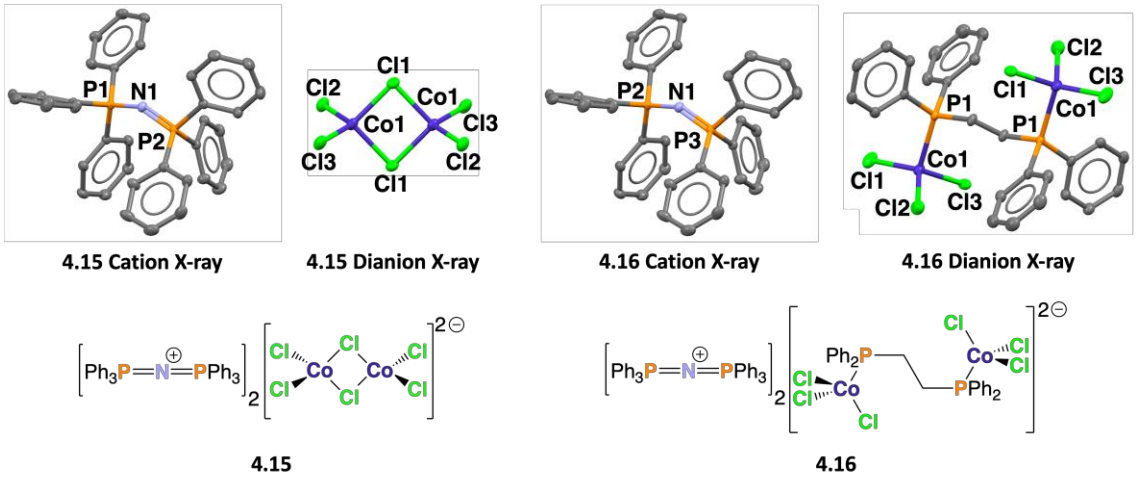


**Figure 4.6.** Solid-state molecular structures of the cations and dianions of complexes **4.15** and **4.16**. Thermal ellipsoids are shown at the 50 % probability level. *NB* hydrogen atoms and a DCM molecule for complex **4.15** have been omitted for clarity. Atom colour: carbon – grey; nitrogen – light blue; cobalt – dark blue and chlorine – green.

The solid-state structure of complex **4.16** is previously unreported, whereas the solid-state structure of complex **4.15** has been described.[9] The key bond lengths and bond angles measured from the solid-state structures of complexes **4.15** and **4.16** are presented in **Table 4.7** and **Table 4.8**, respectively.

**Table 4.7.** Key bond lengths measured from the solid-state molecular structures of complexes **4.15** and **4.16**. *NB* ' is 1 and '' is 2 for complex **4.15**, and ' is 2 and '' is 3 for complex **4.16**.

| Parameter | 4.15 | 4.16 |
|---|---|---|
| P1-Co1 / Å | – | 2.4000(5) |
| Cl1-Co1 / Å | 2.3462(6) | 2.2532(6) |
| Cl2-Co1 / Å | 2.2328(5) | 2.2531(6) |
| Cl3-Co1 / Å | 2.2223(5) | 2.2526(6) |
| P'-N1 / Å | 1.584(1) | 1.581(2) |
| P''-N1 / Å | 1.584(1) | 1.576(2) |

**Table 4.8.** Key bond angles measured from the solid-state molecular structures of complexes **4.15** and **4.16**. *NB* ‘ is 1 and ‘’ is 2 for complex **4.15**, and ‘ is 2 and ‘’ is 3 for complex **4.16**.

| Parameter | 4.15 | 4.16 |
|---|---|---|
| P’-N1-P’’ / ° | 137.77(9) | 142.1(1) |
| Cl1-Co1-Cl1 / ° | 93.80(2) | – |
| Cl2-Co1-Cl3 / ° | 120.28(2) | 118.23(3) |
| Co1-Cl1-Co1 / ° | 86.20(2) | – |
| Cl1-Co1-Cl2 / ° | 111.97(2) | 114.50(2) |
| Cl1-Co1-Cl3 / ° | 109.67(2) | 106.78(2) |
| Cl2-Co1-Cl3 / ° | 120.28(2) | 118.23(3) |
| P1-Co1-Cl1 / ° | – | 104.36(2) |
| P1-Co1-Cl2 / ° | – | 106.10(2) |
| P1-Co1-Cl3 / ° | – | 105.63(2) |

The key bond lengths and bond angles of complex **4.15** (and the [PPN] cation of complex **4.16**) agree with those in the previously reported structure.[9] The [$Cl_3$Co-$PPh_2CH_2CH_2Ph_2$P-$CoCl_3$] dianion in the solid-state structure of complex **4.16** adopts a ‘splayed’ conformation whereby steric clash between the phenyl groups of the two $PPh_2$ moieties and the two distorted tetrahedral $CoCl_3$ moieties is prevented. The Co1-P1 bond distance (2.4000(5) Å) is very similar to the analogous distance 2.390(1) Å reported for the same dianion in complex **1.14** (X = Cl, **b)**, **Scheme 4.5**).[28]

## 4.4 Reaction of $[CoBr(Ph(CH_2)_2N\{PPh_2\}_2)_2]_2[Co_2Br_6]$ (4.10) with Pyridine

It is proposed that zwitterionic cobalt(II) complex **2.14** is afforded *via* the reaction of the $[Co_2Br_6]$ dianion of *in situ* ionic intermediate **4.18** (analogous in structure to complex **4.10**) with one of the two pyridyl groups in each of the two cations in intermediate **4.18** (**Scheme 4.6**). Ionic cobalt(II) complexes (*e.g.*, complexes **4.1** and **4.9** – **4.11**, **Figure 4.3**) are isolated if there is no suitable heteroatom on a pendant donor group of the ‘PNP’ ligands as the proposed reaction (**Scheme 4.6**) cannot occur. The proposed reactivity of the $[Co_2Br_6]$ dianion is reasonable since the reactivity of the $[Co_2X_6]$ dianion of complex **4.15** with dppe has been established in **Section 4.3.4** (**a)**, **Scheme 4.5**).

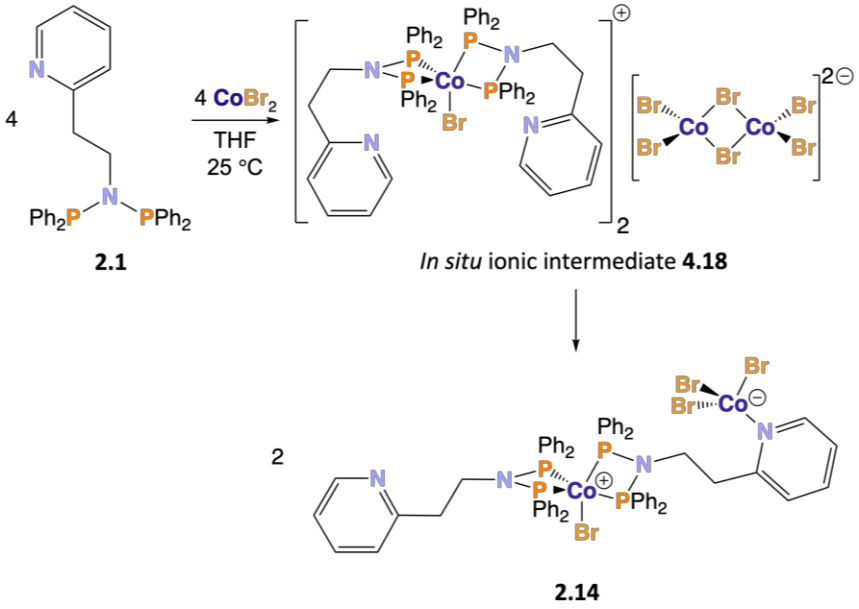


**Scheme 4.6.** Proposed reaction pathway leading to complex **2.14** *via in situ* ionic intermediate **4.18**.

The reaction of pyridine (a model for the pyridyl group in *in situ* ionic intermediate **4.18** in **Scheme 4.6**) with complex **4.10** (produced *in situ* from the 1:1 reaction of compound **2.2** and $CoBr_2$) was studied (**Scheme 4.7**) to verify the existence of *in situ* ionic intermediate **4.18** during the synthesis of zwitterionic cobalt(II) complex **2.14**. If pyridine reacts with the $[Co_2Br_6]$ dianion as proposed in **Scheme 4.7** (producing complex **4.19**), it can be concluded that zwitterionic cobalt(II) complexes with 'PNP' ligands, *e.g.,* **2.14**, are formed *via* an analogous reaction (**Scheme 4.6**).

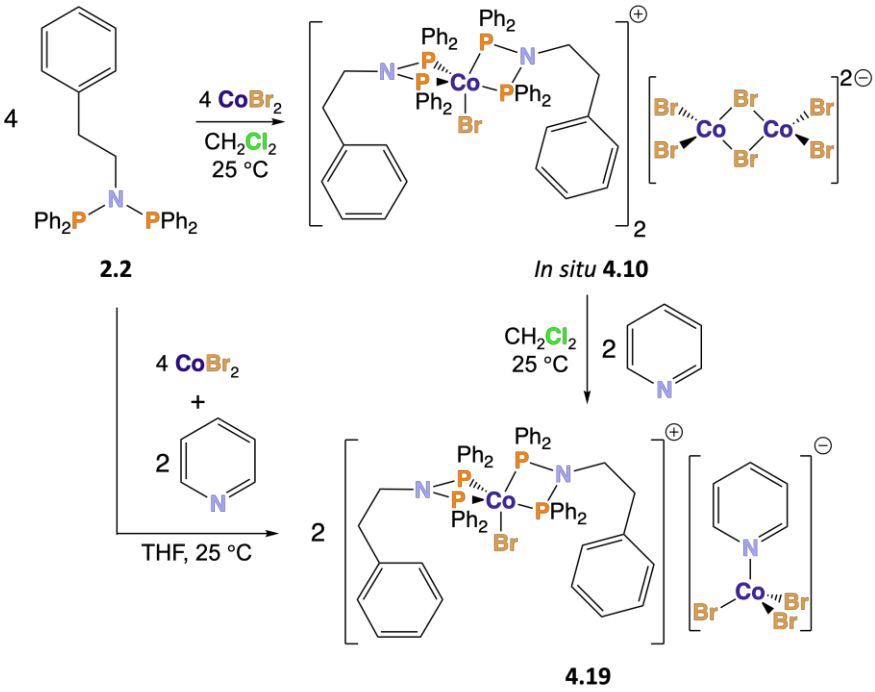


**Scheme 4.7.** Stepwise (in DCM) and 'one pot' (in THF) syntheses of complex **4.19**.

Reaction of pyridine with the $[Co_2Br_6]$ dianion of complex **4.10** was studied by first forming complex **4.10** *in situ* in DCM, from compound **2.2** and $CoBr_2$, followed by pyridine addition after a day of stirring. Additionally, a 'one pot' synthesis was attempted where compound **2.2**, $CoBr_2$ and pyridine were dissolved in THF (from which complex **4.10** precipitates).

Mechanistically, an associative mechanism (involving an intermediate with an increased coordination number, *e.g.,* $L_nMX + Y \rightarrow L_nMXY \rightarrow L_nMY + X$) is expected for the reaction of pyridine with the $[Co_2Br_6]$ dianion (**Scheme 4.8**), as each cobalt(II) in the $[Co_2Br_6]$ dianion can be regarded as having a 15 $e^-$ valence electron count. Other cobalt(II) tetrahedral complexes have been shown by kinetic studies to undergo an associative ligand substitution mechanism.[29]

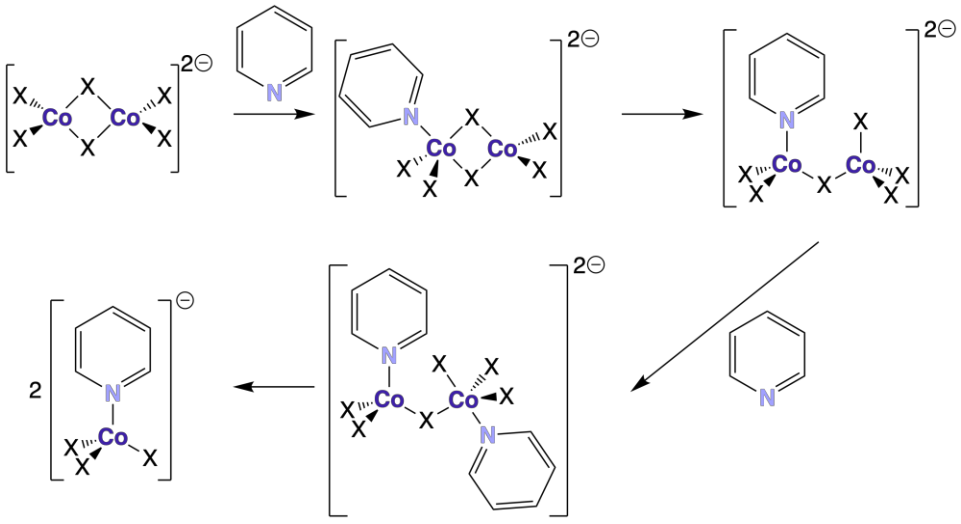

**Scheme 4.8.** Proposed associative mechanism for the reaction of the $[Co_2X_6]$ dianion (X = Cl, Br, I) with two equivalents of pyridine.

## 4.4.1 Solid-State Molecular Structure of $[CoBr(Ph(CH_2)_2N\{PPh_2\}_2)_2][PyCoBr_3]$ (4.19)

Single crystals of complex **4.19** were obtained and a molecular structure determined (**Figure 4.7**). The same molecular structure was obtained from the isolated product of both reaction pathways (**Scheme 4.7**). CHN analysis of the isolated product from both routes in **Scheme 4.7** support the proposed structure of complex **4.19**.

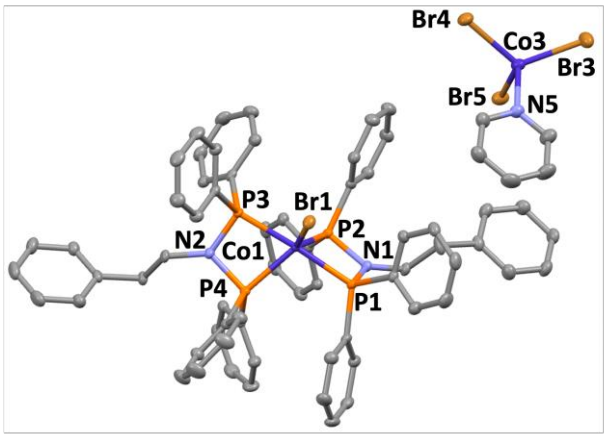


**4.19 X-ray**

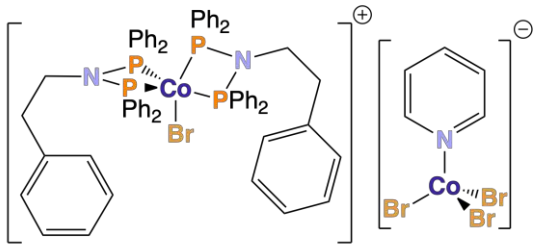


**4.19**

**Figure 4.7.** Solid-state molecular structure of complex **4.19**. Thermal ellipsoids are shown at the 50 % probability level. *NB* hydrogen atoms and DCM molecules are omitted for clarity. Atom colour: carbon – grey; nitrogen – light blue; phosphorus – orange; bromine – orange-brown and cobalt – dark blue.

The key bond lengths and bond angles for the cation and anion of the molecular structure of complex **4.19** (presented in **Table 4.9**) are in agreement with the analogous bond lengths and angles present in the cation of complex **4.10** (**Section 4.2.1**) and the anion of complex **4.14** (**Section 4.3.3**), respectively. The molecular structure of complex **4.19** (**Figure 4.7**) contains a [$PyCoBr_3$] anion consisting of a cobalt(II) centre with three bromide ligands and one pyridine ligand. The [$PyCoBr_3$] anion is afforded from the reaction of the [$Co_2Br_6$] dianion with pyridine as proposed in **Scheme 4.7**. Hence, it can be concluded that zwitterionic cobalt(II) complexes (*e.g.*, complex **2.14**) form as described in **Scheme 4.6**.

**Table 4.9.** Key bond lengths and angles measured from the solid-state molecular structures of complexes **4.19**, **4.10** and **4.11**. *NB* ' has no value, * is 1, ^ is 1, '' is 2 and $ is 3 for complex **4.14**, whilst ' is 3, * is 5, ^ is 3, '' is 4 and $ is 5 for complex **4.19**.

| Parameter | 4.19 | 4.10 | 4.14 |
|---|---|---|---|
| Co1-Br1 / Å | 2.3536(9) | 2.3708(6) | – |
| Co1-P1 / Å | 2.2238(8) | 2.2512(9) | – |
| Co1-P2 / Å | 2.2429(9) | 2.2265(9) | – |
| Co1-P3 / Å | 2.2195(8) | 2.2312(8) | – |
| Co1-P4 / Å | 2.2659(9) | 2.2577(8) | – |
| N1-P1 / Å | 1.686(3) | 1.58(2) | – |
| N1-P2 / Å | 1.709(2) | 1.81(2) | – |
| N2-P3 / Å | 1.684(3) | 1.692(2) | – |
| N2-P4 / Å | 1.720(2) | 1.712(2) | – |
| N*-Co' / Å | 2.051(3) | – | 2.047(2) |
| Co'-Br^ / Å | 2.3842(7) | – | 2.3965(5) |
| Co'-Br'' / Å | 2.3957(5) | – | 2.3898(5) |
| Co'-Br$ / Å | 2.3902(9) | – | 2.3879(5) |
| Br1-Co1-P1 / ° | 94.69(3) | 126.90(3) | – |
| Br1-Co1-P2 / ° | 129.83(3) | 94.47(3) | – |
| Br1-Co1-P3 / ° | 92.89(3) | 96.43(3) | – |
| Br1-Co1-P4 / ° | 122.25(3) | 125.17(3) | – |
| P1-Co1-P2 / ° | 71.57(3) | 71.34(3) | – |
| P1-Co1-P3 / ° | 172.42(4) | 101.62(3) | – |
| P1-Co1-P4 / ° | 104.27(3) | 107.92(3) | – |
| P2-Co1-P3 / ° | 103.60(3) | 169.10(3) | – |
| P2-Co1-P4 / ° | 107.92(3) | 102.39(3) | – |
| P3-Co1-P4 / ° | 71.28(3) | 71.38(3) | – |
| P1-N1-P2 / ° | 100.6(1) | 101(2) | – |
| P3-N2-P4 / ° | 100.3(1) | 100.6(1) | – |
| N*-Co'-Br'' / ° | 105.62(9) | – | 104.74(7) |
| Br^-Co'-Br'' / ° | 117.68(3) | – | 111.99(2) |
| Br^-Co'-Br$ / ° | 113.40(3) | | 113.73(2) |
| N*-Co'-Br$ / ° | 102.41(9) | | 107.46(7) |

## 4.5 Attempted Synthesis of $[CoCl_2\{Py\text{-}o\text{-}(CH_2)_2N(PPh_2)_2\}_2][\{Py\text{-}o\text{-}(CH_2)_2NH_2\}CoCl_3]$ (4.20), $[CoBr_2\{Py\text{-}o\text{-}(CH_2)_2N(PPh_2)_2\}_2][\{Py\text{-}o\text{-}(CH_2)_2NH_2\}CoBr_3]$ (4.21), $[CoCl_2\{Ph(CH_2)_2N(PPh_2)_2\}_2][\{Ph(CH_2)_2NH_2\}CoCl_3]$ (4.22) and $[CoBr_2\{Ph(CH_2)_2N(PPh_2)_2\}_2][\{Ph(CH_2)_2NH_2\}CoBr_3]$ (4.23)

With a view to establishing a rational synthesis of co-crystal **1.20** (**b)**, **Scheme 4.9**),[3] a study of the synthesis of the related co-crystals **4.20** – **4.23** (*via* the 2:1 reaction of either compound **2.1** or **2.2** with either $CoCl_2$ or $CoBr_2$) was undertaken according to **a)**, **Scheme 4.9**. Co-crystals **4.20** – **4.23** could be by-products formed during the 1:1 reaction of 'PNP' compounds with $CoX_2$ (*i.e.*, **Scheme 4.1**, **Section 4.2**). Hence, it is desirable to devise a synthetic protocol to afford co-crystals **4.20** – **4.23** and subsequently characterise them.

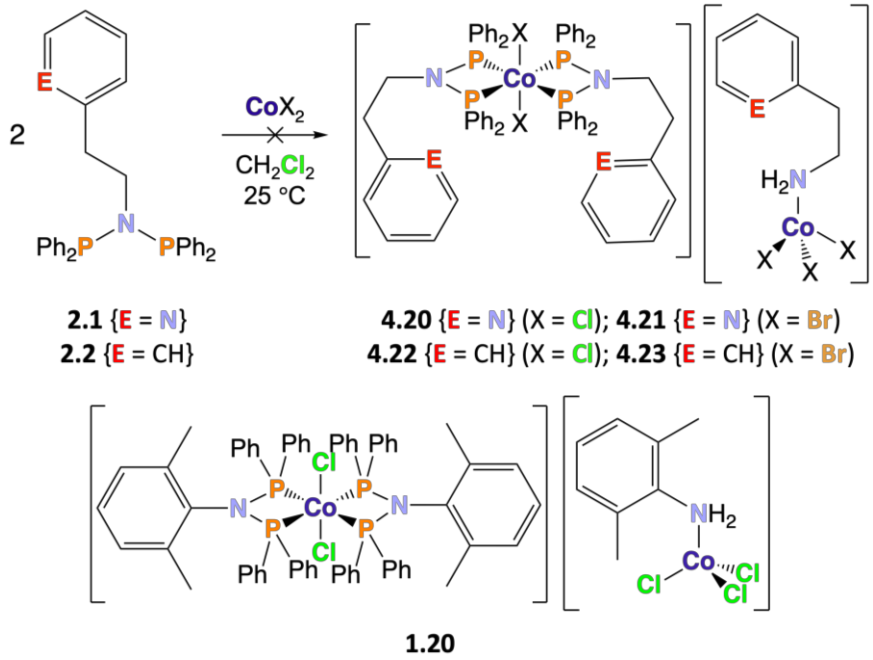


**Scheme 4.9. a)** attempted synthesis of co-crystals **4.20** – **4.23**; **b)** structure of co-crystal **1.20**.[3]

Despite repeated crystallisation attempts, the desired co-crystals **4.20** – **4.23** could not be isolated, with each attempt instead affording complexes **4.7**, **2.14**, **4.9** and **4.11** (**Figure 4.3**), respectively, *i.e.,* the 1:1 'PNP':$CoX_2$ reaction products, despite the 2:1 'PNP':$CoX_2$ reaction stoichiometry. To date, an explanation for the formation of co-crystal **1.20** cannot be devised. The reactivity observed with $\{2,6\text{-}Me_2C_6H_3N(PPh_2)_2\}$ to generate co-crystal **1.20** cannot be replicated using compounds **2.1** and **2.2** studied in this work.[3]

## 4.6 Coordination Chemistry of Py-*o*-$(CH_2)_2N(PPh_2)(Me)$ (2.11) and Py-*o*-$(CH_2)_2N(P\{OPh\}_2)(Me)$ (2.12) with Cobalt(II) Dibromide

Compounds **2.11** and **2.12** were reacted with $CoBr_2$ to afford complexes **4.24** and **4.25** with a view to produce complexes that exhibit $\kappa^2$-*P,N* coordination. However, complexes **4.24** and **4.25** are proposed to react with $H_2O$ to afford complex **4.26** (confirmed by XRD analysis) as shown in **Scheme 4.10**. The origin of $H_2O$ is unclear as the reactions were performed under dry and inert conditions, using dry THF; the same outcome was achieved upon repetition. The N-$PR_2$ bond of complexes **4.24** and **4.25** is hydrolysed and coordination occurs through the newly formed secondary amine moiety and the pyridyl moiety in a $\kappa^2$-*N,N* manner. $PR_2OH$ is presumably produced as a by-product.

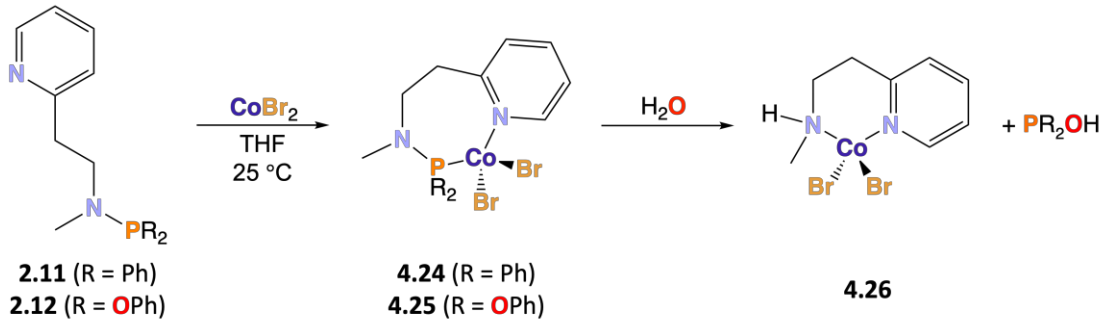


**Scheme 4.10.** Synthesis of complexes **4.24** and **4.25** and their subsequent reaction with $H_2O$ forming complex **4.26**.

The ESI positive ion mass spectrum of the isolated product (complex **4.26** as revealed by the obtained solid-state structure) of the reaction of compound **2.11** with $CoBr_2$ evidences a signal at 523.36 *m/z* corresponding to [**4.24**-Me+H]$^+$. The signal at 523.36 *m/z* evidences the presence of a trace quantity of complex **4.24**, which has not reacted with $H_2O$ to afford complex **4.26**. Hence, complex **4.24** forms in the reaction before P-N bond hydrolysis occurs. An analogous signal is not observed in the ESI positive ion mass spectrum of the isolated product of the reaction of compound **2.12** with $CoBr_2$, suggesting that P-N bond hydrolysis is faster for complex **4.25** than for complex **4.24**. This is likely due to the electron-withdrawing OPh substituents of complex **4.25**, resulting in the phosphorus atom of complex **4.25** being more electron deficient and thereby more susceptible to nucleophilic attack from $H_2O$.

### 4.6.1 Solid-State Molecular Structure of [(MeHN$CH_2CH_2$*o*-Py)$CoBr_2$] (4.26)

Single crystals of complex **4.26** were obtained and a molecular structure determined (**Figure 4.8**). The solid-state structure of the chloro-analogue of complex **4.26**, *i.e.*, [(MeHNCH$_2$CH$_2$*o*-Py)CoCl$_2$], has previously been reported,[30] with the N1-Co1 and N2-Co1 bond distances of 2.034(2) Å and 2.041(3) Å, respectively, showing good similarity with those measured for complex **4.26** (2.028(2) Å and 2.035(3) Å, respectively). The key bond lengths and bond angles measured from the solid-state structure of complex **4.26** are presented in **Table 4.10** and **Table 4.11**, respectively. Further study of complexes **4.24** and **4.25** was abandoned due to their water sensitivity.

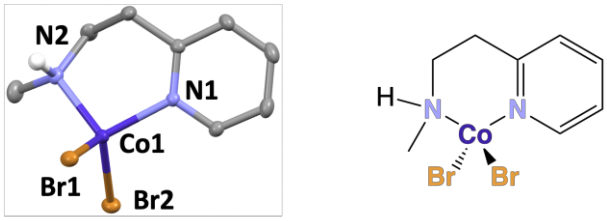


**4.26 X-ray** **4.26**

**Figure 4.8.** Solid-state molecular structure of complex **4.26**. Thermal ellipsoids are shown at the 50 % probability level. *NB* hydrogen atoms (except the NH proton) are omitted for clarity. Atom colour: carbon – grey; nitrogen – light blue; bromine – orange-brown; cobalt – dark blue, and hydrogen – white.

**Table 4.10.** Key bond lengths measured from the solid-state molecular structure of complex **4.26**.

| Bond | Bond Length / Å |
|---|---|
| N1-Co1 | 2.028(2) |
| N2-Co2 | 2.035(3) |
| Br1-Co1 | 2.3837(4) |
| Br2-Co2 | 2.3677(5) |

**Table 4.11.** Key bond angles measured from the solid-state molecular structure of complex **4.26**.

| Angle | Bond Angle / ° |
|---|---|
| Br1-Co1-Br2 | 117.88(2) |
| Br1-Co1-N1 | 111.85(7) |
| Br1-Co1-N2 | 105.81(7) |
| Br2-Co1-N1 | 106.77(7) |
| Br2-Co1-N2 | 113.00(7) |
| N1-Co1-N2 | 100.2(1) |

## 4.7 Coordination Chemistry of Ph(CH$_2$)$_2$N(SPPh$_2$)(PPh$_2$) (2.9) and Ph(CH$_2$)$_2$N(SPPh$_2$)$_2$ (2.10) with Cobalt(II) Dibromide

'SPNP' compound **2.9** was reacted with CoBr$_2$ in a 1:1 ratio (**a)**, **Scheme 4.11**) affording an equilibrium mixture of neutral complex **4.27** and ionic complex **4.28** (analogous to complex **4.10**; **c)**, **Scheme 4.11**). The solid-state molecular structure of complex **4.27** is obtained from XRD analysis of single crystals of the isolated product of the reaction of

compound **2.9** with $CoBr_2$ (**a)**, **Scheme 4.11**). However, the positive ion ESI mass spectrum of the isolated product of the reaction of compound **2.9** with $CoBr_2$ (**a)**, **Scheme 4.11**) evidences no signals assignable to complex **4.27**, instead exhibiting a signal at 1181.96 *m/z* (12.16%) corresponding to cation **4.29** (of complex **4.28**). The presence of the $[Co_2Br_6]$ dianion in complex **4.28** is confirmed by the negative ion ESI mass spectrum exhibiting a signal at 297.84 *m/z*. The magnetic susceptibility measured for the isolated product of the reaction of compound **2.9** with $CoBr_2$ (**a)**, **Scheme 4.11**) *via* the Evans Method (1.13 $\mu_B$ using the molecular weight of **4.27** in the calculation, and 2.21 $\mu_B$ using the molecular weight of **4.28** in the calculation)[23] does not correspond to the calculated magnetic moments for pure complexes **4.27** (3.87 $\mu_B$) and **4.28** (6.92 $\mu_B$) from the spin-only formula (see **Section 4.9**). The lack of agreement between the measured and calculated magnetic moments suggests the presence of multiple paramagnetic species in solution and that complexes **4.27** and **4.28** are in equilibrium in solution (as is the case for complexes **1.42** and **1.43**, **d)** in **Scheme 4.11**).[31,32]

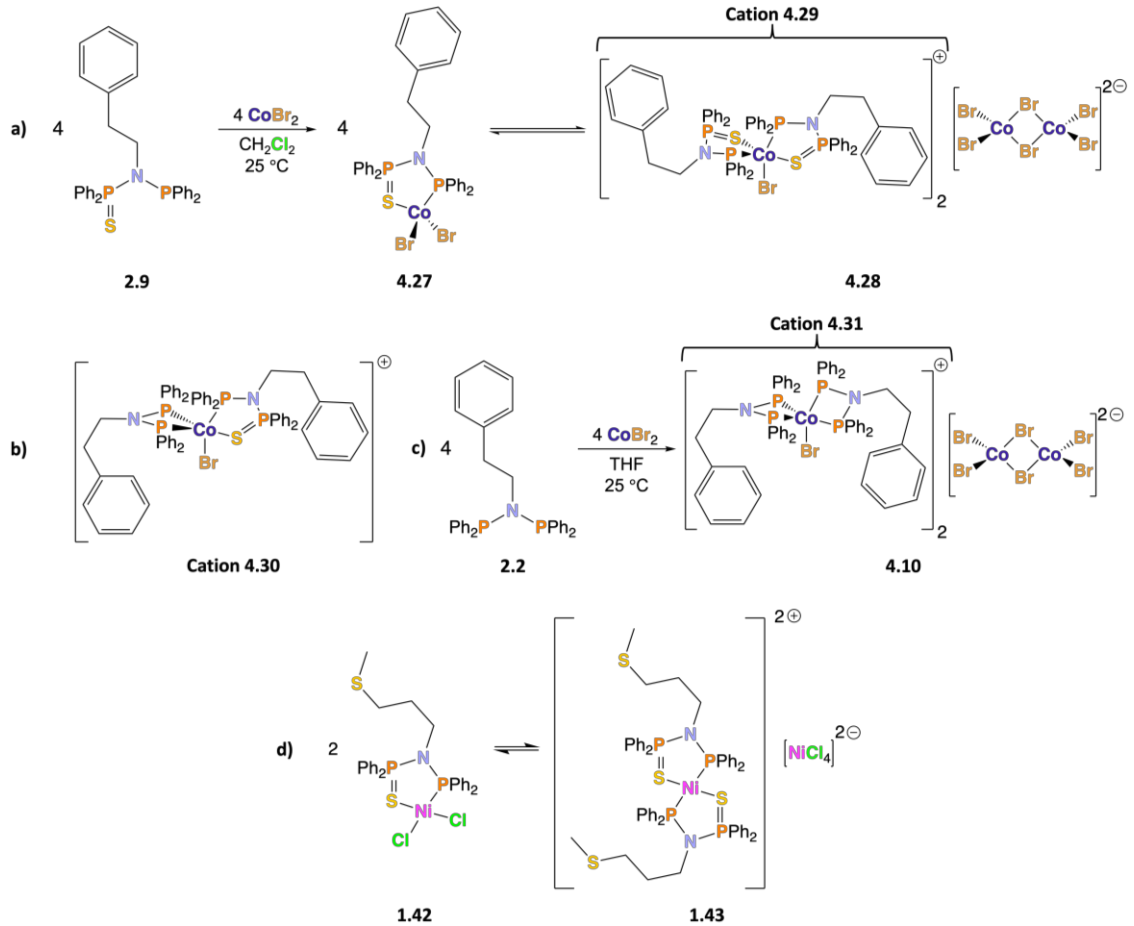


**Scheme 4.11. a)** reaction of compound **2.9** with $CoBr_2$ to afford an equilibrium mixture of complexes **4.27** and **4.28**; **b)** structure of cation **4.30**; **c)** synthesis of complex **4.10**, containing cation **4.31**; **d)** equilibrium mixture of complexes **1.42** and **1.43**.[31,32]

The positive ion ESI mass spectrum of the isolated product of the reaction of compound **2.9** with $CoBr_2$ (**a)**, **Scheme 4.11**) exhibits signals at 1118.30 *m/z* (28.34%) and 1150.08 *m/z* (49.30%). These correspond to cations **4.31** (*i.e.*, the cation of complex **4.10, c)**, **Scheme 4.11**) and **4.30** (**b)**, **Scheme 4.11**), respectively, which contain compound **2.2** (**c)**, **Scheme 4.11**), indicating that compound **2.2** is present in the reaction mixture. Compound **2.2**, present in cations **4.30** and **4.31**, may originate from the sample of compound **2.9** reacted with $CoBr_2$ (**a)**, **Scheme 4.11**) as the $^{31}P\{^1H\}$ NMR spectrum of compound **2.9** (**a)**, **Scheme 4.11**) shows the presence of 4.1% of compound **2.2**. It is also possible that coordination of compound **2.9** to the cobalt(II) centre is promoting the loss of sulfur, resulting in the generation of coordinated compound **2.2**. Greater intensities of the signals in the positive ion ESI mass spectrum corresponding to cations **4.31** and **4.30** relative to the signal corresponding to cation **4.29**, coupled with the small quantity of compound **2.2** present in the sample of compound **2.9** utilised in the reaction of compound **2.9** with $CoBr_2$ (**a)**, **Scheme 4.11**), suggests that complex **4.28** is likely losing sulfur from coordinated **2.9** resulting in the formation of coordinated **2.2**.

Compound **2.10** did not react with $CoBr_2$ (**Scheme 4.12**), as evidenced by the measurement of the magnetic susceptibility of the resultant isolated material *via* the Evans Method[23] suggesting that the isolated material is diamagnetic. Signals observed in the $^{31}P\{^1H\}$ and $^1H$ NMR spectra of the isolated material of **Scheme 4.12** are sharp and well-resolved (and at essentially identical chemical shifts to those seen for compound **2.10**). Hence, a diamagnetic cobalt(II) complex is not formed as broad signals would be observed due to the quadrupolar nature of $^{59}Co$ nuclei ($I$ = 7/2).[33] Instead, the $^{31}P\{^1H\}$ and $^1H$ NMR spectra reveal that the isolated material of **Scheme 4.12** is impure compound **2.10**. Hence, no reaction between compound **2.10** and $CoBr_2$ has taken place.

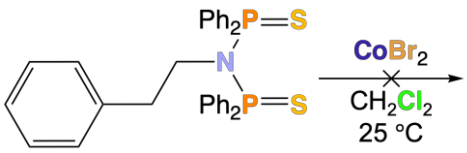


**2.10**

**Scheme 4.12.** Attempted reaction of compound **2.10** with $CoBr_2$.

### 4.7.1 Solid-State Molecular Structure of [(Ph(CH$_2$)$_2$N(SPPh$_2$)(PPh$_2$))CoBr$_2$] (4.27)

Single crystals of complex **4.27** were obtained and a molecular structure determined (**Figure 4.9**). The key bond lengths and bond angles measured from the solid-state structure of complex **4.27** are presented in **Table 4.12** and **Table 4.13**, respectively. The P2-Co1-S1 bite angle of 91.18(3)° is approx. 20° greater than the P-N-P bite angles in complexes **4.1**, **4.5**, **4.7** – **4.11** and **2.14** (**Figure 4.3**), this being due to the fact that complex **4.27** contains 'SPNP' ligand **2.9** rather than an acute bite angle 'PNP' ligand (*i.e.*, RN(PPh$_2$)$_2$). The P2-N1-P1 angle is 118.6(1)°, showing a slight expansion from 114.77(8)° measured in the solid-state structure of compound **2.9** (**Figure 2.2**, **Section 2.4.1**, **Chapter 2**). The P1-N1 bond distance of complex **4.27** of 1.687(2) Å (identical to that measured for compound **2.9**) is shorter than the P2-N1 bond distance of 1.711(2) Å. This P2-N1 bond distance measured for complex **4.27** is slightly shorter than the P2-N1 bond distance of 1.732(1) Å measured for compound **2.9** due to complexation. The P2-S1 bond length measured for compound **2.9** (1.9516(7) Å) is slightly shorter than that measured for complex **4.27** (1.992(1) Å) as a result of complexation. The P2-Co1 bond length of 2.3654(9) Å is close to those measured for complex **4.16** of 2.4000(5) Å (**Figure 4.6**), but longer than those measured for complex **4.7** of ~2.24 – 2.27 Å (**Figure 4.3**). The Co1-S1 bond length is 2.3350(9) Å, which is comparable to the aforementioned P2-Co1 bond length.

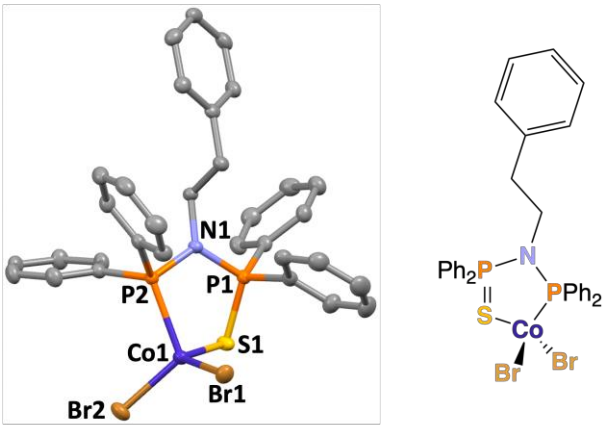


**Figure 4.9.** Solid-state molecular structure of complex **4.27**. Thermal ellipsoids are shown at the 50 % probability level. *NB* hydrogen atoms and disorder are omitted for clarity. Atom colour: carbon – grey; nitrogen – light blue; bromine – orange-brown; cobalt – dark blue, and sulfur – yellow.

**Table 4.12.** Key bond lengths measured from the solid-state molecular structure of complex **4.27**.

| Bond | Bond Length / Å |
|---|---|
| N1-P1 | 1.687(2) |
| N1-P2 | 1.711(2) |
| P2-Co1 | 2.3654(9) |
| P1-S1 | 1.992(1) |
| S1-Co1 | 2.3350(9) |
| Co1-Br1 | 2.3470(4) |
| Co1-Br2 | 2.3444(5) |

**Table 4.13.** Key bond angles measured from the solid-state molecular structure of complex **4.27**.

| Angle | Bond Angle / ° |
|---|---|
| P1-N1-P2 | 118.6(1) |
| S1-Co1-P2 | 91.18(3) |
| S1-Co1-Br1 | 116.00(3) |
| S1-Co1-Br2 | 106.69(3) |
| P2-Co1-Br1 | 111.89(3) |
| P2-Co1-Br2 | 110.81(3) |
| Br1-Co1-Br2 | 117.25(2) |

## 4.7.2 DFT Relative Gibbs Free Energies ($\Delta G_{rel}$) for the Coordination of Py-*o*-$(CH_2)_2N(PPh_2)_2$ (2.1), $Ph(CH_2)_2N(SPPh_2)(PPh_2)$ (2.9) and $Ph(CH_2)_2N(SPPh_2)_2$ (2.10) to Cobalt(II) Dibromide

It is of interest to elucidate the reasoning behind the reaction between compound **2.1** and $CoBr_2$ affording zwitterionic complex **2.14** rather than complex **4.32** (**Scheme 4.13**), and to understand the observation that compound **2.9** coordinates to $CoBr_2$, but compound **2.10** does not. In order to achieve this, the relative gas-phase Gibbs free energies ($\Delta G_{rel}$) for the coordination of compounds **2.1**, **2.9** and **2.10** to $CoBr_2$ have been determined computationally (**Scheme 4.13**). $\Delta G_{rel}$ is calculated using **Equation 4.3**.

$$\Delta G_{rel} = \Sigma G_{product} - \Sigma G_{reactant} \quad \textbf{(4.3)}$$

Values of $G_{product}$ and $G_{reactant}$ were obtained *via* geometry optimisation calculations of compounds **2.1**, **2.9** and **2.10**, complexes **2.14**, **4.27**, hypothetical complexes **4.32** and **4.33**, and $CoBr_2$ as a linear species at the B3LYP/6-31G(d) level. Note that, throughout this thesis, the bond lengths determined from the geometry optimisation calculations evidence good agreement with the bond lengths measured from the solid-state structure of the same compound or complex (when a comparison was possible). Reasoning for the selection of the B3LYP/6-31G(d) level hybrid-DFT functional and basis set is outlined in **Chapter 7**. Optimising $CoBr_2$ as a linear species, despite having a polymeric structure,[34] is a valid approach previously utilised for similar published

calculations, including those involving $NiCl_2$ (also optimised as a linear species despite being polymeric).[32] *NB* the discrete $[Co\{Ph(CH_2)_2N(PPh_2)_2\}_2Br]$ cation and $[Co_2Br_6]$ dianion present in complex **4.10** underwent successful geometry optimisations at the B3LYP/6-31G(d) level. However, the geometry optimisation of the large complex **4.10** containing both charged species at the B3LYP/6-31G(d) level could not be carried out due to the limited computing resources available, preventing determination of $\Delta G_{rel}$. The obtained computational $\Delta G_{rel}$ results are shown in **Scheme 4.13**.

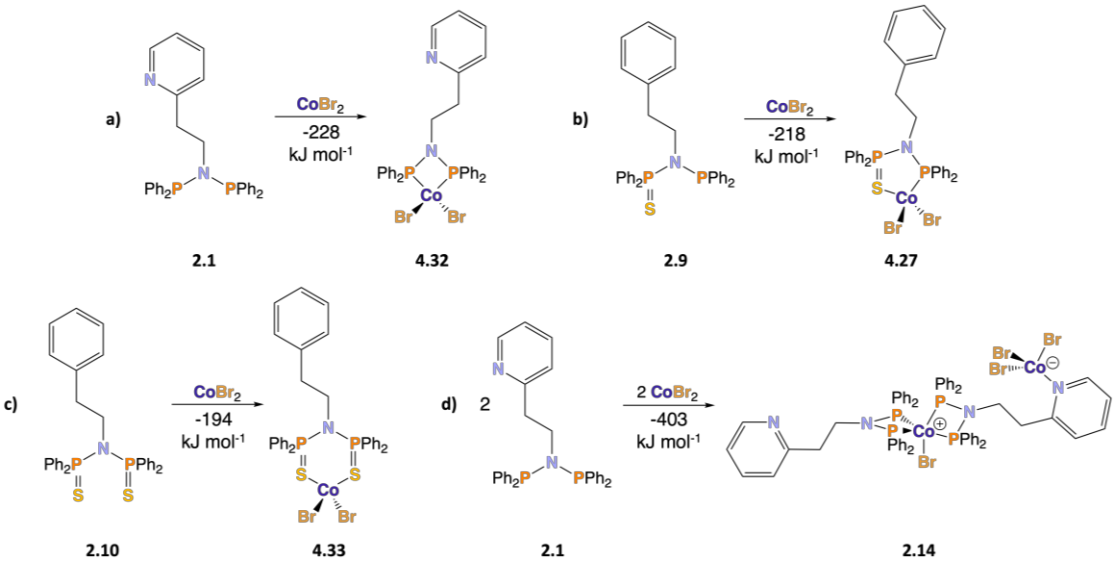


**Scheme 4.13.** The reactions and associated calculated $\Delta G_{rel}$ values for the coordination of **a) 2.1** to afford complex **4.32**, **b) 2.9** to afford complex **4.27**, **c) 2.10** to afford complex **4.33** and **d) 2.1** to afford complex **2.14**, with $CoBr_2$.

The $\Delta G_{rel}$ values of –228 kJ mol$^{-1}$ and –403 kJ mol$^{-1}$ for **a)**, formation of hypothetical complex **4.32**, and **d)**, formation of complex **2.14** (**Scheme 4.13**), respectively, illustrate that the formation of zwitterionic complex **2.14** is significantly more thermodynamically favourable, potentially explaining why complex **4.32** is not observed. Comparison of $\Delta G_{rel}$ values of –228 kJ mol$^{-1}$, –218 kJ mol$^{-1}$ and –194 kJ mol$^{-1}$ for **a)**, **b)** and **c)**, respectively (a valid comparison as the effect of the pyridyl group in **a)** *vs*. the phenyl group in **b)** and **c)** is likely minimised), reveals that the formation of complex **4.27** and hypothetical complexes **4.32** and **4.33** becomes less thermodynamically favourable as the number of sulfur atoms added to the 'PNP' scaffold increases from none in **2.1**, one in **2.9** ('SPNP') to two in **2.10** ('SPNPS'), which may explain why complex **4.33** does not form (**Scheme 4.13**). An analogous study of the coordination chemistry of $NiCl_2$ complexes shows the same trend, with $\Delta E_{rel}$ values of –300 kJ mol$^{-1}$, –245 kJ mol$^{-1}$ and –163 kJ mol$^{-1}$ being obtained for the reactions of 'PNP' ($MeS(CH_2)_3N(PPh_2)_2$), 'SPNP'

($MeS(CH_2)_3N(PPh_2)(SPPh_2)$) and 'SPNPS' ($MeS(CH_2)_3N(SPPh_2)_2$) compounds with $NiCl_2$, respectively.[32]

In conclusion, 'SPNP' compound **2.9** reacts with $CoBr_2$ affording an equilibrium mixture of complexes **4.27** and **4.28** (**a**), **Scheme 4.11**), whereas 'SPNPS' compound **2.10** does not react with $CoBr_2$ (**Scheme 4.12**). Computationally determined $\Delta G_{rel}$ values for the formation of complex **4.27** and hypothetical complex **4.33** provide a rationale for the observed reactivity trend.

## 4.8 Hybrid-DFT Studies to determine the Gibbs free energy change for the formation of [(*P,P*)$CoCl_2$] *vs*. [(*P,P*)$_2$CoCl]Cl complexes

In order to rationalise why the reaction of $CoX_2$ (X = Cl, Br, I) with dppe affords complexes **1.14** and **1.15** ($[CoX(dppe)_2]_2[X_3Co\text{-}PPh_2CH_2CH_2Ph_2P\text{-}CoX_3]$),[28] but the reaction of $CoCl_2$ with dppp affords [(dppp)$CoCl_2$] (**Section 1.1.2**, **Chapter 1**),[35] the Gibbs free energy changes for the formation of neutral complexes **4.34** – **4.36**, as well as their corresponding ionic complexes **4.37** – **4.39**, were determined (**Figure 4.10**). The study of ionic complexes **4.37** – **4.39** of the form [(*P,P*)$_2$CoCl]Cl with the Cl anion, rather than complex **4.9** ($[CoCl(Ph(CH_2)_2N\{PPh_2\}_2)_2]_2[Co_2Cl_6]$), allows for the issues arising from an inability to optimise complexes **4.9** – **4.11**, outlined in **Section 4.7.2**, to be overcome. Complex **4.37** is synthetically accessible, with a published solid-state structure[28] (utilised as a suitable starting point for the geometry optimisations of complexes **4.37** – **4.39**).

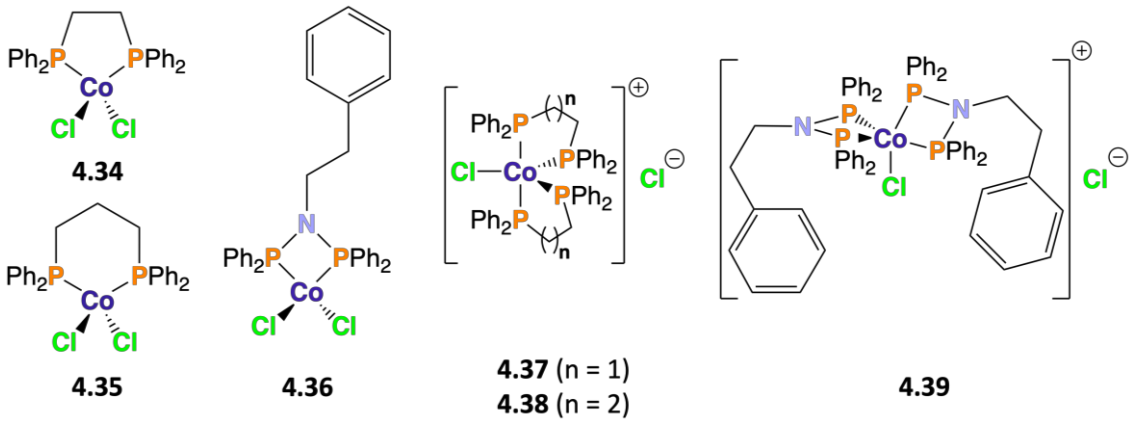


**Figure 4.10.** Structures of complexes **4.34** – **4.39**.

The gas-phase Gibbs free energy changes of formation for complexes **4.34** – **4.39** (obtained by geometry optimisation calculations of complexes **4.34** – **4.39**, their

corresponding ligands, and $CoCl_2$ as a linear species in the quartet state at the B3LYP/6-31G(d) level and utilisation of **Equation 4.3**, **Section 4.7.2**) are shown in **Table 4.14**.

**Table 4.14.** The computationally calculated gas-phase Gibbs free energy change of formation ($\Delta G_F$) of complexes **4.34** – **4.39**.

| Complex | $\Delta G_F$ / kJ mol$^{-1}$ |
|---|---|
| **$[CoCl_2(Ph_2P(CH_2)_2PPh_2)]$ (4.34)** | –235 |
| **$[CoCl_2(Ph_2P(CH_2)_3PPh_2)]$ (4.35)** | –255 |
| **$[CoCl_2(Ph\{CH_2\}_2N(PPh_2)_2)]$ (4.36)** | –230 |
| **$[CoCl(Ph_2P(CH_2)_2PPh_2)_2]Cl$ (4.37)** | –13 |
| **$[CoCl(Ph_2P(CH_2)_3PPh_2)_2]Cl$ (4.38)** | 31 |
| **$[CoCl\{Ph(CH_2)_2N(PPh_2)_2\}_2]Cl$ (4.39)** | –61 |

The data in **Table 4.14** show that the Gibbs free energy of formation is more favourable for neutral complexes **4.34** – **4.36** relative to their analogous ionic complexes **4.37** – **4.39**. Comparison of the energies of neutral and ionic complexes has proven to be challenging previously in the Dyer group as the results are very dependent upon the DFT method utilised. Hence, comparison between a neutral complex and its ionic analogue has been deemed to be unreliable, and has been avoided in this work. Comparison within the neutral complex and ionic complex series' are still useful; comparison of the Gibbs free energies of formation of [(*P,P*)$CoCl_2$] complexes **4.34** – **4.36** clearly shows that the Gibbs free energy of formation decreases, and hence complex stability increases, as the bite angle of the diphosphine in the complex increases. In contrast, comparison of the Gibbs free energies of formation of ionic [$(P,P)_2$CoCl]Cl complexes **4.37** – **4.39** evidences that the Gibbs free energy of formation decreases, and hence complex stability increases, as the bite angle of diphosphine in the complex decreases.

In conclusion, the experimental accessibility of complexes **4.35** (**Figure 4.10**), with larger bite angle dppp ligand, and **4.37** (**Figure 4.10**), **1.14** and **4.9** (**Figure 4.11**), with smaller bite angle dppe and 'PNP' ligands, can be rationalised by computationally determined $\Delta G_F$ values (**Table 4.14**). The aforementioned trends likely stem from diphosphine ligands with smaller bite angles (*e.g.*, ~70 – 85°) better stabilising the trigonal bipyramidal geometry of $[Co(P,P)_2X]^+$, and diphosphine ligands with larger bite angles (~90° and above) better stabilising the tetrahedral geometry of [(*P,P*)$CoCl_2$].

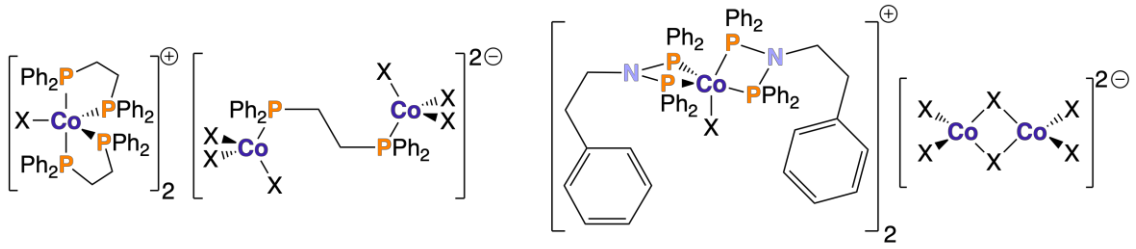


**Figure 4.11.** Structures of complexes **1.14**[28] and **4.9**.

## 4.9 Measuring $\mu_{eff}$ to Determine the Number of Unpaired Electrons in Cobalt Complexes

The effective magnetic moment, $\mu_{eff}$, has been determined *via* the Evans NMR method[23] to further characterise an array of representative cobalt complexes synthesised and discussed in **Chapter 4**. A summary of the measured $\mu_{eff}$ values, as well as the calculated spin-only $\mu_{eff}$ values for the aforementioned cobalt complexes is given in **Table 4.15**. The spin-only $\mu_{eff}$ value for the whole formula unit was predicted by combining the predicted values of $\mu_{eff}$ for each distinct constituent metal centre as shown in **Equation 4.4**:

$$\mu_{eff} = \sqrt{\sum_{i=1}^{x} (n_i(n_i+2))} \qquad \textbf{(4.4)}$$

where $n_i$ is the number of unpaired electrons on metal centre i, with values of i ranging from 1 to the upper limit of summation x. An example of utilising **Equation 4.4** is shown in **Section 7.22**. The spin-only formula assumes that the orbital angular momentum of the d electrons is completely quenched. However, many of the experimentally measured $\mu_{eff}$ values quoted in **Table 4.15** deviate positively from the calculated spin-only $\mu_{eff}$ value, as they theoretically should for many cobalt(I), cobalt(II) and cobalt(III) complexes with $d^8$, $d^7$ and $d^6$ electron configurations, respectively. This is due to the orbital angular momentum of the d electrons being incompletely quenched; this effect is particularly evident when the d subshell is more than half occupied (*i.e.,* $n > 5$ in $d^n$). Here, the spin-orbit coupling interaction ($\lambda$, with $\lambda < 0$ for $n > 5$ in $d^n$) results in the orbital angular momentum (L) and the spin (S) being in concert, *i.e.,* parallel, which augments $\mu_{eff}$ to a value greater than that predicted by the spin-only formula due to the addition

of the magnetic moment arising from the orbital angular momentum to the magnetic moment arising from the spin.[36]

**Table 4.15.** The measured (*via* the Evans NMR method) and calculated $\mu_{eff}$ values for complexes **2.14**, **3.25**, **4.1**, **4.3** – **4.11**, **4.14** – **4.16** and **4.19**. *NB* ^ indicates that 6.92 is calculated for spin-only formula if an ionic structure is assumed. All $\mu_{eff}$ values were measured in $CD_2Cl_2$. $\mu_{eff}$ could not be measured for complex **4.2** due to solubility issues.

| Complex | Measured $\mu_{eff}$ / $\mu_B$ | Predicted Spin-only $\mu_{eff}$ / $\mu_B$ |
|---|---|---|
| **[CoBr(Py-*o*-$(CH_2)_2$N{$PPh_2$}$_2$)({$Br_3$Co}Py-*o*-$(CH_2)_2$N{$PPh_2$}$_2$)] (2.14)** | 4.94 | 4.24 |
| **[N(*n*-Pr)$_4$][({$Cl_3$Co}Py-*o*-$(CH_2)_2$N($PPh_2$)$_2$)$PdCl_2$] (3.25)** | 4.04 | 3.87 |
| **[CoBr(*n*-BuN{$PPh_2$}$_2$)$_2$]$_2$[$Co_2Br_6$] (4.1)** | 6.55 | 4.69 |
| **[CoBr(Ph-$C_6H_4$N{$PPh_2$}$_2$)$_2$]$_2$[$Co_2Br_6$] (4.3)** | 6.28 | 4.69 |
| **[CoBr(Py-*o*-$C_6H_4$N{$PPh_2$}$_2$)$_2$]$_2$[$Co_2Br_6$] (4.4)** | 5.54 | 4.69^ |
| **[CoBr($Me_2$N$(CH_2)_3$N{$PPh_2$}$_2$)({$Br_3$Co}$Me_2$N$(CH_2)_3$N{$PPh_2$}$_2$)] (4.5)** | 5.16 | 4.24 |
| **[(Py-*o*-$(CH_2)_2$N$(CH_2PPh_2)_2$)$CoBr_2$] (4.6)** | 3.61 | 3.87 |
| **[CoCl(Py-*o*-$(CH_2)_2$N{$PPh_2$}$_2$)({$Cl_3$Co}Py-*o*-$(CH_2)_2$N{$PPh_2$}$_2$)] (4.7)** | 5.19 | 4.24 |
| **[CoI(Py-*o*-$(CH_2)_2$N{$PPh_2$}$_2$)({$I_3$Co}Py-*o*-$(CH_2)_2$N{$PPh_2$}$_2$)] (4.8)** | 4.80 | 4.24 |
| **[CoCl(Ph$(CH_2)_2$N{$PPh_2$}$_2$)$_2$]$_2$[$Co_2Cl_6$] (4.9)** | 6.07 | 4.69 |
| **[CoBr(Ph$(CH_2)_2$N{$PPh_2$}$_2$)$_2$]$_2$[$Co_2Br_6$] (4.10)** | 6.00 | 4.69 |
| **[CoI(Ph$(CH_2)_2$N{$PPh_2$}$_2$)$_2$]$_2$[$Co_2I_6$] (4.11)** | 5.83 | 4.69 |
| **[N(*n*-Pr)$_4$][$PyCoBr_3$] (4.14)** | 4.04 | 3.87 |
| **[PPN]$_2$[$Co_2Cl_6$] (4.15)** | 5.47 | 4.00 |
| **[PPN]$_2$[$Cl_3$Co-dppe-$CoCl_3$] (4.16)** | 6.43 | 5.47 |
| **[CoBr(Ph$(CH_2)_2$N{$PPh_2$}$_2$)$_2$][$PyCoBr_3$] (4.19)** | 5.13 | 4.24 |

Complexes **4.14**, **3.25** and **4.6** (**Figure 4.12**) only contain a tetrahedral cobalt(II) ($d^7$) centre with three unpaired electrons. The value of $\mu_{eff}$ is expected to be between 4 – 5 $\mu_B$,[37] which is the case for complexes **4.14** and **3.25**. However, the $\mu_{eff}$ value measured for complex **4.6** is lower than the expected 4 – 5 $\mu_B$ range,[37] with the exact reason for

this being uncertain. The structural assignment of complex **4.6** may be incorrect, but without a solid-state structure this is difficult to say.

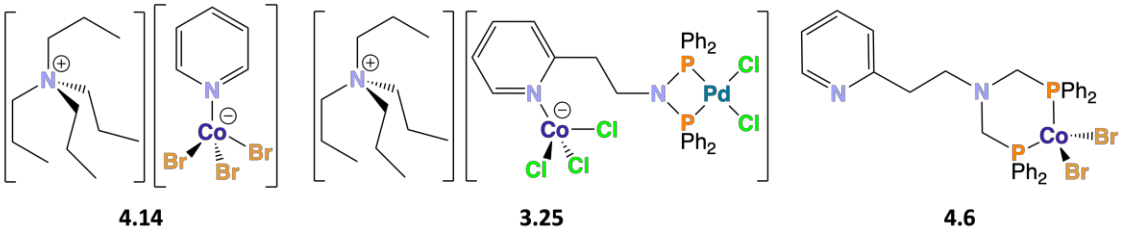

**4.14** **3.25** **4.6**

**Figure 4.12.** Structures of complexes **4.14**, **3.25** and **4.6**.

Homobinuclear complex **4.16** (**Figure 4.13**) has two distorted tetrahedral cobalt(II) centres, therefore a spin-only $\mu_{eff}$ value of 5.47 $\mu_B$ can be predicted (a summative $\mu_{eff}$ value for six unpaired electrons, with three per cobalt(II) centre, assuming no magnetic coupling between the cobalt(II) centres). A $\mu_{eff}$ value of 6.43 $\mu_B$ was measured for complex **4.16**, suggesting a lack of magnetic coupling between the cobalt(II) centres. A lack of magnetic coupling in the [$Cl_3Co$-$PPh_2CH_2CH_2Ph_2P$-$CoCl_3$] dianion in complex **4.16** is evidenced in the reported $\mu_{eff}$ value of 8.39 $\mu_B$ for complex **1.14** (X = Cl, **Figure 4.13**),[28] corresponding to eight unpaired electrons (one per each equivalent of [Co(*P,P*)$_2$Cl] cation and six in the [$Cl_3Co$-$PPh_2CH_2CH_2Ph_2P$-$CoCl_3$] dianion).

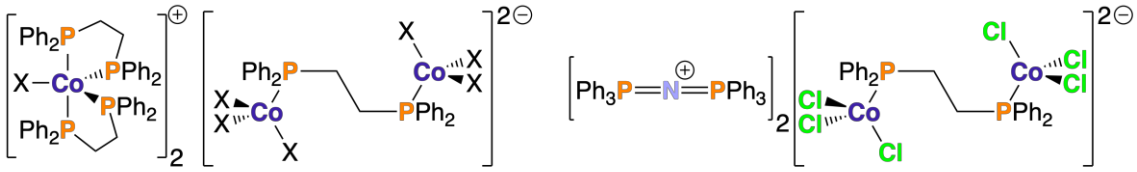

**1.14** **4.16**

**Figure 4.13.** Structures of complexes **1.14**[28] and **4.16**.

Zwitterionic complexes **2.14**, **4.5**, **4.7** and **4.8** (**Figure 4.14**) contain both a cationic distorted trigonal bipyramidal cobalt(II) centre with a single unpaired electron, and an anionic distorted tetrahedral cobalt(II) centre with three unpaired electrons. This results in four unpaired electrons overall, and a summative spin-only $\mu_{eff}$ value of 4.24 $\mu_B$ is calculated. The experimentally-determined $\mu_{eff}$ values for complexes **2.14**, **4.5**, **4.7** and **4.8** are slightly greater than the predicted spin-only $\mu_{eff}$ value of 4.24 $\mu_B$. Additionally, these values are very similar to the $\mu_{eff}$ value of 5.22 $\mu_B$ determined for complex **1.16** (**Figure 4.14**) in the solid-state,[1] verifying that the overall $\mu_{eff}$ is the sum of the magnetic properties of both cobalt(II) centres present in complexes **2.14**, **4.5**, **4.7** and **4.8**. Complex **4.19** (**Figure 4.14**), analogous in structure to zwitterionic complexes **2.14**, **4.5**,

**4.7** and **4.8** with the exception that the two cobalt(II) centres are in different ions, has a measured $\mu_{eff}$ value of 5.13 $\mu_B$. Hence, the $\mu_{eff}$ value of complex **4.19** is the sum of the magnetic properties of both cobalt(II) centres present in the different ions.

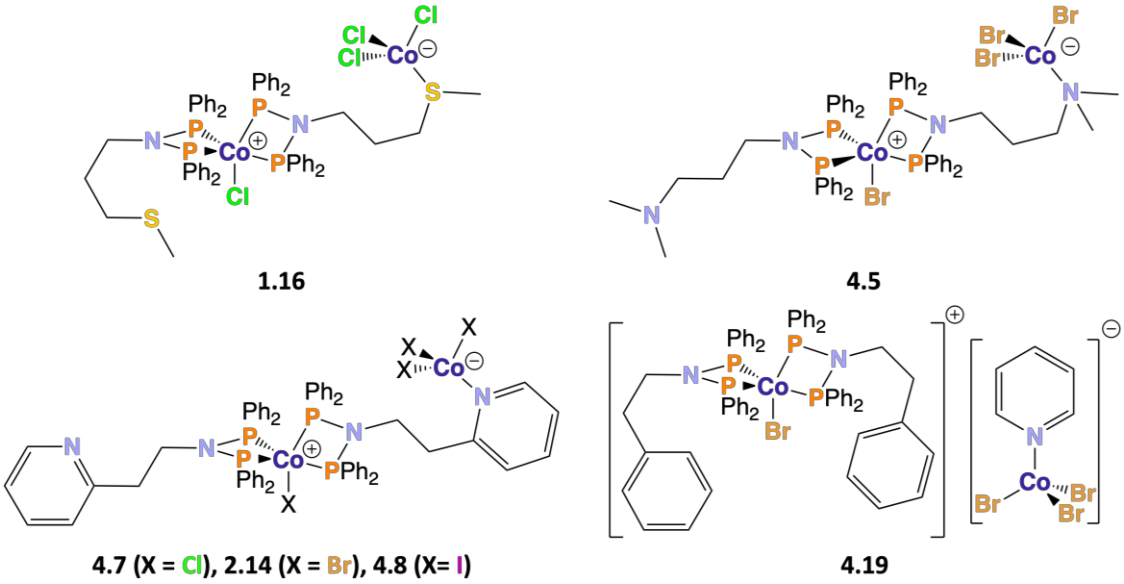


**Figure 4.14.** Structures of complexes **1.16**,[1] **4.5**, **4.7**, **2.14**, **4.8** and **4.19**.

The $\mu_{eff}$ value for complex **4.15** (**Figure 4.15**) has been determined to be 5.47 $\mu_B$, showing good similarity to the $\mu_{eff}$ values of 5.80 $\mu_B$ and 5.9(2) $\mu_B$ previously reported for complex **4.15** in the solid-state[9] and complex **4.40** (**Figure 4.15**) in solution, respectively.[38] A $\mu_{eff}$ value of 5.47 $\mu_B$ suggests that the $[Co_2Cl_6]$ dianion of complex **4.15** contains four unpaired electrons. Six unpaired electrons could be expected, with three unpaired electrons each for both distorted tetrahedral cobalt(II) centres. Hence, the $\mu_{eff}$ values of complex **4.15** suggests that there is antiferromagnetic coupling of two of the unpaired spins across the bridging dihalide (dichloride for complex **4.15**).[38]

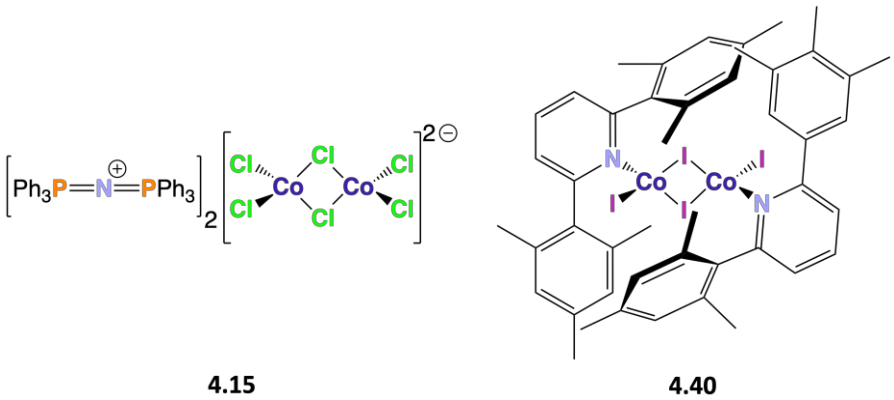


**Figure 4.15.** Structures of complexes **4.15** and **4.40**.[38]

Ionic cobalt(II) complexes **4.1**, **4.3**, **4.4**, and **4.9** – **4.11** (**Figure 4.16**) contain the $[Co_2X_6]$ dianion (with four unpaired electrons) with two distorted tetrahedral cobalt(II) centres and two cationic distorted trigonal bipyramidal cobalt(II) centres (each with one unpaired electron). The $\mu_{eff}$ values determined for complexes **4.1**, **4.3**, **4.4**, and **4.9** – **4.11** are in the range of 5.54 – 6.55 $\mu_B$, which are slightly greater than the spin-only summative $\mu_{eff}$ value of 4.69 $\mu_B$ (for six unpaired electrons in total).

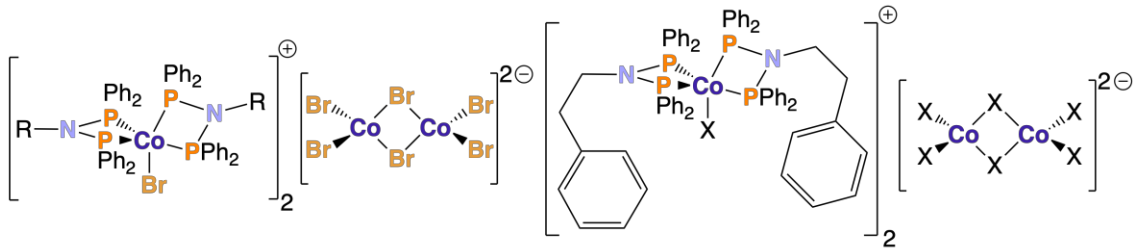


**Figure 4.16.** Structures of complexes **4.1**, **4.3**, **4.4**, and **4.9** – **4.11**.

All of the determined magnetic moments (**Table 4.15**) are entirely consistent with the solid-state structures of the aforementioned complexes being retained in solution and show good similarity with the magnetic moments estimated from the spin-only formula.

## 4.10 Summary

The 1:1 reaction of 'PNP' compounds with cobalt halides has been shown to generate zwitterionic (*e.g.*, $[CoX(Py\text{-}o\text{-}(CH_2)_2N\{PPh_2\}_2)(\{X_3Co\}Py\text{-}o\text{-}(CH_2)_2N\{PPh_2\}_2)]$, complexes **4.7**, **2.14** and **4.8** with X = Cl, Br and I, respectively, from the 1:1 reaction of Py-*o*-$(CH_2)_2N(PPh_2)_2$, compound **2.1**, with $CoX_2$) and ionic (*e.g.*, $[CoX(Ph(CH_2)_2N\{PPh_2\}_2)_2]_2[Co_2X_6]$, complexes **4.9**, **4.10** and **4.11** with X = Cl, Br and I, respectively, from the 1:1 reaction of $Ph(CH_2)_2N(PPh_2)_2$, compound **2.2**, with $CoX_2$) complexes. The same zwitterionic and ionic complexes were isolated from reactions with 'PNP':$CoX_2$ ratios of 1:1 and 2:1. The formation of ionic complexes (afforded when the 'PNP' ligand does not contain a suitable heteroatom allowing for zwitterionic complex formation) has been evidenced for the first time in this work. The solid-state molecular structures of zwitterionic and ionic complexes, determined by XRD analysis of obtained single crystals, are retained in solution as evidenced by $\mu_{eff}$ measurements and ESI mass spectrometric analysis. The formation of zwitterionic complex **2.14** as opposed

to the hypothetical ([(Py-*o*-$(CH_2)_2N(PPh_2)_2$)$CoBr_2$] (complex **4.32**) has been justified by the lower $\Delta G_{rel}$ obtained for complex **2.14** (**Section 4.7.2**). Zwitterionic complex formation *via* an *in situ* ionic complex intermediate (**Scheme 4.6**) has been verified by the synthesis of [$CoBr(Ph(CH_2)_2N\{PPh_2\}_2)_2$][$PyCoBr_3$] (complex **4.19**) from the reaction described in **Scheme 4.7**.

Reaction of Py-*o*-$(CH_2)_2N(PPh_2)(Me)$ and Py-*o*-$(CH_2)_2N(P\{OPh\}_2)(Me)$ (compounds **2.11** and **2.12**, respectively) with $CoBr_2$ afforded [$(MeHNCH_2CH_2o\text{-}Py)CoBr_2$] (complex **4.26**) *via* P-N bond cleavage. $Ph(CH_2)_2N(P\{S\}Ph_2)_2$ (compound **2.10**) did not react with $CoBr_2$, whereas the reaction of $Ph(CH_2)_2N(P\{S\}Ph_2)(PPh_2)$ (compound **2.9**) with $CoBr_2$ affords an equilibrium mixture of [$(Ph(CH_2)_2N(SPPh_2)(PPh_2))CoBr_2$] and [$CoBr\{Ph(CH_2)_2N(SPPh_2)(PPh_2)\}_2]_2[Co_2Br_6$] (complexes **4.27** and **4.28**, respectively). Hence, the reactivity of cobalt complexes containing 'SPNP' ligands will not be further studied. Note that the reactivity of cobalt complexes containing 'PCNCP' ligands will also not be further studied due to the lack of a solid-state structure (and hence complete certainty in the structure) of [(Py-*o*-$(CH_2)_2N(CH_2PPh_2)_2$)$CoBr_2$] (complex **4.6**).

Determination and comparison of the Gibbs free energies of formation of [$CoCl_2(Ph_2P(CH_2)_2PPh_2)$], [$CoCl_2(Ph_2P(CH_2)_3PPh_2)$] and [$CoCl_2(Ph\{CH_2\}_2N(PPh_2)_2)$] (neutral complexes **4.34** – **4.36**, respectively) revealed that the Gibbs free energy of formation decreases as the bite angle of the diphosphine in the complex increases. In contrast, the same analysis for [$CoCl(Ph_2P(CH_2)_2PPh_2)_2$]Cl, [$CoCl(Ph_2P(CH_2)_3PPh_2)_2$]Cl and [$CoCl\{Ph(CH_2)_2N(PPh_2)_2\}_2$]Cl (ionic complexes **4.37** – **4.39**, respectively) evidenced that the Gibbs free energy of formation decreases as the bite angle of diphosphine in the complex decreases. Hence, complexes of the form [(*P,P*)$CoCl_2$] are more stable with larger bite angle diphosphines, whereas complexes of the form [$(P,P)_2$CoCl]Cl are more stable with smaller bite angle diphosphines, agreeing with the synthetic accessibility of complex **4.35**, with larger bite angle dppp ligand, and complexes **4.37**, [$CoX(Ph_2PCH_2CH_2PPh_2)_2]_2[X_3Co\text{-}PPh_2CH_2CH_2Ph_2P\text{-}CoX_3$] (complex **1.14**) and [$CoCl(Ph(CH_2)_2N\{PPh_2\}_2)_2]_2[Co_2Cl_6$] (complex **4.9**), with smaller bite angle dppe and 'PNP' ligands.

## References

1. C. Fliedel, V. Rosa, B. Vileno, N. Parizel, S. Choua, C. Gourlaouen, P. Rosa, P. Turek, P. Braunstein, *Inorg. Chem.*, **2016**, *55*, 4183 – 4198. 10.1021/acs.inorgchem.5b02889
2. D. Naicker, H. B. Friedrich, B. Omondi, *RSC Adv*., **2015**, *5*, 63123 – 63129. 10.1039/C5RA07365K
3. K. Naktode, R. K. Kottalanka, H. Adimulam, T. K. Panda, *J. Coord. Chem*., **2014**, *67*, 3042 – 3053. 10.1080/00958972.2014.953071
4. U. Omoruyi, S. J. Page, S. L. Apps, A. J. P. White, N. J. Long, P. W. Miller, *J. Organomet. Chem*., **2021**, *935*, 121650 – 121661. 10.1016/j.jorganchem.2020.121650
5. R. Pehn, J. Pann, K. Ehrmann, W. Viertl, H. Roithmeyer, M. Bendig, C. Strabler, H. Kopacka, T. Müller, T. Hofer, P. Brüggeller, *Eur. J. Inorg. Chem*., **2020**, 4358 – 4372. 10.1002/ejic.202000778
6. Q. Dong, M. J. Rose, W-Y. Wong, H. B. Gray, *Inorg. Chem*., **2011**, *50*, 10213 – 10224. 10.1021/ic201213c
7. A. Carrick, MChem Thesis, Durham University, **2020**.
8. I. J. Bruno, J. C. Cole, P. R. Edgington, M. Kessler, C. F. Macrae, P. McCabe, J. Pearson, R. Taylor, *Acta Cryst*., **2002**, *B58*, 389 – 397. 10.1107/s0108768102003324
9. J-S. Sun, H. Zhao, X. Ouyang, R. Clérac, J. A. Smith, J. M. Clemente-Juan, C. Gómez-Garcia, E. Coronado, K. R. Dunbar, *Inorg. Chem*., **1999**, *38*, 5841 – 5855. 10.1021/ic990525w
10. W. Harrison, J. Trotter, *J. Chem. Soc., Dalton Trans*., **1973**, 61 – 64. 10.1039/DT9730000061
11. R. Azhakar, R. S. Ghadwal, H. W. Roesky, J. Hey, L. Krause, D. Stalke, *Dalton Trans*., **2013**, *42*, 10277 – 10281. 10.1039/C3DT50939G
12. W. L. Olson, L. F. Dahl, *Acta Cryst*., **1986**, *C42*, 541 – 544. 10.1107/S010827018609546X
13. F. Guo, F. Xia, H-Y. Guan, B-X. Wang, J. Tong, W-S. Guo, *Solid State Sci*., **2011**, *13*, 59 – 65. 10.1016/j.solidstatesciences.2010.10.009
14. A. Crochet, K. M. Fromm, *Z. Anorg. Allg. Chem*., **2010**, *636*, 1484 – 1496. 10.1002/zaac.201000022
15. R. Kapoor, A. Kataria, P. Kapoor, P. Venugopalan, *Transition Met. Chem.,* **2004**, *29*, 425 – 429. 10.1023/B:TMCH.0000027459.47135.ee
16. K. R. Dunbar, A. Quillevéré, S. C. Haefner, *Acta Cryst*., **1991**, *C47*, 2319 – 2321. 10.1107/S0108270191003311
17. O. K. Kireeva, B. M. Bulychev, N. R. Streltsova, V. K. Belsky, A. G. Dunin, *Polyhedron*, **1992**, *11*, 1801 – 1807. 10.1016/S0277-5387(00)83242-8
18. F. Baumann, E. Dormann, Y. Ehleiter, W. Kaim, J. Kärcher, M. Kelemen, R. Krammer, D. Saurenz, D. Stalke, C. Wachter, G. Wolmershäuser, H. Sitzmann, *J. Organomet. Chem*., **1999**, *587*, 267 – 283. 10.1016/S0022-328X(99)00332-0
19. Z. He, X. Xue, Y. Liu, N. Yu, J. P. Krogman, *Dalton Trans*., **2020**, *49*, 12586 – 12591. 10.1039/D0DT00570C
20. K. A. Smart, A. Vanbergen, J. Lednik, C. Y. Tang, H. B. Mansaray, I. Siewert, S. Aldridge, *J. Organomet. Chem*., **2013**, *741-742*, 33 – 39. 10.1016/j.jorganchem.2013.05.020
21. A. Garbagnati, M. Piesch, M. Seidl, G. Balázs, M. Scheer, *Chem. Eur. J*., **2022**, *28*, e202201026. 10.1002/chem.202201026

22. F. H. Köhler, *Paramagnetic Complexes in Solution: The NMR Approach*, *Encyclopedia of Magnetic Resonance*, Wiley, New Jersey, **2011**. 10.1002/9780470034590.emrstm1229
23. D. F. Evans, *J. Chem. Soc*., **1959**, 2003 – 2005. 10.1039/JR9590002003
24. A. W. Addison, T. N. Rao, J. Reedijk, J. van Rijn, G. C. Verschoor, *J. Chem. Soc., Dalton Trans*., **1984**, 1349 – 1356. 10.1039/DT9840001349
25. E. Styczeń, Z. Warnke, D. Wyrzykowski, J. Kłak, J. Mroziński, A. Sikorski, *Struct. Chem*., **2010**, *21*, 269 – 276. 10.1007/s11224-009-9577-y
26. M. Khalfa, A. Oueslati, K. Khirouni, M. Gargouri, A. Rousseau, J. Lhoste, J-F. Bardeau, G. Corbel, *RSC Adv*., **2022**, *12*, 2798 – 2809. 10.1039/D1RA07965D
27. T. Peppel, M. Köckerling, *Cryst. Growth Des*., **2011**, *11*, 5461 – 5468. 10.1021/cg2010419
28. G. Kiefer, H. Vrubel, R. Scopelliti, K. Severin, *Eur. J. Inorg. Chem*., **2013**, 4916 – 4921. 10.1002/ejic.201300551
29. D. R. Eaton, K. Zaw, *Inorg. Chim. Acta*, **1976**, *16*, 61 – 66. 10.1016/S0020-1693(00)91692-X
30. D. Domide, O. Walter, S. Behrens, E. Kaifer, H-J. Himmel, *Eur. J. Inorg. Chem*., **2011**, 860 – 867. 10.1002/ejic.201001095
31. A. Ghisolfi, C. Fliedel, V. Rosa, R. Pattacini, A. Thibon, K. Y. Monakhov, P. Braunstein, *Chem. Asian J*., **2013**, *8*, 1795 – 1805. 10.1002/asia.201300687
32. A. Ghisolfi, C. Fliedel, V. Rosa, K. Y. Monakhov, P. Braunstein, *Organometallics*, **2014**, *33*, 2523 – 2534. 10.1021/om500141k
33. M. T. Mock, R. G. Potter, M. J. O'Hagan, D. M. Camaioni, W. G. Dougherty, W. S. Kassel, D. L. DuBois, *Inorg. Chem*., **2011**, *50*, 11914 – 11928. 10.1021/ic200857x
34. A. Ferrari, F. Giorgio, *Atti della Accademia Nazionale dei Lincei, Classe di Fische, Matematiche e Naturali, Rendiconti*, **1929**, *9*, 782. Found at: https://www.ccdc.cam.ac.uk/structures/Search?Ccdcid=1617119&DatabaseToSearch=Published (31/01/24).
35. K. Heinze, G. Huttner, L. Zsolnai, P. Schober, *Inorg. Chem*., **1997**, *36*, 5457 – 5469. 10.1021/ic9705352
36. A. F. Orchard, *Magnetochemistry*, Oxford Univeristy Press, Oxford, **2003**. 10.1093/hesc/9780198792789.001.0001
37. B. N. Figgis, J. Lewis, *Progress in Inorganic Chemistry*, Interscience, New York, **1964**. 10.1002/9780470166079.ch2
38. J. M. Stauber, A. L. Wadler, C. E. Moore, A. L. Rheingold, J. F. Figueroa, *Inorg. Chem*., **2011**, *50*, 7309 – 7316. 10.1021/ic201205p

# Chapter 5 – Synthesis of Cobalt(I) Complexes of 'PNP' Ligands

## 5.1 Introduction

Building on the coordination chemistry of 'PNP' ligands with $CoX_2$ (X = Cl, Br, I) described in **Chapter 4**, strategies to move towards the preparation of low valent cationic cobalt(I) complexes containing 'PNP' ligands were considered. In this context, studying the reactivity of complexes **4.7** – **4.11** and **2.14** (**Figure 5.1**) is challenging as these complexes contain multiple cobalt(II) centres with vastly different geometries and coordination environments. Multiple cobalt(II) centres results in more potential sites of reactivity and reaction pathways, complicating a reactivity study. Therefore, it is desirable to prepare and study cobalt(II) complexes containing a single cobalt(II) environment.

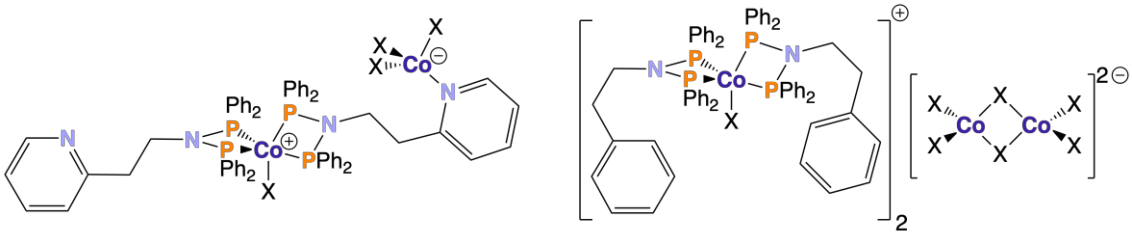


**Figure 5.1.** Structures of complexes **2.14** and **4.7** – **4.11**.

With this in mind, one suitable strategy is to synthesise complexes **5.1** – **5.3** (**Figure 5.2**) containing a single cationic cobalt(II) centre. Reduction of complexes **5.1** – **5.3** with activated zinc is expected to afford cationic cobalt(I) species, and the outcome of these reactions is presented here. Cationic cobalt(II) complexes **5.1** – **5.3** may be suitable for use as pre-catalysts, with many low valent cationic cobalt(I) diphosphine complexes having been explored previously for applications including hydrovinylation,[1] hydroboration[2] and heterodimerisation[3] (**Section 1.1.1**, **Chapter 1**).

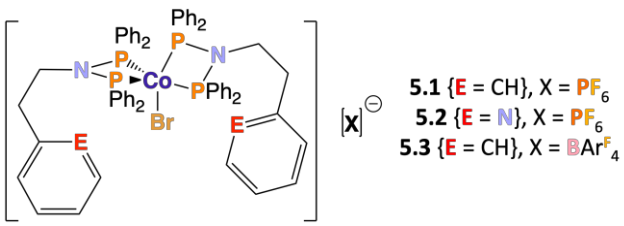


**Figure 5.2.** Structure of complexes **5.1** – **5.3**.

## 5.2 Synthesis of [CoBr(Ph(CH$_2$)$_2$N{PPh$_2$}$_2$)$_2$][PF$_6$] (5.1), [CoBr(Py-*o*-(CH$_2$)$_2$N{PPh$_2$}$_2$)$_2$][PF$_6$] (5.2) and [CoBr(Ph(CH$_2$)$_2$N{PPh$_2$}$_2$)$_2$][BAr$^F_4$] (5.3)

Two equivalents of compound **2.1** or **2.2** were reacted with one equivalent of $CoBr_2$ and one equivalent of $KPF_6$ or $NaBAr^F_4$ (following an adapted literature procedure)[4] to afford complexes **5.1** – **5.3** (**a)**, **Scheme 5.1**). Reaction outcomes were confirmed by solid-state structures (**Section 5.2.1**), CHN analyses, a $\mu_{eff}$ value of 2.10 $\mu_B$ (*cf*. spin-only formula result of 1.73 $\mu_B$) determined for complex **5.2** *via* the Evans Method,[5] and positive ion ESI mass spectrometry evidencing signals at 1118.4 *m/z* and 1120.3 *m/z* for the cations of complexes **5.1**/**5.3** and **5.2**, respectively. It is noteworthy that the attempted synthesis of complex **5.4** (**b)**, **Scheme 5.1**) afforded mono-halide complex **5.3** (UV-Vis and mass spectrum of the isolated product of the attempted 2:1:2 'PNP':$CoBr_2$:$NaBAr^F_4$ reaction described in **b)**, **Scheme 5.4**, are identical to that of complex **5.3**).

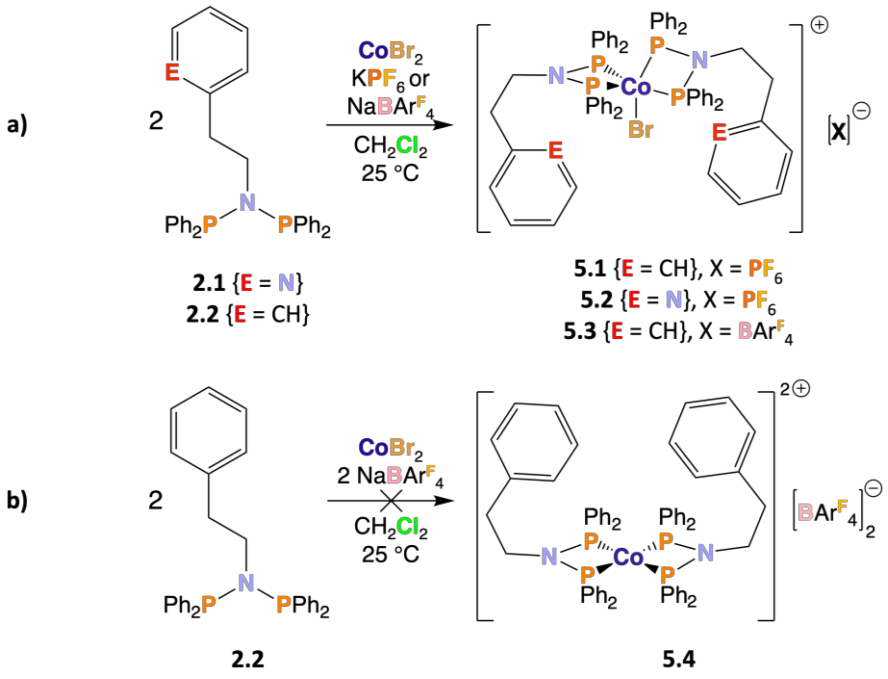


**Scheme 5.1. a)** synthesis of complexes **5.1** – **5.3**; **b)** attempted synthesis of complex **5.4**.

### 5.2.1 Solid-State Molecular Structures of [CoBr(Ph(CH$_2$)$_2$N{PPh$_2$}$_2$)$_2$][PF$_6$] (5.1), [CoBr(Py-*o*-(CH$_2$)$_2$N{PPh$_2$}$_2$)$_2$][PF$_6$] (5.2) and [CoBr(Ph(CH$_2$)$_2$N{PPh$_2$}$_2$)$_2$][BAr$^F_4$] (5.3)

Single crystals of complexes **5.1** – **5.3** were obtained and molecular structures determined (cations shown in **Figure 5.3**). Key bond angles and lengths of the cations of complexes **5.1** – **5.3** (presented in **Table 5.1** and **Table 5.2**, respectively) are very similar

to those measured from analogous structures, *e.g.,* complexes **2.14** ([CoBr(Py-*o*-$(CH_2)_2N\{PPh_2\}_2$)($\{Br_3Co\}$Py-*o*-$(CH_2)_2N\{PPh_2\}_2$)]) and **4.10** ([CoBr(Ph$(CH_2)_2N\{PPh_2\}_2)_2]_2[Co_2Br_6]$), shown in **Figure 5.1**.

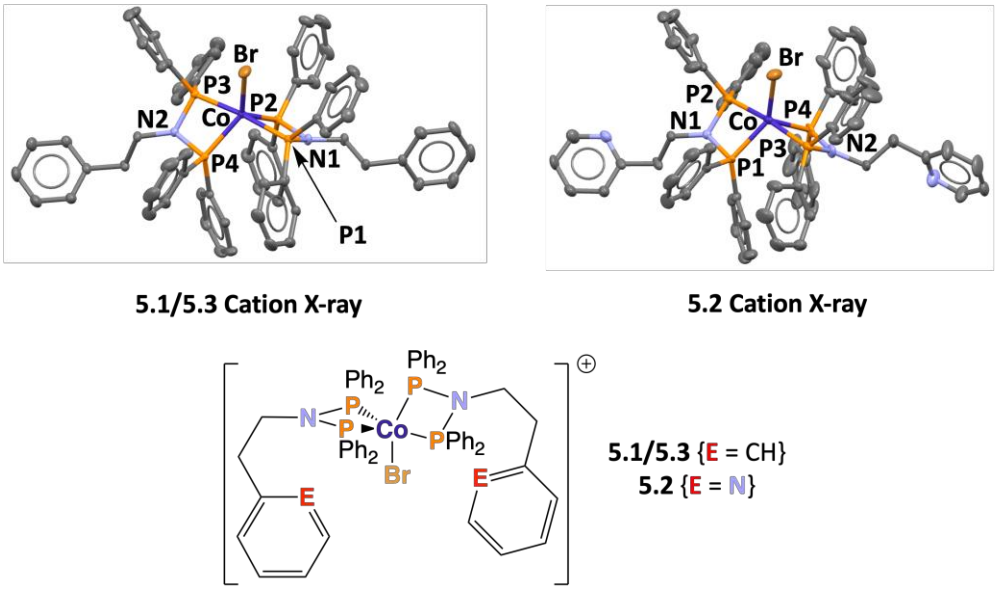


**Figure 5.3.** Solid-state molecular structures of the cations of complexes **5.1** – **5.3**. Thermal ellipsoids are shown at the 50 % probability level. Hydrogen atoms, a single DCM molecule and the $PF_6$ anions are omitted for clarity. Atom colour: carbon – grey; nitrogen – light blue; cobalt – dark blue, and bromine – orange-brown.

**Table 5.1.** Key bond angles measured from the solid-state molecular structures of complexes **5.1** – **5.3**.

| Angle | 5.1 | 5.2 | 5.3 |
|---|---|---|---|
| Br-Co-P1 / ° | 92.42(2) | 132.7(2) | 92.03(2) |
| Br-Co-P2 / ° | 125.61(3) | 96.70(3) | 118.85(2) |
| Br-Co-P3 / ° | 95.77(2) | 91.03(3) | 97.80(2) |
| Br-Co-P4 / ° | 127.27(3) | 117.6(3) | 134.37(2) |
| P1-Co-P2 / ° | 71.54(2) | 71.0(2) | 71.18(2) |
| P1-Co-P3 / ° | 171.81(3) | 99.7(2) | 170.16(3) |
| P1-Co-P4 / ° | 103.29(3) | 109.5(4) | 101.07(3) |
| P2-Co-P3 / ° | 103.57(3) | 172.27(3) | 103.97(3) |
| P2-Co-P4 / ° | 107.09(3) | 104.6(3) | 106.53(3) |
| P3-Co-P4 / ° | 71.49(2) | 71.6(3) | 71.73(2) |
| P1-N1-P2 / ° | 100.19(8) | 105.2(4) | 100.0(1) |
| P3-N2-P4 / ° | 100.82(8) | 102.8(5) | 99.6(1) |

**Table 5.2.** Key bond lengths measured from the solid-state molecular structures of complexes **5.1** – **5.3**.

| Bond | 5.1 | 5.2 | 5.3 |
|---|---|---|---|
| Co-Br / Å | 2.3550(6) | 2.3608(8) | 2.3619(6) |
| Co-P1 / Å | 2.2314(9) | 2.24(1) | 2.2286(6) |
| Co-P2 / Å | 2.2306(8) | 2.2380(8) | 2.2801(8) |
| Co-P3 / Å | 2.2409(8) | 2.2281(9) | 2.2197(7) |
| Co-P4 / Å | 2.2540(6) | 2.31(1) | 2.2237(6) |
| N1-P1 / Å | 1.693(2) | 1.71(1) | 1.702(2) |
| N1-P2 / Å | 1.707(1) | 1.727(6) | 1.724(2) |
| N2-P3 / Å | 1.695(2) | 1.690(3) | 1.714(2) |
| N2-P4 / Å | 1.712(1) | 1.71(1) | 1.696(2) |

## 5.3 Reduction of $[CoBr(Ph(CH_2)_2N\{PPh_2\}_2)_2][PF_6]$ (5.1), $[CoBr(Py\text{-}o\text{-}(CH_2)_2N\{PPh_2\}_2)_2][PF_6]$ (5.2) and $[CoBr(Ph(CH_2)_2N\{PPh_2\}_2)_2][BAr^F{}_4]$ (5.3) with activated zinc

Complexes **5.1** – **5.3** were reduced with 4, 10 or 50 equivalents of activated zinc to afford cationic cobalt(I) complexes **5.5** – **5.7** (**Scheme 5.2**), respectively. A reaction utilising 50 equivalents of activated zinc was attempted in order to result in over-reduction, which would be evidenced by the production of cobalt(0); however, this did not occur. Since experimental evidence suggests that complete reduction occurs with 4, 10 and 50 equivalents of activated zinc (*i.e.*, equivalent $^{31}P\{^1H\}$ NMR and positive ion ESI mass spectra of the isolated products), it was inferred that at least 4 equivalents of activated zinc is required to fully convert the starting material (unlike for reduction reactions of complex **5.1** utilising 1 and 2 equivalents of activated zinc; see **Section 5.3.4** – **5.3.5**).

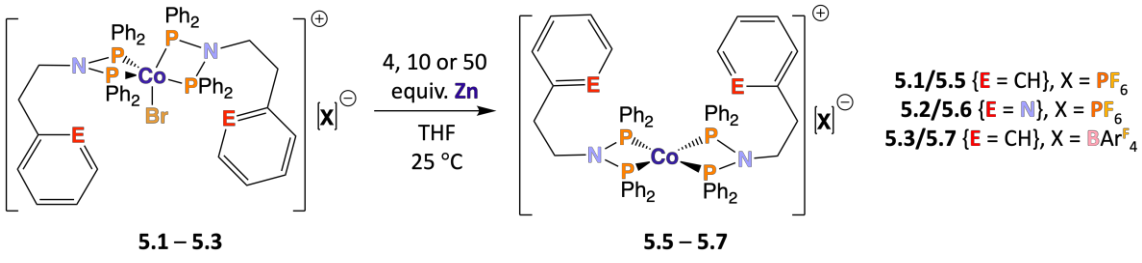


**Scheme 5.2.** Reduction of complexes **5.1** – **5.3** with 4, 10 and 50 equivalents of activated zinc.

Complexes **5.5** – **5.7** are a deep purple colour in both THF solution and in the solid-state as powders; this is in stark contrast to $[CoBr(Py\text{-}o\text{-}(CH_2)_2N\{PPh_2\}_2)(\{Br_3Co\}Py\text{-}o\text{-}$

$(CH_2)_2N\{PPh_2\}_2)]$ (complex **2.14**) and $[CoBr(Ph(CH_2)_2N\{PPh_2\}_2)_2]_2[Co_2Br_6]$ (complex **4.10**; **Figure 5.1**) which are brown and green powders, respectively. Complexes **5.5** – **5.7** are extremely air sensitive, turning bright orange upon exposure to air. Complexes **5.5** – **5.7** are insoluble in most solvents except DCM (which they react with; see **Section 5.3.4**), MeCN (complexes **5.5** – **5.7** turn orange in MeCN), toluene (only complex **5.7** due to the $BAr^F_4$ anion) and THF. Despite multiple attempts, the measured CHN analyses of complexes **5.5** – **5.7** are not in good agreement with the corresponding calculated CHN composition, likely due to the presence of small quantities of impurities produced during the reduction or incomplete removal of activated zinc and zinc bromide (despite employing filtration and, when possible, extraction steps). Attempts to grow single crystals of complexes **5.5** – **5.7** were unsuccessful; even under an inert atmosphere, the deep purple THF solution of complexes **5.5** – **5.7** turns brown as the THF and hexane layers begin to mix.

Characterisation data have been obtained that supports the proposed structures of complexes **5.5** – **5.7** (**Scheme 5.2**). Complexes **5.5** and **5.7** give a signal at 1037.5 *m/z* in their positive ion *m/z* ESI mass spectra, and complex **5.6** presents a signal at 1039.6 *m/z*, corresponding to the $[Co(P,P)_2]$ cation, consistent with removal of the bromide ligand during the reduction process. Determining the magnetic susceptibilities of complexes **5.5** – **5.7** by the Evans NMR Method[5] reveals that the complexes are diamagnetic. A slightly broad ($\nu_{1/2}$ = 105 Hz) singlet is observed in the $^{31}P\{^1H\}$ NMR spectra of complexes **5.5** – **5.7** at $\delta_P$ = 86.6 ppm, 86.8 ppm and 86.7 ppm for complexes **5.5**, **5.6** and **5.7** (**Figure 5.4**), respectively, indicating that all the phosphorus atoms in the $[Co(P,P)_2]$ cations of complexes **5.5** – **5.7** are equivalent. The $^1H$ NMR spectra of complexes **5.5** – **5.7** also exhibits broad peaks. Signal broadening is a result of the 7/2 spin of $^{59}Co$.[6] Together, these magnetic and spectral data are consistent with the $[Co(P,P)_2]$ cations of complexes **5.5** – **5.7** having a square planar geometry (a tetrahedral $[Co(P,P)_2]$ cation would have two unpaired electrons and be paramagnetic). There is no spectroscopic evidence of pyridyl coordination at the cobalt(I) centre in complex **5.6**, hence coordination of the pendant pyridyl moieties is not stabilising the cationic cobalt(I) species.

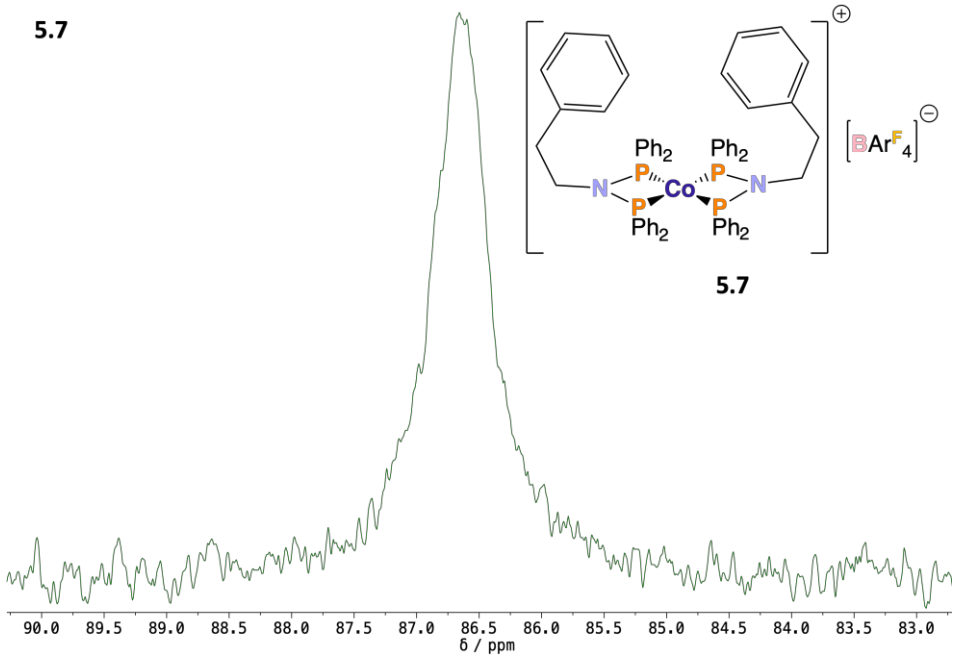


**Figure 5.4.** $^{31}P\{^{1}H\}$ NMR (162 MHz, 290 K, $d_8$-THF) spectra of complex **5.7**.

Square planar cationic cobalt(I) *bis*(diphosphine) complexes have been previously reported, *e.g.*, complexes **5.8 – 5.10** (**Figure 5.5**).[6–8] Hence, the assignment of a square planar geometry for complexes **5.5** – **5.7** has precedence.

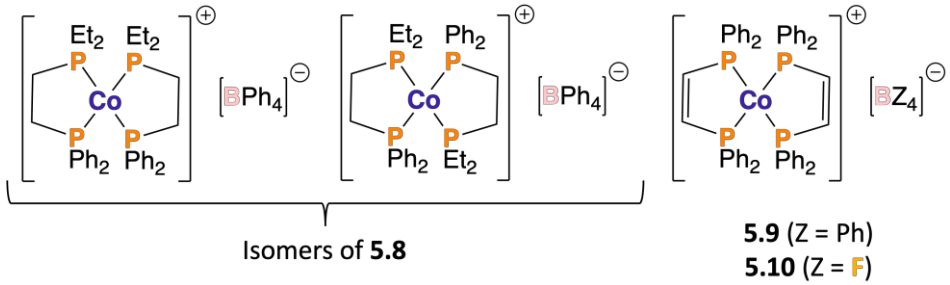


**Figure 5.5.** Structures of complexes **5.8** – **5.10**.[6–8]

## 5.3.1 Reaction of [Co{Ph(CH$_2$)$_2$N(PPh$_2$)$_2$}$_2$][PF$_6$] (5.5), [Co{Py-*o*-(CH$_2$)$_2$N(PPh$_2$)$_2$}$_2$][PF$_6$] (5.6) and [Co{Ph(CH$_2$)$_2$N(PPh$_2$)$_2$}$_2$][BAr$^F_4$] (5.7) with Oxygen

Exposure of deep purple complex **5.7**, as a solid and dissolved in $d_8$-THF, to air and 99.5% pure $O_2$ gas, affords bright orange peroxo-cobalt(III)[9] complex **5.13** (**a**), **Scheme 5.3**), with analogous reactivity being observed for complexes **5.5** – **5.6**. Oxidation of complexes **5.5** – **5.7** to complexes **5.11** – **5.13** occurs during mass spectra acquisition (samples are introduced into the mass spectrometer under air). Hence, signals at 1069.5 *m/z* and 1071.5 *m/z*, corresponding to the [Co(*P,P*)$_2$($\eta^2$-O$_2$)] cation of complexes **5.11**/**5.13** and **5.12**, respectively, are observed in the positive ESI mass spectra of

complexes **5.5**/**5.7** and **5.6**, respectively. $^{31}P\{^{1}H\}$ NMR spectroscopic analysis of complex **5.13** showed two broad ($\nu_{1/2}$ ~230 Hz), unresolved signals at approx. 48 and 75 ppm. The FT-IR spectrum of the powder complex **5.13** evidences a $\nu(O_2)$ stretch at approx. 839 $cm^{-1}$, which is very similar to the $\nu(O_2)$ stretch at 861 $cm^{-1}$ reported for peroxo complex **5.14** (**b**), **Scheme 5.3**).[10] Reaction between cationic $[Co^{I}(P,P)_2]$ species complex **5.10** ($[Co(dppv)_2][BF_4]$, **Figure 5.5**) and $O_2$ (either in air or pure $O_2$ gas) to afford the peroxo complex **5.15** (**c**), **Scheme 5.3**) has previously been reported in the literature.[8]

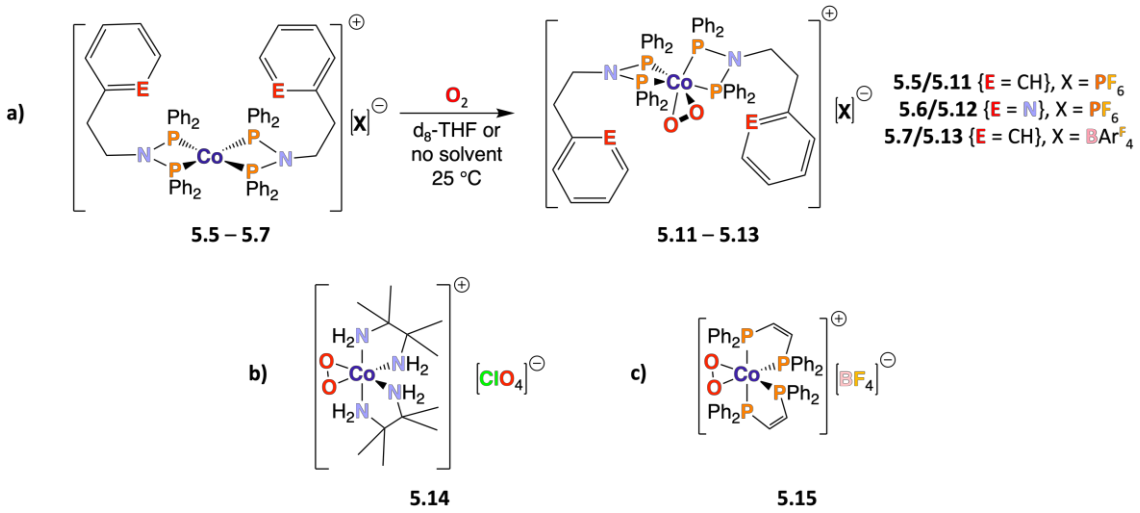


**Scheme 5.3. a)** reaction of complexes **5.5** – **5.7** with $O_2$ to afford peroxo complexes **5.11** – **5.13**; **b)** structure of complex **5.14**;[10] **c)** structure of complex **5.15**.[8]

Complex **5.13** ($[Co(Ph(CH_2)_2N\{PPh_2\}_2)_2(\eta^2\text{-}O_2)][BAr^F{}_4]$) was found to be unstable under atmospheres of both $N_2$ and $O_2$. Overnight standing of a sample of complex **5.13** under an atmosphere of $N_2$ in a Young's NMR tube resulted in an orange to purple colour change, indicating that the bound $O_2$ of complex **5.13** has dissociated to afford complex **5.7** ($[Co(Ph(CH_2)_2N\{PPh_2\}_2)_2][BAr^F{}_4]$), supported by $^{31}P\{^{1}H\}$ NMR analysis showing a singlet at approx. 86.7 ppm. Overnight standing of a sample of complex **5.13** under an atmosphere of 99.5% pure $O_2$ in a Young's NMR tube resulted in an orange to colourless colour change. The obtained $^{31}P\{^{1}H\}$ and $^{1}H$ NMR spectra present extremely broadened signals, indicating that a paramagnetic complex had been produced. The positive ion ESI mass spectrum evidences a signal at 812.3 *m/z* corresponding to $[Co(PhCH_2CH_2N\{OPPh_2\}_2)_3]^{2+}$ (the dication of tri 'PNP' oxidised complex **5.16**, **Figure 5.6**) was observed. Peroxo complexes have previously been reported to oxidise phosphines,[11] with the proposed reaction pathway involving the formation of a hydroperoxo (*i.e.*, Co-O-O-H) intermediate, which presumably forms due to the

presence of water.[11] However, the conversion of complex **5.13** to complex **5.16** occurs in a sealed rigorously dried Young's NMR tube under an atmosphere of dry 99.5% pure $O_2$, meaning that only a negligible amount of water is likely to be present. This potentially suggests that the oxidation of a phosphine by a peroxo complex can occur without water. A small quantity of crystals (~5% yield) of complex **5.16** (**Figure 5.6**) were isolated and XRD analysis performed. Although the atom connectivity was confirmed, the data is of an insufficient quality to allow for full structure refinement.

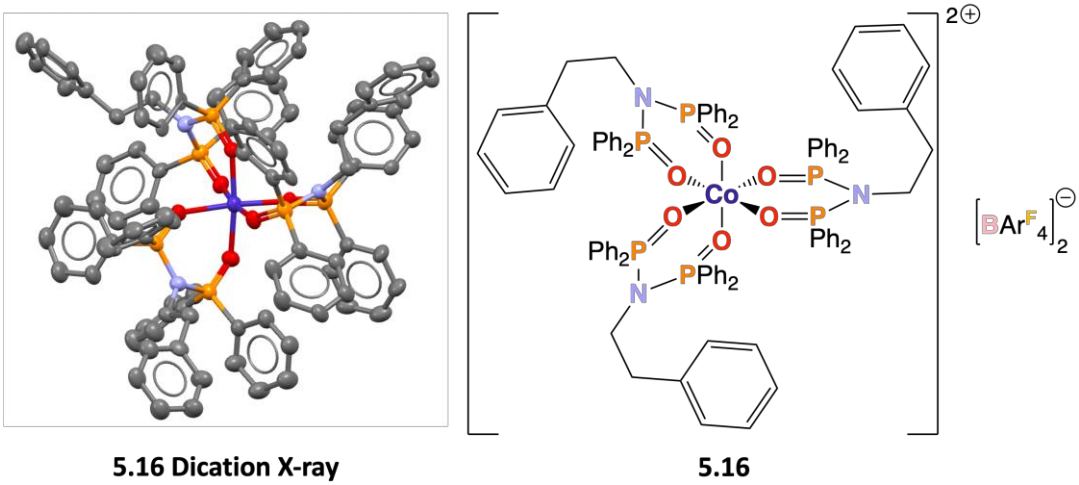


**Figure 5.6.** Connectivity of the dication of complex **5.16**. Atom colour: carbon – grey; nitrogen – light blue; cobalt – dark blue, and oxygen – red. *NB* a solvent mask removed approx. two acetone molecules per asymmetric unit.

## 5.3.2 $^{31}P\{^{1}H\}$ NMR spectroscopic study of the reaction of $Ph(CH_2)_2N(PPh_2)_2$ (2.2) with Oxygen

Since the oxidation of 'PNP' compound **2.2** ($Ph(CH_2)_2N(PPh_2)_2$), *via* a likely hydroperoxo intermediate, was observed in the coordination sphere at cobalt for complex **5.16** (**Figure 5.6**), the reactivity of compound **2.2** with $O_2$ was studied in the absence of a cobalt centre. Compound **2.2** was dissolved in dry $d_8$-THF in a Young's NMR tube, the solution degassed *via* three freeze-pump-thaw cycles, and backfilled with $O_2$ gas. The reaction was then followed by $^{31}P\{^{1}H\}$ NMR spectroscopy (**Figure 5.7**). Partial oxidation of one of the phosphorus atoms of compound **2.2** occurs after approx. 12 hours, affording $Ph(CH_2)_2N(PPh_2)(OPPh_2)$ (compound **5.17**, **Figure 5.7**). The $^{31}P\{^{1}H\}$ NMR spectrum of compound **5.17** contains two doublets at approx. 48.1 ppm and 28.7 ppm, with $^{2}J_{PP}$ = 83.4 Hz; this agrees with analogous data of 49.10 ppm, 32.95 ppm and $^{2}J_{PP}$ = 87.5 Hz measured for *n*-HexN$(PPh_2)(OPPh_2)$.[12] A small amount of $Ph(CH_2)_2N(Ph_2P\{O\})_2$ (compound **5.18**, **Figure 5.7**) also formed after approx. 12 hours, with compound **5.18**

being the major product after *ca*. 2 weeks. The $^{31}P\{^{1}H\}$ spectrum of compound **5.18** presents a singlet at approx. 27.5 ppm; this agrees with analogous chemical shift of 29.42 ppm measured for *n*-HexN($Ph_2P\{O\}$)$_2$.[12] Hence, the oxidation of compound **2.2** can occur under an atmosphere of $O_2$ in the absence of a cobalt centre. However, the oxidation of compound **2.2** under an atmosphere of $O_2$ (**Figure 5.7**) is much slower (days) than the reactivity observed for the cation of complex **5.13** (affording complex **5.16** over a period of ~12 hours). Therefore, the presence of a cobalt centre accelerates the rate of oxidation of compound **2.2** to compound **5.18**, albeit producing a complex where compound **5.18** is coordinating to a cobalt centre.

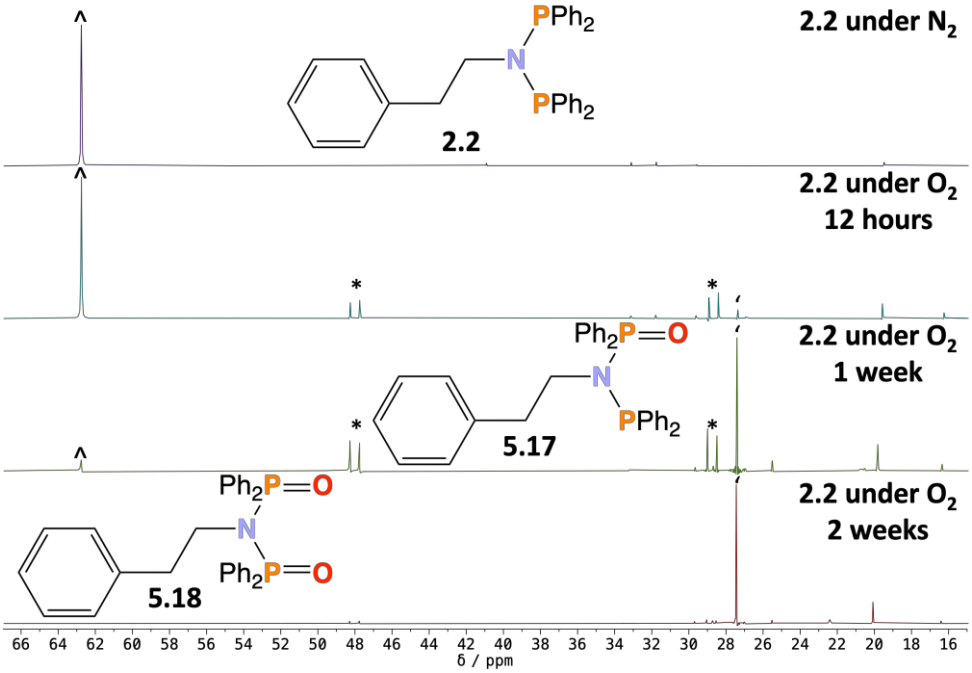


**Figure 5.7.** $^{31}P\{^{1}H\}$ NMR (162 MHz, 290 K, $d_8$-THF) spectra for compound **2.2** (^) under $N_2$ and compound **2.2** under $O_2$ for 12 hours, 1 week and 2 weeks, leading to the formation of compound **5.18** (') *via* compound **5.17** (*).

### 5.3.3 Solid-State Molecular Structure of [Co{Ph(CH$_2$)$_2$N(PPh$_2$)$_2$}$_2$($\eta^2$-O$_2$)][PF$_6$] (5.11)

Single crystals of complex **5.11** were obtained and a molecular structure determined (**Figure 5.8**). Complex **5.11** was synthesised by the reaction of complex **5.5** ([Co(Ph(CH$_2$)$_2$N{PPh$_2$}$_2$)$_2$][PF$_6$]) with $O_2$, described in **a)**, **Scheme 5.3**.

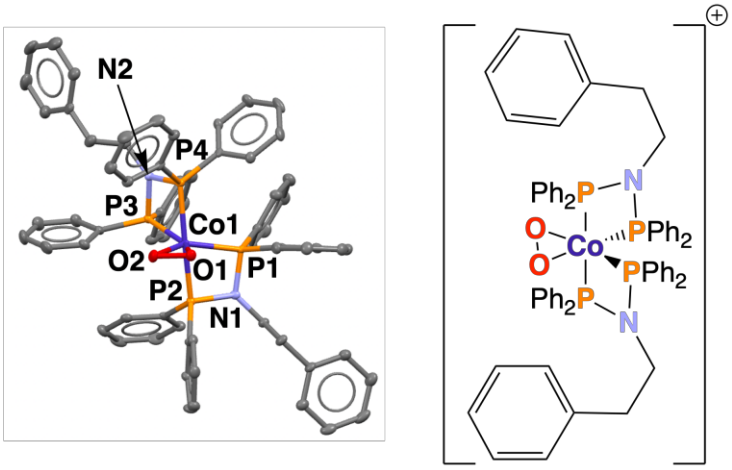


**5.11 Cation X-ray** **5.11 Cation**

**Figure 5.8.** Solid-state molecular structure of the cation of complex **5.11.** Thermal ellipsoids are shown at the 50 % probability level. Hydrogen atoms, three acetone molecules and the $PF_6$ anion are omitted for clarity. Atom colour: carbon – grey; nitrogen – light blue; cobalt – dark blue, and oxygen – red.

Complex **5.11** has Co-O and O1-O2 bond lengths of 1.896(3) Å and 1.418(4) Å, respectively. $[Co(Me_2PCH_2CH_2PMe_2)_2(\eta^2\text{-}O_2)][BPh_4]$ has Co1-O1 and Co1-O2 bond lengths of 1.867(7) Å and 1.859(7) Å, respectively,[13] which are significantly shorter than those in complex **5.11**. The difference in Co-O bond lengths of complexes **5.11** and $[Co(Me_2PCH_2CH_2PMe_2)_2(\eta^2\text{-}O_2)][BPh_4]$ may be due to steric crowding around the cobalt(III) centre in complex **5.11** resulting from the phenyl phosphine substituents (*cf.* less bulky methyl substituents of $[Co(Me_2PCH_2CH_2PMe_2)_2][BPh_4]$). $[Co(Me_2PCH_2CH_2PMe_2)_2][BPh_4]$ has an O1-O2 bond length of 1.41(1) Å[13] showing good similarity to the O1-O2 bond length measured for complex **5.11**. The key bond lengths and bond angles measured from the solid-state structure of the cation of complex **5.11** are presented in **Table 5.3** and **Table 5.4**, respectively.

**Table 5.3.** Key bond lengths measured from the solid-state molecular structure of the cation of complex **5.11**.

| Bond | Bond Length / Å |
|---|---|
| Co1-P1 | 2.222(1) |
| Co1-P2 | 2.243(1) |
| Co1-P3 | 2.229(1) |
| Co1-P4 | 2.242(1) |
| Co1-O1 | 1.896(3) |
| Co1-O2 | 1.896(3) |
| N1-P1 | 1.696(3) |
| N1-P2 | 1.685(3) |
| N2-P3 | 1.694(3) |
| N3-P4 | 1.681(3) |
| O1-O2 | 1.418(4) |

**Table 5.4.** Key bond angles measured from the solid-state molecular structure of the cation of complex **5.11**.

| Angle | Bond Angle / ° |
|---|---|
| P1-Co1-P2 | 71.71(4) |
| P1-Co1-P3 | 108.86(4) |
| P1-Co1-P4 | 101.83(4) |
| P1-Co1-O1 | 105.3(1) |
| P1-Co1-O2 | 146.20(9) |
| P2-Co1-P3 | 103.77(4) |
| P2-Co1-P4 | 170.89(5) |
| P2-Co1-O1 | 92.95(9) |
| P2-Co1-O2 | 93.16(8) |
| P3-Co1-P4 | 71.80(4) |
| P3-Co1-O1 | 145.2(1) |
| P3-Co1-O2 | 103.99(8) |
| P4-Co1-O1 | 95.01(9) |
| P4-Co1-O2 | 95.64(8) |
| O1-Co1-O2 | 43.9(1) |
| P1-N1-P2 | 101.3(2) |
| P3-N2-P4 | 101.9(2) |

### 5.3.4 Solid-State Molecular Structure of $0.75[CoCl\{Ph(CH_2)_2N(PPh_2)_2\}_2][PF_6]\cdot 0.25[CoBr\{Ph(CH_2)_2N(PPh_2)_2\}_2][PF_6]$ (5.19)

Single crystals of complex **5.19** were obtained (from the reduction of complex **5.1** with 1 equiv. of activated zinc in DCM) and a molecular structure determined (**Figure 5.9**). Refinement of the solid-state structure reveals that the halide site is partially occupied by both chloride and bromide ligands in a 0.75:0.25 ratio, *i.e*., the solid-state structure contains a 0.75:0.25 mixture of complexes **5.20** (the chloride analogue of complex **5.1**) and **5.1**.

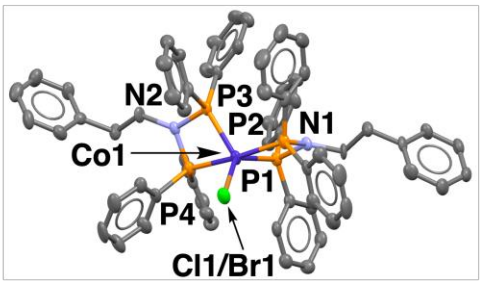


**5.19 Cation X-ray**

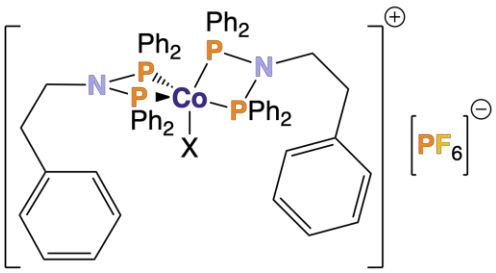


**5.1** (X = Br)
**5.19** (X = 0.75Cl : 0.25Br)
**5.20** (X = Cl)

**Figure 5.9.** Solid-state molecular structure of the cation of complex **5.19**, where X = Cl, Br. Thermal ellipsoids are shown at the 50 % probability level. *NB* hydrogen atoms and DCM molecules are omitted for clarity. Atom colour: carbon – grey; nitrogen – light blue; phosphorus – orange; bromine – orange-brown; chlorine – green; cobalt – dark blue, and fluorine – yellow.

The key bond lengths and angles measured from the solid-state structure of complex **5.19** are presented in **Table 5.5** and **Table 5.6**, respectively. *NB* only bond lengths and bond angles including Br1 in the mixed halide site have been included.

**Table 5.5.** Key bond lengths measured from the solid-state molecular structure of the cation of complex **5.11**.

| Bond | Bond Length / Å |
|---|---|
| Co1-P1 | 2.228(2) |
| Co1-P2 | 2.229(2) |
| Co1-P3 | 2.270(2) |
| Co1-P4 | 2.244(2) |
| Co1-Br1 | 2.288(2) |
| N1-P1 | 1.715(6) |
| N1-P2 | 1.686(5) |
| N2-P3 | 1.706(7) |
| N3-P4 | 1.691(6) |

**Table 5.6.** Key bond angles measured from the solid-state molecular structure of the cation of complex **5.11**.

| Angle | Bond Angle / ° |
|---|---|
| Br1-Co1-P1 | 129.03(7) |
| Br1-Co1-P2 | 93.29(7) |
| Br1-Co1-P3 | 122.92(7) |
| Br1-Co1-P4 | 94.52(7) |
| P1-Co1-P2 | 71.69(7) |
| P1-Co1-P3 | 108.02(8) |
| P1-Co1-P4 | 103.14(8) |
| P2-Co1-P3 | 103.93(8) |
| P2-Co1-P4 | 172.19(8) |
| P3-Co1-P4 | 71.73(7) |
| P1-N1-P2 | 100.3(3) |
| P3-N2-P4 | 102.3(3) |

The reduction of complex **5.1** with 1 equiv. of activated zinc in DCM:THF (10:1) affords a red-yellow solution (*cf*. deep purple solutions observed when using THF as the reaction

solvent, indicating the synthesis of $[Co(Ph(CH_2)_2N\{PPh_2\}_2)_2][PF_6]$, *i.e.*, complex **5.5**, the intermediate in **Scheme 5.4**). This difference in colour has been attributed to the formation of complex **5.20** (**Scheme 5.4**). Since the only source of chlorine in the reaction mixture is DCM, complex **5.20** must form as a result of the *in situ* formation of complex **5.5** and subsequent abstraction of a chlorine atom from DCM (**Scheme 5.4**); note complex **5.1** does not react with DCM.

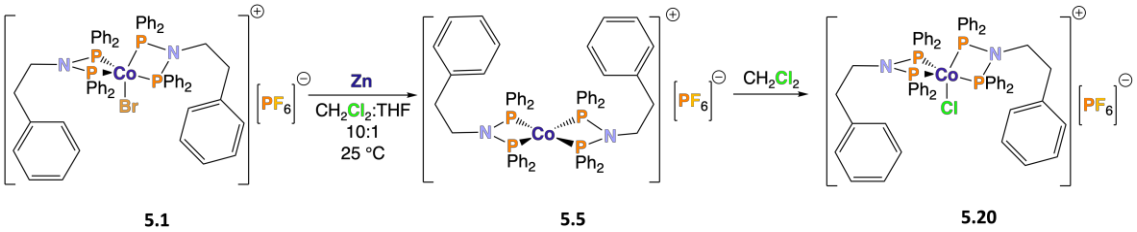


**5.1** **5.5** **5.20**

**Scheme 5.4.** Reduction of complex **5.1** with activated zinc to afford complex **5.5** *in situ*, and the subsequent reaction of complex **5.5** with DCM to afford complex **5.20**.

The reactivity of cationic cobalt(II) species with DCM to form a chloride adduct has been previously reported.[14] For example, the recrystallisation of complex **5.21** from a DCM/ethanol mixture afforded the chloride adduct complex **5.22**, resulting from extraction of a chlorine atom from DCM (**Scheme 5.5**).[14] In contrast, to the best knowledge of the author, the chemistry described in **Scheme 5.4** is the first observed reactivity of a cobalt(I) complex with DCM.

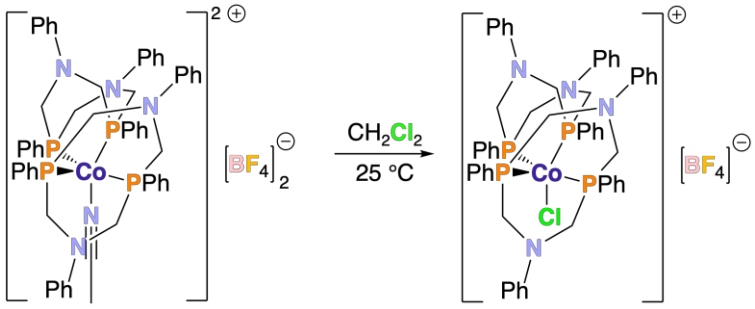


**5.21** **5.22**

**Scheme 5.5.** Reaction of complex **5.21** with DCM.[14]

Halide exchange (**Scheme 5.4**) provides additional evidence for the existence of complex **5.5**, supporting the experimental data discussed in **Section 5.3**. However, incomplete halide exchange (evidenced by 25% bromide ligand in the molecular structure of complex **5.19**, **Figure 5.9**) evidences that 1 equiv. of activated zinc is not enough to completely reduce complex **5.1** to complex **5.5** (first step of **Scheme 5.4**).

### 5.3.5 Solid-State Molecular Structure of 0.76[Co{Ph(CH$_2$)$_2$N(PPh$_2$)$_2$}$_2$($\eta^2$-O$_2$)][PF$_6$]·0.24[CoBr{Ph(CH$_2$)$_2$N(PPh$_2$)$_2$}$_2$][PF$_6$] (5.23)

Single crystals of the isolated product of the reduction of complex **5.1** with 2 equiv. of zinc (first step of **Scheme 5.4**) were obtained, under air, and the molecular structure of complex **5.23** determined (**Figure 5.10**). The presence of a bromide ligand in the molecular structure of complex **5.23** evidences that unreacted complex **5.1** remains. Hence, 2 equiv. of activated zinc is not enough to result in a complete reduction of complex **5.1**. The key bond lengths and bond angles measured from the solid-state structure of complex **5.23** are presented in **Table 5.7** and **Table 5.8**, respectively.

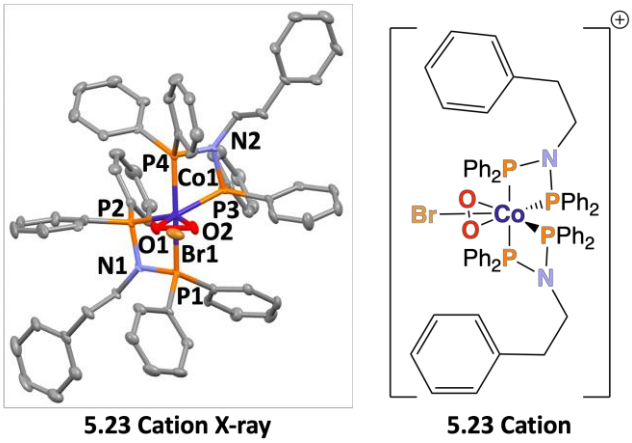


**5.23 Cation X-ray** **5.23 Cation**

**Figure 5.10.** Solid-state molecular structure of the cation of complex **5.23**. Thermal ellipsoids are shown at the 50 % probability level. *NB* hydrogen atoms, three acetone molecules and a $PF_6$ anion are omitted for clarity. Atom colour: carbon – grey; nitrogen – light blue; phosphorus – orange; bromine – orange-brown; cobalt – dark blue, and oxygen – red.

**Table 5.7.** Key bond lengths measured from the solid-state molecular structure of the cation of complex **5.23**.

| Bond | Bond Length / Å |
|---|---|
| Co1-P1 | 2.240(2) |
| Co1-P2 | 2.226(1) |
| Co1-P3 | 2.237(2) |
| Co1-P4 | 2.245(2) |
| Co1-O1 | 1.897(7) |
| Co1-O2 | 1.897(7) |
| N1-P1 | 1.685(5) |
| N1-P2 | 1.695(5) |
| O1-O2 | 1.430(9) |

**Table 5.8.** Key bond angles measured from the solid-state molecular structure of the cation of complex **5.23**.

| Angle | Bond Angle / ° |
|---|---|
| P1-Co1-P2 | 71.69(5) |
| P1-Co1-P3 | 103.68(6) |
| P1-Co1-P4 | 170.70(6) |
| P2-Co1-P3 | 108.78(6) |
| P2-Co1-P4 | 101.79(6) |
| P3-Co1-P4 | 71.71(5) |
| O1-Co1-O2 | 44.3(3) |
| P1-N1-P2 | 101.4(3) |
| P3-N2-P4 | 102.0(3) |

### 5.3.6 UV-Vis Spectroscopic Analysis of [CoBr{Ph(CH$_2$)$_2$N(PPh$_2$)$_2$}$_2$][BAr$^F_4$] (5.3) and [Co{Ph(CH$_2$)$_2$N(PPh$_2$)$_2$}$_2$][BAr$^F_4$] (5.7)

In order to verify the cobalt(I) oxidation state and to probe the origins of the deep purple colour of complex **5.7**, the UV-Vis spectra of complexes **5.3** (brown spectrum in **Figure 5.11**) and **5.7** (purple spectrum in **Figure 5.11**) were obtained. Complex **5.7** has been selected as a representative example of complexes **5.5** – **5.7** for UV-Vis spectroscopic study due to greater solubility of complex **5.7** arising from the BAr$^F_4$ anion relative to that of the $PF_6$ salts complexes **5.5** ([Co(Ph(CH$_2$)$_2$N{PPh$_2$}$_2$)$_2$][PF$_6$]) and **5.6** ([Co(Py-*o*-(CH$_2$)$_2$N{PPh$_2$}$_2$)$_2$][PF$_6$]).

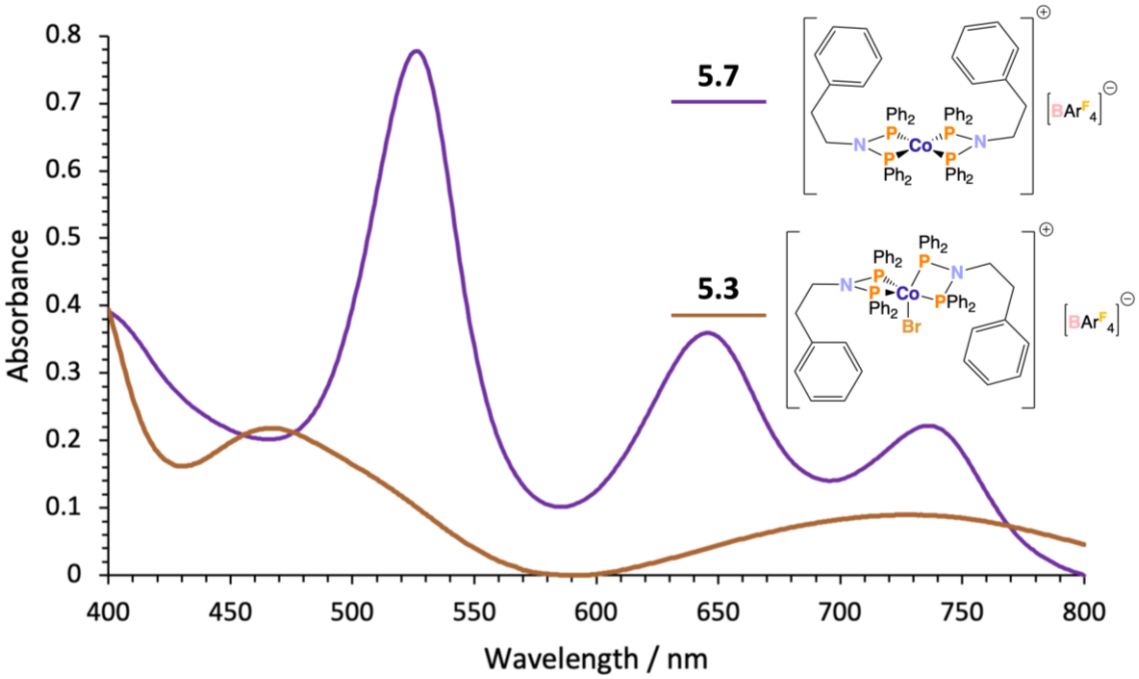


**Figure 5.11.** UV-Vis spectra (0.0001 M) of complexes **5.3** (brown spectrum) and **5.7** (purple spectrum) in THF in the 400 – 800 nm spectral window.

The UV-Vis spectrum of complex **5.3** evidences $\lambda_{max}$ at 466 and 728 nm, whilst the UV-Vis spectrum of complex **5.7** shows $\lambda_{max}$ at 526, 646 and 737 nm (in the 400 – 800 nm spectral window). The UV-Vis spectrum of complex **5.3** shows excellent agreement with $\lambda_{max}$ at 470 and 725 nm reported for complex **5.24** (**Figure 5.12**).[4]

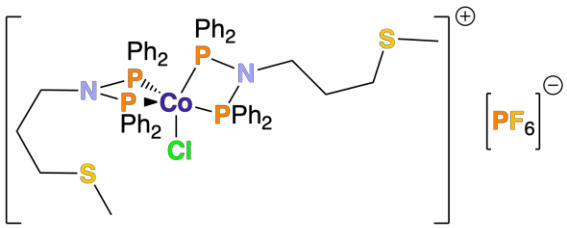


**5.24**

**Figure 5.12.** Structure of complex **5.24**.[4]

The main band of interest in the UV-Vis spectra of complex **5.7** is the band at 526 nm, which has been assigned to $[LCo^{I}]^{+}$, *i.e.*, a cationic cobalt(I) species with coordinating ligands. The band at 526 nm is very similar to a band at 517 nm assigned to $[(dppp)Co^{I}]^{+}$.[3] Together, these data are consistent with complex **5.7** being a cationic cobalt(I) diphosphine species.

The molar absorbance coefficient, $\varepsilon$, for the band at 526 nm in the UV-Vis spectra of complex **5.7**, is estimated to be approx. 7400 $dm^3\ mol^{-1}\ cm^{-1}$. An $\varepsilon$ value of this magnitude indicates that the band at 526 nm is charge transfer in nature, consistent with the very deep purple colour observed for complex **5.7**.

### 5.3.7 Hybrid DFT UV-Vis Spectroscopic Analysis of $[Co\{MeN(PPh_2)_2\}_2][BAr^F_4]$

Hybrid-DFT analysis (at the B3LYP/6-31G(d) level) was carried out to calculate the UV-Vis spectrum of $[Co\{MeN(PPh_2)_2\}_2][BAr^F_4]$ in order to verify the origins and assist with the assignment of the transitions observed experimentally. For ease of computation, a simpler analogue of complex **5.7** with methyl substituents on the nitrogen atoms instead of $CH_2CH_2Ph$ was utilised. This analysis, when coupled with a molecular orbital population analysis using GaussSum,[15] showed that there is a metal-ligand charge transfer at 504 nm (band with greatest oscillator strength in the region of interest, with metal-ligand charge transfer being indicated by the large numerical decrease of 88 on the cobalt(I) centre coupled with the same numerical increase on the ligand fragments; see **Appendix 5** for output data). Considering the change in nitrogen atom substituent from $CH_2CH_2Ph$ in complex **5.7** to Me in $[Co\{MeN(PPh_2)_2\}_2][BAr^F_4]$, the computed value of 504 nm is in good agreement with the experimental value of 526 nm. The major transitions responsible for the computationally calculated band found at 504 nm, with their percentage contribution, are shown in **Figure 5.13**.

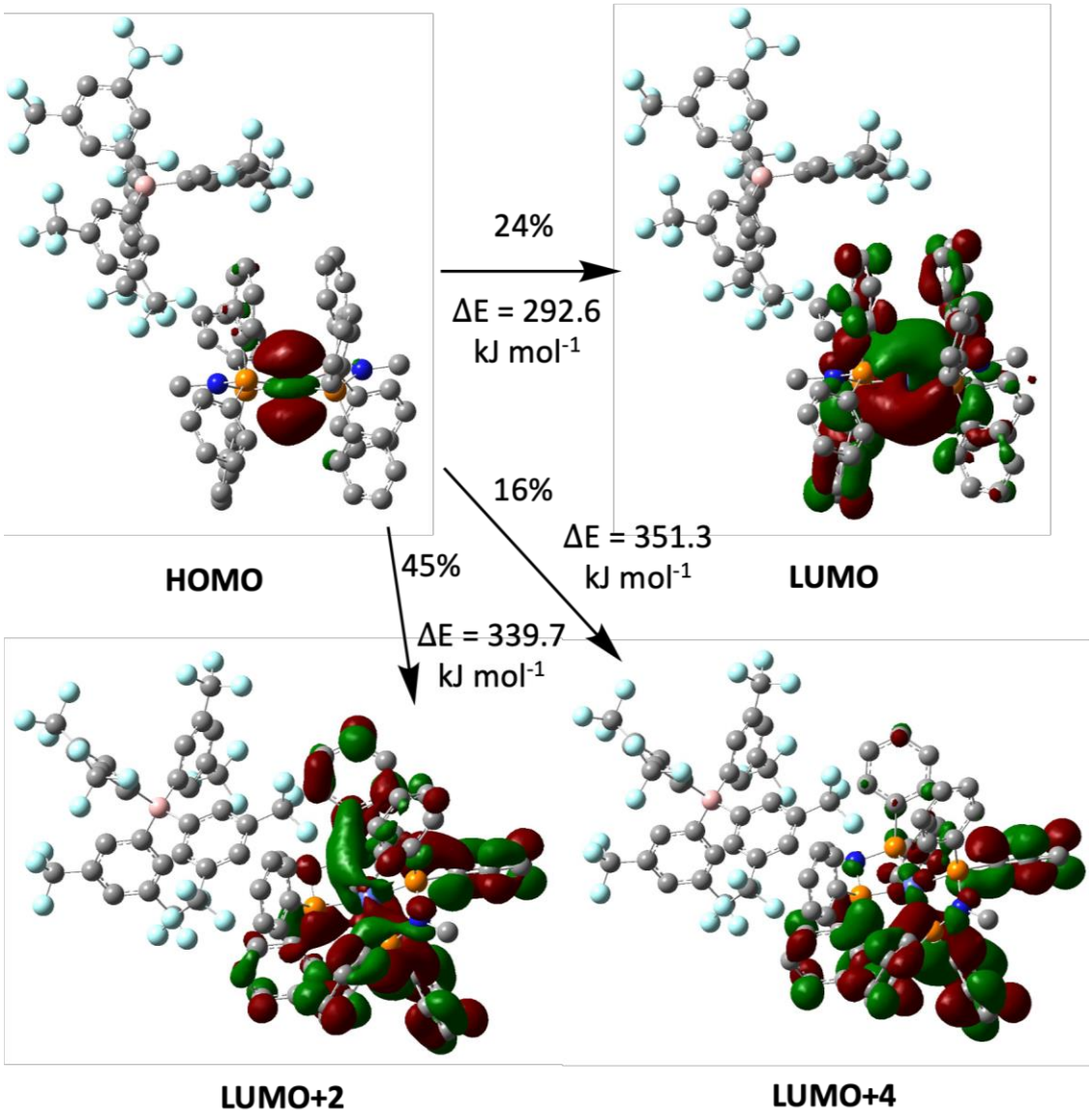


**Figure 5.13.** The three major transitions, with their percentage contributions and computed molecular orbitals, contributing to the band observed at 504 nm in the calculated UV-Vis spectrum of $[Co\{MeN(PPh_2)_2\}_2][BAr^F_4]$.

The data in **Figure 5.13** show that the transitions are occurring from the HOMO (the $3d_z^2$ orbital, purely located on the cobalt(I) centre), to the predominantly ligand-based LUMO (containing the $4_{pz}$ orbital of the cobalt(I) centre), LUMO+2 and LUMO+4 (both with very limited metal orbital character), illustrating that the charge transfer is metal-to-ligand in nature. Although the LUMO contains the $4_{pz}$ orbital of the cobalt(I) centre, the LUMO <- HOMO transition only has a 24% contribution to the computationally calculated band at 504 nm (*cf*. 61% combined contribution for the LUMO+2 <- HOMO and LUMO+4 <- HOMO, *i.e*., transitions involving essentially purely ligand-based LUMOs). Hence, the transitions are still primarily from a metal-based HOMO to ligand-based LUMOs and the overall charge transfer can be regarded as a metal-ligand charge transfer in nature.

## 5.4 Alternative Attempted Strategies to Access Cationic Cobalt(I) Complexes of 'PNP' ligands

As outlined in **Section 5.3**, the reduction of analytically pure complexes **5.1** ([CoBr(Ph(CH$_2$)$_2$N{PPh$_2$}$_2$)$_2$][PF$_6$]), **5.2** ([CoBr(Py-*o*-(CH$_2$)$_2$N{PPh$_2$}$_2$)$_2$][PF$_6$]) and **5.3** ([CoBr(Ph(CH$_2$)$_2$N{PPh$_2$}$_2$)$_2$][BAr$^F_4$]) with activated zinc afforded complexes **5.5** ([Co(Ph(CH$_2$)$_2$N{PPh$_2$}$_2$)$_2$][PF$_6$]), **5.6** ([Co(Py-*o*-(CH$_2$)$_2$N{PPh$_2$}$_2$)$_2$][PF$_6$]) and **5.7** ([Co(Ph(CH$_2$)$_2$N{PPh$_2$}$_2$)$_2$][BAr$^F_4$]) respectively, of which satisfactory CHN analyses could not be obtained. Hence, methodologies to access cationic cobalt(I) complexes containing 'PNP' ligands without utilising zinc as a reductant were attempted to try and circumvent the purification issues presented by residual zinc and the production of zinc halides (as well as phosphorus-containing by-products). *NB* reactions utilising other common reductants (*e.g.*, magnesium, SmI$_2$ and KC$_8$) in place of activated zinc were avoided due to concerns of over-reduction to cobalt(0).[16]

### 5.4.1 Reaction of Py-*o*-(CH$_2$)$_2$N(PPh$_2$)$_2$ (2.1) and Ph(CH$_2$)$_2$N(PPh$_2$)$_2$ (2.2) with CoCl(PPh$_3$)$_3$

Compounds **2.1** and **2.2** were reacted with one equivalent of CoCl(PPh$_3$)$_3$ in an attempt to afford complexes **5.25** and **5.26** (**Scheme 5.6**). However, air sensitive complexes **5.27** and **5.28** are tentatively assigned as the isolated products (**Scheme 5.6**). Complexes **5.27** and **5.28** are the 2:1 'PNP':CoCl(PPh$_3$)$_3$ reaction products, despite the 1:1 'PNP':CoCl(PPh$_3$)$_3$ reaction stoichiometry employed (**Scheme 5.6**). Indeed, the 1:1 reaction of CoCl$_2$ and dppbz with NaBH$_4$ in EtOH provides [CoCl(dppbz)$_2$], *i.e.*, the 2:1 dppbz:CoCl$_2$ product is isolated despite the 1:1 dppbz:CoCl$_2$ reaction stoichiometry.[17] *NB* CoCl(PPh$_3$)$_3$ was synthesised following a literature procedure.[18]

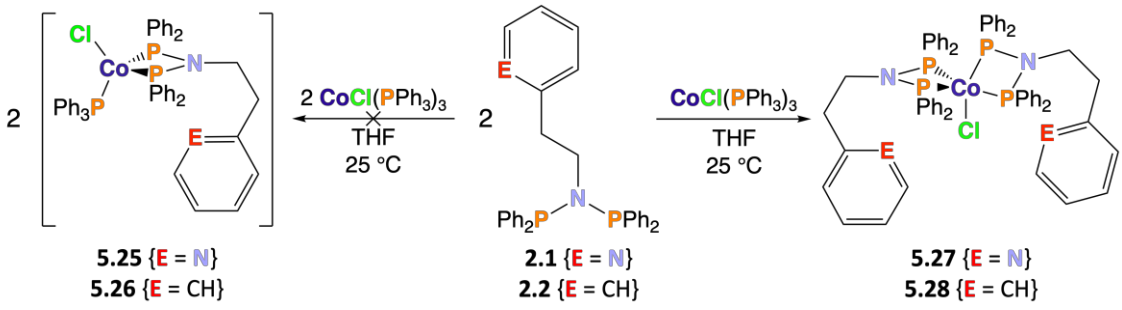


**Scheme 5.6.** Attempted synthesis of complexes **5.25** and **5.26** and proposed synthesis of complexes **5.27** and **5.28**.

The assignment of complexes **5.27** and **5.28** as the isolated product (**Scheme 5.6**) is primarily based on positive ion ESI mass spectrometric analyses of the isolated products. Signals at 1074.5 *m/z* and 1073.3 *m/z* corresponding to $[CoCl\{Py\text{-}o\text{-}(CH_2)_2N(PPh_2)_2\}_2]^+$ and $[CoCl\{Ph(CH_2)_2N(PPh_2)_2\}_2]^+$, *i.e.*, $[M]^+$ of complexes **5.27** and **5.28**, respectively, are evidenced. No signals assignable to complexes **5.25** and **5.26** are observed. Disappointingly, single crystals of complexes **5.27** and **5.28** could not be obtained. The measured CHN analyses of the isolated products (**Scheme 5.6**) were not in good agreement with the calculated CHN composition for target complexes **5.27** and **5.28**, likely due to residual $PPh_3$ (despite washing the crude solids with copious amounts of pentane). Attempted magnetic moment measurements (*via* the Evans NMR method;[5] $d_8$-THF, 294 K) for proposed complexes **5.27** and **5.28** proved to be inconclusive due to several $^1H$ NMR signals appearing in the spectral region of interest (0.5 – 4 ppm for $d_8$-THF) upon addition of the $d_8$-THF lock tube to the sample, suggesting the presence of paramagnetic impurities (or unreacted $CoCl(PPh_3)_3$). Complexes **5.27** and **5.28** should be diamagnetic as the $d^8$ cobalt(I) centre most likely has a distorted trigonal bipyramidal geometry and hence no unpaired electrons (**Figure 5.14**).

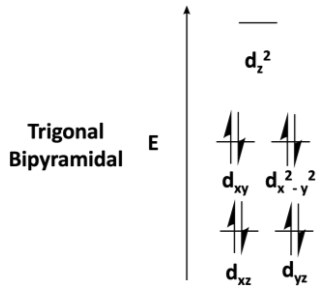


**Figure 5.14.** d-Orbital energy diagram for a trigonal bipyramidal metal centre, showing the orbital occupancy for a $d^8$ electron configuration.[19]

Experimental difficulty, coupled with the air sensitivity of proposed complexes **5.27** and **5.28** ($[CoCl\{Py\text{-}o\text{-}(CH_2)_2N(PPh_2)_2\}_2]$ and $[CoCl\{Ph(CH_2)_2N(PPh_2)_2\}_2]$, respectively), which undergo a green to blue-grey colour change upon exposure to air, has made reliably characterising complexes **5.27** and **5.28** challenging. Hence, further study of complexes **5.27** and **5.28** has been abandoned. Reaction of complexes **5.27** and **5.28** with $ZnCl_2$ in THF would likely afford cationic cobalt(I) complexes **5.29** and **5.30** (**Scheme 5.7**),[20] which are analogous to complexes **5.5** – **5.7** ($[Co(Ph(CH_2)_2N\{PPh_2\}_2)_2][PF_6]$, ($[Co(Py\text{-}o\text{-}(CH_2)_2N\{PPh_2\}_2)_2][PF_6]$) and ($[Co(Ph(CH_2)_2N\{PPh_2\}_2)_2][BAr^F{}_4]$), respectively) apart from the difference in anion (predicted to be the $[ZnCl_3(THF)]$ anion in complexes **5.29** and

**5.30**).[20] Hence, further study of complexes **5.27** and **5.28** seems futile when complexes **5.5** – **5.7** containing the same cation and weakly coordinating anions have been synthesised successfully.

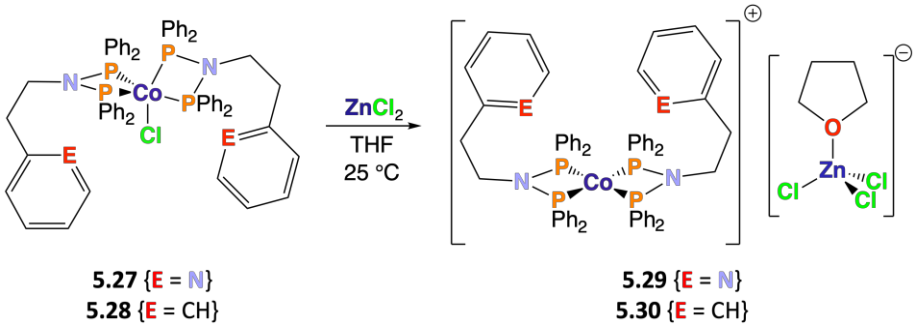


**5.27** {E = N}
**5.28** {E = CH}

**5.29** {E = N}
**5.30** {E = CH}

**Scheme 5.7.** The hypothetical halide abstraction reaction of complexes **5.27** and **5.28** with $ZnCl_2$ to afford complexes **5.29** and **5.30**, respectively.

## 5.4.2 Attempted Synthesis of [CoH{Py-*o*-$(CH_2)_2$N$(PPh_2)_2$}$_2$] (5.31)

Two equivalents of 'PNP' compound **2.1** were reacted with one equivalent of $Co(acac)_2$ and six equivalents of HBPin (pinacolborane) in DCM, in an attempt to prepare cobalt(I) hydride complex **5.31** (**Scheme 5.8**), a target of potential importance in catalytic processes, *e.g.*, selective olefin oligomerisation.[21] This reaction was adapted from a literature procedure that employed the diphosphine dppbz.[22] HBPin was selected as a hydride source as opposed to other common hydride sources, *e.g.*, $NaBH_4$, due to the established coordination of the $BH_4^-$ anion with cobalt centres.[23]

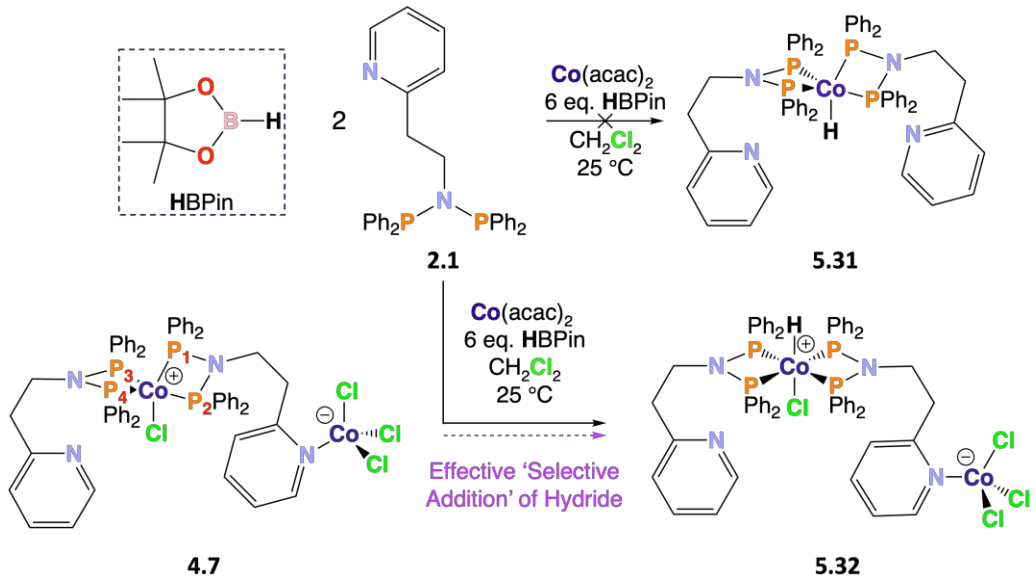


**2.1**

**5.31**

**4.7**

**5.32**

**Scheme 5.8.** Attempted synthesis of complex **5.31** and the synthesis of complex **5.32**.

Instead of the target hydride complex **5.31** it was found that the mixed six coordinate hydride halide complex **5.32** was formed, presumably due to the reaction of a cobalt(I)

intermediate with DCM solvent (see **Section 5.3.4**; DCM is the only source of chlorine atoms in this reaction). Complex **5.32** contains a cationic distorted octahedral cobalt(III) centre with a hydride and chloride ligand with a *trans* relationship and an anionic [PyCo$^{II}$Cl$_3$] moiety analogous to complex **4.7** (**Scheme 5.8**). This transformation (**Scheme 5.8**) can be regarded as a 'selective addition' of a hydride to the cationic cobalt(II) centre of complex **4.7**. Attempts to directly synthesise complex **5.32** from complex **4.7** would be very challenging, if at all possible.

Attempted synthesis of complex **5.31** in THF yielded a sticky solid, which was challenging to isolate. Analytical data ($^1$H and $^{31}$P NMR spectroscopy, CHN and mass spectrometry) evidenced that a complex mixture of products had been produced. Additional attempts to further purify this crude mixture, *e.g.*, washing with pentane and recrystallisation, were unsuccessful. Hence, this reaction was abandoned, as were analogous reactions involving 'PNP' compound **2.2** (Ph(CH$_2$)$_2$N(PPh$_2$)$_2$). An alternative procedure for the formation of hydride complexes, *i.e.*, the reaction of two equivalents of 'PNP' compound **2.1** with Co(NO$_3$)$_2$·6H$_2$O and an excess of NaBH$_4$ (as utilised for the synthesis of [CoH{P(OPh)$_3$}$_4$] using P(OPh)$_3$ as the phosphine)[24] is unsuitable in this case due to the necessity of an alcoholic solvent, *e.g.*, EtOH; metal complexes of 'PNP' ligands are known to undergo alcoholysis of a P-N bond, evidenced in **Section 3.4**, **Chapter 3**.[25]

### 5.4.3 Solid-State Molecular Structure of [Co(H)(Cl)(Py-*o*-(CH$_2$)$_2$N{PPh$_2$}$_2$)({Cl$_3$Co}Py-*o*-(CH$_2$)$_2$N{PPh$_2$}$_2$)] (5.32)

Single crystals of complex **5.32** were obtained from the reaction described in **Scheme 5.8** and a molecular structure determined (**Figure 5.15**). H1 was clearly located during the refinement process and refined freely.

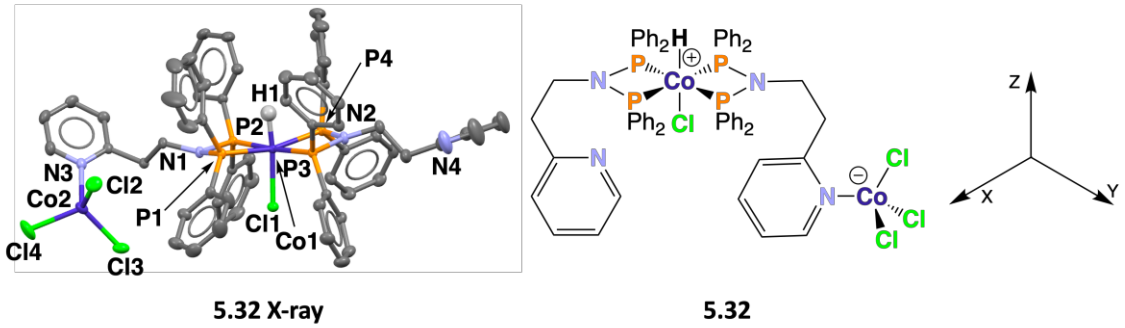


**5.32 X-ray** **5.32**

**Figure 5.15.** Solid-state molecular structure of complex **5.32**. Thermal ellipsoids are shown at the 50 % probability level. *NB* hydrogen atoms (except H1) and DCM molecules are omitted for clarity. Atom colour: carbon – grey; nitrogen – light blue; phosphorus – orange; chlorine – green; cobalt – dark blue, and hydrogen – white.

The key bond lengths and bond angles measured from the solid-state structure of complex **5.32** are presented in **Table 5.9**.

**Table 5.9.** Key bond lengths and bond angles measured from the solid-state molecular structures of complexes **5.32** and **4.7**.

| Parameter | 5.27 | 4.7 |
|---|---|---|
| Cl1-Co1-H1 | 174(1) | – |
| Cl1-Co1-P1 | 90.48(2) | 119.57(3) |
| Cl1-Co1-P2 | 90.05(2) | 95.16(2) |
| Cl1-Co1-P3 | 93.72(2) | 95.26(2) |
| Cl1-Co1-P4 | 103.40(2) | 132.33(3) |
| H1-Co1-P1 | 84(1) | – |
| H1-Co1-P2 | 88(1) | – |
| H1-Co1-P3 | 88(1) | – |
| H1-Co1-P4 | 83(1) | – |
| P1-Co1-P2 | 72.44(2) | 71.35(2) |
| P1-Co1-P3 | 108.45(2) | 103.71(2) |
| P1-Co1-P4 | 166.05(2) | 108.09(2) |
| P2-Co1-P3 | 176.11(2) | 169.57(3) |
| P2-Co1-P4 | 105.69(2) | 100.96(2) |
| P3-Co1-P4 | 72.50(2) | 71.45(2) |
| Cl2-Co2-Cl3 | 113.21(3) | 113.52(3) |
| Cl2-Co2-Cl4 | 111.97(2) | 113.27(3) |
| Cl3-Co2-Cl4 | 110.53(3) | 111.03(3) |
| Cl2-Co2-N3 | 100.14(5) | 100.88(6) |
| Cl3-Co2-N3 | 105.85(5) | 103.39(6) |
| Cl4-Co2-N3 | 114.69(5) | 114.01(6) |
| P1-N1-P2 | 99.35(7) | 101.3(1) |
| P3-N2-P4 | 101.18(8) | 101.0(1) |
| Co1-Cl1 | 2.2806(6) | 2.2264(7) |
| Co1-H1 | 1.42(3) | – |
| Co1-P1 | 2.1927(5) | 2.2687(7) |
| Co1-P2 | 2.2078(5) | 2.2396(7) |
| Co1-P3 | 2.2209(5) | 2.2411(7) |
| Co1-P4 | 2.2073(5) | 2.2397(5) |
| Co2-Cl2 | 2.2575(7) | 2.250(1) |
| Co2-Cl3 | 2.2555(8) | 2.2662(9) |
| Co2-Cl4 | 2.2477(6) | 2.2530(6) |
| Co2-N3 | 2.072(2) | 2.077(2) |
| N1-P1 | 1.700(1) | 1.708(2) |
| N1-P2 | 1.711(1) | 1.694(2) |
| N2-P3 | 1.698(1) | 1.691(2) |
| N2-P4 | 1.691(1) | 1.698(2) |

Comparing the key bond angles and bond lengths of the {Co(H)(Cl)(κ$^2$-*P,P*)$_2$}$^+$ moiety of complex **5.32** with those of the {CoCl(κ$^2$-*P,P*)$_2$}$^+$ moiety of complex **4.7** ([CoCl(Py-*o*-(CH$_2$)$_2$N{PPh$_2$}$_2$)({Cl$_3$Co}Py-*o*-(CH$_2$)$_2$N{PPh$_2$}$_2$)], **Scheme 5.8**), reveals some interesting observations. The PX-Co1 (X = 1 – 4) bond lengths are slightly shorter in complex **5.32** (~2.20 – 2.22 Å) relative to complex **4.7** (~2.24 – 2.27 Å). This could be because P1 – P4 of complex **5.32** are in the XY plane (**Figure 5.15**), hence the phenyl substituents of P1 and P3 (and P2 and P4) are more separated (relative to, for example, the phenyl substituents on P1 and P3 of complex **4.7**, **Scheme 5.8**) and any steric clash between them is less. The greater separation between the P1 and P3 phenyl substituents of complex **5.32** relative to complex **4.7** is evidenced in **Figure 5.16**. As a result, P-Co bond length elongation is not required to reduce steric clash in complex **5.32**.

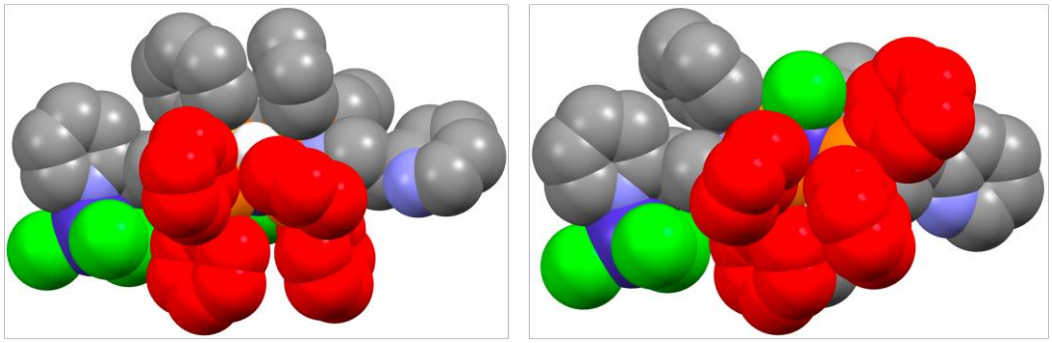


**Figure 5.16.** Space filling models of solid-state structures of complexes **5.32** and **4.7**. The carbon atoms of the P1 and P3 phenyl substituents are red. *NB* hydrogen atoms (except the hydride) and DCM molecules are omitted for clarity. Atom colour: carbon – grey (unless stated to be red); nitrogen – light blue; phosphorus – orange; chlorine – green; cobalt – dark blue, and hydrogen – white.

The P-N bond lengths (~1.69 – 1.71 Å) and P-N-P angles (~101°) in complex **5.32** are essentially unchanged relative to complex **4.7**. The Cl1-Co1 bond is slightly longer in complex **5.32** (2.2806(6) Å) relative to complex **4.7** (2.2264(7) Å), possibly due to the strong *trans* influence of the hydride ligand in complex **5.32**. The H1-Co1 bond length is 1.42(3) Å (very similar to 1.45(2) Å measured for previously reported CoH(dppbz)$_2$).[22] The PX-Co-P(X+1) (where X = 1 or 3) bite angles in complex **5.32** are essentially the same relative to those in complex **4.7** (~71°), but are ~17.5° smaller than the ideal 90° angle between coordinating sites on an octahedral geometry. The small bite angles result in PX-Co-P(X+2) (where X = 1 or 2) bond angles of 108.45(2)° and 105.69(2)° for X = 1 and X = 2, respectively. The P1/3-Co1-Cl1 bond angles of ~90 – 94° are consistent with an octahedral geometry. However, P4-Co1-Cl1 is 103.40(2)°, arising from the deviation of

P4 from the Co(P1-4)$_4$ plane by ~0.434 Å, clearly seen in **Figure 5.15**. The P2/3-Co1-H1 bond angle is 88(1)°, with the P1/4-Co1-H1 bond angle being 84(1)° and 83(1)° for P1 and P4, respectively. This distortion arises due to the H1-Co1 bond being more orientated towards P1, and P4 being displaced from the Co(P1–4)$_4$ plane closer to H1.

### 5.4.4 Synthesis of [Co(H)(Cl)(Py-*o*-(CH$_2$)$_2$N{PPh$_2$}$_2$)$_2$][PF$_6$] (5.33) and [Co(H)(Cl)(Ph(CH$_2$)$_2$N{PPh$_2$}$_2$)$_2$][PF$_6$] (5.34)

Two equivalents of 'PNP' compound **2.1** or **2.2** were reacted with one equivalent of Co(acac)$_2$, six equivalents of HBPin and one equivalent of KPF$_6$ in DCM to afford cationic octahedral cobalt(III) hydride complexes **5.33** and **5.34** (**Scheme 5.9**). The preparation of complexes **5.33** and **5.34** was attempted in order to synthesise a diamagnetic analogue of the octahedral cobalt(III) motif present in complex **5.32** (**Scheme 5.8**), allowing for characterisation by NMR spectroscopic methods.

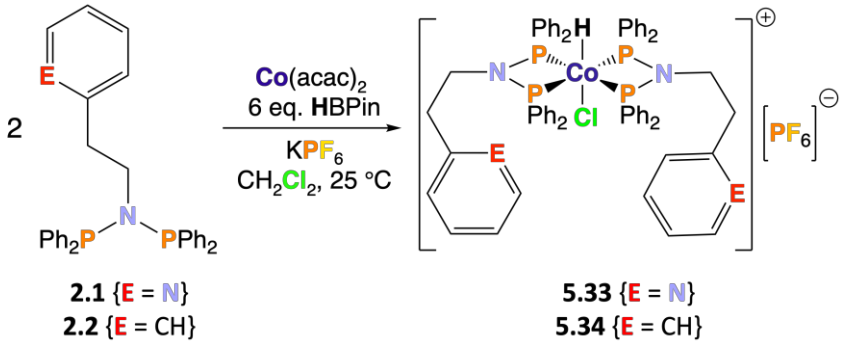


**Scheme 5.9.** Synthesis of complexes **5.33** and **5.34**.

The $^1$H NMR spectra of diamagnetic complexes **5.33** and **5.34** evidence a quintet, at $\delta_H$ = –18.0 ppm for complex **5.33** (**Figure 5.17**), corresponding to the hydride. The quintet arises from coupling of the hydride to four phosphorus atoms with $^2J_{HP}$ = 53 Hz. The spectral data are consistent with the $^1$H NMR spectral data for [Co(H)(Cl)(dppm)$_2$]Cl (quintet at $\delta_H$ = –17.5 ppm with $^2J_{HP}$ = 51 Hz).[26,27] The hydride has been confirmed to come from HBPin and not DCM by conducting the reaction (**Scheme 5.9**) in $CD_2Cl_2$ instead of DCM and monitoring the reaction by $^1$H NMR spectroscopy; the hydride signal is present in the $^1$H NMR spectrum regardless of the reaction solvent.

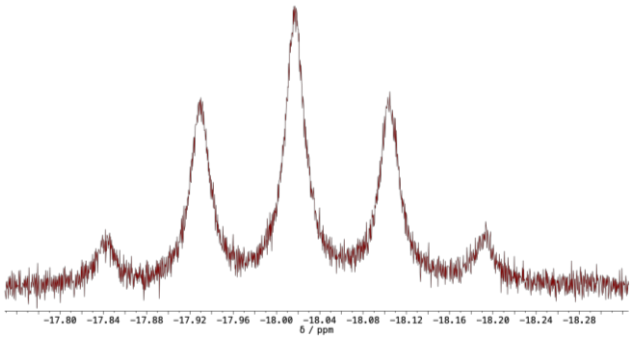


**Figure 5.17.** $^{1}$H NMR (400 MHz, 290 K, $CDCl_3$) spectrum of complex **5.33**, in the –17.80 to –18.25 ppm region, showing the quintet, centred at $\delta_H$ = –18.02 ppm, corresponding to the hydride.

The $^{31}$P NMR spectra of complexes **5.33** and **5.34** show a doublet ($\delta_P$ ~84 ppm, $^{2}J_{HP}$ = 47 Hz) corresponding to the cobalt-bound phosphorus atoms and a septet ($\delta_P$ = –144 ppm) corresponding to $PF_6^-$. Positive ion ESI mass spectrometry reveals signals at 1075.4 *m/z* and 1073.5 *m/z* for the cations of complexes **5.33** and **5.34**, respectively. Hence, $^{31}$P NMR spectroscopic and mass spectrometric evidence together supports the formation of complexes **5.33** and **5.34**. However, measurements of $\mu_{eff}$ *via* the Evans NMR method[5] ($CD_2Cl_2$, 294 K) for complexes **5.33** and **5.34** suggest that paramagnetic impurities are also present (potentially complex **5.32** in the case of compound **5.33**). This is further evidenced from the measured CHN analyses of complexes **5.33** and **5.34** being different from their calculated CHN compositions (for complex **5.33**: ΔC = –1.86, ΔH = –0.42, ΔN = –0.59; for complex **5.34**: ΔC = –1.06, ΔH = 0.06, ΔN = –0.29).

Ultimately, $^{31}$P and $^{1}$H NMR (and mass spectrometric) data evidence the successful synthesis of models for the octahedral cobalt(III) motif present in complex **5.32** ([Co(H)(Cl)(Py-*o*-$(CH_2)_2$N{$PPh_2$}$_2$)({$Cl_3$Co}Py-*o*-$(CH_2)_2$N{$PPh_2$}$_2$)], **Scheme 5.8**). However, the attempts to access cobalt(I) complexes without the use of activated zinc as a reductant presented in **Section 5.4** has highlighted that study of the reactivity of complexes **5.5** – **5.7** ([Co(Ph$(CH_2)_2$N{$PPh_2$}$_2$)$_2$][$PF_6$], ([Co(Py-*o*-$(CH_2)_2$N{$PPh_2$}$_2$)$_2$][$PF_6$]) and ([Co(Ph$(CH_2)_2$N{$PPh_2$}$_2$)$_2$][$BAr^F{}_4$]), respectively, **Section 5.3**) is the most suitable direction for future work, despite the likely presence of zinc-containing impurities. The reactivity of complex **5.7** will be presented in **Chapter 6**.

**Section 5.5** will focus on the isolation and characterisation of the products of the reactions of 'PNP' compounds **2.1** (Py-*o*-$(CH_2)_2$N($PPh_2$)$_2$) and **2.2** (Ph$(CH_2)_2$N($PPh_2$)$_2$) with $ZnBr_2$ to elucidate if the same complexes form during the reductions of complexes **5.1** – **5.3** ([CoBr(Ph$(CH_2)_2$N{$PPh_2$}$_2$)$_2$][$PF_6$], ([CoBr(Py-*o*-$(CH_2)_2$N{$PPh_2$}$_2$)$_2$][$PF_6$]) and

([CoBr(Ph$(CH_2)_2$N{$PPh_2$}$_2$)$_2$][$BAr^F_4$]), respectively, **Section 5.3**) with activated zinc. Studying the reactions of compounds **2.1** and **2.2** with $ZnBr_2$ is important because the reduction of cobalt(II) phosphine halide complexes with activated zinc can lead to the formation of [($\kappa^2$-*P,P*)$ZnX_2$] (X = Cl, Br, I) complexes.[28] [($\kappa^2$-*P,P*)$ZnX_2$] complexes are prepared by the reaction of free phosphine with $ZnX_2$ formed during the reduction with activated zinc.[28] Free phosphine is present as a result of phosphine dissociation from the cobalt(II) complex, or from disproportionation of a cobalt(I) species to produce cobalt(0) and a cobalt(II) complex, followed by phosphine dissociation from the cobalt(II) complex.

## 5.5 Reactivity of Py-*o*-$(CH_2)_2N(PPh_2)_2$ (2.1) and Ph$(CH_2)_2N(PPh_2)_2$ (2.2) with Zinc(II) Dibromide

There has been scarce study of the coordination chemistry of 'PNP' compounds with $ZnX_2$. The only examples the author is aware of are the reaction of compound **5.35** with $ZnCl_2$ affording complex **5.36** with rearrangement of the P-N-P moiety into N=P-P and $\kappa^2$-*N,N* chelation (**a**), **Scheme 5.10**),[29] and the reaction of compounds **5.37** – **5.39** with $ZnEt_2$ affording complexes **5.40** and **5.41**, evidencing $\kappa^2$-*P,P* coordination, or complexes **5.42** and **5.43** (**b**), **Scheme 5.10**).[30]

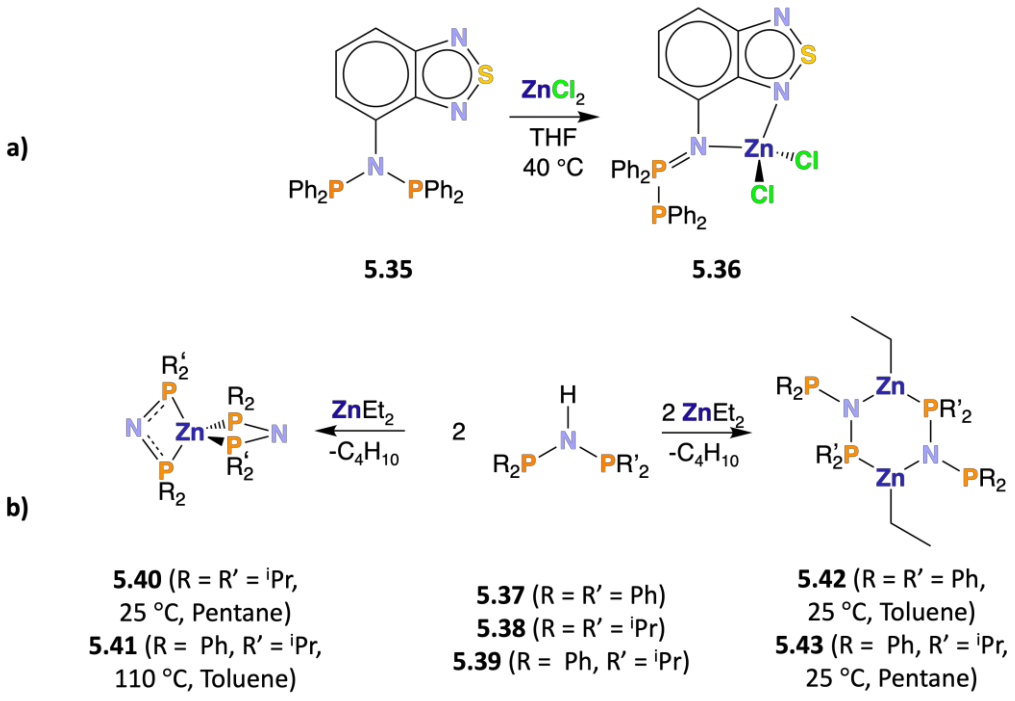


**Scheme 5.10.** Synthesis of complexes **5.36**[29] and **5.40** – **5.43**.[30]

### 5.5.1 Coordination Chemistry of $Ph(CH_2)_2N(PPh_2)_2$ (2.2) with Zinc(II) Dibromide

To further explore the coordination chemistry of 'PNP' compounds with zinc(II), 'PNP' compound **2.2** was reacted with $ZnBr_2$, with a view to potentially afford complex **5.44**, complex **5.45** or complex **5.46** (**Scheme 5.11**).

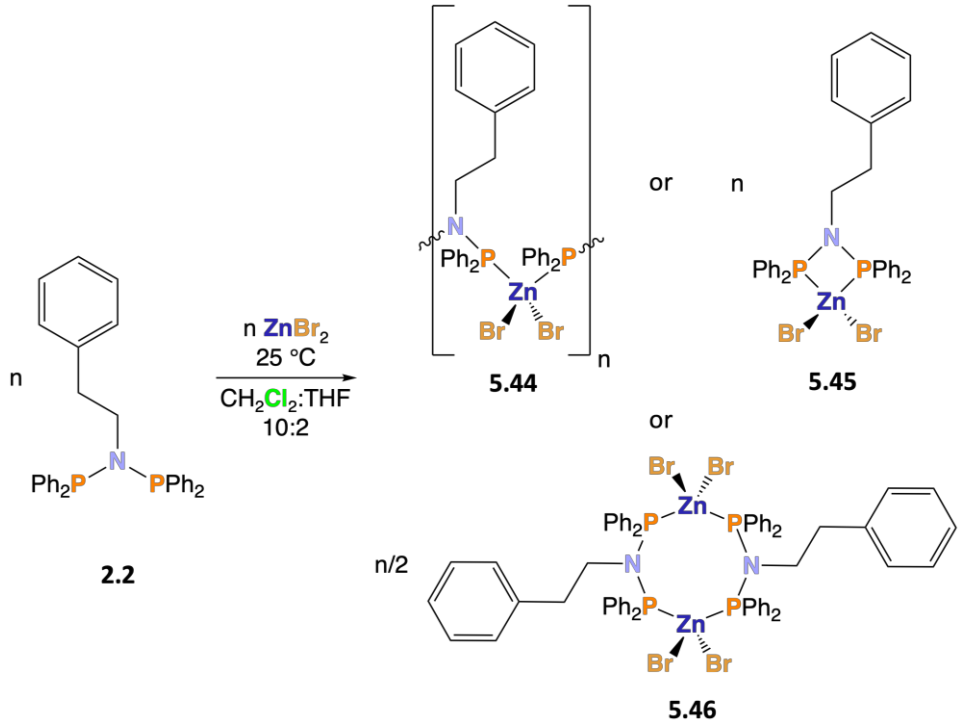


**Scheme 5.11.** Reaction of **2.2** with $ZnBr_2$ affording complex **5.44**, complex **5.45** or complex **5.46**.

Mass spectrometric analysis of the isolated product of the reaction of compound **2.2** with $ZnBr_2$ (**Scheme 5.11**) evidences no signals assignable to complexes **5.44**, **5.45** or **5.46**; only signals corresponding to fragments associated with compound **2.2** are observed. CHN analysis of the isolated product of the reaction of compound **2.2** with $ZnBr_2$ (**Scheme 5.11**) supports a 1:1 ratio of $ZnBr_2$:**2.2** (present in complexes **5.44**, **5.45** and **5.46**). Single crystals of isolated product of the reaction of compound **2.2** with $ZnBr_2$ (**Scheme 5.11**) could not be obtained.

Following the reaction of compound **2.2** with $ZnBr_2$ (**Scheme 5.11**) by $^{31}P\{^1H\}$ NMR spectroscopy evidences a broad ($\nu_{1/2}$ = 101 Hz) singlet with $\delta_P$ = 71.3 ppm relative to $\delta_P$ = 62.7 ppm for compound **2.2** (**Figure 5.18**). The signals in the $^1H$ NMR spectrum of the isolated product of the reaction of compound **2.2** with $ZnBr_2$ (**Scheme 5.11**) are also broadened relative to the sharp signals recorded for compound **2.2**. The $^{31}P\{^1H\}$ and $^1H$ NMR signal broadness is not due to paramagnetism as zinc(II) is $d^{10}$ and diamagnetic.

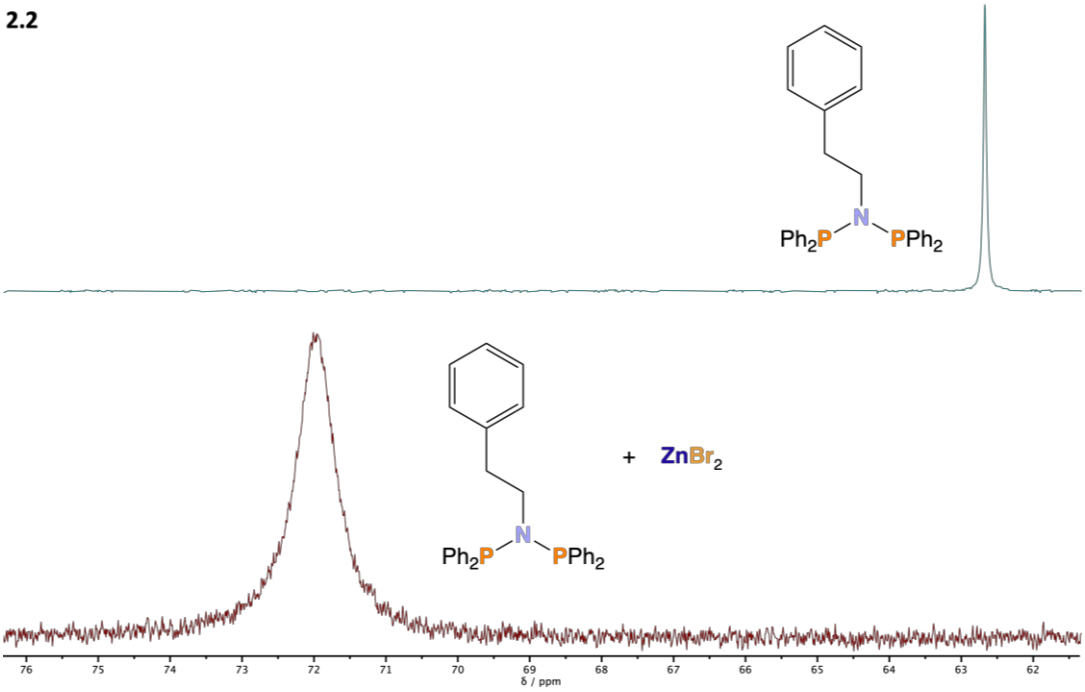


**Figure 5.18.** $^{31}P\{^{1}H\}$ NMR (162 MHz, 290 K) spectra for compound **2.2** ($CDCl_3$) and the isolated product of the reaction of compound **2.2** with $ZnBr_2$ ($CD_2Cl_2$).

A solid-state structure of complex **5.47** (the presumed oxidation product of complex **5.44**) has been obtained (**Section 5.5.2**) whilst attempting to grow single crystals of the isolated product of the reaction of compound **2.2** with $ZnBr_2$ (**Scheme 5.11**) under air. Complex **5.48** is known to oxidise to afford complex **5.49** (**Scheme 5.12**).[31] Hence, it is reasonable to assume that complex **5.44** oxidises to afford complex **5.47**, implying that complex **5.44** is the product of the reaction of compound **2.2** with $ZnBr_2$ (**Scheme 5.11**).

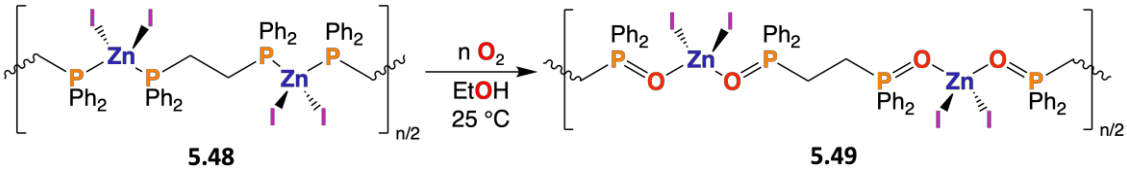


**5.48** **5.49**

**Scheme 5.12.** Reaction of previously reported complex **5.48** with $O_2$ to afford previously reported complex **5.49**.[31]

Coordination polymer complex **5.44** being the isolated product of the reaction of compound **2.2** with $ZnBr_2$ (**Scheme 5.11**) is also supported by the broad $^{31}P\{^{1}H\}$ and $^{1}H$ NMR signals as coordination polymers (*e.g.*, complex **5.48**, **Scheme 5.12**) often exhibit broad signals in their NMR spectra due to poor/hindered rotation along the polymer backbone.[32] Indeed, the structures and NMR spectroscopic analysis of previously reported complexes **5.50**[32] (analogous to complex **5.46**, **Scheme 5.11**) and **5.51**[33] (**Figure 5.19**) further supports the assignment of complex **5.44** as the isolated product of the

reaction of compound **2.2** with $ZnBr_2$ (**Scheme 5.11**). Complex **5.51** (afforded from both the 1:1 and 2:1 reactions of dppm and $ZnI_2$) bears two mono-dentate dppm ligands coordinating at the zinc(II) centre,[33] suggesting that acute bite angle diphosphine ligands do not coordinate at zinc(II) centres in a bidentate manner. Hence, complex **5.45** seems unlikely to be the isolated product (**Scheme 5.11**). The $^{31}P\{^{1}H\}$ and $^{1}H$ NMR spectra of complex **5.50** exhibit sharp signals,[32] suggesting that analogous complex **5.46** (**Scheme 5.11**) is not the isolated product of the reaction of compound **2.2** with $ZnBr_2$. Hence, complex **5.44** is tentatively assigned as the product of the reaction of compound **2.2** with $ZnBr_2$ (**Scheme 5.11**), although in the absence of a solid-state structure certainty is impossible.

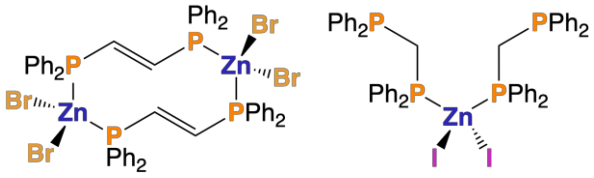


**5.50** **5.51**

**Figure 5.19.** Structures of previously reported complexes **5.50**[32] and **5.51**.[33]

## 5.5.2 Solid-State Molecular Structure of $[(Ph(CH_2)_2N(Ph_2PO)_2)ZnBr_2]_n$ (5.47) metal-organic 1D chain polymer

Single crystals of complex **5.47** (a zinc(II) phosphine oxide coordination polymer) were obtained and a molecular structure determined (**Figure 5.20**). It should be noted that the solid-state structure of complex **5.47** was obtained from one single crystal, which may not be representative of the bulk material of the oxidation product (not enough single crystals were obtained to allow for analysis of the bulk material).

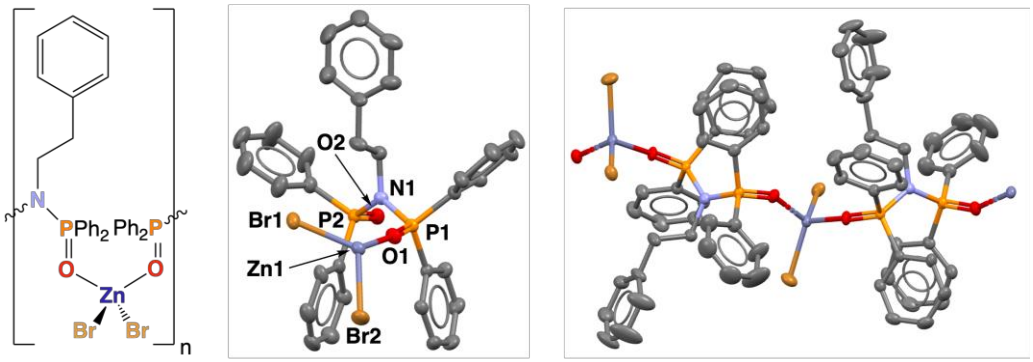


**5.47** **5.47 X-ray**

**Figure 5.20.** Solid-state molecular structure of the repeat unit and a chain segment of complex **5.47**. Thermal ellipsoids are shown at the 50 % probability level. *NB* hydrogen atoms are omitted for clarity. Atom colour: carbon – grey; phosphorus – orange; oxygen – red; zinc – dark blue, and bromide – orange-brown.

**Table 5.10.** Key bond lengths measured from the solid-state molecular structure of complex **5.47**.

| Bond | Bond Length / Å |
|---|---|
| Br1-Zn1 | 2.3562(8) |
| Br2-Zn1 | 2.3469(8) |
| Zn1-O1 | 1.978(3) |
| Zn1-O2 | 1.988(3) |
| P1-O1 | 1.482(3) |
| P2-O2 | 1.492(3) |
| P1-N1 | 1.692(4) |
| P2-N1 | 1.676(5) |

**Table 5.11.** Key bond angles measured from the solid-state molecular structure of complex **5.47**.

| Angle | Bond Angle / ° |
|---|---|
| Br1-Zn1-Br2 | 115.74(3) |
| Br1-Zn1-O1 | 111.3(1) |
| Br1-Zn1-O2 | 112.7(1) |
| Br2-Zn1-O1 | 110.5(1) |
| Br2-Zn1-O2 | 110.5(1) |
| O1-Zn1-O2 | 94.1(1) |
| P1-N1-P2 | 125.6(3) |
| Zn1-O1-P1 | 167.5(2) |
| P2-O2-Zn1 | 151.1(2) |

The key bond lengths and bond angles measured from the solid-state structure of complex **5.47** are presented in **Table 5.10** and **Table 5.11**, respectively. The solid-state structure of complex **5.47** shows that the two P=O bonds in the repeat unit are pointing in opposite directions, minimising steric clash around the P-N-P moiety. The bond angles around the zinc(II) centre are close to 109.5°, evidencing a distorted tetrahedral geometry around the metal in complex **5.47**. The O-Zn bond distances (O2-Zn1 = 1.988(3) Å, O1-Zn1 = 1.978(3) Å) and P=O distances (O1-P1 = 1.482(3) Å, O2-P2 = 1.492(3) Å) show good similarity to analogous distances in complex **5.49** (Zn-O distances: 1.958(2) Å, 1.964(2) Å; P=O distances: 1.493(2) Å, 1.506(9) Å) in **Scheme 5.12**.[31] The P=O bond distances of complex **5.47** are slightly longer than the corresponding distances of 1.471(2) Å and 1.477(2) Å in compound **5.52** (**Figure 5.21**) serving as a model for the $Ph(CH_2)_2N\{P(=O)Ph_2\}_2$ ligand in complex **5.47**, *i.e.*, compound **5.18**, **Figure 5.7**.[34] The P-N bond lengths in complex **5.47** (P1-N1 = 1.692(4) Å, P2-N1 = 1.676(5) Å) show good similarity to those in compound **5.52** (1.689(2) Å and 1.691(2) Å),[34] and are significantly shorter than the P-N bond lengths of 1.725(1) Å and 1.718(1) Å in compound **5.53** (**Figure 5.21**).[35] Hence, oxidation of the phosphorus atom reduces the P-N bond length as phosphorus(V) has a smaller ionic radius than phosphorus(III).[36] The P1-N1-P2 bond angle of complex **5.47** (125.6(3)°) shows good similarity to the P-N-P bond angles measured for compounds **5.52** (124.1(1)°)[34] and **5.53** (122.55(8)°),[35] showing that both

phosphine oxidation and bridging coordination of the phosphine oxide ligand (in complex **5.47**) does not result in compression of the P-N-P bond angle.

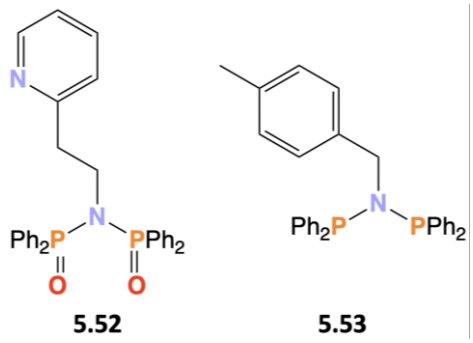


**Figure 5.21.** Structures of compounds **5.52**[34] and **5.53**.[35]

### 5.5.3 Coordination Chemistry of Py-*o*-$(CH_2)_2N(PPh_2)_2$ (2.1) with Zinc(II) Dibromide

Compound **2.1** was reacted with $ZnBr_2$, potentially affording complex **5.54**, **5.55** or **5.56** (**Scheme 5.13**). Both $^{31}P\{^1H\}$ and $^1H$ NMR spectral evidence verifies that the isolated product of the reaction of compound **2.1** with $ZnBr_2$ (**Scheme 5.13**) exhibits *P,N* coordination, despite having a P-N-P moiety allowing for $\kappa^2$-*P,P* coordination.

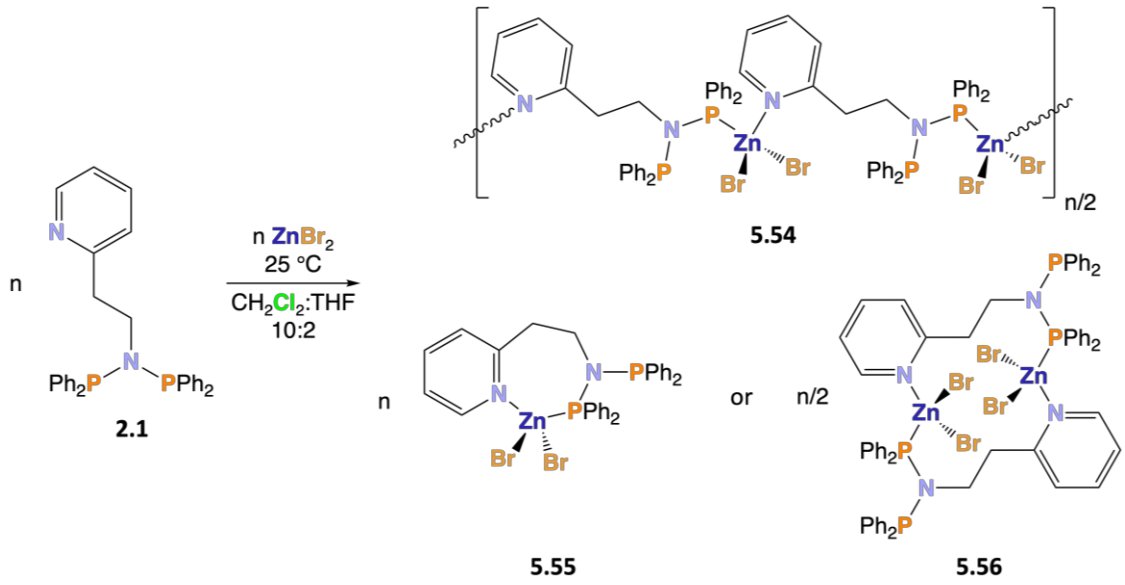


**Scheme 5.13.** Reaction of **2.1** with $ZnBr_2$ affording complex **5.54**, complex **5.55** or complex **5.56**.

The $^{31}P\{^1H\}$ NMR spectrum of the isolated product of the reaction of compound **2.1** with $ZnBr_2$ (**Scheme 5.13**) shows two doublets at $\delta_P$ = 56.3 and 49.5 ppm, with $^2J_{PP}$ = 16 Hz (very similar to $^2J_{P1P2}$ = 22 Hz measured for complex **5.57**, **Figure 5.22**),[37] confirming that the two phosphorus atoms of the P-N-P moiety are inequivalent. Rearrangement of the P-N-P moiety into a N=P-P moiety has not occurred as the aforementioned $^2J_{PP}$ coupling

constant of 16 Hz is smaller than the typical $^{1}J_{PP}$ = 220 – 290 Hz observed for an iminobiphosphine product.[38] The mass spectrum of the isolated product of the reaction of compound **2.1** with $ZnBr_2$ (**Scheme 5.13**) only evidences signals assignable to compound **2.1**. CHN analysis of the isolated product of the reaction of compound **2.1** with $ZnBr_2$ (**Scheme 5.13**) supports a 1:1 ratio of $ZnBr_2$:**2.1** present in complexes **5.54** – **5.56** (**Scheme 5.13**).

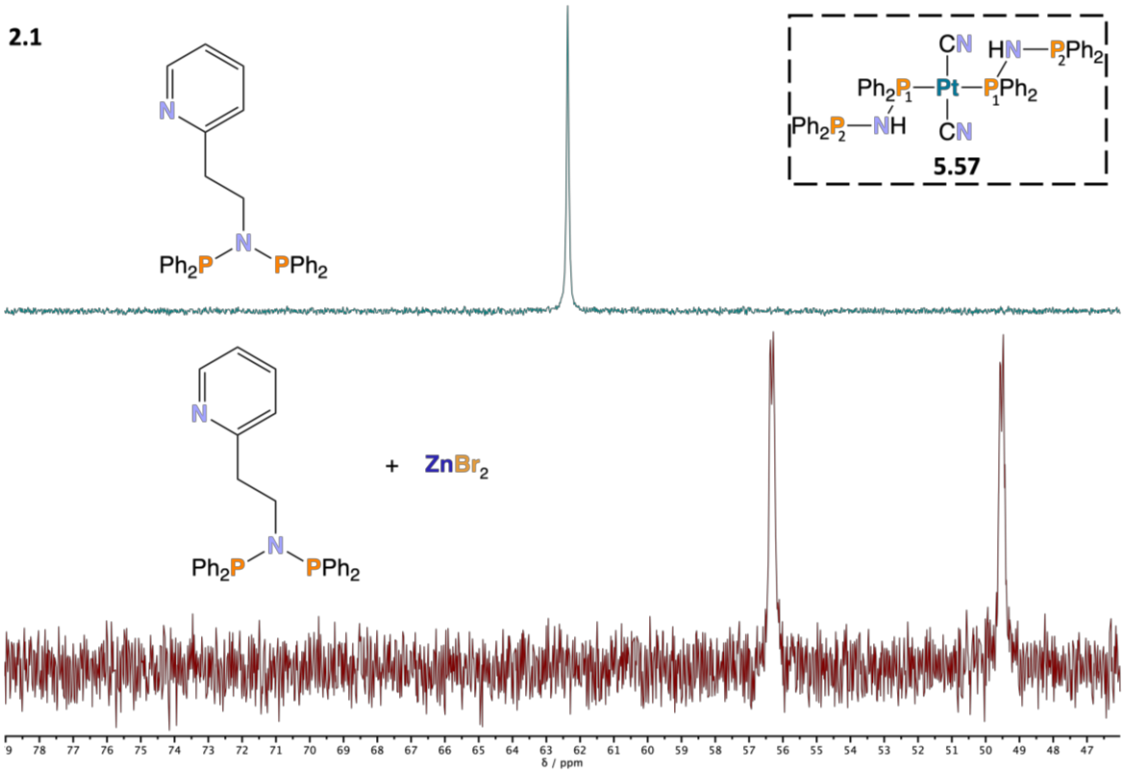


**Figure 5.22.** $^{31}P\{^{1}H\}$ NMR (162 MHz, 290 K, $CDCl_3$) spectra for compound **2.1** and the isolated product of the reaction of compound **2.1** with $ZnBr_2$, and the structure of complex **5.57** in the dashed box.[37]

In order for the zinc(II) centre in the isolated product of the reaction of compound **2.1** with $ZnBr_2$ (**Scheme 5.13**) to attain a tetrahedral geometry with only one phosphorus atom coordinating at zinc(II) (resulting in the doublets observed in the $^{31}P\{^{1}H\}$ NMR spectrum, **Figure 5.22**), another coordinating moiety, *i.e.*, the pyridyl group, must occupy the vacant zinc(II) coordination site. Comparison of the $^{1}H$ NMR spectra (**Figure 5.23**) of compound **2.1** and the isolated product of the reaction of compound **2.1** with $ZnBr_2$ (**Scheme 5.13**) reveals that the signal for the *ortho*-pyridyl proton shifts to a higher frequency from $\delta_H$ = 8.43 ppm in compound **2.1** to 9.17 ppm in the isolated product of the reaction of compound **2.1** with $ZnBr_2$ (**Scheme 5.13**). This evidences that the isolated product of the reaction of compound **2.1** with $ZnBr_2$ (**Scheme 5.13**) contains pyridyl nitrogen atom coordination at the zinc(II) centre. The $\delta_H$ of the *ortho*-pyridyl proton in

complex **3.8** (**Figure 5.23**) is $\delta_H$ = 8.35 ppm, showing only a very slight shift to a lower frequency from the $\delta_H$ of the analogous proton in compound **2.1**, supporting a lack of pyridyl nitrogen coordination in complex **3.8**. Indeed, the signal corresponding to the *ortho*-pyridyl proton in the $^1$H NMR spectra of complex **5.58** (**Figure 5.23**) is at $\delta_H$ = 9.57 ppm[39] relative to $\delta_H$ = 8.43 ppm in the corresponding free ligand.[40] This shift to a higher frequency in $\delta_H$ of 1.14 ppm is also attributed to the coordination of the pyridyl motif to the zinc(II) centre to afford complex **5.58**.

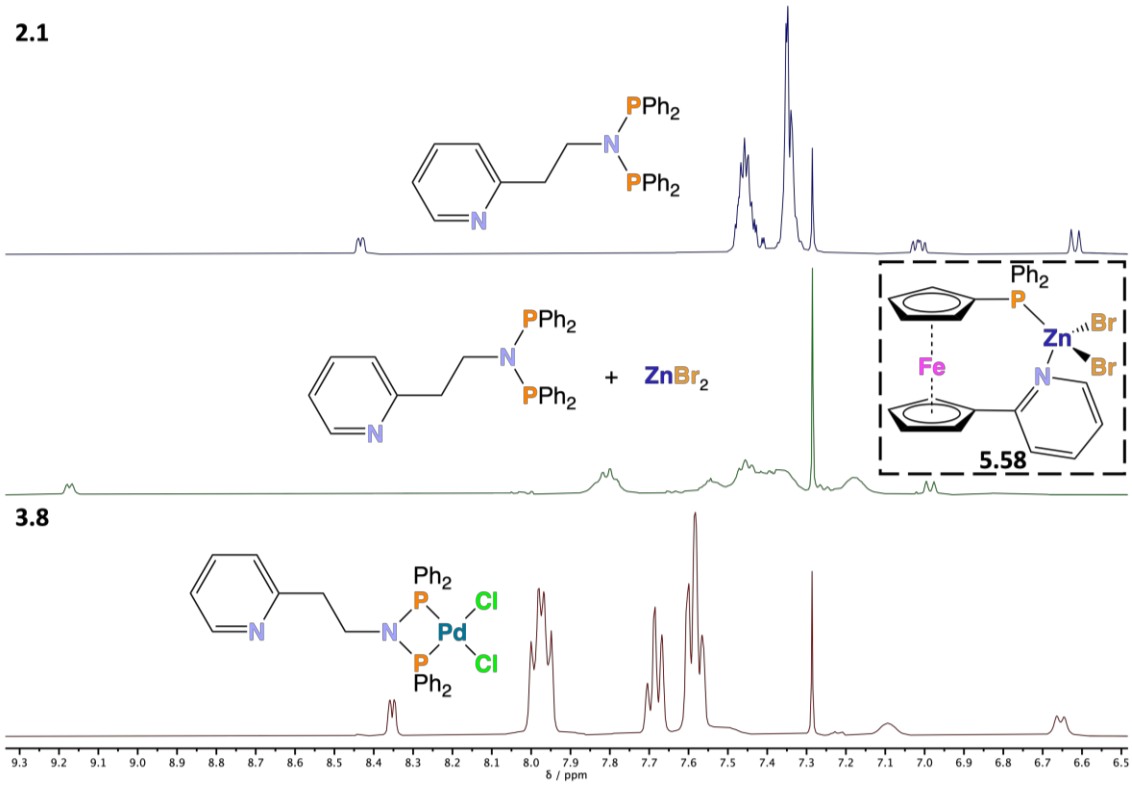


**Figure 5.23.** $^1$H NMR (400 MHz, 290 K, $CDCl_3$) spectra for compound **2.1**, the isolated product of the reaction of compound **2.1** and $ZnBr_2$, and complex **3.8**. The structure of previously reported complex **5.58** is in a black dashed box.[39]

The $^1$H NMR spectrum (**Figure 5.23**) of the isolated product of the reaction of compound **2.1** (Py-*o*-$(CH_2)_2N(PPh_2)_2$) with $ZnBr_2$ (**Scheme 5.13**) shows broad signals, suggesting that coordination polymer **5.54** is the isolated product of the reaction of compound **2.1** with $ZnBr_2$ (**Scheme 5.13**). However, in the absence of a solid-state structure it is impossible to be determine if complex **5.54**, **5.55** or **5.56** is the isolated product of the reaction of compound **2.1** with $ZnBr_2$ (**Scheme 5.13**).

## 5.6 Summary

$[CoBr(Ph(CH_2)_2N\{PPh_2\}_2)_2][PF_6]$ (complex **5.1**), $[CoBr(Py\text{-}o\text{-}(CH_2)_2N\{PPh_2\}_2)_2][PF_6]$ (complex **5.2**) and $[CoBr(Ph(CH_2)_2N\{PPh_2\}_2)_2][BAr^F{}_4]$ (complex **5.3**) have been synthesised and reduced with activated zinc (at least 4 equivalents) affording cationic cobalt(I) complexes $[Co(Ph(CH_2)_2N\{PPh_2\}_2)_2][PF_6]$, $[Co(Py\text{-}o\text{-}(CH_2)_2N\{PPh_2\}_2)_2][PF_6]$ and $[Co(Ph(CH_2)_2N\{PPh_2\}_2)_2][BAr^F{}_4]$ (complexes **5.5** – **5.7**, respectively, **Scheme 5.2**). Complexes **5.5** – **5.7** are very air sensitive and, upon exposure to air, react immediately with dioxygen affording the corresponding peroxo complexes $[Co(Ph(CH_2)_2N\{PPh_2\}_2)_2(\eta^2\text{-}O_2)][PF_6]$, $([Co(Py\text{-}o\text{-}(CH_2)_2N\{PPh_2\}_2)_2(\eta^2\text{-}O_2)][PF_6])$ and $([Co(Ph(CH_2)_2N\{PPh_2\}_2)_2(\eta^2\text{-}O_2)][BAr^F{}_4]$ (complexes **5.11** – **5.13**, respectively, **Scheme 5.3**). UV-Vis spectroscopic analysis of complex **5.7** confirms that complex **5.7** is a cationic cobalt(I) phosphine complex by the presence of a band at 526 nm, assigned to $[\{Ph(CH_2)_2N(PPh_2)_2\}_2Co^I]^+$, which is very similar to a band at 517 nm assigned to $[(dppp)Co^I]^+$ in published work.[3] The molar absorption coefficient has been estimated to be approx. 7400 $dm^3\ mol^{-1}\ cm^{-1}$, indicating that the deep purple colour is due to a charge transfer (revealed to be a metal-to-ligand charge transfer by hybrid-DFT calculations).

The reactions of $Py\text{-}o\text{-}(CH_2)_2N(PPh_2)_2$ (compound **2.1**) and $Ph(CH_2)_2N(PPh_2)_2$ (compound **2.2**) with $CoCl(PPh_3)_3$ were attempted to afford cobalt(I) complexes without utilising activated zinc as a reductant. Characterisation of the resulting isolated products proved inconclusive, with mass spectrometric analysis allowing for the tentative assignment of the isolated products as $[CoCl\{Py\text{-}o\text{-}(CH_2)_2N(PPh_2)_2\}_2]$ and $[CoCl\{Ph(CH_2)_2N(PPh_2)_2\}_2]$ (complexes **5.27** and **5.28**, respectively, **Scheme 5.6**). $[Co(H)(Cl)(Py\text{-}o\text{-}(CH_2)_2N\{PPh_2\}_2)(\{Cl_3Co\}Py\text{-}o\text{-}(CH_2)_2N\{PPh_2\}_2)]$ (complex **5.32**), containing a cationic octahedral cobalt(III) centre, was afforded when attempting to synthesise cobalt(I) hydride species (**Scheme 5.8**). Synthesis of $[Co(H)(Cl)(Py\text{-}o\text{-}(CH_2)_2N\{PPh_2\}_2)_2][PF_6]$ and $[Co(H)(Cl)(Ph(CH_2)_2N\{PPh_2\}_2)_2][PF_6]$ (complexes **5.33** and **5.34**, respectively, **Scheme 5.9**) affords diamagnetic cobalt(III) complexes serving as a model for complex **5.32**, which can be characterised readily by $^1H$ NMR spectroscopy, showing a quintet at $\delta_H \sim -18$ ppm for the cobalt hydride.

The reaction of compounds **2.2** and **2.1** with $ZnBr_2$ were studied, and the resulting isolated products are believed to most likely be coordination polymers $[(Ph(CH_2)_2N(Ph_2P)_2)ZnBr_2]_n$ (complex **5.44**, **Scheme 5.11**) and [(Py-*o*-

$(CH_2)_2N(Ph_2P)_2)ZnBr_2]_n$ (complex **5.54**, **Scheme 5.13**), respectively. A solid-state structure of coordination polymer $[(Ph(CH_2)_2N(Ph_2PO)_2)ZnBr_2]_n$ (complex **5.47**), the presumed oxidation product of coordination polymer **5.44**, has been obtained. Complexes **5.44** and **5.54** are not formed as impurities during the reduction of complexes **5.1**/**5.3** and **5.2** (**Scheme 5.2**), respectively, as the $^{31}P\{^1H\}$ NMR spectra of complexes **5.5**/**5.7** and **5.6** do not contain signals assignable to complexes **5.44** and **5.54**, respectively. Hence, it is likely that the poor agreement between the obtained CHN analyses for complexes **5.5** – **5.7** and the calculated CHN composition for the target complexes **5.5** – **5.7** is due to the presence of trace activated zinc and $ZnBr_2$.

## References


1. R. K. Sharma, T. V. RajanBabu, *J. Am. Chem. Soc*., **2010**, *132*, 3295 – 3297. 10.1021/ja1004703
2. K. Duvvuri, K. R. Dewese, M. M. Parsutkar, S. M. Jing, M. M. Mehta, J. C. Gallucci, T. V. RajanBabu, *J. Am. Chem. Soc*., **2019**, *141*, 7365 – 7375. 10.1021/jacs.8b13812
3. M. Gray, M. T. Hines, M. M. Parsutkar, A. J. Wahlstrom, N. A. Brunelli, T. V. RajanBabu, *ACS Catal*., **2020**, *10*, 4337 – 4348. 10.1021/acscatal.9b05455
4. C. Fliedel, V. Rosa, B. Vileno, N. Parizel, S. Choua, C. Gourlaouen, P. Rosa, P. Turek, P. Braunstein, *Inorg. Chem.*, **2016**, *55*, 4183 – 4198. 10.1021/acs.inorgchem.5b02889
5. D. F. Evans, *J. Chem. Soc*., **1959**, 2003 – 2005. 10.1039/JR9590002003
6. M. T. Mock, R. G. Potter, M. J. O'Hagan, D. M. Camaioni, W. G. Dougherty, W. S. Kassel, D. L. DuBois, *Inorg. Chem*., **2011**, *50*, 11914 – 11928. 10.1021/ic200857x
7. D. A. Kurtz, J. Zhang, A. Sookezian, J. Kallick, M. G. Hill, B. M. Hunter, *Inorg. Chem*., **2021**, *60*, 17445 – 17449. 10.1021/acs.inorgchem.1c03020
8. N. W. Terry III, E. L. Amma, L. Vaska, *J. Am. Chem. Soc*., **1972**, *94*, 653 – 655. 10.1021/ja00757a066
9. M. Dartiguenave, Y. Dartiguenave, M. J. Oliver, A. L. Beauchamp, *J. Coord. Chem*., **1990**, *21*, 275 – 281. 10.1080/00958979009409726
10. A. F. M. M. Rahman, W. G. Jackson, A. C. Willis, *Inorg. Chem*., **2004**, *43*, 7558 – 7560. 10.1021/ic040044z
11. C-M. Lee, M. Sankaralingam, C-H. Chuo, T-H. Tseng, P. P-Y. Chen, M-H. Chiang, X-X. Li, Y-M. Lee, W. Nam, *Dalton Trans*., **2019**, *48*, 5203 – 5213. 10.1039/C9DT00649D
12. Z. Xiao, A. Johnson, K. Singh, K. Suntharalingam, *Angew. Chem. Int. Ed*., **2021**, *60*, 6704 – 6709. 10.1002/anie.202014242
13. T. Ohishi, K. Kashiwabara, J. Fujita, S. Ohba, T. Ishii, Y. Saito, *Bull. Chem. Soc. Jpn*., **1986**, *59*, 385 – 393. 10.1246/bcsj.59.385
14. G. M. Jacobsen, J. Y. Yang, B. Twamley, A. D. Wilson, R. M. Bullock, M. R. DuBois, D. L. DuBois, *Energy Environ. Sci*., **2008**, *1*, 167 – 174. 10.1039/B805309J
15. N. M. O'Boyle, A. L. Tenderholt, K. M. Langer, *J. Comput. Chem*., **2008**, *29*, 839 – 845. 10.1002/jcc.20823

16. J. Rumble, *CRC Handbook of Chemistry and Physics*, CRC Press, Florida, **2023**. ISBN: 9781032425207
17. M. Sun, J-F. Chen, S. Chen, C. Li, *Org. Lett*., **2019**, *21*, 1278 – 1282. 10.1021/acs.orglett.8b04030
18. B. A. Suslick, T. D. Tilley, *J. Am. Chem. Soc*., **2020**, *142*, 11203 – 11218. 10.1021/jacs.0c04072
19. C. E. Housecroft, A. G. Sharpe, *Inorganic Chemistry*, Pearson, London, **2018**. ISBN: 1292134143
20. T. J. Anderson, D. A. Vicic, *Organometallics*, **2004**, *23*, 623 – 625. 10.1021/om034380j
21. P. Cossee, *J. Catal*., **1964**, *3*, 80 – 88. 10.1016/0021-9517(64)90095-8
22. S. Yu, C. Wu, S. Ge, *J. Am. Chem. Soc*., **2017**, *139*, 6526 – 6529. 10.1021/jacs.7b01708
23. J. Pecak, S. Fleissner, L. F. Veiros, E. Pittenauer, B. Stöger, K. Kirchner, *Organometallics*, **2021**, *40*, 278 – 285. 10.1021/acs.organomet.0c00755
24. M. Zhang, C. Wang, C. Zhang, T. Cai, L. Zhu, D. Xia, *New J. Chem*., **2020**, *44*, 15646 – 15653. 10.1039/D0NJ01437K
25. A. Badía, L. R. Falvello, R. Navarro, E. P. Urriolabeitia, *J. Organomet. Chem*., **1997**, *547*, 121 – 128. 10.1016/S0022-328X(97)00206-4
26. D. J. Elliot, D. G. Holah, A. N. Hughes, S. Maciaszek, V. R. Magnuson, K. O. Parker, *Can. J. Chem*., **1988**, *66*, 81 – 85. 10.1139/v88-012
27. D. J. Elliot, D. G. Holah, A. N. Hughes, S. I. Khan, S. Maciaszek, *Inorg. Chim. Acta*, **1985**, *96*, L29 – L30. 10.1016/S0020-1693(00)93727-7
28. C. N. Brodie, PhD thesis, Durham University, **2020**.
29. T. S. Sukhikh, R. M. Khisamov, D. A. Bashirov, V. Y. Komarov, M. S. Molokeev, A. A. Ryadun, E. Benassi, S. N. Konchenko, *Cryst. Growth Des*., **2020**, *20*, 5796 – 5807. 10.1021/acs.cgd.0c00406
30. D. A. Dickie, R. A. Kemp, *Organometallics*, **2014**, *33*, 6511 – 6518. 10.1021/om500856p
31. X. Liu, X-J. Yang, P. Yang, Y. Liu, B. Wu, *Inorg. Chem. Commun*., **2009**, *12*, 481 – 483. 10.1016/j.inoche.2009.03.019
32. A. M. Messinis, S. L. J. Luckham, P. P. Wells, D. Gianolio, E. K. Gibson, H. M. O'Brien, H. A. Sparkes, S. A. Davis, J. Callison, D. Elorriaga, O. Hernandez-Fajado, R. B. Bedford, *Nat. Catal.*, **2019**, *2*, 123 – 133. 10.1038/s41929-018-0197-z
33. C. Rajnák, F. Varga, J. Titiš, J. Moncol, R. Boča, *Inorg. Chem*., **2018**, *57*, 4352 – 4358. 10.1021/acs.inorgchem.7b03193
34. K. Song, H. Gao, F. Liu, J. Pin, L. Guo, S. Zai, Q. Wu, *Eur. J. Inorg. Chem*., **2009**, 3016 – 3024. 10.1002/ejic.200900256
35. L-C. Song, J-P. Li, Z-J. Xie, H-B. Song, *Inorg. Chem*., **2013**, *52*, 11618 – 11626. 10.1021/ic401978h
36. R. D. Shannon, *Acta Cryst*., **1976**, *A32*, 751 – 767. 10.1107/S0567739476001551
37. C. S. Browning, D. H. Farrar, *J. Chem. Soc. Dalton Trans*., **1995**, 521 – 530. 10.1039/DT9950000521
38. Z. Fei, R. Scopelliti, P. J. Dyson, *Dalton Trans*., **2003**, 2772 – 2779. 10.1039/B303645F
39. U. Siemeling, T. Klemann, C. Bruhn, J. Schulz, P. Štěpnička, *Dalton Trans*., **2011**, *40*, 4722 – 4740. 10.1039/C0DT01810D
40. P. Štěpnička, J. Schulz, T. Klemann, U. Siemeling, I. Císarová, *Organometallics*, **2010**, *29*, 3187 – 3200. 10.1021/om100339p

# Chapter 6 – Reactivity of Cationic Cobalt(I) Complexes of 'PNP' Ligands with Ethylene, Carbon Monoxide and Hydrogen

## 6.1 Introduction

Ethylene, carbon monoxide and hydrogen (reagents in hydroformylation) are substrates of interest due to their use in a variety of catalytic processes, *e.g.* hydroformylation.[1] Indeed, many low valent cationic cobalt(I) complexes have been applied to a range of catalytic processes using alkenes as a reagent.[2 – 10] Hence, it is of interest to elucidate the reactivity of cationic cobalt(I) complexes containing 'PNP' ligands with ethylene, carbon monoxide and hydrogen. In order to achieve this, complex **5.7** ($[Co(Ph(CH_2)_2N\{PPh_2\}_2)_2][BAr^F_4]$, selected for further study due to greater solubility arising from $BAr^F_4$ anion relative to complexes **5.5** and **5.6**, *i.e.*, $[Co(Ph(CH_2)_2N\{PPh_2\}_2)_2][PF_6]$ and $[Co(Py\text{-}o\text{-}(CH_2)_2N\{PPh_2\}_2)_2][PF_6]$, respectively) was studied by NMR spectroscopy, under a pressure (generally 1 atm) of the aforementioned gaseous reagents in sealed NMR tubes.

## 6.2 Reaction of $[Co\{Ph(CH_2)_2N(PPh_2)_2\}_2][BAr^F_4]$ (5.7) with ethylene

Complex **5.7** (0.01 g) was dissolved in $d_8$-THF in an NMR tube and the resulting solution degassed by three freeze-pump-thaw cycles before being sealed under vacuum, back-filled with dry ethylene (1 atm or approx. 1 equivalent) and flame–sealed. An immediate colour change from the characteristic deep purple of complex **5.7** to a yellow-brown on contact with ethylene is observed, something that has been attributed to the formation of new alkene complex **6.1** (**Scheme 6.1**). The $^{31}P\{^1H\}$ NMR spectrum at –85 °C (**Figure 6.1**) verifies that the complex **6.1**, *i.e.* the ethylene adduct of complex **5.7**, is diamagnetic (based on the presentation of well-resolved and sharp signals) and contains two unique phosphorus environments, in line with the proposed structure of complex **6.1**. Probing

the structure of ethylene adducts of [Co('PNP')$_2$][X] complexes (where X = $PF_6$ or $BAr^F_4$ anions) affords geometry optimised structures of complexes of the form [Co('PNP')$_2$($\eta^2$-$CH_2CH_2$)][X], *i.e.*, complex **6.1**. Further experimental and computational details to support complex **6.1** being the ethylene adduct of complex **5.7** are discussed in **Section 6.2.1 – 6.2.2**.

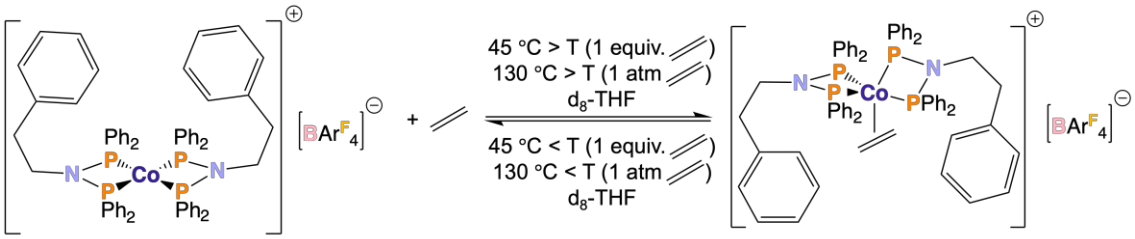


**5.7** **6.1**

**Scheme 6.1.** The reaction of complex **5.7** with ethylene to afford complex **6.1**. *NB* T is temperature.

## 6.2.1 VT-NMR Studies of [Co{Ph(CH$_2$)$_2$N(PPh$_2$)$_2$}$_2$][BAr$^F_4$] (5.7) with ethylene

In order to study the reaction of ethylene with complex **5.7** to afford complex **6.1**, $^{31}P\{^1H\}$ NMR studies were undertaken. The $^{31}P\{^1H\}$ NMR spectrum of complex **6.1** is broad ($\nu_{1/2}$ ~290 Hz) and unresolved at 25 °C, *cf.* the broad ($\nu_{1/2}$ = 105 Hz), but resolved, singlet observed for complex **5.7** at 86.7 ppm (25 °C, **Figure 6.1**). The observation of a broad and unresolved feature in the $^{31}P\{^1H\}$ NMR spectrum for complex **6.1** prompted a $^{31}P\{^1H\}$ VT-NMR study of the reaction of complex **5.7** with 1 atm of ethylene (*i.e.*, formation of complex **6.1**) in $d_8$-THF over the temperature range of –85 to 60 °C (**Figure 6.1**).

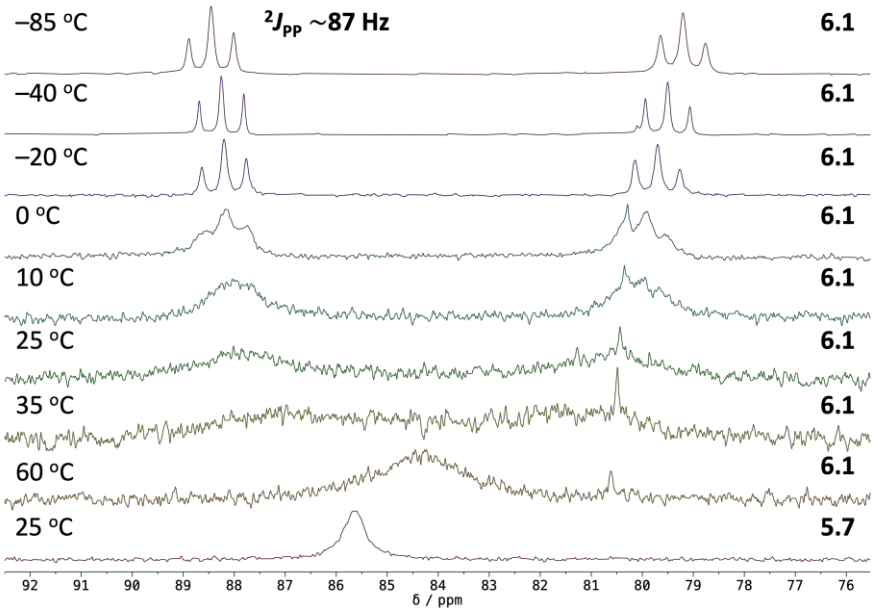


**Figure 6.1.** $^{31}P\{^1H\}$ NMR spectra (162 MHz) of the reaction between complex **5.7** and ethylene (1 atm), *i.e.*, formation of complex **6.1** at various specified temperatures over the –85 to 60 °C range, and complex **5.7** at 25 °C.

The $^{31}P\{^{1}H\}$ NMR spectra acquired at various temperatures (**Figure 6.1**) clearly show that increasing the acquisition temperature to approx. 35 °C from 25 °C results in coalescence, with a broad singlet ($\nu_{1/2}$ ~360 Hz) at approx. 84.3 ppm being observed at 60 °C. Lowering the acquisition temperature from 25 °C results in the development of two resolved triplets (resulting from an $A_2X_2$ spin system) at 88.5 ppm and 79.2 ppm at –85 °C ($^{2}J_{PP}$ ~87 Hz). Since a broad singlet is observed in the $^{31}P\{^{1}H\}$ NMR spectrum of complex **5.7** in the absence of ethylene irrespective of temperature, the observed triplets (**Figure 6.1**) must arise from ethylene complex **6.1** (**Scheme 6.1**).

The NMR spectral data (**Figure 6.1**) are consistent with a temperature-dependent equilibrium between complexes **5.7** and **6.1** (*i.e.*, complex **6.1** forming at lower temperatures and complex **5.7** predominating at elevated temperatures). However, the temperature dependence of the spectral data (**Figure 6.1**) could alternatively be attributed to a Berry *pseudo*rotation[11] or Muetterties process[12 – 14] (**Scheme 6.2**).

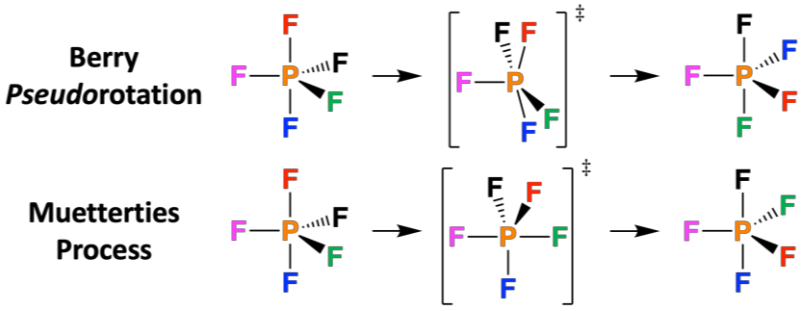


**Scheme 6.2.** General processes Berry *pseudo*rotation[11] and Muetterties[12 – 14] using trigonal bipyramidal $PF_5$ as a representative example.

A Berry *pseudo*rotation[11] or Muetterties process[12 – 14] could interconvert the energetically equivalent Δ and Λ isomers of the cation of complex **6.1** (**Figure 6.2**). An interconversion process slower than the NMR timescale at lower temperatures would result in the observed triplets (**Figure 6.1**; *NB* the Δ and Λ enantiomers have identical $^{31}P\{^{1}H\}$ NMR spectra). An interconversion process faster than the NMR timescale at higher temperatures would result in the broad singlet observed at 60 °C (**Figure 6.1**). Square planar complex **5.7** cannot undergo a Berry *pseudo*rotation or Muetterties process interconversion, unlike the trigonal bipyramidal cation of complex **6.1** (**Figure 6.2**), supporting the observation that the $^{31}P\{^{1}H\}$ NMR spectra of complex **5.7** gives a broad singlet resonance irrespective of temperature. Further experimental and

computational study to determine the origin of the dynamic $^{31}P\{^{1}H\}$ VT-NMR behaviour is discussed in **Section 6.2.3**.

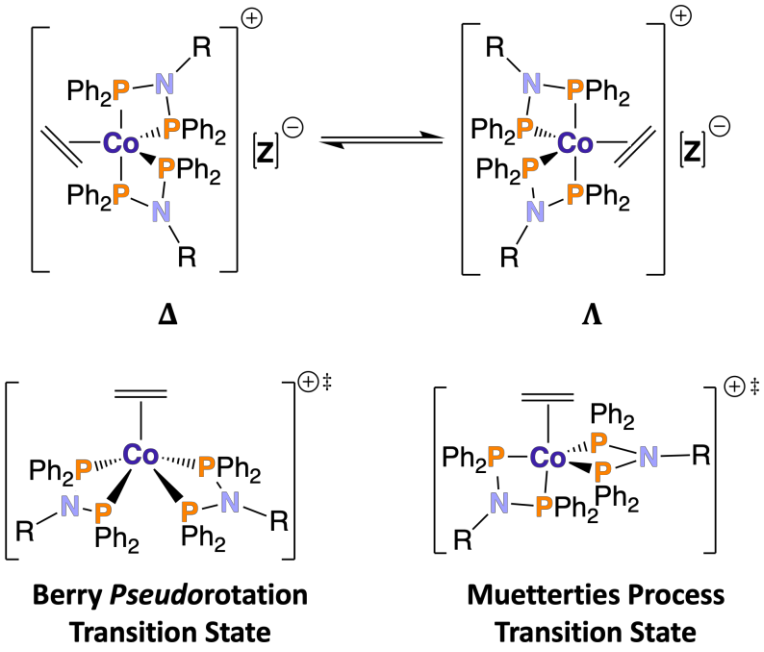


**Figure 6.2.** Interconversion between the Δ and *Λ* enantiomers of the $[Co(RN\{PPh_2\}_2)_2(\eta^2\text{-}CH_2CH_2)]$ cation *via* a Berry *pseudo*rotation or Muetterties process (transition states shown).

The $^{1}H$ NMR spectral data obtained for complex **6.1** during the VT NMR experiments proved difficult to interpret (due to complications arising from the dynamic nature of the system), with no clearly visible signal corresponding to coordinated ethylene being observed. However, the 2D $^{1}H$-$^{1}H$ NOESY spectrum (**a)**, **Figure 6.3**) of complex **6.1** (*i.e.*, from complex **5.7**, $[Co(Ph(CH_2)_2N\{PPh_2\}_2)_2][BAr^F_4]$, in the presence of approx. 1 equivalent of ethylene) in $d_8$-THF shows cross peaks (of the same sign, *i.e.*, colour, as the diagonal)[15] which indicates chemical exchange between uncoordinated ethylene (approx. 5.3 ppm) and cobalt-bound ethylene (approx. 1.8 ppm). Hence, the signal corresponding to coordinated ethylene at 1.8 ppm is not seen in the $^{1}H$ NMR spectrum (**b)**, **Figure 6.3**) of complex **6.1** (formed from complex **5.7** in the presence of approx. 1 equivalent of ethylene) due to being masked by the large THF signal at 1.79 ppm. Indeed, a chemical shift of 1.8 ppm for cobalt-bound ethylene shows good similarity to the signal at a chemical shift of 2.1 ppm corresponding to coordinated ethylene in complexes **6.2** and **6.3** (**c)**, **Figure 6.3**).[16] Cross peaks indicating chemical exchange between uncoordinated and cobalt-bound ethylene are not evidenced in the 2D $^{1}H$-$^{1}H$ NOESY spectrum of complex **6.1** with 1 atm of ethylene. Hence, chemical exchange between uncoordinated and coordinated ethylene is not observed when there is a large excess

of ethylene, as a large excess of ethylene drives the position of equilibrium towards the ethylene complex **6.1** (**Scheme 6.1**).

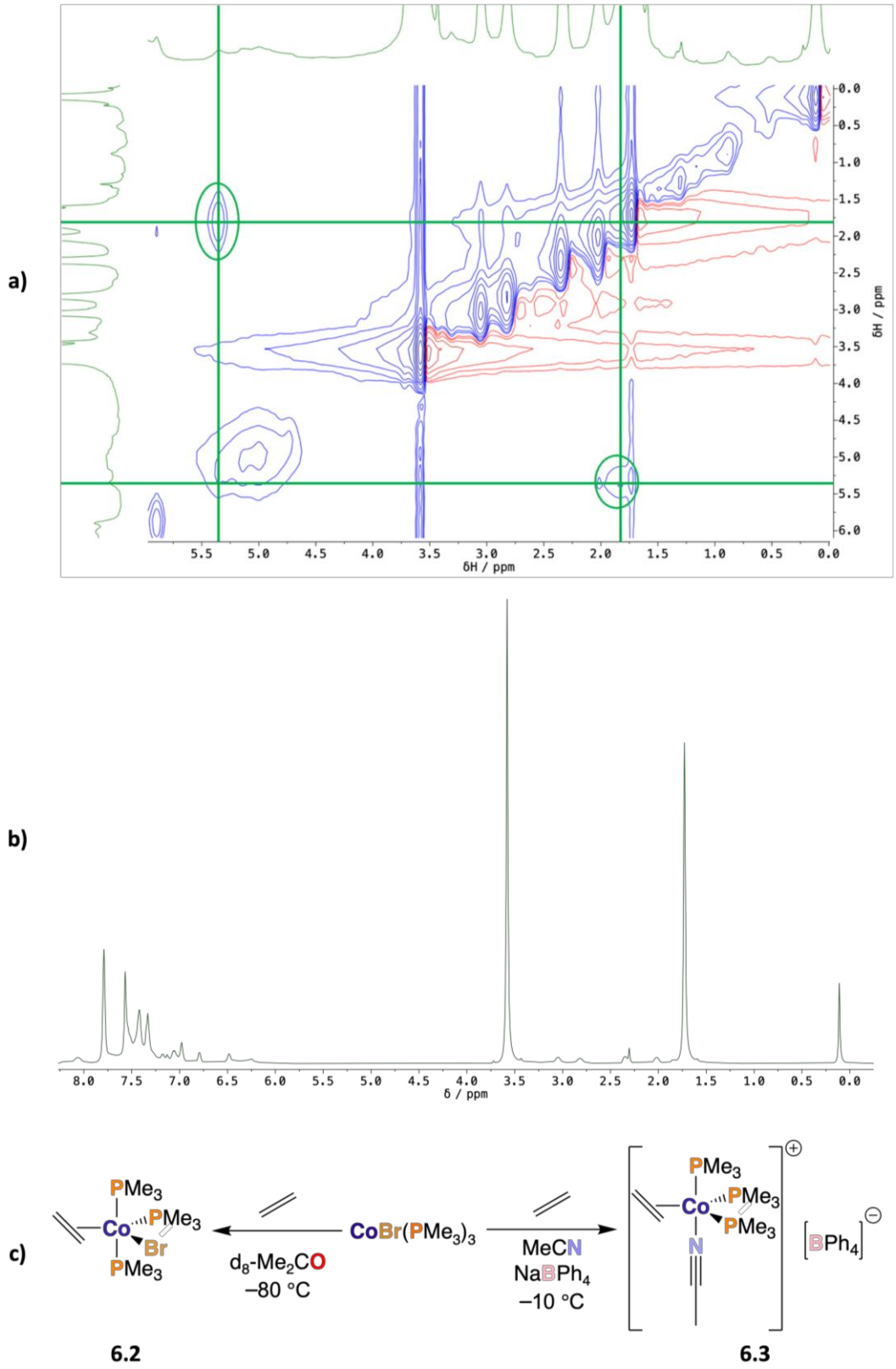


**Figure 6.3. a)** $^{1}$H-$^{1}$H NOESY spectrum of the sample of complex **6.1** (with approx. 1 equivalent of ethylene) in $d_8$-THF at 298.15 K, with the cross peaks evidencing chemical exchange between uncoordinated (approx. 5.3 ppm) and coordinated (approx. 1.8 ppm) ethylene being highlighted in green; **b)** $^{1}$H NMR (400 MHz, 290 K, $d_8$-THF) spectrum of complex **6.1** with approx. 1 equivalent of ethylene; **c)** synthesis of complexes **6.2** and **6.3**.[16]

### 6.2.2 Hybrid-DFT studies probing the structure of [Co{Ph(CH$_2$)$_2$N(PPh$_2$)$_2$}$_2$($\eta^2$-CH$_2$CH$_2$)][BAr$^F_4$] (6.1)

Due to the lability of ethylene, it was not possible to isolate and subsequently obtain a solid-state structure of ethylene complex **6.1** ([Co{Ph(CH$_2$)$_2$N(PPh$_2$)$_2$}$_2$($\eta^2$-CH$_2$CH$_2$)][BAr$^F_4$]). Hence, the structure of complex **6.1** was probed by hybrid-DFT analysis (**Figure 6.4**). The geometry optimisation calculation for complex **6.1** (containing the large [Co{Ph(CH$_2$)$_2$N(PPh$_2$)$_2$}$_2$($\eta^2$-CH$_2$CH$_2$)] cation and BAr$^F_4$ anion) at the B3LYP/6-31G(d) level could not be carried out due to the limited computing resources available. However, the geometry optimisation calculations of analogous complexes **6.6** (containing the same cation as complex **6.1** and smaller $PF_6$ anion) and **6.7** (containing the BAr$^F_4$ anion like complex **6.1** and smaller [Co{MeN(PPh$_2$)$_2$}$_2$($\eta^2$-CH$_2$CH$_2$)] cation) at the B3LYP/6-31G(d) level did complete. The cations of the optimised structures of complexes **6.4** – **6.7** adopt the same trigonal bipyramidal geometry, confirming the geometry around the cobalt(I) centre in complex **6.1**.

The optimised structures of complexes **6.5** – **6.7** have ethylene C=C bond distances of approx. 1.416 Å and average Co-C bond distances of approx. 2.034 Å, showing good agreement with the measured ethylene C=C bond distance of 1.4144 Å and the average Co-C bond distance of 2.027 Å previously reported for related complex [Co(PMe$_3$)$_3$(MeCN)($\eta^2$-CH$_2$CH$_2$)][BPh$_4$] (**6.3**, **c)**, **Figure 6.3**).[16] The similarity in C=C and Co-C bond distances suggests that ethylene is activated to a similar extent in complexes **6.3** and **6.5** – **6.7** through the ethylene C=C bond distance increasing in length relative to that of uncoordinated ethylene (1.3391(13) Å).[17]

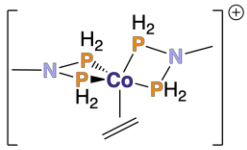

6.4

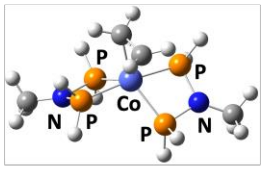

6.4 Cation DFT

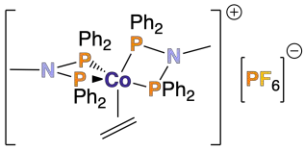

6.5

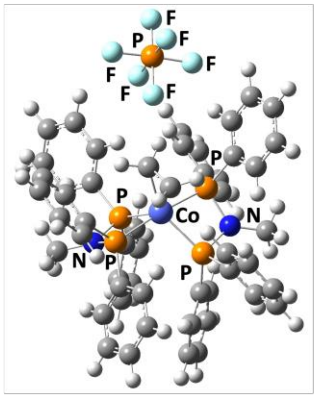

6.5 DFT

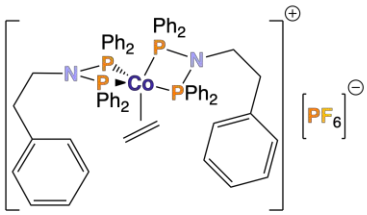

6.6

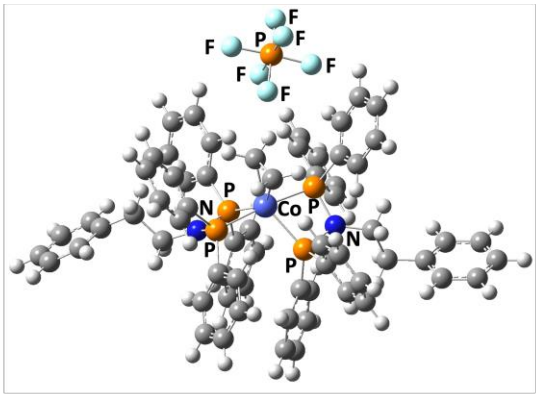

6.6 DFT

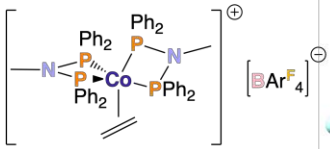

6.7

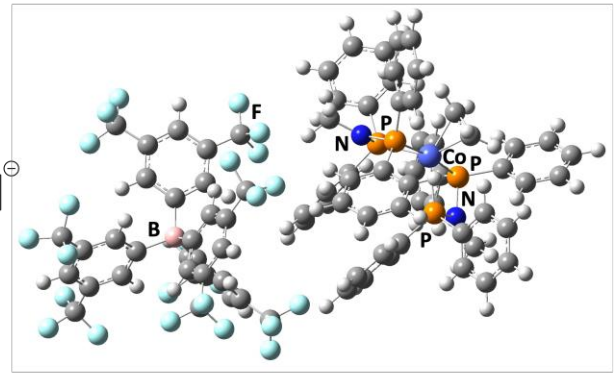

6.7 DFT

**Figure 6.4.** Geometry optimised structures of cation **6.4** and complexes **6.5 – 6.7**, determined by hybrid-DFT analysis at the B3LYP/6-31G(d) level. Atom colour: carbon – grey; nitrogen – dark blue; phosphorus – orange; cobalt – light blue; boron – pink; fluorine – blue-green, and hydrogen – white.

It is noteworthy that the cations of geometry optimised structures **6.4** – **6.7** (**Figure 6.4**) have essentially the same cation geometry as the isoelectronic peroxo complex **5.11** (**Figure 6.5**), with the ethylene $CH_2$ moieties of complexes **6.4** – **6.7** occupying analogous positions of the O atoms of $O_2$ in complex **5.11**.

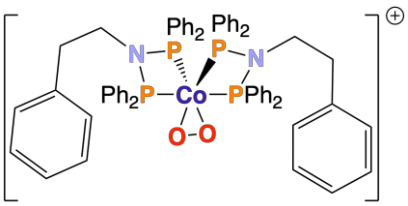


**5.11 Cation**

**Figure 6.5.** Structure of the cation of complex **5.11**.

### 6.2.3 Hybrid-DFT and experimental studies to probe the dynamic $^{31}P\{^{1}H\}$ VT NMR spectroscopic behaviour of $[Co\{Ph(CH_2)_2N(PPh_2)_2\}_2(\eta^2\text{-}CH_2CH_2)][BAr^F{}_4]$ (6.1)

In order to determine the origin of the dynamic $^{31}P\{^{1}H\}$ VT NMR spectroscopic behaviour observed for complex **5.7** in the presence of ethylene (**Figure 6.1**), the transition states for the Berry *pseudo*rotation and Muetterties process for the interconversion of the enantiomers of the (computationally simpler) $[Co\{HN(PH_2)_2\}_2(\eta^2\text{-}CH_2CH_2)]$ cation were determined (**Figure 6.7**). The value of $\Delta G^{\ddagger}$ (the Gibbs free energy of activation) for the Berry *pseudo*rotation is 12.6 kcal $mol^{-1}$ (thermally accessible at room temperature), indicating that the Berry *pseudo*rotation process could be a viable origin for the dynamic $^{31}P\{^{1}H\}$ VT NMR behaviour (**Figure 6.1**). $\Delta G^{\ddagger}$ of 12.6 kcal $mol^{-1}$ compares well with the experimentally determined activation energy of 13 kcal $mol^{-1}$ for racemisation of anion **6.8** (**Figure 6.6**).[14] The value of $\Delta G^{\ddagger}$ for the Muetterties process of the $[Co\{HN(PH_2)_2\}_2(\eta^2\text{-}CH_2CH_2)]$ cation is 19.5 kcal $mol^{-1}$ (**Figure 6.7**), a greater barrier than that determined for the Berry *pseudo*roation process of the same cation ($\Delta G^{\ddagger}$ of 12.6 kcal $mol^{-1}$).

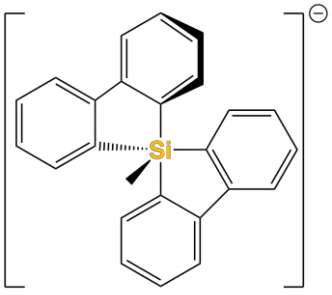


**6.8**

**Figure 6.6.** Structure of anion **6.8**.[14]

The energetic preference for the Berry *pseudo*rotation process likely stems from the preference of ethylene in the $[Co\{RN(PR'_2)_2\}_2(\eta^2\text{-}CH_2CH_2)]$ cation to coordinate in the equatorial plane to maximise $\pi$-back bonding. The loss of $\pi$-back bonding with ethylene occupying an axial position in the transition state for the Muetterties process likely

significantly destabilises this transition state relative to that of the corresponding Berry *pseudo*rotation process (**Figure 6.7**). The Muetterties process transition state contains a *bis*-equatorially bound 'PNP' ligand; the large difference between the approx. 71° P-Co-P angle and the 120° angle between equatorial sites in a trigonal bipyramidal geometry will likely result in significant strain and destabilisation of the transition state.

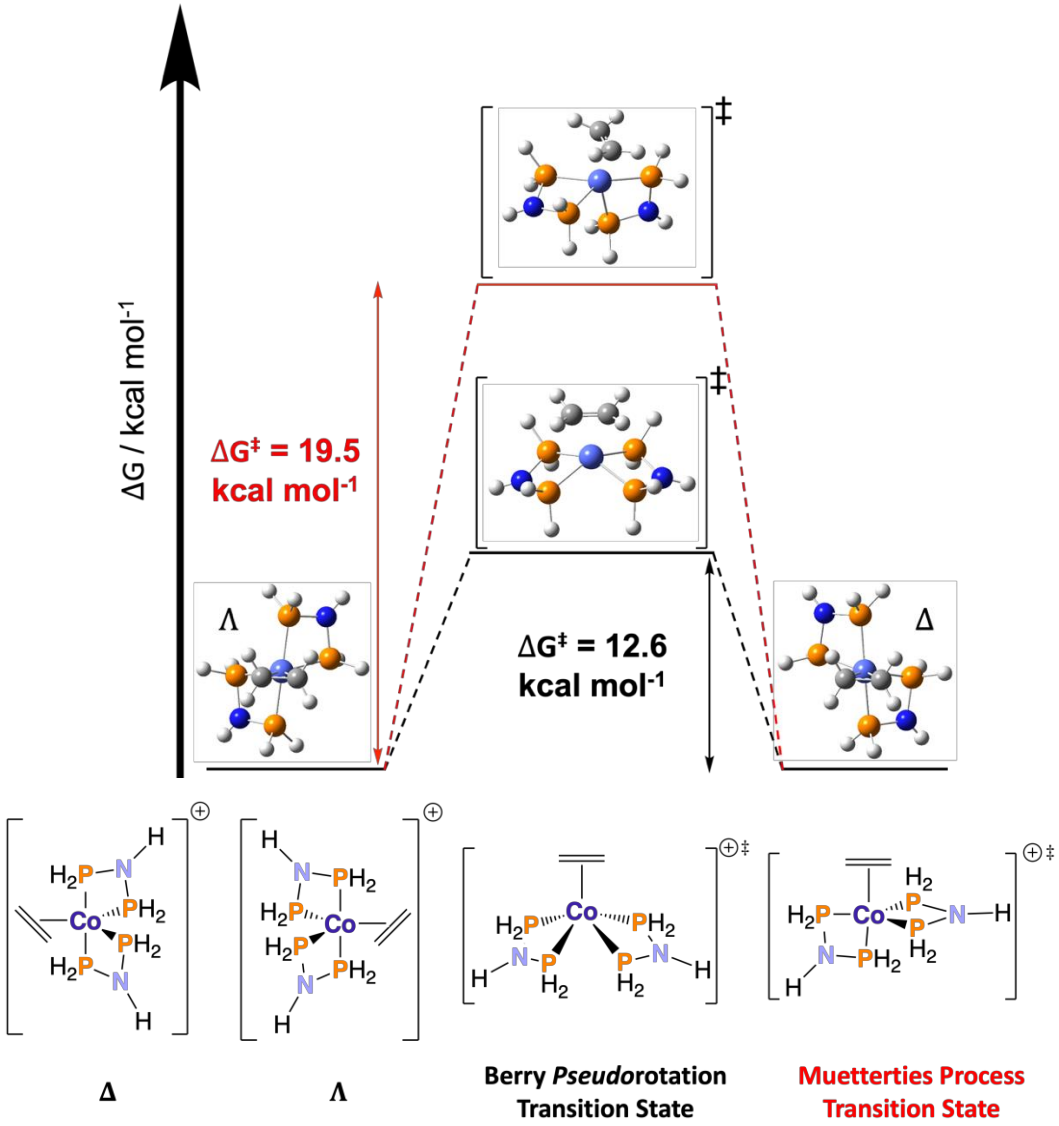


**Figure 6.7.** Racemisation scheme showing the transition states for the interconversion of the Δ and *Λ* enantiomers of $[Co\{HN(PH_2)_2\}_2(\eta^2\text{-}CH_2CH_2)]$ cation *via* a Berry *pseudo*rotation process (black dashed lines) or a Muetterties process (red dashed lines).

Subsequently, the Berry *pseudo*roation transition state was determined for the cation of complex **6.1** (**Figure 6.8**). Computationally, there is a 3.2 kcal $mol^{-1}$ Gibbs free energy difference between the Δ and Λ enantiomers of the cation of complex **6.1**. Hence, there are two $\Delta G^{\ddagger}$ values for the Berry *pseudo*rotation process of 14.4 and 17.6 kcal $mol^{-1}$ for the Λ and Δ enantiomers, respectively. The average value of $\Delta G^{\ddagger}$ is 16 kcal $mol^{-1}$, which

is close to the 12.6 kcal mol$^{-1}$ value of $\Delta G^{\ddagger}$ determined for the simpler [Co{HN(PH$_2$)$_2$}$_2$($\eta^2$-CH$_2$CH$_2$)] cation. Hence, changing the nature of R and R' in the [Co{RN(PR'$_2$)$_2$}$_2$($\eta^2$-CH$_2$CH$_2$)] cation has minimal effect on the activation energy for the Berry *pseudo*rotation process.

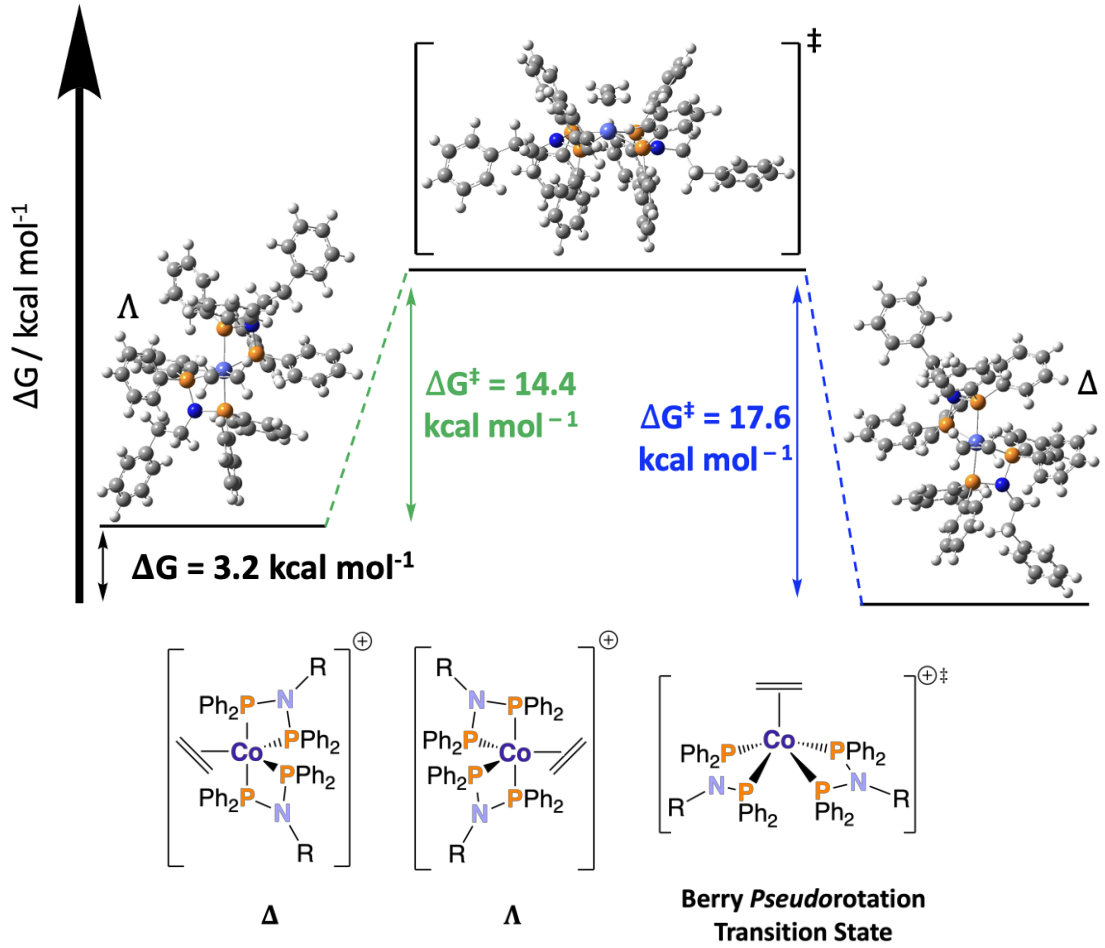


**Figure 6.8.** Racemisation scheme showing the transition state for the interconversion of the Δ and Λ enantiomers of the [Co{RN(PPh$_2$)$_2$}$_2$($\eta^2$-CH$_2$CH$_2$)] cation *via* a Berry *pseudo*rotation process. *NB* R = CH$_2$CH$_2$Ph.

The value of $\Delta G^{\ddagger}$ of 13 kcal mol$^{-1}$ was determined for the process responsible for the temperature dependence of the NMR spectral data (**Figure 6.1**) by using a rate constant determined from the rate of exchange at coalescence, $k_{ex}$, utilising **Equation 6.1**,[18] in the Eyring equation (**Equation 6.2**). This value is in agreement with the computationally determined average $\Delta G^{\ddagger}$ value of 16 kcal mol$^{-1}$ for the Berry *pseudo*rotation process of the cation of complex **6.1**. $\Delta\nu$ in **Equation 6.1** is the frequency difference measured between the two triplets in the $^{31}P\{^1H\}$ NMR spectrum (**Figure 6.1**) at –85 °C (the lower temperature limit).

$$k_{ex} = 2.22\Delta\nu \qquad \textbf{(6.1)}$$

The rate constant determined from **Equation 6.1** can then be applied to **Equation 6.2**, where $k_B$ is the Boltzmann constant, h is Plank's constant, R is the gas constant, and T is the temperature (35 °C, as coalescence is essentially reached at 35 °C in **Figure 6.1**):

$$k_{ex} = \frac{k_B T}{h} \exp\left(\frac{-\Delta G^{\ddagger}}{RT}\right) \qquad \textbf{(6.2)}$$

The excellent agreement between the computational and experimental $\Delta G^{\ddagger}$ values of 16 and 13 kcal $mol^{-1}$, respectively, reinforces the suggestion that the observed fluxionality of complex **6.1** results from a Berry *pseudo*rotation process interconverting the two enantiomers of the [Co{Ph$(CH_2)_2$N$(PPh_2)_2$}$_2$($\eta^2$-$CH_2CH_2$)] cation. However, the existence of a temperature-dependent equilibrium between complex **5.7** and its corresponding ethylene adduct complex **6.1** needs to be assessed experimentally as this equilibrium could possibly be responsible for the dynamic $^{31}P\{^1H\}$ VT NMR behaviour (**Figure 6.1**).

To this end, a sample of complex **6.1** (prepared from complex **5.7**, [Co(Ph$(CH_2)_2$N{$PPh_2$}$_2$)$_2$][$BAr^F{}_4$], in the presence of 1 atm ethylene) was heated in $d_8$-THF in a sealed NMR tube in an oil bath and the temperature increased at 10 °C intervals with a pause of 15 minutes between each temperature. A purple colour, indicating ethylene dissociation from complex **6.1** to afford complex **5.7**, was first observed at approx. 130 °C. Lowering the temperature of the sample resulted in the yellow-brown colour returning, indicating ethylene association to complex **5.7** to afford complex **6.1**, illustrating a temperature–reversible colour change. Hence, the dynamic $^{31}P\{^1H\}$ VT NMR behaviour in the –85 °C to 60 °C temperature range is not due to a temperature–dependent equilibrium between complexes **5.7** and **6.1** (**Scheme 6.1**), but is due to the interconversion of the two enantiomers of the [Co{Ph$(CH_2)_2$N$(PPh_2)_2$}$_2$($\eta^2$-$CH_2CH_2$)] cation *via* the Berry *pseudo*rotation process (**Figure 6.2**). In contrast, heating a 1:1 molar ratio of complex **5.7** and ethylene in $d_8$-THF in a sealed NMR tube evidences a purple colour at approx. 45 °C. As expected, a lower ethylene concentration influences the position of equilibrium (**Scheme 6.1**), resulting in a lower temperature being required to cause ethylene dissociation. The observed colour changes are shown in **Figure 6.9**. *NB* cooling the sample to approx. –78 °C did not result in any colour change.

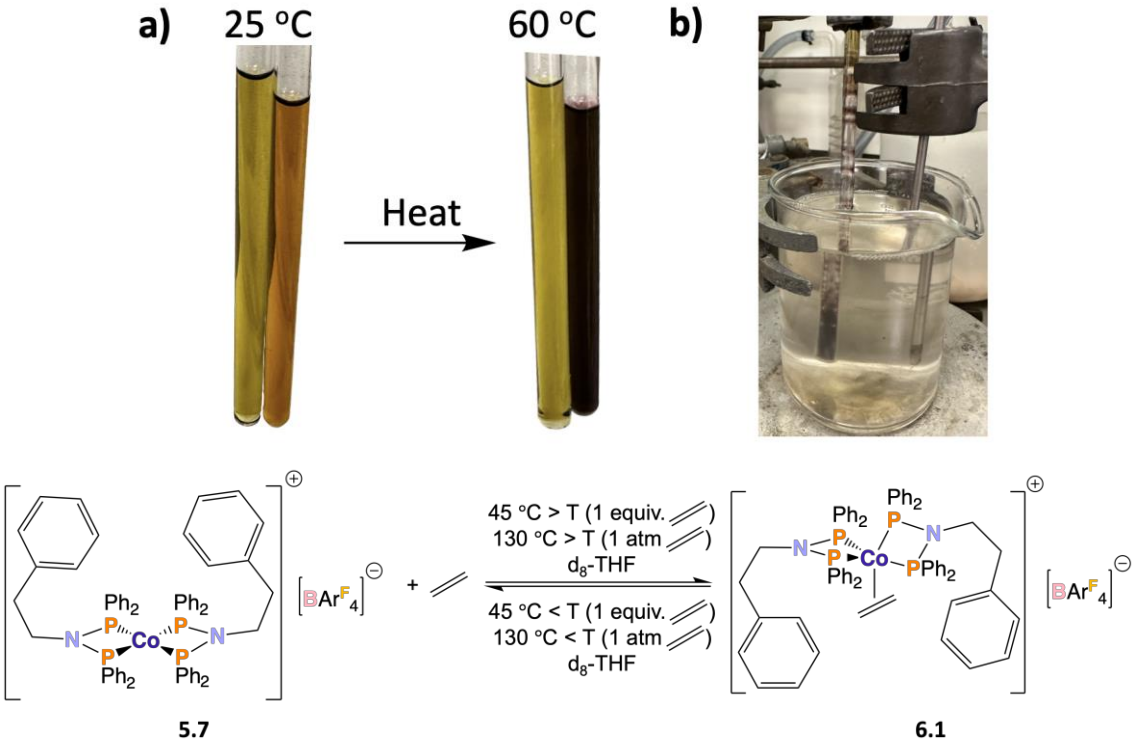


**Figure 6.9. a)** pictures the sealed glass tubes of complex **6.1** in $d_8$-THF with 1 atm of ethylene (tube on the left hand side) and with 1 equivalent of ethylene (tube on the right hand side) at 25 °C to 60 °C, and **b)** a picture of the sealed glass tube of complex **6.1** in $d_8$-THF with 1 atm of ethylene in an oil bath at approx. 130 °C. The equilibrium between complex **5.7** and its ethylene adduct **6.1** is also shown (*NB* T is temperature).

Attempting to study the temperature-dependent colour change shown in **Figure 6.9** by UV-Vis spectroscopy was found to not be possible. Due to the low concentrations required for UV-Vis spectroscopy, it was not possible to add 1 equivalent of ethylene to a specially adapted UV-Vis cell containing complex **5.7**. The lability of ethylene from complex **6.1** renders dilution of a stock solution of complex **6.1** impossible. However, a UV-Vis spectrum of complex **5.7** under 1 atm of ethylene in THF (obtained in a UV-Vis cell allowing for data acquisition of air sensitive samples under an atmosphere of gas) evidences only a single band ($\lambda_{max}$ at 498 nm) in the 400 – 800 nm window. This is significantly different to the UV-Vis spectrum of complex **5.7** in THF in ($\lambda_{max}$ at 526, 646 and 737 nm, **Figure 5.11**), consistent with the aforementioned observed colour change. The lability of ethylene from complex **6.1** is most likely the origin of a lack of signals assignable to complex **6.1** in the positive ion ESI mass spectrum of a sample of complex **5.7** exposed to ethylene (retaining the yellow-brown colour of complex **6.1** prior to mass spectrum acquisition).

It can be concluded that the dynamic behaviour observed by $^{31}P\{^{1}H\}$ VT NMR spectroscopy for complex **5.7** in the presence of 1 atm of ethylene over the temperature

range of –85 – 60 °C (**Figure 6.1**) is due to the two enantiomers of the [Co{Ph(CH$_2$)$_2$N(PPh$_2$)$_2$}$_2$($\eta^2$-CH$_2$CH$_2$)] cation interconverting *via* a Berry *pseudo*rotation process. Treating a sample of complex **5.7** with an equimolar quantity of ethylene also gives rise to a product that is dynamic in nature at temperatures below 45 °C (as indicated by $^{31}$P{$^1$H} spectroscopy). In this case the dynamic behaviour is believed to be more complex and to comprise of both Berry *pseudo*rotation of the [Co{Ph(CH$_2$)$_2$N(PPh$_2$)$_2$}$_2$($\eta^2$-CH$_2$CH$_2$)] cation and also ethylene dissociation at temperatures greater than 45 °C.

## 6.2.4 Reaction of [Co{Ph(CH$_2$)$_2$N(PPh$_2$)$_2$}$_2$][BAr$^F_4$] (5.7) with d$_4$-ethylene

Since the signal corresponding to coordinated ethylene at 1.8 ppm could not be observed in the $^1$H NMR spectrum of complex **6.1** (due to being masked by a large THF signal at 1.79 ppm), the analogous $C_2D_4$ complex, namely complex **6.9**, was synthesised (**Scheme 6.3**) by backfilling a degassed solution of complex **5.7** in (non-deuterated) THF in a NMR tube with an excess of dry d$_4$-ethylene. The NMR tube was then flame–sealed. The $^2$H NMR spectrum of complex **6.9** should only evidence signals corresponding to uncoordinated $C_2D_4$, coordinated $C_2D_4$ and d$_8$-THF (a small amount is naturally present in non-deuterated THF). The signals corresponding to d$_8$-THF should be small and not mask the signal corresponding to coordinated $C_2D_4$, hence a signal corresponding to the coordinated olefin d$_4$-ethylene of complex **6.9** should be observed in the corresponding $^2$H NMR spectrum.

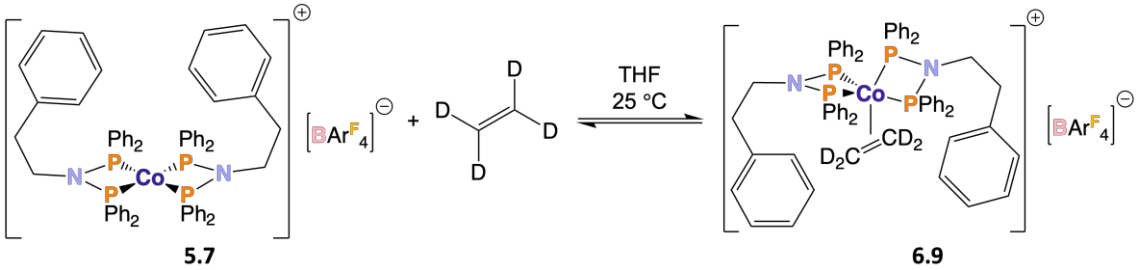


**5.7** **6.9**

**Scheme 6.3.** Synthesis of complex **6.9**.

The obtained $^2$H NMR spectrum (298 K) in **Figure 6.10** show signals at approx. 5.3 ppm (^), corresponding to uncoordinated d$_4$-ethylene, and at approx. 3.56 ppm and 1.77 ppm (*), corresponding to d$_8$-THF. A signal observed at approx. 1.5 ppm (**Figure 6.10**), which is not present in the $^2$H NMR spectrum of d$_4$-ethylene in non-deuterated THF, has been

assigned to coordinated $C_2D_4$ in complex **6.9**. The difference in chemical shift from the predicted approx. 1.8 ppm (based on the determined chemical shift of coordinated ethylene in complex **6.1** from 2D $^1$H-$^1$H NOESY) to approx. 1.5 ppm is likely due to the chemical anisotropy caused by the coordination of $C_2D_4$ containing deuterium atoms, with $I$ = 1, to the $^{59}$Co-centre with $I$ = 7/2.[19] Hence, a signal corresponding to the coordinated olefin $d_4$-ethylene has been observed, confirming $d_4$-ethylene coordination.

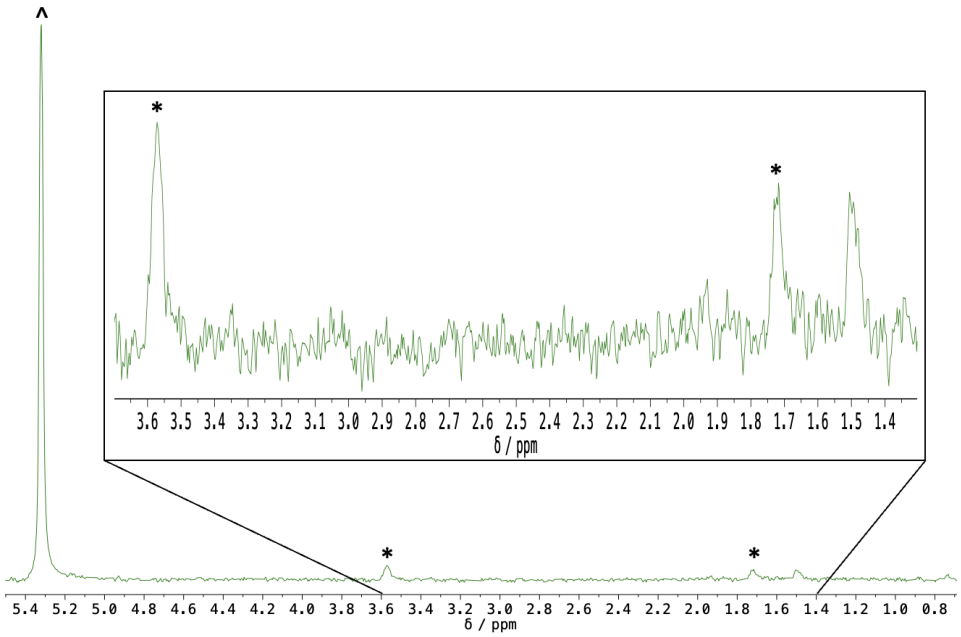


**Figure 6.10.** $^2$H NMR spectrum (162 MHz, 298 K, THF) of complex **6.9**, where ^ is the signal corresponding to uncoordinated $d_4$-ethylene and * are the signals corresponding to $d_8$-THF.

## 6.2.5 Hybrid-DFT studies to determine the Gibbs free energy changes for the association of ethylene to [Co{MeN(PMe$_2$)$_2$}$_2$][PF$_6$] (6.10), [Co{MeN(P{OPh}$_2$)$_2$}$_2$][PF$_6$] (6.11) and [Co{MeN(PPh$_2$)$_2$}$_2$][PF$_6$] (6.12)

In order to probe the effect of the steric bulk and electronic effects of the phosphorus atom substituents on the Gibbs free energy change of ethylene association (ΔG), complexes **6.10** – **6.15** (**Scheme 6.4**) and ethylene were geometry optimised at the B3LYP/6-31G(d) DFT level using a THF solvation model.

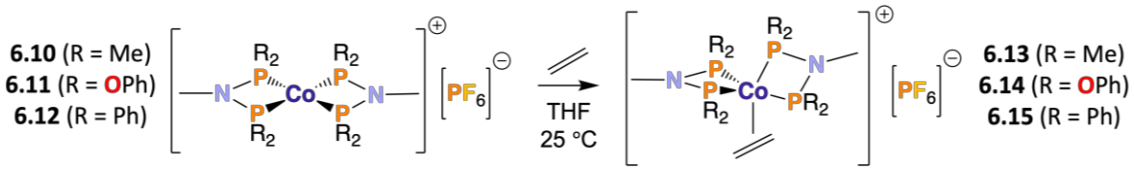


**Scheme 6.4.** The computationally studied reactions of complexes **6.10** – **6.12** with ethylene to afford complexes **6.13** – **6.15**, respectively.

All ΔG values are calculated following **Equation 6.3**, with the results shown in **Table 6.1**.

$$\Delta G = \Sigma G_{product} - \Sigma G_{reactant} \quad \textbf{(6.3)}$$

**Table 6.1.** Calculated Gibbs free energy changes for the association of ethylene to complexes **6.10** – **6.12** in THF at 298.15 K, and the $\%V_{bur}$ (percentage volume buried) in the square planar $[Co\{MeN(PR_2)_2\}_2]$ cation by the two $MeN(PR_2)_2$ ligands determined using the online SambVca 2.1 software.[20]

| R | ΔG / kJ mol$^{-1}$ | $\%V_{bur}$ $[Co\{MeN(PR_2)_2\}_2]^+$ |
|---|---|---|
| Me | –30.0 | 76.4 |
| OPh | –41.6 | 88.1 |
| Ph | –4.4 | 89.2 |

The computationally determined ΔG values (**Table 6.1**) show that changing the phosphorus substituent from Ph to Me results in a lowering of ΔG from –4.4 kJ mol$^{-1}$ to –30.0 kJ mol$^{-1}$, reflecting the lower steric bulk of methyl relative to phenyl groups and hence the less hindered association of ethylene. Examination of the value of $\%V_{bur}$ (percentage volume buried, determined using the SambVca 2.1 software)[20] calculated for the $[Co\{MeN(PR_2)_2\}_2]$ cation also helps rationalise the computationally determined ΔG values (**Table 6.1**). The $\%V_{bur}$ of one of the $Ph(CH_2)_2N(PPh_2)_2$ ligands in $[CoBr(Ph(CH_2)_2N\{PPh_2\}_2)_2][PF_6]$ (complex **5.1**) is shown in **b)**, **Figure 6.11**, with the result suggesting (highly sterically hindered regions appear in red) that little steric congestion exists around the metal centre as a result of the 'PNP' ligand. The smaller value of $\%V_{bur}$ for the $[Co\{MeN(PR_2)_2\}_2]$ cation with R = Me (76.4) relative to R = Ph (89.2) evidences the lower steric bulk of methyl relative to phenyl groups, resulting in greater accessibility of the cobalt(I) centre for ethylene coordination and a more favourable ΔG.

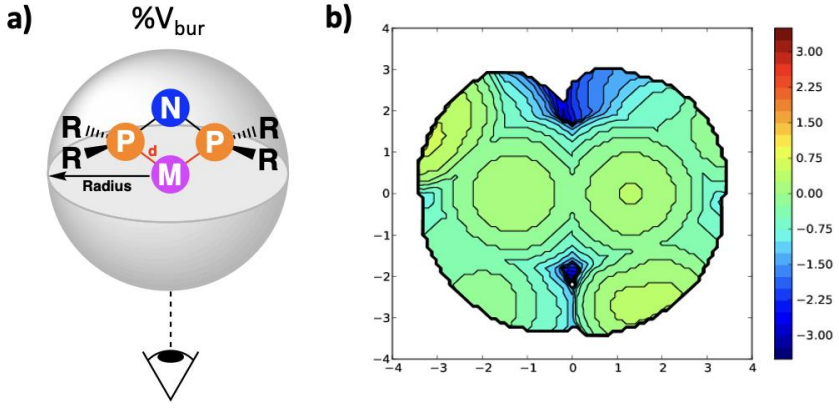


**Figure 6.11. a)** representation of the percentage volume buried, with direction shown for the view of steric maps (a representative example shown in **b)** for one of the $Ph(CH_2)_2N(PPh_2)_2$ ligands in complex **5.1**). *NB* radius is 3.5 Å and metal centre-ligand distance is 2 Å.

The phenoxy phosphorus substituent (*i.e.*, complexes **6.11** and **6.14**, **Scheme 6.4**) results in a ΔG of –41.6 kJ mol$^{-1}$ (the most favourable in **Table 6.1**), reflecting the electron-

withdrawing nature of the phenoxy groups relative to methyl and phenyl as the $\%V_{bur}$ values of 88.1 and 89.2 for the $[Co\{MeN(PR_2)_2\}_2]$ cation with R = OPh and Ph, respectively, are essentially identical. Hence, there is practically no difference in the steric congestion around the cobalt(I) centre in the $[Co\{MeN(PR_2)_2\}_2]$ cation (with R = OPh or Ph). Phosphines with electron-withdrawing substituents, *e.g.*, phenoxy, could stabilise the cationic electron-rich low oxidation state cobalt(I) centre and reduce the amount of electron density at the cobalt(I) centre, making coordination of a L-type ligand, *i.e.*, ethylene, more favourable.

### 6.2.6 Hybrid-DFT studies to determine the Gibbs free energy changes for the association of THF, ethylene, $N_2$, MeCN, CO and $H_2O$ to $[Co\{MeN(PPh_2)_2\}_2][PF_6]$ (6.12)

The reactivity of complex **6.12** ($[Co(MeN\{PPh_2\}_2)_2][PF_6]$), a computationally simpler model of complex **5.7** ($[Co(Ph(CH_2)_2N\{PPh_2\}_2)_2][BAr^F{}_4]$) with THF, ethylene, $N_2$, MeCN, CO and $H_2O$, *i.e.*, L in **Scheme 6.5**, has been probed by calculating the Gibbs free energies of association of L to complex **6.12**. Since complex **5.7** is synthesised in THF solvent, under a $N_2$ atmosphere and potentially in the presence of trace amounts of $H_2O$, it is useful to computationally assess the coordination potential of THF, $N_2$ and $H_2O$ with complex **6.12** as THF, $N_2$ and $H_2O$ may coordinate to the cobalt centre of the $[Co('PNP')_2]$ cation. From experiment, MeCN is believed to coordinate to complex **5.7** as a purple-to-orange colour change is observed when complex **5.7** is dissolved in MeCN (**Section 5.3**). Verification of coordination of MeCN to complex **5.7** can be provided by the computational assessment of the coordination of MeCN to complex **6.12**. Computational assessment of the coordination of CO to complex **6.12** is also of interest as CO is a commonly utilised substrate for many catalytic applications (*e.g.*, hydroformylation)[1] and a large negative Gibbs free energy of association is expected due to the $\pi$-accepting ability of CO.

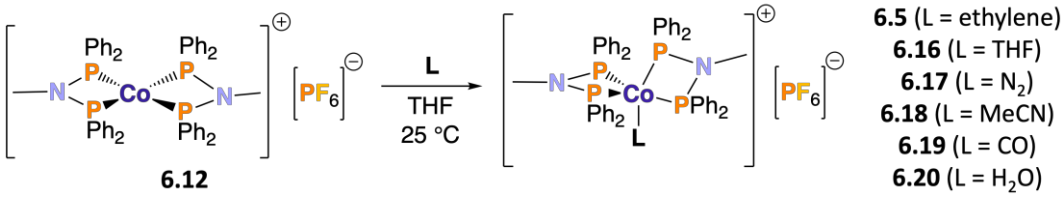


**Scheme 6.5.** The association of molecule **L** to complex **6.12** to afford complexes **6.5** and **6.16** – **6.20** (L = ethylene, THF, $N_2$, MeCN, CO and $H_2O$).

In order to determine the Gibbs free energies of formation of complexes **6.5** and **6.16** – **6.20** (**Scheme 6.5**), THF, ethylene, $N_2$, MeCN, CO and $H_2O$, complexes **6.5**, **6.12** and **6.16** – **6.20** underwent geometry optimisations at the B3LYP/6-31G(d) level (with a THF solvation model). The Gibbs free energies of association were calculated using **Equation 6.3** (**Section 6.2.5**), and the obtained values of ΔG are shown in **Table 6.2**.

**Table 6.2.** Calculated Gibbs free energy changes for the formation of complexes **6.5** and **6.16** – **6.20** (THF, 298.15 K).

| Complex | L | ΔG / kJ mol$^{-1}$ |
|---|---|---|
| **6.5** | Ethylene | –4.38 |
| **6.16** | Tetrahydrofuran | 51.3 |
| **6.17** | Dinitrogen | 2.95 |
| **6.18** | Acetonitrile | –4.62 |
| **6.19** | Carbon monoxide | –91.9 |
| **6.20** | Water | 15.7 |

The formation of complexes **6.17** ([Co(MeN{$PPh_2$}$_2$)$_2$($N_2$)][$PF_6$]) and **6.18** ([Co(MeN{$PPh_2$}$_2$)$_2$(MeCN)][$PF_6$]) are accompanied by very small ΔG values that are very close to the ΔG value for the formation of complex **6.5** (with analogous ethylene complex **6.1**, [Co{Ph($CH_2$)$_2$N($PPh_2$)$_2$}$_2$($\eta^2$-$CH_2CH_2$)][$BAr^F{}_4$], established experimentally to exist at room temperature). It is therefore possible that $N_2$ and MeCN could also coordinate to complex **6.12** ([Co(MeN{$PPh_2$}$_2$)$_2$][$PF_6$]), and hence also to complexes **5.5** ([Co(Ph($CH_2$)$_2$N{$PPh_2$}$_2$)$_2$][$PF_6$]), **5.6** ([Co(Py-*o*-($CH_2$)$_2$N{$PPh_2$}$_2$)$_2$][$PF_6$]), and **5.7** ([Co(Ph($CH_2$)$_2$N{$PPh_2$}$_2$)$_2$][$BAr^F{}_4$]). The computationally obtained IR spectrum of complex **6.17** reveals a $\nu$($N_2$) stretch at 2251 cm$^{-1}$. A peak corresponding to this stretch is not observed in the experimental IR spectrum (acquired in a nujol mull) of complex **5.7** prepared in a glovebox under $N_2$ atmosphere. Hence, this suggests that $N_2$ does not coordinate to complexes **5.5** – **5.7**. Positive ion ESI mass spectra of solutions of complexes **5.5** – **5.7** evidence no signal for the [Co('PNP')$_2$(MeCN)] cation, although this does not confirm that MeCN does not coordinate to complexes **5.5** – **5.7**.

Computationally, complex **6.19** ([Co(MeN{$PPh_2$}$_2$)$_2$(CO)][$PF_6$]) has a ΔG of formation of –91.9 kJ mol$^{-1}$, reflecting the $\pi$-accepting ability and small, linear nature of carbon monoxide. The ΔG of formation of complexes **6.16** ([Co(MeN{$PPh_2$}$_2$)$_2$(THF)][$PF_6$]) and **6.20** ([Co(MeN{$PPh_2$}$_2$)$_2$($H_2O$)][$PF_6$]), with larger and non-linear molecules THF and $H_2O$,

respectively, are larger positive values (**Table 6.2**), evidencing the greater steric bulk of THF and $H_2O$ (particularly THF) relative to smaller molecules like MeCN. This suggests that THF, the solvent for the ethylene coordination reactions (**Scheme 6.1**), and $H_2O$ do not coordinate to complex **6.12** and complexes **5.5** – **5.7**.

## 6.3 Reaction of $[Co\{Ph(CH_2)_2N(PPh_2)_2\}_2][BAr^F{}_4]$ (5.7) with CO

Since CO was found to likely coordinate to complex **6.12** computationally (**Section 6.2.6**), the reactivity of CO with complex **5.7** was probed experimentally. A solution of complex **5.7** in $d_8$-THF was degassed by three freeze-pump-thaw cycles and backfilled with 1 atm of CO gas. This results in a purple-to-orange colour change, consistent with the formation of complex **6.21** (**Scheme 6.6**).

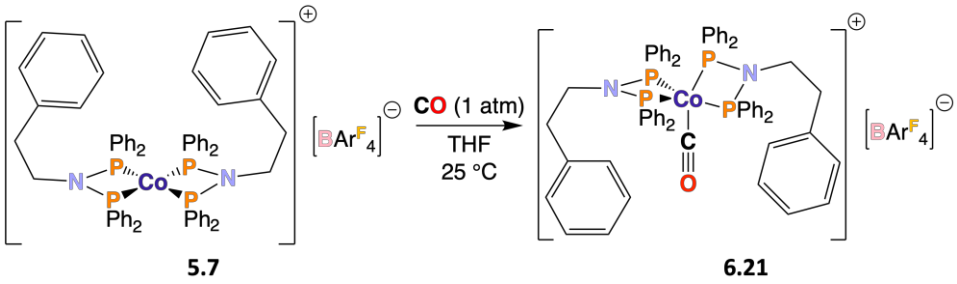


**Scheme 6.6.** Synthesis of complex **6.21**.

The positive ion ESI spectrum of isolated complex **6.21** exhibits a signal at 1066.1 *m/z*, indicating the coordination of a single CO ligand (**Scheme 6.6**). The FT-IR spectrum of complex **6.21** evidences a single $\nu_{CO}$ stretching frequency of 1951 $cm^{-1}$, agreeing with the computational value of 2010 $cm^{-1}$ and 1955 $cm^{-1}$ previously reported for complex **6.22**[21] (**Figure 6.12**). The cation of complex **6.21** has a $C_2$ point group, and group theory analysis indicates that one CO stretching frequency should be expected. 'Free' CO exhibits a $\nu_{CO}$ of 2143 $cm^{-1}$,[22] hence complex **6.21** evidences a reduction in $\nu_{CO}$ relative to 'free' CO. A reduction in $\nu_{CO}$ relative to 'free' CO indicates C-O bond weakening upon coordination to the $[Co\{Ph(CH_2)_2N(PPh_2)_2\}_2]$ cation as a result of synergic bonding.

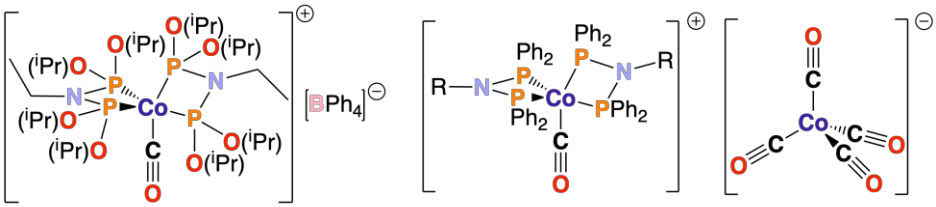


**Figure 6.12.** Structures of complexes **6.22** – **6.25**.[21,23,24]

A singlet resonance in the $^{31}P\{^{1}H\}$ and $^{31}P$ NMR spectra of complex **6.21** at 81.6 ppm shows excellent agreement with singlet resonances in the $^{31}P\{^{1}H\}$ and $^{31}P$ NMR spectra ($\delta_P$ ~76 – 84 ppm)[23,24] for analogous previously reported complexes **6.23** – **6.25** (**Figure 6.12**) containing the [Co('PNP')$_2$(CO)] cation. Solid-state structures of complexes **6.23** – **6.25** show a trigonal bipyramidal [Co{RN(PPh$_2$)$_2$}$_2$(CO)] cation.[23,24]

The observation of a singlet (as opposed to two signals, *cf*. the $^{31}P\{^{1}H\}$ spectrum of complex **6.1**, [Co{Ph(CH$_2$)$_2$N(PPh$_2$)$_2$}$_2$($\eta^2$-CH$_2$CH$_2$)][BAr$^F_4$], at temperatures below approx. 35 °C) in the $^{31}P\{^{1}H\}$ and $^{31}P$ NMR spectra of complex **6.21** suggests that the rate of exchange between the two enantiomers of the [Co{Ph(CH$_2$)$_2$N(PPh$_2$)$_2$}$_2$(CO)] cation of complex **6.21**, *via* Berry *pseudo*rotation, is faster than the NMR timescale. Determination of the Berry *pseudo*rotation transition state at the B3LYP/6-31G(d) DFT level (**Figure 6.13**) demonstrates activation barriers of 2.5 and 4.3 kcal mol$^{-1}$ for interconversion between Δ and Λ enantiomers.

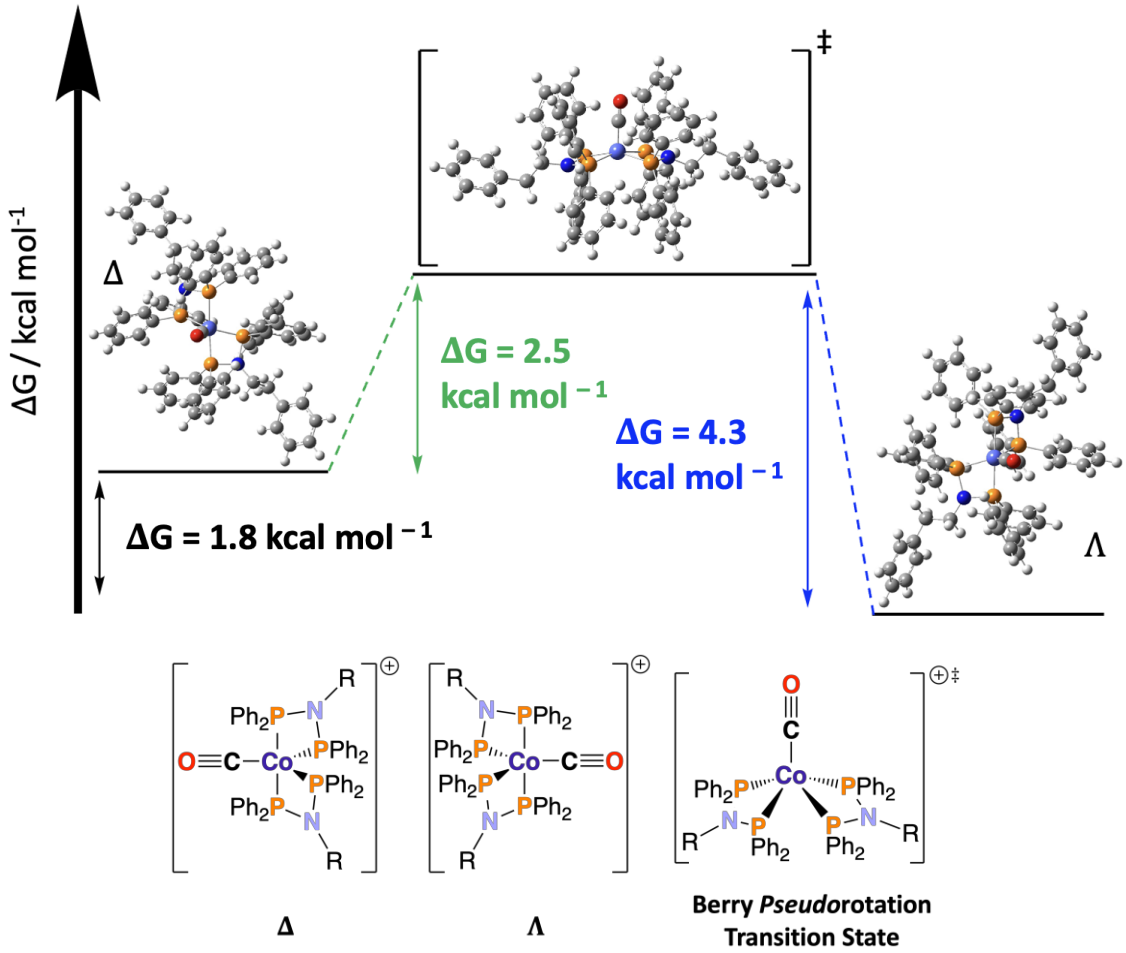


**Figure 6.13.** Racemisation scheme showing the transition state for the interconversion of the Δ and *Λ* enantiomers of the [Co{RN(PPh$_2$)$_2$}$_2$(CO)] cation of complex **6.21** *via* a Berry *pseudo*rotation process. *NB* R = CH$_2$CH$_2$Ph.

The activation barriers of 2.5 and 4.3 kcal $mol^{-1}$ are negligible, allowing for rapid interconversion between the two enantiomers of the $[Co\{Ph(CH_2)_2N(PPh_2)_2\}_2(CO)]$ cation at room temperature. This is consistent with the observation of a singlet in the $^{31}P\{^1H\}$ and $^{31}P$ NMR spectra of complex **6.21**. The highlighted fluxional nature of analogous trigonal bipyramidal cobalt(I) complexes is well established.[25]

The activation barriers of 2.5 and 4.3 kcal $mol^{-1}$ (**Figure 6.13**) are much smaller than the analogous activation barriers for the $[Co\{Ph(CH_2)_2N(PPh_2)_2\}_2(\eta^2\text{-}CH_2CH_2)]$ cation of complex **6.1** (14.4 and 17.6 kcal $mol^{-1}$ for the $\Lambda$ and $\Delta$ enantiomers, respectively), likely stemming from ethylene having greater steric bulk than CO due to ethylene coordinating in a 'side on' manner (**Figure 6.8**).

## 6.4 Reaction of $[Co\{Ph(CH_2)_2N(PPh_2)_2\}_2][BAr^F{}_4]$ (5.7) with $H_2$ and HD

In order to study the coordination chemistry of cationic cobalt(I) complexes containing 'PNP' ligands with $H_2$, a solution of the complex $[Co(Ph(CH_2)_2N\{PPh_2\}_2)_2][BAr^F{}_4]$ (**5.7**) in $d_8$-THF was degassed by three freeze-pump-thaw cycles and backfilled with 1 atm of $H_2$ gas. This resulted in a purple-to-yellow colour change ascribed to the formation of the corresponding $H_2$ adduct. Additionally, complex **5.7** was reacted with HD in order to measure the value of $J_{HD}$ coupling of the resulting HD adduct of complex **5.7**, to provide insight into the nature of the Co-(H)(E) or Co($\eta^2$-HE) interaction (where E = H or D). The $H_2$ and HD adducts of complex **5.7** could not be isolated and were primarily studied by *in situ* NMR spectroscopy. HD gas was synthesised *via* a 1:1 reaction of NaH and $D_2O$,[26] passed through a drying column of anhydrous $CaCl_2$ and used to backfill a solution of complex **5.7** in $d_8$-THF, degassed by three freeze-pump-thaw cycles, in a Young's NMR tube. However, a mixture of HD and $H_2$ gas (presumably due to the presence of $H_2O$ in $D_2O$) was produced in an approx. $2H_2$:3HD ratio determined from integration of the $^1H$ NMR signals corresponding to $H_2$ (a singlet at 4.58 ppm) and HD (a 1:1:1 triplet at 4.54 ppm). Hence, the reaction of complex **5.7** with HD gas (**Scheme 6.7**) produces a mixture of the HD and $H_2$ adducts of complex **5.7**.

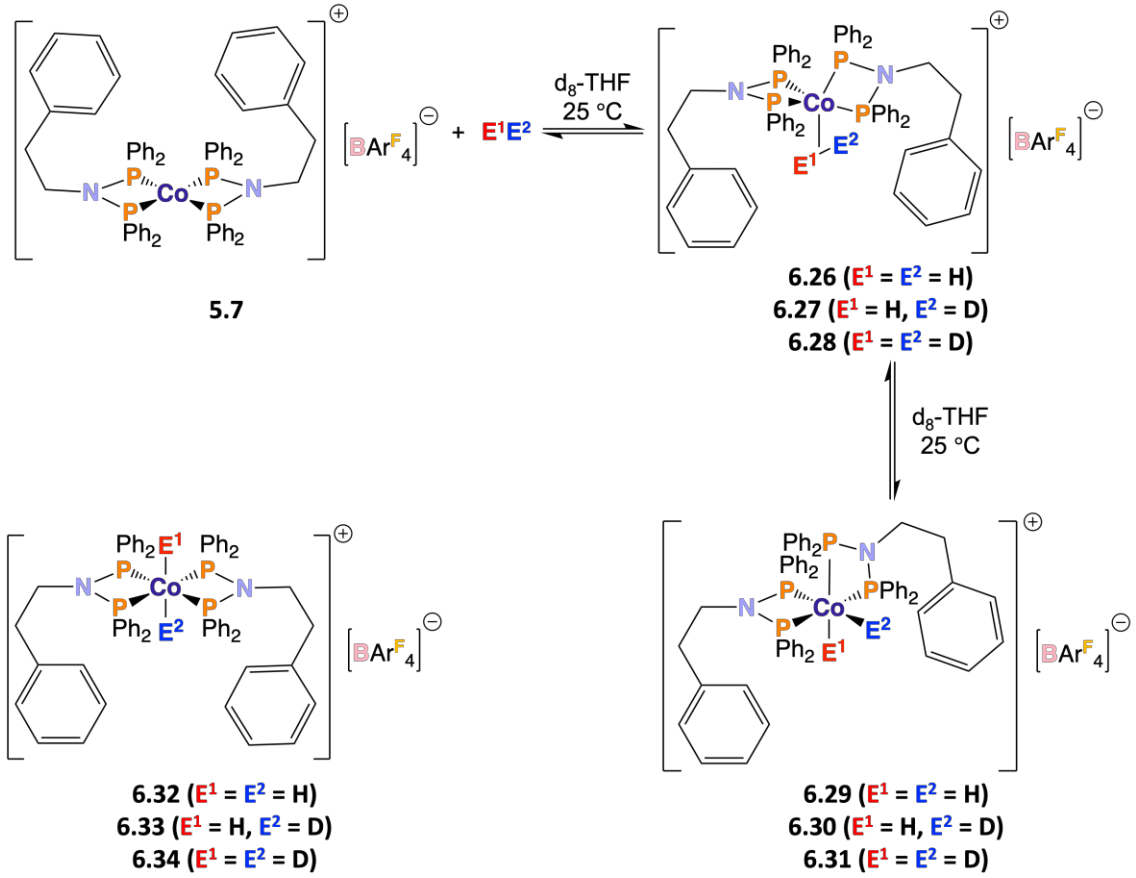


**Scheme 6.7.** Synthesis of the $H_2$, HD and $D_2$ adducts of complex **5.7**, and structures of complexes **6.26** – **6.34**.

The $^1$H NMR spectrum presented in **a)**, **Figure 6.14** evidences the presence of two cobalt-bound hydrogen atoms as a quintet at $\delta_H$ = –6.25 ppm with $^2J_{PH}$ ~36 Hz and an integral of two is present. $\delta_H$ = –6.25 ppm is within the typical $\delta_H$ range of –5 to –25 ppm expected for hydride or $\eta^2$-$H_2$ complexes.[27] The $^1$H{$^{31}$P} spectrum shown in **b)**, **Figure 6.14** shows a singlet, revealing that the quintet in the $^1$H NMR spectrum displayed in **a)**, **Figure 6.14** arises due to the cobalt-interacting hydrogen atoms coupling to the four phosphorus atoms. The $^1$H{$^{31}$P} NMR spectrum shown in **d)**, **Figure 6.14** presents one new singlet (in addition to that previously mentioned at –6.25 ppm) at approx. –6.16 ppm corresponding to the HD adduct of complex **5.7**, evidencing a lack of H-D coupling. A $J_{HD}$ value of 10 – 35 Hz is considered definitive evidence of a $\eta^2$-HD ligand,[28,29] and *trans*-dihydride species (*i.e.*, complex **6.33**, **Scheme 6.7**) exhibit large $J_{HD}$ values.[30] Hence, a lack of H-D coupling suggests that complexes **6.26** – **6.27** (containing $\eta^2$-$H_2$ and $\eta^2$-HD ligands, respectively) and *trans*-dihydride complexes **6.32** – **6.33** (**Scheme 6.7**) are not observed experimentally. Therefore, it is likely that *cis*-dihydride complexes **6.29** – **6.30** are the $H_2$/HD adducts of complex **5.7** ([Co(Ph(CH$_2$)$_2$N{PPh$_2$}$_2$)$_2$][BAr$^F_4$]). Two

overlapping quintets are observed in the $^{1}$H NMR spectrum shown in **c)**, **Figure 6.14**. The ratio of the HD and $H_2$ adducts of complex **5.7** is 2:3 (determined by $^{1}$H NMR signal integration in **d)**, **Figure 6.14**), which is the inverse of the approx. $2H_2$:3HD ratio from HD synthesis, suggesting that H-D scrambling may be taking place.

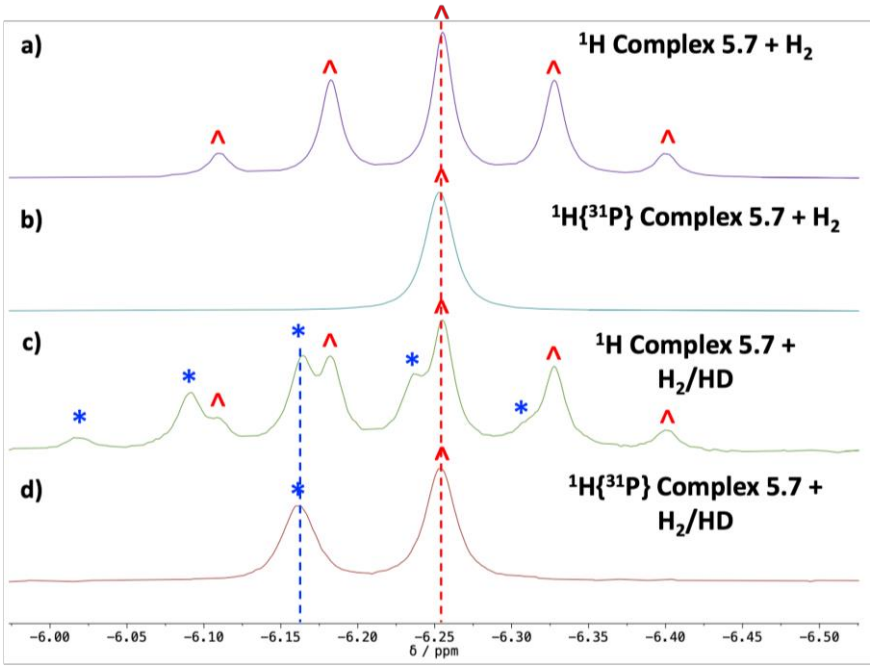


**Figure 6.14.** $^{1}$H (400 MHz, 290 K, $d_8$-THF) spectra of **a)** complex **5.7 + $H_2$** and **c)** complex **5.7 + $H_2$/HD**, and $^{1}$H{$^{31}$P} (400 MHz, 290 K, $d_8$-THF) spectra of **b)** complex **5.7 + $H_2$** and **d)** complex **5.7 + $H_2$/HD**. ^ and * indicate signals corresponding to complex **5.7 + $H_2$** and complex **5.7 + HD**, respectively. *NB* approx. $2H_2$:3HD ratio added to sample of complex **5.7**.

The $^{31}$P NMR spectrum shown in **a)**, **Figure 6.15** evidences a broad triplet ($^{2}J_{PH}$ ~35 Hz) at $\delta_P$ = 100 ppm (assigned to the $H_2$ adduct of complex **5.7**), indicating chemical equivalence of all four phosphorus atoms, and coupling between the phosphorus atoms and the two cobalt-bound hydrogen atoms. The $^{31}$P{$^{1}$H} NMR spectrum presented in **b)**, **Figure 6.15** evidences a singlet at $\delta_P$ = 100 ppm. The $^{31}$P{$^{1}$H} NMR spectrum shown in **d)**, **Figure 6.15** evidences a broad signal with peaks $\alpha$, $\beta$, and $\gamma$, assigned to the $H_2$, HD and $D_2$ adducts of complex **5.7** ([Co(Ph$(CH_2)_2$N{$PPh_2$}$_2$)$_2$][$BAr^F_4$]), respectively. The $^{31}$P NMR spectrum displayed in **c)**, **Figure 6.15** evidences a doublet ($^{2}J_{HP}$ ~38.6 Hz) assigned to the HD adduct of complex **5.7**. This signal is a doublet due to P-H coupling (and a lack of P-D coupling) and masks peaks $\alpha$ and $\gamma$ visible in the $^{31}$P{$^{1}$H} NMR spectrum shown in **d)**, **Figure 6.15**.

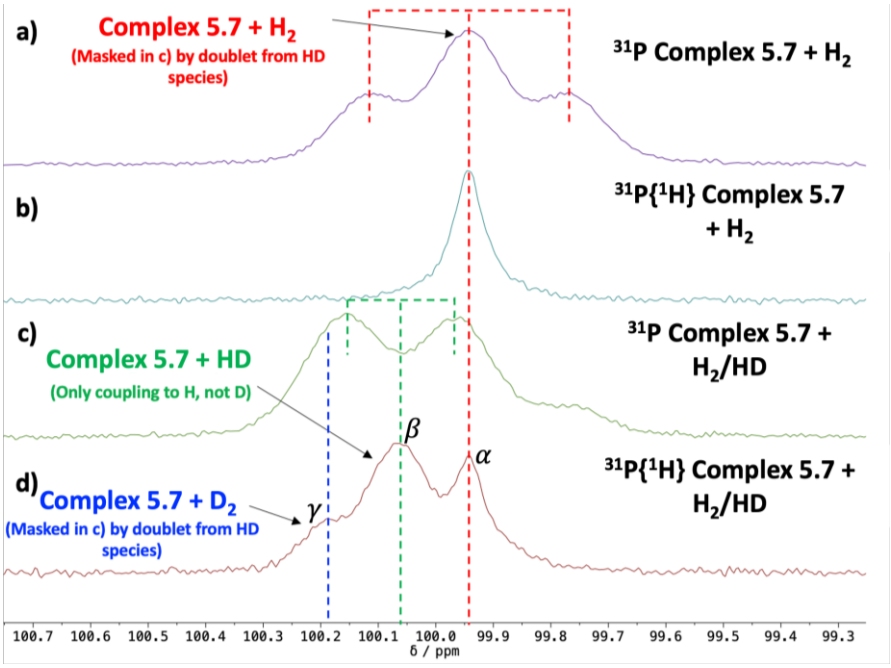


**Figure 6.15.** $^{31}P$ NMR spectra (162 MHz, 294 K) of **a)** complex **5.7 + $H_2$** and **c)** complex **5.7 + $H_2$/HD**, and $^{31}P\{^1H\}$ spectra (162 MHz, 294 K) of **b)** complex **5.7 + $H_2$** and **d)** complex **5.7 + $H_2$/HD**. $\alpha$, $\beta$, and $\gamma$ represent signals corresponding to complex **5.7 + $H_2$**, complex **5.7 + HD**, and complex **5.7 + $D_2$**, respectively. *NB* approx. $2H_2$:3HD ratio added to sample of complex **5.7**.

A signal assigned to the $D_2$ adduct of complex **5.7** appears in the $^{31}P\{^1H\}$ NMR spectrum obtained one day after exposure of complex **5.7** to $H_2$/HD (**b)**, **Figure 6.16**), and at a greater intensity in the $^{31}P\{^1H\}$ NMR spectrum obtained after 3 weeks (**c)**, **Figure 6.16**). The $^{31}P\{^1H\}$ NMR spectral data (**Figure 6.16**) suggest that $D_2$ is produced as a result of H-D scrambling, implying occurrence of H-D and H-H bond cleavage, providing evidence for *cis*-dihydride complexes **6.29** – **6.30** being the $H_2$/HD adducts of complex **5.7**.

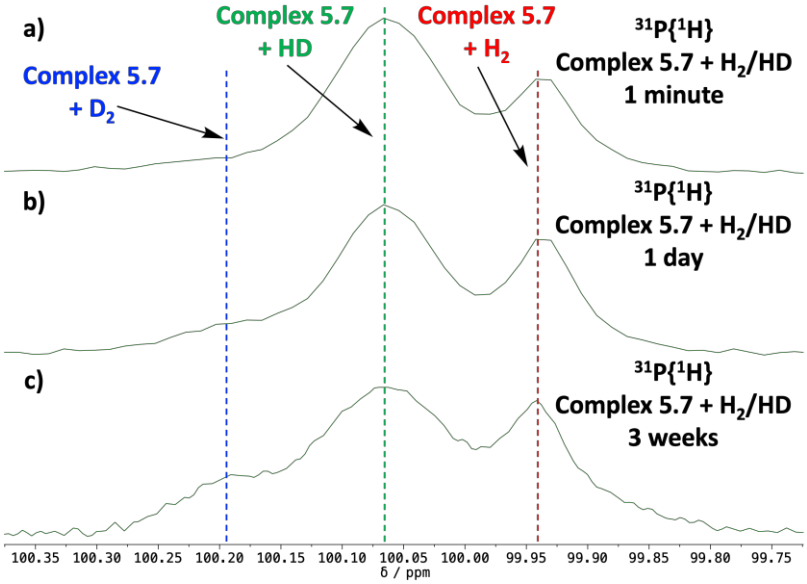


**Figure 6.16.** $^{31}P\{^1H\}$ spectra (162 MHz, 294 K) of complex **5.7 + $H_2$/HD** acquired after 1 minute, 1 day and 3 weeks. *NB* approx. $2H_2$:3HD ratio added to sample of complex **5.7**.

The 2D $^{1}$H-$^{1}$H NOESY spectrum (**Figure 6.17**) evidences chemical exchange (indicated by cross peaks of the same sign, *i.e.*, colour, as the diagonal)[15] between 'free' $H_2$/HD and $H_2$/HD interacting with complex **5.7**. Chemical exchange is observed only when there is an excess of $H_2$/HD gas.

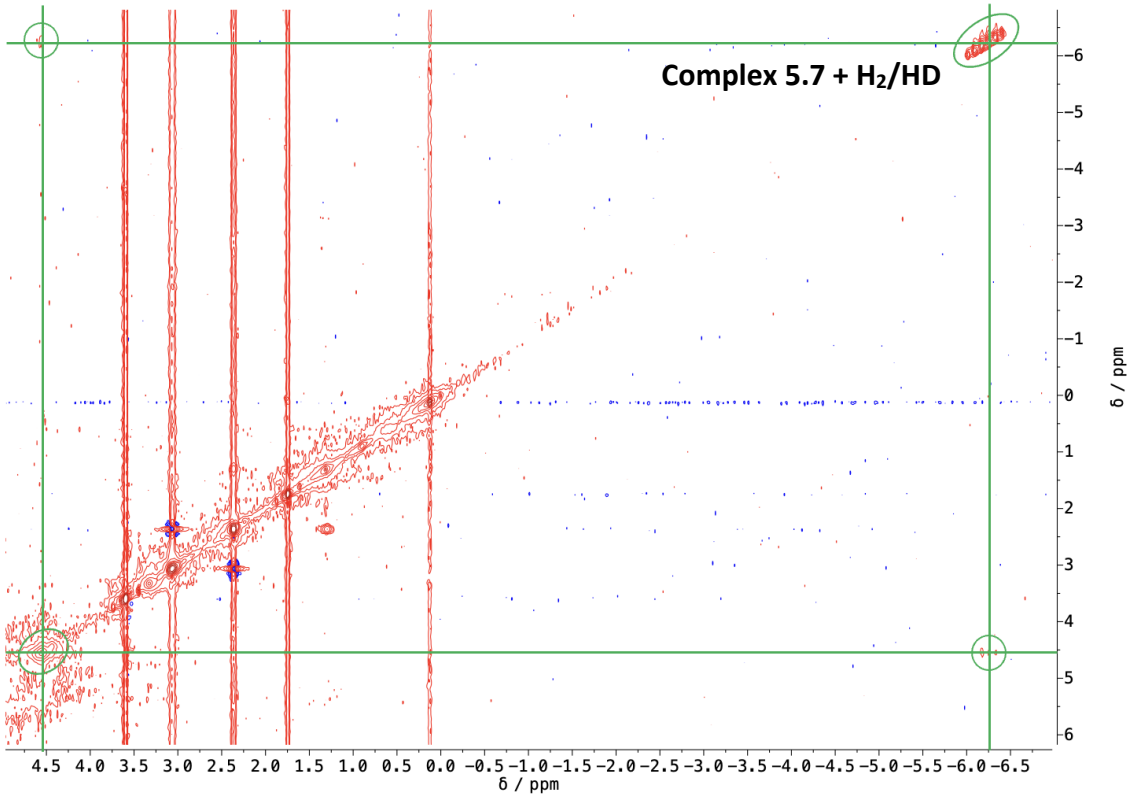


**Figure 6.17.** $^{1}$H-$^{1}$H NOESY spectrum of the sample of the $H_2$/HD adducts of complex **5.7** in $d_8$-THF at 298.15 K, with the cross peaks evidencing chemical exchange between uncoordinated (approx. 4.5 ppm) and coordinated (approx. –6.2 ppm) $H_2$/HD being highlighted in green. *NB* approx. $2H_2$:3HD ratio added to sample of complex **5.7**.

Chemical exchange of $H_2$/HD must occur through the association and dissociation of $\eta^2$-HE (E = H or D). Hence, the observation of chemical exchange suggests that dihydrogen complexes **6.26** – **6.27** are observed experimentally. The spectral data suggest that complexes **6.26** ([Co(Ph(CH$_2$)$_2$N{PPh$_2$}$_2$)$_2$($\eta^2$-H$_2$)][BAr$^F_4$]) and **6.29** ([Co(Ph(CH$_2$)$_2$N{PPh$_2$}$_2$)$_2$(*cis*-(H)$_2$)][BAr$^F_4$]), and complexes **6.27** ([Co(Ph(CH$_2$)$_2$N{PPh$_2$}$_2$)$_2$($\eta^2$-HD)][BAr$^F_4$]) and **6.30** ([Co(Ph(CH$_2$)$_2$N{PPh$_2$}$_2$)$_2$(*cis*-(H)(D))][BAr$^F_4$]), are both present in equilibrium (**Scheme 6.8**), with complexes **6.28** ([Co(Ph(CH$_2$)$_2$N{PPh$_2$}$_2$)$_2$($\eta^2$-D$_2$)][BAr$^F_4$]) and **6.31** ([Co(Ph(CH$_2$)$_2$N{PPh$_2$}$_2$)$_2$(*cis*-(D)$_2$)][BAr$^F_4$]) being produced as a result of H-D scrambling. However, complexes **6.26** – **6.31** have two unique phosphorus environments and hence would be expected to exhibit two signals in their proton-coupled and proton-decoupled $^{31}$P NMR spectra,

which is not the case (even when cooled to –85 °C). Therefore, the $H_2$, HD and $D_2$ adducts of complex **5.7** must be fluxional (as was observed for the $[Co\{Ph(CH_2)_2N(PPh_2)_2\}_2(CO)]$ cation in **Section 6.3**) to result in the four phosphorus atoms and two hydrogen atoms interacting with the cobalt centre to be equivalent.

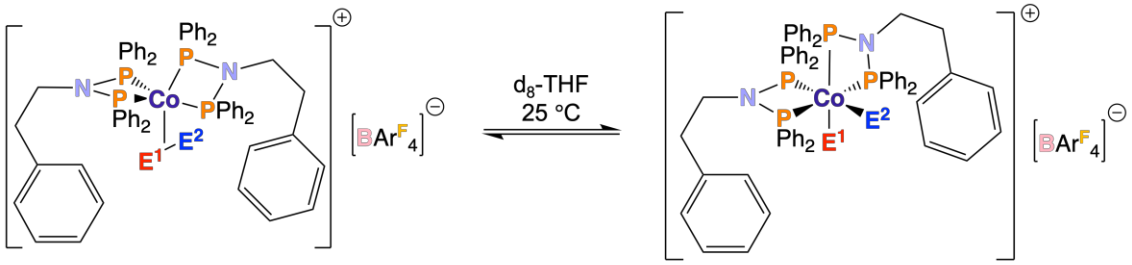


**6.26** ($E^1 = E^2 = H$), **6.27** ($E^1 = H$, $E^2 = D$), **6.28** ($E^1 = E^2 = D$) ⇌ **6.29** ($E^1 = E^2 = H$), **6.30** ($E^1 = H$, $E^2 = D$), **6.31** ($E^1 = E^2 = D$)

**Scheme 6.8.** Equilibrium between complexes **6.26** – **6.28** and **6.29** – **6.31**.

As a result of the fluxional behaviour and $H_2$ exchange, a $T_{1(min)}$ relaxation time for the dihydrogen/hydride resonance (obtained from an inversion recovery experiment) of the $H_2$/HD adducts of complex **5.7** ($[Co(Ph(CH_2)_2N\{PPh_2\}_2)_2][BAr^F_4]$) could not be reliably obtained. The $T_{1(min)}$ relaxation time is a quantity classically utilised to distinguish between dihydride, with $T_{1(min)} > 50$ ms, and dihydrogen, with $T_{1(min)} < 35$ ms, species.[31] Note that the $T_{1(min)}$ relaxation time criterion has been found to be generally unsuitable for cobalt complexes due to cobalt's high magnetogyric ratio (which significantly impacts the relaxation time of species in or close to the cobalt centre).[32] The fluxional behaviour of the $[Co\{Ph(CH_2)_2N(PPh_2)_2\}_2(H_2)]$ cation will be explored computationally in **Section 6.4.1**.

### 6.4.1 Hybrid-DFT studies probing the structure of the $H_2$ adduct of $[Co\{Ph(CH_2)_2N(PPh_2)_2\}_2][BAr^F_4]$ (5.7)

The fluxional behaviour of the $H_2$ adduct of complex **5.7** (*i.e.*, the equilibrium mixture of complexes **6.26** and **6.29**, **Scheme 6.8**) may arise from the $[Co\{Ph(CH_2)_2N(PPh_2)_2\}_2(\eta^2\text{-}H_2)]$ cation of complex **6.26** undergoing a Berry *pseudo*rotation (**a**), **Scheme 6.9**), interconverting between Δ and Λ enantiomers. Alternatively, the octahedral $[Co\{Ph(CH_2)_2N(PPh_2)_2\}_2(cis\text{-}(H)_2)]$ cation of complex **6.29** may undergo a Bailer twist[33] (**b**), **Scheme 6.9**) interconverting between Δ and Λ enantiomers.

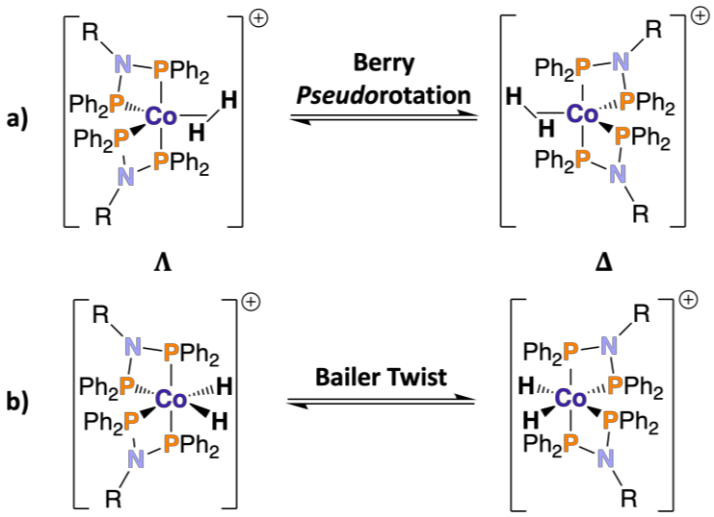


**Scheme 6.9. a)** Berry *pseudo*rotation of the [Co{Ph(CH$_2$)$_2$N(PPh$_2$)$_2$}$_2$($\eta^2$-H$_2$)] cation and **b)** Bailer twist of the [Co{Ph(CH$_2$)$_2$N(PPh$_2$)$_2$}$_2$(*cis*-(H)$_2$)] cation (*NB* R = CH$_2$CH$_2$Ph).

In order to probe the fluxional processes suggested in **a)** and **b)** (**Scheme 6.9**), the optimised geometries of the Δ and Λ enantiomers of the [Co{Ph(CH$_2$)$_2$N(PPh$_2$)$_2$}$_2$($\eta^2$-H$_2$)] and [Co{Ph(CH$_2$)$_2$N(PPh$_2$)$_2$}$_2$(*cis*-(H)$_2$)] cations need to be obtained *via* geometry optimisation calculations at the B3LYP/6-31G(d) level. However, attempted geometry optimisation calculations of the [Co{Ph(CH$_2$)$_2$N(PPh$_2$)$_2$}$_2$($\eta^2$-H$_2$)] cation afforded the lower energy minima [Co{Ph(CH$_2$)$_2$N(PPh$_2$)$_2$}$_2$(*cis*-(H)$_2$)] cation. Hence, further computational study of the [Co{Ph(CH$_2$)$_2$N(PPh$_2$)$_2$}$_2$($\eta^2$-H$_2$)] cation directly, including the hypothesised Berry *pseudo*rotation, was not possible. The [Co{Ph(CH$_2$)$_2$N(PPh$_2$)$_2$}$_2$($\eta^2$-H$_2$)] cation, however, could be observed indirectly from scan calculations of the H$_2$ adduct of the cation of complex **5.7** ([Co(Ph(CH$_2$)$_2$N{PPh$_2$}$_2$)$_2$][BAr$^F{}_4$]) at the B3LYP/6-31G(d) level, allowing for the production of plots illustrating the effect of H-H distance and H-Co-H angle upon the energy of the H$_2$ adduct of the cation of complex **5.7** (**a)** and **b)**, **Figure 6.18**, respectively.

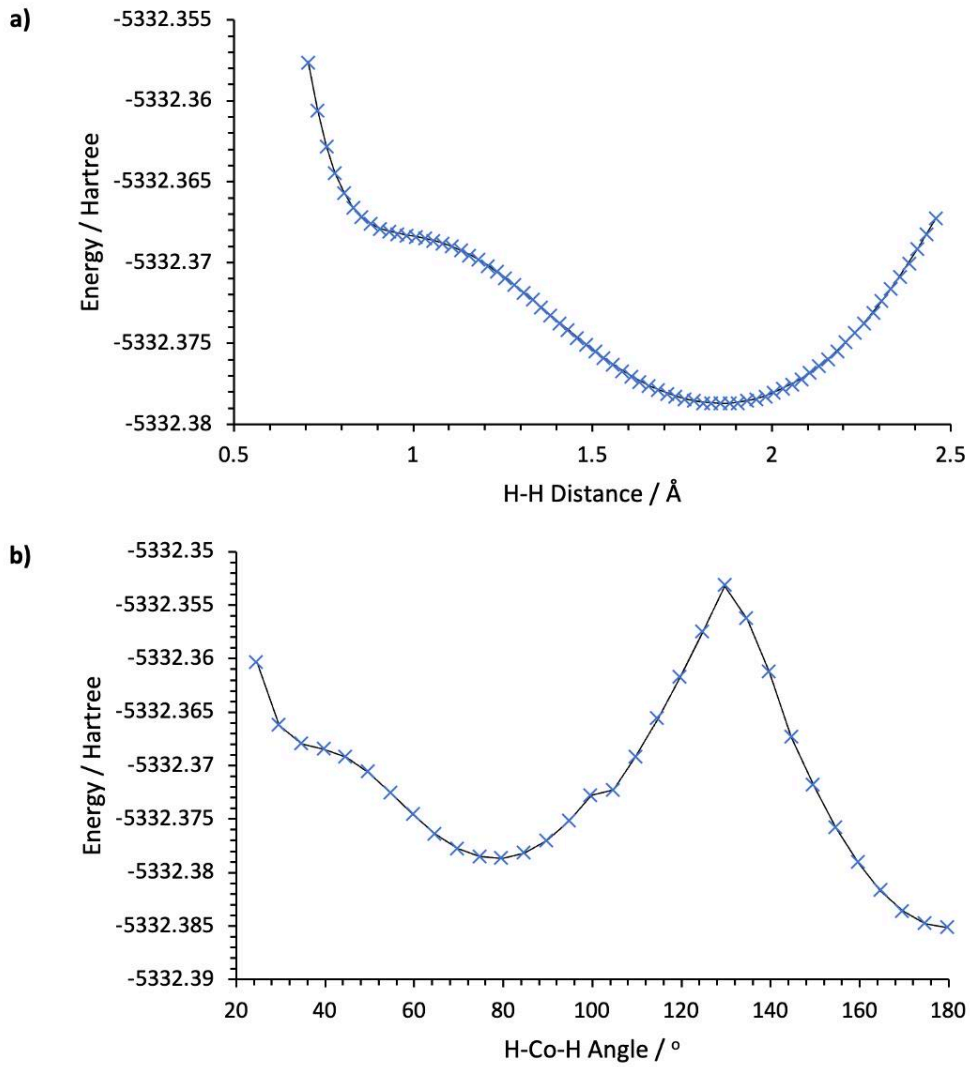


**Figure 6.18. a)** H-H distance *vs*. energy, and **b)** H-Co-H angle *vs*. energy, both for the $H_2$ adduct of the $[Co\{Ph(CH_2)_2N(PPh_2)_2\}_2]$ cation of complex **5.7**.

The H-H distance *vs*. energy plot of the $H_2$ adduct of the $[Co\{Ph(CH_2)_2N(PPh_2)_2\}_2]$ cation (**a)**, **Figure 6.18**) evidences a minimum at approx. 1.86 Å, and the H-Co-H angle *vs*. energy plot of the $H_2$ adduct of the $[Co\{Ph(CH_2)_2N(PPh_2)_2\}_2]$ cation (**b)**, **Figure 6.18**) evidences a minimum at approx. 80°, corresponding to the $[Co\{Ph(CH_2)_2N(PPh_2)_2\}_2(cis\text{-}(H)_2)]$ cation, but no minimum corresponding to the $[Co\{Ph(CH_2)_2N(PPh_2)_2\}_2(\eta^2\text{-}H_2)]$ cation is evidenced. Instead, plateaus in the H-H distance *vs*. energy plot of the $H_2$ adduct of the $[Co\{Ph(CH_2)_2N(PPh_2)_2\}_2]$ cation (**a)**, **Figure 6.18**) in the approx. 0.9 – 1.1 Å region and in the H-Co-H angle *vs*. energy plot of the $H_2$ adduct of the $[Co\{Ph(CH_2)_2N(PPh_2)_2\}_2]$ cation (**b)**, **Figure 6.18**) in the approx. 32 – 44° region are identified (sensible H-H distance and H-Co-H angle ranges for a $\eta^2$-$H_2$ ligand).[34 – 36] The plots (**Figure 6.18**) evidence an approx. 6.7 kcal $mol^{-1}$ energy difference between the $[Co\{Ph(CH_2)_2N(PPh_2)_2\}_2(\eta^2\text{-}H_2)]$ cation and

the [Co{Ph(CH$_2$)$_2$N(PPh$_2$)$_2$}$_2$(*cis*-(H)$_2$)] cation (from geometry optimised structure: H-H distance ~1.868 Å, H-Co-H angle ~79.1°). This very small 6.7 kcal mol$^{-1}$ energy difference between the [Co{Ph(CH$_2$)$_2$N(PPh$_2$)$_2$}$_2$(*cis*-(H)$_2$)] cation and the [Co{Ph(CH$_2$)$_2$N(PPh$_2$)$_2$}$_2$($\eta^2$-H$_2$)] cation (*cf*. 5.8 kcal mol$^{-1}$ activation barrier for the inversion of ammonia)[37] results in the [Co{Ph(CH$_2$)$_2$N(PPh$_2$)$_2$}$_2$($\eta^2$-H$_2$)] cation effectively being at a minimum in energy, supporting the facile interconversion inferred to occur between complexes **6.26** ([Co(Ph(CH$_2$)$_2$N{PPh$_2$}$_2$)$_2$($\eta^2$-H$_2$)][BAr$^F{}_4$]) and **6.29** ([Co(Ph(CH$_2$)$_2$N{PPh$_2$}$_2$)$_2$(*cis*-(H)$_2$)][BAr$^F{}_4$]) from NMR spectral data (**Section 6.4**).

Since the geometry optimisation calculations of the Δ and Λ enantiomers of the [Co{Ph(CH$_2$)$_2$N(PPh$_2$)$_2$}$_2$(*cis*-(H)$_2$)] cation were successful, the Bailer twist transition state between the two enantiomers could be located at the B3LYP/6-31G(d) level (**Figure 6.19**). The Bailer twist transition state has a computationally determined H-H distance of ~0.8 Å, evidencing significant $\eta^2$-H$_2$ ligand character.

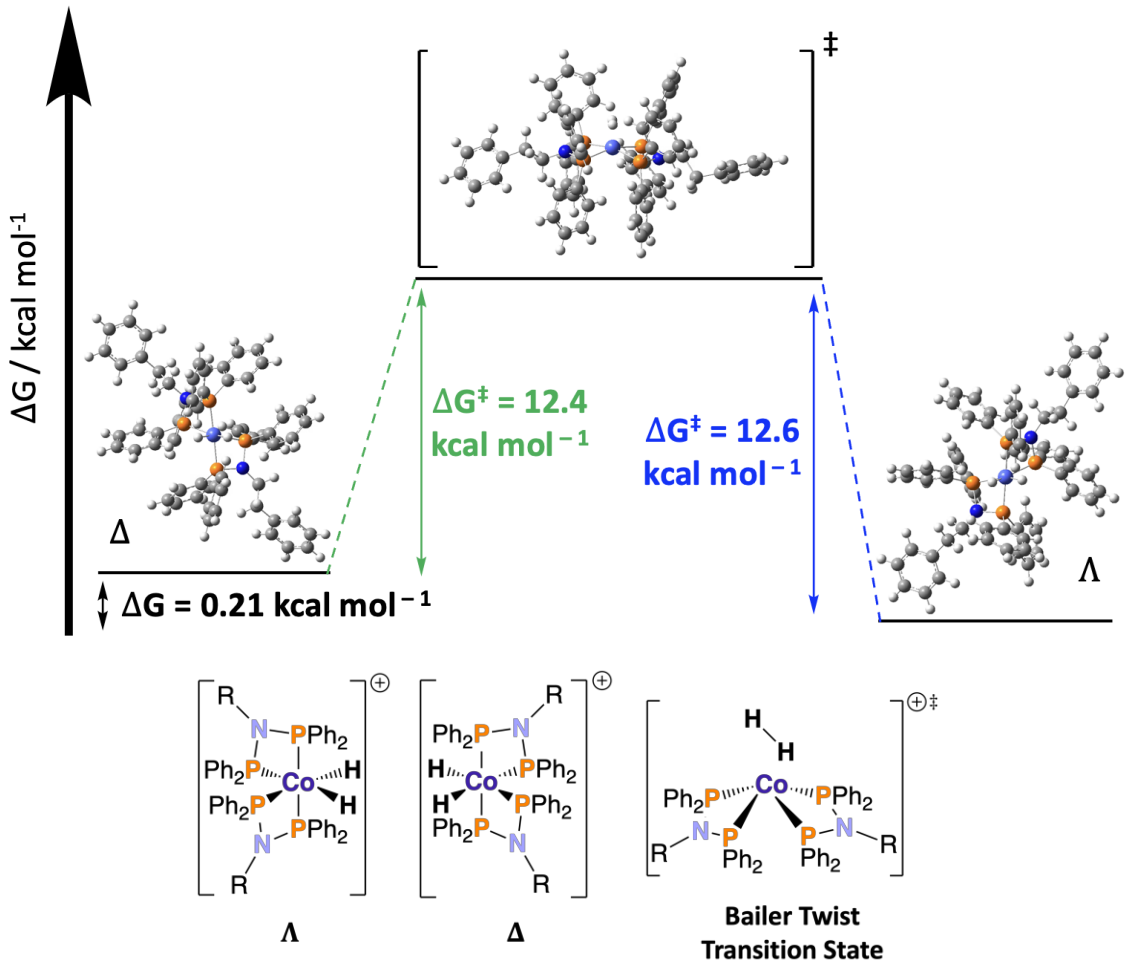


**Figure 6.19.** Racemisation scheme showing the transition state for the interconversion of the Δ and Λ enantiomers of [Co{RN(PPh$_2$)$_2$}$_2$(*cis*-(H)$_2$)] cation *via* a Bailer twist process. *NB* R = CH$_2$CH$_2$Ph.

The Gibbs free energy of activation ($\Delta G^{\ddagger}$) of the computationally identified Bailer twist process interconverting the Δ and Λ enantiomers of the [Co{Ph(CH$_2$)$_2$N(PPh$_2$)$_2$}$_2$(*cis*-(H)$_2$)] cation was found to be approx. 13 kcal mol$^{-1}$. The $\Delta G^{\ddagger}$ value of 13 kcal mol$^{-1}$ is the same as the $\Delta G^{\ddagger}$ value determined for the Berry *pseudo*rotation process interconverting the Δ and Λ enantiomers of the [Co{Ph(CH$_2$)$_2$N(PPh$_2$)$_2$}$_2$($\eta^2$-CH$_2$CH$_2$)] cation, and temperature–dependent effects were observed in the $^{31}$P{$^1$H} NMR spectra of complex **6.1** ([Co{Ph(CH$_2$)$_2$N(PPh$_2$)$_2$}$_2$($\eta^2$-CH$_2$CH$_2$)][BAr$^F_4$]). Hence, a lack of temperature–dependent effects being observed in the NMR spectra of the H$_2$ adduct of complex **5.7** (*e.g.*, when cooling to –85 °C) suggests that the Bailer twist of the [Co{Ph(CH$_2$)$_2$N(PPh$_2$)$_2$}$_2$(*cis*-(H)$_2$)] cation is not the fluxional process responsible for the four phosphorus atoms and two hydrogen atoms interacting with the cobalt centre in the H$_2$ adduct of complex **5.7** ([Co(Ph(CH$_2$)$_2$N{PPh$_2$}$_2$)$_2$][BAr$^F_4$]) to be equivalent. Instead, it is likely that the Berry *pseudo*rotation process interconverting between the Δ and Λ enantiomers of the [Co{Ph(CH$_2$)$_2$N(PPh$_2$)$_2$}$_2$($\eta^2$-H$_2$)] cation would have a small $\Delta G^{\ddagger}$ (*cf*. the $\Delta G^{\ddagger}$ value of approx. 3.4 kcal mol$^{-1}$ for the [Co{Ph(CH$_2$)$_2$N(PPh$_2$)$_2$}$_2$(CO)] cation, **Figure 6.13**) due to the small size of the $\eta^2$-H$_2$ ligand and would hence be the fluxional process responsible for the observed spectroscopic equivalence.

## 6.5 Reaction of [Co{Ph(CH$_2$)$_2$N(PPh$_2$)$_2$}$_2$][BAr$^F_4$] (5.7) with syngas

Continuing the study of the reactivity of complex [Co(Ph(CH$_2$)$_2$N{PPh$_2$}$_2$)$_2$][BAr$^F_4$] (**5.7**), the reactivity with syngas (50:50 CO:H$_2$) was probed as cobalt complexes are ubiquitous in olefin hydroformylation reactions involving syngas and alkenes.[1] Complex **5.7** reacted exclusively with CO (affording complex **6.21**, [Co(Ph(CH$_2$)$_2$N{PPh$_2$}$_2$)$_2$CO][BAr$^F_4$], **Scheme 6.6**) when a degassed (by three freeze–pump–thaw cycles) solution of complex **5.7** in d$_8$-THF was backfilled with syngas. The computationally–determined ΔG values for the formation of CO adduct complex **6.19** (–91.9 kJ mol$^{-1}$, probed in **Section 6.2.6**) and H$_2$ adduct complex **6.35** (ΔG = –8 kJ mol$^{-1}$) support the exclusive reaction of complex **5.7** with CO (**Scheme 6.10**). *NB* complex **6.35**, with the *cis*-(H)$_2$ moiety rather than with the $\eta^2$-H$_2$ moiety due to computational limitations, was utilised for this computational study due to the fact that the energy between the [Co{Ph(CH$_2$)$_2$N(PPh$_2$)$_2$}$_2$(*cis*-(H)$_2$)] cation and the [Co{Ph(CH$_2$)$_2$N(PPh$_2$)$_2$}$_2$($\eta^2$-H$_2$)] is so small (6.7 kcal mol$^{-1}$; **Section 6.4.1**).

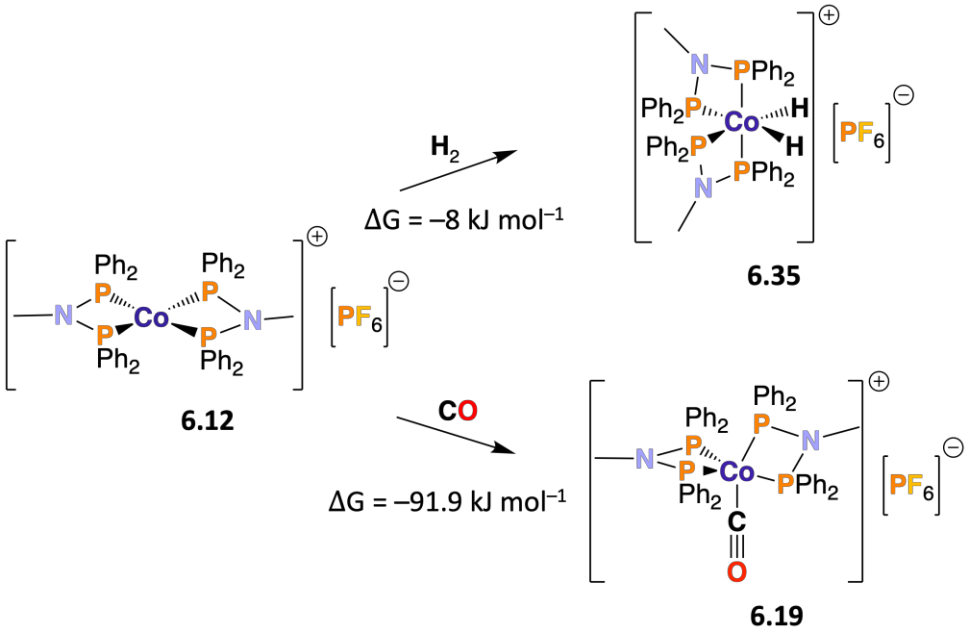


**Scheme 6.10.** Computationally studied synthesis of complexes **6.19** and **6.35**.

Hence, there is a large thermodynamic preference for the formation of complex **6.19** relative to complex **6.35** (**Scheme 6.10**), which is reflected in the experimental observation of the exclusive formation of complex **6.21** ([Co(Ph(CH$_2$)$_2$N{PPh$_2$}$_2$)$_2$CO][BAr$^F$$_4$]) from the reaction of complex **5.7** ([Co(Ph(CH$_2$)$_2$N{PPh$_2$}$_2$)$_2$][BAr$^F$$_4$]) with syngas. The exclusive formation of complex **6.21** is likely responsible for complex **5.7** leading to no conversion when screened for hydroformylation catalysis by Jake Backhouse (Dyer group member). The origin of the lack of catalytic activity of complex **5.7** is assumed to originate from the [Co{RN(PR'$_2$)$_2$}$_2$] cation containing two equivalents of 'PNP' ligand (RN(PR'$_2$)$_2$) coordinating at the cobalt(I) centre in a $\kappa^2$-*P,P* manner, resulting in a sterically congested environment.

## 6.6 Summary

The reaction of [Co(Ph(CH$_2$)$_2$N{PPh$_2$}$_2$)$_2$][BAr$^F$$_4$] (complex **5.7**) with ethylene was found to afford [Co{Ph(CH$_2$)$_2$N(PPh$_2$)$_2$}$_2$($\eta^2$-CH$_2$CH$_2$)][BAr$^F$$_4$] (complex **6.1**). Complex **6.1** exhibits temperature–dependent behaviour by $^{31}$P{$^1$H} NMR spectroscopy, something found to be due to the [Co{Ph(CH$_2$)$_2$N(PPh$_2$)$_2$}$_2$($\eta^2$-CH$_2$CH$_2$)] cation of complex **6.1** undergoing a Berry *pseudo*rotation. Good agreement between the experimentally (*via* the rate of exchange at coalescence) and computationally determined Gibbs free energies of activation for the Berry *pseudo*rotation process of 13 and 16 kcal mol$^{-1}$, respectively,

was obtained. Reaction of complex **5.7** with $d_4$-ethylene evidenced a signal at approx. 1.5 ppm in the $^2$H NMR spectrum, assigned to cobalt-coordinated $d_4$-ethylene.

The reaction of complex **5.7** with CO (1 atm) affords fluxional species [Co{Ph(CH$_2$)$_2$N(PPh$_2$)$_2$}$_2$(CO)][BAr$^F{}_4$] (complex **6.21**) with a $\nu_{CO}$ stretching frequency of 1951 cm$^{-1}$. Complex **6.21** has a small $\Delta G^{\ddagger}$ ~3.4 kcal mol$^{-1}$ for the Berry *pseudo*rotation between the $\Delta$ and $\Lambda$ enantiomers of the [Co{Ph(CH$_2$)$_2$N(PPh$_2$)$_2$}$_2$CO] cation. The reactions of complex **5.7** with $H_2$ and HD is proposed to form equilibrium mixtures of [Co(Ph(CH$_2$)$_2$N{PPh$_2$}$_2$)$_2$($\eta^2$-H$_2$)][BAr$^F{}_4$] and [Co(Ph(CH$_2$)$_2$N{PPh$_2$}$_2$)$_2$(*cis*-(H)$_2$)][BAr$^F{}_4$] (complexes **6.26** and **6.29**, respectively) and [Co(Ph(CH$_2$)$_2$N{PPh$_2$}$_2$)$_2$($\eta^2$-HD)][BAr$^F{}_4$] and [Co(Ph(CH$_2$)$_2$N{PPh$_2$}$_2$)$_2$(*cis*-(H)(D))][BAr$^F{}_4$] (complexes **6.27** and **6.30**, respectively), *i.e.*, the corresponding dihydrogen and *cis*-dihydride species. The reaction of complex **5.7** with syngas (50:50 CO:$H_2$) affords exclusively complex **6.21**, reflecting the thermodynamic preference for CO coordination relative to $H_2$ coordination due to the $\pi$-accepting capability of CO.

## References


1. D. M. Hood, R. A. Johnson, D. J. Vinyard, F. R. Fronczek, G. G. Stanley, *J. Am. Chem. Soc*., **2023**, *145*, 19715 – 19726. 10.1021/jacs.3c04866
2. M. E. Farmer, L. E. Ehehalt, T. P. Pabst, M. T. Tudge, P. J. Chirik, *Organometallics*, **2021**, *40*, 3599 – 3607. 10.1021/acs.organomet.1c00473
3. J. H. Herbort, R. F. Lalisse, C. M. Hadad, T. V. RajanBabu, *ACS Catal*., **2021**, *11*, 9605 – 9617. 10.1021/acscatal.1c02530
4. S. Biswas, J. P. Page, K. R. Dewese, T. V. RajanBabu, *J. Am. Chem. Soc*., **2015**, *137*, 14268 – 14271. 10.1021/jacs.5b10364
5. M. M. Parsutkar, T. V. RajanBabu, *J. Am. Chem. Soc*., **2021**, *143*, 12825 – 12835. 10.1021/jacs.1c06245
6. C. S. MacNeil, H. Zhong, T. P. Pabst, M. Shevlin, P. J. Chirik, *ACS Catal*., **2022**, *12*, 4680 – 4687. 10.1021/acscatal.2c01059
7. M. Gray, M. T. Hines, M. M. Parsutkar, A. J. Wahlstrom, N. A. Brunelli, T. V. RajanBabu, *ACS Catal*., **2020**, *10*, 4337 – 4348. 10.1021/acscatal.9b05455
8. S. M. Jing, V. Balasanthiran, V. Pagar, J. C. Gallucci, T. V. RajanBabu, *J. Am. Chem. Soc*., **2017**, *139*, 18034 – 18043. 10.1021/jacs.7b10055
9. R. K. Sharma, T. V. RajanBabu, *J. Am. Chem. Soc*., **2010**, *132*, 3295 – 3297. 10.1021/ja1004703
10. K. Duvvuri, K. R. Dewese, M. M. Parsutkar, S. M. Jing, M. M. Mehta, J. C. Gallucci, T. V. RajanBabu, *J. Am. Chem. Soc*., **2019**, *141*, 7365 – 7375. 10.1021/jacs.8b13812
11. R. S. Berry, *J. Chem. Phys*., **1960**, *32*, 933 – 938. 10.1063/1.1730820
12. E. L. Muetterties, *J. Am. Chem. Soc*., **1969**, *91*, 1636 – 1643. 10.1021/ja01035a009
13. E. L. Muetterties, *J. Am. Chem. Soc*., **1969**, *91*, 4115 – 4122. 10.1021/ja01043a017

14. E. P. A. Couzijn, D. W. F. van den Engel, J. C. Slootweg, F. J. J. de Kanter, A. W. Ehlers, M. Schakel, K. Lammertsma, *J. Am. Chem. Soc*., **2009**, *131*, 3741 – 3751. 10.1021/ja809154g
15. P. J. Hore, *Nuclear Magnetic Resonance*, Oxford University Press, Oxford, **1995**. ISBN: 978–0–19–870341–9
16. B. Capelle, A. L. Beauchamp, M. Dartiguenave, Y. Dartiguenave, H-F. Klein, *J. Am. Chem. Soc*., **1982**, *104*, 3891 – 3897. 10.1021/ja00378a018
17. C. Karunatilaka, B. S. Tackett, J. Washington, S. G. Kukolich, *J. Am. Chem. Soc*., **2007**, *129*, 10522 – 10530. 10.1021/ja0727969
18. J. A. Iggo, *NMR Spectroscopy in Inorganic Chemistry*, Oxford University Press, Oxford, **1999**. ISBN: 9780198558903
19. M. T. Mock, R. G. Potter, M. J. O'Hagan, D. M. Camaioni, W. G. Dougherty, W. S. Kassel, D. L. DuBois, *Inorg. Chem*., **2011**, *50*, 11914 – 11928. 10.1021/ic200857x
20. L. Falivene, Z. Cao, A. Petta, L. Serra, A. Poater, R. Oliva, V. Scarano, L. Cavallo, *Nat. Chem*., **2019**, *11*, 872 – 879. 10.1038/s41557-019-0319-5
21. G. de Leeuw, J. S. Field, R. J. Haines, E. M. Minshall, *S. Afr. J. Chem.*, **1988**, *41*, 9 – 16. 10.10520/AJA03794350_1527
22. N. Mina-Camilde, C. Manzanares I., J. F. Caballero, *J. Chem. Educ*., **1996**, *73*, 804 – 807. 10.1021/ed073p804
23. Z-Z. Zhang, A. Yu, H-P. Xi, R-J. Wang, H-G. Wang, *J. Organomet. Chem*., **1994**, *470*, 223 – 229. 10.1016/0022-328X(94)80170-3
24. J. Zhao, P. Wu, E. Lai, J. Li, Y. Chen, W. Jiang, B. Wang, H. Zhu, *Chem. Asian J*., **2021**, *16*, 3453 – 3461. 10.1002/asia.202100688
25. D. L. DuBois, D. W. Meek, *Inorg. Chem*., **1976**, *15*, 3076 – 3083. 10.1021/ic50166a029
26. M. T. Bautista, E. P. Cappellani, S. D. Drouin, R. H. Morris, C. T. Schweitzer, A. Sella, J. Zubkowski, *J. Am. Chem. Soc*., **1991**, *113*, 4876 – 4887. 10.1021/ja00013a025
27. P. Hrobárik, V. Hrobárikova, F. Meier, M. Repisky, S. Komorovsky, M. Kaupp, *J. Phys. Chem. A*, **2011**, *115*, 5654 – 5659. 10.1021/jp202327z
28. D. M. Heinekey, A. Liegeois, M. van Roon, *J. Am. Chem. Soc*., **1994**, *116*, 8388 – 8389. 10.1021/ja00097a065
29. D. M. Heinekey, M. van Roon, *J. Am. Chem. Soc*., **1996**, *118*, 12134 – 12140. 10.1021/ja962702n
30. S. Gründemann, H-H. Limbach, G. Buntkowsky, S. Sabo-Etienne, B. Chaudret, *J. Phys. Chem. A*, **1999**, *103*, 4752 – 4754. 10.1021/jp990601g
31. R. H. Crabtree, *Acc. Chem. Res*., **1990**, *23*, 95 – 101. 10.1021/ar00172a001
32. P. J. Desrosiers, L. Cai, Z. Lin, R. Richards, J. Halpern, *J. Am. Chem. Soc*., **1991**, *113*, 4173 – 4184. 10.1021/ja00011a019
33. A. Rodger, B. F. G. Johnson, *Inorg. Chem*., **1988**, *27*, 3061 – 3062. 10.1021/ic00291a001
34. D. Sellmann, A. Hille, F. W. Heinemann, M. Moll, M. Reiher, B. A. Hess, W. Bauer, *Chem. Eur. J*., **2004**, *10*, 4214 – 4224. 10.1002/chem.200400120
35. R. C. Cammarota, J. Xie, S. A. Burgess, M. V. Vollmer, K. D. Vogiatzis, J. Ye, J. C. Linehan, A. M. Appel, C. Hoffmann, X. Wang, V. G. Young, C. C. Lu, *Chem. Sci*., **2019**, *10*, 7029 – 7042. 10.1039/C9SC02018G
36. S. Lachaize, A. Caballero, L. Vendier, S. Sabo-Etienne, *Organometallics*, **2007**, *26*, 3713 – 3721. 10.1021/om700295g

37. A. M. Halpern, B. R. Ramachandran, E. D. Glendening, *J. Chem. Educ*., **2007**, *84*, 1067 – 1072. 10.1021/ed084p1067

# Chapter 7 – Experimental

All syntheses were performed using standard Schlenk-line and glovebox (*Saffron Scientific; Innovative Technologies*) techniques under an inert, dry nitrogen atmosphere. Dry solvents, obtained from an Innovative Technologies SPS facility (except THF, which was dried by heating at reflux over Na wire, with benzophenone indicator, and subsequently distilled), were degassed using three freeze-pump-thaw cycles. All other reagents were used as received, including solvents for NMR spectroscopy (excluding $CDCl_3$, which was dried over $CaH_2$ and isolated by vacuum transfer), unless mentioned otherwise. Solution phase NMR spectra were collected on a Varian Mercury 400 or Bruker Advance 400 at ambient probe temperature (290 K), and chemical shifts (ppm) referenced to residual proton ($^1H$) impurities in the deuterated solvent, $^{13}C$ shift of the solvent for $^{13}C$, or (external) 85% $H_3PO_4$ for $^{31}P$ and $^{31}P\{^1H\}$; chemical shifts are reported in ppm and NMR coupling constants are reported in Hz. Infrared spectra were collected on a FT-IR Perkin-Elmer Spectrum RXI. Elemental analyses were performed by Emily Unsworth of Durham University (Exeter CE-440 Elemental Analyser). ESI mass spectra were acquired using a Waters TQD Mass Spectrometer and Waters Acquity UPLC in $CH_2Cl_2$, MeCN or THF. ASAP mass spectra were acquired using a LCT Premier XE mass spectrometer or Waters Xevo QToF mass spectrometer (all at Durham University). Crystallographic data were obtained in Durham University by either Dr Andrei Batsanov, Dr Dmitry Yufit or Dr Toby Blundell using a Bruker D8-Venture, with Cryosteam 700+ and HELIX (Oxford Cryosystems) and ancillary attachments, and Mo-K$\alpha$ ($\lambda$ 0.71073 Å) at –180(1) °C. All calculations were performed on the Olex2 software package, except for refinements which used SHELXT.[1] Images were produced on Mercury, with ORTEPS set at 50%.[2] CSD searches were conducted using Conquest.[3] Butylamine and cobalt(II) iodide were purchased from Alfa Aesar; phenethylamine, elemental selenium, cobalt(II) acetylacetonate, tetrapropylammonium bromide, tetrapropylammonium chloride, trifluoroacetic acid, pyridine, *bis*(triphenylphosphoranylidene) ammonium chloride, ammonium hexafluorophosphate, *tetrakis*(acetonitrile)palladium(II) tetrafluoroborate, 1,2-*bis*(diphenylphosphino)ethane, potassium hexafluorophosphate, zinc, sodium borohydride, zinc(II) bromide, cobalt(II) bromide, deuterium oxide and sodium hydride

were purchased from Sigma Aldrich; 3-aminomethylpyridine, 3-(dimethylamino)-1-propylamine, 2-(aminoethyl)pyridine, 4-(-2-pyridyl)aniline, 4-aminobiphenyl, *N*-Methyl-*N*-(2-pyridin-2-ylethyl)amine, pinacolborane (HBPin), sodium *tetrakis*[3,5-*bis*(trifluoromethyl)phenyl]borate and $Ph_2PCl$ (purified by vacuum transfer) were purchased from Fluorochem; triethylamine (dried over KOH, distilled and degassed), paraformaldehyde, triphenylphosphine and cobalt(II) chloride hexahydrate were purchased from Fisher Scientific; cobalt(II) chloride was purchased from ACROS Organics, and were all used as received unless mentioned otherwise. All liquid reagents were degassed before use and were not further purified unless mentioned. All hybrid-DFT calculations were performed using the B3LYP 6-31G(d) basis set. Hamilton8 supercomputer (Durham University) was used for all calculations except those involved in determining molecular orbitals, which were ran on a Windows PC *via* Gaussian16.[4] GaussView6 [5] was used to analyse the results and prepare input gjf files; mol2 files from crystallographic studies were used where appropriate to generate the input file.

## 7.1 Synthesis of $Ph(CH_2)_2N(PPh_2)_2$ (2.2), *n*-$BuN(PPh_2)_2$ (2.3), $NMe_2(CH_2)_3N(PPh_2)_2$ (2.4), Py-*m*-$CH_2N(PPh_2)_2$ (2.5), Ph-$C_6H_4N(PPh_2)_2$ (2.6) and Py-*o*-$C_6H_4N(PPh_2)_2$ (2.7)

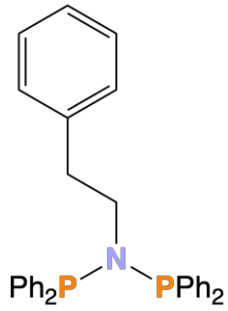


**2.2**

**Synthesis of $Ph(CH_2)_2N(PPh_2)_2$ (2.2):** Phenethylamine (1.21 g, 10.0 mmol) was degassed in a Schlenk flask by three freeze-pump-thaw cycles, and $NEt_3$ (11.2 mL, 80.0 mmol) was added. Both amines were dissolved in THF (40 mL), and the resulting solution cooled to –40 °C in an acetone/dry ice bath. $PPh_2Cl$ (3.6 mL, 20.0 mmol) was added dropwise, and after the complete addition the resulting slurry was stirred overnight at room temperature. The reaction was filtered to remove $NEt_3$·HCl, the solvent removed *in vacuo*, and the crude oil was stirred in MeOH (20 mL) to precipitate the product as a white solid (3.383 g, 6.91 mmol, 69%), which was isolated by filtration and dried *in*

*vacuo*; $\delta_H$ (400 MHz, $CDCl_3$) 7.41 – 7.48 (8H, m, aryl), 7.32 – 7.38 (12H, m, aryl), 7.05 – 7.17 (3H, m, phenyl), 6.72 – 6.77 (2H, m, phenyl), 3.34 – 3.45 (2H, m, $(PPh_2)_2N$-C$\underline{H}_2$), 2.23 – 2.31 (2H, m, Ph-C$\underline{H}_2$); $\delta_P$ $^{31}P\{^1H\}$ (162 MHz, $CDCl_3$) 62.7 (2P, s); $\delta_C$ (100.57 MHz, $CDCl_3$) 139.5 (t, *J* = 5.7 Hz, aryl-C), 139.3 (s, aryl-C), 132.9 (t, *J* = 11.0 Hz, aryl-C), 129.0 (s, aryl-C), 128.8 (s, aryl-C), 128.32 (d, *J* = 3.1 Hz, aryl-C), 128.28 (s, aryl-C), 126.2 (s, aryl-C), 54.9 (s, $CH_2$), 38.3 (t, *J* = 3.0 Hz, $CH_2$); selected $\nu_{max}$ / $cm^{-1}$ 3051 (aromatic C-H stretch), 2981 (C-H stretch), 1605, 1478 (aromatic C=C), 1433 (P-Ph), 1090 (C-N), 863 (P-N-P); Anal. calc. for $C_{32}H_{29}NP_2$ (489.54) (%): C, 78.51; H, 5.97; N, 2.86 Found (%): C, 78.12; H, 6.06; N, 2.83; MS (ESI): positive ion *m/z* 490.5 (89.76% $[M+H]^+$), 521.4 (13.57% $[M+O_2]^+$). NMR spectroscopic data and CHN elemental analyses are consistent with published data.[6]

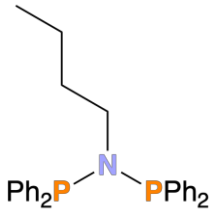


**2.3**

**Synthesis of *n*-BuN$(PPh_2)_2$ (2.3):** Compound **2.3** was synthesised following the same method outlined for the preparation of compound **2.2**, except butylamine (0.73 g, 10.0 mmol) was used. Compound **2.3** was gained as a white solid (2.427 g, 5.50 mmol, 55%); $\delta_H$ (400 MHz, $CDCl_3$) 7.27 – 7.42 (20H, m, phenyl), 3.16 – 3.27 (2H, m, $(PPh_2)_2NC\underline{H}_2$), 1.00 – 1.10 (2H, m, $(PPh_2)_2NCH_2C\underline{H}_2$), 0.87 – 0.97 (2H, m, $C\underline{H}_2CH_3$), 0.60 (3H, t, $^2J_{HH}$ = 7.30 Hz, $C\underline{H}_3$); $\delta_P$ $^{31}P\{^1H\}$ (162 MHz, $CDCl_3$) 62.0 (2P, s); $\delta_C$ (100.57 MHz, $CDCl_3$) 139.7 (t, *J* = 5.9 Hz, aryl-C), 132.9 (t, *J* = 11.0 Hz, aryl-C), 128.8 (s, aryl-C), 128.2 (t, *J* = 3.2 Hz, aryl-C), 52.9 (s, $CH_2$), 33.6 (t, *J* = 3.2 Hz, $CH_2$), 20.1 (s, $CH_2$), 13.8 (s, $CH_3$); selected $\nu_{max}$ / $cm^{-1}$ 3055 (aromatic C-H stretch), 2953 (C-H stretch), 1600, 1477 (aromatic C=C), 1453, 1374 ($CH_3$ bend), 1432 (P-Ph), 1091 (C-N), 856 (P-N-P); Anal. calc. for $C_{28}H_{29}NP_2$ (441.49) (%): C, 76.17; H, 6.62; N, 3.17 Found (%): C, 75.42; H, 6.72; N, 3.03; MS (ESI): positive ion *m/z* 442.4 (72.77% $[M+H]^+$), 458.4 (45.14% $[M+H+O]^+$). NMR spectroscopic data are consistent with published data.[7]

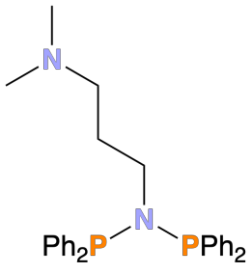

**2.4**

**Synthesis of $NMe_2(CH_2)_3N(PPh_2)_2$ (2.4):** Compound **2.4** was synthesised following the same method outlined for the preparation of compound **2.2**, except 3-(dimethylamino)-1-propylamine (1.02 g, 10.0 mmol) was used, and the crude oil was dissolved in MeOH (20 mL), which once removed *in vacuo* resulted in the isolation of the product as a white solid (2.905 g, 6.17 mmol, 62%); $\delta_H$ (400 MHz, $CDCl_3$) 7.36 – 7.43 (8H, m, phenyl), 7.27 – 7.34 (12H, m, phenyl), 3.22 – 3.34 (2H, m, $(PPh_2)_2NC\underline{H}_2$), 1.94 (6H, s, $N(C\underline{H}_3)_2$), 1.85 (2H, t, $^2J_{HH}$ = 7.2 Hz, $C\underline{H}_2NMe_2$), 1.21 – 1.30 (2H, m, $C\underline{H}_2CH_2NMe_2$); $\delta_P$ $^{31}P\{^1H\}$ (162 MHz, $CDCl_3$) 62.5 (2P, s); $\delta_C$ (100.57 MHz, $CDCl_3$) 139.5 (t, *J* = 6.1 Hz, aryl-C), 132.7 (t, *J* = 11.0 Hz, aryl-C), 128.7 (s, aryl-C), 128.1 (t, *J* = 3.1 Hz, aryl-C), 57.2 (s, alkyl-C), 51.1 (t, *J* = 10.9 Hz, alkyl-C), 45.4 (s, alkyl-C), 29.3 (s, alkyl-C); selected $\nu_{max}$ / $cm^{-1}$ 3052 (aromatic C-H stretch), 2969 (C-H stretch), 1603, 1478 (aromatic C=C), 1431 (P-Ph), 1090 (C-N), 861 (P-N-P); Anal. calc. for $C_{29}H_{32}N_2P_2$ (470.54) (%): C, 74.03; H, 6.86; N, 5.95 Found (%): C, 73.60; H, 6.82; N, 5.54; MS (ESI): positive ion *m/z* 471.4 (100.00% $[M+H]^+$), 487.4 (61.12% $[M+H+O]^+$), 503.4 (4.92% $[M+H+O_2]^+$). Although previously synthesised, no characterisation data were reported.[8]

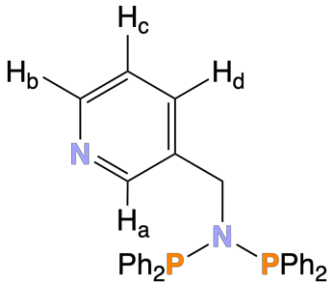

**2.5**

**Synthesis of Py-*m*-$CH_2N(PPh_2)_2$ (2.5):** 3-Aminomethylpyridine (1.08 g, 10.0 mmol) was degassed in a Schlenk flask by three freeze-pump-thaw cycles, and $NEt_3$ (11.2 mL, 80.0 mmol) was added. Both amines were dissolved in DCM (40 mL), and the resulting solution cooled to –40 °C in an acetone/dry ice bath. $PPh_2Cl$ (3.6 mL, 20.0 mmol) was added dropwise, and after the complete addition the resulting slurry was stirred

overnight at room temperature. The reaction was filtered to remove $NEt_3$·HCl, the solvent removed *in vacuo*, and the residue washed with $H_2O$ (3 × 20 mL), and recrystallised from the minimum amount of EtOH in the freezer overnight, affording compound **2.5** as a white solid (1.983 g, 4.16 mmol, 42%). The product was isolated by filtration and dried *in vacuo*; $\delta_H$ (400 MHz, $CDCl_3$) 8.33 (1H, d, $^2J_{HH}$ = 3.7 Hz, $H_b$), 7.91 (1H, s, $H_a$), 7.22 – 7.42 (20H, m, phenyl), 6.87 – 7.02 (2H, m, $H_c$ + $H_d$), 4.52 (2H, d, $^3J_{HP}$ = 10.4 Hz, $(PPh_2)_2NC\underline{H}_2$); $\delta_P$ $^{31}P\{^1H\}$ (162 MHz, $CDCl_3$) 61.2 (2P, s); $\delta_C$ (100.57 MHz, $CDCl_3$) 150.3 (s, py-C), 148.1 (s, py-C), 138.9 (dd, *J* = 4.3 Hz, 18.0 Hz, aryl-C), 136.4 (s, py-C), 135.2 (s, py-C), 132.8 (d, *J* = 22.0 Hz, aryl-C), 129.0 (s, aryl-C), 128.2 (d, J = 6.7 Hz, aryl-C), 122.8 (s, py-C), 58.4 (s, $CH_2$); selected $\nu_{max}$ / $cm^{-1}$ 3049 (aromatic C-H stretch), 2979 (C-H stretch), 1606, 1479 (aromatic C=C), 1584, 1571 (C=N), 1434 (P-Ph), 1093 (C-N), 862 (P-N-P); Anal. calc. for $C_{30}H_{26}N_2P_2$ (476.50) (%): C, 75.62; H, 5.50; N, 5.88 Found (%): C, 75.40; H, 5.45; N, 5.91; MS (ESI): positive ion *m/z* 477.3 (100% $[M+H]^+$), 493.4 (15.20% $[M+H+O]^+$). NMR and FT-IR spectroscopic data are consistent with published data.[9]

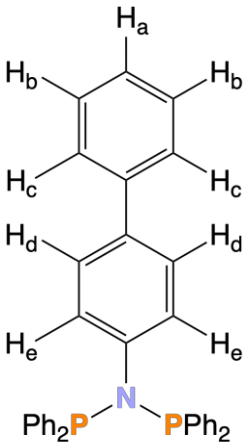


**2.6**

**Synthesis of Ph-$C_6H_4N(PPh_2)_2$ (2.6):** 4-aminobiphenyl (1.69 g, 10.0 mmol), and $NEt_3$ (11.2 mL, 80.0 mmol) were dissolved in THF (40 mL), and the resulting solution cooled to –40 °C in an acetone/dry ice bath. $PPh_2Cl$ (3.6 mL, 20.0 mmol) was added dropwise, and after the complete addition the reaction mixture was allowed to warm to room temperature and stir overnight. The reaction mixture was filtered, the solvent removed *in vacuo*, the crude product washed with $Et_2O$ (3 × 10 mL) and dried *in vacuo*, affording compound **2.6** as a cream solid (2.395 g, 4.5 mmol, 45%); $\delta_H$ (400 MHz, $CDCl_3$) 7.18 – 7.50 (27H, m, phenyl, $H_a$, $H_b$, $H_c$, $H_d$), 6.73 (2H, d, *J* = 8.5 Hz, $H_e$); $\delta_P$ $^{31}P\{^1H\}$ (162 MHz, $CDCl_3$) 68.5 (2P, s); $\delta_C$ (100.57 MHz, $CDCl_3$) 140.5 (s, aryl-C), 139.2 (s, aryl-C), 139.2 (d, *J*

= 13.6 Hz, aryl-C), 139.1 (d, *J* = 6.9 Hz, aryl-C), 133.3 (t, *J* = 11.5 Hz, aryl-C), 129.2 (t, *J* = 3.2 Hz, aryl-C), 129.1 (s, aryl-C), 128.7 (s, aryl-C), 128.0 (t, *J* = 3.2 Hz, aryl-C), 127.0 (s, aryl-C), 126.8 (s, aryl-C), 116.3 (s, aryl-C); selected $\nu_{max}$ / $cm^{-1}$ 3052 (aromatic C-H stretch), 1604, 1464 (aromatic C=C), 1434 (P-Ph), 1092 (C-N); Anal. calc. for $C_{36}H_{29}NP_2$ (537.58) (%): C, 80.43; H, 5.44; N, 2.61 Found (%): C, 79.59; H, 5.04; N, 2.53; MS (ESI): positive ion *m/z* 538.4 (5.79% $[M+H]^+$).

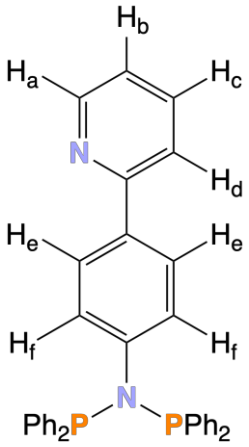


**2.7**

**Synthesis of Py-*o*-$C_6H_4N(PPh_2)_2$ (2.7):** Compound **2.7** was afforded by the same synthetic method outlined for the synthesis of compound **2.6**, using 4-(-2-pyridyl)aniline (1.70 g, 10.0 mmol), affording compound **2.7** as a beige solid (3.103 g, 5.8 mmol, 58%); $\delta_H$ (400 MHz, $CDCl_3$) 8.63 (1H, dq, *J* = 0.89 Hz, 4.91 Hz, $H_a$), 7.70 (1H, td, *J* = 1.8 Hz, 7.7 Hz, $H_c$), 7.57 – 7.63 (3H, m, $H_d$ + $H_e$), 7.38 – 7.45 (8H, m, phenyl), 7.27 – 7.36 (12H, m, phenyl), 7.18 (1H, ddd, *J* = 0.9 Hz, 4.8 Hz, 7.4 Hz, $H_b$), 6.76 (2H, d, *J* = 8.6 Hz, $H_f$); $\delta_P$ $^{31}P\{^1H\}$ (162 MHz, $CDCl_3$) 68.8 (2P, s); $\delta_C$ (100.57 MHz, $CDCl_3$) 156.9 (s, aryl-C), 149.5 (s, aryl-C), 139.0 (t, *J* = 6.6 Hz, aryl-C), 136.6 (s, aryl-C), 135.9 (s, aryl-C), 133.3 (t, *J* = 11.6 Hz, aryl-C), 129.1 (s, aryl-C), 128.6 (d, *J* = 6.6 Hz, aryl-C), 128.1 (t, *J* = 3.3 Hz, aryl-C), 126.7 (s, aryl-C), 121.8 (s, aryl-C), 120.2 (s, aryl-C), 116.0 (s, aryl-C); selected $\nu_{max}$ / $cm^{-1}$ 3049 (aromatic C-H stretch), 2981 (C-H stretch), 1601, 1464 (aromatic C=C), 1585, 1561 (C=N), 1434 (P-Ph), 1093 (C-N); Anal. calc. for $C_{35}H_{28}N_2P_2$ (538.57) (%): C, 78.06; H, 5.24; N, 5.20 Found (%): C, 78.86; H, 5.00; N, 5.66; MS (ESI): positive ion *m/z* 355.4 (100% $[M-PPh_2+2H]^+$), 539.4 (12.34% $[M+H]^+$).

## 7.2 Synthesis of Py-*o*-$(CH_2)_2N(CH_2PPh_2)_2$ (2.8)

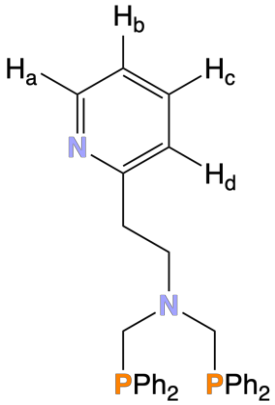


**2.8**

**Synthesis of Py-*o*-$(CH_2)_2N(CH_2PPh_2)_2$ (2.8):** $PPh_2H$ (4.28 g, 23.0 mmol), paraformaldehyde (0.351 g, 11.7 mmol) and 2-(2-aminoethyl)pyridine (1.43 g, 11.7 mmol) were dissolved in MeOH (20 mL) and toluene (30 mL), and the resulting mixture was refluxed overnight. After cooling to room temperature, the solvent was removed *in vacuo*, the crude residue washed with hexane (3 × 10 mL) and dried *in vacuo*. Upon standing, the product solidified, gaining compound **2.8** as an off-white solid (4.602 g, 8.87 mmol, 76%); $\delta_H$ (400 MHz, $CDCl_3$) 8.50 (1H, dq, $J$ = 0.90 Hz, 4.95 Hz, $H_a$), 7.48 (1H, td, $J$ = 1.9 Hz, 7.7 Hz, $H_c$), 7.38 – 7.44 (8H, m, phenyl), 7.25 – 7.32 (12H, m, phenyl), 7.07 (1H, ddd, $J$ = 1.0 Hz, 4.9 Hz, 7.6 Hz, $H_b$), 6.96 (1H, dt, $J$ = 1.0 Hz, 7.8 Hz, $H_d$), 3.65 (4H, d, $^2J_{HP}$ = 3.2 Hz, $Ph_2P$-C<u>H</u>$_2$), 3.34 (2H, t, $^3J_{HH}$ = 7.6 Hz, $(CH_2PPh_2)_2NC$<u>H</u>$_2$), 2.92 (2H, t, $^3J_{HH}$ = 7.6 Hz, Py-C<u>H</u>$_2$); $\delta_P$ $^{31}P\{^1H\}$ (162 MHz, $CDCl_3$) –28.5 (2P, s); $\delta_C$ (100.57 MHz, $CD_2Cl_2$) 160.3 (s, aryl-C), 149.1 (s, aryl-C), 138.3 (d, $J$ = 13.3 Hz, aryl-C), 135.9 (s, aryl-C), 133.1 (d, $J$ = 18.7 Hz, aryl-C), 128.5 (s, aryl-C), 128.3 (d, $J$ = 6.9 Hz, aryl-C), 123.1 (s, aryl-C), 120.9 (s, aryl-C), 58.5 (dd, $J$ = 5.3 Hz, 9.4 Hz, $CH_2$), 56.1 (t, $J$ = 9.2 Hz, $CH_2$), 35.0 (s, $CH_2$); selected $\nu_{max}$ / $cm^{-1}$ 3051 (aromatic C-H stretch), 2978 (C-H stretch), 1605, 1470 (aromatic C=C), 1583, 1567 (C=N), 1432 (P-Ph), 1091 (C-N); Anal. calc. for $C_{33}H_{32}N_2P_2$ (518.58) (%): C, 76.43; H, 6.22; N, 5.40 Found (%): C, 75.78; H, 6.33; N, 5.50; MS (ESI): positive ion *m/z* 199.2 (70.37% $[PPh_2CH_2]^+$), 333.3 (100.00% $[M\text{-}PPh_2]^+$), 349.4 (57.69% $[M\text{-}PPh_2\text{+}O]^+$).

## 7.3 Synthesis of $Ph(CH_2)_2N(SPPh_2)(PPh_2)$ (2.9) and $Ph(CH_2)_2N(SPPh_2)_2$ (2.10)

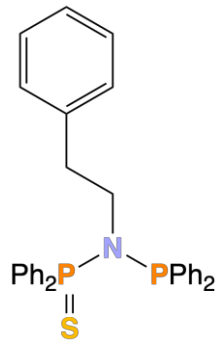


**2.9**

**Synthesis of $Ph(CH_2)_2N(SPPh_2)(PPh_2)$ (2.9):** $Ph(CH_2)_2N(PPh_2)_2$ (**2.2**, 1.00 g, 2.04 mmol) and $S_8$ (0.066 g, 0.26 mmol) were dissolved in THF (20 mL) and stirred overnight. The reaction mixture was filtered, the volume reduced to approx. 5 mL *in vacuo*, the remaining solution layered with MeOH (15 mL) and left to stand overnight, affording compound **2.9** as a white crystalline powder (0.414 g, 0.79 mmol, 39%), which was isolated by filtration and dried *in vacuo*; $\delta_H$ (400 MHz, $CD_2Cl_2$) 8.03 – 8.11 (4H, m, phenyl), 7.43 – 7.60 (16 H, m, phenyl), 7.06 – 7.13 (3H, m, phenyl), 6.53 – 6.58 (2H, m, phenyl), 3.60 – 3.70 (2H, m, $(PPh_2)_2N$-C<u>H</u>$_2$), 1.98 – 2.07 (2H, m, Ph-C<u>H</u>$_2$); $\delta_P$ $^{31}P\{^1H\}$ (162 MHz, $CD_2Cl_2$) 71.0 (1P, d, $^2J_{PP}$ = 88.3 Hz, S<u>P</u>NP), 51.9 (1P, d, $^2J_{PP}$ = 88.3 Hz, SPN<u>P</u>); $\delta_C$ (100.57 MHz, $CD_2Cl_2$) 138.8 (s, aryl-C), 136.5 (dd, *J* = 5.0 Hz, 18.2 Hz, aryl-C), 135.3 (d, *J* = 3.64 Hz, aryl-CC), 134.2 (d, *J* = 3.60 Hz, aryl-CC), 132.9 (d, *J* = 20.9 Hz, aryl-C), 132.4 (dd, *J* = 3.06 Hz, 11.1 Hz, aryl-C), 131.7 (d, *J* = 3.10 Hz, aryl-C), 129.5 (s, aryl-C), 128.5 (dd, *J* = 5.95 Hz, 6.05 Hz, aryl-C), 128.3 (s, aryl-C), 128.1 (d, *J* = 1.85 Hz, aryl-C), 126.0 (s, aryl-C), 39.2 (s, $CH_2$), 37.0 (s, $CH_2$); selected $\nu_{max}$ / $cm^{-1}$ 3055 (aromatic C-H stretch), 2985 (C-H stretch), 1603, 1478 (aromatic C=C), 1434 (P-Ph), 1097 (C-N), 862 (P-N-P) 697 (P=S); Anal. calc. for $C_{32}H_{29}NP_2S$ (521.60) (%): C, 73.69; H, 5.60; N, 2.69 Found (%): C, 72.53; H, 5.81; N, 2.89; MS (ESI): positive ion *m/z* 336.3 (5.39% $[M\text{-}PPh_2]^+$), 490.3 (30.74% $[M\text{-}S+H]^+$), 522.3 (55.23% $[M\text{-}S+2O+H]^+$). Note poor agreement in CHN analysis for carbon likely due to trace amounts of unreacted compound **2.2** and compound **2.10**.

Single crystals suitable for XRD analysis were obtained by diffusion following dissolution of a sample of compound **2.9** in THF and layering this with hexane.

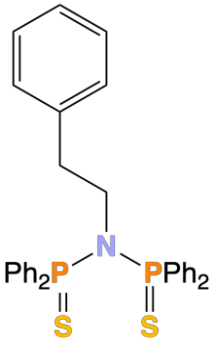


**2.10**

**Synthesis of $Ph(CH_2)_2N(SPPh_2)_2$ (2.10):** $Ph(CH_2)_2N(PPh_2)_2$ (**2.2**, 0.500 g, 1.02 mmol) and $S_8$ (0.066 g, 0.26 mmol) were dissolved in THF (20 mL) and stirred overnight. The reaction mixture was filtered, the solvent removed *in vacuo*, the crude product washed with $Et_2O$ (3 × 10 mL) and dried *in vacuo*, affording compound **2.10** as a white powder (0.318 g, 0.57 mmol, 56%); $\delta_H$ (400 MHz, $CD_2Cl_2$) 7.94 – 8.03 (8H, m, phenyl), 7.49 – 7.56 (4H, m, phenyl), 7.38 – 7.45 (8H, m, phenyl), 7.05 – 7.11 (3H, m, phenyl), 6.40 – 6.46 (2H, m, phenyl), 3.58 – 3.75 (2H, m, $(PPh_2)_2N$-C$\underline{H}_2$), 2.59 – 2.67 (2H, m, Ph-C$\underline{H}_2$); $\delta_P$ $^{31}P\{^1H\}$ (162 MHz, $CD_2Cl_2$) 69.0 (2P, s); $\delta_C$ (100.57 MHz, $CD_2Cl_2$) 138.1 (s, aryl-C), 133.8 (s, aryl-C), 133.1 (t, *J* = 6.02 Hz, aryl-C), 132.8 (s, aryl-C), 131.8 (t, *J* = 1.37 Hz, aryl-C), 128.3 (d, *J* = 21.1 Hz, aryl-C), 128.0 (t, *J* = 7.08 Hz, aryl-C), 126.3 (s, aryl-C), 38.3 (s, $CH_2$), 36.9 (s, $CH_2$); selected $\nu_{max}$ / $cm^{-1}$ 3054 (aromatic C-H stretch), 2984 (C-H stretch), 1602, 1479 (aromatic C=C), 1434 (P-Ph), 1100 (C-N), 866 (P-N-P) 685 (P=S); Anal. calc. for $C_{32}H_{29}NP_2S_2$ (553.66) (%): C, 69.42; H, 5.28; N, 2.53 Found (%): C, 69.44; H, 5.25; N, 2.46; MS (ESI): positive ion *m/z* 123.9 (100% $[M\text{-}2SPPh_2+3H]^+$).

Single crystals suitable for XRD analysis were obtained by dissolving a sample of the solid isolated from the reaction of compound **2.10** with $CoBr_2$ in acetone and allowing the solvent to evaporate.

## 7.4 Synthesis of Py-*o*-$(CH_2)_2N(PPh_2)(Me)$ (2.11) and Py-*o*-$(CH_2)_2N(P\{OPh\}_2)(Me)$ (2.12)

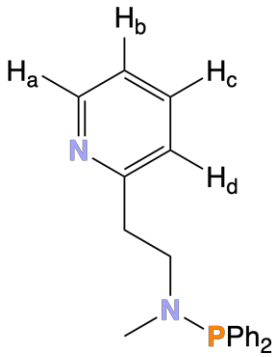


**2.11**

**Synthesis of Py-*o*-$(CH_2)_2N(PPh_2)(Me)$ (2.11):** *N*-Methyl-*N*-(2-pyridin-2-ylethyl)amine (0.759 g, 5.57 mmol) and $NEt_3$ (7 mL, 50 mmol) were dissolved in THF (30 mL), and the resulting solution cooled to –40 °C in an acetone/dry ice bath. $PPh_2Cl$ (1 mL, 5.57 mmol) was added dropwise, and after the complete addition the reaction mixture was allowed to warm to room temperature and stir overnight. The reaction mixture was filtered, the solvent removed *in vacuo*, the crude product washed with $Et_2O$ (3 × 10 mL) and dried *in vacuo*, affording compound **2.11** as a pale yellow oil (1.28 g, 4.00 mmol, 72%); $\delta_H$ (400 MHz, $CD_2Cl_2$) 8.56 (1H, ddd, *J* = 0.76 Hz, 1.08 Hz, 4.75 Hz, $H_a$), 7.60 (1H, td, *J* = 1.90 Hz, 7.60 Hz, $H_c$), 7.36 – 7.42 (10H, m, phenyl), 7.11 – 7.18 (2H, m, $H_b$ + $H_d$), 3.52 – 3.61 (2H, m, $(PPh_2)_2N$-C$\underline{H}_2$), 2.99 – 3.06 (2H, m, Py-C$\underline{H}_2$), 2.63 (3H, d, $^3J_{HP}$ = 5.67 Hz, Me); $\delta_P$ $^{31}P\{^1H\}$ (162 MHz, $CD_2Cl_2$) 64.4 (1P, s); $\delta_C$ (100.57 MHz, $CD_2Cl_2$) 160.2 (s, aryl-C), 149.3 (s, aryl-C), 139.5 (d, *J* = 15.1 Hz, aryl-C), 136.0 (s, aryl-C), 131.9 (d, *J* = 19.6 Hz, aryl-C), 128.3 (s, aryl-C), 128.1 (d, *J* = 5.67 Hz, aryl-C), 123.3 (s, aryl-C), 121.1 (s, aryl-C), 56.8 (d, *J* = 30.6 Hz, Me), 38.1 (d, *J* = 5.7 Hz, $CH_2$), 36.8 (s, $CH_2$); selected $\nu_{max}$ / $cm^{-1}$ 3055 (aromatic C-H stretch), 2980 (C-H stretch), 1605, 1473 (C=C), 1586, 1563 (C=N), 1438 (P-Ph), 860 (P-N-P); MS (ESI): positive ion *m/z* 137.2 (85.3% $[M\text{-}PPh_2+H]^+$), 215.3 (49.5% $[M\text{-}CH_2CH_2Py+H]^+$), 242.3 (10.2% $[M\text{-}Ph]^+$). Note that compound **2.11** is very waxy, which hindered sample transfer to the tin capsules, required for CHN analysis to be obtained; consequently no reliable data could be obtained. NMR spectroscopic data are consistent with previously published data.[10]

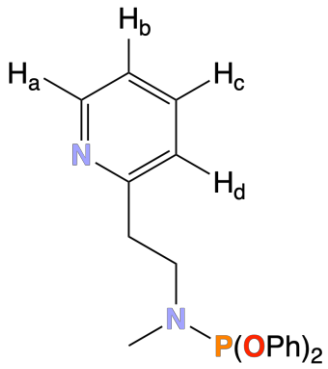


**2.12**

**Synthesis of Py-*o*-(CH$_2$)$_2$N(P{OPh}$_2$)(Me) (2.12):** *N*-Methyl-*N*-(2-pyridin-2-ylethyl)amine (0.703 g, 5.16 mmol) and NEt$_3$ (7 mL, 50 mmol) were dissolved in THF (30 mL), and the resulting solution cooled to –40 °C in an acetone/dry ice bath. P(OPh)$_2$Cl (1 mL, 5.16 mmol) was added dropwise, and after the complete addition the reaction mixture was allowed to warm to room temperature and stir overnight. The reaction mixture was filtered, the solvent removed *in vacuo*, the crude product washed with Et$_2$O (3 × 10 mL) and dried *in vacuo*, affording compound **2.12** as a pale yellow oil (1.25 g, 3.55 mmol, 69%); $\delta_H$ (400 MHz, $CD_2Cl_2$) 8.57 (1H, d, $J$ = 3.98 Hz, $H_a$), 7.59 (1H, td, $J$ = 1.84 Hz, 7.68 Hz, $H_c$), 7.04 – 7.44 (12H, m, phenyl + $H_b$ + $H_d$), 3.58 – 3.68 (2H, m, (PPh$_2$)$_2$N-C$\underline{H}_2$), 3.01 – 3.07 (2H, m, Py-C$\underline{H}_2$), 2.90 (3H, d, $^3J_{HP}$ = 7.14 Hz, Me); $\delta_P$ $^{31}$P{$^1$H} (162 MHz, $CD_2Cl_2$) 140.1 (1P, s); $\delta_C$ (100.57 MHz, $CD_2Cl_2$) 159.5 (s, aryl-C), 153.8 (d, $J$ = 6.91 Hz, aryl-C), 149.4 (s, aryl-C), 136.1 (s, aryl-C), 129.6 (s, aryl-C), 123.4 (s, aryl-C), 123.0 (d, $J$ = 1.26 Hz, aryl-C), 121.3 (s, aryl-C), 120.1 (d, $J$ = 8.45 Hz, aryl-C), 48.7 (d, $J$ = 30.4 Hz, Me), 37.6 (d, $J$ = 4.39 Hz, $CH_2$), 30.9 (d, $J$ = 10.6 Hz, $CH_2$); selected $\nu_{max}$ / cm$^{-1}$ 3058 (aromatic C-H stretch), 2982 (C-H stretch), 1601, 1476 (C=C), 1590, 1566 (C=N); MS (ESI): positive ion *m/z* 137.2 (45.0% [M-P(OPh)$_2$+2H]$^+$), 259.3 (9.73% [M-OPh]$^+$). Note that compound **2.12** is very waxy, which hindered sample transfer to the tin capsules, required for CHN analysis to be obtained; consequently no reliable data could be obtained.

## 7.5 Attempted synthesis of Py-*o*-(CH$_2$)$_2$N(P{OPh}$_2$)$_2$ (2.13)

**Synthesis of P(OPh)$_2$Cl:** PCl$_3$ (2.19 mL, 25.0 mmol) and P(OPh)$_3$ (13.1 mL, 50.0 mmol) were added to a Schlenk flask, followed by $CF_3CO_2H$ (0.08 mL, 5.0 mmol). The reaction mixture was heated at reflux overnight. Following this, the reaction mixture was allowed to cool and was transferred *via* cannula into a distillation apparatus. P(OPh)$_2$Cl was

collected by vacuum distillation (at approx. 120 °C) as a colourless liquid (6 mL, 31.0 mmol, 41%, density = 1.304 g $mL^{-1}$); $\delta_H$ (400 MHz, $CDCl_3$) 7.40 – 7.47 (4H, m, phenyl), 7.24 – 7.31 (6H, m, phenyl); $\delta_P$ $^{31}P\{^1H\}$ (162 MHz, $CDCl_3$) 158.2 (1P, s); $\delta_C$ (100.57 MHz, $CDCl_3$) 151.1 (s, aryl-C), 129.8 (s, aryl-C), 125.3 (d, *J* = 1.46 Hz, aryl-C), 121.2 (d, *J* = 6.25 Hz, aryl-C). NMR spectroscopic data are consistent with previously published data.[11]

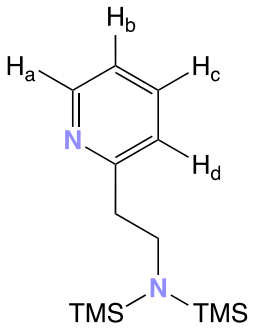


**Synthesis of Py-*o*-$(CH_2)_2N(TMS)_2$:** 2-Aminoethylpyridine (0.618 g, 5.05 mmol) was added to a Schlenk flask and degassed by freeze-pump thaw method (three cycles). To this, THF (20 mL) and $NEt_3$ (6 mL, 43.0 mmol) were added. This mixture was cooled to approx. –40 °C in a acetone/dry ice bath, stirred and $Me_3SiCl$ (2 mL, 15.8 mmol) added slowly dropwise. The mixture was allowed to warm to room temperature and was stirred overnight. A $^1H$ NMR spectrum of the crude reaction mixture was acquired by removing an aliquot of the reaction mixture under nitrogen using a needle and syringe and transferring to a previously evacuated and $N_2$-back-filled NMR tube (located in a large Schlenk), removing the solvent *in vacuo* and dissolving the sample in $CDCl_3$. Upon confirmation of reaction completion, the reaction mixture was filtered using a cannula filter, volatile components removed *in vacuo*, and the product extracted in hexane (3 × 10 mL), affording the product as a colourless oil (1.13 g, 4.24 mmol, 84%); $\delta_H$ (400 MHz, $CD_2Cl_2$) 8.53 (1H, dq, *J* = 0.84 Hz, 4.90 Hz, $H_a$), 7.62 (1H, td, *J* = 1.90 Hz, 7.65 Hz, $H_c$), 7.11 – 7.17 (2H, m, $H_b$ + $H_d$), 3.13 – 3.20 (2H, m, $(PPh_2)_2N$-C<u>H</u>$_2$), 2.80 – 2.88 (2H, m, Py-C<u>H</u>$_2$), 0.19 (18H, s, $Si(CH_3)_3$); $\delta_C$ (100.57 MHz, $CD_2Cl_2$) 160.3 (s, py-C), 149.3 (s, py-C), 136.0 (s, py-C), 122.8 (s, py-C), 121.0 (s, py-C), 46.0 (s, $CH_2$), 44.2 (s, $CH_2$), 1.78 (s, $Si(CH_3)_3$); MS (ESI): positive ion *m/z* 123.3 (100.0% $[M\text{-}2TMS+3H]^+$), 267.5 (1.18% $[M+H]^+$). NMR spectroscopic data are consistent with published data.[12]

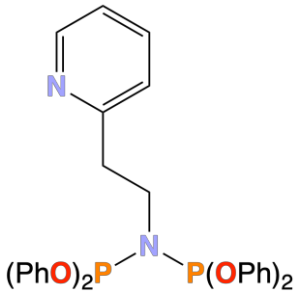

**2.13**

**Attempted synthesis of Py-*o*-$(CH_2)_2N(P\{OPh\}_2)_2$ (2.13) – Method 1:** 2-Aminoethylpyridine (0.630 g, 5.16 mmol) was added to a Schlenk flask and degassed by freeze-pump thaw method (three cycles). To this, THF (20 mL) and $NEt_3$ (6 mL, 43.0 mmol) were added. This mixture was cooled to approx. –40 °C in a Cardice/acetone bath, stirred and $P(OPh)_2Cl$ (2 mL, 10.3 mmol) added slowly dropwise. The mixture was allowed to warm to room temperature and was stirred overnight. Crude $^{31}P\{^1H\}$ NMR analysis revealed a mixture of *o*-$PyCH_2CH_2NH(P\{OPh\}_2$, compound **2.13** and unreacted $P(OPh)_2Cl$, hence the reaction mixture was refluxed overnight. Since this did not alter the crude $^{31}P\{^1H\}$ NMR significantly, the reaction was abandoned.

**Attempted synthesis of Py-*o*-$(CH_2)_2N(P\{OPh\}_2)_2$ (2.13) – Method 2:** Py-*o*-$(CH_2)_2N(TMS)_2$ (0.69 g, 2.6 mmol) and $NEt_3$ (6 mL, 43.0 mmol) were dissolved in THF (20 mL), the mixture cooled to approx. –40 °C in a acetone/dry ice bath, stirred and $P(OPh)_2Cl$ (1 mL, 5.2 mmol) added slowly dropwise. The mixture was allowed to warm to room temperature and was stirred overnight. Volatilities were removed *in vacuo*, affording a product tentatively assigned to be compound **2.13** as a sticky, waxy, pale yellow oil; $\delta_P$ $^{31}P\{^1H\}$ (162 MHz, $CD_2Cl_2$) 129.6 (2P, s). Due to the complexities of the $^1H$ and $^{13}C$ NMR spectra, they cannot be assigned reliably. The sticky, waxy nature of the product prevented removal of the majority of the product from the Schlenk flask, hence an accurate yield cannot be reported. FT-IR and CHN analysis cannot be acquired for the same reason. MS (ESI): positive ion analysis did not evidence any useful signals. Further study of compound **2.13** was abandoned.

## 7.6 Synthesis of Phosphine Selenides of $Ph(CH_2)_2N(PPh_2)_2$ (2.2), *n*-$BuN(PPh_2)_2$ (2.3), $NMe_2(CH_2)_3N(PPh_2)_2$ (2.4), Py-*m*-$CH_2N(PPh_2)_2$ (2.5), Ph-$C_6H_4N(PPh_2)_2$ (2.6), and Py-*o*-$C_6H_4N(PPh_2)_2$ (2.7), Py-*o*-$(CH_2)_2N(CH_2PPh_2)_2$ (2.8), $Ph(CH_2)_2N(SPPh_2)(PPh_2)$ (2.9), Py-*o*-$(CH_2)_2N(PPh_2)(Me)$ (2.11) and Py-*o*-$(CH_2)_2N(P\{OPh\}_2)(Me)$ (2.12)

**General Procedure 1:** An excess of elemental grey selenium was added to a sample of **2.2 – 2.9**, **2.11** and **2.12** in $CDCl_3$ in an NMR tube, and the NMR tube was sonicated for 40 mins at 30 °C. The $|^1J_{SeP}|$ coupling constants (**Table 2.2**, **Chapter 2**) were measured from the obtained $^{31}P\{^1H\}$ NMR spectra. All selenides were synthesised following **General Procedure 1**.

## 7.7 Synthesis of $[Ph(CH_2)_2N(PPh_2)_2PdCl_2]$ (3.1), [*n*-$BuN(PPh_2)_2PdCl_2$] (3.2), $[NMe_2(CH_2)_3N(PPh_2)_2PdCl_2]$ (3.3), [Py-*m*-$CH_2N(PPh_2)_2PdCl_2$] (3.4), [Ph-$C_6H_4N(PPh_2)_2PdCl_2$] (3.5), [Py-*o*-$C_6H_4N(PPh_2)_2PdCl_2$] (3.6), and $[Py\text{-}o\text{-}(CH_2)_2N(CH_2PPh_2)_2PdCl_2]$ (3.7)

**General Procedure 2: 2.2** – **2.8** and $[(MeCN)_2PdCl_2]$ (0.100 g, 0.385 mmol) were dissolved in DCM (~15 mL) and stirred overnight. The solution was concentrated to ~10 mL, layered with $Et_2O$ (~20 mL) and left standing for approx. 1 – 2 days to gain the product as single crystals suitable for XRD analysis. The product was isolated by filtration and dried *in vacuo*. Note that complexes **3.2** – **3.4** and **3.6** are too insoluble in common organic solvents to allow for $^{13}C$ NMR spectra to be obtained (solvents tried: $CD_2Cl_2$, $CDCl_3$ and $d_8$-THF).

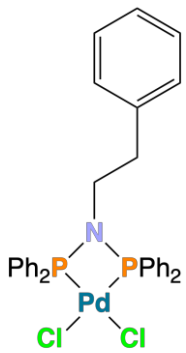


**3.1**

**Synthesis of $[Ph(CH_2)_2N(PPh_2)_2PdCl_2]$ (3.1):** Follows **General Procedure 2**, using $Ph(CH_2)_2N(PPh_2)_2$ (compound **2.2**, 0.188 g, 0.385 mmol), gaining complex **3.1** as a brown

solid (0.149 g, 0.223 mmol, 58%); $\delta_H$ (400 MHz, $CDCl_3$) 7.89 – 7.99 (8H, m, phenyl), 7.64 – 7.72 (4H, m, phenyl), 7.53 – 7.62 (8H, m, phenyl), 7.11 – 7.19 (3H, m, $CH_2CH_2\underline{Ph}$), 6.67 – 6.75 (2H, m, $CH_2CH_2\underline{Ph}$), 3.14 – 3.41 (2H, m, $(PPh_2)_2N\text{-}C\underline{H_2}$), 2.18 – 2.27 (2H, m, $PhC\underline{H_2}$); $\delta_P$ $^{31}P\{^1H\}$ (162 MHz, $CDCl_3$) 31.1 (2P, s); $\delta_C$ (100.57 MHz, $CD_2Cl_2$) 136.8 (s, aryl-C), 133.6 (s, aryl-C), 133.58 (t, $J$ = 6.8 Hz, aryl-C), 129.6 (t, $J$ = 6.3 Hz, aryl-C), 128.7 (s, aryl-C), 128.1 (s, aryl-C), 127.2 (s, aryl-C), 127.0 (s, aryl-C), 50.8 (s, $CH_2$), 36.0 (s, $CH_2$); selected $\nu_{max}$ / $cm^{-1}$ 3045 (aromatic C-H stretch), 2963 (C-H stretch), 1605, 1481 (aromatic C=C), 1434 (P-Ph), 1098 (C-N), 798 (P-N-P); Anal. calc. for $C_{32}H_{29}Cl_2NP_2Pd$ (666.86) (%): C, 57.64; H, 4.38; N, 2.10 Found (%): C, 56.77; H, 4.04; N, 2.23; MS (ESI): positive ion *m/z* 1296.2 (10.69% $[2M\text{-}Cl+H]^+$).

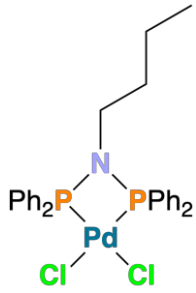


**3.2**

**Synthesis of [*n*-BuN(PPh$_2$)$_2$PdCl$_2$] (3.2):** Follows **General Procedure 2**, using *n*-BuN$(PPh_2)_2$ (compound **2.3**, 0.170 g, 0.385 mmol), gaining complex **3.2** as a yellow powder (0.142 g, 0.229 mmol, 60%); $\delta_H$ (400 MHz, $CDCl_3$) 7.83 – 7.93 (8H, m, phenyl), 7.63 – 7.70 (4H, m, phenyl), 7.51 – 7.59 (8H, m, phenyl), 2.92 – 3.07 (2H, m, $(PPh_2)_2NC\underline{H_2}$), 1.05 – 1.16 (2H, m, $(PPh_2)_2NCH_2C\underline{H_2}$), 0.84 – 0.95 (2H, m, $C\underline{H_2}CH_3$), 0.59 (3H, t, $^3J_{HH}$ = 7.3 Hz, $CH_3$); $\delta_P$ $^{31}P\{^1H\}$ (162 MHz, $CDCl_3$) 31.4 (2P, s); selected $\nu_{max}$ / $cm^{-1}$ 3053 (aromatic C-H stretch), 2969 (C-H stretch), 1611, 1480 (aromatic C=C), 1456, 1376 ($CH_3$ bend), 1434 (P-Ph), 1099 (C-N), 837 (P-N-P); Anal. calc. for $C_{28}H_{29}Cl_2NP_2Pd$ (618.81) (%): C, 54.35; H, 4.72; N, 2.26 Found (%): C, 53.20; H, 4.50; N, 2.48; MS (ESI): positive ion *m/z* 582.3 (100.00% $[M\text{-}Cl]^+$), 616.1 (37.78% $[M\text{-}H]^+$), 1200.2 (57.02% $[2M\text{-}Cl+H]^+$).

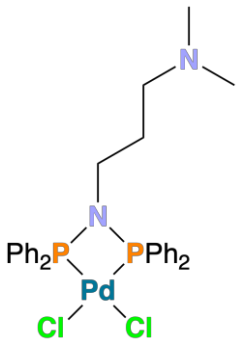

**3.3**

**Synthesis of [$NMe_2(CH_2)_3N(PPh_2)_2PdCl_2$] (3.3):** Follows **General Procedure 2**, using $NMe_2(CH_2)_3N(PPh_2)_2$ (compound **2.4**, 0.181 g, 0.385 mmol), gaining complex **3.3** as a light brown powder (0.137 g, 0.211 mmol, 55%); $\delta_H$ (400 MHz, $CD_2Cl_2$) 7.89 – 8.00 (8H, m, phenyl), 7.69 – 7.78 (4H, m, phenyl), 7.59 – 7.67 (8H, m, phenyl), 3.11 – 3.28 (2H, m, $(PPh_2)_2NC\underline{H}_2$), 1.96 (8H, s, $N(C\underline{H}_3)_2$ + $C\underline{H}_2NMe_2$), 1.16 – 1.28 (2H, m, $C\underline{H}_2CH_2NMe_2$); $\delta_P$ $^{31}P\{^1H\}$ (162 MHz, $CD_2Cl_2$) 30.5 (2P, s); selected $\nu_{max}$ / $cm^{-1}$ 3054 (aromatic C-H stretch), 2980 (C-H stretch), 1605, 1477 (aromatic C=C), 1433 (P-Ph), 1099 (C-N), 812 (P-N-P); Anal. calc. for $C_{29}H_{32}Cl_2N_2P_2Pd$ (647.86) (%): C, 53.76; H, 4.98; N, 4.32 Found (%): C, 52.65; H, 4.91; N, 3.97; MS (ESI): positive ion *m/z* 645.2 (100% $[M\text{-}H]^+$), 1258.3 (10.57% $[2M\text{-}Cl+H]^+$).

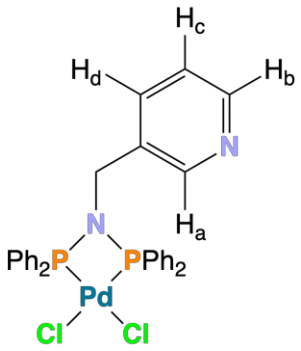

**3.4**

**Synthesis of [Py-*m*-$CH_2N(PPh_2)_2PdCl_2$] (3.4):** Follows **General Procedure 2**, using Py-*m*-$CH_2N(PPh_2)_2$ (compound **2.5**, 0.183 g, 0.385 mmol), except 0.130 g of complex **3.4** precipitated during the reaction. The precipitate was isolated by filtration, and the filtrate layered (without concentration) with $Et_2O$ (~20 mL), gaining a second crop of complex **3.4** as single crystals suitable for XRD analysis. Complex **3.4** was isolated as a yellow powder (0.200 g, 0.306 mmol, 79%); $\delta_H$ (400 MHz, $CD_2Cl_2$) 8.29 (1H, dd, *J* = 1.3 Hz, 4.4 Hz, $H_b$), 7.50 – 7.95 (21H, m, phenyl + $H_a$), 6.78 (1H ,dd, *J* = 4.8 Hz, 8.0 Hz, $H_c$),

6.59 (1H, dt, $J$ = 1.9 Hz, 7.9 Hz, $H_d$), 4.33 (2H, t, $^3J_{HP}$ = 12.6 Hz, $(PPh_2)_2NC\underline{H}_2$); $\delta_P$ $^{31}P\{^1H\}$ (162 MHz, $CD_2Cl_2$) 34.3 (2P, s); selected $\nu_{max}$ / $cm^{-1}$ 3056 (aromatic C-H stretch), 2981 (C-H stretch), 1603, 1478 (aromatic C=C), 1586, 1575 (C=N), 1434 (P-Ph), 1099 (C-N), 811 (P-N-P); Anal. calc. for $C_{30}H_{26}Cl_2N_2P_2Pd$ (653.82) (%): C, 55.11; H, 4.01; N, 4.28 Found (%): C, 54.44; H, 3.80; N, 4.74; MS (ESI): positive ion $m/z$ 650.4 (100% $[M\text{-}H]^+$).

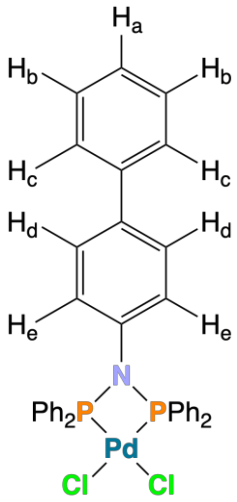


**3.5**

**Synthesis of [Ph-$C_6H_4N(PPh_2)_2PdCl_2$] (3.5):** Follows **General Procedure 2**, using Ph-$C_6H_4N(PPh_2)_2$ (compound **2.6**, 0.207 g, 0.385 mmol), gaining complex **3.5** as a brown solid (0.179 g, 0.250 mmol, 65%); $\delta_H$ (400 MHz, $CDCl_3$) 7.92 – 8.01 (8H, m, phenyl), 7.64 – 7.71 (4H, m, *para*-phenyl), 7.52 – 7.58 (8H, m, phenyl), 7.30 – 7.47 (7H, m, $H_a$ + $H_b$ + $H_c$ + $H_d$), 6.62 (2H, d, $J$ = 8.6 Hz, $H_e$); $\delta_C$ (100.57 MHz, $CDCl_3$) 139.0 (s, aryl-C), 133.9 (t, $J$ = 6.6 Hz, aryl-C), 133.6 (s, aryl-C), 129.4 (t, $J$ = 6.3 Hz, aryl-C), 128.9 (s, aryl-C), 128.1 (s, aryl-C), 127.9 (s, aryl-C), 127.2 (s, aryl-C), 126.7 (s, aryl-C), 126.6 (s, aryl-C), 126.2 (t, $J$ = 3.2 Hz aryl-C), 118.8 (s, aryl-C); $\delta_P$ $^{31}P\{^1H\}$ (162 MHz, $CDCl_3$) 34.8 (2P, s); selected $\nu_{max}$ / $cm^{-1}$ 3053 (aromatic C-H stretch), 2983 (C-H stretch), 1605, 1483 (aromatic C=C), 1434 (P-Ph), 1098 (C-N), 833 (P-N-P); Anal. calc. for $C_{36}H_{29}Cl_2NP_2Pd$ (714.90) (%): C, 60.48; H, 4.09; N, 1.96 Found (%): C, 60.41; H, 3.84; N, 2.15; MS (ESI): positive ion $m/z$ 712.2 (65.71% $[M\text{-}H]^+$).

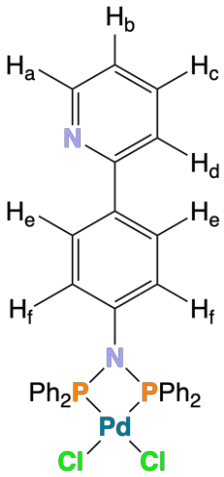


**3.6**

**Synthesis of [Py-*o*-$C_6H_4N(PPh_2)_2PdCl_2$] (3.6):** Follows **General Procedure 2**, using Py-*o*-$C_6H_4N(PPh_2)_2$ (compound **2.7**, 0.207 g, 0.385 mmol), gaining complex **3.6** as a brown solid (0.132 g, 0.18 mmol, 48%); $\delta_H$ (400 MHz, $CDCl_3$) 8.64 (1H, d, *J* = 5.1 Hz, $H_a$), 7.91 – 8.01 (8H, m, phenyl), 7.71 – 7.75 (3H, m, $H_e$ + pyridyl-H), 7.63 – 7.70 (4H, m, *para*-phenyl), 7.57 – 7.62 (1H, m, pyridyl-H), 7.50 – 7.58 (8H, m, phenyl), 7.23 – 7.27 (1H, m, $H_b$), 6.67 (2H, d, *J* = 8.5 Hz, $H_f$); $\delta_P$ $^{31}P\{^1H\}$ (162 MHz, $CDCl_3$) 35.0 (2P, s); selected $\nu_{max}$ / $cm^{-1}$ 3052 (aromatic C-H stretch), 2981 (C-H stretch), 1603, 1480 (aromatic C=C), 1585, 1571 (C=N), 1434 (P-Ph), 1097 (C-N), 832 (P-N-P); Anal. calc. for $C_{35}H_{28}Cl_2N_2P_2Pd$ (715.89) (%): C, 58.72; H, 3.94; N, 3.91 Found (%): C, 58.19; H, 3.78; N, 4.11; MS (ESI): positive ion *m/z* 713.0 (89.48% $[M-H]^+$).

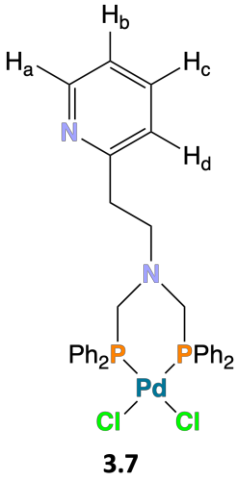


**3.7**

**Synthesis of [Py-*o*-$(CH_2)_2N(CH_2PPh_2)_2PdCl_2$] (3.7):** Follows **General Procedure 2**, using **Py-*o*-$(CH_2)_2N(CH_2PPh_2)_2$** (**2.8**, 0.200 g, 0.385 mmol), gaining **3.7** as a brown solid (0.185 g, 0.266 mmol, 69%); $\delta_H$ (400 MHz, $CD_2Cl_2$) 8.50 (1H, dq, *J* = 0.8 Hz, 4.9 Hz, $H_a$), 7.42 – 7.90 (21H, m, phenyl + $H_c$), 7.17 (1H, ddd, *J* = 0.9 Hz, 4.9 Hz, 7.6 Hz, $H_b$), 6.86 (1H,

dt, J = 1.0 Hz, 7.8 Hz, $H_d$), 3.43 – 3.50 (4H, m, $Ph_2P$-C$\underline{H}_2$), 3.17 (2H, t, $^3J_{HH}$ = 7.6 Hz, $(CH_2PPh_2)_2NC\underline{H}_2$), 2.84 (2H, t, $^3J_{HH}$ = 7.6 Hz, Py-C$\underline{H}_2$); $\delta_C$ (100.57 MHz, $CD_2Cl_2$) 158.7 (s, aryl-C), 149.4 (s, aryl-C), 136.4 (s, aryl-C), 133.9 (m, aryl-C), 131.5 (s, aryl-C), 129.2 (s, aryl-C), 128.6 (m, aryl-C), 123.3 (s, aryl-C), 121.6 (s, aryl-C), 56.7 (d, *J* = 2.5 Hz, $CH_2$), 56.3 (d, *J* = 3.0 Hz, $CH_2$), 33.7 (s, $CH_2$); $\delta_P$ $^{31}P\{^1H\}$ (162 MHz, $CD_2Cl_2$) 8.10 (2P, s); selected $\nu_{max}$ / $cm^{-1}$ 3052 (aromatic C-H stretch), 2982 (C-H stretch), 1604, 1475 (aromatic C=C), 1588, 1567 (C=N), 1435 (P-Ph), 1099 (C-N); Anal. calc. for $C_{33}H_{32}Cl_2N_2P_2Pd$ (695.90) (%): C, 56.96; H, 4.64; N, 4.03 Found (%): C, 56.56; H, 4.67; N, 3.39; MS (ESI): positive ion *m/z* 661.4 (64.82% $[M\text{-}Cl+2H]^+$).

## 7.8 Synthesis and Deprotonation of [(H-Py-*o*-$(CH_2)_2N(PPh_2)_2)PdCl_2][CF_3CO_2]$ (3.9), [(H-Py-*o*-$(CH_2)_2N(CH_2PPh_2)_2)PdCl_2][CF_3CO_2]$ (3.10), [(H-$NMe_2(CH_2)_3N(PPh_2)_2)PdCl_2][PF_6]$ (3.11) and [(H-$NMe_2(CH_2)_3N(PPh_2)_2)PdCl_2][CF_3CO_2]$ (3.12)

Note that complexes **3.9** – **3.12** are too insoluble in common organic solvents to allow for $^{13}C$ NMR spectra to be obtained (solvents tried: $CD_2Cl_2$, $CDCl_3$ and $d_8$-THF).

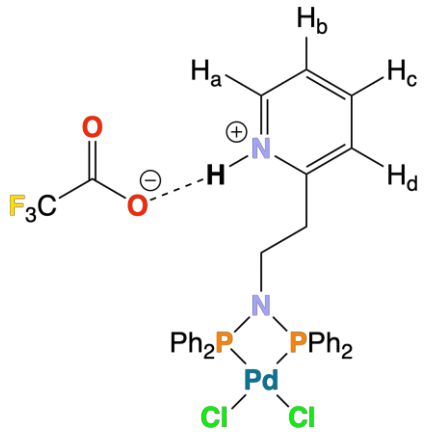


**3.9**

**Synthesis of [(H-Py-*o*-$(CH_2)_2N(PPh_2)_2)PdCl_2][CF_3CO_2]$ (3.9):** [(Py-*o*-$(CH_2)_2N(PPh_2)_2)PdCl_2$] (**3.8**, 0.068 g, 0.1 mmol) and TFA (8 $\mu$L, 0.1 mmol) were dissolved in DCM (15 mL) and the reaction mixture stirred overnight. The reaction mixture was concentrated to approx. 5 mL and layered with hexane (10 mL). Following diffusion, this provided crystals of complex **3.9** which were isolated by filtration and dried *in vacuo*, affording complex **3.9**, as a yellow solid (0.028 g, 0.036 mmol, 36%); $\delta_H$ (400 MHz,

$CD_2Cl_2$) 12.0 (1H, s, br, $\nu_{1/2}$ ~440 Hz, $Py^+$-H), 8.69 (1H, d, $J$ = 5.5 Hz, $H_a$), 8.18 (1H, td, $J$ = 1.4 Hz, 7.9 Hz, $H_c$), 7.98 – 8.08 (8H, m, phenyl), 7.59 – 7.81 (13H, m, phenyl + $H_b$), 6.95 (1H, d, $J$ = 7.9 Hz, $H_d$), 3.58 – 3.73 (2H, m, $CH_2N(PPh_2)_2$), 2.51 – 2.63 (2H, m, Py-$CH_2$); $\delta_P$ $^{31}P\{^1H\}$ (162 MHz, $CD_2Cl_2$) 32.1 (2P, s); $\delta_F$ $^{19}F$ (376.33 MHz, $CD_2Cl_2$) –76.0 (3F, s, $CF_3CO_2^-$); selected $\nu_{max}$ / $cm^{-1}$ 3454 (O-H + N-H stretch, br), 3054 (aromatic C-H stretch), 2963 (C-H stretch), 1686 (C=O stretch, br), 1623, 1480 (aromatic C=C), 1586, 1570 (C=N), 1435 (P-Ph), 1099 (C-N), 833 (P-N-P); Anal. calc. for $C_{33}H_{29}Cl_2F_3N_2O_2P_2Pd$ (781.87) (%): C, 50.69; H, 3.74; N, 3.58 Found (%): C, 49.45; H, 3.24; N, 3.53; MS (ESI): positive ion *m/z* 632.3 (100.00% $[M\text{-}Cl\text{-}CO_2CF_3]^+$), 1299.3 (8.94% $[2M\text{-}Cl\text{+}H\text{-}2CO_2CF_3]^+$); negative ion *m/z* 113.1 (100.00% $[CF_3CO_2]^-$).

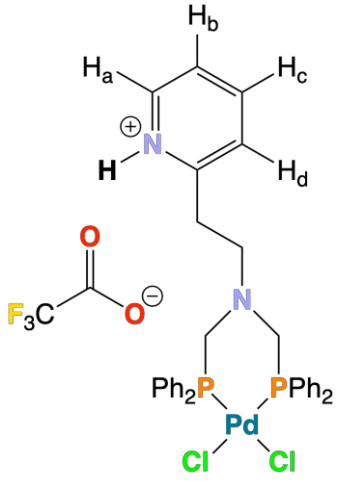


**3.10**

**Synthesis of [(H-Py-*o*-$(CH_2)_2N(CH_2PPh_2)_2$)$PdCl_2$][$CF_3CO_2$] (3.10):** Complex **3.10** was synthesised following the procedure outlined for complex **3.9**, using [(Py-*o*-$(CH_2)_2N(CH_2PPh_2)_2$)$PdCl_2$] (complex **3.7**, 0.054 g, 0.078 mmol) and TFA (6 $\mu$L, 0.078 mmol), affording **3.10** as yellow crystals (0.023 g, 0.028 mmol, 36%); $\delta_H$ (400 MHz, $CD_2Cl_2$) 15.9 (1H, s, br, $\nu_{1/2}$ ~440 Hz, $Py^+$-H), 8.68 (1H, d, $J$ = 5.7 Hz, $H_a$), 7.96 (1H, td, $J$ = 1.6 Hz, 7.8 Hz, $H_c$), 7.79 – 7.93 (8H, m, phenyl), 7.59 – 7.64 (1H, m, $H_b$), 7.52 – 7.59 (4H, m, *para*-phenyl), 7.40 – 7.50 (8H, m, phenyl), 7.14 (1H, d, $J$ = 8.0 Hz, $H_d$), 3.58 – 3.70 (4H, m, $Ph_2P$-$CH_2$), 2.98 – 3.15 (4H, m, $(CH_2PPh_2)_2NCH_2CH_2$); $\delta_P$ $^{31}P\{^1H\}$ (162 MHz, $CD_2Cl_2$) 8.91 (2P, s); $\delta_F$ $^{19}F$ (376.33 MHz, $CD_2Cl_2$) –76.0 (3F, s, $CF_3CO_2^-$); selected $\nu_{max}$ / $cm^{-1}$ 3417 (O-H + N-H stretch, br), 3055 (aromatic C-H stretch), 2963 (C-H stretch), 1682 (C=O stretch), 1627, 1481 (aromatic C=C), 1587, 1574 (C=N), 1435 (P-Ph), 1098 (C-N); Anal. calc. for $C_{35}H_{33}Cl_2F_3N_2O_2P_2Pd$ (809.92) (%): C, 51.90; H, 4.11; N, 3.46 Found (%): C, 50.69; H, 3.27;

N, 3.41; MS (ESI): positive ion *m/z* 660.4 (100.00% $[M\text{-}Cl\text{-}CO_2CF_3]^+$), 1355.3 (5.74% $[2M\text{-}Cl\text{-}2CO_2CF_3]^+$); negative ion *m/z* 113.1 (100.00% $[CF_3CO_2]^-$).

Crystals suitable for XRD analysis were obtained by letting a DCM solution of complex **3.10** stand for approx. 3 days in a sealed Young's NMR tube under $N_2$.

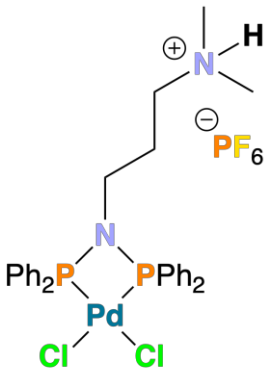


**3.11**

**Synthesis of $[(H\text{-}NMe_2(CH_2)_3N(PPh_2)_2)PdCl_2][PF_6]$ (3.11):** $[(NMe_2(CH_2)_3N(PPh_2)_2)PdCl_2]$ (**3.3**, 0.050 g, 0.077 mmol) and $NH_4PF_6$ (0.013 g, 0.077 mmol) were dissolved in DCM (10 mL) and the reaction mixture stirred overnight. The reaction mixture was filtered, concentrated to approx. 5 mL, and layered with $Et_2O$ (10 mL). After standing for *ca*. 2 days, single crystals suitable for XRD analysis were isolated by filtration and dried *in vacuo*, affording complex **3.11** as yellow crystals (0.013 g, 0.016 mmol, 21%); $\delta_H$ (400 MHz, $CD_2Cl_2$) 7.17 – 8.00 (21H, m, phenyl + $N^+$-H), 3.07 – 3.24 (2H, m, $(PPh_2)_2NCH_2$), 2.20 – 2.58 (8H, m, br, $\nu_{1/2}$ ~40 Hz, $N(CH_3)_2$ + $CH_2NMe_2$), 1.46 (2H, s, br, $\nu_{1/2}$ ~40 Hz, $CH_2CH_2NMe_2$); $\delta_P$ $^{31}P\{^1H\}$ (162 MHz, $CD_2Cl_2$) 30.7 (2P, s, PNP), –144.4 (1P, spt, $^1J_{FP}$ = 711 Hz, $PF_6^-$); $\delta_F$ $^{19}F$ (376.33 MHz, $CD_2Cl_2$) –73.0 (6F, d, $^1J_{PF}$ = 713 Hz, $PF_6^-$); selected $\nu_{max}$ / $cm^{-1}$ 3055 (aromatic C-H stretch), 2980 (C-H stretch), 2855 (N-H stretch), 1623, 1480 (aromatic C=C), 1436 (P-Ph), 1099 (C-N), 833 (P-F stretch), 812 (P-N-P), 556 (P-F bend); Anal. calc. for $C_{29}H_{33}Cl_2F_6N_2P_3Pd$ (793.83) (%): C, 43.88; H, 4.19; N, 3.53 Found (%): C, 42.80; H, 3.40; N, 3.74; MS (ESI): positive ion *m/z* 648.3 (100.00% $[M\text{-}PF_6]^+$), 1259.3 (5.06% $[2M\text{-}Cl\text{-}2PF_6]^+$); negative ion *m/z* 145.1 (100.00% $[PF_6]^-$).

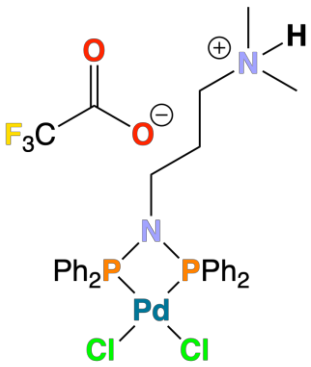

**3.12**

**Synthesis of [(H-NMe$_2$(CH$_2$)$_3$N(PPh$_2$)$_2$)PdCl$_2$][CF$_3$CO$_2$] (3.12):** Complex **3.12** was synthesised following the procedure outlined for complex **3.9**, using [(NMe$_2$(CH$_2$)$_3$N(PPh$_2$)$_2$)PdCl$_2$] (complex **3.3**, 0.068 g, 0.105 mmol) and TFA (8 $\mu$L, 0.105 mmol), affording **3.12** as yellow crystals (0.024 g, 0.032 mmol, 30%); $\delta_H$ (400 MHz, CDCl$_3$) 11.1 (1H, s, br, $\nu_{1/2}$ ~440 Hz, N$^+$-H), 7.75 – 7.95 (8H, m, phenyl), 7.55 – 7.65 (4H, m, *para*-phenyl), 7.44 – 7.55 (8H, m, phenyl), 3.13 – 3.30 (2H, m, (PPh$_2$)$_2$NCH$_2$), 2.72 – 2.88 (2H, m, CH$_2$NMe$_2$), 2.49 (6H, d, $J$ = 4.1 Hz, N(CH$_3$)$_2$), 1.37 – 1.53 (2H, m, CH$_2$CH$_2$NMe$_2$); $\delta_P$ $^{31}$P{$^1$H} (162 MHz, CDCl$_3$) 30.8 (2P, s); $\delta_F$ $^{19}$F (376.33 MHz, CD$_2$Cl$_2$) –76.0 (3F, s, CF$_3$CO$_2^-$); selected $\nu_{max}$ / cm$^{-1}$ 3445 (O-H, br), 3052 (aromatic C-H stretch), 2981 (C-H stretch), 2653 (N-H stretch, br), 1673 (C=O stretch, br), 1486 (aromatic C=C), 1435 (P-Ph), 1099 (C-N), 798 (P-N-P); Anal. calc. for C$_{31}$H$_{33}$Cl$_2$F$_3$N$_2$O$_2$P$_2$Pd (761.88) (%): C, 48.87; H, 4.37; N, 3.68 Found (%): C, 48.45; H, 3.86; N, 3.79; MS (ESI): positive ion *m/z* 613.5 (87.47% [M-Cl+H-CO$_2$CF$_3$]$^+$), 649.5 (100.00% [M+H-CO$_2$CF$_3$]$^+$), 1259.3 (12.09% [2M-Cl-2CO$_2$CF$_3$]$^+$); negative ion *m/z* 113.1 (100.00% [CF$_3$CO$_2$]$^-$).

**Deprotonation of complexes 3.9 – 3.12:** Protonated palladium complex (0.01 mmol) was dissolved in CDCl$_3$ (0.7 mL) in a Young's NMR tube, and NEt$_3$ (1.6 $\mu$L, 0.01 mmol) was added. The Young's NMR tube was sonicated for approx. 10 mins, and subsequently $^1$H and $^{31}$P NMR spectra acquired.

## 7.9 Synthesis of [(Ph(CH$_2$)$_2$NHPPh$_2$)(MeOPPh$_2$)PdCl$_2$] (3.23)

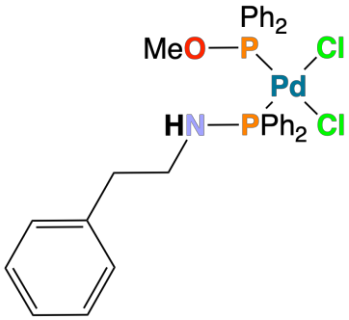

**3.23**

**Synthesis of [(Ph(CH$_2$)$_2$NHPPh$_2$)(MeOPPh$_2$)PdCl$_2$] (3.23):** [(Ph(CH$_2$)$_2$N(PPh$_2$)$_2$)PdCl$_2$] (**3.1**, 0.025 g, 0.038 mmol) was dissolved in MeOH (15 mL) and stirred overnight. The solvent was removed *in vacuo*, the crude product dissolved in DCM (5 mL) and layered with hexane (10 mL), affording of complex **3.23** as a brown solid (0.003 g, 0.0043 mmol, 11%); $\delta_H$ (400 MHz, $CD_2Cl_2$) 7.78 – 7.87 (4H, m, *para*-phenyl), 7.55 – 7.65 (8H, m, phenyl), 7.43 – 7.55 (8H, m, phenyl), 7.18 – 7.30 (3H, m, $CH_2CH_2$Ph), 7.03 – 7.09 (2H, m, $CH_2CH_2$Ph), 5.01 – 5.11 (1H, m, NH), 2.80 – 2.89 (2H, m, (PPh$_2$)N-C$H_2$), 2.75 (3H, d, $J$ = 11.5 Hz, OMe), 2.63 – 2.69 (2H, m, PhC$H_2$); $\delta_P$ $^{31}P\{^1H\}$ (162 MHz, $CD_2Cl_2$) 111.9 (0.19 P, s, [(MeOPPh$_2$)$_2$PdCl$_2$]), 108.8 (1 P, d, $^2J_{PP}$ = 30.0 Hz, [(Ph(CH$_2$)$_2$NHPPh$_2$)(MeOPPh$_2$)PdCl$_2$]), 58.1 (1P, d, $^2J_{PP}$ = 30.0 Hz, [(Ph(CH$_2$)$_2$NHPPh$_2$)(MeOPPh$_2$)PdCl$_2$]). *NB* due to the presence of a notable amount of [(MeOPPh$_2$)$_2$PdCl$_2$]) and other irremovable trace impurities, a reliable CHN and FT-IR analysis could not be obtained, and the percentage yield has been calculated assuming all the mass of the isolated product is due to complex **3.23**.

## 7.10 Synthesis of [N(*n*-Pr)$_4$][({Cl$_3$Co}Py-*o*-(CH$_2$)$_2$N(PPh$_2$)$_2$)PdCl$_2$] (3.25)

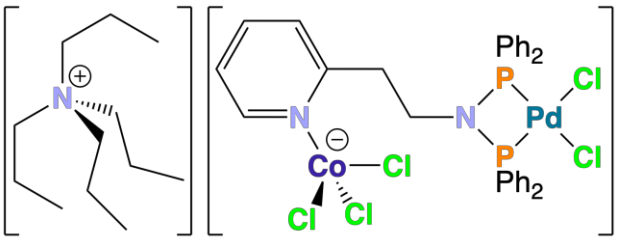

**3.25**

**Synthesis of [N(*n*-Pr)$_4$][({Cl$_3$Co}Py-*o*-(CH$_2$)$_2$N(PPh$_2$)$_2$)PdCl$_2$] (3.25):** [(Py-*o*-(CH$_2$)$_2$N(PPh$_2$)$_2$)PdCl$_2$] (**3.8**, 0.257 g, 0.385 mmol) was dissolved in DCM (15 mL) and added *via* cannula transfer a Schlenk containing CoCl$_2$ (0.05 g, 0.385 mmol) and [N(*n*-Pr)$_4$]Cl (0.085 g, 0.385 mmol), with the resulting reaction mixture being stirred

overnight. The reaction mixture was filtered, concentrated to approx. 5 mL, layered with hexane, filtered after standing for 2 days and dried *in vacuo*, affording complex **3.25** as a green powder (0.219 g, 0.215 mmol, 56%); $\mu_{eff}$ ($CD_2Cl_2$, 294 K) = 4.04 $\mu_B$; $\delta_P$ $^{31}P\{^1H\}$ (162 MHz, $CD_2Cl_2$) 30.0 (2P, s); selected $\nu_{max}$ / $cm^{-1}$ 3055 (aromatic C-H stretch), 2971 (C-H stretch), 1605, 1478 (aromatic C=C), 1585, 1570 (C=N), 1435 (P-Ph), 1099 (C-N), 839 (P-N-P); Anal. calc. for $C_{43}H_{56}Cl_5CoN_3P_2Pd$ (1019.49) (%): C, 50.66; H, 5.54; N, 4.12 Found (%): C, 50.65; H, 5.41; N, 4.28; MS (ESI): positive ion *m/z* 186.3 (88.40% $[NEt_4]^+$), 631.5 (100.00% $[M\text{-}CoCl_3\text{-}Cl\text{-}NEt_4]^+$).

Single crystals of complex **3.25** were obtained following diffusion of a saturated acetone solution of **3.25** layered with hexane.

## 7.11 Synthesis of $[(Py\text{-}o\text{-}(CH_2)_2N(PPh_2)(Me))PdCl_2]$ (3.29) and $[(Py\text{-}o\text{-}(CH_2)_2N(P\{OPh\}_2)(Me))PdCl_2]$ (3.30)

Note that complexes **3.29** and **3.30** are too insoluble in common organic solvents to allow for $^{13}C$ NMR spectra to be obtained (solvents tried: $CD_2Cl_2$, $CDCl_3$ and $d_8$-THF).

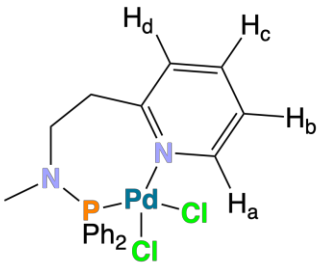


**3.29**

**Synthesis of $[(Py\text{-}o\text{-}(CH_2)_2N(PPh_2)(Me))PdCl_2]$ (3.29):** Py-*o*-$(CH_2)_2N(PPh_2)(Me)$ (**2.11**, 0.123 g, 0.385 mmol) and $[(MeCN)_2PdCl_2]$ (0.100 g, 0.385 mmol) were dissolved in DCM (15 mL) and stirred overnight. The solution was concentrated to 10 mL, layered with $Et_2O$ (20 mL) and left standing overnight to gain complex **3.29** (0.141 g, 0.283 mmol, 74%) as yellow single crystals suitable for XRD analysis. The product was isolated by filtration and dried *in vacuo*; $\delta_H$ (400 MHz, $CD_2Cl_2$) 8.80 (1H, d, *J* = 5.96 Hz, $H_a$), 7.87 – 8.04 (3H, m, phenyl + pyridyl), 7.47 – 7.68 (9H, m, phenyl + pyridyl), 7.35 – 7.42 (1H, m, phenyl or pyridyl), 4.81 (1H, tdd, *J* = 1.80 Hz, 6.33 Hz, 13.8 Hz, Py-C<u>H</u>--Pd), 3.38 (1H, ddd, *J* = 1.32 Hz, 5.50 Hz, 14.2 Hz, alkyl-CH), 2.91 – 3.16 (2H, m, $CH_2$), 2.07 (3H, d, *J* = 9.71 Hz, Me); $\delta_P$ $^{31}P\{^1H\}$ (162 MHz, $CD_2Cl_2$) 59.7 (2P, s); selected $\nu_{max}$ / $cm^{-1}$ 3051 (aromatic C-H stretch), 2958 (C-H stretch), 1604, 1483 (aromatic C=C), 1569 (C=N), 1436 (P-Ph), 1095

(C-N); Anal. calc. for $C_{20}H_{21}Cl_2N_2PPd$ (497.70) (%): C, 48.27; H, 4.25; N, 5.63 Found (%): C, 45.82; H, 4.18; N, 5.85; MS (ESI): positive ion *m/z* 430.1 (100.0% $[M\text{-}2Cl+4H]^+$).

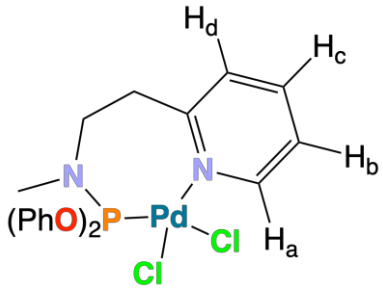


**3.30**

**Synthesis of [(Py-*o*-$(CH_2)_2$N(P{OPh}$_2$)(Me))$PdCl_2$] (3.30):** Complex **3.30** was afforded by the same synthetic method outlined for complex **3.29**, using Py-*o*-$(CH_2)_2$N(P{OPh}$_2$)(Me) (compound **2.12**, 0.136 g, 0.385 mmol), affording complex **3.30** as (0.136 g, 0.26 mmol, 67%) as yellow single crystals suitable for XRD analysis; $\delta_H$ (400 MHz, $CDCl_3$) 9.11 (1H, d, *J* = 5.70 Hz, $H_a$), 7.60 – 7.78 (3H, m, phenyl + pyridyl), 7.21 – 7.46 (9H, m, phenyl + pyridyl), 6.98 – 7.04 (1H, m, phenyl or pyridyl), 4.71 (1H, tdd, *J* = 1.90 Hz, 5.23 Hz, 14.2 Hz, Py-CH--Pd), 3.40 – 3.47 (1H, m, alkyl-CH), 3.19 – 3.30 (1H, m, alkyl-CH), 2.93 – 3.17 (1H, m, alkyl-CH), 2.72 (3H, d, *J* = 7.81 Hz, Me); $\delta_P$ $^{31}P\{^1H\}$ (162 MHz, $CDCl_3$) 83.8 (2P, s); selected $\nu_{max}$ / $cm^{-1}$ 3066 (aromatic C-H stretch), 2961 (C-H stretch), 1608, 1483 (aromatic C=C), 1585 (C=N), 1426 (P-Ph), 1102 (C-N); Anal. calc. for $C_{20}H_{21}Cl_2N_2O_2PPd$ (529.69) (%): C, 45.35; H, 4.00; N, 5.29 Found (%): C, 44.32; H, 3.99; N, 5.45; MS (ESI): positive ion *m/z* 137.1 (100.0% $[M\text{-}P(OPh)_2PdCl_2+2H]^+$), 353.5 (21.0% $[M\text{-}PdCl_2+H]^+$).

## 7.12 Synthesis of [CoBr(*n*-BuN{$PPh_2$}$_2$)$_2$]$_2$[$Co_2Br_6$] (4.1), [CoBr(Py-*m*-$CH_2$N{$PPh_2$}$_2$)$_2$]$_2$[$Co_2Br_6$] (4.2), [CoBr(Ph-$C_6H_4$N{$PPh_2$}$_2$)$_2$]$_2$[$Co_2Br_6$] (4.3), [CoBr(Py-*o*-$C_6H_4$N{$PPh_2$}$_2$)$_2$]$_2$[$Co_2Br_6$] (4.4), [CoBr($Me_2$N($CH_2$)$_3$N{$PPh_2$}$_2$)({$Br_3$Co}$Me_2$N($CH_2$)$_3$N{$PPh_2$}$_2$)] (4.5), [(Py-*o*-($CH_2$)$_2$N($CH_2PPh_2$)$_2$)$CoBr_2$] (4.6), [CoX(Py-*o*-($CH_2$)$_2$N{$PPh_2$}$_2$)({$X_3$Co}Py-*o*-($CH_2$)$_2$N{$PPh_2$}$_2$)] (4.7, X = Cl; 4.8, X = I) and [CoX(Ph($CH_2$)$_2$N{$PPh_2$}$_2$)$_2$]$_2$[$Co_2X_6$] (4.9, X = Cl; 4.10, X = Br; 4.11, X = I)

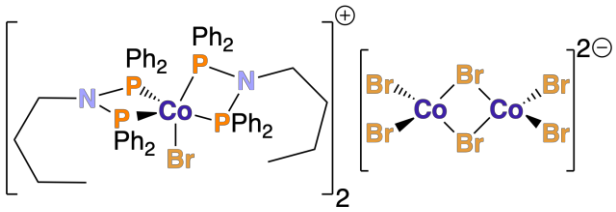

**4.1**

**Synthesis of [CoBr(*n*-BuN{$PPh_2$}$_2$)$_2$]$_2$[$Co_2Br_6$] (4.1):** $CoBr_2$ (0.109 g, 0.5 mmol) and *n*-BuN($PPh_2$)$_2$ (**2.3**, 0.221 g, 0.5 mmol) were dissolved in THF (~15 mL) and the resultant solution was stirred overnight. The solvent was removed *in vacuo*, the crude residue washed with hexane (2 × 10 mL) and $Et_2O$ (2 × 10 mL) and the product dried *in vacuo*, affording complex **4.1** as a black solid (0.252 g, 0.1 mmol, 76%); $\mu_{eff}$ ($CD_2Cl_2$, 294 K) = 7.02 $\mu_B$; selected $\nu_{max}$ / $cm^{-1}$ 3053 (aromatic C-H stretch), 2958 (C-H stretch), 1606, 1481 (aromatic C=C), 1461, 1379 ($CH_3$ bend), 1433 (P-Ph), 1089 (C-N), 857 (P-N-P); Anal. calc. for $C_{112}H_{116}Br_8Co_4N_4P_8$ (2640.94) (%): C, 50.94; H, 4.43; N, 2.12 Found (%): C, 50.00; H, 4.52; N, 1.97; MS (ESI): positive ion *m/z* 471.3 (100.00% [$CH_3(CH_2)_3N(OPPh_2)_2$-2H]$^+$), 1021.4 (20.26% [CoBr{$CH_3(CH_2)_3N(PPh_2)_2$}$_2$]$^+$); negative ion *m/z* 297.8 (100% [$Co_2Br_6$]$^{2-}$).

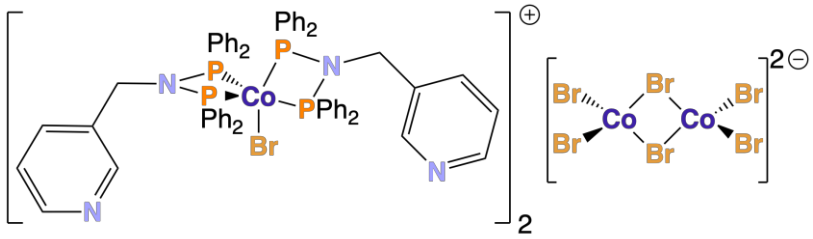

**4.2**

**Synthesis of [CoBr(Py-*m*-$CH_2$N{$PPh_2$}$_2$)$_2$]$_2$[$Co_2Br_6$] (4.2):** Complex **4.2** was synthesised following the same method as that outlined for the preparation of complex **4.1**, using Py-*m*-$CH_2$N{$PPh_2$}$_2$ (**2.5**, 0.237 g, 0.5 mmol), affording complex **4.2** as a green solid (0.202 g, 0.0726 mmol, 58%); selected $\nu_{max}$ / $cm^{-1}$ 3053 (aromatic C-H stretch),

2981 (C-H stretch), 1605, 1480 (aromatic C=C), 1585, 1571 (C=N), 1433 (P-Ph), 1091 (C-N), 860 (P-N-P); Anal. calc. for $C_{120}H_{104}Br_8Co_4N_8P_8$ (2780.96) (%): C, 51.83; H, 3.77; N, 4.03 Found (%): C, 51.63; H, 4.03; N, 4.15; MS (ESI): positive ion *m/z* 506.2 (100.00% $[C_5H_4NCH_2N(OPPh_2)_2)\text{-}2H]^+$), 1092.3 (54.33% $[CoBr\{C_5H_4NCH_2N(PPh_2)_2\}_2]^+$); negative ion *m/z* 297.7 (100.00% $[Co_2Br_6]^{2-}$). Magnetic moment not determined due to solubility issues.

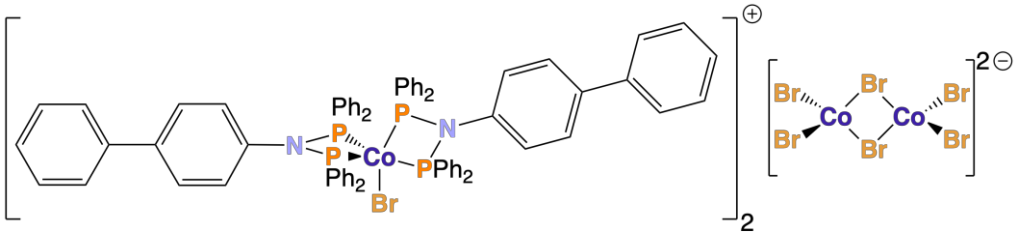

**4.3**

**Synthesis of $[CoBr(Ph\text{-}C_6H_4N\{PPh_2\}_2)_2]_2[Co_2Br_6]$ (4.3):** $CoBr_2$ (0.109 g, 0.5 mmol) and $Ph\text{-}C_6H_4N(PPh_2)_2$ (**2.6**, 0.269 g, 0.5 mmol) were dissolved in THF (~15 mL) and the resultant solution was stirred overnight. The solvent was removed *in vacuo*, the crude product being washed with hexane (2 × 10 mL) and $Et_2O$ (2 × 10 mL) and dried *in vacuo*, affording complex **4.3** as a dark brown solid (0.203 g, 0.07 mmol, 54%); $\mu_{eff}$ ($CD_2Cl_2$, 294 K) = 6.93 $\mu_B$; selected $\nu_{max}$ / $cm^{-1}$ 3050 (aromatic C-H stretch), 1605, 1482 (aromatic C=C), 1433 (P-Ph), 1091 (C-N), 829 (P-N-P); Anal. calc. for $C_{144}H_{116}Br_8Co_4N_4P_8$ (3025.28) (%): C, 57.17; H, 3.87; N, 1.85 Found (%): C, 58.26; H, 4.29; N, 1.64; MS (ESI): positive ion *m/z* 1212.4 (100.00% $[C_{72}H_{58}BrCoN_2P_4]^+$); negative ion *m/z* 297.8 (100.00% $[Co_2Br_6]^{2-}$).

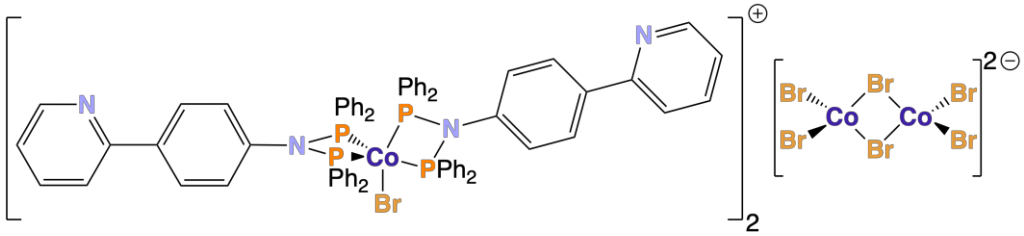

**4.4**

**Synthesis of $[CoBr(Py\text{-}o\text{-}C_6H_4N\{PPh_2\}_2)_2]_2[Co_2Br_6]$ (4.4):** $CoBr_2$ (0.109 g, 0.5 mmol) and $Py\text{-}o\text{-}C_6H_4N(PPh_2)_2$ (**2.7**, 0.269 g, 0.5 mmol) were dissolved in THF (~15 mL) and the resultant solution was stirred overnight. The solvent was removed *in vacuo*, then the crude product washed with hexane (2 × 10 mL) and $Et_2O$ (2 × 10 mL) and dried *in vacuo*, affording complex **4.4** as a dark brown solid (0.100 g, 0.03 mmol, 26%); $\mu_{eff}$ ($CD_2Cl_2$, 294 K) = 7.11 $\mu_B$; selected $\nu_{max}$ / $cm^{-1}$ 3049 (aromatic C-H stretch), 1605, 1474 (aromatic C=C), 1585, 1571 (C=N), 1433 (P-Ph), 1090 (C-N), 828 (P-N-P); Anal. calc. for $C_{140}H_{112}Br_8Co_4N_8P_8$

(3029.25) (%): C, 55.51; H, 3.73; N, 3.70 Found (%): C, 55.21; H, 4.11; N, 3.67; MS (ESI): positive ion *m/z* 1216.3 (13.65% $[C_{70}H_{56}BrCoN_4P_4]^+$); negative ion *m/z* 297.8 (100.00% $[Co_2Br_6]^{2-}$).

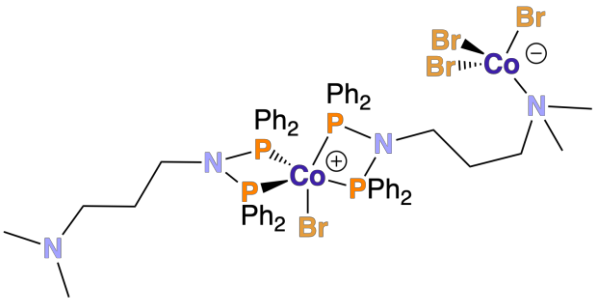


**4.5**

**Synthesis of [CoBr(Me$_2$N(CH$_2$)$_3$N{PPh$_2$}$_2$)({Br$_3$Co}Me$_2$N(CH$_2$)$_3$N{PPh$_2$}$_2$)] (4.5):** $CoBr_2$ (0.109 g, 0.5 mmol) and $NMe_2(CH_2)_3N(PPh_2)_2$ (**2.4**, 0.235 g, 0.5 mmol) were dissolved in THF (~15 mL) and the resultant solution was stirred overnight. A brown precipitate formed, which was isolated by filtration and dried *in vacuo*, affording complex **4.5** as a dark brown solid (0.207 g, 0.15 mmol, 60%); $\mu_{eff}$ ($CD_2Cl_2$, 294 K) = 5.16 $\mu_B$; selected $\nu_{max}$ / $cm^{-1}$ 3056 (aromatic C-H stretch), 2971 (C-H stretch), 1605, 1480 (aromatic C=C), 1433 (P-Ph), 1091 (C-N), 851 (P-N-P); Anal. calc. for $C_{58}H_{64}Br_4Co_2N_4P_4$ (1378.56) (%): C, 50.53; H, 4.68; N, 4.06 Found (%): C, 50.11; H, 5.00; N, 4.24; MS (ESI): positive ion *m/z* 500.2 (100.00% $[((CH_3)_2N(CH_2)_3N(OPPh_2)_2)\text{-}2H]^+$), 1080.4 (22.75% $[CoBr\{(CH_3)_2N(CH_2)_3N(PPh_2)_2\}_2]^+$); negative ion *m/z* 297.8 (33.24% $[CoBr_3]^-$).

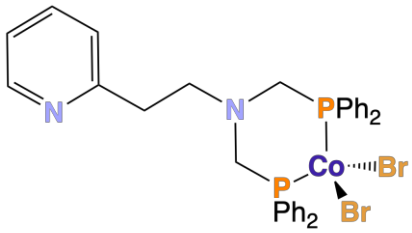


**4.6**

**Synthesis of [(Py-*o*-(CH$_2$)$_2$N(CH$_2$PPh$_2$)$_2$)CoBr$_2$] (4.6):** $CoBr_2$ (0.113 g, 0.52 mmol) and Py-*o*-$(CH_2)_2N(CH_2PPh_2)_2$ (**2.8**, 0.268 g, 0.52 mmol) were dissolved in DCM (~15 mL) and the resultant solution was stirred overnight. The solution was concentrated to approx. 5 mL and layered with hexane (15 mL), which afforded the product as crystals after approx. 18 hours, which were isolated by filtration and dried *in vacuo*, gaining a dark green solid (0.225 g, 0.31 mmol, 59%); $\mu_{eff}$ ($CD_2Cl_2$, 294 K) = 3.61 $\mu_B$; selected $\nu_{max}$ / $cm^{-1}$ 3051 (aromatic C-H stretch), 2978 (C-H stretch), 1605, 1482 (aromatic C=C), 1588, 1568 (C=N), 1433 (P-Ph), 1093 (C-N); Anal. calc. for $C_{33}H_{32}Br_2N_2P_2Co$ (737.32) (%): C, 53.76; H,

4.37; N, 3.80 Found (%): C, 54.03; H, 4.42; N, 3.67; MS (ESI): positive ion *m/z* 333.3 (98.56% $[M\text{-}PPh_2CoBr_2]^+$), 656.3 (8.62% $[M\text{-}Br]^+$).

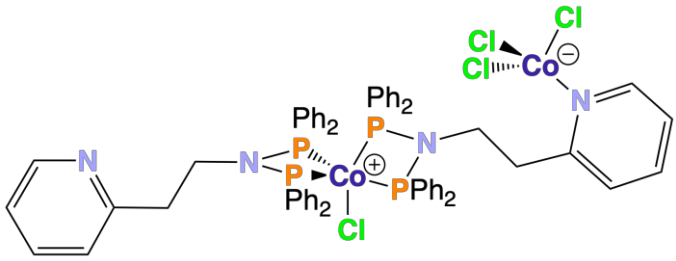

**4.7**

**Synthesis of [CoCl(Py-*o*-$(CH_2)_2$N{$PPh_2$}$_2$)({$Cl_3Co$}Py-*o*-$(CH_2)_2$N{$PPh_2$}$_2$)] (4.7):** $CoCl_2$ (0.065 g, 0.5 mmol) and Py-*o*-$(CH_2)_2$N{$PPh_2$}$_2$ (**2.1**, 0.245 g, 0.5 mmol) were dissolved in THF (~15 mL) and the resultant solution was stirred overnight. A dark green precipitate formed, which was isolated by filtration and dried *in vacuo*, gaining complex **4.7** as a green solid (0.171 g, 0.14 mmol, 55%); $\mu_{eff}$ ($CD_2Cl_2$, 294 K) = 5.19 $\mu_B$; selected $\nu_{max}$ / $cm^{-1}$ 3056 (aromatic C-H stretch), 2973 (C-H stretch), 1604, 1481 (C=C), 1588, 1569 (C=N), 1434 (P-Ph), 834 (P-N-P); Anal. calc. for $C_{62}H_{56}Cl_4Co_2N_4P_4$ (1240.72) (%): C, 60.02; H, 4.55; N, 4.55 Found (%): C, 59.93; H, 4.68; N, 4.29; MS (ESI): positive ion *m/z* 520.2 (100.00% $[M\text{-}Co_2Cl_4C_{31}H_{30}N_2P_2\text{+}O_2]^+$), 1074.4 (27.55% $[M\text{-}CoCl_3]^+$); negative ion *m/z* 163.9 (100.00% $[CoCl_3]^-$).

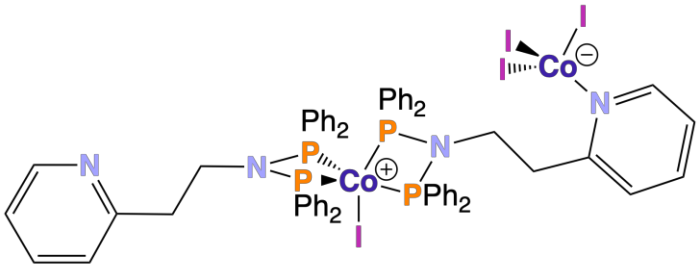

**4.8**

**Synthesis of [CoI(Py-*o*-$(CH_2)_2$N{$PPh_2$}$_2$)({$I_3Co$}Py-*o*-$(CH_2)_2$N{$PPh_2$}$_2$)] (4.8):** $CoI_2$ (0.156 g, 0.5 mmol) and Py-*o*-$(CH_2)_2$N{$PPh_2$}$_2$ (**2.1**, 0.245 g, 0.5 mmol) were dissolved in THF (~15 mL) and the resultant solution was stirred overnight. A maroon precipitate formed, which was isolated by filtration and dried *in vacuo*, gaining complex **4.8** as a red solid (0.251 g, 0.16 mmol, 62%); $\mu_{eff}$ ($CD_2Cl_2$, 294 K) = 4.80 $\mu_B$; selected $\nu_{max}$ / $cm^{-1}$ 3053 (aromatic C-H stretch), 2970 (C-H stretch), 1603, 1480 (C=C), 1587, 1569 (C=N), 1433 (P-Ph), 835 (P-N-P); Anal. calc. for $C_{62}H_{56}Co_2I_4N_4P_4$ (1606.54) (%): C, 46.35; H, 3.51; N, 3.49 Found (%): C, 46.81; H, 3.12; N, 4.25; MS (ESI): positive ion *m/z* 520.2 (100.00% [M-

$Co_2I_4C_{31}H_{30}N_2P_2+O_2]^+$), 1166.3 (56.07% $[M\text{-}CoI_3]^+$); negative ion *m/z* 439.8 (56.47% $[CoI_3]^-$).

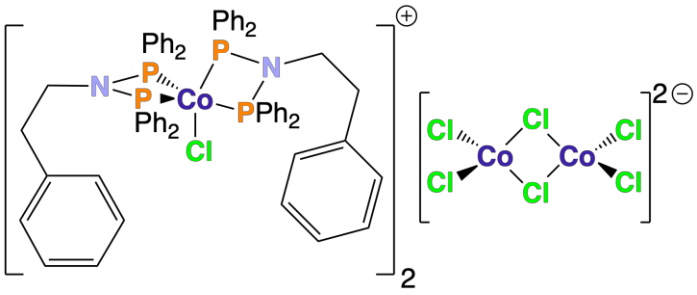

**4.9**

**Synthesis of $[CoCl(Ph(CH_2)_2N\{PPh_2\}_2)_2]_2[Co_2Cl_6]$ (4.9):** $CoCl_2$ (0.065 g, 0.5 mmol) and $Ph(CH_2)_2N\{PPh_2\}_2$ (**2.2**, 0.245 g, 0.5 mmol) were dissolved in THF (~15 mL) and the resultant solution was stirred overnight. A brown precipitate formed, which was isolated by filtration and dried *in vacuo*, gaining complex **4.9** as a brown solid (0.259 g, 0.10 mmol, 84%); $\mu_{eff}$ ($CD_2Cl_2$, 294 K) = 7.07 $\mu_B$; selected $\nu_{max}$ / $cm^{-1}$ 3056 (aromatic C-H stretch), 2981 (C-H stretch), 1602, 1480 (aromatic C=C), 1433 (P-Ph), 1090 (C-N), 831 (P-N-P); Anal. calc. for $C_{128}H_{116}Cl_8Co_4N_4P_8$ (2477.49) (%): C, 62.06; H, 4.72; N, 2.26 Found (%): C, 62.33; H, 4.39; N, 2.48; MS (ESI): positive ion *m/z* 1072.3 (100.00% $[CoCl\{Ph(CH_2)_2N(PPh_2)_2\}_2]^+$); negative ion *m/z* 163.9 (100.00% $[Co_2Cl_6]^{2-}$).

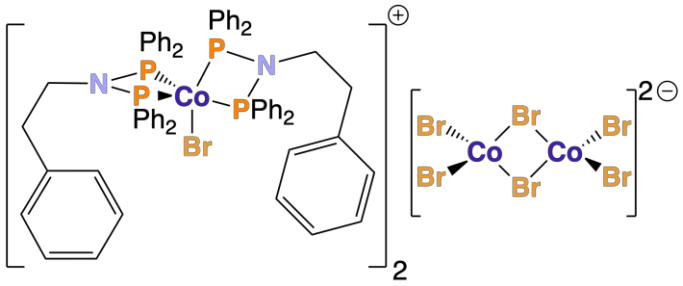

**4.10**

**Synthesis of $[CoBr(Ph(CH_2)_2N\{PPh_2\}_2)_2]_2[Co_2Br_6]$ (4.10):** $CoBr_2$ (0.109 g, 0.5 mmol) and $Ph(CH_2)_2N\{PPh_2\}_2$ (**2.2**, 0.245 g, 0.5 mmol) were dissolved in THF (~15 mL) and the resultant solution was stirred overnight. A green precipitate formed, which was isolated by filtration and dried *in vacuo*, gaining complex **4.10** as a green solid (0.080 g, 0.03 mmol, 23%); $\mu_{eff}$ ($CD_2Cl_2$, 294 K) = 6.82 $\mu_B$; selected $\nu_{max}$ / $cm^{-1}$ 3055 (aromatic C-H stretch), 2981 (C-H stretch), 1604, 1481 (aromatic C=C), 1433 (P-Ph), 1089 (C-N), 823 (P-N-P); Anal. calc. for $C_{128}H_{116}Br_8Co_4N_4P_8$ (2823.79) (%): C, 54.27; H, 4.13; N, 1.98 Found (%): C, 54.29; H, 4.34; N, 2.12; MS (ESI): positive ion *m/z* 519.3 (100.00%

[$Ph(CH_2)_2N(OPPh_2)_2$-2H]$^+$), 1116.4 (47.60% [$CoBr\{Ph(CH_2)_2N(PPh_2)_2\}_2$]$^+$); negative ion *m/z* 297.7 (100.00% $[Co_2Br_6]^{2-}$).

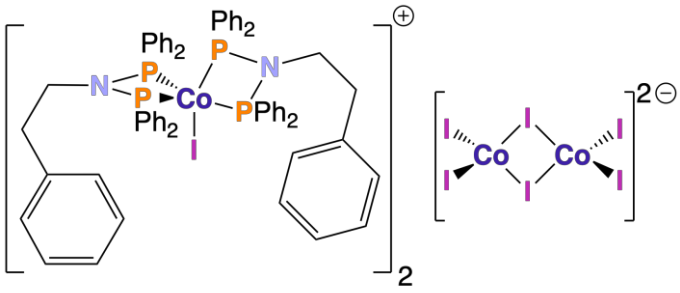

**4.11**

**Synthesis of [$CoI(Ph(CH_2)_2N\{PPh_2\}_2)_2$]$_2$[$Co_2I_6$] (4.11):** $CoI_2$ (0.156 g, 0.5 mmol) and $Ph(CH_2)_2N\{PPh_2\}_2$ (**2.2**, 0.245 g, 0.5 mmol) were dissolved in THF (~15 mL) and the resultant solution was stirred overnight. A red precipitate formed, which was isolated by filtration and dried *in vacuo*, gaining complex **4.11** as a red solid (0.178 g, 0.06 mmol, 44%); $\mu_{eff}$ ($CD_2Cl_2$, 294 K) = 6.89 $\mu_B$; selected $\nu_{max}$ / $cm^{-1}$ 3053 (aromatic C-H stretch), 2980 (C-H stretch), 1602, 1480 (aromatic C=C), 1433 (P-Ph), 1088 (C-N), 825 (P-N-P); Anal. calc. for $C_{128}H_{116}Co_4I_8N_4P_8$ (3209.12) (%): C, 47.91; H, 3.64; N, 1.75 Found (%): C, 48.17; H, 3.60; N, 2.23; MS (ESI): positive ion *m/z* 519.2 (72.41% [$Ph(CH_2)_2N(OPPh_2)_2$-2H]$^+$), 1164.7 (100.00% [$CoI\{Ph(CH_2)_2N(PPh_2)_2\}_2$]$^+$); negative ion *m/z* 439.0 (1.41% $[Co_2I_6]^{2-}$).

Single crystals suitable for XRD analysis of compounds **4.1**, **4.5** and **4.7** – **4.11** were gained by dissolving a sample of the respective compound in DCM and layering this with hexane.

## 7.13 Attempted Synthesis of Complex [N(*n*-Pr)$_4$]$_2$[$Co_2Br_6$] (4.12)

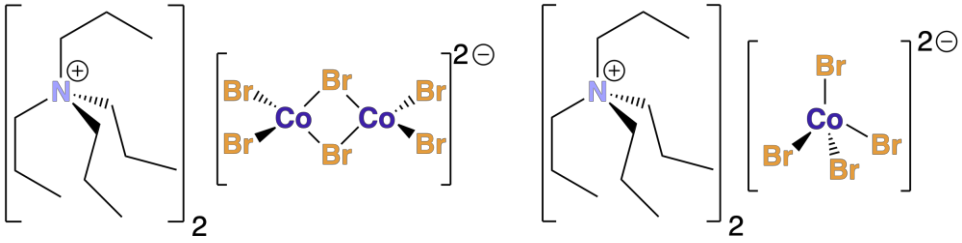

**4.12** **4.13**

**Attempted synthesis of [N(*n*-Pr)$_4$]$_2$[$Co_2Br_6$] (4.12):** [N(*n*-Pr)$_4$]Br (0.329 g, 1.24 mmol, which had been heated at 110 °C under vacuum for approx. 15 hours) and $CoBr_2$ (0.271 g, 1.24 mmol) were dissolved in DCM and stirred overnight. A blue-green precipitate formed, which was isolated by filtration and dried *in vacuo*, providing complex **4.13** and

one unreacted equivalent of $CoBr_2$ as a blue green solid. Single crystals suitable for XRD analysis of $[N(n\text{-}Pr)_4]_2[CoBr_4]$ (complex **4.13**) were grown by dissolving a sample in $H_2O$ and allowing the solvent to slowly evaporate; Anal. calc. for $C_{24}H_{56}Br_4CoN_2$ + $CoBr_2$ (970.02) (%): C, 29.72; H, 5.82; N, 2.89 Found (%): C, 29.83; H, 5.44; N, 1.17.

## 7.14 Synthesis of Complex $[N(n\text{-}Pr)_4][PyCoBr_3]$ (4.14)

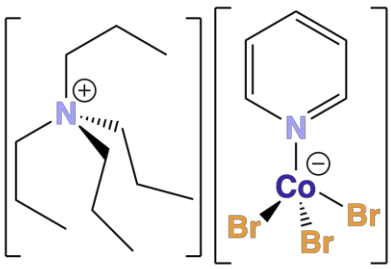


**4.14**

**Synthesis of $[N(n\text{-}Pr)_4][PyCoBr_3]$ (4.14):** $[N(n\text{-}Pr)_4]Br$ (0.329 g, 1.24 mmol, which had been heated at 110 °C under vacuum for approx. 15 hours), $CoBr_2$ (0.271 g, 1.24 mmol) and pyridine (0.1 mL, 1.24 mmol) were dissolved in DCM, forming a deep blue solution which was stirred overnight. The reaction mixture was concentrated to approx. 5 mL and layered with hexane (15 mL), gaining a blue solid which was isolated by filtration and dried *in vacuo*, affording complex **4.14** as a blue powder (0.607 g, 1.07 mmol, 87%); $\mu_{eff}$ ($CD_2Cl_2$, 294 K) = 4.04 $\mu_B$; selected $\nu_{max}$ / $cm^{-1}$ 3055 (aromatic C-H stretch), 2981 (C-H stretch), 1605, 1485 (aromatic C=C), 1587, 1570 (C=N), 1093 (C-N); Anal. calc. for $C_{17}H_{33}Br_3CoN_2$ (564.11) (%): C, 36.20; H, 5.90; N, 4.97 Found (%): C, 36.11; H, 5.60; N, 4.97; MS (ESI): positive ion *m/z* 186.3 (100.00% $[N(n\text{-}Pr)_4]^+$); negative ion *m/z* 297.8 (100.00% $[CoBr_3]^-$).

Single crystals suitable for XRD analysis were obtained by dissolving a sample in DCM and layering it with hexane.

## 7.15 Synthesis of Complex $[PPN]_2[Co_2Cl_6]$ (4.15)

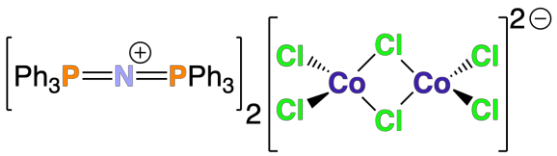

**4.15**

**Synthesis of $[PPN]_2[Co_2Cl_6]$ (4.15):** [PPN]Cl (0.574 g, 1 mmol) and $CoCl_2$ (0.130 g, 1 mmol) were dissolved in DCM (15 mL) and stirred overnight. The reaction mixture was concentrated to approx. 5 mL and layered with hexane (15 mL), affording complex **4.15** as blue crystals, which were isolated by filtration and dried *in vacuo*, suitable for XRD analysis (0.510 g, 0.36 mmol, 72%); $\delta_H$ (400 MHz, $CD_2Cl_2$) 7.30 (12H, s, br, $\nu_{1/2}$ ~17 Hz, *para*-phenyl), 7.00 – 7.18 (48H, m, *ortho*- + *meta*-phenyl); $\delta_P$ $^{31}P\{^1H\}$ (162 MHz, $CD_2Cl_2$) 21.0 (4P, $[Ph_3\underline{P}{=}N{=}\underline{P}Ph_3]^+$); $\delta_C$ (100.57 MHz, $CD_2Cl_2$) 134.6 (s, aryl-C), 132.6 (t, $J$ = 5.5 Hz, aryl-C), 130.5 (s, aryl-C), 130.4 (d, $J$ = 6.7 Hz, aryl-C); $\mu_{eff}$ ($CD_2Cl_2$, 294 K) = 5.47 $\mu_B$; selected $\nu_{max}$ / $cm^{-1}$ 3056 (aromatic C-H stretch), 1587, 1481 (aromatic C=C), 1437 (P-Ph); Anal. calc. for $C_{72}H_{60}Cl_6Co_2N_2P_4$ (1407.75) (%): C, 61.43; H, 4.30; N, 1.99 Found (%): C, 63.72; H, 4.02; N, 2.28; MS (ESI): positive ion *m/z* 538.3 (100.00% $[PPN]^+$); negative ion *m/z* 163.9 (100.00% $[Co_2Cl_6]^{2-}$). IR data are consistent with the literature, NMR data previously unobtained.[13]

## 7.16 Synthesis of Complex $[PPN]_2[Cl_3Co\text{-}PPh_2CH_2CH_2PPh_2\text{-}CoCl_3]$ (4.16)

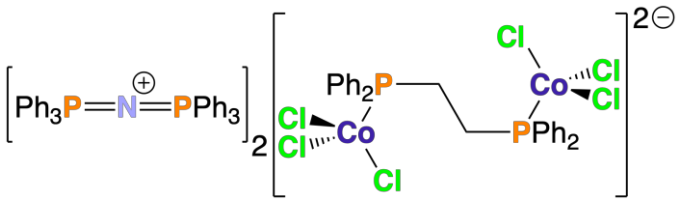

**4.16**

**Synthesis of $[PPN]_2[Cl_3Co\text{-}PPh_2CH_2CH_2PPh_2\text{-}CoCl_3]$ (4.16):** $[PPN]_2[Co_2Cl_6]$ (0.05 g, 0.0355 mmol) and dppe (0.014 g, 0.0355 mmol) were dissolved in DCM (15 mL) and stirred overnight. The reaction mixture was concentrated to approx. 5 mL and layered with hexane (15 mL), affording the product as crystals which were isolated by filtration and dried *in vacuo*, affording complex **4.16** as blue crystals suitable for XRD analysis (0.036 g, 0.0199 mmol, 56%); $\delta_P$ $^{31}P\{^1H\}$ (162 MHz, $CD_2Cl_2$) 21.4 (4P, $[Ph_3\underline{P}{=}N{=}\underline{P}Ph_3]^+$); $\delta_C$

(100.57 MHz, $CD_2Cl_2$) 135.1 (s, PPN aryl-C), 133.0 (t, *J* = 5.5 Hz, PPN aryl-C), 130.8 (s, PPN aryl-C), 130.7 (d, *J* = 6.5 Hz, PPN aryl-C); $\mu_{eff}$ ($CD_2Cl_2$, 294 K) = 6.43 $\mu_B$; selected $\nu_{max}$ / $cm^{-1}$ 3052 (aromatic C-H stretch), 1587, 1482 (aromatic C=C), 1435 (P-Ph); Anal. calc. for $C_{72}H_{60}Cl_6Co_2N_2P_4$ (1806.17) (%): C, 65.17; H, 4.69; N, 1.55 Found (%): C, 63.80; H, 4.43; N, 1.78; MS (ESI): positive ion *m/z* 538.8 (100.00% $[PPN]^+$); negative ion *m/z* 163.8 (1.03% $[CoCl_3]^-$). *NB* signals associated with the dppe ligand are not observed in the $^{13}C$ NMR spectra, something that has been attributed to paramagnetism of the cobalt(II) centres.

## 7.17 Synthesis of $[CoBr(Ph(CH_2)_2N\{PPh_2\}_2)_2][PyCoBr_3]$ (4.19)

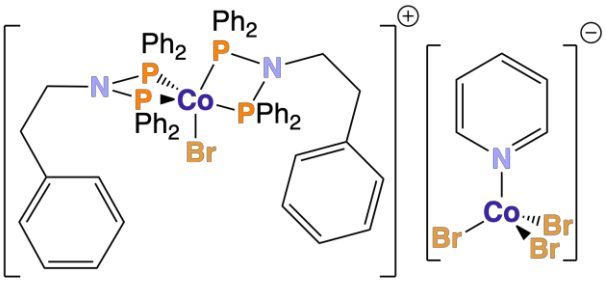


**4.19**

**DCM Route:** $CoBr_2$ (0.109 g, 0.5 mmol) and $Ph(CH_2)_2N\{PPh_2\}_2$ (**2.2**, 0.245 g, 0.5 mmol) were dissolved in DCM (10 mL) and stirred overnight. The reaction was filtered, pyridine (0.02 mL, 0.25 mmol) was added to the filtrate, and the resulting mixture was again stirred overnight. The solvent was removed *in vacuo*, the crude product washed with hexane (2 × 10 mL) and $Et_2O$ (2 × 10 mL) and dried *in vacuo*, affording complex **4.19** as a green solid (0.181 g, 0.121 mmol, 48%); $\mu_{eff}$ ($CD_2Cl_2$, 294 K) = 5.13 $\mu_B$; selected $\nu_{max}$ / $cm^{-1}$ 3053 (aromatic C-H stretch), 2981 (C-H stretch), 1604, 1481 (aromatic C=C), 1433 (P-Ph), 1087 (C-N), 864 (P-N-P); Anal. calc. for $C_{69}H_{63}Br_4Co_2N_3P_4$ (1495.66) (%): C, 55.41; H, 4.25; N, 2.81 Found (%): C, 55.72; H, 4.37; N, 3.06; MS (ESI): positive ion *m/z* 519.2 (100.00% $[Ph(CH_2)_2N(OPPh_2)_2\text{-}2H]^+$), 1116.3 (67.96% $[CoBr\{Ph(CH_2)_2N(PPh_2)_2\}_2]^+$); negative ion *m/z* 297.7 (100.00% $[CoBr_3]^-$).

**THF Route:** $CoBr_2$ (0.109 g, 0.5 mmol), $Ph(CH_2)_2N\{PPh_2\}_2$ (**2.2**, 0.245 g, 0.5 mmol) and pyridine (0.02 mL, 0.25 mmol) were dissolved in THF (10 mL) and stirred overnight. A green precipitate formed, which was isolated by filtration and dried *in vacuo*, affording complex **4.19** as a green solid (0.145 g, 0.097 mmol, 39%); selected $\nu_{max}$ / $cm^{-1}$ 3055

(aromatic C-H stretch), 2971 (C-H stretch), 1607, 1480 (aromatic C=C), 1433 (P-Ph), 1091 (C-N), 858 (P-N-P); Anal. calc. for $C_{69}H_{63}Br_4Co_2N_3P_4$ (1495.66) (%): C, 55.41; H, 4.25; N, 2.81 Found (%): C, 55.09; H, 4.07; N, 3.09; same MS and magnetic moment data as reported for DCM route.

## 7.18 Attempted Synthesis of $[CoX_2\{Py\text{-}o\text{-}(CH_2)_2N(PPh_2)_2\}_2][\{Py\text{-}o\text{-}(CH_2)_2NH_2\}CoX_3]$ (X = Cl, 4.20; X = Br, 4.21) and $[CoX_2\{Ph(CH_2)_2N(PPh_2)_2\}_2][\{Ph(CH_2)_2NH_2\}CoX_3]$ (X = Cl, 4.22; X = Br, 4.23)

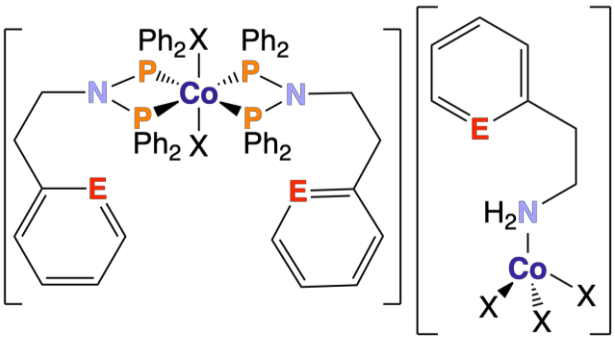


**4.20** {E = N} (X = Cl); **4.21** {E = N} (X = Br)
**4.22** {E = CH} (X = Cl); **4.23** {E = CH} (X = Br)

**Attempted synthesis of $[CoX_2\{Py\text{-}o\text{-}(CH_2)_2N(PPh_2)_2\}_2][\{Py\text{-}o\text{-}(CH_2)_2NH_2\}CoX_3]$ and $[CoX_2\{Ph(CH_2)_2N(PPh_2)_2\}_2][\{Ph(CH_2)_2NH_2\}CoX_3]$ (4.20 – 4.23):** Py-*o*-$(CH_2)_2N(PPh_2)_2$ or $Ph(CH_2)_2N(PPh_2)_2$ (compounds **2.1** or **2.2**, respectively, 0.245 g, 0.5 mmol) and $CoBr_2$ (0.055 g, 0.25 mmol) or $CoCl_2$ (0.032 g, 0.25 mmol) were dissolved in DCM (10 mL) and stirred overnight. The reaction mixture was concentrated to approx. 2 mL and stored at –18 °C for 3 days. After no crystals were produced, the reaction mixture was layered with hexane, affording crystals of one of $[CoCl(Py\text{-}o\text{-}(CH_2)_2N\{PPh_2\}_2)(\{Cl_3Co\}Py\text{-}o\text{-}(CH_2)_2N\{PPh_2\}_2)]$, $[CoBr(Py\text{-}o\text{-}(CH_2)_2N\{PPh_2\}_2)(\{Br_3Co\}Py\text{-}o\text{-}(CH_2)_2N\{PPh_2\}_2)]$, $[CoCl(Ph(CH_2)_2N\{PPh_2\}_2)_2]_2[Co_2Cl_6]$ or $[CoBr(Ph(CH_2)_2N\{PPh_2\}_2)_2]_2[Co_2Br_6]$ (complexes **4.7**, **2.14**, **4.9** and **4.10**, respectively) as confirmed by both XRD and mass spectroscopic analysis. At this point, the reactions were abandoned.

## 7.19 Synthesis of Complex [(MeHNCH$_2$CH$_2$*o*-Py)CoBr$_2$] (4.26)

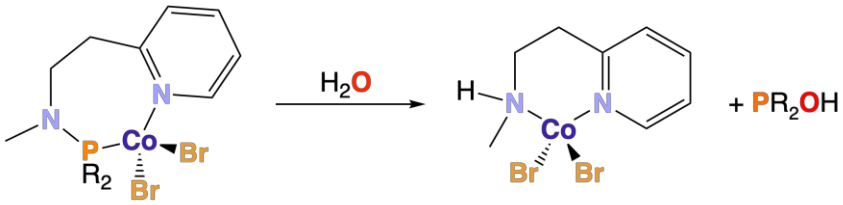


**4.24** (R = Ph)
**4.25** (R = OPh)

**4.26**

**Synthesis of [(MeHNCH$_2$CH$_2$*o*-Py)CoBr$_2$] (4.26):** Either Py-*o*-(CH$_2$)$_2$N(PPh$_2$)(Me) (compound **2.11**, 0.146 g, 0.46 mmol) or Py-*o*-(CH$_2$)$_2$N(P{OPh}$_2$)(Me) (**2.12**, 0.161 g, 0.46 mmol) was dissolved in THF (20 mL) alongside CoBr$_2$ (0.100 g, 0.46 mmol), and the reaction stirred overnight. The reaction mixture was concentrated (10 mL), and layered with hexane (20 mL), which upon standing overnight afforded single crystals suitable for XRD analysis of complex **4.26** (the hydrolysis product of complexes **4.24** and **4.25**); MS (ESI): positive *m/z* 137.2 (100.00% [PyCH$_2$CH$_2$NH$_2$Me]$^+$), 523.4 (62.67% [({Me}PPh$_2$NCH$_2$CH$_2$*o*-Py)CoBr$_2$-Me+H]$^+$). Due to the reaction outcome not changing upon repetition and changing solvent, *etc*., the reaction was abandoned.

## 7.20 Synthesis of [(Ph(CH$_2$)$_2$N(SPPh$_2$)(PPh$_2$))CoBr$_2$] (4.27)

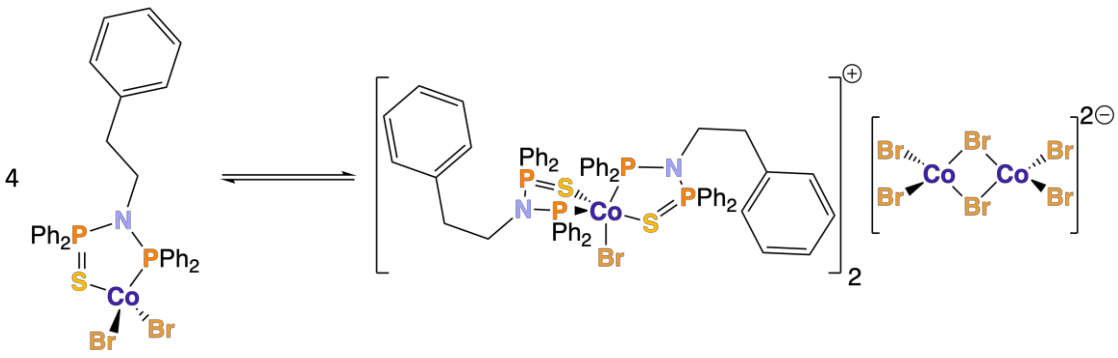

**4.27** **4.28**

**Synthesis of [(Ph(CH$_2$)$_2$N(SPPh$_2$)(PPh$_2$))CoBr$_2$] (4.27):** Ph(CH$_2$)$_2$N(SPPh$_2$)(PPh$_2$) (**2.9**; 0.200 g, 0.384 mmol) and CoBr$_2$ (0.084 g, 0.384 mmol) were dissolved in DCM (20 mL) and the reaction mixture stirred overnight. The reaction mixture was concentrated (10 mL), and layered with hexane (20 mL), which upon standing overnight afforded single crystals suitable for XRD analysis of complex **4.27** (0.186 g, 0.251 mmol, 65%). Since complex **4.27** is likely to be in equilibrium with [CoBr{Ph(CH$_2$)$_2$N(SPPh$_2$)(PPh$_2$)}$_2$]$_2$[Co$_2$Br$_6$]

(complex **4.28**), a reliable $\mu_{eff}$ could not be obtained; selected $\nu_{max}$ / $cm^{-1}$ 3055 (aromatic C-H stretch), 2981 (C-H stretch), 1603, 1481 (aromatic C=C), 1435 (P-Ph), 1097 (C-N), 871 (P-N-P) 689 (P=S); Anal. calc. for $C_{32}H_{29}Br_2CoNP_2S$ (740.34) (%): C, 51.92; H, 3.95; N, 1.89 Found (%): C, 51.64; H, 4.50; N, 1.99; MS (ESI): positive ion *m/z* 522.3 (25.59% $[Ph(CH_2)_2N(SPPh_2)(PPh_2)+H]^+$), 1118.30 (28.34% $[CoBr\{Ph(CH_2)_2N(PPh_2)_2\}_2]^+$), 1150.08 (49.30% $[CoBr\{Ph(CH_2)_2N(PPh_2)_2\}\{Ph(CH_2)_2N(SPPh_2)(PPh_2)\}]^+$), 1181.96 *m/z* (12.16% $[CoBr\{Ph(CH_2)_2N(SPPh_2)(PPh_2)\}_2]^+$); negative ion *m/z* 297.8 (100.00% $[Co_2Br_6]^{2-}$).

## 7.21 Attempted Reaction of $Ph(CH_2)_2N(SPPh_2)_2$ (2.10) with $CoBr_2$

**Attempted reaction of $Ph(CH_2)_2N(SPPh_2)_2$ (2.10) with $CoBr_2$:** $Ph(CH_2)_2N(SPPh_2)_2$ (**2.10**, 0.100 g, 0.183 mmol) and $CoBr_2$ (0.040 g, 0.183 mmol) were dissolved in DCM (20 mL) and the reaction mixture stirred overnight. The reaction mixture was filtered, and the solvent removed *in vacuo*. Since the obtained $^1H$ and $^{31}P\{^1H\}$ NMR spectra of the isolated product are essentially identical to those obtained for compound **2.10**, it was concluded that no reaction had taken place and hence the reaction was abandoned.

## 7.22 Measuring $\mu_{eff}$ *via* the Evans Method

**General Procedure 3:** A sample of a complex with a known concentration (for this work, typically 4 – 10 mg in 0.7 mL) was prepared in $CD_2Cl_2$ (or $d_8$-THF for samples which are known to or are predicted to react with $CD_2Cl_2$), and added to a Young's NMR tube containing a sealed capillary tube filled with the same deuterated solvent. A $^1H$ NMR spectrum (400 MHz) of the sample of a given complex is obtained, and the frequency difference, Δv, between the residual solvent in the sealed capillary tube (standard) and the bulk solvent containing the chemical species, is measured. The measured value of Δv can then be used to calculate $\chi_g$, as shown in **Equation 7.1**:

$$\chi_g = \frac{\Delta v}{sFvc} + \chi_o \qquad \textbf{(7.1)}$$

$\chi_g$ is the mass magnetic susceptibility, sF is the shape factor ($4\pi/3$ for a cylindrical sample in a superconducting NMR spectrometer), c is the sample concentration in the NMR tube, and $\chi_o$ is the mass susceptibility of the solvent. The molar mass susceptibility,

$\chi_m$, can be corrected from $\chi_m$' (itself being obtained by multiplying $\chi_g$ by the relative molecular mass) by subtracting the diamagnetic contribution, $\chi_D$ (determined by using $\chi_{Di}$ values for each atom present in the chemical species).[14] Finally, $\chi_m$ can be used to calculate the effective magnetic moment, $\mu_{eff}$, following **Equation 7.2**:

$$\mu_{eff} = \sqrt{\frac{3kT\chi_m}{N_A}} = 2.828\sqrt{\chi_m T} \qquad \textbf{(7.2)}$$

k is Boltzmann's constant, T is the temperature (in K), and $N_A$ is Avogadro's constant.[15,16]

**Example of utilising Equation 4.4:** Complex **2.14** contains a trigonal bipyramidal cobalt(II) centre with one unpaired electron ($n_1 = 1$) and a tetrahedral centre with three unpaired electrons ($n_2 = 3$). Hence, complex **2.14** contains two cobalt centres and the upper limit of summation (x) is therefore two. The value of $\mu_{eff}$ is determined as follows: $\mu_{eff} = \sqrt{\{[(1(1+2)]+[(3(3+2)]\}} = 4.24\ \mu_B$.

## 7.23 Synthesis of [CoBr(Ph(CH$_2$)$_2$N{PPh$_2$}$_2$)$_2$][PF$_6$] (5.1), [CoBr(Py-*o*-(CH$_2$)$_2$N{PPh$_2$}$_2$)$_2$][PF$_6$] (5.2) and [CoBr(Ph(CH$_2$)$_2$N{PPh$_2$}$_2$)$_2$][BAr$^F{}_4$] (5.3)

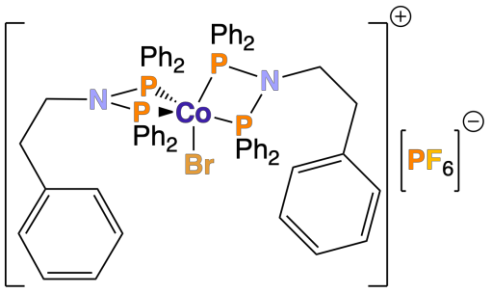


**5.1**

**Synthesis of [CoBr(Ph(CH$_2$)$_2$N{PPh$_2$}$_2$)$_2$][PF$_6$] (5.1):** CoBr$_2$ (0.109 g, 0.5 mmol), Ph(CH$_2$)$_2$N{PPh$_2$}$_2$ (**2.2**, 0.490 g, 1 mmol) and KPF$_6$ (0.092 g, 0.5 mmol) were dissolved in DCM (15 mL) and stirred over a weekend. The reaction mixture was filtered, concentrated to approx. 5 mL, and layered with hexane (15 mL). This provided single crystals suitable for XRD analysis which were isolated by filtration and dried *in vacuo*, affording complex **5.1** as dark brown crystals suitable for XRD analysis (0.396 g, 0.31 mmol, 63%); selected $\nu_{max}$ / cm$^{-1}$ 3053 (aromatic C-H stretch), 2982 (C-H stretch), 1638, 1474 (aromatic C=C), 1433 (P-Ph), 1090 (C-N), 832 (P-F stretch), 556 (P-F bend); Anal.

calc. for $C_{64}H_{58}BrCoF_6N_2P_5$ (1262.88) (%): C, 60.87; H, 4.63; N, 2.22 Found (%): C, 60.76; H, 4.57; N, 2.76; MS (ESI): positive ion *m/z* 519.2 (100.00% $[Ph(CH_2)_2N(OPPh_2)_2\text{-}2H]^+$), 1118.4 (44.96% $[CoBr\{Ph(CH_2)_2N(PPh_2)_2\}_2]^+$); negative ion *m/z* 145.0 (100.00% $[PF_6]^-$).

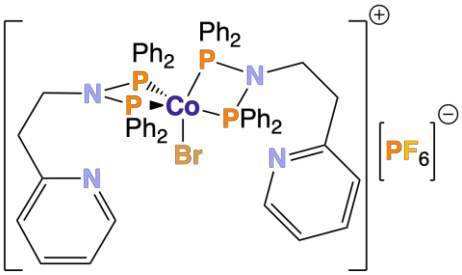


**5.2**

**Synthesis of [Co(Py-*o*-$(CH_2)_2$N{$PPh_2$}$_2$)$_2$Br][$PF_6$] (5.2):** Complex **5.2** was synthesised following the same method as that outlined for complex **5.1**, using Py-*o*-$(CH_2)_2$N{$PPh_2$}$_2$ (**2.1**, 0.491 g, 1 mmol), affording complex **5.2** as dark brown crystals suitable for XRD analysis (0.415 g, 0.33 mmol, 66%); $\mu_{eff}$ ($CD_2Cl_2$, 294 K) = 2.10 $\mu_B$; selected $\nu_{max}$ / $cm^{-1}$ 3055 (aromatic C-H stretch), 2981 (C-H stretch), 1603, 1481 (aromatic C=C), 1585, 1571 (C=N), 1434 (P-Ph), 1088 (C-N), 832 (P-F stretch), 556 (P-F bend); Anal. calc. for $C_{62}H_{56}BrCoF_6N_4P_5$ (1264.85) (%): C, 58.87; H, 4.46; N, 4.43 Found (%): C, 58.53; H, 4.40; N, 4.33; MS (ESI): positive ion *m/z* 520.2 (100.00% $[Py(CH_2)_2N(OPPh_2)_2\text{-}2H]^+$), 1120.3 (15.63% $[CoBr\{Py(CH_2)_2N(PPh_2)_2\}_2]^+$); negative ion *m/z* 145.0 (100.00% $[PF_6]^-$).

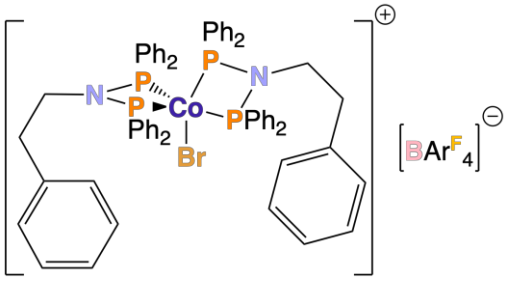


**5.3**

**Synthesis of [CoBr(Ph$(CH_2)_2$N{$PPh_2$}$_2$)$_2$][$BAr^F_4$] (5.3):** Complex **5.3** was synthesised following the same method as that outlined for complex **5.1**, using Ph$(CH_2)_2$N{$PPh_2$}$_2$ (**2.2**, 0.494 g, 1.01 mmol), $CoBr_2$ (0.110 g, 0.503 mmol) and $NaBAr^F_4$ (0.447 g, 0.504 mmol) instead of $KPF_6$, affording complex **5.3** as dark brown crystals (0.745 g, 0.376 mmol, 75%); selected $\nu_{max}$ / $cm^{-1}$ 3056 (aromatic C-H stretch), 2978 (C-H stretch), 1610, 1482 (aromatic C=C), 1436 (P-Ph), 1088 (C-N), 864 (P-N-P); $\lambda_{max}$ (THF) / nm 466, 728; Anal. calc. for $C_{96}H_{70}BBrCoF_{24}N_2P_4$ (1981.13) (%): C, 58.20; H, 3.56; N, 1.41; Found (%): C, 58.10; H, 3.47; N, 1.53; MS (ESI): positive ion *m/z* 519.2 (100.00% $[Ph(CH_2)_2N(OPPh_2)_2$-

2H]$^+$), 1118.1 (61.31% [CoBr{Ph(CH$_2$)$_2$N(PPh$_2$)$_2$}$_2$]$^+$); negative ion *m/z* 863.3 (100.00% [BAr$^F$$_4$]$^-$).

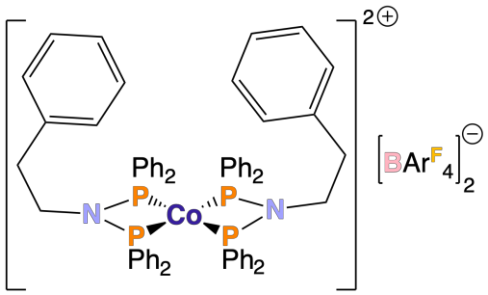


**5.4**

**Attempted synthesis of [Co(Ph(CH$_2$)$_2$N{PPh$_2$}$_2$)$_2$][BAr$^F$$_4$]$_2$ (5.4):** CoBr$_2$ (0.109 g, 0.5 mmol), Ph(CH$_2$)$_2$N{PPh$_2$}$_2$ (**2.2**, 0.490 g, 1 mmol) and NaBAr$^F$$_4$ (0.894 g, 1.008 mmol) were dissolved in DCM (15 mL) and stirred over a weekend. The reaction mixture was filtered, and the solvent removed *in vacuo*. The UV-Vis spectrum of the resulting material was identical to that of complex **5.3**, and positive ion ESI mass spectrometric analysis only evidences signals seen for complex **5.3**, confirming that complex **5.3** was afforded; MS (ESI): positive ion *m/z* 519.1 (100.00% [Ph(CH$_2$)$_2$N(OPPh$_2$)$_2$-2H]$^+$), 1118.0 (25.76% [CoBr{Ph(CH$_2$)$_2$N(PPh$_2$)$_2$}$_2$]$^+$); negative ion *m/z* 863.3 (100.00% [BAr$^F$$_4$]$^-$).

## 7.24 Synthesis of [Co(Ph(CH$_2$)$_2$N{PPh$_2$}$_2$)$_2$][PF$_6$] (5.5), [Co(Py-*o*-(CH$_2$)$_2$N{PPh$_2$}$_2$)$_2$][PF$_6$] (5.6) and [Co(Ph(CH$_2$)$_2$N{PPh$_2$}$_2$)$_2$][BAr$^F$$_4$] (5.7)

**Condition screen for the reduction of [CoBr(Ph(CH$_2$)$_2$N{PPh$_2$}$_2$)$_2$][PF$_6$] (5.1) to [Co(Ph(CH$_2$)$_2$N{PPh$_2$}$_2$)$_2$][PF$_6$] (5.5):** [CoBr(Ph(CH$_2$)$_2$N{PPh$_2$}$_2$)$_2$][PF$_6$] (complex **5.1**) and activated zinc powder (see **Table 7.2** for **5.1** : zinc ratios attempted) were dissolved in 10 mL of THF. The solvent was removed *in vacuo*, the product washed with Et$_2$O (3 × 10 mL), and dried *in vacuo* affording [Co(Ph(CH$_2$)$_2$N{PPh$_2$}$_2$)$_2$][PF$_6$] (complex **5.5**) as a purple powder. It was concluded that at least 4 equiv. of activated zinc was required for the reduction, and this was taken forward for the synthesis of [Co(Ph(CH$_2$)$_2$N{PPh$_2$}$_2$)$_2$][PF$_6$] (**5.5**), [Co(Py-*o*-(CH$_2$)$_2$N{PPh$_2$}$_2$)$_2$][PF$_6$] (**5.6**) and [Co(Ph(CH$_2$)$_2$N{PPh$_2$}$_2$)$_2$][BAr$^F$$_4$] (**5.7**).

Some reactions were attempted using DCM (10 mL) and THF (1 mL) as the solvent; the solvent was removed *in vacuo*, dissolved in DCM (5 mL), filtered, and layered with hexane (10 mL). Single crystals of $0.75[Co\{Ph(CH_2)_2N(PPh_2)_2\}_2Cl][PF_6]\cdot 0.25[Co\{Ph(CH_2)_2N(PPh_2)_2\}_2Br][PF_6]$ (complex **5.19**) were obtained for the reaction with 1 equiv. of zinc when attempted in DCM, evidencing an incomplete reaction.

**Table 7.1.** Screened quantities to optimise the reaction of complex **5.1** with activated zinc. *Visible brown colour in solution, *i.e.*, did not turn the characteristic deep purple observed during reduction. ^Solid-state structures to evidence incomplete reduction (see **Section 5.3.4** and **Section 5.3.5** for the 1 equiv., with DCM solvent, and 2 equiv. reactions, respectively).

| Mass of 5.1 / g | Mass of Zn / g | Equivalents of Zn |
|---|---|---|
| 1.263 | 0.033 | 0.5* |
| 0.05 | 0.003 | 1^ |
| 0.05 | 0.005 | 2^ |
| 0.05 | 0.010 | 4 |
| 0.100 | 0.052 | 10 |
| 0.100 | 0.260 | 50 |

Note that complexes **5.5** – **5.7** are not soluble enough in common organic solvents to allow for $^{13}C$ NMR spectra to be obtained (solvents tried: $d_8$-THF and toluene-$d_8$, the latter in case the of complex **5.7**). The range of possible deuterated solvents suitable to use for NMR spectroscopic study of complexes **5.5** – **5.7** is limited by the reactivity of complexes **5.5** – **5.7** with halogenated solvents (and their likely reactivity with MeCN).

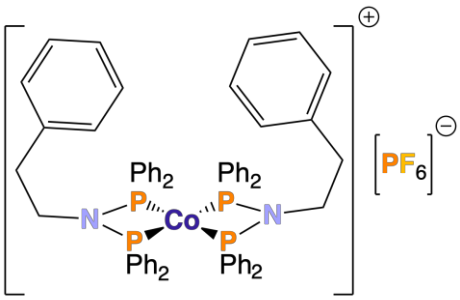


**5.5**

**Synthesis of $[Co(Ph(CH_2)_2N\{PPh_2\}_2)_2][PF_6]$ (5.5):** $[CoBr(Ph(CH_2)_2N\{PPh_2\}_2)_2][PF_6]$ (complex **5.1**, 0.05 g, 0.0395 mmol) and activated zinc powder (0.02 g, 0.158 mmol) were dissolved in THF, producing a deep purple solution, which was stirred overnight. The solvent was removed *in vacuo*, the product washed with $Et_2O$ (3 × 10 mL) and dried *in*

*vacuo* affording complex **5.5** as a purple powder (0.017 g, 0.014 mmol, 36%). Note that trace excess activated zinc could not be completely removed, despite attempts to extract complex **5.5** in various solvents, *e.g.,* toluene. Hence, the percentage yield is calculated assuming all the mass is due to complex **5.5**, and CHN analyses showing good agreement with the calculated composition of complex **5.5** could not be acquired. $\delta_P$ $^{31}P\{^1H\}$ (162 MHz, $d_8$-THF) 86.6 (4P, s, br, $\nu_{1/2}$ = 105 Hz, Co-P), –143.9 (1P, septet, $^1J_{FP}$ = 704 Hz, $\underline{P}F_6^-$); $\delta_F$ $^{19}F$ (376.33 MHz, $d_8$-THF) –72.6 (6F, d, $^1J_{PF}$ = 703 Hz, $P\underline{F}_6^-$); MS (ESI): positive ion *m/z* 519.1 (100.00% $[Ph(CH_2)_2N(OPPh_2)_2\text{-}2H]^+$), 1037.5 (30.23% $[Co\{Ph(CH_2)_2N(PPh_2)_2\}_2]^+$), 1069.5 (27.21% $[Co\{Ph(CH_2)_2N(PPh_2)_2\}_2O_2]^+$); negative ion *m/z* 145.0 (100.00% $[PF_6]^-$). $^1H$ NMR spectrum cannot be reliably assigned due to exhibiting numerous broad signals.

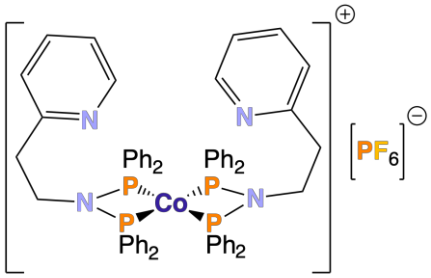


**5.6**

**Synthesis of $[Co(Py\text{-}o\text{-}(CH_2)_2N\{PPh_2\}_2)_2][PF_6]$ (5.6):** Complex **5.6** was synthesised following the same method as that outlined for $[Co(Ph(CH_2)_2N\{PPh_2\}_2)_2][PF_6]$ (complex **5.5**), using $[Co(Py\text{-}o\text{-}(CH_2)_2N\{PPh_2\}_2)_2Br][PF_6]$ (complex **5.2**, 0.05 g, 0.0395 mmol), affording complex **5.6** as a purple powder (0.028 g, 0.024 mmol, 60%). Note that excess activated zinc could again not be completely removed. Hence, the percentage yield is calculated assuming all the mass is due to complex **5.6**; a meaningful CHN analysis could not be acquired. $\delta_P$ $^{31}P\{^1H\}$ (162 MHz, $d_8$-THF) 86.8 (4P, s, br, $\nu_{1/2}$ = 105 Hz, Co-P), –143.9 (1P, septet, $^1J_{FP}$ = 704 Hz, $\underline{P}F_6^-$); $\delta_F$ $^{19}F$ (376.33 MHz, $d_8$-THF) –72.6 (6F, d, $^1J_{PF}$ = 703 Hz, $P\underline{F}_6^-$); MS (ESI): positive ion *m/z* 520.1 (100.00% $[Py(CH_2)_2N(OPPh_2)_2\text{-}2H]^+$), 1039.6 (24.08% $[Co\{Py(CH_2)_2N(PPh_2)_2\}_2]^+$), 1071.5 (35.77% $[Co\{Py(CH_2)_2N(PPh_2)_2\}_2O_2]^+$); negative ion *m/z* 145.0 (100.00% $[PF_6]^-$). $^1H$ NMR spectrum cannot be reliably assigned due to exhibiting numerous broad signals.

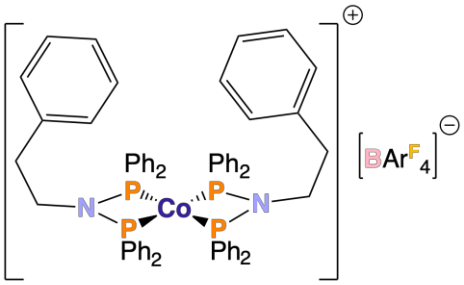

**5.7**

**Synthesis of [Co(Ph(CH$_2$)$_2$N{PPh$_2$}$_2$)$_2$][BAr$^F$$_4$] (5.7):** [CoBr(Ph(CH$_2$)$_2$N{PPh$_2$}$_2$)$_2$][BAr$^F$$_4$] (complex **5.3**, 0.100 g, 0.05 mmol) and activated zinc (0.033 g, 0.5 mmol) were dissolved in THF (20 mL), and the reaction mixture stirred overnight. The reaction mixture was filtered, the solvent removed *in vacuo*, the product extracted in toluene (3 × 10 mL) and the solvent removed *in vacuo*, affording complex **5.7** as a purple powder (0.052 g, 0.027 mmol, 55%). Note that excess activated zinc could again not be completely removed. Hence, the percentage yield is calculated assuming all the mass is due to complex **5.7**, and a meaningful CHN analysis could not be acquired. $\delta_H$ (400 MHz, d$_8$-THF) 7.80 (8H, s, br, $\nu_{1/2}$ = 10 Hz, *o*-BAr$^F$$_4$), 7.54-7.63 (13H, m, phenyl + *p*-BAr$^F$$_4$), 7.42-7.49 (15H, m, phenyl), 7.36 (15H, t, *J* = 7.6 Hz, phenyl), 7.00-7.14 (7H, m, phenyl), 6.69-6.77 (4H, m, phenyl), 2.87-3.00 4H, s, br, $\nu_{1/2}$ = 27 Hz, (PPh$_2$)$_2$N-C<u>H</u>$_2$), 2.21 – 2.30 (4H, m, Ph-C<u>H</u>$_2$); $\delta_P$ $^{31}$P{$^1$H} (162 MHz, d$_8$-THF) 86.7 (4P, s, br, $\nu_{1/2}$ = 105 Hz, Co-<u>P</u>); $\delta_F$ $^{19}$F (79.47 MHz, d$_8$-THF) –63.4 (C<u>F</u>$_3$-BAr$^F$$_4$); $\delta_B$ $^{11}$B{$^1$H} (100.60 MHz, d$_8$-THF) –6.52 (<u>B</u>Ar$^F$$_4^-$); selected $\nu_{max}$ / cm$^{-1}$ 3059 (aromatic C-H stretch), 2963 (C-H stretch), 1604, 1478 (aromatic C=C), 1436 (P-Ph), 1098 (C-N), 837 (P-N-P); $\lambda_{max}$ (THF) / nm 526 ($\varepsilon$ / dm$^3$ mol$^{-1}$ cm$^{-1}$ ~7400), 646, 737; MS (ESI): positive ion *m/z* 519.2 (100.00% [Ph(CH$_2$)$_2$N(OPPh$_2$)$_2$-2H]$^+$), 1037.5 (31.37% [Co{Ph(CH$_2$)$_2$N(PPh$_2$)$_2$}$_2$]$^+$), 1069.6 (25.64% [Co{Ph(CH$_2$)$_2$N(PPh$_2$)$_2$}$_2$O$_2$]$^+$); negative ion *m/z* 863.3 (100.00% [BAr$^F$$_4$]$^-$). The sample exhibited no change in the $^{31}$P{$^1$H} spectrum at various temperatures across the range –85 – 60 °C.

## 7.25 Synthesis of [Co{Ph(CH$_2$)$_2$N(PPh$_2$)$_2$}$_2$O$_2$][BAr$^F$$_4$] (5.13)

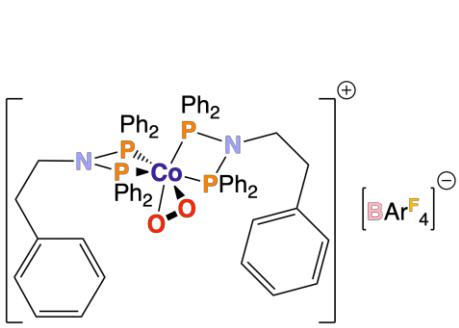

5.13

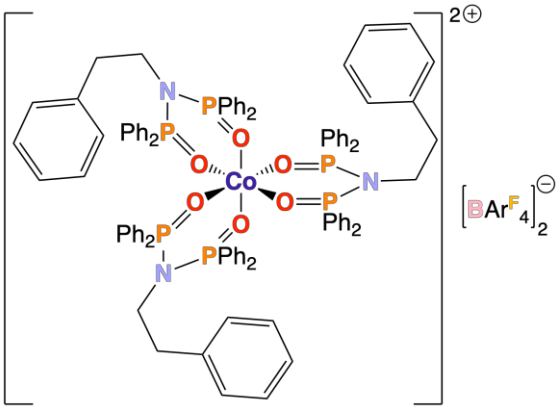

5.16

**Synthesis of [Co{Ph(CH$_2$)$_2$N(PPh$_2$)$_2$}$_2$O$_2$][BAr$^F$$_4$] (5.13) in solution:** [Co(Ph(CH$_2$)$_2$N{PPh$_2$}$_2$)$_2$][BAr$^F$$_4$] (complex **5.7**, 0.01 g, 0.00526 mmol) was dissolved in d$_8$-THF (0.7 mL) in a Young's NMR tube in the glovebox. The sample was brought out of the glovebox, and the resulting solution was subject to three freeze-pump-thaw cycles. The Young's NMR tube was backfilled with 99.5% pure O$_2$ gas, and sealed under a 1 atm pressure of O$_2$. An immediate colour change from deep purple to orange was observed (as had been seen when powder samples of complexes **5.5** – **5.7** had been exposed to air). The solution underwent three freeze-pump-thaw cycles to remove excess O$_2$; $\delta_P$ $^{31}$P{$^1$H} (162 MHz, d$_8$-THF) 74.9 (2P, s, br, $\nu_{1/2}$ ~230 Hz), 48.2 (2P, s, br, $\nu_{1/2}$ ~230 Hz); this is the same as the $^{31}$P{$^1$H} NMR spectrum obtained for a sample of complex **5.13** when complex **5.7** is exposed to air. The $^1$H NMR spectra could not be assigned reliably due to complications arising from exchange between the two enantiomers of the [Co{Ph(CH$_2$)$_2$N(PPh$_2$)$_2$}$_2$O$_2$] cation. A $^{31}$P{$^1$H} NMR spectrum the next day revealed a broad singlet at 86.7 ppm, assigned to complex **5.7**, with a purple colour exhibited by the sample correlating with this observation. Hence, the sample was subject to three freeze-pump-thaw cycles and was backfilled with 1 atm pressure of 99.5% pure O$_2$, resulting in the orange colour being regained. A $^{31}$P{$^1$H} NMR spectrum the next day evidenced a paramagnetic spectrum; this, along with the colourless colour of the sample indicates the formation of complex **5.16**; MS (ESI): positive ion *m/z* 812.3 (100.00% [Co{Ph(CH$_2$)$_2$N(OPPh$_2$)$_2$}$_3$]$^{2+}$).

**Synthesis of [Co{Ph(CH$_2$)$_2$N(PPh$_2$)$_2$}$_2$O$_2$][BAr$^F$$_4$] (5.13) in solid-state:** [Co(Ph(CH$_2$)$_2$N{PPh$_2$}$_2$)$_2$][BAr$^F$$_4$] (complex **5.7**, 0.01 g, 0.00526 mmol) was added to a Young's NMR tube and sealed under vacuum. The Young's NMR tube was backfilled with

99.5% pure $O_2$ gas, and sealed under a 1 atm pressure of $O_2$. An immediate colour change from deep purple to orange was observed (as had been seen when powder samples of complexes **5.5** – **5.7** had been exposed to air). Excess $O_2$ was removed *in vacuo*, and the sample brought back into the glovebox. A portion of this sample was dissolved in $d_8$-THF (0.7 mL), affording the same $^{31}P\{^1H\}$ NMR spectroscopic data described in the above section; selected $\nu_{max}$ / $cm^{-1}$ 3058 (aromatic C-H stretch), 2964 (C-H stretch), 1610, 1485 (aromatic C=C), 1438 (P-Ph), 1113 (C-N), 839 (O-O); MS (ESI): positive ion *m/z* 519.0 (23.57% $[Ph(CH_2)_2N(OPPh_2)_2\text{-}2H]^+$), 1037.6 (34.20% $[Co\{Ph(CH_2)_2N(PPh_2)_2\}_2]^+$), 1069.6 (94.61% $[Co\{Ph(CH_2)_2N(PPh_2)_2\}_2O_2]^+$); negative ion *m/z* 863.3 (100.00% $[BAr^F{}_4]^-$). Reported characterisation data agrees with that obtained from the bright orange powder gained upon exposure of complex **5.7** to air. CHN analysis could not be obtained, likely due to trace contaminants present in the starting material.

Single crystals suitable for XRD analysis of $[Co\{Ph(CH_2)_2N(PPh_2)_2\}_2O_2][PF_6]$ (complex **5.11**, afforded by exposure of $[Co(Ph(CH_2)_2N\{PPh_2\}_2)_2][PF_6]$, complex **5.5**, to air) were obtained, following diffusion, by dissolving a sample of complex **5.11** in acetone and layering with hexane.

## 7.26 Reaction of $Ph(CH_2)_2N(PPh_2)_2$ (2.2) with $O_2$ to afford $Ph(CH_2)_2N(P\{O\}Ph_2)(PPh_2)$ (5.17) and $Ph(CH_2)_2N(P\{O\}Ph_2)_2$ (5.18)

**Reaction of 2.2 with $O_2$:** $Ph(CH_2)_2N(PPh_2)_2$ (**2.2**, 0.02 g, 0.041 mmol) was dissolved in $d_8$-THF (0.7 mL) in a Young's NMR tube inside the glovebox. The sample was brought out of the glovebox, and the resulting solution underwent three freeze-pump-thaw cycles. The Young's NMR tube was backfilled with 99.5% pure $O_2$ gas, and sealed under a 1 atm pressure of $O_2$. The reaction was then followed by $^{31}P\{^1H\}$ NMR spectroscopy over a period of two weeks, showing the gradual conversion of compound **2.2** to $Ph(CH_2)_2N(P\{O\}Ph_2)_2$ (compound **5.18**) *via* $Ph(CH_2)_2N(P\{O\}Ph_2)(PPh_2)$ (compound **5.17**); $\delta_P$ $^{31}P\{^1H\}$ (162 MHz, $d_8$-THF) 27.5 (2P, $Ph(CH_2)_2N(\underline{P}\{O\}Ph_2)_2$, s).

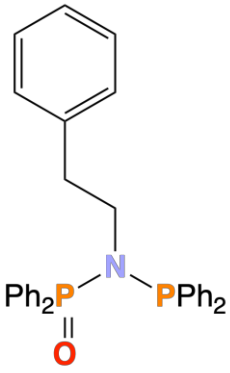


**5.17**

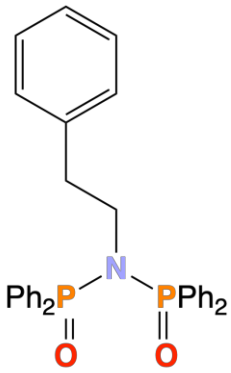


**5.18**

## 7.27 Synthesis of $CoCl(PPh_3)_3$

**Synthesis of $CoCl(PPh_3)_3$:** A slight modification of a known synthetic method was employed.[17] $CoCl_2.6H_2O$ (0.5 g, 2.10 mmol) and $PPh_3$ (1.75 g, 6.67 mmol) were dissolved in degassed EtOH (30 mL) and heated at reflux for 30 minutes under an inert atmosphere. After cooling to room temperature, $NaBH_4$ (0.067 g, 1.77 mmol), dissolved in degassed EtOH (10 mL), was added slowly portion-wise over approx. 20 minutes, with the reaction mixture being stirred for approx. 50 minutes after complete addition. The reaction was filtered, the crude solid washed with EtOH (until the EtOH washes were colourless), $H_2O$ (3 × 20 mL), hexane (1 × 10 mL), and then dried *in vacuo*, affording $CoCl(PPh_3)_3$ as a brown solid (0.858 g, 0.97 mmol, 55%); $\delta_P$ $^{31}P\{^1H\}$ (162 MHz, $CD_2Cl_2$) – 5.59 (3P, s, br, $\nu_{1/2}$ ~80 Hz); Anal. calc. for $C_{54}H_{45}ClCoP_3$ (881.24) (%): C, 73.60; H, 5.15; Found (%): C, 73.14; H, 5.14; MS (ESI): positive ion *m/z* 263.2 (56.52% $[PPh_3+H]^+$), 293.2 (32.42% $[PPh_3+2O]^+$), 650.2 (3.29% $[M\text{-}H\text{-}PPh_3+2O]^+$). CHN data are in good agreement with previously published data.[17]

## 7.28 Synthesis of $[CoCl\{Py\text{-}o\text{-}(CH_2)_2N(PPh_2)_2\}_2]$ (5.27) and $[CoCl\{Ph(CH_2)_2N(PPh_2)_2\}_2]$ (5.28)

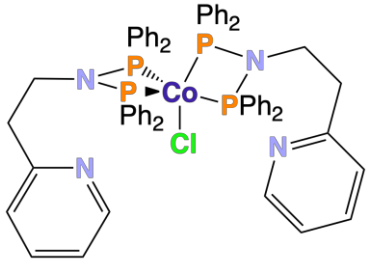


**5.27**

**Synthesis of [CoCl{Py-*o*-$(CH_2)_2N(PPh_2)_2$}$_2$] (5.27):** $CoCl(PPh_3)_3$ (0.220 g, 0.25 mmol) and Py-*o*-$(CH_2)_2N(PPh_2)_2$ (**2.1**, 0.123 g, 0.25 mmol) were dissolved in approx. 5 mL of THF and stirred overnight. The solvent was removed *in vacuo*, pentane (5 mL) was added, and the resulting suspension was stirred over a weekend. After filtration, the crude solid was washed with pentane (3 × 10 mL) and dried *in vacuo*, affording complex **5.27** brown solid (0.099 g, 0.09 mmol, 74%); Anal. calc. for $C_{62}H_{56}ClCoN_4P_4$ (1075.44) (%): C, 69.24; H, 5.25; N, 5.21 Found (%): C, 67.68; H, 4.31; N, –0.65; MS (ESI): positive ion *m/z* 523.3 (100.00% $[Py(CH_2)_2N(OPPh_2)_2+H]^+$), 1074.5 (7.48% $[CoCl\{Py(CH_2)_2N(PPh_2)_2\}_2]^+$).

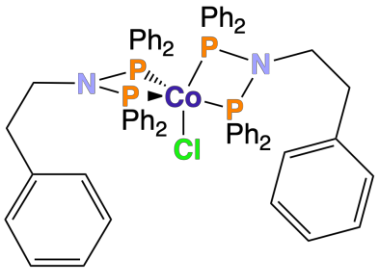


**5.28**

**Synthesis of [CoCl{Ph$(CH_2)_2N(PPh_2)_2$}$_2$] (5.28):** Complex **5.28** was synthesised following the procedure outlined for [CoCl{Py-*o*-$(CH_2)_2N(PPh_2)_2$}$_2$] (complex **5.27**), using Ph$(CH_2)_2N(PPh_2)_2$ (**2.2**, 0.122 g, 0.25 mmol), affording complex **5.28** as a brown solid (0.100 g, 0.09 mmol, 75%); Anal. calc. for $C_{64}H_{58}ClCoN_2P_4$ (1073.46) (%): C, 71.61; H, 5.45; N, 2.61 Found (%): C, 68.94; H, 4.88; N, 1.95; MS (ESI): positive ion *m/z* 519.0 (40.42% $[Ph(CH_2)_2N(OPPh_2)_2-2H]^+$), 1073.3 (57.86% $[CoCl\{Ph(CH_2)_2N(PPh_2)_2\}_2]^+$).

## 7.29 Synthesis of [Co(H)(Cl)(Py-*o*-$(CH_2)_2N\{PPh_2\}_2$)({$Cl_3Co$}Py-*o*-$(CH_2)_2N\{PPh_2\}_2$)] (5.32)

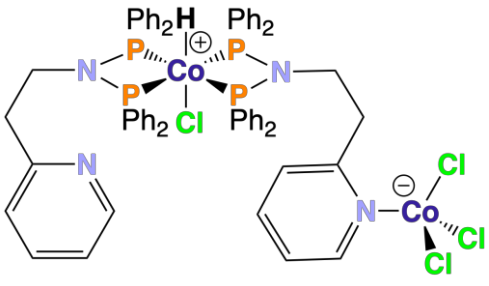


**5.32**

**Synthesis of [Co(H)(Cl)(Py-*o*-$(CH_2)_2N\{PPh_2\}_2$)({$Cl_3Co$}Py-*o*-$(CH_2)_2N\{PPh_2\}_2$)] (5.32):** Py-*o*-$(CH_2)_2N\{PPh_2\}_2$ (**2.1**, 0.245 g, 0.5 mmol), $Co(acac)_2$ (0.064 g, 0.25 mmol) and HBPin (0.192 g, 1.5 mmol) were dissolved in DCM (15 mL) and stirred overnight. The solvent was

removed *in vacuo*, the crude product washed with pentane (3 × 10 mL), and dried *in vacuo*, affording complex **5.32** as a green powder (0.113 g, 0.091 mmol, 36%); $\mu_{eff}$ ($CD_2Cl_2$, 294 K) = 4.31 $\mu_B$; selected $\nu_{max}$ / $cm^{-1}$ 3054 (aromatic C-H stretch), 2972 (C-H stretch), 1603, 1481 (C=C), 1588, 1569 (C=N), 1434 (P-Ph), 834 (P-N-P); Anal. calc. for $C_{62}H_{57}Cl_4Co_2N_4P_4$ (1241.73) (%): C, 59.97; H, 4.63; N, 4.51 Found (%): C, 58.60; H, 4.56; N, 3.94; MS (ESI): positive ion *m/z* 520.5 (100.00% $[Py(CH_2)_2N(OPPh_2)_2\text{-}2H]^+$), 1075.4 (33.65% $[Co(H)(Cl)\{Py(CH_2)_2N(PPh_2)_2\}_2]^+$); negative ion *m/z* 163.8 (100.00% $[CoCl_3]^-$). *NB* yield determined based on the reaction stoichiometry of Py-*o*-$(CH_2)_2N\{PPh_2\}_2$ (**2.1**).

Single crystals suitable for XRD analysis were obtained, following diffusion, by dissolving the sample in DCM and layering with hexane.

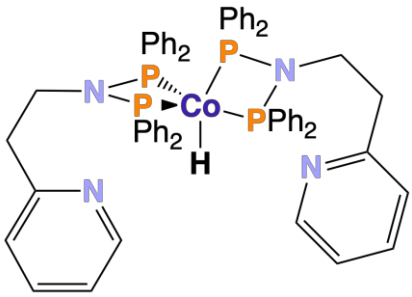


**5.31**

**Attempted synthesis of [CoH{Py-*o*-$(CH_2)_2N(PPh_2)_2\}_2$] (5.31):** the procedure outlined for the synthesis of complex **5.32** was repeated using THF (15 mL) as the solvent instead of DCM; the resulting reaction mixture was stirred overnight. The reaction was filtered, the solvent removed *in vacuo*, and the crude product washed with pentane (3 × 10 mL). Attempts at recrystallising the product (*e.g.*, using THF and pentane) were futile. The product was dried *in vacuo*, affording a sticky black solid which was difficult to isolate and characterise ($^1H$ and $^{31}P$ NMR spectroscopy, CHN and mass spectroscopy evidencing that a complicated mixture of products was produced). The reaction was abandoned at this point.

## 7.30 Synthesis of [Co(H)(Cl)(Py-*o*-$(CH_2)_2N\{PPh_2\}_2)_2$][$PF_6$] (5.33) and [Co(H)(Cl)(Ph$(CH_2)_2N\{PPh_2\}_2)_2$][$PF_6$] (5.34)

Note that complexes **5.33** and **5.34** are not soluble enough in common organic solvents to allow for $^{13}C$ NMR spectra to be obtained (solvents tried: $CD_2Cl_2$, $CDCl_3$, and $d_8$-THF).

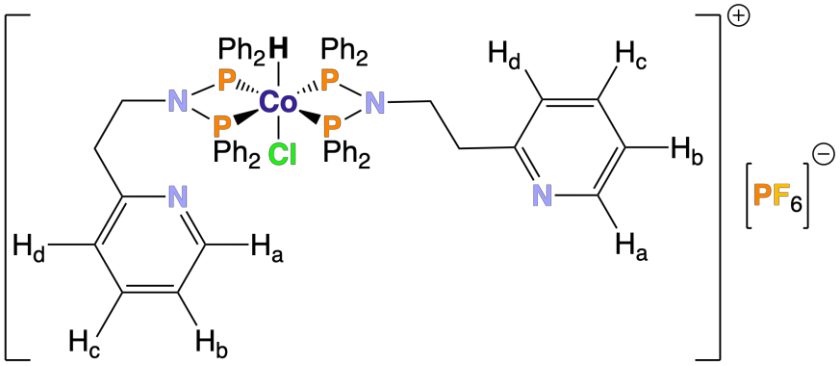

**5.33**

**Synthesis of [Co(H)(Cl)(Py-*o*-(CH$_2$)$_2$N{PPh$_2$}$_2$)$_2$][PF$_6$] (5.33):** Py-*o*-(CH$_2$)$_2$N{PPh$_2$}$_2$ (**2.1**, 0.245 g, 0.5 mmol), Co(acac)$_2$ (0.064 g, 0.25 mmol), HBPin (0.192 g, 1.5 mmol) and KPF$_6$ (0.046 g, 0.25 mmol) were dissolved in DCM (15 mL) and stirred overnight. The reaction mixture was filtered, the solvent removed *in vacuo* and the crude product washed with Et$_2$O (3 × 10 mL), affording complex **5.33** as a brown solid (0.103 g, 0.08 mmol, 34%); $\delta_H$ (400 MHz, CDCl$_3$) 8.35 (2H, s, br, $\nu_{1/2}$ ~40 Hz, H$_a$), 7.09 – 7.67 (42H, m, phenyl + H$_c$), 7.02 (2H, s, br, $\nu_{1/2}$ ~50 Hz, H$_b$), 6.73 (2H, s, br, $\nu_{1/2}$ ~50 Hz, H$_d$), 3.40 (4H, s, br, $\nu_{1/2}$ ~70 Hz, (PPh$_2$)$_2$NC<u>H</u>$_2$), 2.64 (4H, s, br, $\nu_{1/2}$ ~50 Hz, Py-C<u>H</u>$_2$), –18.02 (1H, quin, $^2J_{PH}$ = 52.6 Hz, Co-H); $\delta_P$ $^{31}$P (162 MHz, CDCl$_3$) 83.9 (4P, d, $^2J_{PH}$ = 48.4 Hz, Co-P), –143.9 (1P, spt, $^1J_{FP}$ = 714 Hz, <u>P</u>F$_6^-$); $\delta_F$ $^{19}$F (376.33 MHz, CDCl$_3$) –73.0 (6F, d, $^1J_{PF}$ = 714 Hz, PF$_6^-$); $\mu_{eff}$ (CD$_2$Cl$_2$, 294 K) = 3.47 $\mu_B$; selected $\nu_{max}$ / cm$^{-1}$ 3053 (aromatic C-H stretch), 2981 (C-H stretch), 1620, 1481 (aromatic C=C), 1588, 1570 (C=N), 1435 (P-Ph), 1095 (C-N), 835 (P-F stretch), 557 (P-F bend); Anal. calc. for C$_{62}$H$_{57}$ClCoF$_6$N$_4$P$_5$ (1221.41) (%): C, 60.97; H, 4.70; N, 4.59 Found (%): C, 59.11; H, 4.28; N, 4.00; MS (ESI): positive ion *m/z* 520.1 (55.72% [Py(CH$_2$)$_2$N(OPPh$_2$)$_2$-2H]$^+$), 1075.4 (100.00% [Co(H)(Cl){Py(CH$_2$)$_2$N(PPh$_2$)$_2$}$_2$]$^+$); negative ion *m/z* 145.0 (100.00% [PF$_6$]$^-$).

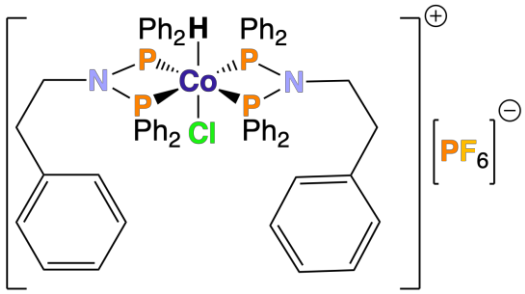

**5.34**

**Synthesis of [Co(H)(Cl)(Ph(CH$_2$)$_2$N{PPh$_2$}$_2$)$_2$][PF$_6$] (5.34):** Complex **5.34** was synthesised following the same procedure outlined for [Co(H)(Cl)(Py-*o*-

$(CH_2)_2N\{PPh_2\}_2)_2][PF_6]$ (complex **5.33**), using $Ph(CH_2)_2N\{PPh_2\}_2$ (**2.2**, 0.245 g, 0.5 mmol), affording complex **5.34** as a brown solid (0.112 g, 0.09 mmol, 37%); $\delta_H$ (400 MHz, $CDCl_3$) 6.99 – 7.69 (48H, m, phenyl), 6.77 (2H, m, phenyl), 3.11 (4H, s, br, $\nu_{1/2}$ ~40 Hz, $(PPh_2)_2NC\underline{H}_2$), 2.40 – 2.48 (4H, m, Ph-C$\underline{H}_2$), –18.00 (1H, q, $^2J_{PH}$ = 52.6 Hz, Co-H); $\delta_P$ $^{31}$P (162 MHz, $CDCl_3$) 83.9 (4P, d, $^2J_{PH}$ = 48.3 Hz, Co-P), –143.9 (1P, spt, $^1J_{FP}$ = 711 Hz, $\underline{P}F_6^-$); $\delta_F$ $^{19}$F (376.33 MHz, $CDCl_3$) –73.0 (6F, d, $^1J_{PF}$ = 714 Hz, $PF_6^-$); $\mu_{eff}$ ($CD_2Cl_2$, 294 K) = 2.47 $\mu_B$; selected $\nu_{max}$ / $cm^{-1}$ 3053 (aromatic C-H stretch), 2981 (C-H stretch), 1603, 1481 (aromatic C=C), 1434 (P-Ph), 1093 (C-N), 832 (P-F stretch), 556 (P-F bend); Anal. calc. for $C_{64}H_{59}ClCoF_6N_2P_5$ (1219.43) (%): C, 63.04; H, 4.88; N, 2.30 Found (%): C, 61.98; H, 4.94; N, 2.01; MS (ESI): positive ion *m/z* 519.1 (100.00% $[Ph(CH_2)_2N(OPPh_2)_2\text{-}2H]^+$), 1073.5 (58.42% $[Co(H)(Cl)\{Ph(CH_2)_2N(PPh_2)_2\}_2]^+$); negative ion *m/z* 145.0 (100.00% $[PF_6]^-$).

**Synthesis of $[Co(H)(Cl)(Py\text{-}o\text{-}(CH_2)_2N\{PPh_2\}_2)_2][PF_6]$ (5.33) in $CD_2Cl_2$:** Py-*o*-$(CH_2)_2N\{PPh_2\}_2$ (**2.1**, 0.03 g, 0.061 mmol), $Co(acac)_2$ (0.008 g, 0.031 mmol), HBPin (0.024 g, 0.186 mmol) and $KPF_6$ (0.006 g, 0.031 mmol) were dissolved in $CD_2Cl_2$ (0.7 mL) in a Young's NMR tube and the reaction sonicated for approx. 30 minutes. $^1$H and $^{31}$P NMR spectroscopic data matched that reported for the reaction conducted in DCM (see synthesis of $[Co(H)(Cl)(Py\text{-}o\text{-}(CH_2)_2N\{PPh_2\}_2)_2][PF_6]$ above).

## 7.31 Synthesis of Complexes $[\{Ph(CH_2)_2N(PPh_2)_2\}ZnBr_2]_n$ (5.44) and $[(Py\text{-}o\text{-}(CH_2)_2N(Ph_2P)_2)ZnBr_2]_n$ (5.54)

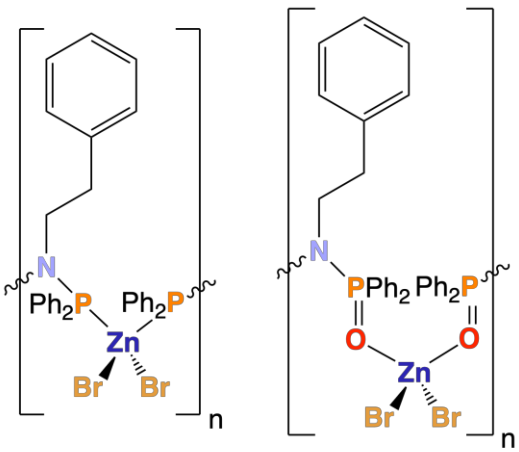


**5.44** **5.47**

**Synthesis of $[\{Ph(CH_2)_2N(PPh_2)_2\}ZnBr_2]_n$ (5.44):** $Ph(CH_2)_2N(PPh_2)_2$ (**2.2**, 0.218 g, 0.444 mmol) and $ZnBr_2$ (0.100 g, 0.444 mmol) were dissolved in THF (2 mL) and DCM (10 mL)

and stirred overnight. The solvent was removed *in vacuo*, and the crude product washed with hexane (2 × 10 mL), affording complex **5.44** as a white powder (0.186 g, 0.260 mmol, 59%); $\delta_H$ (400 MHz, $CDCl_3$) 7.70 – 7.85 (8H, m, phenyl), 7.49 – 7.64 (12H, m, phenyl), 7.08 – 7.19 (3H, m, phenyl), 6.62 – 6.70 (2H, m, phenyl), 3.16 – 3.31 (2H, m, $(PPh_2)_2NC\underline{H}_2$), 2.02 – 2.14 (2H, m, Ph-$C\underline{H}_2$); $\delta_C$ (100.57 MHz, $CD_2Cl_2$) 137.7 (s, aryl-C), 136.9 (s, aryl-C), 133.2 (t, *J* = 8.2 Hz, aryl-C), 132.1 (s, aryl-C), 129.2 (t, *J* = 4.9 Hz, aryl-C), 128.5 (s, aryl-C), 128.2 (s, aryl-C), 126.6 (s, aryl-C), 67.9 (s, $CH_2$), 37.1 (s, $CH_2$); $\delta_P$ $^{31}P\{^1H\}$ (162 MHz, $CDCl_3$) 71.3 (2P, s, br, $\nu_{1/2}$ = 101 Hz, PNP); selected $\nu_{max}$ / $cm^{-1}$ 3054 (aromatic C-H stretch), 2981 (C-H stretch), 1603, 1481 (C=C), 1434 (P-Ph); Anal. calc. for n $C_{32}H_{29}Br_2NP_2Zn$ (714.73) (%): C, 53.78; H, 4.09; N, 1.96 Found (%): C, 54.40; H, 4.36; N, 2.05; MS (ASAP): positive ion *m/z* 490.1 (100.00% $[Ph(CH_2)_2N(PPh_2)_2+H]^+$).

Single crystals suitable for XRD analysis of $[(Ph(CH_2)_2N(Ph_2PO)_2)ZnBr_2]_n$ (complex **5.47**) were obtained by layered a DCM solution of $[\{Ph(CH_2)_2N(PPh_2)_2\}ZnBr_2]_n$ (complex **5.44**) with hexane under atmospheric conditions.

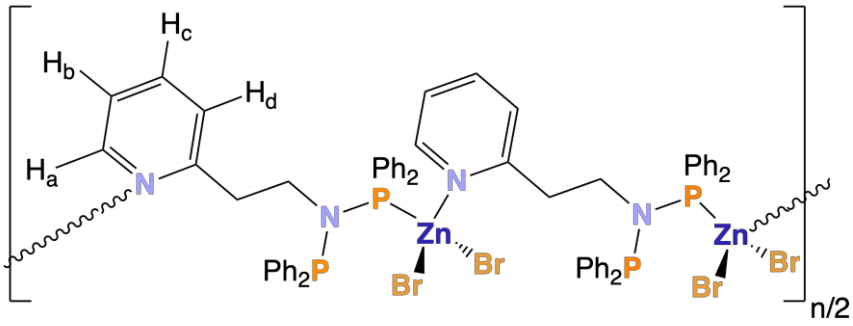


**5.54**

**Synthesis of $[(Py\text{-}o\text{-}(CH_2)_2N(Ph_2P)_2)ZnBr_2]_n$ (5.54):** Complex **5.54** was prepared in the same manner as compound **5.44**, using Py-*o*-$(CH_2)_2N(Ph_2P)_2$ (compound **2.1**, 0.109 g, 0.222 mmol) and $ZnBr_2$ (0.050 g, 0.222 mmol) were dissolved in THF (2 mL) and DCM (10 mL) and stirred overnight. The solvent was removed *in vacuo*, and the crude product washed with hexane (2 × 10 mL), affording complex **5.54** as a white powder (0.163 g, 0.228 mmol, 51%); $\delta_H$ (400 MHz, $CDCl_3$) 9.17 (1H, d, *J* = 5.3 Hz, $H_a$), 7.75 – 7.88 (4H, m, phenyl and pyridyl), 7.30 – 7.60 (14H, m, phenyl and pyridyl), 7.10 – 7.23 (4H, m, phenyl and pyridyl), 6.99 (1H, d, *J* = 7.9 Hz, phenyl or $H_d$), 3.92 – 4.05 (2H, m, $(PPh_2)_2NC\underline{H}_2$), 3.11 (2H, t, *J* = 6.1 Hz, Py-$C\underline{H}_2$); $\delta_C$ (100.57 MHz, $CD_2Cl_2$) 158.7 (s, aryl-C), 149.4 (s, aryl-C), 136.4 (s, aryl-C), 135.7 (s, aryl-C), 134.8 (s, aryl-C) 133.9 (m, aryl-C), 131.5 (s, aryl-C), 129.2 (s, aryl-C), 128.6 (m, aryl-C), 125.5 (s, aryl-C), 124.3 (s, aryl-C), 123.3 (s, aryl-C),

121.6 (s, aryl-C), 56.3 (s, $CH_2$), 33.7 (s, $CH_2$); $\delta_P$ $^{31}P\{^1H\}$ (162 MHz, $CDCl_3$) 56.3 (1P, d, $^2J_{PP}$ = 16 Hz), 49.5 (1P, d, $^2J_{PP}$ = 16 Hz); selected $\nu_{max}$ / $cm^{-1}$ 3053 (aromatic C-H stretch), 2981 (C-H stretch), 1608, 1482 (C=C), 1586, 1571 (C=N), 1434 (P-Ph); Anal. Calc. for n $C_{31}H_{28}Br_2N_2P_2Zn$ (715.71) (%): C, 52.02; H, 3.94; N, 3.91 Found (%): C, 52.24; H, 3.10; N, 3.94; MS (ASAP): positive ion *m/z* 490.1 (100.00% [Py-*o*-$(CH_2)_2N(PPh_2)_2]^+$).

## 7.32 Synthesis of $[Co\{Ph(CH_2)_2N(PPh_2)_2\}_2(\eta^2\text{-}CH_2CH_2)][BAr^F_4]$ (6.1)

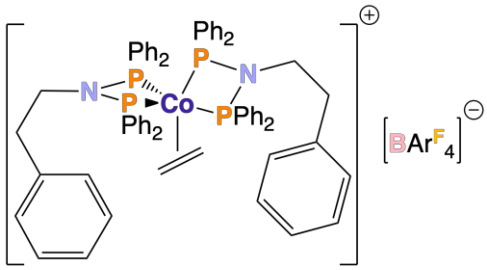


**6.1**

**Reaction of $[Co\{Ph(CH_2)_2N(PPh_2)_2\}_2][BAr^F_4]$ (5.7) with 1 atm of ethylene:** $[Co\{Ph(CH_2)_2N(PPh_2)_2\}_2][BAr^F_4]$ (complex **5.7**, 0.01 g, 0.00526 mmol) was dissolved in $d_8$-THF (0.7 mL) in a Young's NMR tube inside the glovebox. The sample was brought out of the glovebox, and the resulting solution subject to three freeze-pump-thaw cycles. The Young's NMR tube was backfilled with 1 atm of ethylene gas, affording $[Co\{Ph(CH_2)_2N(PPh_2)_2\}_2(\eta^2\text{-}CH_2CH_2)][BAr^F_4]$ (**6.1**). The sample was subject to a variable temperature $^{31}P\{^1H\}$ NMR spectroscopic study (**Figure 6.1**, **Chapter 6**). Acquired $^{31}P[^1H]$ spectra were essentially identical to their $^{31}P\{^1H\}$ counterparts. The $^1H$ NMR spectra could not be assigned reliably due to complications arising from exchange between the two enantiomers of the $[Co\{Ph(CH_2)_2N(PPh_2)_2\}_2(\eta^2\text{-}CH_2CH_2)]$ cation, and the sample was too low a concentration to achieve a $^{13}C$ NMR spectrum; $\delta_P$ $^{31}P\{^1H\}$ (162 MHz, 298 K, $d_8$-THF) 88.0 (s, br, $\nu_{1/2}$ = 105 Hz, $[Co\{Ph(CH_2)_2N(\underline{P}Ph_2)_2\}_2(\eta^2\text{-}CH_2CH_2)]^+$), 80.5 (s, br, $\nu_{1/2}$ = 105 Hz, $[Co\{Ph(CH_2)_2N(\underline{P}Ph_2)_2\}_2(\eta^2\text{-}CH_2CH_2)]^+$).

**Attempted isolation of $[Co\{Ph(CH_2)_2N(PPh_2)_2\}_2(\eta^2\text{-}CH_2CH_2)][BAr^F_4]$ (6.1):** $[Co\{Ph(CH_2)_2N(PPh_2)_2\}_2][BAr^F_4]$ (complex **5.7**, 0.05 g, 0.026 mmol) was dissolved in THF (10 mL) in a Schlenk flask, and the resulting solution subjected to three freeze-pump-thaw cycles. The Schlenk flask was backfilled with 1 atm of ethylene gas, affording

$[Co\{Ph(CH_2)_2N(PPh_2)_2\}_2(\eta^2\text{-}CH_2CH_2)][BAr^F{}_4]$ (**6.1**). Attempting to remove volatilities *in vacuo* resulted in a return to the deep purple colour of complex **5.7**, indicating that the coordinated ethylene had been removed. No further attempts at isolating complex **6.1** were made.

**Reaction of $[Co\{Ph(CH_2)_2N(PPh_2)_2\}_2][BAr^F{}_4]$ (5.7) with 1 equiv. of ethylene:** $[Co\{Ph(CH_2)_2N(PPh_2)_2\}_2][BAr^F{}_4]$ (complex **5.7**, 0.01 g, 0.00526 mmol) was dissolved in $d_8$-THF (0.7 mL) in a Young's NMR tube inside the glovebox. The sample was brought out of the glovebox, and the resulting solution subject to three freeze-pump-thaw cycles. The Young's NMR tube was backfilled with (approx.) 1 eq. of ethylene gas (this was achieved by filling a 7 $cm^3$ glass bulb, attached to the Schlenk line and the Young's NMR tube, with a pressure of ethylene at 14 mmHg, with this pressure being determined using pV = nRT), affording $[Co\{Ph(CH_2)_2N(PPh_2)_2\}_2(\eta^2\text{-}CH_2CH_2)][BAr^F{}_4]$ (**6.1**). The $^1H$ and $^{31}P\{^1H\}$ NMR data are identical to those seen for the same sample with 1 atm of ethylene.

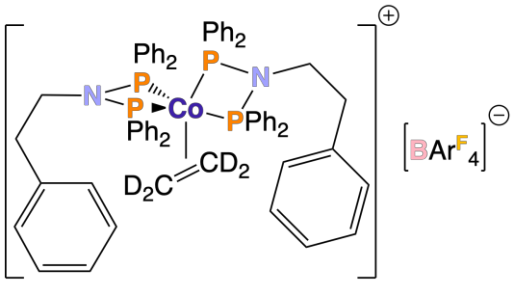


**6.9**

**Reaction of $[Co\{Ph(CH_2)_2N(PPh_2)_2\}_2][BAr^F{}_4]$ (5.7) with $d_4$-ethylene:** $[Co\{Ph(CH_2)_2N(PPh_2)_2\}_2][BAr^F{}_4]$ (complex **5.7**, 0.01 g, 0.00526 mmol) was dissolved in THF (0.7 mL) in a Young's NMR tube inside the glovebox. The sample was brought out of the glovebox, and the resulting solution subject to three freeze-pump-thaw cycles. The Young's NMR tube was backfilled with an excess of $d_4$-ethylene gas, affording $[Co\{Ph(CH_2)_2N(PPh_2)_2\}_2(\eta^2\text{-}CD_2CD_2)][BAr^F{}_4]$ (**6.9**); $\delta_D$ (76.67 MHz, THF) 5.34 (s, $C_2D_4$), 3.56 (s, $d_8$-THF), 1.77 (s, $d_8$-THF), 1.52 (s, $Co(\eta^2\text{-}CD_2CD_2)$); $\delta_P$ $^{31}P\{^1H\}$ (162 MHz, 298 K, $d_8$-THF) 87.9 (s, br, $\nu_{1/2}$ = 496 Hz, $[Co\{Ph(CH_2)_2N(\underline{P}Ph_2)_2\}_2(\eta^2\text{-}CD_2CD_2)]^+$), 80.6 (s, br, $\nu_{1/2}$ = 396 Hz, $[Co\{Ph(CH_2)_2N(\underline{P}Ph_2)_2\}_2(\eta^2\text{-}CD_2CD_2)]^+$).

## 7.33 Synthesis of [Co{Ph(CH$_2$)$_2$N(PPh$_2$)$_2$}$_2$(CO)][BAr$^F_4$] (6.21)

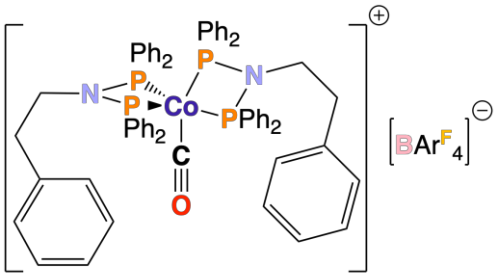

**6.21**

**Reaction of [Co{Ph(CH$_2$)$_2$N(PPh$_2$)$_2$}$_2$][BAr$^F_4$] (5.7) with 1 atm of CO:** [Co{Ph(CH$_2$)$_2$N(PPh$_2$)$_2$}$_2$][BAr$^F_4$] (complex **5.7**, 0.01 g, 0.00526 mmol) was dissolved in d$_8$-THF (0.7 mL) in a Young's NMR tube inside the glovebox. The sample was brought out of the glovebox, and the resulting solution subject to three freeze-pump-thaw cycles. The Young's NMR tube was backfilled with 1 atm of CO gas, affording [Co{Ph(CH$_2$)$_2$N(PPh$_2$)$_2$}$_2$(CO)][BAr$^F_4$] (complex **6.21**). The sample was studied by $^1$H and $^{31}$P{$^1$H} NMR spectroscopy (the sample was too low a concentration to achieve a $^{13}$C NMR spectrum) and the solvent was removed *in vacuo*, isolating complex **6.21** as an orange powder (0.008 g, 0.00415 mmol, 79%); $\delta_H$ (400 MHz, d$_8$-THF) 7.80 – 7.87 (16H, m, phenyl), 7.46 – 7.70 (20H, m, phenyl), 7.21 (9H, t, *J* = 7.58 Hz, phenyl), 6.95 – 7.03 (13H, m, phenyl), 6.51 – 6.58 (4H, m, phenyl), 2.75 – 2.88 (4H, m, (PPh$_2$)$_2$N-C<u>H</u>$_2$), 1.87 – 1.97 (4H, m, Ph-C<u>H</u>$_2$); $\delta_P$ $^{31}$P{$^1$H} (162 MHz, d$_8$-THF) 81.6 (4P, s); selected $\nu_{max}$ / cm$^{-1}$ 3057 (aromatic C-H stretch), 2962 (C-H stretch), 1951 (C-O) 1609, 1487 (aromatic C=C), 1436 (P-Ph), 1090 (C-N), 839 (P-N-P); MS (ESI): positive ion *m/z* 519.1 (55.99% [Ph(CH$_2$)$_2$N(OPPh$_2$)$_2$-2H]$^+$), 1066.1 (100.00% [Co{Ph(CH$_2$)$_2$N(PPh$_2$)$_2$}$_2$CO]$^+$); negative ion *m/z* 863.3 (100.00% [BAr$^F_4$]$^-$). CHN analyses in good agreement with the calculation composition for complex **6.21** could not be obtained, most likely due to trace contaminants present in the starting material.

## 7.34 Reaction of [Co{Ph(CH$_2$)$_2$N(PPh$_2$)$_2$}$_2$][BAr$^F_4$] (5.7) with H$_2$

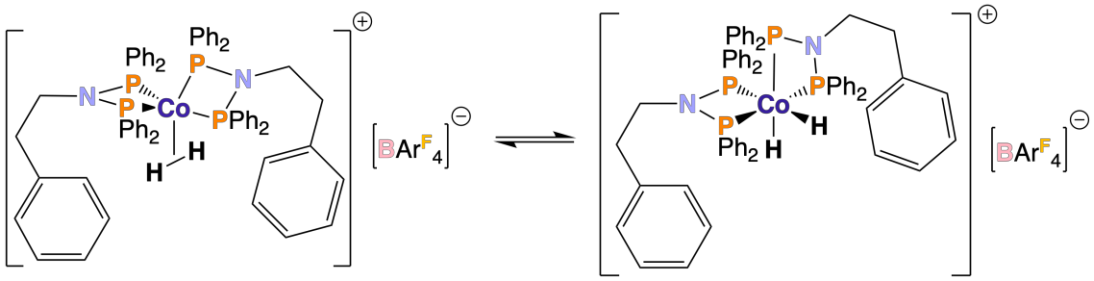

**6.26** **6.29**

**Reaction of [Co{Ph(CH$_2$)$_2$N(PPh$_2$)$_2$}$_2$][BAr$^F$$_4$] (5.7) with 1 atm of H$_2$:** [Co{Ph(CH$_2$)$_2$N(PPh$_2$)$_2$}$_2$][BAr$^F$$_4$] (complex **5.7**, 0.01 g, 0.00526 mmol) was dissolved in d$_8$-THF (0.7 mL) in a Young's NMR tube inside the glovebox. The sample was brought out of the glovebox, and the resulting solution underwent three freeze-pump-thaw cycles. The Young's NMR tube was backfilled with 1 atm of H$_2$ gas, affording an equilibrium mixture of [Co(Ph(CH$_2$)$_2$N{PPh$_2$}$_2$)$_2$($\eta^2$-H$_2$)][BAr$^F$$_4$] and [Co(Ph(CH$_2$)$_2$N{PPh$_2$}$_2$)$_2$(*cis*-(H)$_2$)][BAr$^F$$_4$] (complexes **6.26** and **6.29**, respectively). The sample was studied by $^1$H and $^{31}$P{$^1$H} NMR spectroscopy (the sample was too low a concentration to achieve a $^{13}$C NMR spectrum); $\delta_H$ (400 MHz, d$_8$-THF) 7.80 – 7.86 (9H, m, phenyl), 7.54 – 7.60 (12 H, m, phenyl), 7.44 (15H, s, br, $\nu_{1/2}$ = 16 Hz, phenyl), 7.32 – 7.38 (15H, m, phenyl), 7.05 – 7.18 (7H, m, phenyl), 6.78 – 6.83 (4H, m, phenyl), 3.00 – 3.12 (4H, m, (PPh$_2$)$_2$N-C<u>H</u>$_2$), 2.33 – 2.45 (4H, m, Ph-C<u>H</u>$_2$), –6.25 (2H, quin, $^2J_{PH}$ = 36.3 Hz, Co(H$_2$)); $\delta_H$ $^1$H{$^{31}$P} (400 MHz, d$_8$-THF) –6.25 (2H, s, Co(H$_2$)); $\delta_P$ $^{31}$P{$^1$H} (162 MHz, d$_8$-THF) 99.9 (4P, s); $\delta_P$ $^{31}$P (162 MHz, d$_8$-THF) 99.9 (4P, t, $^2J_{PH}$ = 34.1 Hz); MS (ESI): positive ion *m/z* 519.1 (100.00% [Ph(CH$_2$)$_2$N(OPPh$_2$)$_2$-2H]$^+$), 1037.5 (57.13.23% [Co{Ph(CH$_2$)$_2$N(PPh$_2$)$_2$}$_2$]$^+$), 1069.5 (40.48% [Co{Ph(CH$_2$)$_2$N(PPh$_2$)$_2$}$_2$O$_2$]$^+$); negative ion *m/z* 863.3 (100.00% [BAr$^F$$_4$]$^-$). Attempts to isolate the H$_2$ adduct of complex **5.7** resulted in complex **5.7**, *i.e.*, removal of the coordinated H$_2$ *in vacuo*.

## 7.35 Reaction of [Co{Ph(CH$_2$)$_2$N(PPh$_2$)$_2$}$_2$][BAr$^F$$_4$] (5.7) with HD

**Synthesis of HD gas:** 60% NaH in mineral oil (0.13 mol, 3.21 g in 5.35 g) was added to a 50 mL three-necked round bottom flask (with a stopper on one neck, a tap connected to a Schlenk line in another neck, and a frit containing CaCl$_2$ (5 g), serving as a drying column for the gas, and a tap connected to a T-piece with a Young's NMR tube, containing d$_8$-THF, 0.7 mL, degassed and under own vapour pressure, and double-skinned balloon). The setup was put under vacuum and backfilled with nitrogen gas,

with this process being repeated three times. The apparatus was closed off from the Schlenk line, and $N_2$-sparged $D_2O$ (0.13 mol, 2.42 $cm^3$) was added cautiously and dropwise *via* a syringe through a suba seal into the 50 mL flask, producing HD gas, which was collected in the balloons. Once the balloon were inflated, the tap on the Young's NMR tube (sealed under vacuum) was opened, allowing for the HD gas to enter the tube. After a minute, the Young's NMR tube was sealed, and the sample was studied by NMR spectroscopy; $\delta_H$ (400 MHz, $d_8$-THF) 4.58 (s, $H_2$), 4.54 (t, $^1J_{HD}$ = 42.6 Hz, HD). A mixture of $H_2$ and HD gas (in a $H_2$:HD ratio of approx. 2:3, determined from the integrals measured from the $^1$H NMR spectrum) was produced.

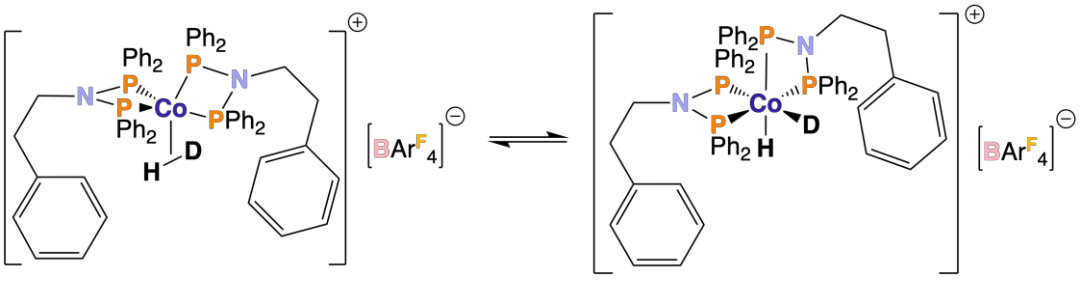

**6.27** **6.30**

**Reaction of [Co{Ph(CH$_2$)$_2$N(PPh$_2$)$_2$}$_2$][BAr$^F_4$] (5.7) with HD:** 60% NaH in mineral oil (0.13 mol, 3.21 g in 5.35 g) was added to a 50 mL three-necked round bottom flask (with a stopper on one neck, a tap connected to a Schlenk line in another neck, and a frit containing $CaCl_2$ (5 g), serving as a drying column for the gas, and a tap connected to a T-piece with a Young's NMR tube, containing [Co{Ph(CH$_2$)$_2$N(PPh$_2$)$_2$}$_2$][BAr$^F_4$] (complex **5.7**, 0.01 g, 0.00526 mmol) and $d_8$-THF, 0.7 mL, degassed and under own vapour pressure, and double-skinned balloon). The setup was put under vacuum and backfilled with nitrogen gas, with this process being repeated three times. The apparatus was closed off from the Schlenk line, and $N_2$-sparged $D_2O$ (0.13 mol, 2.42 $cm^3$) was added cautiously and dropwise *via* a syringe through a suba seal into the 50 mL flask, producing HD gas which was collected in the balloons. Once the balloon was inflated, the tap on the Young's NMR tube (sealed under vacuum) was opened, allowing for the HD gas to enter the tube, affording an equilibrium mixture of [Co(Ph(CH$_2$)$_2$N{PPh$_2$}$_2$)$_2$($\eta^2$-HD)][BAr$^F_4$] (**6.27**) and [Co(Ph(CH$_2$)$_2$N{PPh$_2$}$_2$)$_2$(*cis*-(H)(D))][BAr$^F_4$] (**6.30**). After a minute, the Young's NMR tube was sealed, and the sample is studied by NMR spectroscopy; $\delta_H$ (400 MHz, $d_8$-THF) 7.80 – 7.86 (10H, m, phenyl), 7.54 – 7.61 (12 H, m, phenyl), 7.44 (14H,

s, br, $\nu_{1/2}$ = 16 Hz, phenyl), 7.31 – 7.38 (15H, m, phenyl), 7.03 – 7.11 (5H, m, phenyl), 6.78 – 6.82 (3H, m, phenyl), 3.00 – 3.13 (4H, m, $(PPh_2)_2N$-C<u>H</u>$_2$), 2.33 – 2.42 (4H, m, Ph-C<u>H</u>$_2$), –5.99 – –6.44 (2H, m, Co($H_2$) + Co(HD)); $\delta_H$ $^1H\{^{31}P\}$ (400 MHz, $d_8$-THF) –6.16 (2H, s, Co(HD)), –6.25 (2H, s, Co($H_2$)); $\delta_P$ $^{31}P\{^1H\}$ (162 MHz, $d_8$-THF) 99.7 – 100.3 (m, [Co{Ph$(CH_2)_2$N$(PPh_2)_2$}$_2$($D_2$)][$BAr^F_4$], [Co{Ph$(CH_2)_2$N$(PPh_2)_2$}$_2$(HD)][$BAr^F_4$], [Co{Ph$(CH_2)_2$N$(PPh_2)_2$}$_2$($H_2$)][$BAr^F_4$]); $\delta_P$ $^{31}P$ (162 MHz, $d_8$-THF) 100.1 (4P, d, $^2J_{PH}$ = 37.1 Hz, [Co{Ph$(CH_2)_2$N$(PPh_2)_2$}$_2$(HD)][$BAr^F_4$]). Note that the integrals of the $^1H$ NMR spectrum are not reliable due to there being a mixture of complexes [Co{Ph$(CH_2)_2$N$(PPh_2)_2$}$_2$($H_2$)][$BAr^F_4$], [Co{Ph$(CH_2)_2$N$(PPh_2)_2$}$_2$(HD)][$BAr^F_4$] and [Co{Ph$(CH_2)_2$N$(PPh_2)_2$}$_2$($D_2$)][$BAr^F_4$].

## 7.36 Reaction of [Co{Ph$(CH_2)_2$N$(PPh_2)_2$}$_2$][$BAr^F_4$] (5.7) with syngas to afford [Co{Ph$(CH_2)_2$N$(PPh_2)_2$}$_2$(CO)][$BAr^F_4$] (6.21)

**Reaction of [Co{Ph$(CH_2)_2$N$(PPh_2)_2$}$_2$][$BAr^F_4$] (5.7) with syngas:** [Co{Ph$(CH_2)_2$N$(PPh_2)_2$}$_2$][$BAr^F_4$] (complex **5.7**, 0.01 g, 0.00526 mmol) was dissolved in $d_8$-THF (0.7 mL) in a Young's NMR tube inside the glovebox. The sample was brought out of the glovebox, and the resulting solution subject to three freeze-pump-thaw cycles. The Young's NMR tube was backfilled with 1 atm of syngas, affording [Co{Ph$(CH_2)_2$N$(PPh_2)_2$}$_2$(CO)][$BAr^F_4$] (complex **6.21**) exclusively (no evidence of [Co(Ph$(CH_2)_2$N{$PPh_2$}$_2$)$_2$($\eta^2$-$H_2$)][$BAr^F_4$] and [Co(Ph$(CH_2)_2$N{$PPh_2$}$_2$)$_2$(*cis*-$(H)_2$)][$BAr^F_4$], *i.e.*, complexes **6.26** and **6.29**, respectively). An immediate colour change from deep purple to orange was observed. The $^1H$ and $^{31}P\{^1H\}$ NMR spectroscopic data is consistent with that mentioned in **Section 7.33**.

## 7.37 Rationale for selection of DFT method and basis set

A ground-state DFT B3LYP method with a 6-31G(d) basis set was chosen for all calculations in this project. This approach was taken since optimisation of the structure of complex **5.1** ([CoBr(Ph$(CH_2)_2$N{$PPh_2$}$_2$)$_2$][$PF_6$]) using these parameter gave the best agreement with the experimentally determined solid-state structure of complex **5.1**. Although slight alterations in the basis set improved some parameters, this occurred at

the expense of others, hence the ground state DFT B3LYP method with a 6-31G(d) basis set was chosen as a best compromise.

## 7.38 Syntheses and characterisation data for previously synthesised Py-*o*-$(CH_2)_2N(PPh_2)_2$ (2.1), [CoBr(Py-*o*-$(CH_2)_2N\{PPh_2\}_2$)($\{Br_3Co\}$Py-*o*-$(CH_2)_2N\{PPh_2\}_2$)] (2.14) and [{Py-*o*-$(CH_2)_2N(PPh_2)_2\}PdCl_2$] (3.8)

Py-*o*-$(CH_2)_2N(PPh_2)_2$ (compound **2.1**), [CoBr(Py-*o*-$(CH_2)_2N\{PPh_2\}_2$)($\{Br_3Co\}$Py-*o*-$(CH_2)_2N\{PPh_2\}_2$)] (complex **2.14**) and [{Py-*o*-$(CH_2)_2N(PPh_2)_2\}PdCl_2$] (complex **3.8**) were previously synthesised in the MChem project of the author of this thesis.[18] Further original work (not previously submitted for as part of the author's MChem thesis at Durham University) has been undertaken in this thesis. The syntheses and characterisation data for compound **2.1** and complexes **2.14** and **3.8** are included for completeness.

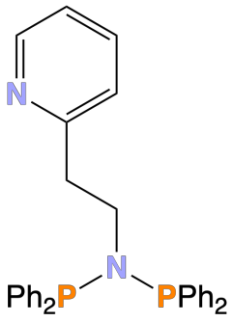


**2.1**

**Synthesis of Py-*o*-$(CH_2)_2N(PPh_2)_2$ (2.1):** 2-(2-aminoethyl)pyridine (1.22 g, 10.0 mmol) and triethylamine (11.2 mL, 80.0 mmol) were dissolved in DCM (~15 mL), and the resulting solution cooled to –40 °C in an acetone/dry ice bath. Chlorodiphenylphosphine (3.6 mL, 20.0 mmol) was added dropwise. Salt formed immediately, and after the complete addition the resulting yellow slurry was allowed to warm to room temperature and stirred for 2 days. The resulting mixture was then filtered, the volatile components removed *in vacuo* from the filtrate, and the product extracted from the crude oil that formed with toluene (2 × 20 mL). The solvent was removed *in vacuo*, gaining the product as a yellow waxy solid (1.410 g, 2.87 mmol, 29%). $\delta_H$ (400 MHz, $CD_2Cl_2$) 2.52 (2H, m, Py-C<u>H</u>$_2$), 3.66 (2H, m, C<u>H</u>$_2$N$(PPh_2)_2$), 6.66 (1H, dt, $J_{HH}$ = 1.0 Hz, 7.8 Hz, H-3Py), 7.04 (1H, ddd, $J_{HH}$ = 1.1 Hz, 4.9 Hz, 7.6 Hz, H-4Py), 7.34-7.42 (12H, m, phenyl), 7.46-7.53 (9H, m, phenyl

+ H-5Py), 8.43 (1H, dq, $J_{HH}$ = 0.9 Hz, 4.9 Hz, H-6Py); $\delta_P$ $^{31}P\{^1H\}$ (162 MHz, $CD_2Cl_2$) 62.7 (2P, s); $\delta_C$ (376.45 MHz, $CD_2Cl_2$) 39.9 (t, $J$ = 3.1 Hz, $CH_2$), 53.0 (s, $CH_2$), 121.0 (s, py-C), 122.9 (s, py-C), 128.1 (t, $J$ = 3.1 Hz, aryl-C), 128.8 (s, aryl-C), 132.8 (dd, $J$ = 11.0 Hz, 12.1 Hz, aryl-C), 135.9 (s, py-C), 139.5 (dd, $J$ = 6.3 Hz, 7.4 Hz, aryl-C), 149.2 (s, py-C), 159.3 (s, py-C); selected $\nu_{max}$ / $cm^{-1}$ 3052 (aromatic C-H stretch), 2983 (C-H stretch), 1604, 1475 (C=C), 1587, 1565 (C=N), 1435 (P-Ph), 858 (P-N-P); Anal. calc. for $C_{31}H_{28}Cl_2N_2P_2$ (490.53) (%): C, 75.91; H, 5.75; N, 5.71 Found (%): C, 75.60; H, 5.48; N, 5.61; MS (ESI): positive ion *m/z* 491.4 (100.00% $[M+H]^+$).

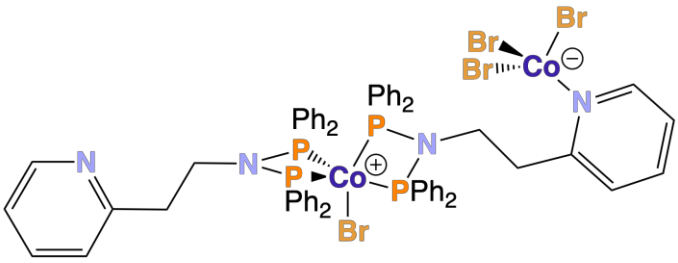


**2.14**

**Synthesis of [CoBr(Py-*o*-$(CH_2)_2$N{$PPh_2$}$_2$)({$Br_3$Co}Py-*o*-$(CH_2)_2$N{$PPh_2$}$_2$)] (2.14):** $CoBr_2$ (0.109 g, 0.5 mmol) and Py-*o*-$(CH_2)_2$N$(PPh_2)_2$, **2.1**, (0.245 g, 0.5 mmol) were dissolved in THF and stirred at room temperature overnight. A precipitate formed, which was isolated by filtration and dried *in vacuo*, affording the cobalt(II) complex **2.14** as a light brown solid (0.198 g, 0.140 mmol, 56%); $\mu_{eff}$ ($CD_2Cl_2$, 294 K) = 4.94 $\mu_B$; selected $\nu_{max}$ / $cm^{-1}$ 1603, 1480 (C=C), 1586, 1569 (C=N), 1433 (P-Ph), 835 (P-N-P); Anal. calc. for $C_{62}H_{56}Br_4CoN_4P_4$ (1418.54) (%): C, 52.50; H, 3.98; N, 3.95 Found (%): C, 51.91; H, 3.91; N, 3.92; MS (ESI): positive ion *m/z* 520.2 (100.00% $[M\text{-}Co_2Br_4C_{31}H_{30}N_2P_2+O_2]^+$), 1120.4 (30.84% $[M\text{-}CoBr_3]^+$); negative ion *m/z* 297.7 (100.00% $[CoBr_3]^-$).

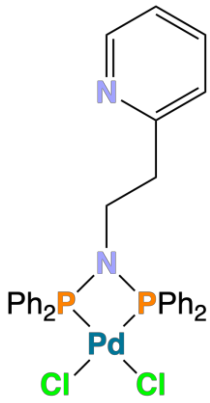


**3.8**

**Synthesis of [{Py-*o*-$(CH_2)_2N(PPh_2)_2$}$PdCl_2$] (3.8):** Py-*o*-$(CH_2)_2N(PPh_2)_2$, **2.1**, (0.195 g, 0.397 mmol) and $[(MeCN)_2PdCl_2]$ (0.102 g, 0.397 mmol) were stirred in DCM (10 mL) overnight. The reaction mixture was concentrated to 5 mL and layered with $Et_2O$ (15 mL), affording crystals after 18 hours. These were isolated by filtration, and the product dried *in vacuo*, affording complex **3.8** as yellow crystals (0.173 g, 0.259 mmol, 65%). $\delta_H$ (400 MHz, $CD_2Cl_2$) 8.33 (1H, dq, $J_{HH}$ = 0.7 Hz, 4.8 Hz, H-6Py), 7.94-8.04 (8H, m, phenyl), 7.71-7.79 (4H, m, phenyl), 7.60-7.68 (8H, m, phenyl), 7.48 (1H, t, $J_{HH}$ = 7.5 Hz, H-4Py), 7.07 (1H, t, $J_{HH}$ = 5.7 Hz, H-5Py), 6.67 (1H, d, $J_{HH}$ = 7.9 Hz, H-3Py), 3.49-3.64 (2H, m, $C\underline{H}_2N(PPh_2)_2$), 2.45-2.56 (2H, m, Py-$C\underline{H}_2$); $\delta_P$ $^{31}P\{^1H\}$ (162 MHz, $CD_2Cl_2$) 30.9 (2P, s); selected $\nu_{max}$ / $cm^{-1}$ 1603, 1473 (C=C), 1589, 1568 (C=N), 1433 (P-Ph), 842 (P-N-P), 331, 286 (Pd-Cl); Anal. calc. for $C_{31}H_{28}Cl_2N_2P_2PdCl_2 \cdot CH_2Cl_2$ (752.77) (%): C, 51.06; H, 4.02; N, 3.72 Found (%): C, 50.59; H, 4.04; N, 3.72; MS (ESI): positive ion *m/z* 632.2 (100.00% $[M-Cl+H]^+$).

## References


1. G. M. Sheldrick, *Acta Crystallogr. Sect. A: Found. Crystallogr.*, **2008**, *64*, 112 – 122. 10.1107/S0108767307043930
2. C. F. Macrae, I. Sovago, S. J. Cottrell, P. T. A. Galek, P. McCabe, E. Pidcock, M. Platings, G. P. Shields, J. S. Stevens, M. Towler and P. A. Wood, *J. Appl. Crystallogr.*, **2020**, *53*, 226 – 235. 10.1107/S1600576719014092
3. I. J. Bruno, J. C. Cole, P. R. Edgington, M. Kessler, C. F. Macrae, P. McCabe, J. Pearson, R. Taylor, *Acta Cryst.*, **2002**, *B58*, 389 – 397. 10.1107/s0108768102003324
4. M. J. Frisch, G. W. Trucks, H. B. Schlegel, G. E. Scuseria, M. A. Robb, J. R. Cheeseman, G. Scalmani, V. Barone, G. A. Petersson, H. Nakatsuji, X. Li, M. Caricato, A. V. Marenich, J. Bloino, B. G. Janesko, R. Gomperts, B. Mennucci, H. P. Hratchian, J. V. Ortiz, A. F. Izmaylov, J. L. Sonnenberg, D. Williams-Young, F. Ding, F. Lipparini, F. Egidi, J. Goings, B. Peng, A. Petrone, T. Henderson, D. Ranasinghe, V. G. Zakrzewski, J. Gao, N. Rega, G. Zheng, W. Liang, M. Hada, M. Ehara, K. Toyota, R. Fukuda, J. Hasegawa, M. Ishida, T. Nakajima, Y. Honda, O. Kitao, H. Nakai, T. Vreven, K. Throssell, J. A. Montgomery, Jr., J. E. Peralta, F. Ogliaro, M. J. Bearpark, J. J. Heyd, E. N. Brothers, K. N. Kudin, V. N. Staroverov, T. A. Keith, R. Kobayashi, J. Normand, K. Raghavachari, A. P. Rendell, J. C. Burant, S. S. Iyengar, J. Tomasi, M. Cossi, J. M. Millam, M. Klene, C. Adamo, R. Cammi, J. W. Ochterski, R. L. Martin, K. Morokuma, O. Farkas, J. B. Foresman, D. J. Fox, Gaussian, Inc., Wallingford CT, **2016**.
5. GaussView, Version 6.1, R. Dennington, T. A. Keith, J. M. Millam, Semichem Inc., Shawnee Mission, KS, **2016**.
6. P. Wang, H. Liu, Y-Q. Li, X-L. Zhao, Y. Lu, Y. Liu, *Catal. Sci. Technol.*, **2016**, *6*, 3854 – 3861. 10.1039/C5CY01827G
7. H. Lee, S. H. Hong, *Appl. Catal., A*, **2018**, *560*, 21 – 27. 10.1016/j.apcata.2018.04.030

8. P-H. Zhao, M-Y. Hu, J-R. Li, Z-Y. Ma, Y-Z. Wang, J. He, Y-L. Li, X-F. Liu, *Organometallics*, **2019**, *38*, 385 – 394. 10.1021/acs.organomet.8b00759
9. L-C. Song, L. Feng, Y-Q. Guo, *Dalton Trans*., **2019**, *48*, 1443 – 1453. 10.1039/C8DT04211J
10. Y. Shaikh, J. Gurnham, K. Albahily, S. Gambarotta, I. Korobkov, *Organometallics*, **2012**, *31*, 7427 – 7433. 10.1021/om3007135
11. Y. Xu, Y. J. Hong, D. J. Tantillo, M. K. Brown, *Org. Lett*., **2017**, *19*, 3703 – 3706. 10.1021/acs.orglett.7b01420
12. J. R. Ascenso, C. G. de Azevedo, A. R. Dias, M. T. Duarte, I. Eleutério, M. J. Ferreira, P. T. Gomes, A. M. Martins, *J. Organomet. Chem*., **2001**, *632*, 17 – 26. 10.1016/S0022-328X(01)00837-3
13. J-S. Sun, H. Zhao, X. Ouyang, R. Clérac, J. A. Smith, J. M. Clemente-Juan, C. Gómez-Garcia, E. Cornado, K. R. Dunbar, *Inorg. Chem*., **1999**, *38*, 5841 – 5855. 10.1021/ic990525w
14. G. A. Bain, J. F. Berry, *J. Chem. Educ*., **2008**, *85*, 532 – 536. 10.1021/ed085p532
15. D. F. Evans, *J. Chem. Soc*., **1959**, 2003 – 2005. 10.1039/JR9590002003
16. D. F. Evans, G. V. Fazakerley, R. F. Phillips, *J. Chem. Soc. A*, **1971**, 1931 – 1934. 10.1039/J19710001931
17. B. A. Suslick, T. D. Tilley, *J. Am. Chem. Soc*., **2020**, *142*, 11203 – 11218. 10.1021/jacs.0c04072
18. A. Carrick, MChem Thesis, Durham University, **2020**.

# Chapter 8 – Conclusions and Future Outlook

## 8.1 Conclusions

The main aim of the work presented in this thesis (outlined in **Section 1.4**, **Chapter 1**) was to study the structures and reactivity of acute bite angle ligand complexes to develop an understanding of the effects of acute bite angle ligands on cobalt complexes. This aim has been achieved by probing the coordination chemistry of acute bite angle 'PNP' ligands, mainly Py-*o*-$(CH_2)_2N(PPh_2)_2$ (compound **2.1**) and $Ph(CH_2)_2N(PPh_2)_2$ (compound **2.2**), with cobalt(II) halides, and subsequently accessing low valent cationic cobalt(I) species containing 'PNP' ligands for a reactivity study. The 1:1 reaction of compound **2.1** with $CoX_2$ (X = Cl, Br, I) affords zwitterionic complexes [CoX(Py-*o*-$(CH_2)_2N\{PPh_2\}_2$)({$X_3Co$}Py-*o*-$(CH_2)_2N\{PPh_2\}_2$)] (complexes **4.7**, **2.14** and **4.8** with X = Cl, Br and I, respectively). In contrast, the 1:1 reaction of compound **2.2** with $CoX_2$ affords ionic complexes $[CoX(Ph(CH_2)_2N\{PPh_2\}_2)_2]_2[Co_2X_6]$ (complexes **4.9**, **4.10** and **4.11** with X = Cl, Br and I, respectively), which are presented for the first time in this work. The same complexes are isolated irrespective of the 'PNP':$CoX_2$ ratio (1:1 and 2:1 screened). The reaction of complex **4.10** with pyridine to afford $[CoBr(Ph(CH_2)_2N\{PPh_2\}_2)_2][PyCoBr_3]$ (complex **4.19**) verifies that zwitterionic complexes are afforded *via* an *in situ* formed ionic complex ($[CoBr(Py\text{-}o\text{-}(CH_2)_2N\{PPh_2\}_2)_2]_2[Co_2Br_6]$, complex **4.18**, in the case of complex **2.14**) which undergoes an intramolecular reaction.

Moving towards accessing low valent cationic cobalt(I) complexes containing 'PNP' ligands, $[CoBr(Ph(CH_2)_2N\{PPh_2\}_2)_2][PF_6]$, $[CoBr(Py\text{-}o\text{-}(CH_2)_2N\{PPh_2\}_2)_2][PF_6]$ and $[CoBr(Ph(CH_2)_2N\{PPh_2\}_2)_2][BAr^F{}_4]$ (complexes **5.1** – **5.3**, respectively), containing a single cationic cobalt(II) centre, were accessed. Reduction of complexes **5.1** – **5.3** with activated zinc affords cobalt(I) species $[Co(Ph(CH_2)_2N\{PPh_2\}_2)_2][PF_6]$, $[Co(Py\text{-}o\text{-}(CH_2)_2N\{PPh_2\}_2)_2][PF_6]$ and $[Co(Ph(CH_2)_2N\{PPh_2\}_2)_2][BAr^F{}_4]$ (complexes **5.5** – **5.7**, respectively) suitable for a reactivity study. Indeed, complex **5.7** has been shown to react with dioxygen, ethylene, carbon monoxide and dihydrogen, affording $[Co\{Ph(CH_2)_2N(PPh_2)_2\}_2(\eta^2\text{-}O_2)][BAr^F{}_4]$ (complex **5.13**), $[Co\{Ph(CH_2)_2N(PPh_2)_2\}_2(\eta^2$-

$CH_2CH_2$)][$BAr^F_4$] (complex **6.1**), [Co{Ph($CH_2$)$_2$N($PPh_2$)$_2$}$_2$(CO)][$BAr^F_4$] (complex **6.21**), and an equilibrium mixture of [Co(Ph($CH_2$)$_2$N{$PPh_2$}$_2$)$_2$($\eta^2$-$H_2$)][$BAr^F_4$] (complex **6.26**) and [Co(Ph($CH_2$)$_2$N{$PPh_2$}$_2$)$_2$(*cis*-(H)$_2$)][$BAr^F_4$] (complex **6.29**). Hence, low valent cationic cobalt(I) complexes containing 'PNP' ligands have been accessed and their reactivity with a range of substrates has been probed. One equivalent of ethylene coordinates to complex **5.7** when exposed to a large excess of ethylene. As a result, complex **5.7** does not catalyse ethylene oligomerisation. Attempts at using complex **5.7** for hydroformylation catalysis by Jake Backhouse (Dyer group member) led to no conversion, presumably because complex **5.7** reacts with CO affording complex **6.21** (**Scheme 6.6**), which is not catalytically active. Hence, application of complex **5.7** as a catalyst for catalytic processes including olefin oligomerisation and hydroformylation appears to be limited.

It is also noteworthy that side aims of studying the coordination chemistry of 'PNP' ligands with palladium(II) dichloride and selenium were successful. The reactivity of compounds **2.2** and **2.1** with zinc(II) dibromide, with the structures of the obtained complexes being tentatively assigned as coordination polymers [(Ph($CH_2$)$_2$N($Ph_2P$)$_2$)$ZnBr_2$]$_n$ (complex **5.44**) and [(Py-*o*-($CH_2$)$_2$N($Ph_2P$)$_2$)$ZnBr_2$]$_n$ (complex **5.54**), respectively.

## 8.2 Future Outlook

As mentioned in **Section 6.5**, **Chapter 6**, the origin of the lack of catalytic activity of complex **5.7** likely originates from two equivalents of 'PNP' ligand coordinating at the cobalt(I) centre in a $\kappa^2$-*P,P* manner in the [Co{RN(PR'$_2$)$_2$}$_2$] cation. Hence, the cobalt(I) centre of the [Co{RN(PR'$_2$)$_2$}$_2$] cation is sterically and coordinatively congested. A strategy to potentially produce cationic cobalt(I) complexes with one equivalent of 'PNP' ligand coordinating at the cobalt(I) centre (which, accordingly, would be less sterically congested, and potentially more suitable for catalytic applications) is to synthesise complexes of the form of complex **8.1** (**Scheme 8.1**). This strategy has been successfully implemented for other diphosphines in place of 'PNP' compounds in **Scheme 8.1**.[1]

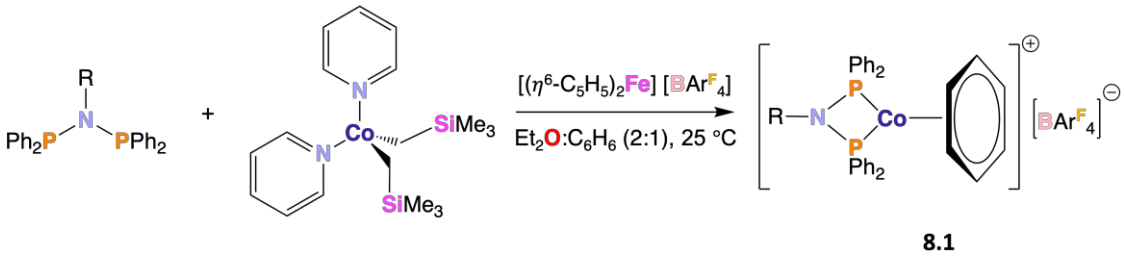


**Scheme 8.1.** Synthesis of complex **8.1**.

The synthesis of compounds **8.2** and **8.3** (**Figure 8.1**) and a subsequent study of their coordination chemistry with $CoBr_2$ would also be of interest. The cobalt(II) bromide complex of compound **8.2** could potentially exhibit $\kappa^2$-*P,N*, $\kappa^2$-*P,S*, or $\kappa^2$-*S,N* coordination, whereas compound **8.3** may coordinate to cobalt(II) bromide in a $\kappa^2$-*S,N* manner as $\kappa^2$-*S,S* coordination has been established to not occur due to the lack of reaction between $Ph(CH_2)_2N(P\{S\}Ph_2)_2$ (compound **2.10**) and cobalt(II) bromide (**Scheme 4.12**, **Chapter 2**).

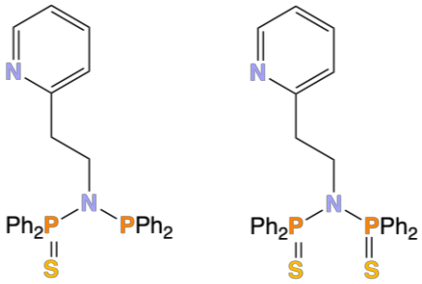


**Figure 8.1.** Structures of compounds **8.2** and **8.3**.

Probing the reactivity of complex **5.7** with $CO_2$ (**Scheme 8.2**) may also be of interest as it is likely that cobalt(III) complex **8.4** would be produced. If accessible, complex **8.4**, like $[Ni(\eta^2\text{-}CO_2)(PCy_3)_2]$, may be capable of catalysing organozinc coupling with $CO_2$.[2]

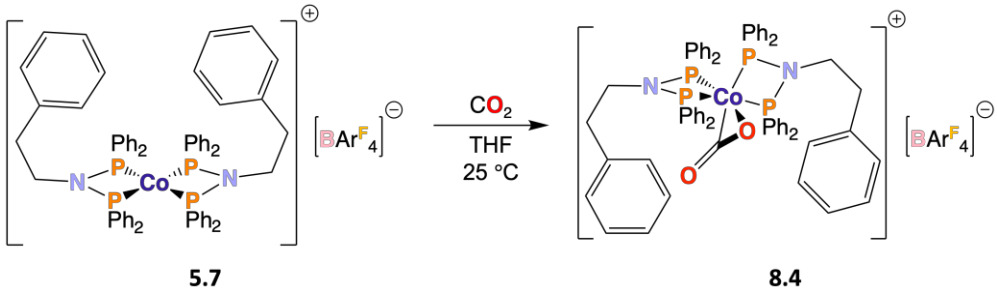


**Scheme 8.2.** Reaction of complex **5.7** with $CO_2$.

## References


1. C. S. MacNeil, H. Zhong, T. P. Pabst, M. Shevlin, P. J. Chirik, *ACS Catal.*, **2022**, *12*, 4680 – 4687. 10.1021/acscatal.2c01059
2. C. S. Yeung, V. M. Dong, *J. Am. Chem. Soc.*, **2008**, *130*, 7826 – 7827. 10.1021/ja803435w

# Appendices

## Appendix 1 – Conferences Attended

**OWPC-21 –** Online Workshop on Phosphorus Chemistry 2021, March 29th – 31st
Poster: Catalytic Alkene Carbonylation: Design, Synthesis and Application of Multi-functional Ligands

**Dalton 2021 –** joint interest group meeting, 29th June – 1st July 2021
Poster: Coordination chemistry of *Bis*(diphenylphosphino)amine-type ligands with cobalt(II) halides

**Scottish Dalton Meeting 2021 –** 26th August 2021
Flash: Coordination chemistry of *Bis*(diphenylphosphino)amine-type ligands with cobalt(II) halides

**Durham Postgraduate Symposium 2022** – June 22nd – 23rd 2022
Poster: Synthesis and Reactivity of *bis*(Diphenylphosphino)amine-type Ligand Cobalt Complexes

**Liverpool Summer School in Catalysis: Fundamentals and Practice 2022** – July 18th – 22nd 2022
Poster: Synthesis and Reactivity of *bis*(Diphenylphosphino)amine-type Ligand Cobalt Complexes

**RSC Sir Geoffrey Wilkinson Dalton Poster Symposium 2022** – 7th September 2022
Poster: Synthesis and Reactivity of *bis*(Diphenylphosphino)amine-type Ligand Cobalt Complexes

**18th European Workshop on Phosphorus Chemistry** – September 14th – 16th 2022
Talk: Coaxing Cobalt with '*PNP*' Ligands

**Dalton 2023** – April 18th – 20th 2023
Talk: Coaxing Cobalt with '*PNP*' Ligands

**Durham Postgraduate Symposium 2023** – June 21st 2023
Talk: Coaxing Cobalt with '*PNP*' Ligands

**7th SaFE National Teachers and Educators Hybrid Conference** – 4th July 2023
Theme: The Next Generation of Chemistry Teachers – Enthusing Early Career Chemistry Teachers. Developing Student Transitions

**Dalton Young Members Event 2023** – August 17th – 18th 2023
Poster: Coaxing Cobalt with '*PNP*' Ligands

## Appendix 2 – Seminars Attended

*Substituted Shape-Shifters and 8pi/6pi Synthesis*
Dr Thomas Fallon, University of Adelaide, Australia, 21st October 2020

*Much ado about a ring: The curious case of tropylium ion*
Dr Vinh Nguyen, University of New South Wales, Australia, 25th November 2020

*The role of ammonia in a future carbon-free energy landscape*
Dr Laura Torrente Murciano, University of Cambridge, 24th February 2021

*Early transition metal complexes for the treatment of cancer – a necessary evil?*
Dr Rianne Lord, University of East Anglia, 10th March 2021

*Linking Structure and Function in Materials for Energy and the Environment*
Dr John Griffin, Lancaster University, 17th March 2021

*Amazing Phosphorus Ligands for Innovations in Carbonylation Chemistry*
Prof Matthias Beller, Leibniz Institute for Catalysis, 21st September 2021

*How Do You Write Chemoselectivity? Of Course With a P!*
Prof Christian Hackenberger, Leibniz-Forschungsinstitut für Molekulare Pharmakologie, 21st September 2021

*The Unique Properties of Organophosphorus Compounds for Optoelectronics*
Prof Muriel Hissler, Rennes Institute of Chemical Sciences, 21st September 2021

*Phosphorus Sustainability: Addressing Environmental Challenges of P Deficiencies and Excesses*
Prof Helen Jarvie, University of Waterloo, 21st September 2021

*Conversion of butanol to propene via a triple flow cascade dehydration, isomerisation and metathesis*
Dr Yiping Shi, University of Durham, 10th November 2021

*Zeolite catalysis for the conversion of mandelic acid into bioplastic monomers*
Sam Meacham, University of Durham, 10th November 2021

*Improving the selectivity of nickel-based catalysts for vapour-phase furfural hydrogenation*
Kathryn MacIntosh, University of Durham, 10th November 2021

*From phosphorescence to delayed fluorescence in one step: tuning photophysical properties by quanternisation of an $sp^2$ nitrogen atom*
Dr Anastasia Klimash, 19th November 2021

*Twists and Turns in Stereoselective Synthesis*

Dr Roly Armstrong, Newcastle University, 1st December 2021

*Shape Selective Mass Spectrometry*
Dr Jackie Mosley, Teesside University, 28th January 2022

*Making "Difficult-to-Make" Molecules: Photochemistry as an Enabling Tool*
Dr Susannah Coote, Lancaster Univeristy, 23rd February 2022

*Design of anisotropic or hierarchical nanostructures for healthcare and energy applications*
Dr Sunjie Le, University of Leeds, 16th March 2022

*From molecules to crystal treasures: Lessons learnt along the pathways*
Dr Aurora Cruz-Cabeza, University of Manchester, 25th March 2022

*Understanding and Exploring Selectivity in the Ir-Catalysed C-H Borylation of Heterocycles*
Prof Patrick Steel, Durham University, 4th May 2022

*New Synthetic Chemistry for the Exploration of 3-D Pharmaceutical Space*
Prof Peter O'Brien, University of York, 4th May 2022

*Functionalization of N-Heterocycles using Li, Mg and Zn Organometallics*
Prof Paul Knockel, Ludwig-Maximilians Universität München, 4th May 2022

*Applications of Thiyl-Radicals for Peptide Synthesis*
Dr Eoin Scanlan, Trinity College Dublin, 11th May 2022

*Dissociation Dynamics of Complex Ions*
Dr Jemma Gibbard, Durham University, 9th November 2022
*Advancing the Field of Bio-Derived Polymers Synthesised by Living Anionic Polymerisation*
Llyod Shaw, Durham University, 9th November 2022

*Keeping You Smelling Nice for Longer – The Chemistry of Slow Release Perfumes*
Beth Beck, Durham University, 9th November 2022

*Characterising the Hygroscopicity of Chloride and Carbonate Containing Aerosols to Quantify Multicomponent Droplets*
C Day, Northumbria University, 9th November 2022

*Nanostructural and Water Transport in Epoxy Barrier Coatings*
Dr Suzanne Morsch, University of Manchester, 16th November 2022

*NMR Data Analysis By and For Synthetic Chemists: Is there a Better Way?*
Dr Alan Kenwright, Durham University, 22nd November 2022

*Redox-controlled Photochemistry and Photo-assisted Electrochemistry*
Prof Franti Hartl, University of Reading, 25th January 2023

*Can Data Save Us? Exploring the Role of Informatics on Materials Research*
Dr Taylor Sparks, University of Utah, 1st February 2023

*Innovation in Research and Applied Technology in Organic Synthesis: Prospecting for Bioactive Compounds and Certified Reference Materials*
Prof Fernanda Gadini Finelli, University of Rio de Janeiro, 8th February 2023

*Advanced Electrocatalysts for Sustainable Energy Technologies*
Dr Laurie King, Manchester Metropolitan University, 22nd February 2023

*Sustainable Processes and Catalysis for the Net Zero Transition*
Dr Stephen Poulston, Johnson Matthey, 22nd February 2023

*Catalysis Using Renewable Resources to Make Recyclable and Degradable Plastics, Elastics and Adhesives*
Prof Charlotte Williams, University of Oxford, 22nd February 2023

*Evaluation and Development of Methodologies for the Synthesis of Chiral Phosphorus Acid Organocatalysts*
Prof Jean-Luc Montchamp, College of Science and Engineering, 8th March 2023

*New Approaches for Reductive Elimination? – Exploring Phosphine-Alkene Ligand Chemistry*
Prof Philip W Dyer, Durham University, 8th March 2023

*High Performance Luminescent Materials Using Structural Constraint*
Prof Zachary Hudson, University of British Columbia, 13th March 2023
*Synthetic Biology Approaches to New Chemistry*
Prof Michelle Chang, University of California, Berkeley, 23rd March 2023

*Polymers for Cells: a Journey Towards a Better Understanding of Cell Behaviour*
Dr Maria Chiara Arno, University of Birmingham, 10th May 2023

*How to build a molecular machine*
Dr Stefan Borsley, University of Manchester, 20th June 2023

*From charge transfer processes in biopolymers to functional protein-based materials*
Prof Nadav Amdursky, Technion, Israel Institute of Technology, 27th June 2023

## Appendix 3 – Publications in Preparation

1. A. Carrick, A. S. Batsanov, D. S. Yufit, P. W. Dyer, A study into the coordination of DPPA-type ligands with cobalt(II) halides. In preparation.

## Appendix 4 – Crystallographic Data

| Compound | 2.9: 0.12 2.9 Ox | 2.10 | **3.1**·DCM |
|---|---|---|---|
| Identification code | 23srv152 | 23srv155 | 21srv159 |
| Empirical formula | $C_{32}H_{29}NO_{0.12}P_2S$ | $C_{32}H_{29}NP_2S_2$ | $C_{33}H_{31}Cl_4NP_2Pd$ |
| Formula weight | 523.44 | 553.62 | 751.73 |
| Temperature/K | 120.00 | 120.00 | 120 |
| Crystal system | monoclinic | triclinic | monoclinic |
| Space group | $P2_1/c$ | P-1 | $P2_1/n$ |
| a/Å | 10.2714(2) | 10.2020(2) | 11.1660(3) |
| b/Å | 18.5374(4) | 11.2112(3) | 16.5810(5) |
| c/Å | 14.8905(4) | 13.3545(3) | 17.3397(5) |
| α/° | 90 | 87.7200(10) | 90 |
| β/° | 106.5610(10) | 71.4640(10) | 91.9076(12) |
| γ/° | 90 | 70.7860(10) | 90 |
| Volume/$Å^3$ | 2717.61(11) | 1363.94(6) | 3208.55(16) |
| Z | 4 | 2 | 4 |
| $\rho_{calc}g/cm^3$ | 1.279 | 1.348 | 1.556 |
| $\mu/mm^{-1}$ | 0.259 | 0.336 | 1.036 |
| F(000) | 1100.0 | 580.0 | 1520.0 |
| Crystal size/$mm^3$ | 0.368 × 0.132 × 0.044 | 0.202 × 0.201 × 0.163 | 0.259 × 0.12 × 0.095 |
| Radiation | Mo Kα (λ = 0.71073) | Mo Kα (λ = 0.71073) | Mo Kα (λ = 0.71073) |
| 2Θ range for data collection/° | 4.394 to 65.242 | 3.858 to 74.702 | 4.4 to 69.938 |
| Index ranges | -15 ≤ h ≤ 15, -28 ≤ k ≤ 28, -22 ≤ l ≤ 22 | -17 ≤ h ≤ 17, -19 ≤ k ≤ 18, -22 ≤ l ≤ 22 | -18 ≤ h ≤ 17, -26 ≤ k ≤ 26, -27 ≤ l ≤ 27 |
| Reflections collected | 76348 | 66548 | 74884 |
| Independent reflections | 9927 [$R_{int}$ = 0.0659, $R_{sigma}$ = 0.0427] | 13082 [$R_{int}$ = 0.0374, $R_{sigma}$ = 0.0354] | 14018 [$R_{int}$ = 0.0485, $R_{sigma}$ = 0.0408] |
| Data/restraints/ parameters | 9927/0/335 | 13082/0/334 | 14018/0/371 |
| Goodness-of-fit on $F^2$ | 1.079 | 1.026 | 1.026 |
| Final R indexes [I>=2σ (I)] | $R_1$ = 0.0542, $wR_2$ = 0.1110 | $R_1$ = 0.0403, $wR_2$ = 0.0965 | $R_1$ = 0.0317, $wR_2$ = 0.0641 |
| Final R indexes [all data] | $R_1$ = 0.0724, $wR_2$ = 0.1179 | $R_1$ = 0.0570, $wR_2$ = 0.1037 | $R_1$ = 0.0462, $wR_2$ = 0.0689 |
| Largest diff. peak/hole / e $Å^{-3}$ | 0.71/-0.46 | 0.55/-0.33 | 0.56/-0.69 |

| **Compound** | **3.3** | **3.4**·DCM | **3.5**·2DCM |
|---|---|---|---|
| Identification code | 21srv179 | 21srv183 | 21srv366 |
| Empirical formula | $C_{29}H_{32}Cl_2N_2P_2Pd$ | $C_{31}H_{28}Cl_4N_2P_2Pd$ | $C_{38}H_{33}Cl_6NP_2Pd$ |
| Formula weight | 647.80 | 738.69 | 884.69 |
| Temperature/K | 120 | 120 | 120 |
| Crystal system | orthorhombic | orthorhombic | monoclinic |
| Space group | $Pna2_1$ | $Pna2_1$ | C2/c |
| a/Å | 19.8695(5) | 20.6994(5) | 17.1508(4) |
| b/Å | 9.9715(3) | 8.5461(2) | 16.2438(4) |
| c/Å | 14.5270(4) | 17.6036(4) | 14.4493(3) |
| α/° | 90 | 90 | 90 |
| β/° | 90 | 90 | 115.2488(8) |
| γ/° | 90 | 90 | 90 |
| Volume/Å$^3$ | 2878.22(14) | 3114.06(13) | 3640.91(15) |
| Z | 4 | 4 | 4 |
| $\rho_{calc}$g/cm$^3$ | 1.495 | 1.576 | 1.614 |
| μ/mm$^{-1}$ | 0.963 | 1.067 | 1.068 |
| F(000) | 1320.0 | 1488.0 | 1784.0 |
| Crystal size/mm$^3$ | 0.184 × 0.132 × 0.087 | 0.212 × 0.054 × 0.045 | 0.27 × 0.267 × 0.238 |
| Radiation | Mo Kα (λ = 0.71073) | Mo Kα (λ = 0.71073) | Mo Kα (λ = 0.71073) |
| 2Θ range for data collection/° | 4.1 to 74.836 | 5.156 to 68.992 | 5.906 to 73.988 |
| Index ranges | -32 ≤ h ≤ 33, -16 ≤ k ≤ 15, -24 ≤ l ≤ 24 | -32 ≤ h ≤ 32, -13 ≤ k ≤ 13, -28 ≤ l ≤ 27 | -28 ≤ h ≤ 29, -27 ≤ k ≤ 26, -23 ≤ l ≤ 22 |
| Reflections collected | 90152 | 71531 | 55829 |
| Independent reflections | 13798 [$R_{int}$ = 0.0340, $R_{sigma}$ = 0.0244] | 13170 [$R_{int}$ = 0.0530, $R_{sigma}$ = 0.0438] | 8595 [$R_{int}$ = 0.0320, $R_{sigma}$ = 0.0241] |
| Data/restraints/ parameters | 13798/1/329 | 13170/2/377 | 8595/0/287 |
| Goodness-of-fit on F$^2$ | 1.043 | 1.047 | 1.040 |
| Final R indexes [I>=2σ (I)] | $R_1$ = 0.0258, $wR_2$ = 0.0580 | $R_1$ = 0.0367, $wR_2$ = 0.0828 | $R_1$ = 0.0246, $wR_2$ = 0.0551 |
| Final R indexes [all data] | $R_1$ = 0.0294, $wR_2$ = 0.0597 | $R_1$ = 0.0466, $wR_2$ = 0.0877 | $R_1$ = 0.0293, $wR_2$ = 0.0570 |
| Largest diff. peak/hole / e Å$^{-3}$ | 0.72/-0.53 | 0.96/-0.73 | 0.59/-0.57 |

| **Compound** | **3.6**·1.5DCM | **3.7**·DCM | **3.9**·DCM |
|---|---|---|---|
| Identification code | 21srv367 | 21srv024 | 22srv171 |
| Empirical formula | $C_{36.5}H_{31}Cl_5N_2P_2Pd$ | $C_{33.36}H_{32.72}Cl_{2.72}N_2P_2Pd$ | $C_{34}H_{31}Cl_4F_3N_2O_2P_2Pd$ |
| Formula weight | 843.22 | 726.22 | 866.75 |
| Temperature/K | 120 | 120 | 120.00 |
| Crystal system | orthorhombic | orthorhombic | monoclinic |
| Space group | $P2_12_12_1$ | $P2_12_12_1$ | $P2_1/n$ |
| a/Å | 10.1267(2) | 8.0011(3) | 9.2629(5) |
| b/Å | 14.6938(3) | 17.5756(7) | 27.5491(15) |
| c/Å | 24.9097(5) | 22.6361(9) | 14.5836(8) |
| α/° | 90 | 90 | 90 |
| β/° | 90 | 90 | 101.602(2) |
| γ/° | 90 | 90 | 90 |
| Volume/Å$^3$ | 3706.56(13) | 3183.2(2) | 3645.5(3) |
| Z | 4 | 4 | 4 |
| $\rho_{calc}$g/cm$^3$ | 1.511 | 1.515 | 1.579 |
| μ/mm$^{-1}$ | 0.976 | 0.938 | 0.939 |
| F(000) | 1700.0 | 1476.0 | 1744.0 |
| Crystal size/mm$^3$ | 0.257 × 0.094 × 0.083 | 0.206 × 0.146 × 0.024 | 0.18 × 0.13 × 0.02 |
| Radiation | Mo Kα (λ = 0.71073) | Mo Kα (λ = 0.71073) | Mo Kα (λ = 0.71073) |
| 2Θ range for data collection/° | 4.288 to 69.954 | 4.972 to 66 | 4.108 to 60 |
| Index ranges | -16 ≤ h ≤ 15, -23 ≤ k ≤ 23, -39 ≤ l ≤ 40 | -12 ≤ h ≤ 12, -26 ≤ k ≤ 26, -34 ≤ l ≤ 34 | -13 ≤ h ≤ 13, -38 ≤ k ≤ 38, -20 ≤ l ≤ 20 |
| Reflections collected | 89393 | 92973 | 131547 |
| Independent reflections | 16268 [$R_{int}$ = 0.0457, $R_{sigma}$ = 0.0384] | 12022 [$R_{int}$ = 0.0642, $R_{sigma}$ = 0.0424] | 10603 [$R_{int}$ = 0.0579, $R_{sigma}$ = 0.0267] |
| Data/restraints/ parameters | 16268/28/460 | 12022/11/457 | 10603/12/464 |
| Goodness-of-fit on F$^2$ | 1.034 | 1.026 | 1.226 |
| Final R indexes [I>=2σ (I)] | $R_1$ = 0.0344, $wR_2$ = 0.0720 | $R_1$ = 0.0360, $wR_2$ = 0.0626 | $R_1$ = 0.0483, $wR_2$ = 0.0937 |
| Final R indexes [all data] | $R_1$ = 0.0408, $wR_2$ = 0.0743 | $R_1$ = 0.0498, $wR_2$ = 0.0671 | $R_1$ = 0.0537, $wR_2$ = 0.0955 |
| Largest diff. peak/hole / e Å$^{-3}$ | 1.18/-0.54 | 0.52/-0.85 | 0.73/-1.37 |

| **Compound** | **3.10**·2DCM | **3.11**·DCM | **3.25** |
|---|---|---|---|
| Identification code | 22srv061 | 22srv049 | 22srv090 |
| Empirical formula | $C_{36.5}H_{36}Cl_5F_3N_2O_2P_2Pd$ | $C_{29.33}H_{33.67}Cl_{2.67}F_6N_2P_3Pd$ | $C_{43}H_{56}Cl_5CoN_3P_2Pd$ |
| Formula weight | 937.26 | 822.09 | 1019.42 |
| Temperature/K | 120.00 | 120.00 | 120.00 |
| Crystal system | monoclinic | monoclinic | monoclinic |
| Space group | P2/c | $P2_1/c$ | $P2_1/c$ |
| a/Å | 21.1390(6) | 22.2356(7) | 16.3268(7) |
| b/Å | 11.2934(3) | 22.9563(7) | 8.6193(4) |
| c/Å | 17.7410(5) | 20.2843(6) | 33.1966(14) |
| α/° | 90 | 90 | 90 |
| β/° | 101.9250(10) | 92.7649(12) | 98.3830(10) |
| γ/° | 90 | 90 | 90 |
| Volume/Å$^3$ | 4143.9(2) | 10342.0(5) | 4621.7(4) |
| Z | 4 | 12 | 4 |
| $\rho_{calc}$g/cm$^3$ | 1.502 | 1.584 | 1.465 |
| μ/mm$^{-1}$ | 0.895 | 0.940 | 1.140 |
| F(000) | 1892.0 | 4968.0 | 2092.0 |
| Crystal size/mm$^3$ | 0.14 × 0.05 × 0.01 | 0.16 × 0.12 × 0.08 | 0.14 × 0.02 × 0.0008 |
| Radiation | Mo Kα (λ = 0.71073) | Mo Kα (λ = 0.71073) | Mo Kα (λ = 0.71073) |
| 2Θ range for data collection/° | 4.11 to 60 | 3.994 to 60 | 4.886 to 51.998 |
| Index ranges | -29 ≤ h ≤ 29, -15 ≤ k ≤ 15, -24 ≤ l ≤ 24 | -31 ≤ h ≤ 31, -32 ≤ k ≤ 32, -28 ≤ l ≤ 28 | -20 ≤ h ≤ 20, -10 ≤ k ≤ 10, -40 ≤ l ≤ 40 |
| Reflections collected | 98846 | 236499 | 65386 |
| Independent reflections | 12090 [$R_{int}$ = 0.0683, $R_{sigma}$ = 0.0406] | 30128 [$R_{int}$ = 0.0593, $R_{sigma}$ = 0.0373] | 9079 [$R_{int}$ = 0.1051, $R_{sigma}$ = 0.0692] |
| Data/restraints/ parameters | 12090/6/482 | 30128/56/1222 | 9079/0/526 |
| Goodness-of-fit on $F^2$ | 1.063 | 1.037 | 1.043 |
| Final R indexes [I>=2σ (I)] | $R_1$ = 0.0567, $wR_2$ = 0.1374 | $R_1$ = 0.0507, $wR_2$ = 0.1198 | $R_1$ = 0.0486, $wR_2$ = 0.0884 |
| Final R indexes [all data] | $R_1$ = 0.0702, $wR_2$ = 0.1449 | $R_1$ = 0.0736, $wR_2$ = 0.1334 | $R_1$ = 0.0905, $wR_2$ = 0.1068 |
| Largest diff. peak/hole / e Å$^{-3}$ | 2.02/-1.29 | 1.85/-1.20 | 0.67/-0.49 |

| **Compound** | **3.29**·DCM | **3.30** | **4.1**·3DCM |
|---|---|---|---|
| Identification code | 22srv230 | 22srv233 | 21srv160c |
| Empirical formula | $C_{21}H_{23}Cl_4N_2PPd$ | $C_{20}H_{21}Cl_2N_2O_2PPd$ | $C_{115}H_{122}Br_8Cl_6Co_4N_4P_8$ |
| Formula weight | 582.58 | 529.66 | 2895.62 |
| Temperature/K | 120.00 | 120.00 | 120 |
| Crystal system | orthorhombic | monoclinic | triclinic |
| Space group | Pbca | $P2_1/c$ | P-1 |
| a/Å | 9.0393(2) | 10.4481(2) | 12.0169(4) |
| b/Å | 16.8788(4) | 12.6348(3) | 24.1352(8) |
| c/Å | 30.3005(7) | 15.5868(3) | 24.2559(8) |
| α/° | 90 | 90 | 61.7826(12) |
| β/° | 90 | 91.4480(10) | 75.9875(13) |
| γ/° | 90 | 90 | 77.1106(13) |
| Volume/Å$^3$ | 4623.02(18) | 2056.95(7) | 5965.7(5) |
| Z | 8 | 4 | 2 |
| $\rho_{calc}$g/cm$^3$ | 1.674 | 1.710 | 1.612 |
| μ/mm$^{-1}$ | 1.346 | 1.259 | 3.516 |
| F(000) | 2336.0 | 1064.0 | 2900.0 |
| Crystal size/mm$^3$ | 0.206 × 0.08 × 0.072 | 0.191 × 0.18 × 0.106 | 0.438 × 0.128 × 0.064 |
| Radiation | Mo Kα (λ = 0.71073) | Mo Kα (λ = 0.71073) | Mo Kα (λ = 0.71073) |
| 2Θ range for data collection/° | 4.826 to 74.664 | 5.742 to 74.558 | 3.738 to 58 |
| Index ranges | -14 ≤ h ≤ 15, -28 ≤ k ≤ 27, -51 ≤ l ≤ 48 | -16 ≤ h ≤ 16, -20 ≤ k ≤ 21, -24 ≤ l ≤ 26 | -16 ≤ h ≤ 16, -32 ≤ k ≤ 32, -33 ≤ l ≤ 33 |
| Reflections collected | 104869 | 47659 | 104038 |
| Independent reflections | 11229 [$R_{int}$ = 0.0660, $R_{sigma}$ = 0.0503] | 9648 [$R_{int}$ = 0.0338, $R_{sigma}$ = 0.0308] | 31682 [$R_{int}$ = 0.0472, $R_{sigma}$ = 0.0583] |
| Data/restraints/ parameters | 11229/0/263 | 9648/0/254 | 31682/57/1385 |
| Goodness-of-fit on $F^2$ | 1.077 | 1.046 | 1.051 |
| Final R indexes [I>=2σ (I)] | $R_1$ = 0.0508, $wR_2$ = 0.0969 | $R_1$ = 0.0273, $wR_2$ = 0.0573 | $R_1$ = 0.0482, $wR_2$ = 0.0927 |
| Final R indexes [all data] | $R_1$ = 0.0829, $wR_2$ = 0.1066 | $R_1$ = 0.0373, $wR_2$ = 0.0607 | $R_1$ = 0.0736, $wR_2$ = 0.1005 |
| Largest diff. peak/hole / e Å$^{-3}$ | 1.04/-1.64 | 0.71/-0.85 | 1.41/-0.97 |

| **Compound** | **4.5**·DCM | **4.7**·4DCM | **4.8**·3DCM |
|---|---|---|---|
| Identification code | 21srv180 | 21srv281 | 21srv221 |
| Empirical formula | $C_{59}H_{66}Br_4Cl_2Co_2N_4P_4$ | $C_{64.7}H_{61.4}Cl_{8.7}Co_2N_4P_4$ | $C_{65}H_{62}Cl_6Co_2I_4N_4P_4$ |
| Formula weight | 1463.43 | 1445.13 | 1861.22 |
| Temperature/K | 120 | 120.0 | 120 |
| Crystal system | triclinic | triclinic | triclinic |
| Space group | P-1 | P-1 | P-1 |
| a/Å | 11.7700(6) | 11.5474(7) | 11.6309(4) |
| b/Å | 16.1821(8) | 17.1235(10) | 17.7474(6) |
| c/Å | 17.3247(8) | 19.7255(12) | 20.0867(7) |
| α/° | 74.1194(17) | 65.107(2) | 65.7961(11) |
| β/° | 85.3665(17) | 89.573(2) | 73.3159(12) |
| γ/° | 85.9732(18) | 71.176(2) | 72.7477(12) |
| Volume/Å$^3$ | 3159.4(3) | 3311.1(3) | 3545.8(2) |
| Z | 2 | 2 | 2 |
| $\rho_{calc}$g/cm$^3$ | 1.538 | 1.449 | 1.743 |
| μ/mm$^{-1}$ | 3.280 | 0.992 | 2.567 |
| F(000) | 1472.0 | 1479.0 | 1816.0 |
| Crystal size/mm$^3$ | 0.15 × 0.082 × 0.038 | 0.447 × 0.085 × 0.022 | 0.681 × 0.126 × 0.064 |
| Radiation | Mo Kα (λ = 0.71073) | Mo Kα (λ = 0.71073) | MoKα (λ = 0.71073) |
| 2Θ range for data collection/° | 4.246 to 53.998 | 3.768 to 62.998 | 3.982 to 60.068 |
| Index ranges | -15 ≤ h ≤ 14, -20 ≤ k ≤ 20, -22 ≤ l ≤ 22 | -16 ≤ h ≤ 16, -25 ≤ k ≤ 25, -28 ≤ l ≤ 28 | -16 ≤ h ≤ 16, -24 ≤ k ≤ 24, -28 ≤ l ≤ 28 |
| Reflections collected | 62072 | 87628 | 61843 |
| Independent reflections | 13762 [$R_{int}$ = 0.0416, $R_{sigma}$ = 0.0410] | 22004 [$R_{int}$ = 0.0621, $R_{sigma}$ = 0.0608] | 20668 [$R_{int}$ = 0.0624, $R_{sigma}$ = 0.0677] |
| Data/restraints/ parameters | 13762/42/790 | 22004/1/767 | 20668/110/860 |
| Goodness-of-fit on F$^2$ | 1.088 | 1.013 | 1.033 |
| Final R indexes [I>=2σ (I)] | $R_1$ = 0.0546, $wR_2$ = 0.1262 | $R_1$ = 0.0489, $wR_2$ = 0.1034 | $R_1$ = 0.0442, $wR_2$ = 0.0937 |
| Final R indexes [all data] | $R_1$ = 0.0769, $wR_2$ = 0.1364 | $R_1$ = 0.0729, $wR_2$ = 0.1134 | $R_1$ = 0.0630, $wR_2$ = 0.1008 |
| Largest diff. peak/hole / e Å$^{-3}$ | 1.59/-0.95 | 0.82/-0.95 | 1.15/-1.07 |

| **Compound** | **4.9**·2DCM | **4.10**·8DCM | **4.11**·8DCM |
|---|---|---|---|
| Identification code | 21srv285 | 21srv178 | 21srv222 |
| Empirical formula | $C_{130}H_{120}Cl_{12}Co_4N_4P_8$ | $C_{136}H_{132}Br_8Cl_{16}Co_4N_4P_8$ | $C_{136}H_{132}Cl_{16}Co_4I_8N_4P_8$ |
| Formula weight | 2647.17 | 3512.41 | 3888.33 |
| Temperature/K | 120 | 120 | 120 |
| Crystal system | triclinic | triclinic | triclinic |
| Space group | P-1 | P-1 | P-1 |
| a/Å | 11.8837(3) | 11.8240(4) | 12.0333(5) |
| b/Å | 13.8584(3) | 19.4940(6) | 14.7190(6) |
| c/Å | 20.7044(5) | 31.9203(11) | 21.4908(8) |
| α/° | 78.7260(10) | 83.8356(12) | 80.0853(15) |
| β/° | 74.1320(10) | 83.7957(13) | 82.6962(16) |
| γ/° | 69.5842(9) | 86.4443(12) | 82.5404(15) |
| Volume/Å$^3$ | 3054.82(13) | 7262.7(6) | 3696.4(3) |
| Z | 1 | 2 | 1 |
| $\rho_{calc}$g/cm$^3$ | 1.439 | 1.606 | 1.747 |
| μ/mm$^{-1}$ | 0.953 | 3.081 | 2.536 |
| F(000) | 1360.0 | 3512.0 | 1900.0 |
| Crystal size/mm$^3$ | 0.509 × 0.239 × 0.064 | 0.537 × 0.08 × 0.041 | 0.204 × 0.063 × 0.014 |
| Radiation | Mo Kα (λ = 0.71073) | Mo Kα (λ = 0.71073) | Mo Kα (λ = 0.71073) |
| 2Θ range for data collection/° | 3.856 to 66.28 | 3.824 to 60.316 | 4.118 to 60.184 |
| Index ranges | -18 ≤ h ≤ 18, -21 ≤ k ≤ 21, -31 ≤ l ≤ 31 | -16 ≤ h ≤ 16, -27 ≤ k ≤ 27, -45 ≤ l ≤ 45 | -16 ≤ h ≤ 16, -20 ≤ k ≤ 20, -30 ≤ l ≤ 30 |
| Reflections collected | 68215 | 182175 | 90624 |
| Independent reflections | 23267 [$R_{int}$ = 0.0393, $R_{sigma}$ = 0.0516] | 42877 [$R_{int}$ = 0.0519, $R_{sigma}$ = 0.0516] | 21662 [$R_{int}$ = 0.0519, $R_{sigma}$ = 0.0535] |
| Data/restraints/ parameters | 23267/6/730 | 42877/76/1689 | 21662/19/833 |
| Goodness-of-fit on F$^2$ | 1.021 | 1.020 | 1.093 |
| Final R indexes [I>=2σ (I)] | $R_1$ = 0.0425, $wR_2$ = 0.0934 | $R_1$ = 0.0456, $wR_2$ = 0.0997 | $R_1$ = 0.0597, $wR_2$ = 0.1215 |
| Final R indexes [all data] | $R_1$ = 0.0604, $wR_2$ = 0.1000 | $R_1$ = 0.0701, $wR_2$ = 0.1089 | $R_1$ = 0.0839, $wR_2$ = 0.1298 |
| Largest diff. peak/hole / e Å$^{-3}$ | 0.56/-0.47 | 1.22/-1.60 | 1.44/-1.96 |

| Compound | 4.13 | 4.14 | 4.15 |
|---|---|---|---|
| Identification code | 21srv368 | 21srv370 | 22srv037 |
| Empirical formula | $C_{24}H_{56}Br_4CoN_2$ | $C_{17}H_{33}Br_3CoN_2$ | $C_{74}H_{64}Cl_{10}Co_2N_2P_4$ |
| Formula weight | 751.27 | 564.11 | 1577.51 |
| Temperature/K | 120 | 120 | 120.00 |
| Crystal system | monoclinic | orthorhombic | monoclinic |
| Space group | C2/c | $Pca2_1$ | $P2_1/n$ |
| a/Å | 32.6980(9) | 14.0421(4) | 11.0569(3) |
| b/Å | 14.1480(4) | 11.3373(3) | 12.3902(3) |
| c/Å | 14.8115(4) | 14.1904(4) | 25.6951(6) |
| α/° | 90 | 90 | 90 |
| β/° | 109.5790(11) | 90 | 91.1592(9) |
| γ/° | 90 | 90 | 90 |
| Volume/Å$^3$ | 6455.8(3) | 2259.10(11) | 3519.44(15) |
| Z | 8 | 4 | 2 |
| $\rho_{calc}$g/cm$^3$ | 1.546 | 1.659 | 1.489 |
| μ/mm$^{-1}$ | 5.497 | 6.067 | 0.987 |
| F(000) | 3048.0 | 1124.0 | 1612.0 |
| Crystal size/mm$^3$ | 0.374 × 0.26 × 0.23 | 0.259 × 0.253 × 0.045 | 0.28 × 0.17 × 0.13 |
| Radiation | MoKα (λ = 0.71073) | Mo Kα (λ = 0.71073) | Mo Kα (λ = 0.71073) |
| 2Θ range for data collection/° | 3.168 to 64 | 4.618 to 63.996 | 3.982 to 59.998 |
| Index ranges | -48 ≤ h ≤ 48, -21 ≤ k ≤ 20, -22 ≤ l ≤ 22 | -20 ≤ h ≤ 20, -16 ≤ k ≤ 16, -21 ≤ l ≤ 21 | -15 ≤ h ≤ 15, -17 ≤ k ≤ 17, -36 ≤ l ≤ 36 |
| Reflections collected | 62265 | 59272 | 83699 |
| Independent reflections | 11203 [$R_{int}$ = 0.0389, $R_{sigma}$ = 0.0325] | 7819 [$R_{int}$ = 0.0447, $R_{sigma}$ = 0.0306] | 10246 [$R_{int}$ = 0.0391, $R_{sigma}$ = 0.0227] |
| Data/restraints/ parameters | 11203/18/330 | 7819/1/217 | 10246/0/415 |
| Goodness-of-fit on $F^2$ | 1.015 | 1.035 | 1.066 |
| Final R indexes [I>=2σ (I)] | $R_1$ = 0.0263, $wR_2$ = 0.0479 | $R_1$ = 0.0255, $wR_2$ = 0.0457 | $R_1$ = 0.0324, $wR_2$ = 0.0738 |
| Final R indexes [all data] | $R_1$ = 0.0416, $wR_2$ = 0.0512 | $R_1$ = 0.0325, $wR_2$ = 0.0477 | $R_1$ = 0.0374, $wR_2$ = 0.0759 |
| Largest diff. peak/hole / e Å$^{-3}$ | 0.73/-0.54 | 0.44/-0.55 | 0.58/-0.42 |

| **Compound** | **4.16** | **4.19**·2.6DCM | **4.26** |
|---|---|---|---|
| Identification code | 22srv127 | 21srv243 | 22srv231 |
| Empirical formula | $C_{98}H_{84}Cl_6Co_2N_2P_6$ | $C_{71.6}H_{68.2}Br_4Cl_{5.2}Co_2N_3P_4$ | $C_8H_{12}Br_2CoN_2$ |
| Formula weight | 1806.05 | 1716.41 | 354.95 |
| Temperature/K | 120.00 | 120 | 120.00 |
| Crystal system | triclinic | monoclinic | monoclinic |
| Space group | P-1 | $P2_1/n$ | $P2_1/c$ |
| a/Å | 12.0205(3) | 18.3763(6) | 13.1024(4) |
| b/Å | 12.9884(3) | 23.4798(8) | 6.7551(2) |
| c/Å | 15.5087(3) | 35.0514(12) | 13.7347(4) |
| α/° | 97.8273(9) | 90 | 90 |
| β/° | 112.4955(8) | 100.7733(12) | 104.7550(10) |
| γ/° | 96.3601(8) | 90 | 90 |
| Volume/Å$^3$ | 2180.87(9) | 14857.1(9) | 1175.54(6) |
| Z | 1 | 8 | 4 |
| $\rho_{calc}$g/cm$^3$ | 1.375 | 1.535 | 2.006 |
| μ/mm$^{-1}$ | 0.723 | 2.914 | 8.217 |
| F(000) | 932.0 | 6890.0 | 684.0 |
| Crystal size/mm$^3$ | 0.18 × 0.11 × 0.06 | 0.406 × 0.087 × 0.087 | 0.532 × 0.311 × 0.278 |
| Radiation | Mo Kα (λ = 0.71073) | Mo Kα (λ = 0.71073) | Mo Kα (λ = 0.71073) |
| 2Θ range for data collection/° | 3.726 to 59.994 | 3.832 to 58 | 6.158 to 67.518 |
| Index ranges | -16 ≤ h ≤ 16, -18 ≤ k ≤ 18, -21 ≤ l ≤ 21 | -25 ≤ h ≤ 25, -32 ≤ k ≤ 31, -47 ≤ l ≤ 47 | -20 ≤ h ≤ 20, -10 ≤ k ≤ 10, -21 ≤ l ≤ 21 |
| Reflections collected | 66202 | 308095 | 39905 |
| Independent reflections | 12677 [$R_{int}$ = 0.0370, $R_{sigma}$ = 0.0288] | 39471 [$R_{int}$ = 0.0590, $R_{sigma}$ = 0.0385] | 4680 [$R_{int}$ = 0.0604, $R_{sigma}$ = 0.0335] |
| Data/restraints/ parameters | 12677/0/514 | 39471/7/1710 | 4680/0/119 |
| Goodness-of-fit on F$^2$ | 1.024 | 1.120 | 1.065 |
| Final R indexes [I>=2σ (I)] | $R_1$ = 0.0412, $wR_2$ = 0.1013 | $R_1$ = 0.0483, $wR_2$ = 0.0934 | $R_1$ = 0.0388, $wR_2$ = 0.0751 |
| Final R indexes [all data] | $R_1$ = 0.0491, $wR_2$ = 0.1060 | $R_1$ = 0.0713, $wR_2$ = 0.1027 | $R_1$ = 0.0586, $wR_2$ = 0.0831 |
| Largest diff. peak/hole / e Å$^{-3}$ | 2.04/-1.05 | 1.27/-0.82 | 1.26/-1.09 |

| **Compound** | **4.27** | **5.1**·0.5DCM | **5.2**·0.5DCM |
|---|---|---|---|
| Identification code | 23srv175 | 21srv355 | 21srv354 |
| Empirical formula | $C_{32}H_{29}Br_2CoNP_2S$ | $C_{64.5}H_{59}BrClCoF_6N_2P_5$ | $C_{62.5}H_{57}BrClCoF_6N_4P_5$ |
| Formula weight | 740.31 | 1305.27 | 1307.26 |
| Temperature/K | 120.00 | 120 | 120 |
| Crystal system | monoclinic | monoclinic | monoclinic |
| Space group | $P2_1/n$ | $P2_1/n$ | $P2_1/n$ |
| a/Å | 9.7944(3) | 11.6342(3) | 11.4937(3) |
| b/Å | 19.4469(6) | 33.6871(8) | 33.3785(7) |
| c/Å | 16.6465(5) | 16.3153(4) | 16.2719(4) |
| α/° | 90 | 90 | 90 |
| β/° | 104.6940(10) | 108.3933(9) | 107.7431(8) |
| γ/° | 90 | 90 | 90 |
| Volume/Å$^3$ | 3066.97(16) | 6067.7(3) | 5945.6(2) |
| Z | 4 | 4 | 4 |
| $\rho_{calc}$g/cm$^3$ | 1.603 | 1.429 | 1.460 |
| μ/mm$^{-1}$ | 3.361 | 1.178 | 1.203 |
| F(000) | 1484.0 | 2672.0 | 2672.0 |
| Crystal size/mm$^3$ | 0.14 × 0.06 × 0.03 | 0.229 × 0.168 × 0.046 | 0.397 × 0.136 × 0.03 |
| Radiation | Mo Kα (λ = 0.71073) | Mo Kα (λ = 0.71073) | Mo Kα (λ = 0.71073) |
| 2Θ range for data collection/° | 4.188 to 59.998 | 3.882 to 63 | 3.916 to 58 |
| Index ranges | -13 ≤ h ≤ 13, -27 ≤ k ≤ 27, -23 ≤ l ≤ 23 | -17 ≤ h ≤ 17, -49 ≤ k ≤ 49, -23 ≤ l ≤ 23 | -15 ≤ h ≤ 15, -45 ≤ k ≤ 45, -22 ≤ l ≤ 22 |
| Reflections collected | 75138 | 147805 | 103074 |
| Independent reflections | 9064 [$R_{int}$ = 0.0563, $R_{sigma}$ = 0.0360] | 20175 [$R_{int}$ = 0.0438, $R_{sigma}$ = 0.0299] | 15791 [$R_{int}$ = 0.0504, $R_{sigma}$ = 0.0363] |
| Data/restraints/ parameters | 9064/0/378 | 20175/194/780 | 15791/290/963 |
| Goodness-of-fit on F$^2$ | 1.099 | 1.020 | 1.023 |
| Final R indexes [I>=2σ (I)] | $R_1$ = 0.0409, $wR_2$ = 0.0795 | $R_1$ = 0.0409, $wR_2$ = 0.0906 | $R_1$ = 0.0534, $wR_2$ = 0.1179 |
| Final R indexes [all data] | $R_1$ = 0.0602, $wR_2$ = 0.0857 | $R_1$ = 0.0539, $wR_2$ = 0.0965 | $R_1$ = 0.0731, $wR_2$ = 0.1287 |
| Largest diff. peak/hole / e Å$^{-3}$ | 1.15/-1.25 | 0.94/-1.15 | 1.01/-1.17 |

| **Compound** | **5.3** | **5.11**·3OC(CH$_3$)$_2$ | **5.19**·3DCM |
|---|---|---|---|
| Identification code | 23srv090 | 23srv076 | 21srv446 |
| Empirical formula | $C_{96}H_{70}BBrCoF_{24}N_2P_4$ | $C_{73}H_{76}CoF_6N_2O_5P_5$ | $C_{67}H_{64}Br_{0.25}Cl_{6.75}CoF_6N_2P_5$ |
| Formula weight | 1981.07 | 1389.13 | 1484.24 |
| Temperature/K | 120.00 | 120.00 | 120.0 |
| Crystal system | triclinic | monoclinic | triclinic |
| Space group | P-1 | $P2_1/c$ | P-1 |
| a/Å | 12.8535(5) | 17.6827(7) | 11.5759(8) |
| b/Å | 18.1906(6) | 11.3220(4) | 14.9694(10) |
| c/Å | 19.6418(7) | 33.6445(13) | 19.9811(13) |
| α/° | 74.3080(10) | 90 | 80.781(2) |
| β/° | 81.8800(10) | 95.6670(10) | 81.751(2) |
| γ/° | 83.6640(10) | 90 | 81.586(2) |
| Volume/Å$^3$ | 4364.5(3) | 6702.8(4) | 3355.3(4) |
| Z | 2 | 4 | 2 |
| $\rho_{calc}$g/cm$^3$ | 1.507 | 1.377 | 1.469 |
| μ/mm$^{-1}$ | 0.828 | 0.445 | 0.852 |
| F(000) | 2006.0 | 2896.0 | 1519.0 |
| Crystal size/mm$^3$ | 0.316 × 0.223 × 0.076 | 0.446 × 0.081 × 0.053 | 0.13 × 0.05 × 0.014 |
| Radiation | Mo Kα (λ = 0.71073) | Mo Kα (λ = 0.71073) | Mo Kα (λ = 0.71073) |
| 2Θ range for data collection/° | 3.822 to 61.016 | 3.798 to 57.398 | 3.916 to 52 |
| Index ranges | -18 ≤ h ≤ 18, -25 ≤ k ≤ 25, -28 ≤ l ≤ 28 | -23 ≤ h ≤ 23, -15 ≤ k ≤ 15, -45 ≤ l ≤ 45 | -14 ≤ h ≤ 14, -18 ≤ k ≤ 18, -24 ≤ l ≤ 24 |
| Reflections collected | 164746 | 109721 | 52650 |
| Independent reflections | 26627 [$R_{int}$ = 0.0961, $R_{sigma}$ = 0.0688] | 17261 [$R_{int}$ = 0.1325, $R_{sigma}$ = 0.0940] | 13191 [$R_{int}$ = 0.1276, $R_{sigma}$ = 0.1473] |
| Data/restraints/ parameters | 26627/709/1311 | 17261/0/835 | 13191/76/829 |
| Goodness-of-fit on F$^2$ | 1.045 | 1.199 | 1.022 |
| Final R indexes [I>=2σ (I)] | $R_1$ = 0.0553, $wR_2$ = 0.1030 | $R_1$ = 0.0953, $wR_2$ = 0.1567 | $R_1$ = 0.0888, $wR_2$ = 0.1486 |
| Final R indexes [all data] | $R_1$ = 0.0899, $wR_2$ = 0.1147 | $R_1$ = 0.1318, $wR_2$ = 0.1687 | $R_1$ = 0.1765, $wR_2$ = 0.1797 |
| Largest diff. peak/hole / e Å$^{-3}$ | 0.56/-0.75 | 0.58/-0.53 | 1.05/-0.65 |

| **Compound** | **5.23**·3OC(CH$_3$)$_2$ | **5.32**·DCM | **5.47** |
|---|---|---|---|
| Identification code | 23srv070 | 21srv286 | 21srv428 |
| Empirical formula | $C_{73}H_{76}Br_{0.24}CoF_6N_2O_{4.53}P_5$ | $C_{63}H_{59}Cl_6Co_2N_4P_4$ | $C_{32}H_{29}Br_2NO_2P_2Zn$ |
| Formula weight | 1400.55 | 1326.58 | 746.69 |
| Temperature/K | 120.00 | 150 | 120.0 |
| Crystal system | monoclinic | triclinic | orthorhombic |
| Space group | $P2_1/c$ | P-1 | $P2_12_12_1$ |
| a/Å | 17.7352(12) | 11.9094(5) | 10.6084(4) |
| b/Å | 11.3289(8) | 14.2646(6) | 15.3952(7) |
| c/Å | 33.583(2) | 18.9925(8) | 18.8859(8) |
| α/° | 90 | 97.8859(16) | 90 |
| β/° | 95.572(2) | 102.6242(17) | 90 |
| γ/° | 90 | 91.4158(18) | 90 |
| Volume/Å$^3$ | 6715.7(8) | 3113.7(2) | 3084.4(2) |
| Z | 4 | 2 | 4 |
| $\rho_{calc}$g/cm$^3$ | 1.385 | 1.415 | 1.608 |
| μ/mm$^{-1}$ | 0.585 | 0.936 | 3.521 |
| F(000) | 2914.0 | 1362.0 | 1496.0 |
| Crystal size/mm$^3$ | 0.568 × 0.058 × 0.047 | 0.159 × 0.152 × 0.093 | 0.09 × 0.07 × 0.06 |
| Radiation | Mo Kα (λ = 0.71073) | Mo Kα (λ = 0.71073) | Mo Kα (λ = 0.71073) |
| 2Θ range for data collection/° | 3.514 to 50.054 | 3.71 to 65 | 4.664 to 59.996 |
| Index ranges | -21 ≤ h ≤ 21, -13 ≤ k ≤ 13, -39 ≤ l ≤ 39 | -18 ≤ h ≤ 18, -21 ≤ k ≤ 21, -28 ≤ l ≤ 28 | -14 ≤ h ≤ 14, -21 ≤ k ≤ 21, -26 ≤ l ≤ 26 |
| Reflections collected | 117291 | 67297 | 75306 |
| Independent reflections | 11859 [$R_{int}$ = 0.1224, $R_{sigma}$ = 0.0633] | 22500 [$R_{int}$ = 0.0372, $R_{sigma}$ = 0.0466] | 8984 [$R_{int}$ = 0.0863, $R_{sigma}$ = 0.0539] |
| Data/restraints/ parameters | 11859/0/845 | 22500/0/723 | 8984/0/361 |
| Goodness-of-fit on F$^2$ | 1.208 | 1.033 | 1.040 |
| Final R indexes [I>=2σ (I)] | $R_1$ = 0.0966, $wR_2$ = 0.2003 | $R_1$ = 0.0454, $wR_2$ = 0.0999 | $R_1$ = 0.0399, $wR_2$ = 0.0790 |
| Final R indexes [all data] | $R_1$ = 0.1154, $wR_2$ = 0.2088 | $R_1$ = 0.0611, $wR_2$ = 0.1066 | $R_1$ = 0.0532, $wR_2$ = 0.0837 |
| Largest diff. peak/hole / e Å$^{-3}$ | 0.76/-0.68 | 0.66/-0.95 | 0.60/-0.50 |

## Appendix 5 – GaussSum UV-Vis Data

Transition discussed in **Section 5.3.7**, **Chapter 5**, is in bold, with -88 highlighted in yellow.

HOMO is 436

| No. | Energy (cm-1) | Wavelength (nm) | Osc. Strength | Symmetry | Major contribs | Minor contribs | Co | me1 | me2 | ph1 | ph2 | ph3 | ph4 | ph5 | ph6 | ph7 | ph8 | pnp1 | pnp2 | B | bph1 | bph2 | bph3 | bph4 |
|---|---|---|---|---|---|---|---|---|---|---|---|---|---|---|---|---|---|---|---|---|---|---|---|---|
| 1 | 11877.3205215 | 841.940737554 | 0.0109 | Singlet-A | HOMO->LUMO (68%) | HOMO->L+2 (7%), HOMO->L+4 (7%), HOMO->L+19 (6%), HOMO->L+20 (2%) | 103-->24 (-79) | 0-->0 (0) | 0-->0 (0) | 0-->7 (7) | 0-->3 (3) | 0-->7 (7) | 0-->4 (4) | 0-->2 (2) | 1-->6 (5) | 0-->12 (12) | 0-->2 (2) | -3-->14 (17) | -3-->14 (17) | 0-->0 (0) | 0-->0 (0) | 0-->2 (2) | 0-->0 (0) | 0-->2 (2) |
| 2 | 13567.8586046 | 737.035982714 | 0.003 | Singlet-A | H-1->LUMO (66%) | H-1->L+2 (6%), H-1->L+4 (8%), H-1->L+19 (7%), H-1->L+20 (3%) | 87-->24 (-63) | 0-->0 (0) | 0-->0 (0) | 0-->7 (7) | 0-->3 (3) | 0-->6 (6) | 1-->4 (3) | 0-->2 (2) | 1-->6 (5) | 0-->12 (12) | 0-->2 (2) | 4-->14 (10) | 5-->14 (9) | 0-->0 (0) | 0-->0 (0) | 0-->2 (2) | 0-->0 (0) | 0-->3 (3) |
| 3 | 16619.860564 | 601.689765176 | 0.0031 | Singlet-A | H-2->LUMO (65%) | H-2->L+2 (6%), H-2->L+4 (7%), H-2->L+19 (6%), H-2->L+20 (2%) | 79-->24 (-55) | 0-->0 (0) | 0-->0 (0) | 0-->7 (7) | 1-->3 (2) | 0-->7 (7) | 1-->4 (3) | 1-->2 (1) | 0-->6 (6) | 0-->12 (12) | 1-->2 (1) | 8-->14 (6) | 8-->14 (6) | 0-->0 (0) | 0-->0 (0) | 0-->2 (2) | 0-->0 (0) | 0-->2 (2) |
| 4 | 19291.9753873 | 518.350236265 | 0.0011 | Singlet-A | HOMO->L+1 (94%) | 103-->3 (-100) | 0-->1 (1) | 0-->0 (0) | 0-->25 (25) | 0-->6 (6) | 0-->12 (12) | 0-->27 (27) | 0-->0 (0) | 1-->0 (-1) | 0-->0 (0) | 0-->1 (1) | -3-->0 (3) | -3-->25 (28) | 0-->0 (0) | 0-->0 (0) | 0-->0 (0) | 0-->0 (0) | 0-->0 (0) | 0-->0 (0) |
| **5** | **19816.2357661** | **504.636708911** | **0.0301** | **Singlet-A** | **HOMO->LUMO (24%), HOMO->L+2 (45%), HOMO->L+4 (16%)** | **HOMO->L+19 (4%)** | **103-->15 (-88)** | **0-->0 (0)** | **0-->0 (0)** | **0-->14 (14)** | **0-->10 (10)** | **0-->5 (5)** | **0-->12 (12)** | **0-->5 (5)** | **1-->3 (2)** | **0-->6 (6)** | **0-->7 (7)** | **-3-->9 (12)** | **-3-->12 (15)** | **0-->0 (0)** | **0-->0 (0)** | **0-->1 (1)** | **0-->0 (0)** | **0-->1 (1)** |
| 6 | 21436.603614 | 466.491809061 | 0.0064 | Singlet-A | H-10->LUMO (47%) | H-12->LUMO (3%), H-11->LUMO (6%), H-10->L+2 (5%), H-10->L+4 (7%), H-10->L+19 (7%), H-10->L+20 (3%) | 56-->24 (-32) | 1-->0 (-1) | 0-->0 (0) | 0-->7 (7) | 1-->3 (2) | 1-->6 (5) | 0-->4 (4) | 2-->2 (0) | 12-->6 (-6) | 1-->12 (11) | 2-->2 (0) | 4-->13 (9) | 4-->14 (10) | 0-->0 (0) | 2-->0 (-2) | 13-->2 (-11) | 1-->0 (-1) | 1-->3 (2) |
| 7 | 21823.7497399 | 458.216398153 | 0.0178 | Singlet-A | H-1->L+1 (12%), H-1->L+2 (17%), HOMO->L+3 (43%) | H-1->LUMO (8%), H-1->L+4 (7%) | 95-->9 (-86) | 0-->0 (0) | 0-->0 (0) | 0-->10 (10) | 0-->7 (7) | 0-->3 (3) | 0-->9 (9) | 0-->22 (22) | 1-->3 (2) | 0-->12 (12) | 0-->4 (4) | 0-->13 (13) | 1-->8 (7) | 0-->0 (0) | 0-->0 (0) | 0-->0 (0) | 0-->0 (0) | 0-->0 (0) |

8 21888.2740942 456.865623894 0.0276 Singlet-A H-1->LUMO (14%), H-1->L+2 (25%), HOMO->L+3 (38%) H-1->L+4 (8%), H-1->L+19 (2%) 94-->11 (-83) 0-->0 (0) 0-->0 (0) 0-->8 (8) 0-->8 (8) 0-->3 (3) 0-->7 (7) 0-->20 (20) 1-->4 (3) 0-->12 (12) 0-->5 (5) 1-->14 (13) 2-->7 (5) 0-->0 (0) 0-->0 (0) 0-->0 (0) 0-->0 (0) 0-->1 (1)

9 22214.1220835 450.16408762 0.0077 Singlet-A H-1->L+1 (77%) H-1->LUMO (2%), H-1->L+3 (5%), HOMO->L+3 (8%) 89-->4 (-85) 0-->1 (1) 0-->0 (0) 0-->21 (21) 0-->5 (5) 0-->10 (10) 1-->22 (21) 0-->6 (6) 1-->1 (0) 0-->3 (3) 0-->1 (1) 3-->3 (0) 4-->22 (18) 0-->0 (0) 0-->0 (0) 0-->0 (0) 0-->0 (0) 0-->0 (0)

10 23362.6555904 428.03353246 0.0036 Singlet-A HOMO->L+2 (34%), HOMO->L+4 (62%) 103-->8 (-95) 0-->0 (0) 0-->0 (0) 0-->23 (23) 0-->15 (15) 0-->2 (2) 0-->18 (18) 0-->9 (9) 1-->1 (0) 0-->4 (4) 0-->6 (6) -3-->5 (8) -3-->9 (12) 0-->0 (0) 0-->0 (0) 0-->0 (0) 0-->0 (0) 0-->0 (0)

11 24841.0698588 402.559151311 0.002 Singlet-A H-2->L+1 (92%) 79-->3 (-76) 0-->1 (1) 0-->0 (0) 0-->25 (25) 1-->6 (5) 0-->12 (12) 1-->27 (26) 1-->0 (-1) 0-->0 (0) 0-->0 (0) 1-->1 (0) 8-->0 (-8) 8-->25 (17) 0-->0 (0) 0-->0 (0) 0-->0 (0) 0-->0 (0) 0-->0 (0)

12 25116.1049191 398.150908838 0.0687 Singlet-A H-2->LUMO (18%), H-2->L+2 (38%), H-2->L+4 (13%), H-1->L+3 (12%) H-2->L+3 (2%), H-2->L+19 (3%) 80-->13 (-67) 0-->0 (0) 0-->0 (0) 0-->12 (12) 1-->10 (9) 0-->4 (4) 1-->11 (10) 1-->11 (10) 0-->3 (3) 0-->8 (8) 1-->6 (5) 7-->10 (3) 7-->10 (3) 0-->0 (0) 0-->0 (0) 0-->0 (0) 0-->0 (0) 0-->1 (1)

13 25258.0584986 395.913248858 0.0242 Singlet-A H-1->L+3 (73%) H-2->LUMO (5%), H-2->L+2 (5%), H-1->L+1 (4%) 86-->8 (-78) 0-->0 (0) 0-->1 (1) 0-->4 (4) 0-->5 (5) 0-->1 (1) 1-->3 (2) 0-->34 (34) 1-->4 (3) 0-->17 (17) 0-->2 (2) 4-->18 (14) 5-->3 (-2) 0-->0 (0) 0-->0 (0) 0-->0 (0) 0-->0 (0) 0-->0 (0)

14 25854.908776 386.773749102 0.0023 Singlet-A HOMO->L+5 (48%), HOMO->L+6 (10%), HOMO->L+7 (28%) HOMO->L+2 (4%), HOMO->L+4 (4%) 103-->3 (-100) 0-->1 (1) 0-->0 (0) 0-->24 (24) 0-->14 (14) 0-->8 (8) 0-->28 (28) 0-->4 (4) 1-->1 (0) 0-->6 (6) 0-->6 (6) -3-->2 (5) -3-->3 (6) 0-->0 (0) 0-->0 (0) 0-->0 (0) 0-->0 (0) 0-->0 (0)

15 26091.2292237 383.270558633 0.0038 Singlet-A HOMO->L+5 (34%), HOMO->L+6 (54%) HOMO->L+7 (4%) 103-->3 (-100) 0-->1 (1) 0-->0 (0) 0-->21 (21) 0-->20 (20) 0-->3 (3) 0-->13 (13) 0-->9 (9) 1-->4 (3) 0-->19 (19) 0-->2 (2) -3-->4 (7) -3-->2 (5) 0-->0 (0) 0-->0 (0) 0-->0 (0) 0-->0 (0) 0-->0 (0)

16 26363.0380663 379.318953106 0.0023 Singlet-A H-1->L+2 (34%), H-1->L+4 (59%) 87-->8 (-79) 0-->0 (0) 0-->0 (0) 0-->23 (23) 0-->15 (15) 0-->2 (2) 1-->18 (17) 0-->9 (9) 1-->1 (0)

0-->4 (4) 0-->6 (6) 4-->5 (1) 5-->9 (4) 0-->0 (0) 0-->0 (0) 0-->0 (0) 0-->0 (0) 0-->0 (0)
17 26484.8277851 377.574665811 0.0008 Singlet-A HOMO->L+5 (11%), HOMO->L+6 (26%), HOMO->L+7 (55%) 103-->2 (-101) 0-->0 (0) 0-->0 (0) 0-->9 (9) 0-->15 (15) 0-->12 (12) 0-->27 (27) 0-->7 (7) 1-->2 (1) 0-->10 (10) 0-->9 (9) -3-->4 (7) -3-->2 (5) 0-->0 (0) 0-->0 (0) 0-->0 (0) 0-->0 (0) 0-->0 (0)
18 27458.3389809 364.18808898 0.0061 Singlet-A HOMO->L+8 (74%), HOMO->L+9 (11%) H-2->L+3 (8%), HOMO->L+10 (2%) 101-->2 (-99) 0-->0 (0) 0-->0 (0) 0-->23 (23) 0-->6 (6) 0-->13 (13) 0-->25 (25) 0-->9 (9) 1-->2 (1) 0-->11 (11) 0-->6 (6) -2-->3 (5) -2-->1 (3) 0-->0 (0) 0-->0 (0) 0-->0 (0) 0-->0 (0) 0-->0 (0)
19 27576.9024819 362.622307076 0.0004 Singlet-A H-2->L+3 (73%), HOMO->L+9 (11%) H-2->L+2 (3%), HOMO->L+8 (3%) 82-->6 (-76) 0-->0 (0) 0-->1 (1) 0-->4 (4) 1-->5 (4) 0-->3 (3) 1-->3 (2) 1-->34 (33) 0-->5 (5) 0-->17 (17) 1-->6 (5) 6-->17 (11) 6-->1 (-5) 0-->0 (0) 0-->0 (0) 0-->0 (0) 0-->0 (0) 0-->0 (0)
20 27849.5178789 359.072643321 0.0005 Singlet-A HOMO->L+8 (16%), HOMO->L+9 (65%) H-2->L+3 (6%), HOMO->L+10 (4%) 102-->2 (-100) 0-->0 (0) 0-->0 (0) 0-->13 (13) 0-->7 (7) 0-->15 (15) 0-->8 (8) 0-->13 (13) 1-->4 (3) 0-->10 (10) 0-->22 (22) -2-->4 (6) -2-->3 (5) 0-->0 (0) 0-->0 (0) 0-->0 (0) 0-->0 (0) 0-->0 (0)
21 28241.5033314 354.088799121 0.0002 Singlet-A H-3->LUMO (99%) 0-->29 (29) 0-->0 (0) 0-->0 (0) 0-->5 (5) 0-->1 (1) 0-->8 (8) 0-->2 (2) 0-->0 (0) 0-->7 (7) 0-->15 (15) 0-->0 (0) 0-->16 (16) 0-->17 (17) 3-->0 (-3) 22-->0 (-22) 4-->0 (-4) 64-->0 (-64) 8-->0 (-8)
22 28671.3968421 348.779658524 0.0031 Singlet-A HOMO->L+10 (70%) H-1->L+5 (4%), H-1->L+7 (2%), HOMO->L+9 (4%), HOMO->L+11 (8%) 102-->2 (-100) 0-->0 (0) 0-->1 (1) 0-->3 (3) 0-->5 (5) 0-->5 (5) 0-->7 (7) 0-->42 (42) 1-->3 (2) 0-->17 (17) 0-->13 (13) -3-->2 (5) -2-->1 (3) 0-->0 (0) 0-->0 (0) 0-->0 (0) 0-->0 (0) 0-->0 (0)
23 28780.28169 347.460115495 0.0002 Singlet-A H-2->L+2 (33%), H-2->L+4 (59%) 79-->8 (-71) 0-->0 (0) 0-->0 (0) 0-->23 (23) 1-->15 (14) 0-->2 (2) 1-->18 (17) 1-->9 (8) 0-->1 (1) 0-->4 (4) 1-->6 (5) 8-->5 (-3) 8-->9 (1) 0-->0 (0) 0-->0 (0) 0-->0 (0) 0-->0 (0) 0-->0 (0)
24 28832.7077279 346.828334486 0.0004 Singlet-A H-4->LUMO (99%) 0-->29 (29) 0-->0 (0) 0-->0 (0) 0-->5 (5) 0-->1 (1) 0-->8 (8) 0-->2 (2) 0-->0 (0) 0-->7 (7) 0-->15 (15) 0-->0 (0) 0-->16 (16) 0-->17 (17) 4-->0 (-4) 7-->0 (-7) 29-->0 (-29) 7-->0 (-7) 52-->0 (-52)
25 29047.251206 344.266654668 0.0062 Singlet-A H-1->L+5 (74%), H-1->L+7 (11%) H-1->L+4 (2%), HOMO->L+10 (4%) 88-->2 (-86) 0-->1 (1) 0-->0 (0) 0-->33 (33) 0-->13 (13) 0-->6 (6) 1-->30 (29) 0-->4 (4) 1-->0

(-1) 0-->4 (4) 0-->4 (4) 4-->1 (-3) 5-->2 (-3) 0-->0 (0) 0-->0 (0) 0-->0 (0) 0-->0 (0) 0-->0 (0)